88th ANNUAL

NEW YORK STATE GEOLOGICAL ASSOCIATION

FIELD CONFERENCE

JOINT CONFERENCE WITH FRIENDS OF THE GRENVILLE

"GEOLOGIC DIVERSITY IN THE NEW YORK METROPOLITAN AREA"

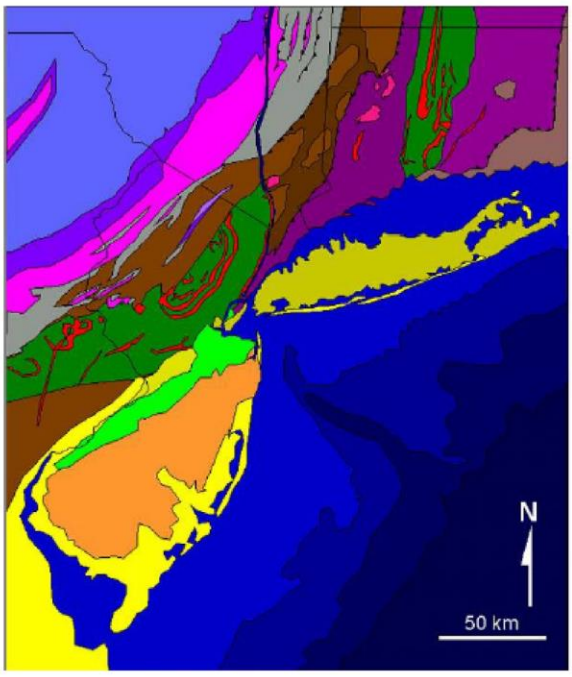

SEPTEMBER 30-OCTOBER 2, 2016

http://www.nysga-online.net/

Image courtesy of the U.S. Geological Survey

88th ANNUAL

NEW YORK STATE GEOLOGICAL ASSOCIATION

FIELD CONFERENCE

JOINT CONFERENCE WITH FRIENDS OF THE GRENVILLE

"GEOLOGIC DIVERSITY IN THE NEW YORK METROPOLITAN AREA"

SEPTEMBER 30-OCTOBER 2, 2016

Hosts: Rutgers University-Newark & Hofstra University

Organizers: Alexander E. Gates & J Bret Bennington

Field Volume Editor: Alexander E. Gates

http://www.nysga-online.net/

image courtesy of the U.S. Geological Survey

SPONSORS OF THE CONFERENCE

FIELD TRIPS

Trip Title **Page**

Friday, September 30

Tectonic evolution of the western Hudson Highlands basement, New York,

Jeff Chiarenzelli, David Valentino, Alexander Gates and Matthew Gorring……6

Saturday, October 1

A-1 Cretaceous Fossil Localities in Central New Jersey, J Bret Bennington……..43

A-2 Environmental Geology of the Hackensack Meadowlands Estuary, NJ,

Francisco Artigas, Joseph Grzyb and Michael Stepowyj……..63

Electrical Environmental Geophysics in Northern New Jersey, Dimitris Ntarlagiannis……..75

A-3 Crystalline Megaboudins Along the Leading Edge of the

Taconic Thrust Sheet, Orange County, NY**,** Alexander Gates……91

A-4 *Petrogenesis and Tectonics of pre-, syn-, and post-Ottawan Granitoids

of the western Hudson Highlands, NY, Matthew Gorring, Alexander Gates

and David Valentino……112

A-5 Stratigraphy, Structure and Tectonics of New York City as Viewed Through

Its Parks and Engineering Projects, Charles Merguerian and Mickey Merguerian……142

A-6 New Insights on rift basin development, mass extinction, and carbon

sequestration from outcrops, and new core, drill holes and seismic lines

from the northern Newark Basin (New York and New Jersey), Paul Olsen,

Sean T. Kinney, Natalia V. Zakharova, Roy W. Schlische,

Martha O. Withjack, Dennis V. Kent, David S. Goldberg and Brian E. Slater……190

Sunday, October 2

B-1 Geology of Staten Island, NY, Alan Benimoff……276

B-2 Naturally occurring filtration systems sequestering metal contaminants

from historical tailing wastes at the Sterling Lake Smelter Complex,

Hudson Highlands, NewYork, Sivajini Gilchrist and Alexander Gates……294

B-3 *Late Proterozoic Shear Zones in the Western Hudson Highlands, NY,

Michael Kalczynski and Alexander Gates……305

B-4 Lower to Middle Devonian rocks of the Delaware Water Gap

National Recreation Area, New Jersey: fracture and lithologic control

on rock-shelters, karst and groundwater flow, Don Monteverde and Don Witte……334

B-5 New Insights on rift basin development, mass extinction,

and carbon sequestration from outcrops, and new core, drill holes

and seismic lines from the northern Newark Basin (New York and New Jersey),

Paul Olsen et al. Continued……190

B-6 Late- and Post- Igneous Mineralization of the Orange Mountain Basalt

and the co-Magmatic Lower Palisades Sill, John Puffer,

Karin A. Block, Chris Laskowich and Michael Dorsey……418

** denotes joint NYSGA-FOG field trips*

TECTONIC EVOLUTION OF THE WESTERN HUDSON HIGHLANDS, NEW YORK

JEFFREY R. CHIARENZELLI
St. Lawrence University, Canton, NY 13617

DAVID W. VALENTINO
Department of Atmospheric and Geological Sciences, State University of New York at Oswego, Oswego, NY 13126

ALEXANDER E. GATES
Department of Earth and Environmental Sciences, Rutgers University, Newark, NJ 07102

MATTHEW L. GORRING
Department of Earth and Environmental Studies, Montclair State University, Upper Montclair, NJ 07043

INTRODUCTION

The New York Geological Association field conference in 2001 was organized to be run in southern New York State and northern New Jersey. Although the field guide for the conference was published by the association, the decision was made to postpone the field conference due to the attacks that took place on September 11th that year. In the end, the field trips were not run that year. Between 2001 and 2006, a considerable amount of geologic mapping was complete in the western Hudson Highlands supported by new geochronology and geochemistry, so a field excursion was prepared for the 2006 National Geological Society of America meeting held in Philadelphia (Gates et al., 2006). That field trip was canceled due to low attendance.

Over the past decade, the authors of this field guide have continued to examine the rocks of the Hudson Highlands but also in the context of the rocks exposed in the southernmost Adirondacks. This field trip is a continuation of the trip and field guide that was prepared by Gates et al. (2001) but never held. With the integration of continued bedrock mapping in the western Hudson Highlands, coupled with new geochronology and geochemistry, our objective with this trip is to provide a general tectonic overview to support other field trips on basement geology being run during this field conference. With the heavy emphasis on basement geology this year, it's worth noting that the NYSGA field conference is being run in conjunction with the annual field conference of the Friends of the Grenville.

LITHOTECTONIC UNITS

Early mapping in the region of the Hudson Highlands divide the bedrock according to lithology (Dallmeyer, 1974), resulting in geologic maps of rock types, with no apparent tectonic connections. Later mapping (Gundersen, 1986), using a strategy of "lumping" rock bodies a lithologic assemblages with common tectonic affinity, resulted in the definition of lithotectonic units, or lithofacies. Applying this system of grouping lithologies by inferred tectonic association, the bedrock geology of the western Hudson Highlands, NY was remapped and recompiled for the purpose of discovering tectonic

boundaries and associations. During a decade-long field project funded by the USGS StateMap program through the New York State Museum, the following 7.5 minute quadrangles were completed as open-file reports: Sloatsburg, Theills, Monroe, Popolopen Lake, Maybrook, Cornwall and part of Greenwood Lake and Warwick. Figure 1 is a simplified version of some of the new geological maps for this region.

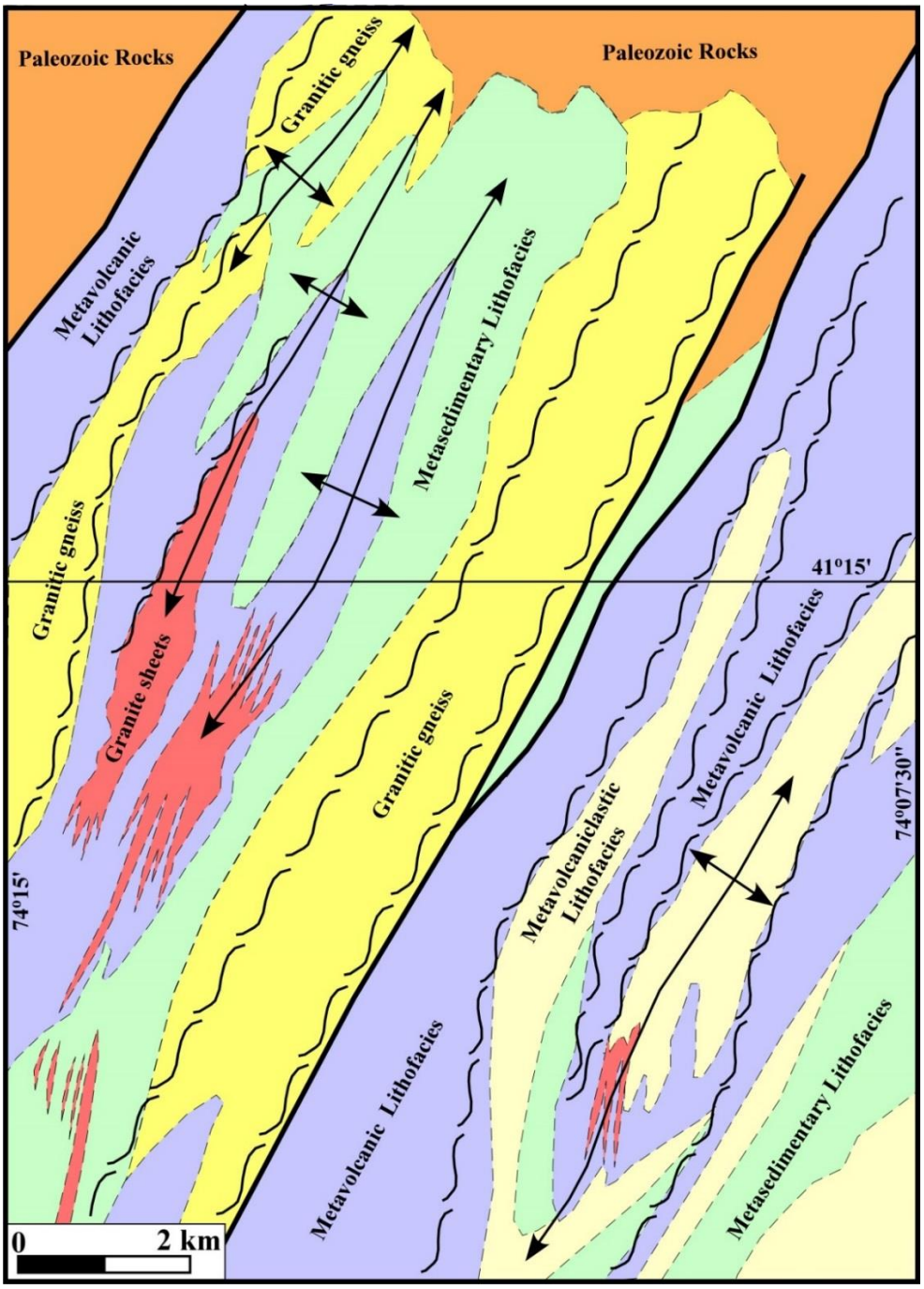

Figure 1. Geologic map of the western Hudson Highlands basement. Ductile shear zones are represented by the dashed "S" lines.

Metasedimentary Lithofacies

The metasedimentary lithofacies includes a suite of granulite facies metamorphic rocks with protoliths that were most likely sedimentary. This lithofacies includes bodies of quartzite, minor marble, pelitic, semipelitic and psammitic gneisses (Figure 2A), and calcsilicate gneiss (Figure 2B). The meta-pelite and psammite consist of interlayered biotite-garnet gneiss with medium to coarse quartz, plagioclase, K-feldspar and local sillimanite, and cordierite with thin granitic layers. Within the metapelite are zones of graphite-pyrite-garnet gneiss with biotite, quartz, K-feldspar, plagioclase, and minor sillimanite. Some metapelites include migmatite with biotite-garnet melanosomes and thin layers of course granite both parallel and cross cutting the dominant gneissocity. The pelitic gneiss is often interlayered with semipelitic and psammitic gneiss and may include quartzite layers (10-50 cm thick), discontinuous layers (10-20 cm thick) of diopside and diopside-garnet marble, and calcsilicate gneiss. The calcsilicate gneiss is quartzofeldspathic with salite, apatite, sphene, scapolite, and hornblende, and is commonly migmatitic. Some calcsilicate gneiss bodies are 10's of meters thick and were mapped as separate rock bodies. All of these roock bodies are dominated by coarse gneissocity that includes intrafolial pegmatites that exhibit rootless isoclinal folding. The contacts of this gneiss body assemblage with the regional quartzofeldspathic gneiss and rocks of the metavolcanic lithofacies can be sharp or gradational.

A.

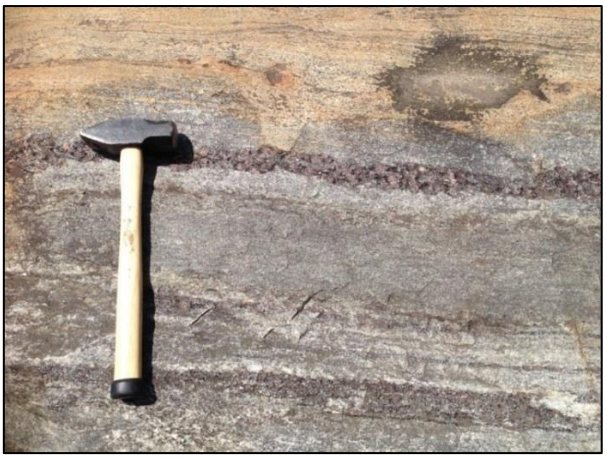

B.

Figure 2. Photographs of metasedimentary rock outcrops. A. Psammitic gneiss with concentrations of garnet and biotite. B. Calcsilicate gneiss with K-feldspar-quartz leucosomes.

Metavolcanic Lithofacies

The metavolcanic lithofacies includes bodies of gneiss that are made up of a mineralogically and chemically diverse assemblage of interlayered rocks at decimeter to meter scale (Figure 3). This assemblage of rocks consists of interlayered black and pale gray mafic, intermediate, and felsic gneiss. The mafic gneiss is medium to coarse grained with well-developed foliation defined by aligned augite, hornblende, plagioclase, and ortho and clino-pyroxene, and local concentrations of magnetite. The intermediate gneiss consists of medium to coarse-grained plagioclase, quartz, and minor hornblende and/or pyroxene. These two gneisses are intimately interlayered at the outcrop scale, and may include minor layers of felsic gneiss consisting of quartz, K-feldspar, plagioclase with minor hornblende.

Figure 3. Outcrop photograph of interlayered mafic, intermediate and felsic gneiss defining the metavolcanic lithofacies.

The gneissic layering ranges in thickness from 5 cm to 1.5 m with varying proportions of each rock type. Local interlayers of quartzite and calcsilicate gneiss also occur. This assemblage of rocks was inferred to have a volcanic origin, hence the metavolcanic lithofaices, based on the diverse range of rock compositions that are dominated by mafic and intermediate lithologies, and supported by being interlayered at the outcrop scale. The contacts of the metavolcanic lithofacies with metavolcaniclastic lithofacies (Figure 4) and metasedimentary lithofacies rocks are generally gradational but can be sharp locally.

Metavolcaniclastic Lithofacies

About 30% of the western Hudson Highlands is underlain by medium to coarse grained quartzofeldspathic gneiss (Figure 4). The gneiss is characterized by massive to layered quartz-plagioclase aggregates with minor amounts of biotite, and/or hornblende, and trace magnetite, K-

feldspar, or garnet. Compositional layering in the gneiss is defined by the proportion of mafic minerals. Gates et al. (2001) reported on some layering containing gradual increase in mica with sharp contacts possibly representing original sedimentary compositional variation. In places, the quartzofelspathic gneiss contains layers of amphibolite that are parallel to compositional layering and pervasive foliation. Locally the gneiss is interlayered with quartzite and amphibolite layers near the contacts with the metasedimentary and metavolcanic lithofacies bodies, respectively. A second foliation is directly associated with steeply dipping km-scale ductile shear zones that are well developed in the quartzofeldspatic gneiss. Commonly small pockets of granite occur between foliation boudins in the gneiss. The unit is also host to cross cutting pegmatites ranging from decimeter to several meters thick. Based on the mineral composition and the occurrence of compositional layers in the quartzofeldspathic gneiss, the unit is interpreted to represent a sequence of volcaniclastic metasedimentary rocks.

Figure 4. Outcrop photograph of strongly foliated quartzofeldspathic gneiss with an amphibolite layer.

Granitic gneiss

In the westernmost blocks of the Hudson Highlands, there are multiple northeast striking bodies of grantic gneiss that are greatly impacted by steeply dipping ductile shear zones and are considered mylonites (Figure 1). Although mineralogically similar to the quartzofeldspathic rocks, these rocks contain relict plutonic textures such as megacrysts of plagioclase and K-feldpspar that form asymmetric augen that form rotated porphyroclasts. Additionally, these granitic gneiss bodies do not contain the compositional layering that is so prominent. To characterize the geochemistry of the granitic gneiss

body, a suite of samples was collected where the body is exposed on Route 17A. As might be expected, the granitic gneisses have a relatively limited range in major oxide and trace element chemistry. For example, SiO_2 content ranges from 64.54 to 71.87% which is quite silicic. Details of the geochemistry are described below.

Figure 5. Outcrop photographs of granitic gneiss of the western Hudson Highlands. A. Strongly foliated course grained gneiss with minor leucosome where the foliation is disrupted. B. Course grained granitic gneiss with relict megacrysts of K-feldspar that form both symmetric and asymmetric augen.

Granite Sheets

There is a suite of granite sheets that are concordant to the local folation, and appear to have intruded all of the units previously described (Figure 1). The sheets range in thickness from 5 to 50 m and are laterally continuous for several kilometers. The granite is generally medium to coarse grained, locally megacrystic, and the margins of the sheets contain mylonitic foliation that is concordant with the adjacent rock bodies (Figure 6). The granite sheets commonly contain xenoliths of the local country rock. Where the granite is mylonitic, the contact with the quartzofeldspathic gneiss is difficult to determine. Although there are a few exceptions, most of the granite sheets occur in the hinge regions of km-scale upright folds in the western Hudson Highlands (Figures 1). Based on these field relations, it was concluded that the granite sheets were intruded during deformation (Thomas et al., 2001; Linguanti et al., 2011).

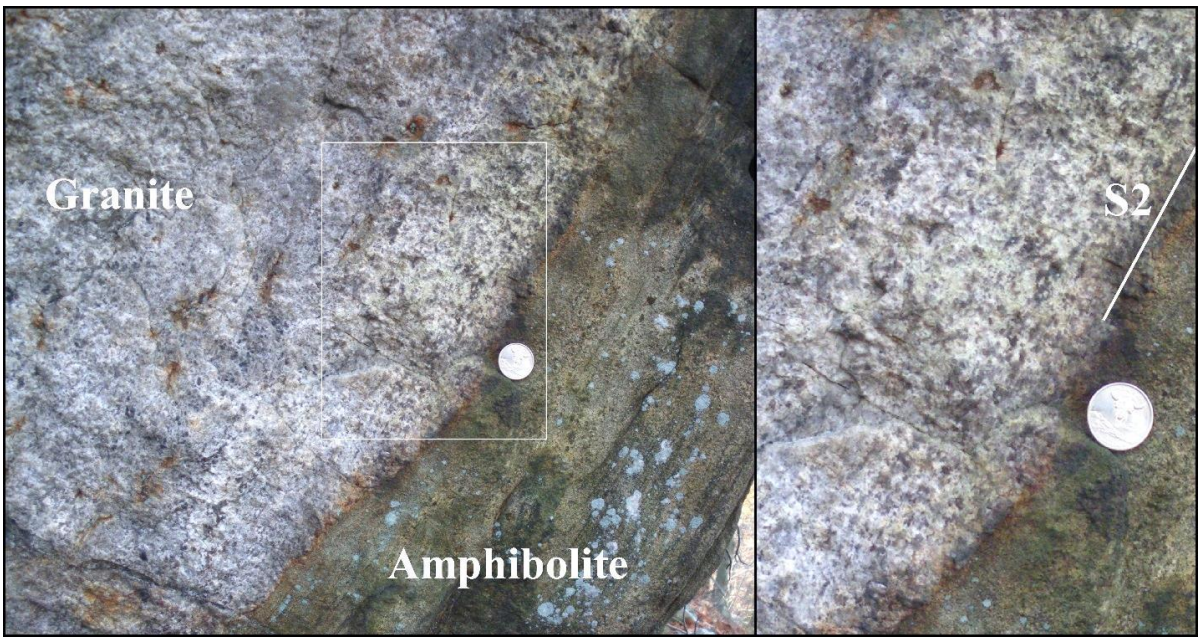

Figure 6. Photograph of the contact between the granite sheet at Tiger Hill and the local amphibolite. Note the weakly developed foliation in the margin of the granite that is parallel to the S2 foliation in the amphibolite.

Lake Tioroti Diorite

Coarse- to very coarse-grained black and white speckled diorite contains plagioclase, pyroxene, hornblende, and biotite locally. The diorite grades to lower pyroxene, anorthositic compositions locally. Texture ranges from granoblastic to foliated and mylonitic with S-C fabric. The diorite locally contains xenoliths of country rock with ductile contacts that are partially melted to form a rind of coarse to pegmatitic granite around them and filling fractures in the diorite. The primary occurrence of this diorite is on the west shore of Lake Tioroti, and based on cross cutting relations and occurrence of local xenoliths, the diorite was used to determine the relative, and absolute age, of igneous activity and regional metamorphism and deformation (Figure 7).

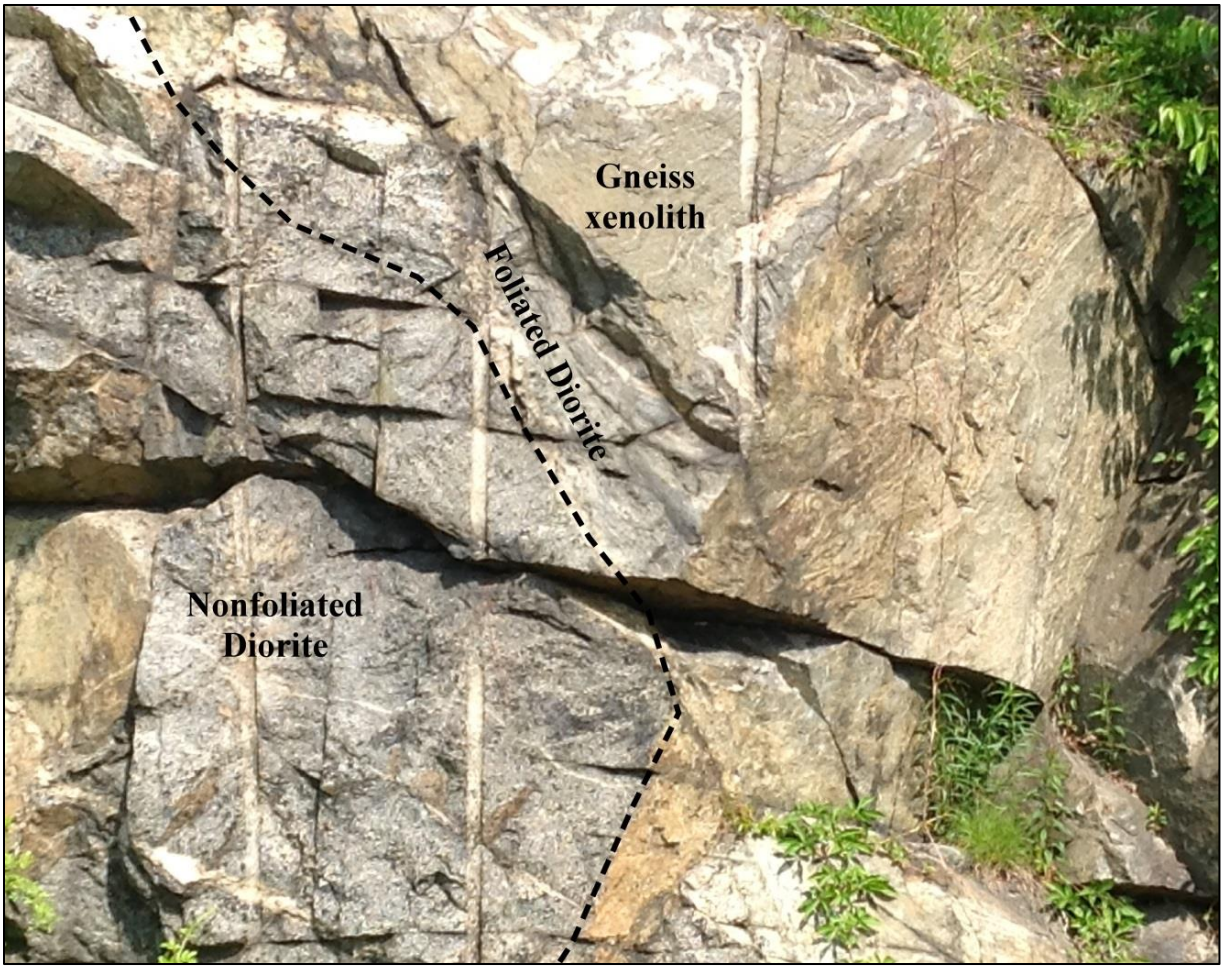

Figure 7. Outcrop photograph of Lake Tioroti diorite where it contains a xenolith of foliated gneiss (presumed to be S1 foliation) and also contains mylonitic foliation (S2) associated with the local dextral shear zone (D2).

Pegmatites

There are two generations of pegmatite dikes in the western Hudson Highlands. Early dikes are white and contain white K-feldspar, quartz, muscovite, and garnet locally. They are largely parallel to subparallel gneissic foliation, display boudinage and contain internal foliation and plastically deformed grains. Their thickness ranges from 10cm to 1m. A second suite of pegmatite dikes cross-cut the pervasive regional foliation and foliation associated with ductile shear zones (Figure 8). These late pegmatite dikes are very coarse grained with pink K-feldspar, quartz, and locally muscovite, magnetite, pyroxene, titanite, and/or garnet, and occasionally contain elongate hornblende aggregates that define a magmatic lineation or are plumose. These pegmatites are highly discordant, commonly associated within zones of brittle shear, and contain xenoliths of fault rocks. They exhibit no internal deformational fabric, and the thickness ranges from 1m to 10m.

Figure 8. Outcrop photograph of the contact between quartzofeldspathic gneiss and a hornblende pegmatite. The geochronology for both of these units is discussed below.

DEFORMATION AND METAMORPHISM

The basement rocks of the western Hudson Highlands experienced at least two major deformational events accompanied by emplacement of igneous bodies and high-grade metamorphism. All of the major rock units described above contain a penetrative foliation (S1) that is parallel to compositional layering and includes intrafolial isoclinal and sheath folds (F1). This foliation is defined by planar aggregates of recrystallized minerals and the pervasive gneissosity is associated with this foliation. Depending on the bulk composition, minerals such as biotite, amphibole, sillimanite, and/or pyroxene are aligned in the strongly foliated quartz-feldspar matrix. Stillwell (2005) reported on garnet-biotite exchange thermometry with temperatures ranging from 650-800^{o}C for pelitic gneiss samples collected across the entire western Hudson Highlands. These results are consistent with the presence of sillimanite, K-feldspar, biotite and locally cordierite.

Small pegmatite bodies are commonly parallel to subparallel to the gneissosity and exhibit well developed pinch and swell, and are locally asymmetric relative to the foliation. Aggregates of hornblende and pyroxene define porphyroclasts, and rocks containing intrafolial asymmetric isoclinal folds that exhibit vergence that is consistent locally. Mesoscopic and megascopic folds are recumbent and shallowly reclined. They are tight to isoclinal and commonly asymmetric with missing lower limbs. Although the attitude of the foliation and intrafolial folds were impacted by later deformation, the overall asymmetric fold consistency suggests northwestward nappe-like ductile flow during the first deformation event. The sparse kinematic indicators described above are consistent with the vergence of folds.

Overall, the S1 high grade metamorphic fabric has a variable orientation across the western Hudson Highlands due to map-scale folding (F2) associated with younger km-scale transcurrent shear zones (Figure 1). One of the map-scale F2 folds occurs at the southern end of Lake Tiorti and another excellent example occurs in the region southwest of Sterling Lake. Both of these map-scale folds are developed in the transition zone to the large ductile shear zones.

The second deformational event is characterized by a system of subvertical to steeply dipping, northeast striking anastomosing ductile shear zones (Figure 1). These shear zones cross cut and have transposed the foliation of the first deformational event. They range from 0.5 to 2 km in thickness though the boundaries exhibit wide strain gradient in some areas and are difficult to determine. The shear zones are developed in all of the major lithotectonic units and are defined by well-developed S-C mylonite with shallowly northeast plunging mineral lineations defined by recrystallized aggregates of feldspar, quartz and/or mafic minerals. Although the shear zones cross cut all lithotectonic units, they are best developed the granitic gneiss and the quartzofeldspathic gneiss of metavolcaniclastic lithofacies.

The Lake Tioroti diorite and the granite sheets also locally contain minor S-C mylonite, indicating that the diorite and granite bodies intruded before or during the development of the D2 shear zones. Kinematic indicators within the mylonite include C-S fabric, rotated porphyroclasts, shear bands, and asymmetric boudins. There are well-developed mesoscopic sheath folds with shallow northeast plunge, and megascopic drag folds adjacent to the main shear zone. Additionally, there are highly attenuated upright folds that occur within the shear zone foliation and many exhibit a small amount of granite that was intruded parallel to the fold limbs.

Figure 9. Outcrop photograph of granitic gneiss within the Indian Hill shear zone. The view is looking down into the ground at subvertical foliation that exhibits asymmetric boundins consistent with dextral shear. The end of the hammer handle is pointing approximately 035.

Kinematic analysis was conducted on all of the segments of shear zone within the anastomosing network, and the results are consistently dextral. Minerals within the sheared rocks include amphibole and biotite as well as quartz and feldspar, all of which show plastic deformation but with full recovery, suggesting that the shear zones initiated under a minimum of amphibolite metamorphic conditions.

Meso- and macroscopic gentle to open upright folds also occur adjacent to the shear zones locally (Figures 10 and 11). These folds plunge gently from due north to north-northeast. The folds occur in well-layered metavolcanic and metasedimentary sequences directly adjacent to the shear zone boundary. In the area of Harriman State Park, upright folds form an en-echelon array with the hinge axes oblique to the north relative to the northeast strike of the shear zones. In the Sterling Forest region of the westernmost Hudson Highlands, there are upright map-scale folds defined by the map pattern of the local metasedimentary and metavolcanic rocks. The hinge regions of these upright folds are also the locations where granite sheets are most prevalent, and they are subparallel to the fold hinges, similar to observations at the outcrop described above. The granite sheets have variably developed mylonite at the contact with highly sheared country rock, suggesting syn-kinematic emplacement in the hinge of the upright folds.

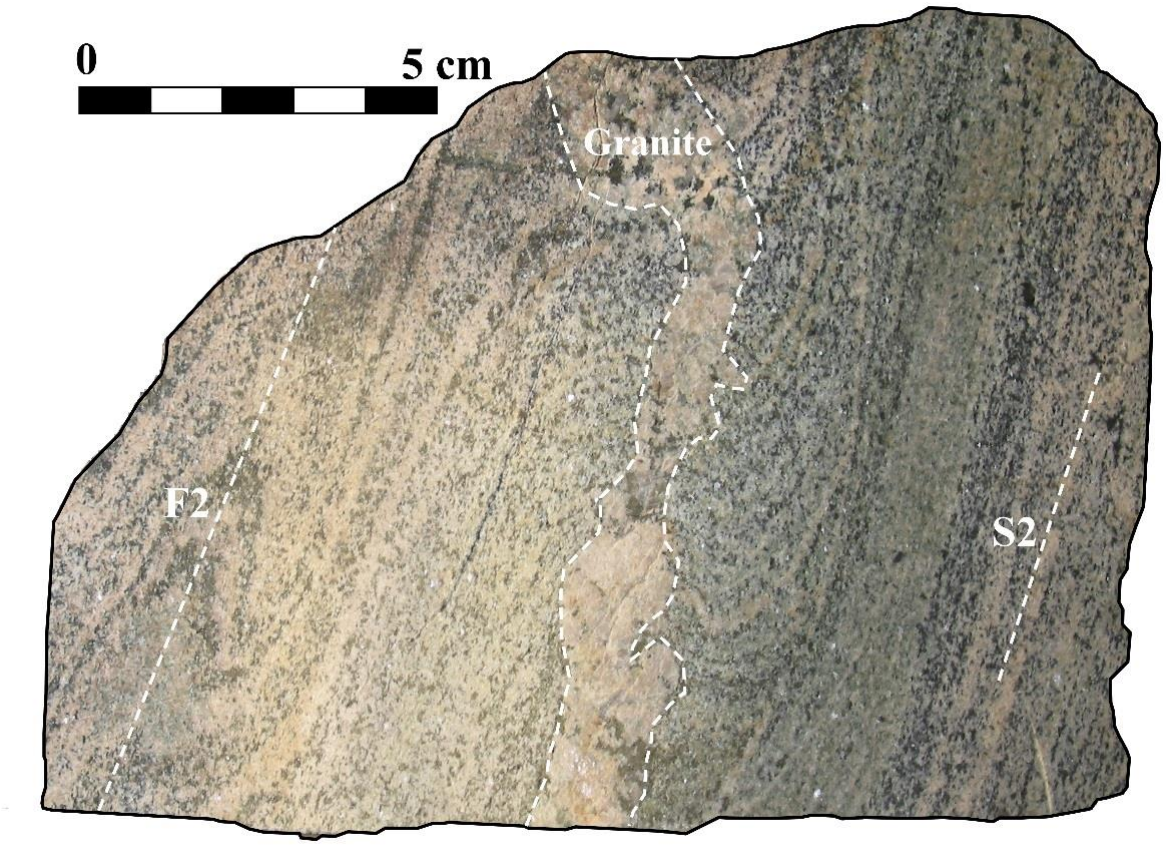

Figure 10. Cut slab of quartzofeldspathic gneiss exhibiting F2 folds and small F2-parallel granite. This is a small-scale example of the structural emplacement of the granite sheets into upright folds formed between the dextral shear zones.

Figure 11. Upright open antiform developed in quartzofeldspathic gneiss. The hinge axis of this fold is oriented oblique to the local Fingerboard shear zone (Gates and Valentino, 2011).

Late stage concordant to slightly discordant brittle fracture zones occur within several of the D2 mylonite zones and are highly mineralized. They contain randomly oriented, coarse to megacrystic intergrowths of salite and phlogopite followed by magnetite and scapolite and cemented by calcite in areas of marble. Other zones contain hornblende and clinopyroxene followed by magnetite that are contained within quartz. Zones that connect the magnetite deposits are thinner and typically composed of randomly oriented to aligned clinopyroxene with only minor magnetite, phlogopite and/or quartz. They are commonly intruded by late pegmatites that contain mineralized rock as xenoliths. Thicknesses of the zones range from 2 m to 15 m. Some of the mineralized zones are more than 5 km long and occur along the length of the ductile shear zone. The veins parallel the zones but clearly cut the mylonitic foliation with ragged to planar contacts.

GEOCHRONOLOGY

Metasedimentary Lithofacies

Semi-pelitic gneiss. Zircon separated from a semi-pelitic gneiss are rounded and average about 125 microns in diameter. In back scattered electron mode small rounded to oval cores, often displaying oscillatory zoning, are within much larger areas of diffuse or unzoned zircon rims. The uranium content of 13 cores averages 613±520 ppm and the U/Th ratios are 3.24±1.82 ppm. The rims of 22 grains averaged1487±872 ppm and the U/Th ratios were 57.2±50.6. The grains range of 95.1 to 102.4% concordant.

Figure 12 shows all of the data points plotted on a concordia diagram. Grains range in age from 2041-991 Ma. Several distinct clusters or groupings of analyses occur and Figure 3c gives the weighted means for several possible groupings which yield ages of 1331±10, 1030.5±2.5, and 1005.9±4.6 Ma. Similar values were obtained for concordia plots and concordant ages. The wide distribution of ages suggests that the semi-pelitic gneiss is of supracrustal origin. However, BSE images suggest thick metamorphic rims have grown on or replaced the bulk of the volume of detrital grains. Similar conclusions where reached for zircon from the Irving Pond quartzite in the Adirondack Highlands analyzed by Peck et al. (2013). For comparison, relatively intact detrital zircons were found by Chiarenzelli et al. (2015) in upper amphibolite facies quartz-rich metasedimentary rocks from the Adirondack Lowlands.

Based on age, U-content, U-Th ratios, and core versus rim relations the zircon spots analyzed can be separated into those thought to yield detrital versus metamorphic ages. The youngest clearly detrital analysis has a $^{207}Pb/^{206}Pb$ age of 1264±12.7 Ma and provides a maximum age for deposition of the precursor of the semi-pelitic gneiss. This age agrees well with existing geochronological information from rocks of the Grenville Supergroup including the Franklin Marble. However, the relatively small number of analyses in this study (n = 35) limit the degree of confidence in this and other interpretations.

A cluster of 7 grains yielding an age of 1331±10 Ma matches well with tonalitic arc magmatism known many areas in the Grenville Province and Grenville rocks in Appalachian inliers, and are perhaps part of the Dysart-Mt. Holly Suite. Cluster ages of 1030.5±2.5 and 1005.9±4.6 Ma agree well with estimates of late Ottawan metamorphism (see sample G-2) and late intrusion (see sample G-1) in the Hudson Highlands.

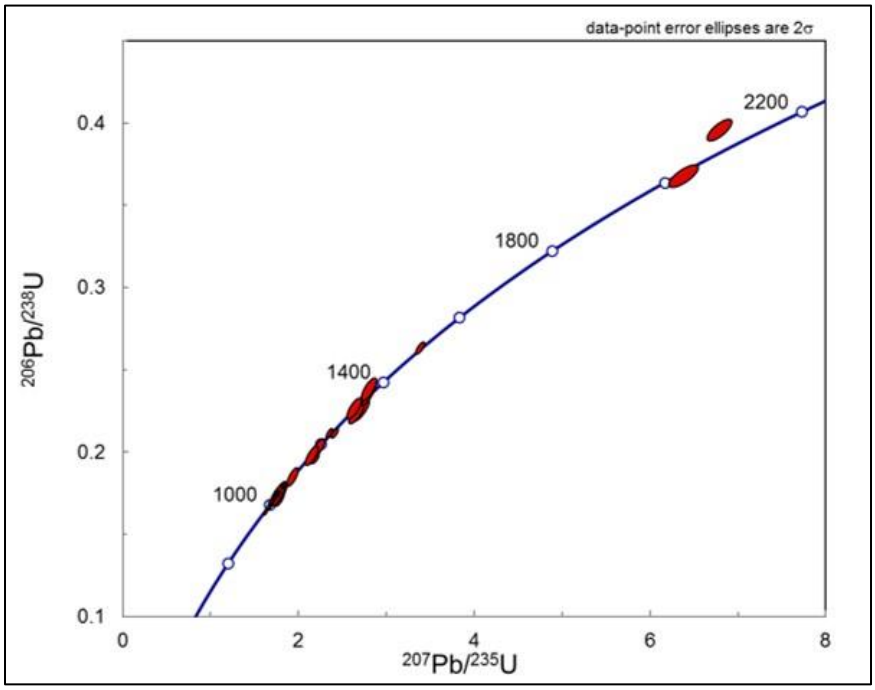

Figure 12. Concordia diagram for zircons analyzed from semi-pelitic gneiss.

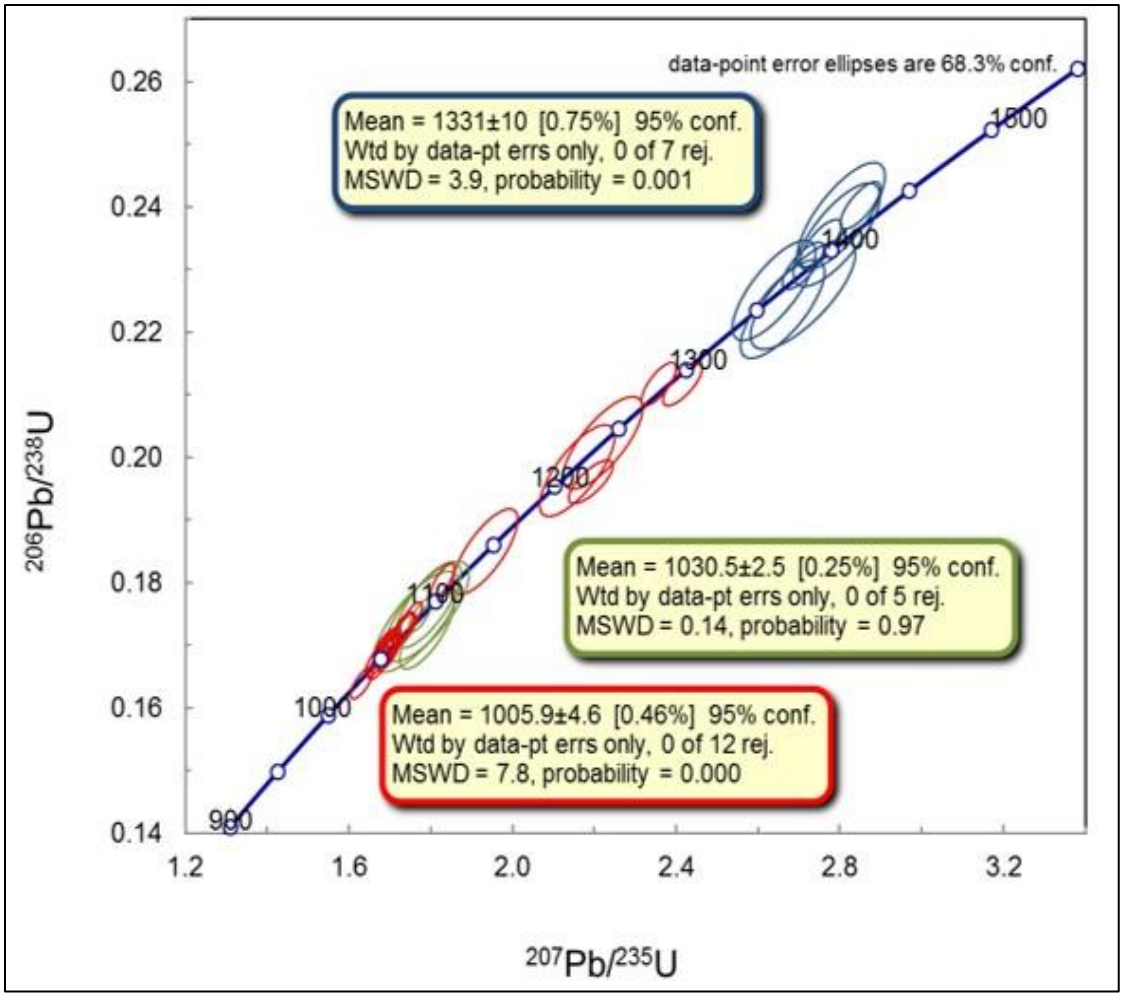

Figure 13. Geochronological results from sample G-5 a semi-pelitic gneiss located near Mombasha Lake. This enlargement of the younger analyses showing possible groupings based on the clustering of data point. Color coded ellipses correspond to results of weighted mean calculation. The two younger groupings (1030.5±2.5 and 1005.9±4.6 Ma) are interpreted as metamorphic. The oldest grouping shown in the diagram (1331±10 Ma) is believed to represent a population of detrital material derived from tonalitic rocks equivalent to Dysart-Mt. Holly Suite.

Quartzite. Zircons separated from a sample of quartzite have complex shapes varying from euhedral to faceted to rounded. Some grains occur as clusters and/or with other zircons nucleated off them. The majority of grains are somewhat rounded, dipyramid crystals about 150 microns in length. When viewed in cathodoluminscence mode several types of zoning, cores, rims, and considerable variation in brightness (i.e. CL response) is observed (Figure 14A). The uranium content of the grains is highly variable ranging from 99-1544 ppm, as is their U/Th ratios which range from 0.85-172.0. The grains range from 70 to 168% concordant. After filtering for concordancy values between 95-105%, of the 92 grains analyzed, only 49 analyses are considered suitable for further consideration. Collectively these characteristics indicate a detrital origin for the vast majority of analyses and considerable post-depositional disturbance of U-Pb isotopic systematics.

Figure 14B shows all of the data points plotted on a probability histogram. Analyses yield ages ranging from 2749±10 to 960±8 Ma. A variety of small "peaks" and several distinctive gaps in the data occur between 2052 and 2606 Ma and 1226-1303 Ma on the calculated histogram. The first gap indicates a lack of a later (ca. 2100-2500 Ma) Paleoproterozoic source. The second gap is believed to represent detrital ages from those of metamorphic or hybrid age. Analyses in the age range 1800-1500 Ma dominate the population, indicating a source(s) of this range. Curiously both Shawinigan and Ottawa ages are poorly represented, indicating few metamorphic grains or rims were analyzed, perhaps because of the preferential targeting of grain cores.

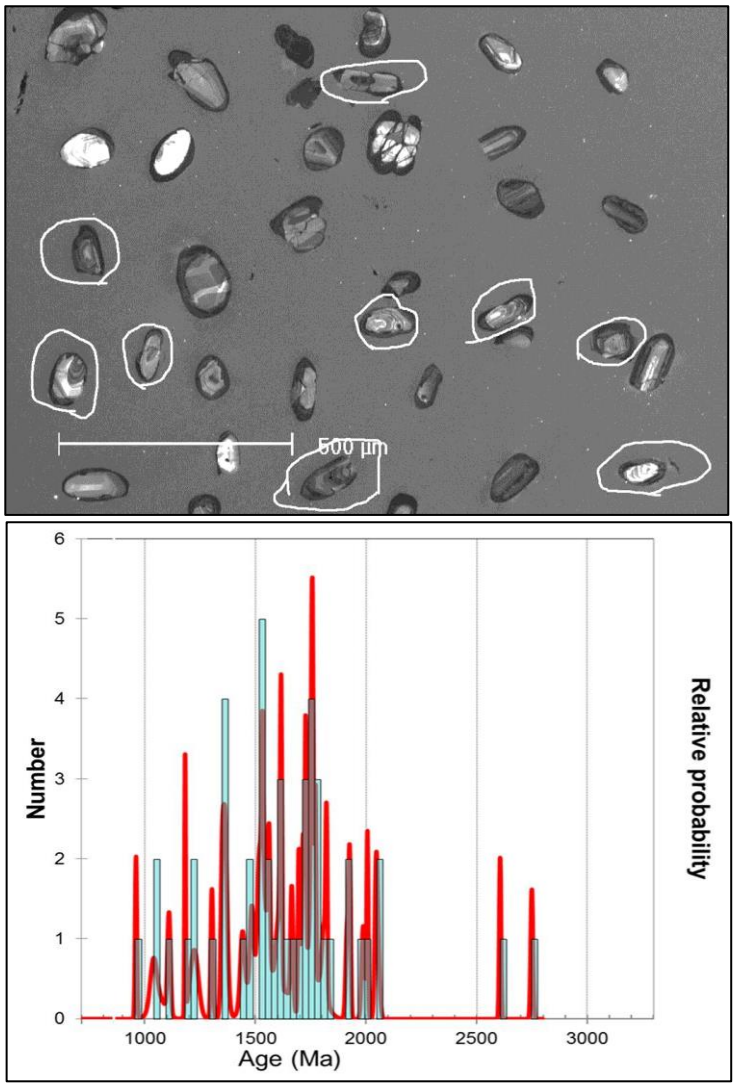

Figure 14. Geochronological results from a quartzite taken from the supracrustal sequence near Bear Mountain. A total of 49 analyses are displayed. A. Cathodoluminsce (CL) image of typical zircon grains separated from the quartzite. Note variety in shape, zoning types, and cathodoluminsce response. Grains outlined in white were selected for analyzsis. B. Probability histogram shows the range of ages from analyses of zircons from the quartzite. Note large gaps between Archean and Proterozoic time. Ages younger than 1303 Ma are interpreted metamorphic or hybrid (see text).

In comparison with the semi-pelitic gneiss, zircons from the quartzite appear to better represent original detrital populations, with far fewer analyses that are likely of metamorphic origin. Similar findings were noted by Chiarenzelli et al. (2015) who attributed the preservation of more detrital grains a function of the minimal reactivity and melting of high-grade quartzose rocks compared to those of pelitic origin. While the relatively small number (n = 49) of usable detrital ages prohibits detailed interpretation of potential source(s), those of significance include a small Neoarchean component and various Meso- to Paleoproterozoic components, particularly those ranging in age from 1800-1500 Ma. Also present are a significant amount of ca. 1350 Ma grains thought to be derived from Dysart-Mt. Holly terrane equivalents. The youngest grain interpreted as detrital gives an age 1303±10 Ma providing a maximum depositional age for the quartzite.

Granitic gneiss

Zircon separated from a granitic mylonite from the Indian Hill shear zone (Allers et al., 2001) averages approximately 200 microns in length, forming modified euhedral prisms (Figure 15A). In back scattered electron mode dark zoned and rounded cores are overgrown by partial to complete, bright rims up to tens of microns across at their widest point. Fine and wide oscillatory zoning is visible in the cores. The uranium content of the cores averages 588±514 ppm and the U/Th ratios are very consistent at 2.46±0.71. In total 22 grains and grain fragments were analyzed and yielded data points ranging from 96.4 to 103.4% concordant. The uranium content of rims average is high, averaging 1565±107 ppm and the U/Th ratios were 13.7±6.4. In total, 3 bright rims were analyzed and yielded data points ranging from 96.6-105.1% concordant.

Figure 15B shows all of the data points plotted on a concordia diagram. Two distinct clusters occur and yield $^{207}Pb/^{206}Pb$ ages at least 126 Ma apart and hence were grouped accordingly. In addition, distinct differences in BSE response, U content, and U/Th ratios were noted between the two groupings. The older, upper group of 22 analyses yields $^{207}Pb/^{206}Pb$ ages between 1235 to 1159 Ma. A Concordia plot (Figure 15B) yields a lower intercept of 1178±110 Ma (MSWD of 1.3). A weighted mean of 1184±10 Ma is considerably more precise but with an MSWD of 39 unlikely to accurately represent the age of the zircons in this group.

Alternatively, the spread of analyses along concordia is likely the result of disturbance within the Indian Hill Shear Zone. High-grade mylonitic rocks deformed and metamorphosed shortly after or during their intrusion can display zircon arrays that fan out along concordia indicating continued growth or Pb-loss over an extended period. Later or recent Pb-loss can further add further complexity to zircon arrays by causing additional Pb-loss along steeper chords. We conclude that granitic rocks that form the protolith to those in Indian Hill Shear Zone where intruded shortly before metamorphism and deformation associated with the Shawinigan Orogeny, considered to have occurred between 1210-1150 Ma. Exactly when requires additional research but their time of crystallization is constrained by the 207 Pb/206Pb ages of the oldest and youngest core analyses of 1235 to 1159 Ma.

Analysis of the three bright rims yields a concordant age of 1023±6.3 Ma with an MSWD of 0.73. A weighted mean of 1012±17 Ma with an MSWD of 1.6 agrees within analytical error (Figures 15E and 15F). These results are believed to reflect the timing of late zircon growth likely associated with the latest stages of the Ottawan Orogeny (1090-1020 Ma).

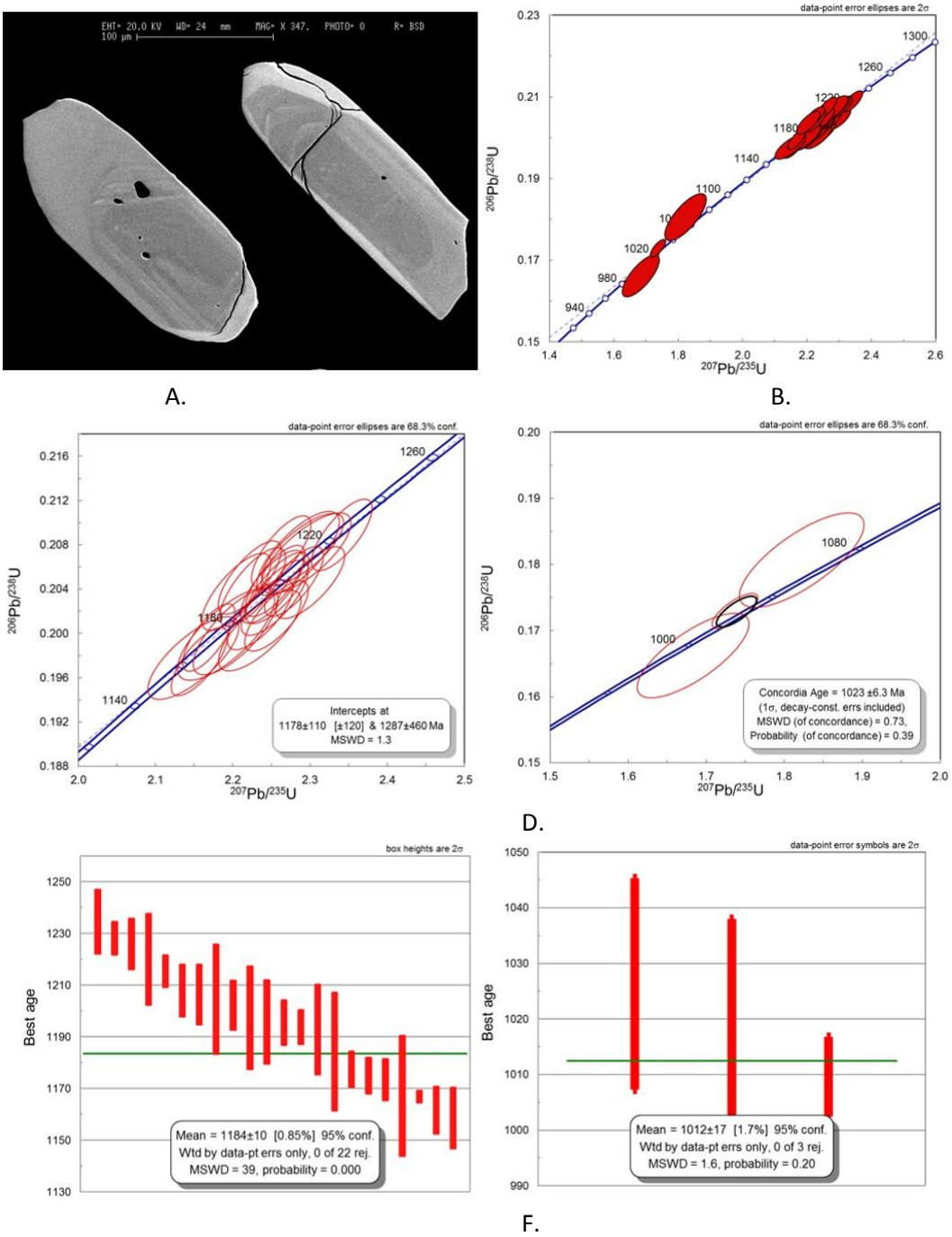

Figure 15. Geochronological results from sample G-2 a quartzofeldspathic gneiss from the Indian Hill Shear Zone. A. BSE images of typical zircon grains separated from the quartzofeldspathic gneiss. B. Concordia diagram showing all U-Th-Pb analyses performed on zircons and their clustering into two major groupings. C. Blow up of the upper, older group of analyses showing both their spread along concordia and above and below it. D. Blow up of the lower grouping of three grains showing their concordant age (black circle). E. Weighted mean of the upper grouping, not the wide spread of ages and high MSWD not indicative of a single population. F. Weighted mean of the lower grouping.

Lake Tiorati Diorite

Zircon separated from the Lake Tiorati diorite average approximately 150 microns in long dimension, are primarily equant, and show faint zoning (Figure 16A). Some are euhedral showing square cross-sections; others appear to be fractured fragments of larger grains. Their uranium content averages 463±159 ppm and the U/Th ratios are very consistent at 2.60±1.32. In total, 18 grains and grain fragments were analyzed and yielded data points ranging from 97.5 to 103.2% concordant. For these reasons the zircons are considered of igneous origin having been derived from crystallization from an intermediate to mafic magma. Little or no evidence of metamorphic rims, grains, or resetting was noted.

Plotting all 18 grains analyzed on a standard Concordia diagram yield an upper intercept age of 1004±12 Ma (MSWD of 0.32). A concordant age calculated from the same data set yielded an age of 1006.8±5.0 Ma (MSWD of 0.027; Figure 16B). A weighted mean calculated from the same data set yielded an age of 1008.1±4.6 Ma (MSWD of 4.5; Figure 16C). All three methods of calculating the age of the zircons from the Lake Tiorati diorite yield ages within analytical error of each other. The concordant age of 1006.8±5.0 Ma is taken as the time of crystallization. Thus the rock crystallized approximately 1007 Ma and the zircons have retained relatively closed U-Th-Pb isotopic systems since.

A.

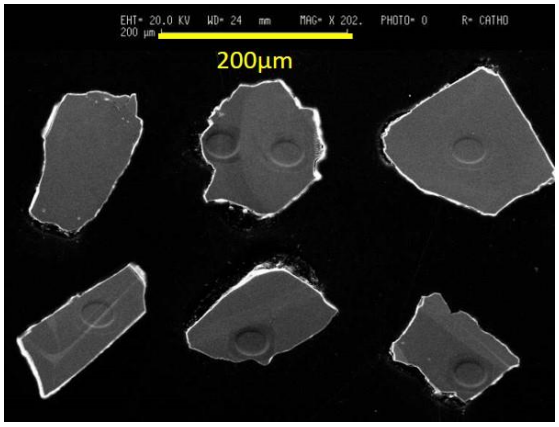

B.

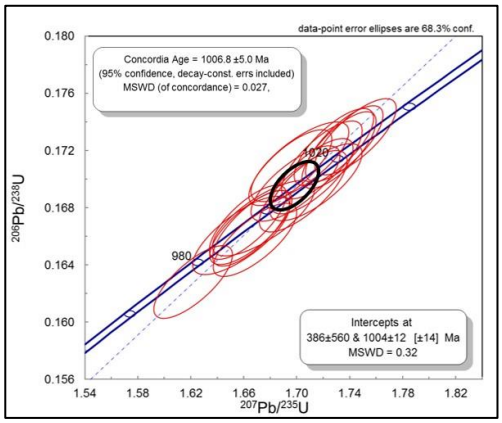

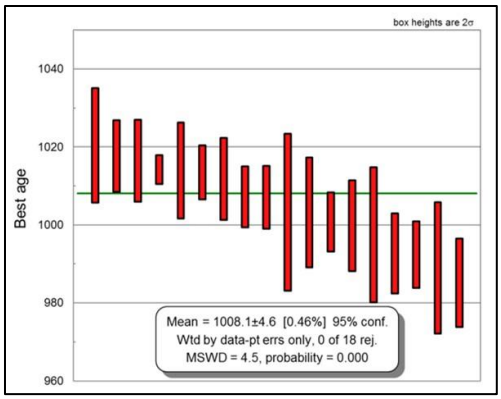

Figure 16. Geochronological results from sample G-1 Lake Tiorati Diorite. A) BSE images of typical zircon grains and fragments separated from the Lake Tiorati diorite. Note SHRIMP ablation pits. B) Concordia diagram showing all U-Th-Pb analyses performed on zircons and their clustering. The black circle outlines the calculated concordant age derived from all the analyses. C) The weighted mean calculated from all U-Th-Pb analyses of zircon.

Pegmatite

Zircons were separated from one of the larger pegmatite bodies that cross cuts the mylonitic foliation of the Indian Hill shear zone. The zircon uranium content averages 362.4±287 ppm and the U/Th ratios are very consistent at 2.87±0.93. In total, 12 grains and grain fragments were analyzed and yielded data points ranging from 94.8 to 104.2% concordant. For these reasons, the zircons are considered of igneous origin having been derived from crystallization from a granitic magma. Little or no evidence of metamorphic rims, grains, or resetting was noted.

Plotting all 12 grains analyzed on a standard Concordia diagram yield an upper intercept age of 990±17 Ma (MSWD of 0.72). A concordant age calculated from the same data set yielded 981.6±3.5 Ma (MSWD of 2.5). A weighted mean calculated from the same data set yielded an age of 992±14 Ma (MSWD of 0.72). All three methods of calculating the age of the zircons from the pegmatite yield ages within analytical error of each other. The concordant age of 981.6±3.5 Ma is taken as the time of crystallization. Thus the rock crystallized approximately 980 Ma and the zircons have retained relatively closed U-Th-Pb isotopic systems since.

A.

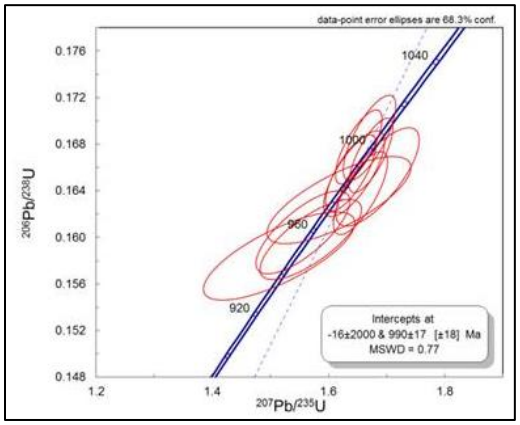

B.

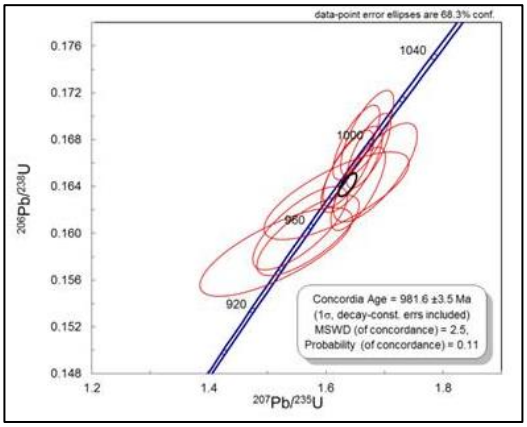

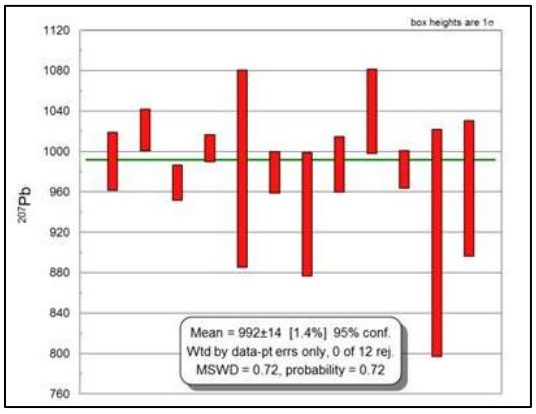

Figure 17. Geochronological results from a sample of hornblende pegmatite that cross cuts the Indian Hill shear zone along Route 17A. A total of 12 analyses are displayed. A. Cathodoluminsce (CL) image of typical zircon grains separated from the pegmatite. B. Concordia diagram showing all U-Th-Pb analyses performed on zircons and their clustering. C. A concordant age calculated from the U-Th-Pb analyses represent by the black circle. D. The weighted mean calculated from all U-Th-Pb analyses of zircon.

Mineralized Zone

Zircon separates from a magnetite vein within one of the mineralized zones exhibit several different distinct morphologies and sizes, including high U cores, low-U rims, and large clear zircon grains. Their uranium content ranges between 135.5 to 2731 ppm and the U/Th ratios between 1.87 and 11.6. In total, 21 grains and grain fragments were analyzed and one was eliminated from further consideration because of its concordancy of only 90%. Two general clusters or groupings of ages can be seen on the concordia diagram (Figure 18A). In detail, several fairly coherent groupings were identified. The interpretation of the ages is equivocal.

A single analysis of a core yielded a 207Pb/206Pb age of 1217.2 ± 15.6 Ma and is reasonably interpreted as a xenocrystic zircon (Figure 18B). Seven, high-U, grain cores, six of which plotted slightly above concordia yielded a concordia intercept of 1164.5±7.2 Ma with an MSWD of 1.4 (Figure 18B). If the single most concordant grain of the grouping is used to calculate a concordant age an analytically indistinguishable age of 1170±8.5 Ma with an MSWD of 0.95 is obtained.

A grouping of six slightly discordant, lower U rims, in the lower cluster yielded an upper intercept age of 1026.8±4.3 Ma with a MSWD of 2.5 (Figure 18A). A weighted mean calculated from the same six grains yields an analytical indistinguishable age of 1037±14 Ma (MSWD of 0.17). A final grouping of grains yielded a weighted mean of 949±31 Ma (MSWD of 1.6). An analytically indistinguishable concordant age of 964±5.1 Ma with an MSWD of 6.6 was calculated and is shown on Figure 18C.

The simplest interpretation of the data summarized above is that an older rock experienced several generations of zircon growth associated with Grenville and later metamorphic events (Figure 19). Thus the age of the rock us taken as ca. 1170±8.5 Ma with the addition of zircon rims at 1026.8±4.3 Ma and discrete pegmatitic or hydrothermal zircon at 964±5.1 Ma.

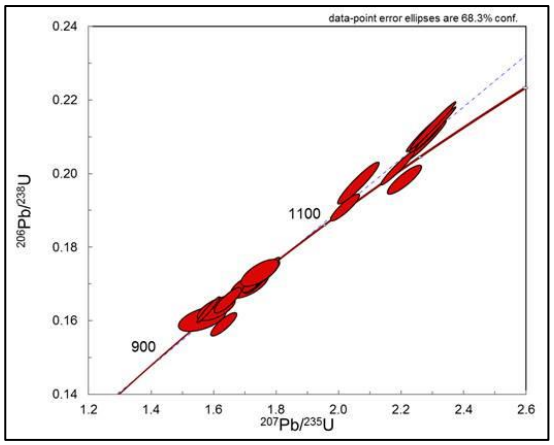

B.

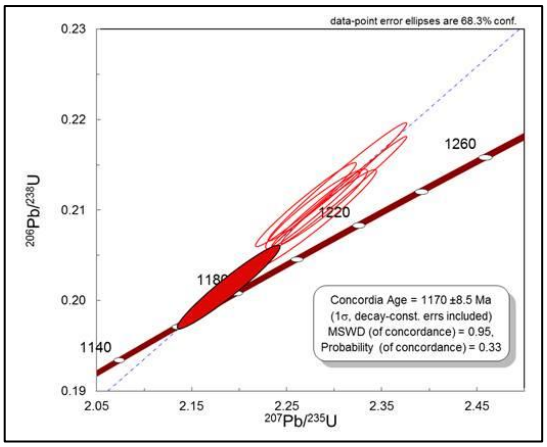

C.

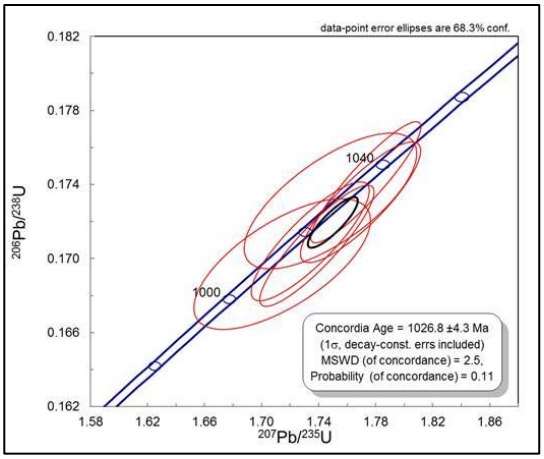

Figure 18. Geochronological results from a mineralized vein sample with magnetite from the Hogan Camp mine area. A. A total of 20 analyses are displayed on a concordia diagram and show two distinct groupings. B. A concordia diagram showing the concordant age of 1170±8 Ma (filled circle). C. Concordia diagram showing the concordant age (black ellipse) calculated from six zircon analyses.

Ar/Ar thermochronology

Gates et al. (2001) reported on Ar/Ar thermochronology for mineralized brittle-ductile zones in the western Hudson Highlands. A summary of that work is included here. The Ar/Ar thermochronology was completed on hornblende and biotite samples from the mineralized rocks in the Hogencamp mine area. The samples analyzed at the Ar/Ar thermochronology lab at Massachusetts Institute of Technology, using standard step-wise heating techniques. Two hornblende and one biotite from the gangue minerals produced ages of 914 $\pm$ 3.6 Ma, 922 $\pm$ 3.4 Ma, and 840 $\pm$ 5.0 Ma, respectively. While hornblende and biotite from an undeformed pegmatite within the mineralized vein produced ages of 923 $\pm$ 2.8 Ma and 794 $\pm$ 3.0 Ma. The relatively tight cooling ages for the mineralized and pegmatite hornblende suggest a genetic tie between the two with both mineralization and pegmatite crystallization occurring about the same time. Gates et al. (2001) inferred a very slow cooling rate from these results, however, the 45 Ma difference in the biotite cooling temperatures are perplexing suggesting problems with the results.

COMPARATIVE GEOCHEMISTRY

There is a discrepancy in the overall results of the zircon geochronology from the lithotectonic units. Figure 19 summarizes the U-Pb ages, superimposed on the major tectonic events of the Grenville Province (after River, 2008). The detrital zircon cores produced ages that predate the Elzeverian Orogeny, and the rims appear to have grown during the Ottawan Orogeny.

The granitic gneiss sample of the Indian Hill shear zones produced a range of zircon core ages that span the Shawinigan Orogeny in addition to some metamorphic rims that grew toward the end of the same event. Additionally, that sample produced zircon rim ages that overlap with the Ottawan Phase of the Grenville Orogeny. It appears that rock bodies that are currently juxtaposed contain zircons that produced very different histories. Therefore, we decided to examine the geochemistry of these units in detail to possibly explain this discrepancy.

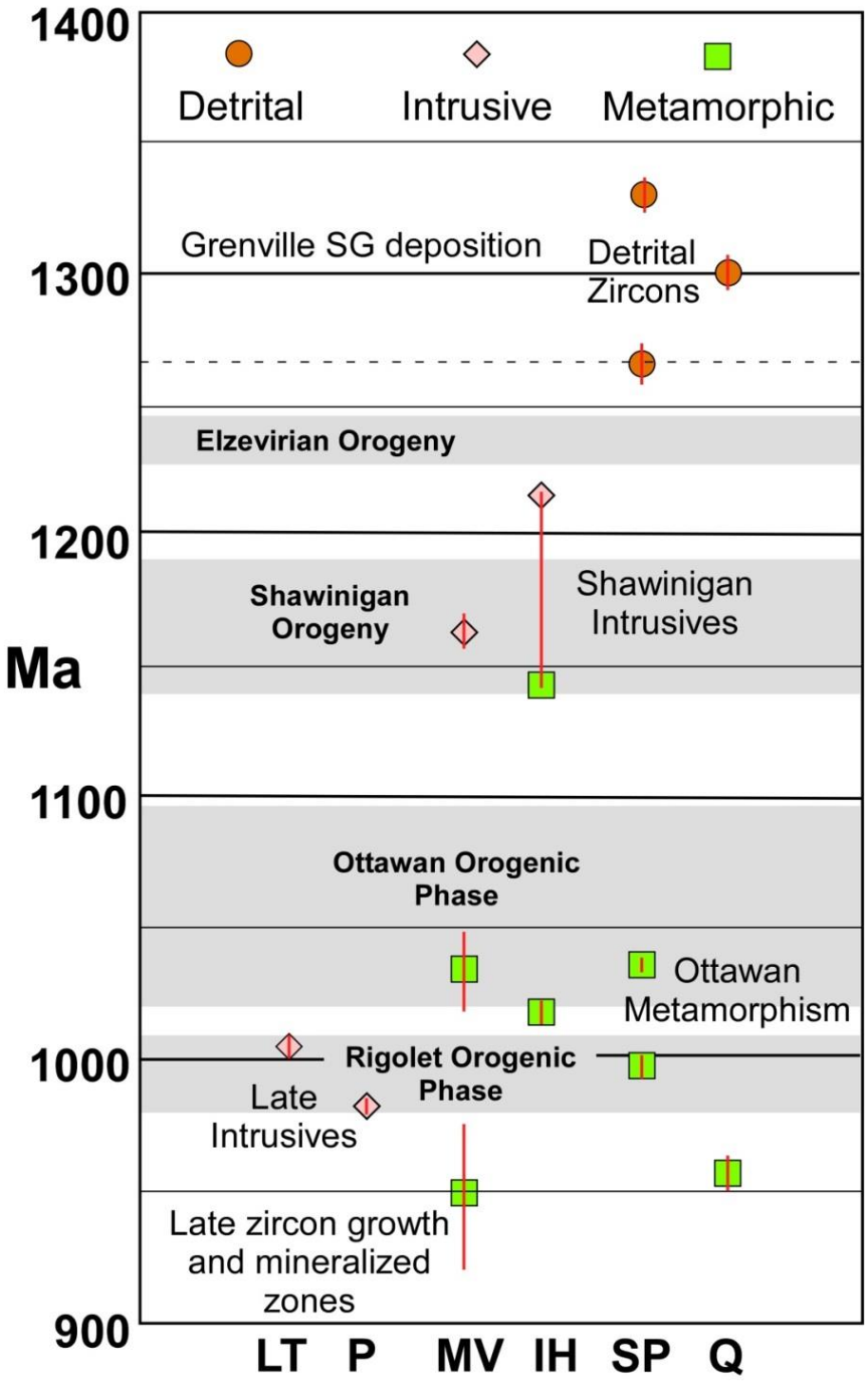

Figure 19. Summary of zircon U-Pb geochronology. Lake Tioroti (LT-diorite), P-pegmatite, Mineralized vein (MV-magnetite vein), Granitic gneiss within the Indian Hill shear zone (IH-granitic gneiss), Metasedimentary rocks (SP-semi-pelitic gneiss , Q-quartzite). Gray domains denote orogenic events are phases in the Canadian Grenville Province (after River, 2008).

Suites (ten samples each) of rock samples were selected from the sequence of metapelitic and metapsammitic gneisss, and from the granitic gneiss, and analyzed for whole rock major oxide and trace element compositions. The granitic gneiss is strongly deformed but reasonable homogeneous and most likely has a plutonic origin. In addition, rock samples from the metasedimentary lithofacies ranging in lithology from pelitic gneiss to quartzite were collected near Bear Mountain. The metasedimentary rocks range from 71.88 to 91.54 % SiO_2. This is consistent with the interpretation that these rocks have a supracrustal origin. In fact, some of the supracrustal rocks are so enriched in silica that the role of the concentration of quartz during weathering is indisputable. The granitic gneiss samples range from 64.54 to 71.87% SiO_2. This range is consistent with a granite origin for this gneiss body.

Igneous rocks can be subdivided based on the trend of a given related suite on an alkali-iron-magneisum (AFM) plot. Figure 20 displays both suites of geochemical analyses and shows a clear distinction in their trends. The granitic gneiss samples plot along the tie line between alkalis and iron, indicating an iron enrichment trend. This type of trend is seen in granitic rocks of anorogenic or "A"-type affinity such as the granitic members of the Anorthosite-mangerite-charnockite-granite or AMCG suite in the Adirondacks and elsewhere in the Grenville Province. Although the second suite of rocks are interpreted as metasedimentary in origin, it is also instructive to examine their trend on the AFM plot as a signature of their source terrane. Figure 20 shows a calc-akaline trend for these rocks, suggesting derivation by erosion of an arc terrane.

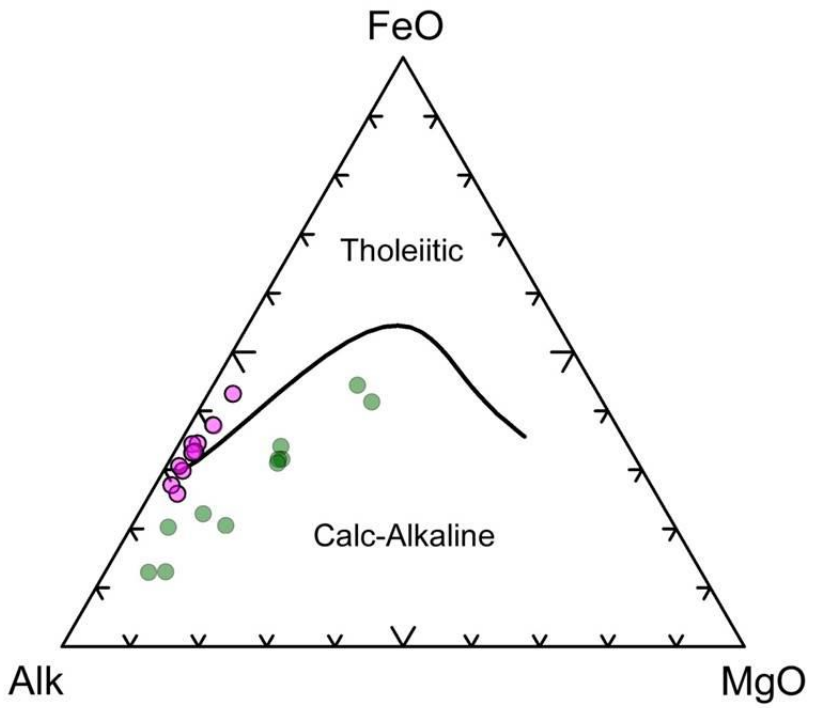

Figure 20. AFM diagram after Irvine and Barager (1971) showing samples of the granitic gneiss from the Indian Hill shear zone (pink or dark circles) and the Supracrustal sequence (green or pale). The granitic gneisses show a strong iron differentiation trend similar to granitic members of the Anorthosite-Mangerite-Charnockite-Granite (AMCG) suite in the Adirondacks and elsewhere. The supracustal rocks show a calc-alkaline trend suggesting derivation from arc-related volcanic and/or plutonic rocks.

Examination of the rare earth element concentrations normalized to the Post-Archean Australian Shale (PAAS) composite of Taylor and McLennan (1985) provides insight into the origin of the two suites (Figure 21). Comparison of the REE trends shows no overlap in concentration and some distinct differences in patterns between the two suites. The granitic gneiss lies above "1" for each of the REE with several samples close to an order of magnitude more concentrated than PAAS. In addition, a distinctly negative europium anomaly can be seen on the diagram. This is characteristic of a fractionated felsic igneous rock from which plagioclase feldspar has been separated. The metasedimentary rock samples lie between "1" and "0.1" on the same diagram and approximately half of the samples have a strongly positive europium anomaly. The lower concentrations of REE is consistent with a detrital origin for the suite and can readily be explained by dilution by greater amounts of detrital quartz in arenaceous rocks. Quartz contains little or no trace elements including the REEs, so high silica clastic detrital rocks typically have lower REEs and other trace elements than more mud-rich rocks. The positive europium anomaly shown by several samples of the metasedimentary rocks indicates erosion of plagioclase-rich rocks that would be associated with an arc terrane.

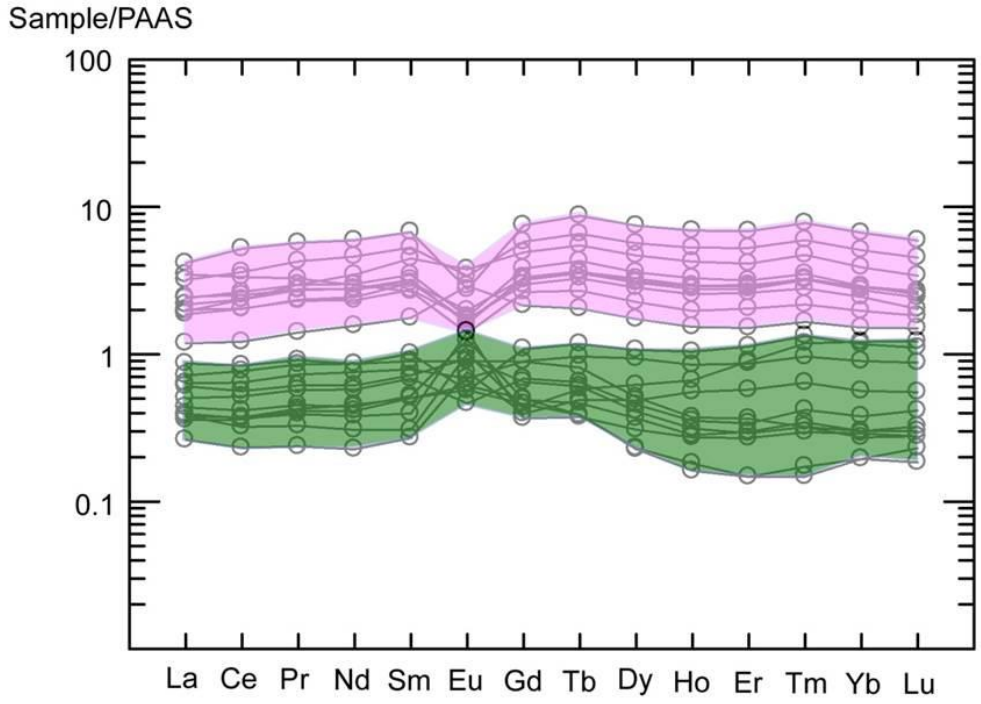

Figure 21. Rare earth element spidergram showing samples from the Indian Hill granitic gneiss (top field) and the supracrustal rocks (lower field). The rare earth element concentrations are normalized by the Post-Archean Australia Shale (PAAS) composite after Taylor and McLelland (1985). Major differences include the greater concentration of rare earth elements in the granitic gneisses and a negative, rather than positive, Europium anomaly. The concentration and pattern of the supracrustal rocks suggests dilution by quartz (SiO_2 up to 91.45%) and erosion of a plagioclase-rich terrane.

Tectonic discrimination diagrams have found widespread utility in evaluating the setting of a variety of igneous rocks over the past several decades. Application to ancient orogenic settings and highly metamorphosed rocks may be useful particularly when other factors are considered along with the

discrimination diagrams. In Figure 22 the data from both suites of rocks is plotted on a discrimination diagram that uses Rb concentrations plotted against the sum of Y and Nb to subdivide granites into four fields. The granitic gneiss samples plot in the With-in Plate Granite (WPG) field confirming their trace element signature is also consistent with an "A"-type origin. The metasedimentary rock samples plot within the Volcanic Arc Granitic (VAG) field consistent with other data suggesting the metasedimentary sequence was derived from the erosion of an arc terrane.

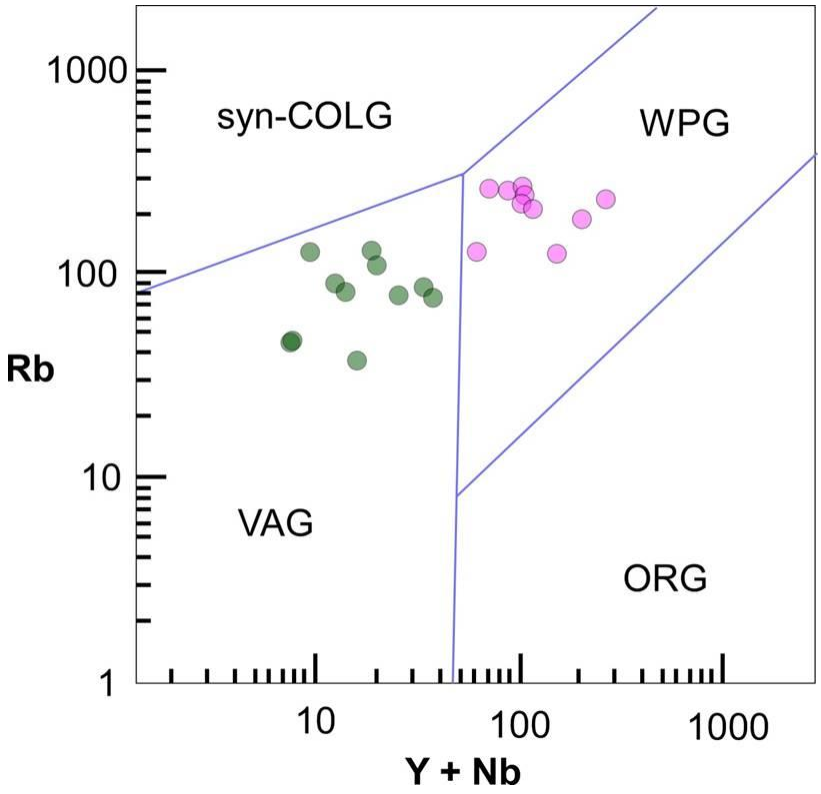

Figure 22. Rb versus Y + Nb tectonic discrimination diagram showing samples from the granitic gneisse (WPG field) and the supracrustal sequence (VAG field) after Pearce et al. (1984). The results are consistent with the granitic gneisses having an "A" type protolith and derivation of the supracrustal rocks by erosion of an arc terrane.

Finally, in Figure 23 both suites are plotted on a discrimination diagram designed to distinguish between the sources of granites. Based on the concentration of Zr versus Ga and Al the field is subdivided into an "A"-type granite field and one that combines both sedimentary (S-type) and igneous (I-type) granites. As is shown in the figure, the granitic gneiss samples fall exclusively within the upper right hand corner where "A"-type granites plot, whereas the metasedimentary rock samples plot within the S & I type fields. This suggests immobile trace elements can be used to differentiate the ultimate source region of both spots.

Geochemical investigation indicates that the granitic gneisses are chemically consistent within narrow limits and have the typical major and trace element signature found in "A"-type granites. They show a strong iron enrichment trend on the AFM diagram and fall within the with-in plate or "A"-type fields on discrimination diagrams. They show an enriched in REE over PAAS and have a negative europium

anomaly. Both of these characteristics are believed to be due to fractionation and the enrichment of trace elements due to their felsic composition and possibly the extent of partial melting of their source. Although the zircon systematics of these rocks defy a simple explanation, the age of the zircon cores is consistent with timing of "A"-type or AMCG granite intrusion in the Adirondacks and Grenville Province This magmatism began about ca. 1185 Ma and continued to at least 1150 Ma elsewhere and perhaps in the Hudson Highlands as well.

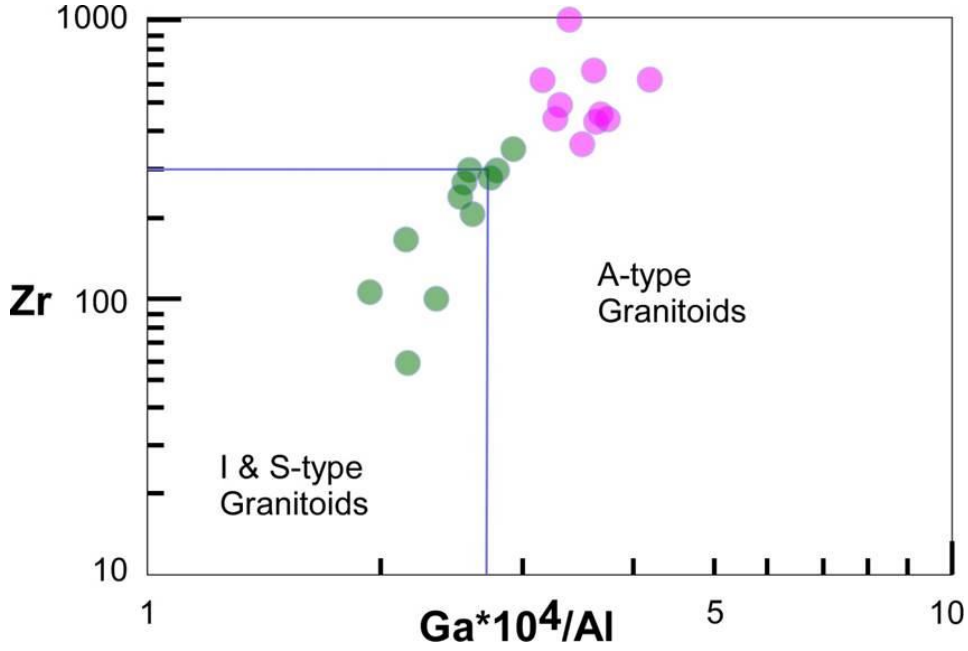

Figure 23. Tectonic discrimination diagram showing Zr vs. Ga*1000/Al concentrations for the granitic gneisses (A-type Granitoid field) and the supracrustal sequence (cluster in the I & S-type Granitoid field with two samples in the A-type field) after Whalen et al. (1987).

Rocks of the metasedimentary lithofacies have chemical characteristics indicative of a supracrustal sequence ranging from pelitic to quartz-rich. In addition, the major and trace element characteristics indicate they were derived from an arc terrane. They have substantially lower REE than the PAAS composite and this reflects the inclusion of coarser-grain clastic rocks in the suite. On the AFM plot and tectonic discrimination diagrams they show a calc-alkaline trend and arc related geochemistry. The metasedimentary rocks are interpreted to be part of the Grenville Supergroup which was deposited in a series of back-arc basins (Gundersen, 1986; Gates et al., 2001) between 1250-1300 Ma. A viable source for the clastic material they contain would be an arc or arc fragments of the widespread Dysart-Mt. Holly Complex ranging in age from 1300-1350 Ma and/or local metavolcanic equivalents.

TECTONIC CONCLUSIONS

1. The lithotectonic units in the western Hudson Highlands represent a complex sequence of deposition, volcanism and intrusions, superimposed by multiple regional deformation events that occurred deep in the crust. Detrital zircons from two separate bodies of metasedimentary rocks yielded provenances ranging in age from 1.2 to 2.7 Ga. The younger detrital ages are consistent with the Grenville Supergroup, however the wide range of older ages with Archean sources. Gates et al. (2006) proposed

that the range of ages suggests deposition in a passive margin with a possible Amazonian contribution. It was suggested by Gates et al. (2006) that the Archean ages may reflect an Amazonian source contribution to the detrital material. As well, this interpretation is supported by the metasedimentary lithotectonic rock assemblage including quartzite, marble, calcsilicate and pelities is consistent with this interpretation.

2. The metavolcanic and metavolcaniclastic rocks most likely represent the remains of a volcanic arc, including the granitic intrusive rocks that are now granitic gneiss. The granitic gneiss body yielded a range of ziron ages of 1235 to 1159 Ma, suggesting that the granite intruded before or during the Shawinigan Orogeny, but the geochemistry suggests the body is related to the A-type suite of plutons associated with the AMCG rocks of the Adirondacks and Grenville Province. The sample of granitic gneiss is from the Indian Hill shear zone, and the span of ages is attributed to subsequent mylonitic deformation and metamorphism.

3. Gorring et al. (2003), suggested that the Lake Tioroti diorite and other minor granitic bodies in the western Hudson Highlands were associated with localized transtensional deformation within the transcurrent shear system. The age of the Lake Tioriti diorite is 1008 Ma, and the shear zone fabric occurs along the margin of the body, suggesting that shearing and intrusion were linked. This is the same structural relationship that was observed for the granite sheets that occur in the hinges of transpressional folds between the dextral shear zones. The intrusion of igneous bodies during dextral shearing requires elements of dilation, but the location of the bodies in the cores of upright folds suggests that the bodies migrated to domains of vertical escape in an overall transpressional tectonic environment. Constrained by cross cutting pegmatite, the high-grade ductile dextral transpression in the western Hudson Highlands was over by 980 Ma. But, lower temperature brittle-ductile deformation in the same shear system continued and was accompanied by mineralization.

FIELD GUIDE AND ROAD LOG

Meeting Point: This field trip begins at the upper parking lot for the Sterling Forest visitor center within the Sterling Forest State Park.

Meeting Point Coordinates: 41.197°N, 74.256°W

Meeting Time: 9:00AM

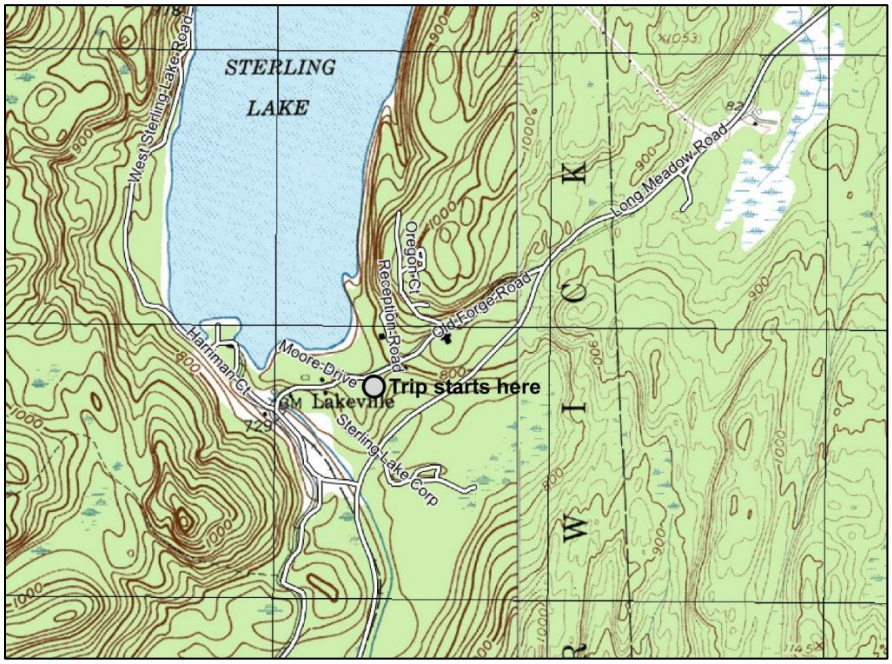

Figure 24. Topographic map showing the starting location for the field trip near the Sterling Forest visitor center on Old Forge Road.

Distance in miles (km)		
Cumulative	Point to point	Route Description
0.0 (0.0)	0.0 (0.0)	Turn right when exiting the parking lot onto Old Forge Road.
0.5 (0.8)	0.5 (0.8)	Turn right onto Long Meadow Road and follow the intersection with Route 72.
4.7 (7.6)	4.2 (0.8)	Turn left onto Route 72.
6.0 (9.7)	1.3 (2.1)	Turn left onto Eagle Valley Road.
6.1 (9.8)	0.1 (0.2)	Park in the gravel lot on the left side of road. Walk about 0.1 miles along the road until you reach the dirt road under the power line. Follow the power line road about 0.1 miles up-hill to the left. Stop 1 is located under the first tower that you encounter along the dirt road.

Stop 1. Metavolcanic Lithofacies, Eagle Valley Road, Sloatsburg, NY

Location Coordinates: (41.160°N, 74.213°W)

Figure 25. Topographic map showing the location of Stop 1 on Eagle Valley Road.

This outcrop contains interlayered mafic, intermediate composition gneiss and grantic gneiss layers. All of the rock types are contain a penetrative foliation that is interpreted to be the regional S1. The folding of this foliation is associated with regional dextral transpression. This stop is located between two of the larger dextral shear zones. The assemblage of rock compositions interlayered at the meter to sub-meter scale is interpreted to represent metavolcanic rocks.

Distance in miles (km) Cumulative	Point to point	Route Description
6.2 (10.0)	0.1 (0.2)	Back track on Eagle Valley Road to the intersection with Route 72 and turn left.
7.9 (12.7)	1.7 (2.7)	Follow signs for Route 17 north.
8.9 (14.3)	1.0 (1.6)	Turn right onto Seven Lakes Drive and enter Harriman State Park.
12.2 (19.6)	3.3 (5.3)	Pull over on the right side of road between two large outcrops. This is Stop 2.

Stop 2. Metasedimentary Lithofacies, Seven Lakes Drive, Sloatsburg, NY

Location Coordinates: (41.190°N, 74.143°W)

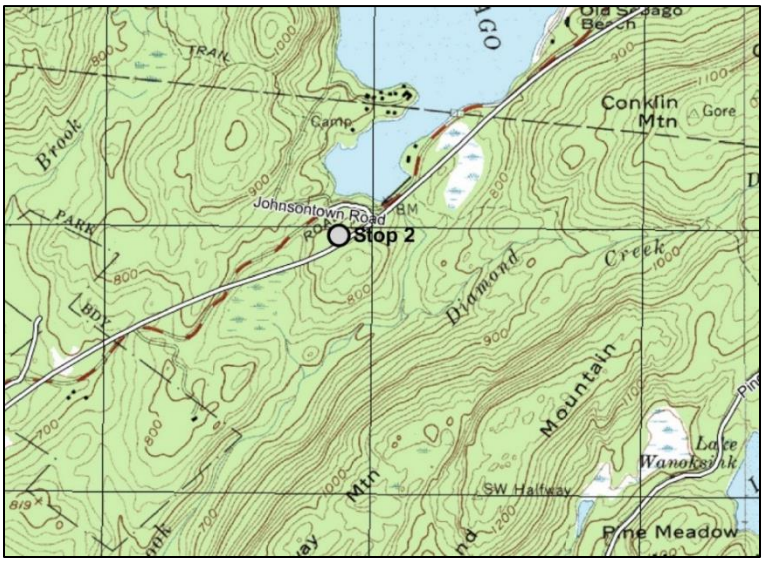

Figure 26. Topographic map showing the location of Stop 2 on Seven Lakes Drive.

The rocks at this stop include sillimanite-garnet-biotite gneiss, and graphite-pyrite bearing metapsammitic gneiss. The presence of sulfides accounts for the rusty weathered outcrop surface. The dominant foliation in this gneiss is the regional S1 with minor crenulations and open folds that are subparallel to mineral lineations. Gates et al. (2006) interpreted these rocks to represent low energy sedimentary deposits in a restricted marine basin.

Figure 27. Outcrop photograph of interlayered pelitic, semi-pelitic and psammitic gneiss bearing abundant sulfides.

Distance in miles (km) Cumulative	Point to point	Route Description
15.9 (25.6)	3.7 (6.0)	Approach Kanawauke Circle from the south. Proceed north on Seven Lakes Dr.
18.4 (29.6)	2.5 (4.0)	Pass the Tioriti diorite outcrop on left. Refer to Gates et al. (2002); Gorring et al. (2003); and Gates et al. (2006) for description of this outcrop. This trip will proceed north.
19.2 (30.9)	0.8 (1.3)	Approach Tioriti Circle from the south. Proceed north on Seven Lakes Drive.
22.9 (36.9)	3.7 (6.0)	Approach the intersection with Route 6. Seven Lake Drive merges with Route 6. You will exit the circle half way around and continue east until the two roads split. Take the exit for Seven Lakes Drive, toward Bear Mountain Park.
23.7 (38.1)	0.8 (1.3)	At the end of the exit road, park on the wide shoulder to Seven Lakes Drive. Carefully walk back on the exit road and onto Route 6 until you read the end of a very long outcrop on the left. This is the beginning of Stop 3. Examine the outcrop as you slowly proceed back to the vehicles.

Stop 3. Metasedimentary Lithofacies, Palisades Interstate Parkway, Doodletown, NY

Location Coordinates: (41.307°N, 74.028°W)

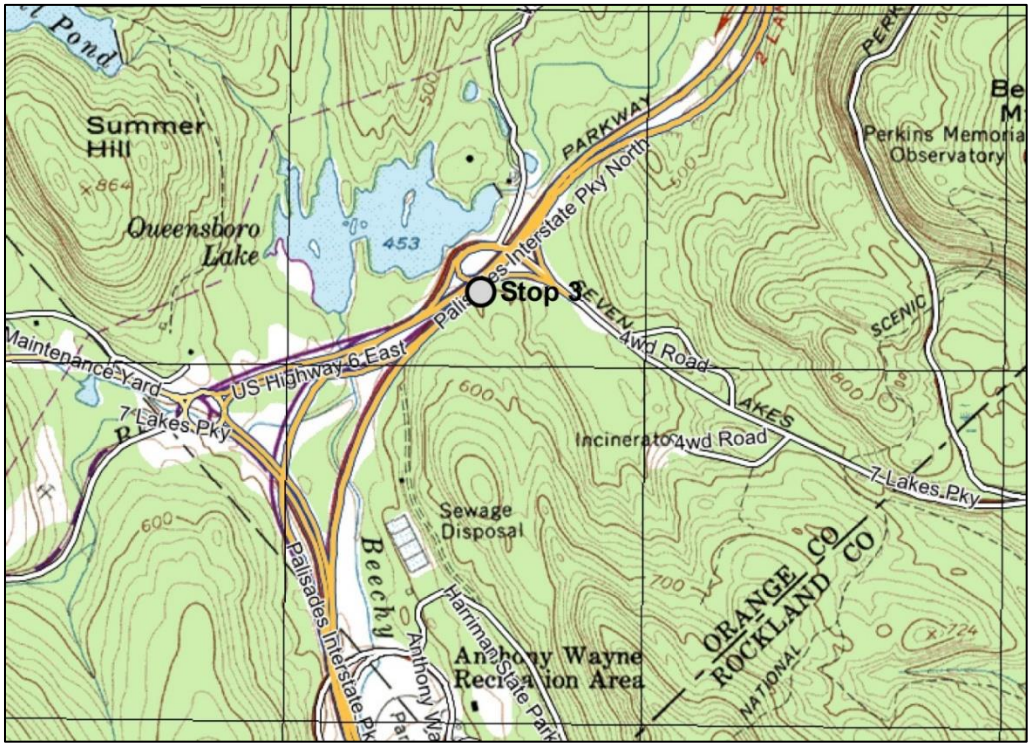

Figure 28. Topographic map showing the location of the supracrustal rocks at Stop 3.

An extensive sequence of interlayered quartzite, semi-pelitic gneiss and pelitic gneiss outcrop at Stop 3 along the Palisades Interstate Parkway. The compositional layering most likely represents the compositional variation of the sedimentary protoliths. The pelitic layers contain biotite, garnet, sillimanite and K-feldspar, while the quartzite layers contain primarily recrystallized quartz and K-feldspar and garnets. Samples from this outcrop were analyzed to characterize the geochemistry of this unit, and one sample of quartzite was used for U-Pb geochronology. The results of this work is discussed above.

Distance in miles (km)		
Cumulative	Point to point	Route Description
31.6 (50.7)	7.8 (12.6)	Back track on Seven Lakes Drive to the Kanawauke Circle in Harriman State Park. Turn right onto Kanawauke Road.
32.1 (51.7)	0.6 (1.0)	Optional stop. Turn left into the parking lot. Walk 0.4 miles farther on Kanawauke Road to examine an outcrop of the Metavolcanic Lithofacies. Refer to the NYSGA 2001 Guidebook, Trip 3, Stop 3. Proceed west on Kanawauke Dr.
36.8 (59.2)	4.7 (7.6)	Kanawauke Drive will pass under the NY Thruway and end at a stop sign. Proceed straight onto Route 17A.
37.5 (60.4)	0.7 (1.1)	Park on the wide shoulder of Route 17A. There are abundant outcrops on the north side of the highway. This is Stop 4.

Stop 4. Granitic Gneiss of the Indian Hill Shear Zone, Route 17A, Tuxedo Park, NY

Location Coordinates: (41.234°N, 74.193°W)

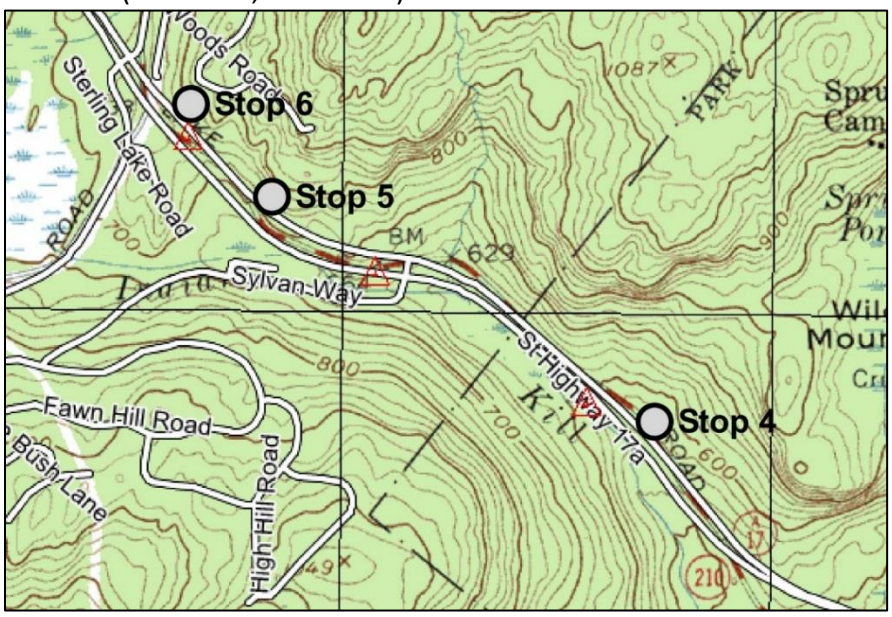

Figure 29. Topographic map showing the locations of Stops 4, 5 and 6 along Route 17A.

There are numerous outcrops of granitic gneiss along the west bound lanes of Route 17A (Figure 29). Stop 4 is a series of outcrops within the first kilometer along the road. This area is underlain by highly deformed granitic gneiss, and a complete cross section of the Indian Hill ductile shear zone (Allers et al., 2001). The granitic gneiss contains a steeply east dipping penetrative foliation defined by recrystallized planar aggregates of quartz, K-feldspar and plagioclase, with subhorizontal mineral lineations. In places, there is well developed S-C fabric, and relict feldspar grains forming asymmetric augen. Using oriented samples, kinematic analysis of these macroscopic structures reveals a dominant dextral shear sense. In places, the foliation is disrupted by minor leucosomes, forming asymmetric boudins (Figure 9) with the same shear sense. Commonly, there are amphibolite layers ranging from a few cm to a meter wide within the granitic gneiss. The amphibolite layers are internally foliated with boundaries that are parallel to the penetrative foliation in the granitic gneiss. One thicker layer has an array of granite-filled en-echelon veins that also consistent with dextral shear (Figure 30).

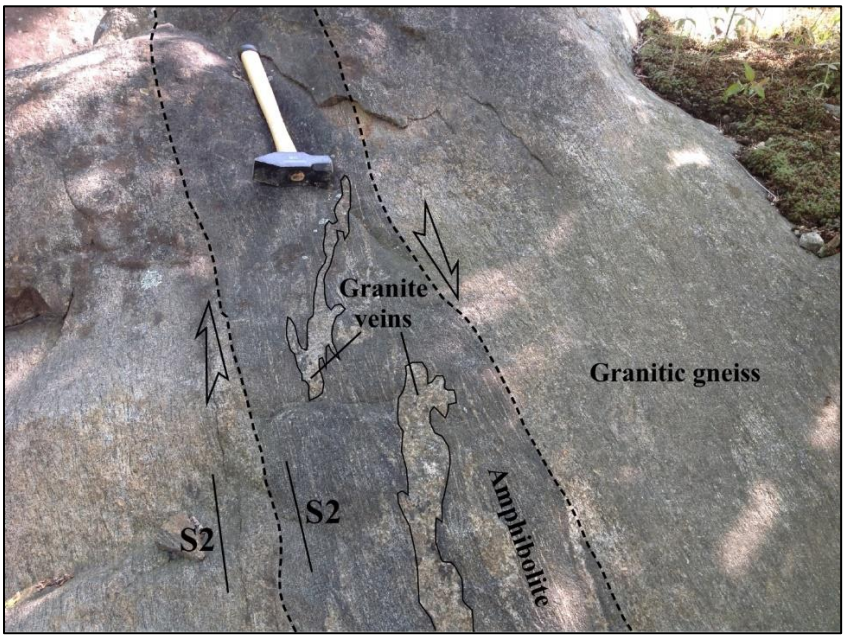

Figure 30. Outcrop photograph of strongly foliated granitic gneiss with an amphibolite layer that has dextral en-echelon granite veins. View is looking into the ground and the hammer handle trends approximately 215 degrees.

Distance in miles (km)		
Cumulative	Point to point	Route Description
38.0 (61.2)	0.5 (0.8)	Proceed west on Route 17A. Park on wide shoulder just past the blind curve. There are a pair of outcrops on both sides of the highway. Be especially cautious when crossing the double lakes of Route 17A. This is Stop 5.

Stop 5. Granitic Gneiss and Pegmatite, Route 17A, Tuxedo Park, NY

Location Coordinates: (41.238°N, 74.202°W)

Stop 5 is a series of outcrops that are on both sides of the west bound lanes of Route 17A. At this location, the grantic gneiss of Stop 4 is cross cut by a pegmatite that is several meters thick. The contact is well exposed on both sides of the highway, however for those of you that are allergic to poison ivy, it is recommended that you carefully cross the highway to view the pegmatite –granitic gneiss contact on the south side of the highway. The pegmatite contains typical K-feldspar and quartz in a addition to large hornblende crystals that form a nearly subhorizontal lineation that relects growth direction. This location is where samples were collected for U-Pb zircon geochronology previously discussed in this field guide.

Distance in miles (km)		
Cumulative	Point to point	Route Description
38.2 (61.5)	0.2 (0.3)	Proceed west on Route 17A and park on the wide shoulder. This is Stop 6.

Stop 6. Calcsilicate Gneiss, Route 17A, Tuxedo Park, NY

Location Coordinates: (41.240°N, 74.205°W)

The granitic gneiss is in sharp contact with calcsilicate gneiss between Stop 5 and 6 along Route 17A. The calcsilicate gneiss contains plagioclase, quartz, diopside and epidote in the prominent dark layers that are strongly foliated. Lighter layers are leucosomes of K-feldspar and quartz that are parallel to the penetrative foliation (Figure 31). In most places, and especially at this location, the calcsilicate gneiss occurs as a minor migmatite. Typically, the calcsilicate gneiss is interlayered with other metasedimentary lithologies such as pelites, psammites and marble. But, this body is one of the thickest, reaching upward of several hundred meters and was traced for more than 5 kilometers to the northeast along the margin of the granitic gneiss. The foliation in this calcsilicate appears to be composite where S2 (gneissocity) has been transposed parallel to the local shear zone (S2).

Figure 31. Outcrop photograph of calcsilicate gneiss with the typical melanosomes of diopside-quartz-plagioclase- epidote and leucosomes of K-feldspar-quartz.

Distance in miles (km) Cumulative	Point to point	Route Description
38.8 (62.4)	0.6 (1.0)	Turn left onto Long Meadow Road.
39.6 (63.7)	0.8 (1.3)	Turn right onto Ironwood Drive.
40.8 (65.7)	1.2 (1.9)	Proceed to the end of Ironwood Drive and park. Walk the dirt road to the about 0.2 miles to the large outcrops of granite under the power-line tower. This is Stop 7.

Stop 7. Bare Mountain Granite, Ironwood Drive, Tuxedo Park, NY

Location Coordinates: (41.232°N, 74.237°W)

A series of granite sheets underlie the hills on the north and south side of the Ironwood Drive valley (Figure 33). The sheets range in thickness from a few meters upward of several hundred meters. Note the serrated topography on the south flank of Hogback Mountain in the topographic map above. Each of the promontories on the side of the mountain is underlain by the more resistant granite. The granite at Bare Mountain is one of the thicker granite sheets. Excellent outcrops occur on the western flank of Bare Mountain and for those interested in a good climb it would be worth the time to scale the face to examine a cross section of the granite. However, the same granite is readily accessible along the dirt road that follows the powerline. At this location, the granite is pink to white, leucocratic, containing quartz, K-feldspar and plagioclase with only trace amount of biotite or hornblende. In places, there are K-feldspar megacrysts upward of 10 cm in diameter. Although not exposed at this location, the contact with the local country rock is sharp, but the granite has a weakly to moderately developed mylonitic foliation.

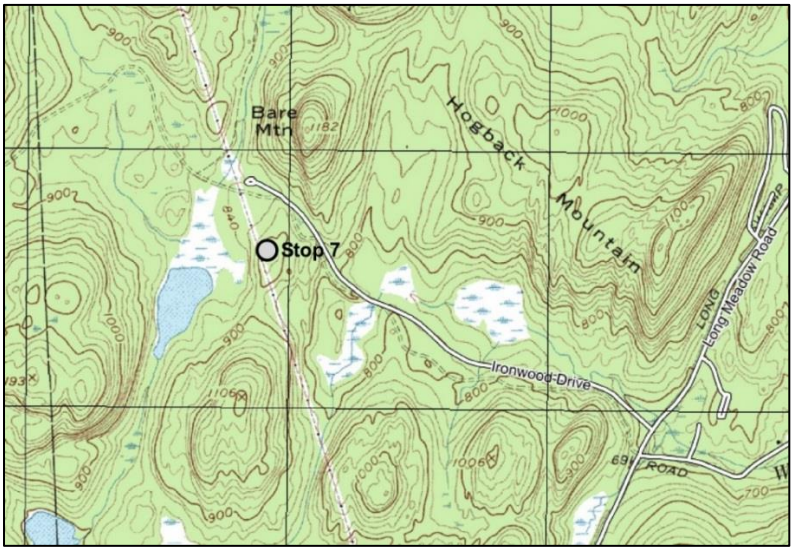

Figure 32. Topographic map showing the location of the Bare Mountain granite at Stop 7 at the end of Ironwood Drive in the Sterling Forest.

Figure 33. Bare Mountain granite outcrops at Stop 7 with pressure release sheet joints.

Distance in miles (km) Cumulative	Point to point	Route Description
42.0 (67.6)	1.2 (1.9)	Proceed back on Ironwood Dr. to Long Meadow Rd. Turn left.
44.3 (71.3)	2.3 (3.7)	Optional stop. This is an outcrop of a smaller granite sheet. Refer to the 2003 NYSGA Guidebook, Appendix A, Trip A6, Stop 2 for details (Gorring et al., 2003).
44.4 (71.5)	0.1 (0.2)	Turn right onto Old Forge Road and proceed to the parking lot.
44.8 (72.1)	0.4 (0.6)	Parking lot where the trip started.

REFERENCES CITED

Allers, T., Valentino, D., Gates, A. and Chiarenzelli, J., 2001, Structural analysis of the Indian Hill shear zone, Hudson Highlands, NY, Geological Society of America, Abstracts with Programs, v. 33, p. 79.

Chiarenzelli, J., Kratzmann, D., Selleck, B., and de Lorraine, W., 2015, Age and provenance of Grenville Supergroup rocks, Trans-Adirondack Basin, constrained by detrital zircons: Geology, v. 43; no. 2; p. 183–186.

Dallmeyer, R. D., 1974, Metamorphic history of the northeastern Reading Prong, New York and Northern New Jersey, Jourournal of Petrology, v. 15, p. 325-359.

Gates, A. E. and Valentino, D. W., 2011, Bedrock geology of the Highlands, *in* (ed. Lathrop, R. G., Jr.) The

Highlands, Critical Resources, Treasured Landscapes, Rutgers University Press, New Brunswick, NJ, p. 9-25.

Gates, A. E., Valentino, D. W., Gorring, M. L. and Hamilton, M., 2001, The assembly of the Supercontinent Rodinia in the western Hudson Highlands, New York State Geological Association, Field Trip Guidebook, v. 73, p. 174-204.

Gates, A. E., Valentino, D. W., Gorring, M. L., Tern, E. R. and Chiarenzelli, J. R., 2006, Rodinian collision and escape tectonics in the Hudson Highlands, New York, Geological Society of America, Field Guide 8, p. 65-82.

Gorring, M. L., Valentino, D. W., Solar, G. S. and Gates, A. E., 2003, Late Ottawan ductile shearing and granitoid emplacement in the Hudson Highlands, NY, New York State Geological Association, Field Trip Guidebook, v. 75, Appendix A., p. 1-27.

Gundersen, L.C., 1986, Geology and geochemistry of the Precambrian rocks of the Reading Prong, New York and New Jersey - Implications for the genesis of iron-uranium-rare earth deposits, In USGS Research on Energy Resources - 1986 Programs and Abstracts (Carter, L.M.H., ed.), U.S.G.S. Circular 974, 19 p.

Irvine, T.N., and Baragar, W.R.A., 1971, A guide to the chemical classification of the common volcanic rocks: Canadian Journal of Earth Sciences, v. 8, p. 523-548.

Linguanti, C., Valentino, D., Gorring, M. and Gates, A., 2011, Synorogenic emplacement of granite sheets, Hudson Highlands, New York, Geological Society of America, Abstracts with Programs, v. 43, p. 149.

Peck, W., Selleck, B., Wong, M., Chiarenzelli, J., Harpp, K., Hollocher, K., Lackey, J., Catalano, J., Regan, S., and Stocker, A., 2013, Orogenic to postorogenic (1.20–1.15 Ga) magmatism in the Adirondack Lowlands and Frontenac terrane, southern Grenville Province, USA and Canada: Geosphere, v. 9, p. 1637-1663.

Rivers, T., 2008, Assembly and preservation of lower, mid, and upper orogenic crust in the Grenville Province—Implications for the evolution of large hot long-duration orogens, Precambrian Research, v. 167, p. 237-259.

Stilwell, S., 2006, Geothermometry of pelitic rocks from the western Hudson Highlands, New York, State University of New York at Oswego, B.S. Thesis, 72 p.

Pearce, J.A., Harris, N.B.W., and Tindle, A.G., 1984, Trace element discrimination diagrams for the tectonic interpretation of granitic rocks: Journal of Petrology, v. 25, p. 956-983.

Taylor S. R., McLennan S. M., 1985, The continental crust: its composition and evolution. Blackwell Scientific Publication, Carlton, 312 p.

Thomas, J., Valentino, D. and Gates, A., 2001, Structural control on the intrusion of granite sheets in the Hudson Highlands, NY, Geological Society of America, Abstracts with Programs, v. 33, p. 29.

Whalen, J.B., Currie, K.L., and Chappell, B.W., 1987, S-type granites: geochemical characteristics, discrimination and petrogenesis. Contributions to Mineralogy and Petrology, v. 95, p. 407-419.

TRIP A1: SEQUENCE STRATIGRAPHY, SEDIMENTOLOGY, AND PALEONTOLOGY OF THE UPPER CRETACEOUS NAVESINK FORMATION, NEW JERSEY

J BRET BENNINGTON
Department of Geology, Environment, and Sustainability, Hofstra University, Hempstead, NY 11549

INTRODUCTION

Overview of the Navesink Formation

The Navesink Formation is an 8 meter thick interval of fossiliferous glauconitic sand exposed along the eastern margin of the Cretaceous outcrop belt in New Jersey (Figure 1). At the northern end of the outcrop belt in Monmouth County, the Navesink Formation is accessable along the banks of Big Brook between Hillsdale Road and Boundary Road and along the banks of Poricy Brook, at Poricy Park on the Middletown-Lincroft Road. These two localities have long been known to fossil hunters as accessable places to collect Late Cretaceous marine fossils. Less widely appreciated is the fact that the Navesink Formation contains an excellent sedimentological record of the transition from an inner shelf to an outer shelf environment during a sea-level rise. The changes in environment that occurred with the

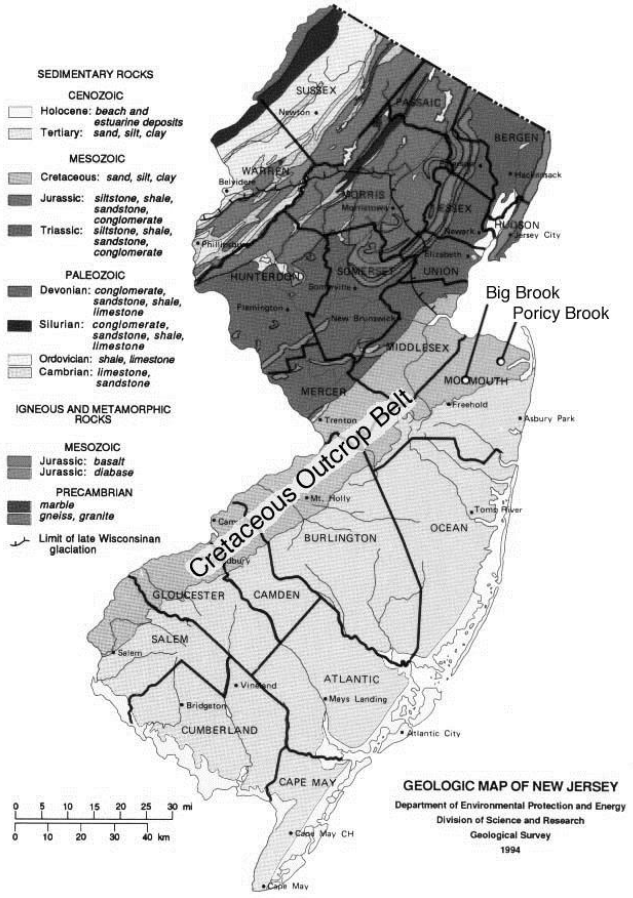

Figure 1. Geologic map of New Jersey showing Cretaceous outcrop belt and field trip stream exposure locations.

changes in sea level are recorded in a sequence of sedimentary facies defined by distinctive suites of sediments, trace fossils, and macrofossils. Our objective on this field trip is to examine the various features that define each facies, as well as the characteristics of the transitions between facies. The explanations for the transitions between facies and the sequence stratigraphic interpretation of the Navesink are incompletely understood and provide opportunities for discussion and debate. Likewise, the mechanisms of shell bed formation in the upper Navesink remain an unsolved mystery – was the primary control on shell accumulation biological, sedimentological, or environmental?

The Navesink Formation in Time and Stratigraphy

The age of the Navesink sediments has been estimated to range from approximately 70 million years at the base of the formation to approximately 66 million years at the top on the basis of Sr-isotope age estimates (Sugarman et al., 1995). Stratigraphically, the Navesink is placed at the base of the Maastrichtian Stage of the Upper Cretaceous, and is thus the beginning of the end of the Mesozoic (Figure 2). The Navesink is also the basal formation in the last of six depositional cycles developed during the Late Cretaceous on the Atlantic Coastal Plain. These sequences of marine sediments were deposited during cycles of sea level rise and fall (transgression and regression) and are separated from each other by disconformity surfaces representing intervals during which the coastal plain was exposed

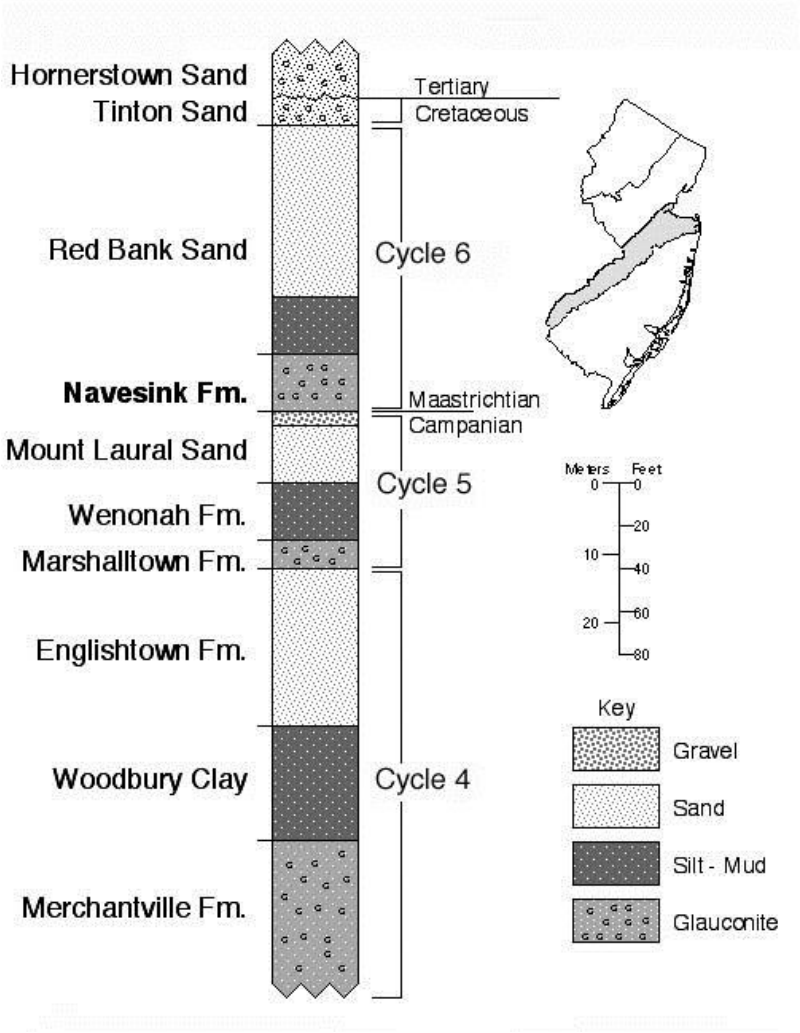

Figure 2. Stratigraphic formations and cycles in the uppermost Cretaceous of the New Jersey coastal plain (after Owens et al., 1970 and Owens and Gohn, 1985).

and eroding. The Navesink records the marine transgression that initiated deposition of cycle 6 and grades continuously into the overlying Red Bank Sand, which was deposited during the regressive part of the cycle (Figure 2). The majority of sediment in the Navesink Formation consists of glauconite, which occurs as dark green, lobate, sand-sized grains with surface cracks. Glauconite is an iron-rich mica mineral that forms diagenetically at the sediment-water interface from clay minerals likely originally encapsulated into fecal pellets. Formation of glauconite sands occurs on the continental shelf during prolonged intervals of sediment starvation (Odin and Fullagar, 1998). Deposition rates for the upper Navesink Formation have been estimated to be approximately 1 m/Ma based on formation thickness and strontium isotope dates from different stratigraphic horizons (Sugarman et al., 1995). The low rate of sediment accumulation and scarcity of terrigenous sediment argue that the Navesink was deposited under sediment starved conditions during a transgression.

The Navesink Formation and Sequence Stratigraphy

A Sequence Stratigraphic Primer (based on Nichols, 1999)

Sequence stratigraphy is a method for understanding the formation of sedimentary strata within the context of cycles of relative sea level rise (transgression) and fall (regression). A stratigraphic sequence is basically a package of strata deposited during a single cycle of sea level rise and fall. Sequences are bounded above and below by unconformities, meaning that they are deposited between episodes of significant sea level fall. Sea level fall of several tens of meters will cause subaerial exposure of the coastal plain and downcutting and erosion by rivers draining out to the receding shoreline. On the shelf, deep water sediments will be overlain by shallow water sediments. If sea level fall is extensive enough to expose the entire shelf, then a widespread unconformity surface will develop – a sequence boundary. There is no cycle order (length or time scale) implicit in the definition of a sequence - one could conceivably define a sequence for any order of cycle. In practice, however, sequences are reserved for packages of strata bounded by regionally significant unconformities marked by significant erosion on the shelf and coastal plain.

Systems tracts are packages of strata within a sequence that can be attributed to formation during particular phases of rising and falling relative sea level (Fig. 3). Systems tracts have also been called facies tracts because they contain strata from related depositional environments.

Lowstand systems tract (LST): During a relative fall in sea level the shoreline moves seaward, exposing the continental shelf. Valleys are eroded into the coastal plain and shelf and submarine canyons are eroded into the slope. Sediment bypasses the shelf and slope and is deposited as turbidity currents in **submarine fans** on the basin floor. Sediment fans can also be deposited on the slope. As relative sea level stops falling sediments may begin to fill the valleys carved on the shelf, creating a **lowstand wedge**. Together, the lowstand wedge, slope fan, and basin-floor fan deposits form the LST. On most of the shelf, the LST may exist only as a surface of unconformity.

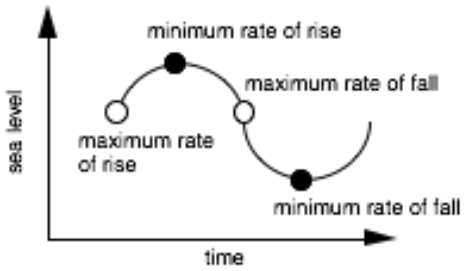

Figure 3. Cycle of sea level rise and fall

Transgressive Systems Tract (TST): As sea level starts to rise, base level increases and fluvial deposits form in incised valleys. The shelf becomes flooded again, creating a **marine flooding surface or transgressive surface (TS)** as the shoreline migrates landward, reworking the lowstand deposits or the surface of erosion developed during sea level fall. This reworked unconformity surface defines the beginning of a new sequence on the shelf and is called a **sequence boundary**. Above the sequence boundary, marine deposits of the TST are often thin due to sediment starvation as clastic sediments become trapped in flood plains and estuaries flooded during the time of maximum rate of rising sea level. This causes the deposition of a condensed section on the continental shelf characterized by authigenic sediments such as glauconite. As the rate of sea level rise begins to decline, rivers begin to build deltas out from the shoreline and clastic sediments begin prograding across the shelf. At some point prior to the beginning of renewed deposition of shelf clastics, the **maximum flooding surface (MFS)** – stratigraphic level of maximum relative sea level – is deposited. Shortly above the MFS the renewed deposition of allogenic sediments is shown by increasing quantities of terrigenous mud and sand.

Highstand Systems Tract (HST): This systems tract is characterized by aggradation of shelf sediments and then movement of the shoreline landward again as the rate of sea level rise slows, stops, and then reverses. Often this is the thickest part of the sequence because clastics stored in estuaries during sea level rise are flushed out onto the shelf during early sea level fall. The upper boundary of the HST is a sequence boundary, formed as sea level fall accelerates and begins to expose the coastal plain and shelf to erosion once again.

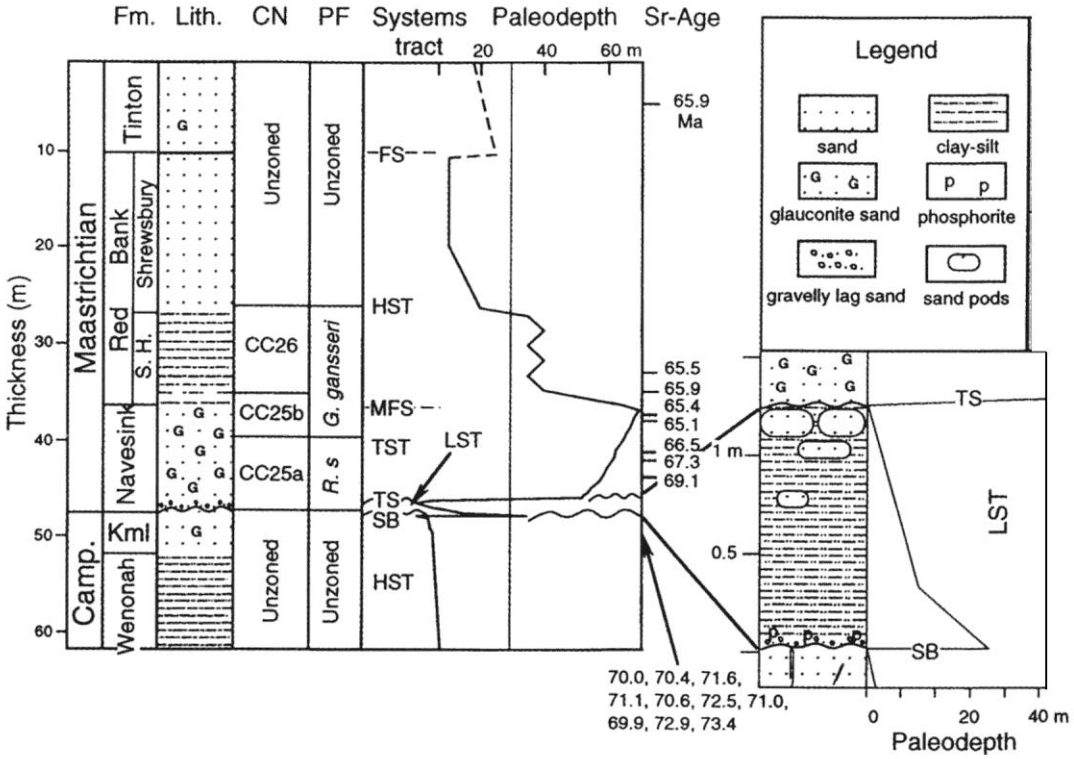

Figure 4. Sequence stratigraphic interpretation of the Navesink sequence from Miller et al., 1999, Fig. 2).

Sequence Stratigraphic Interpretation of the Navesink

The Navesink Formation has long been understood to be the transgressive interval in a sedimentary cycle that includes the overlying Red Bank and Tinton sands (e.g. Owens et al., 1968). Becker et. al. (1996) identified a transgressive lag deposit at the base of the Navesink at Big Brook and other localities and argued that this lag deposit represents a significant erosional unconformity. Miller et al. (1999) identify this lag as a major sequence boundary (Fig. 4). Unfortunately, the lag deposit is not exposed where it is easily accessible (it outcrops about a mile upstream from the Boundary Road bridge and is usually covered by slumping) and we will not be able to view it. Above this sequence boundary the Navesink Formation preserves deposits of the transgressive systems tract (TST). Martino and Curran (1990) describe two distinct lithofacies within the Navesink, a 0-4 meter transgressive sheet sand overlain by muddy, glauconite sand. Miller et al. (1999) describe one meter of clay-silt with reworked sand pods at the base of the Navesink (Fig. 4), which they interpret to be a deposit of the lowstand systems tract (LST). The difference between these two interpretations lies in the placement of the transgressive surface (TS) which represents the initial flooding of the shelf during sea level rise. Martino and Curran (1990) place the TS directly above the erosional lag at the sequence boundary, whereas Miller et al. (1999; 2004) place the TS about 1.5 meters higher in the section, above what they interpret to be a regressive lowstand tract deposit (Figure 4). Miller et al. (2004) find evidence for two systems tracts within the Navesink sequence based on analysis of two boreholes from the New Jersey coastal plain with to distinct transgressive systems tracts, but this is not apparent in the outcrops visited on this field trip.

Navesink Sedimentary Facies

We have been studying the sedimentology and paleontology of the Navesink Formation at different stratigraphic levels, paying particular attention to bounding surfaces between facies. Our work has found evidence for four distinct lithofacies and biofacies overlying the transgressive lag at the base of the Navesink (Figure 5). Together, these facies appear to show a progressive but discontinuous rise in sea level beginning with the erosional lag at the sequence boundary (Bonelli and Bennington, 2000).

Facies A) A thin basal interval of fine quartz sand with abundant carbonaceous matter, mud and some glauconite (average 15% by weight – Fig. 6). This interval is extensively burrowed, with the distinctive trace fossil *Spongeliomorpha* (similar in form to the better known *Ophiomorpha* but with unlined burrow walls marked by longitudinal ridges [Bromley, 1996]). The claws of the callianassid crustacean *Protocallianassa sp.* are occasionally preserved within the burrows at the Big Brook locality. We interpret this facies to be sands deposited in an inner shelf environment. These muddy sands must have been sufficiently cohesive to permit callianassids to excavate burrows without the need to line the burrow walls with fecal pellets, which would have produced *Ophiomorpha* traces (Bromley, 1996).

Facies B) A fining-upward interval of muddy, fine to very fine quartz sand with abundant carbonaceous matter and some glauconite (average 15% by weight – Fig. 6). This facies is characterized by a diverse bivalve fauna, including both epifaunal and burrowing forms, preserved as composite molds in the unlithified sediment. Genera identified include *Inoceramus*, *Trigonia*, *Crassatellites*, *Lima*, *Periplomya* (?), and *Linearea*. Burrows consisting of small (5 mm diameter), sand-lined tubes are found in this facies. We interpret this Facies B to represent a deeper water inner shelf environment inhabited by a diverse fauna of epifaunal and infaunal mollusks.

Facies C) Fine quartz sands that include increasing numbers of glauconite grains (average 25% by weight – Fig. 6) and a decrease in carbonaceous matter. The sediments are extensively bioturbated with dense burrows of *Thallassinoides*. Also present are phosphatic grains. Macrofossils in this interval include gryphaeid oysters, pectens and common belemnites. The contact between Facies B and Facies C appears to be erosional and is marked by irregular sandy blobs of uncertain origin, phosphatic pebbles, belemnite guards, and large, branching burrows (*Thallasinoides*) that penetrate vertically, piping dark, glauconitic sands from Facies C down into the lighter mud-rich sediments of Facies B. This contact appears to mark a significant decrease in the rate of sediment influx combined with current winnowing of the upper surface of Facies B. Similar contacts have been observed in Tertiary sediments on the New Jersey slope, where they are interpreted to be current eroded firmgrounds (Savrda et al., 2001). The sandy blobs may be the remnants of a lag layer of quartz sand produced by winnowing, possibly concentrated into horizontal burrows. Facies C appears to represent a transitional environment between inner and outer shelf depths. The boundary between Facies C and D is considered by some authors to be a transgressive surface, characterized by reworked sediments and marking the start of the transgressive systems tract (Miller et al., 1999; Miller et al., 2004).

Facies D) Glauconite sands (average 90% by weight – Fig. 6) with little to no detrital quartz grains. The sediments are extensively bioturbated with dense burrows of *Thallassinoides*. This facies includes two shell-rich intervals with abundant gryphaeid oysters. The lower interval is dominated by articulated individuals of the oyster *Exogyra costata* and contains few other species. The upper fossiliferous interval is more diverse and dominated by the oysters *Pycnodonte mutabilis* and *Agerostrea mesenterica*, with an accessory fauna of *Choristothyris* brachiopods and small pectens. Benthic and planktic foraminifera are very abundant in the upper shell bed. Also common are the spines from burrowing echinoids, although echinoid body fossils are not found. Of the large oysters, almost 100% show evidence of biocorrosion, primarily in the form of clionid borings, but also present are borings attributable to lithophagid bivalves, acrothoracican barnacles, and polychaete annelids. Encrusting organisms are also common and include several species of bryozoa, serpulid annelids, and small oysters. Many large oyster valves are almost completely biodegraded and some show evidence of having remained partially buried for extended periods of time. Most bivalved specimens are disarticulated, although approximately even valve ratios are present in samples. These observations suggest a benthic environment undisturbed by wave activity or pulses of substantial sediment input, where shells remained exposed on the sediment surface for long periods of time or became partly buried by the activities of burrowing organisms. The upper shell bed is a backlap shellbed deposited near the position of the maximum flooding surface (MFS) (Bennington et al., 1999). Modern sediments composed almost exclusively of glauconite grains are found in current swept, open marine environments of the middle to outer shelf at depths greater than 60 m, with the optimum depth of glauconite formation found to be approximately 200 m near the top of the continental slope (Odin and Fullagar, 1988).

Facies E) Similar to facies D but with increasing amounts of very fine quartz sand, showing the transition to the overlying Red Bank Formation.

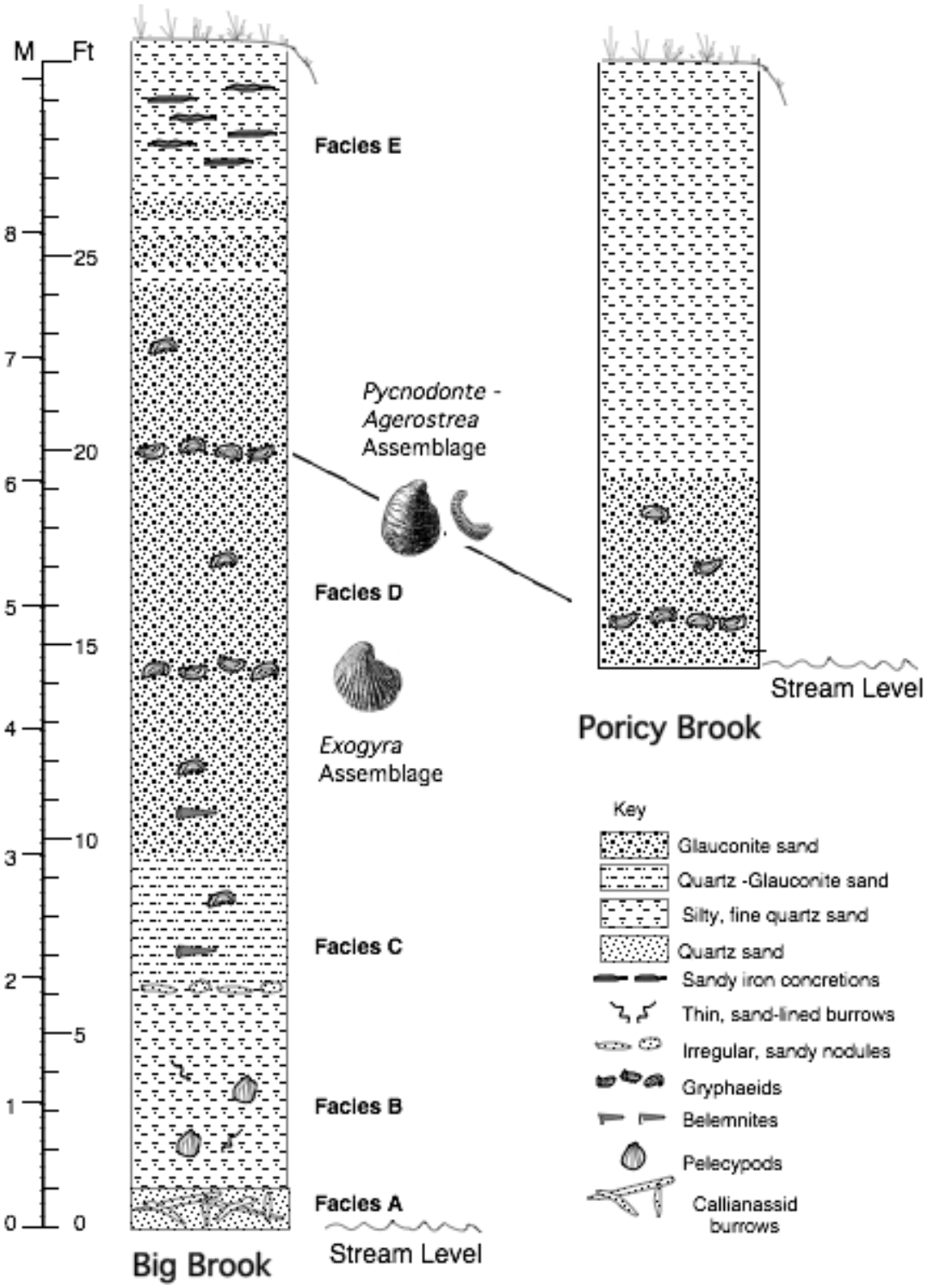

Figure 5. Summary diagram of the Navesink Formation at the Big Brook and Poricy Brook localities visited on this field trip.

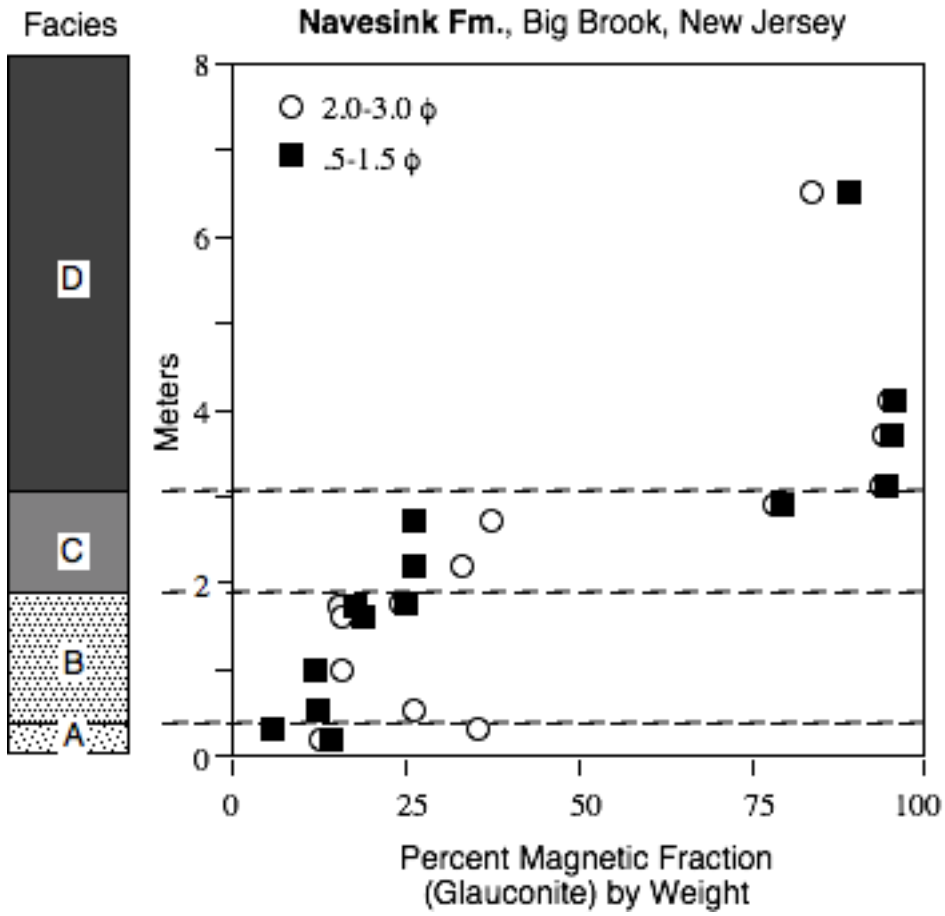

Figure 6. Percentage of coarse to fine glauconite grains by weight in sediments from different facies in the Navesink Formation at Big Brook, New Jersey. Each data point is the mean of separate runs on three splits from a single sample. 95% confidence intervals around each value are +/- 4% or less for all samples.

Navesink Paleontology

The Navesink Formation is the most fossiliferous and accessible Cretaceous unit in the northern Atlantic Coastal Plain. It is well known to both professional paleontologists and amateur collectors for its abundant invertebrate and vertebrate faunas. Public familiarity with the Navesink is enhanced by exposures along Big Brook and Poricy Brook in Monmouth County, NJ where fossil collecting is permitted on county land. The long history of collecting in the Navesink has produced a number of rare finds and an extensive faunal list for the formation (see Rose, 2000; Kuehne, 1999; Lauginiger, 1986).

Vertebrate Fossils

Vertebrate fossils consist chiefly of common shark teeth and less common bony fish, and marine reptile teeth. The greatest abundance of vertebrate remains are reported to originate from a lag deposit at the base of the formation that is not usually exposed (Rose, 2000). However, the occasional shark tooth has been found in bulk samples of sediment collected from the upper glauconite sand interval of the Navesink, so it seems likely that vertebrate remains are scattered throughout the unit. The most reliable way to recover vertebrate fossils from the Navesink is to sieve the stream sediments through a 1 cm^2

mesh, carefully inspecting the remaining gravel for shiny black pieces of tooth and bone. The most abundant shark teeth found are from the genera *Cretolamna* (mackeral shark) *Scapanorhychus* (goblin shark) *and Squalicorax*. Also commonly found are sawfish rostral spines from the genus *Ischyrhiza* and spike-like teeth from the bony fish *Enchodus*. More unusual finds may include conical mosasaur teeth, the flat teeth of shell-crushing fish and rays, and bones and shell plates from marine turtles. Dinosaur remains have been recovered from the Navesink, but they are extremely rare. To date, isolated bones and teeth from the genera *Ornithomimus* (ornithomimosaurid theropod), *Dryptosaurus* (tyrannosaurid theropod?), *Hadrosaurus* (ornithopod), and the dorsal osteoscute of an ankylosaur have been found (Rose, 2000).

Invertebrate Fossils

Invertebrate fossils and burrows are found throughout the Navesink Formation (see the description of facies above). At the localities visited on this field trip aragonitic mollusks, while abundant in the lower interval of the formation, are poorly preserved occuring as molds and composite molds in clay-rich sands. Small chalky specimens of the pelecypod *Chlamys venustus* are common in the lower glauconitic sands, but the most abundant species are those with calcite shells, including the guards of the squid *Belemnitella americana*, the large gryphaeid oysters *Exogyra costata* and *Pycnodonte mutabilis*, the small ostreid oyster *Agerostrea mesenterica*, and the brachiopod *Choristothyris plicata*. These last four species compose most of the fauna of two shell beds within the upper Navesink we will observe on this field trip. The most prominent shell bed is a 30 cm thick concentration of shells that forms the uppermost shell bed in the Navesink and appears to be widespread, occurring at approximately the same stratigraphic level along both Poricy Brook and Big Brook, at localities 10 kilometers distant. A study that sampled this shell bed at a hierarchy of spatial scales concluded that the fossil assemblage was statistically indistinguishable between the two localities (Bennington, 2003), supporting the correlation of the shell bed and suggesting that its formation was a regional event (Figure 6). Bennington et al. (1999) interpreted this shell bed to be a “backlap”

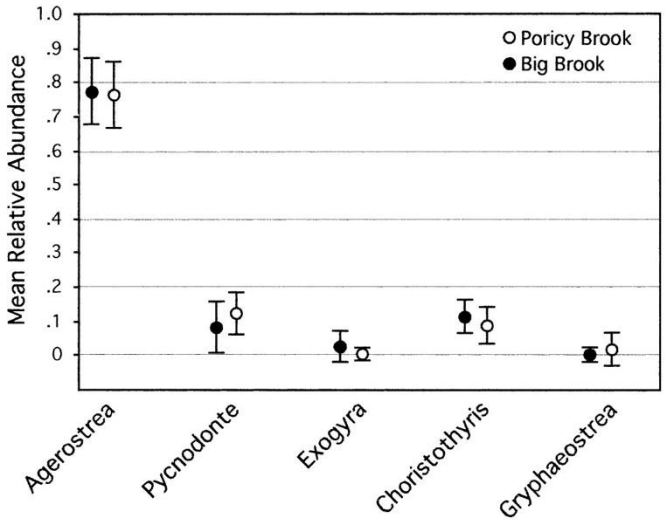

Figure 6. Comparison from Bennington 2003 of the mean relative abundance and 95% cluster confidence intervals for the five most abundant species between the uppermost Navesink shell bed at the Poricy Brook and Big Brook Boundary Road localities.

shell bed deposited during maximum transgression under conditions of sediment starvation below wave base and in the absence of substantial current winnowing. Evidence for this includes the observation that most of the large oyster shells are extensively biocorroded by the boring sponge *Cliona*, yet specimens are commonly found partially articulated or with both valves in close proximity. Thus, shells

appear to have been exposed on the sediment surface for significant periods of time, but were relatively undisturbed by currents. What is not clear are the exact mechanisms that generated the concentration of shells, given that sedimentation rates in the upper Navesink appear to have been uniformly slow. One possibility is that the benthic environment of the upper Navesink was relatively dysaerobic, perhaps due to thermal stratification of the overlying ocean, preventing the colonization of the benthos by macroinvertebrates except during relatively brief intervals of bottom oxygenation. However, the extensively bioturbated fabric of the glauconitic sands argues for an actively burrowing infauna (spines from burrowing echinoids are common) which does not corraborate a dysaerobic benthos. For now, the mechanism of shell bed generation in the upper Navesink remains a puzzle.

Preservation of Shell Color in *Pycnodonte* oysters

One of the most interesting attributes of the oyster fauna of the Navesink Formation is the preservation of orginal shell coloration in many specimens of *Pycnodonte*. Distinct bands of reddish pigmentation extend radially from the umbo to the margin of the shell. The pattern of banding is highly variable from individual to individual, ranging from thick bands that cover most of the shell to a few grouped bands or a single thin band. Color bands in *Pycnodonte convexa* have been reported previously in specimens from Utah and New Jersey (Stokes and Stifel, 1964) and are also found in specimens from the Coon Creek Formation in Mississippi, which is correlative with the Navesink. Although shell coloration is rarely preserved in fossils, radial color bands have been noted in a variety of fossil gryphaeids and in one gryph-shaped ostreid (Stenzel, 1971), suggesting that this may have been a common color pattern in these oysters.

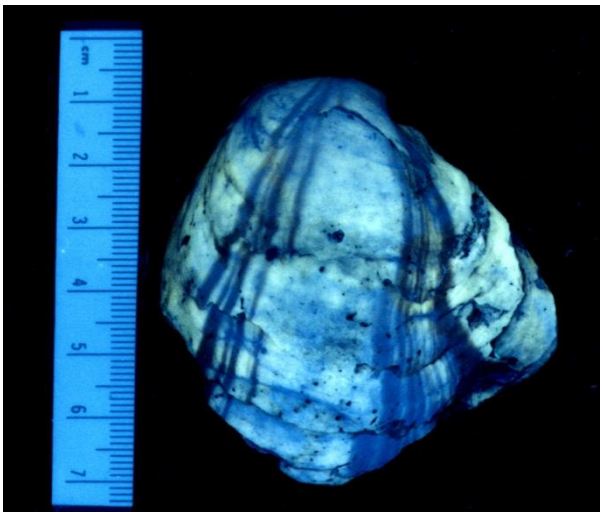

Figure 7. Specimen of *Pycnodonte* photographed under longwave UV light. Note the prominent radial bands of pigmented shell displaced laterally along intervals of shell growth disruption caused by damage to the former margin fo the shell.

Careful observation of the color banding in *Pycnodonte* reveals that the radial bands are displaced laterally along distinct growth disruptions marked by abrupt thickening, healed, crenellated breaks, and localized, abrupt changes in the slope of the outer shell surface (Figure 7). These disruptions are best explained as the result of damage to the shell margin by durophagous predators such as crabs. If the shell margin was broken irregularly and then later repaired, but with the mantle in a slightly different position, the newly formed shell bands, although of the same number and width as before, would begin regrowing in a different position along the margin of the shell after the break. Modern oysters are commonly preyed upon by crabs and lobsters that snip away at and crush the shell margin (LaBarbera,

1981) and Cretaceous oysters commonly bear indentations and other signs of breakage-induced shell repair (Dietl et al., 2000). LaBarbera (1981) demonstrated that modern crab species (blue crabs and stone crabs) will attack and attempt to consume resin models of extinct gryph-shaped oysters based on visual rather than olfaclatory sensing. This raises the possibility that the color banding on gryphaeid oysters served to break up the visual outline of the shell, providing a form of camouflage. In any case, the color band disruptions provide a unique record of the frequency and timing of crustacean attacks throughout the life of the oyster. Many *Pycnodonte* valves show multiple disruptions throughout the life of the oyster, suggesting that crustacean attacks, although a constant threat, were not often lethal.

Microfossils

Microfossils, including benthic and planktonic foraminifera, ostracods, burrowing echinoid spines, and fish scales are common in the glauconitic sediments of the upper Navesink Formation. Wet sieving sediments, particularly those associated with the uppermost shell layer, yields an abundance of specimens useful for introducing students to the study of micropaleontology (Baker, 1995).

REFERENCES CITED

Baker, J.E.B., 1995, Simple methods for extracting microfossils of the Navesink Formation (Cretaceous; N.J.): *in* Contributions to the Paleontology of New Jersey, J.E.B. Baker, ed., The Geological Association of New Jersey, v. 12, p. 302-305.

Becker, M. A., Slattery, W., and Chamberlain, J. A. Jr. (1996) Reworked Campanian and Maastrichtian macrofossils in a sequence bounding, transgressive lag deposit, Monmouth County, New Jersey: Northeastern Geology and Environmental Sciences, v.18, p. 243-252.

Bennington, J B., 2002, Cretaceous oysters on the half-shell: a record of durophagous predation preserved in *Pycnodonte convexa*: Geological Society of America, Abstracts with Programs, v. 34 (6): 541.

Bennington, J B., 2003, Transcending patchiness in the comparative analysis of paleocommunities: A test case from the Upper Cretaceous of New Jersey: PALAIOS, v. 18, p.22-33.

Bennington, J B., Bonelli, J., Chandler, J., and Selss, M. 1999, Paleoecological evidence for the formation of a backlap shell bed during maximum flooding, Upper Cretaceous Navesink formation, New Jersey: Geological Society of America, Abstracts with Programs, v. 31 (7): A468.

Bennington, J B., Selss, M., and Vinnik, A., 2000, Original color banding preserved in the Cretaceous oyster *Pycnodonte convexa* records repeated disruption to shell growth, possibly related to episodes of predation: Geological Society of America, Abstracts with Programs, v. 32 (7): A371.

Bonelli, J., and Bennington, J B., 2000, Sequence stratigraphic interpretation of the Upper Cretaceous Navesink formation, central New Jersey: Evidence from macrofossil distribution and taphonomy: Geological Society of America, Abstracts with Programs, v. 32 (1): A6.

Bromley, R., G., 1996 Trace Fossils: Chapman and Hall, 361 pp.

Dietl, G. P., Alexander, R. R., and Bien, W. F., 2000, Escalation in Late Cretaceous - early Paleocene oysters (Gryphaeidae) from the Atlantic Coastal Plain: Paleobiology, v. 26, p. 215-237.

Kuehne, D.F., 1999, Upper Cretaceous Macroinvertebrate faunas of the northern Atlantic Coastal Plain: The Mosasaur, Delaware Valley Paleontological Society, Philadelphia, v. 6, p. 29-79.

LaBarbera, M., 1981, The ecology of Mesozoic Gryphaea, Exogyra, and Ilymatogyra (Bivalvia: Mollusca) in a modern ocean: Paleobiology, v. 7, p. 510-526.

Lauginiger, E.M., 1986, An Upper Cretaceous vertebrate assemblage from Big Brook, New Jersey: The Mosasaur, Delaware Valley Paleontological Society, Philadelphia, v. 3, p. 53-61.

Martino, R.L., and Curran, H. A., 1990, Sedimentology, ichnology, and paleoenvironments of the Upper Cretaceous Wenonah and Mt. Laurel Formations, New Jersey: Journal of Sedimentary Petrology, v.60, p. 125-144.

Miller, K.G., Barrera, E., Olsson, R. K., Sugarman, P. J., and Savin, S. M., 1999, Does ice drive early Maastrichtian eustacy?: Geology, v. 27, p.783-786.

Miller, K.G., Sugarman, P.J., Browning, J.V., Kominz, M.A., Olsson, R.K.,Feigenson, M.D., and Hernandez, J.C., 2004, Upper Cretaceous sequences and sea-level history, New Jersey Coastal Plain: GSA Bulletin, v. 116, p.368-393.

Nichols, G., 1999, Sedimentology and Stratigraphy: London, Blackwell Science Ltd.

Odin, G.S. and Fullagar, P.D., 1988, Geological significance of the glaucony facies: *in* Odin, G.S., ed., Green Marine Clays: Amsterdam, Elsevier, p. 295-232.

Owens, J.P., Minard, J.P., and Sohl, N.F., 1968, Cretaceous deltas in the northern New Jersey coastal plain: *in* Finks, R.M., ed., Guidebook to Field Excursions at the 40th Annual Meeting of the New York State Geological Association, New York State Geological Association, p. 33-49.

Owens, J.P., Minard, J.P., Sohl, N. F., and Mello, J.F., 1970, Stratigraphy of the outcropping post-Magothy Upper Cretaceous Formations in southern New Jersey and northern Delmarva Peninsula, Delaware and Maryland: U.S. Geological Survey Professional Paper 674.

Owens, J.P. and Gohn, J.S., 1985, Depositional history of the Cretaceous Series in the U.S. Atlantic Coastal Plain: stratigraphy, paleoenvironments, and tectonic controls of sedimentation: *in* Poag, C.W., ed., Geological Evolution of the United States Atlantic Margin: New York, Van Nostrand Reinhold, p. 25-86.

Rose, E., ed., 2000, Big Brook: Upper Cretaceous Geology and Paleontology: The New York Paleontological Society, Spring Field Trip Guidebook.

Savrda, C.,E., Browning, J.V., Krawinkel, H., and Hesselbo, S.P., 2001, Firmground ichnofabrics in deep-water sequence stratigraphy, Tertiary clinoform-toe deposits, New Jersey slope: PALAIOS, v.16, p. 294-305.

Stenzel, H. B., 1971, Oysters: Treatise on Invertebrate Paleontology, Part N, Mollusca 6, Vol. 3, Raymond C. Moore, ed., The Geological Society of America and University of Kansas Press.

Stokes, W. L. and Stifel, P. B., 1964, Color markings of fossil *Gryphaea* from the Cretaceous of Utah and New Jersey: Journal of Paleontology, v.38, p.889-890.

Sugarman, P.J., Miller, K.G., Bukry, D., and Feigenson, M.D., 1995, Uppermost Campanian-Maestrichtian strontium isotopic, biostratigraphic, and sequence stratigraphic framework of the New Jersey Coastal Plain, GSA Bulletin, v.107, p. 19-37.

SEQUENCE STRATIGRAPHY, SEDIMENTOLOGY, AND PALEONTOLOGY OF THE UPPER CRETACEOUS NAVESINK FORMATION, NEW JERSEY

J BRET BENNINGTON
Department of Geology, Environment, and Sustainability, Hofstra University, Hempstead, NY 11549

FIELD GUIDE AND ROAD LOG

Meeting Point: north side of parking lot of the Double Tree Inn, 425 Route 59, Nanuet, NY 10954

Meeting Point Coordinates: 41.090773°N, 73.995446°W

Meeting Time: 8:30 AM

Distance in miles (km)

Cumu-lative	Point to Point	Route Description
0.0 (0.0)	0.0 (0.0)	Assemble at the north side of the hotel parking lot. Follow exit road 150 ft to Rt. 59. Exit turning right onto Rt. 59.
0.3 (.48)	0.3 (.48)	Merge onto Palisades Interstate Parkway N toward Bear Mountain.
1.3 (2.1)	1.0 (1.6)	Take exit 9W to merge onto I87 N toward Albany.
3.9 (6.3)	2.6 (4.2)	Take exit 14A to merge onto Garden State Pkwy toward New Jersey.
64.9 (104.4)	61 (98)	Take exit 114 toward Holmdel, Middletown, NJ.
65.3 (105.1)	0.4 (.6)	At the end of the exit road, turn left onto Red Hill Rd.
65.6 (105.4)	0.3 (.5)	Turn right on Dwight Rd.
67.4 (108.5)	1.8 (2.9)	Turn left onto Middletown-Lincroft Rd.
68 (109.5)	0.6 (1.0)	Turn right onto Oak Hill Rd.
68.8 (110.7)	0.8 (1.3)	Turn right into entrance to Poricy Park.

STOP 1, Poricy Park Nature Center, 345 Oak Hill Road**,** Middletown, NJ 07748

Location Coordinates: 40.369853°N, 74.097626°W

Meeting Time: approximately 10:00 AM

The Poricy Park Nature Center is located on the grounds of the Poricy Park Conservancy, a 250 acre tract of open space – the largest in Monmouth County. The nature center features an exhibit showcasing the common fossils recovered from the Navesink Formation. As the rest of the field trip stops are not located far from the nature center, we can carpool from here to cut down on the number of vehicles at subsequent stops. Bathrooms are also available in the nature center.

Distance in miles (km)

Cumu-lative	Point to Point	Route Description
68.8 (110.7)	0.0 (0.0)	Depart the nature center, turning left onto Oak Hill Rd.
69.2 (111.4)	0.4 (.65)	Turn left onto Middletown-Lincroft Road.
69.5 (111.8)	0.3 (.5)	Pull off into gravel parking area on left (SE) side of road.

STOP 2, Poricy Park Fossil Beds, Middletown, NJ

Location Coordinates: 40.369261°N, 74.116148°W

The Poricy Brook fossil locality is located in Monmouth County, NJ on the Middletown-Lincroft Road / Hwy 50. Fossil collecting is permitted within the rules stipulated by the park.

Sediments and Fossils

Only the uppermost section of the Navesink (Facies D – Figure 5 in the corresponding paper) is exposed at Poricy Brook. The upper shell bed is exposed at stream level and large specimens of *Pycnodonte* can be seen weathering out of the clayey glauconitic sands. Careful disaggregation of the shell bed sediments will reveal *Agerostrea* , *Exogyra*, and the brachiopod *Choristothyris*. Shell bed sediments also contain an abundant microfauna which can be extracted by soaking the sediment in household bleach for several days and then washing through a fine mesh to remove the clays. Careful examination of specimens of *Pycnodonte* will show that many contain faint red bands of original coloration preserved in the shell. In addition, most *Pycnodonte* record evidence of repeated predation attempts shown as irregular disruptions in the growth lines in the shell and displacements of the preserved color bands (Bennington, 2002; Bennington et al., 2000). Digging into the cut banks of the stream to obtain fossils is against the rules of the park, but I will try to obtain permission to collect some fresh specimens so we can observe the original shell coloration. Sieving the stream sediments will produce valves and fragments of the larger oysters as well as smaller specimens of belemnites, oysters, and brachiopods.

Distance in miles (km)

Cumu-lative	Point to Point	Route Description
69.5 (111.8)	0.0 (0.0)	Depart, turn left (south) onto Middletown-Lincroft Rd.
71.4 (114.9)	1.9 (3.1)	Turn right onto West Front Street.
72.5 (116.7)	1.1 (1.8)	Turn left onto Everett Road at the end of West Front Street.
73.0 (117.5)	0.5 (.8)	Turn right onto Main Street.
75.5 (121.5)	2.5 (4.0)	Turn left onto State Route 34.
78.0 (125.5)	0.5 (.8)	Turn right onto Clover Hill Road.
79.4 (127.8)	1.4 (2.2)	Turn left onto Hillsdale Road.
80.5 (129.5)	1.1 (1.8)	Pull into parking area on right (east) side of Hillsdale Road.

STOP 3, Big Brook Hillsdale Road Locality, Colts Neck, NJ

Location Coordinates: 40.320442°N, 74.214300°W

The Navesink Formation is exposed in cut banks along Big Brook in Monmouth County, NJ and can be accessed from the Hillsdale Road entrance to the Big Brook Nature Preserve. Fossil collecting is permitted within the rules stipulated by the preserve. Walk upstream from the bridge on Hillsdale Road to the first large cut bank.

Sediments and Fossils

This section exposes the middle interval of the Navesink Formation, from the top of Facies B at stream level to midway through Facies D (Figure 5 in the corresponding paper). The contact between Facies B and C can be clearly seen as a break in the slope of the cut bank wall about 30 cm from stream level. Belemnite guards are easy to find in the sediments directly above the contact. About midway up the cut bank wall is the lower shell layer containing articulated specimens of *Exogyra costata*. The upper shell bed is exposed near the top of the slope downstream from the bridge. Burrows in the upper interval of Facies B can be observed to have originated above in Facies C, piping the darker, more glauconite-rich, sediment of Facies C downward into Facies B. Specimens of the pectin *Chlamys venustus* can be observed in the lower interval of Facies C. The contact between Facies B and C, which we will also see at Stop 4, is interpreted by some researchers (e.g. Miller et al., 1999; 2004) to be a transgressive surface of erosion as evidenced by a sharp disconformity, reworked sandy sediment, and phosphate nodules. The increase in abundance of fossil from pelagic organisms, in particular belemnite squid quards, suggests a significant decrease in sedimentation rate across the Facies B-C boundary.

Distance in miles (km)

Cumu-	Point to	Route Description

lative	Point	
80.5 (129.5)	0.0 (0.0)	Depart, turn right (south) onto Hillsdale Rd.
81.1 (130.5)	0.6 (1.0)	Turn right onto Crine Road at the end of Hillsdale Road.
81.6 (131.3)	0.5 (.8)	Turn right onto Boundary Road.
82.1 (132.1)	0.5 (.8)	Pull over on the right side of Boundary Road, just before the bridge.

STOP 4, Big Brook Boundary Road Locality, Colts Neck, NJ

Location Coordinates: 40.319194°N, 74.22304°W

Here the Navesink Formation can be accessed via a path down to the stream on the southeast side of the bridge over Big Brook at Boundary Road. Fossil collecting is permitted within the rules stipulated by the Big Brook Preserve. Walk **downstream** from the bridge on Boundary Road observing the sediments exposed in the cut banks. Avoid going upstream of the bridge – this reach is bordered by private property on the north side of the stream and the landowner is hostile toward fossil collectors.

Sediments and Fossils

Walking downstream from the bridge, one can observe Facies A through Facies D (Figure 5 in the corresponding paper) in various locations along the stream banks. At stream level the callianassid burrows (*Ophiomorpha*) typical of Facies A weather out of the sediment in relief and their branching structure can be observed. Just above eye level the contact between Facies B and C is marked by a horizon of light, sandy blobs. Belemnite guards can usually be found weathering out of the sediment in the first meter above the Facies B-C contact. The *Exogyra* shell bed observed at the last stop is also present here, but it is difficult to access. Climbing the vegetated slope of a large slump at the first large cut bank downstream of the bridge allows access to the upper shell bed, although it may be covered by loose sediment. Although the fossiliferous lag that marks the sequence boundary at the base of the Navesink is below stream level at this location, weathering of this horizon farther upstream creates a steady supply of vertebrate fossils that are washed downstream. Sieving the stream gravels in the downstream vicinity of the bridge will produce a variety of shark teeth, as well as fish teeth and the occasional bone or tooth fragment from a marine reptile.

Return to Meeting Headquarters

Distance in miles (km)

Cumu-lative	Point to Point	Route Description
82.1.5 (132.1)	0.0 (0.0)	Depart, make a u-turn and head south on Boundary Road.
82.6 (132.9)	0.5 (.8)	Turn right onto Vanderburg Road.
84.0 (135.2)	1.4 (2.3)	At the end of the road, turn left onto North Main Street.

84.3 (135.7)	0.3 (.5)	Turn right to merge onto NJ-18 N toward New Brunswick.
89.4 (143.9)	5.1 (8.2)	Take exit 30 onto US-9 N toward the Amboys, New York.
96.6 (155.5)	7.2 (11.6)	Turn right to merge onto Garden State Parkway N.
99.0 (159.3)	2.4 (3.9)	Keep left on Garden State Parkway N.
145.0 (233.4)	46 (74)	Continue onto Gov Thomas E Dewey Thruway N.
146.3 (235.4)	1.3 (2.1)	Take exit to merge onto I-87 S toward New York City.
146.8 (236.3)	.5 (.8)	Keep left to merge onto I-87 S toward Tappan Zee Bridge.
147.7 (237.7)	0.9 (1.4)	Take exit 14 onto NY-59 toward Nanuet, Spring Valley.
148.0 (238.2)	0.3 (0.5)	Turn left onto W Route 59 toward Nanuet.
149.6 (240.8)	1.6 (2.6)	Meeting headquarters, Double Tree Inn, Nanuet is on the right.

REFERENCES CITED

Bennington, J B. (2002) Cretaceous oysters on the half-shell: a record of durophagous predation preserved in *Pycnodonte convexa*. Geological Society of America, Abstracts with Programs, v. 34 (6): 541.

Bennington, J B., Selss, M., and Vinnik, A. (2000). Original color banding preserved in the Cretaceous oyster *Pycnodonte convexa* records repeated disruption to shell growth, possibly related to episodes of predation. Geological Society of America, Abstracts with Programs, v. 32 (7): A371.

Miller, K.G., Barrera, E., Olsson, R. K., Sugarman, P. J., and Savin, S. M., 1999, Does ice drive early Maastrichtian eustacy?: Geology, v. 27, p.783-786.

Miller, K.G., Sugarman, P.J., Browning, J.V., Kominz, M.A., Olsson, R.K.,Feigenson, M.D., and Hernandez, J.C., 2004, Upper Cretaceous sequences and sea-level history, New Jersey Coastal Plain: GSA Bulletin, v. 116, p.368-393.

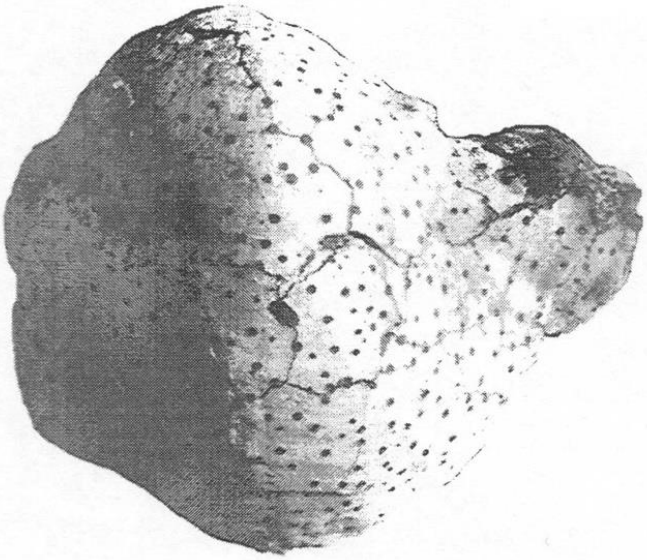

Pycnodonte mutabilis **Morton**
left valve, note the small holes made by the boring sponge *Cliona cretacica*, x3/4

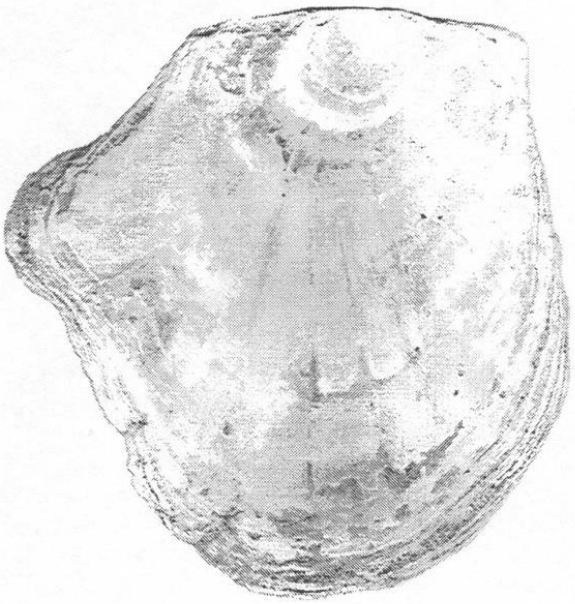

Pycnodonte mutabilis **(Morton**
right valve, note the glove-like shape, x1

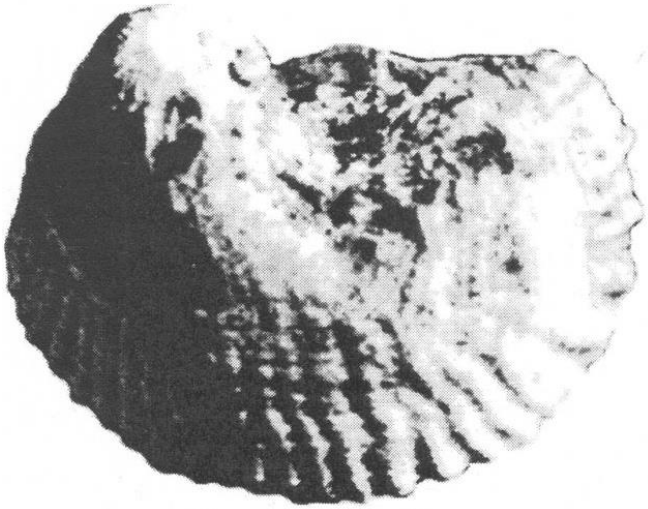

Exogyra costata **Say**
left valve exterior, x1

Belemnitella americana **Morton**
complete guard of a belemnite, x1

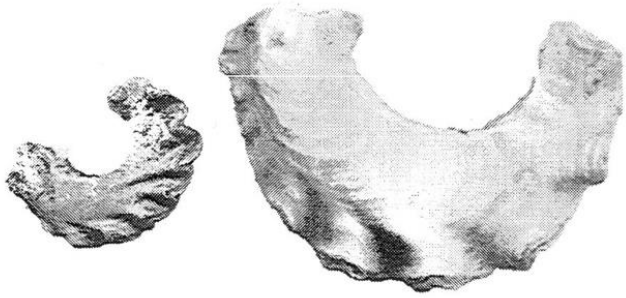

Agerostrea mesenterica **Morton**
right valves x1, middle x3, & edge view, x1

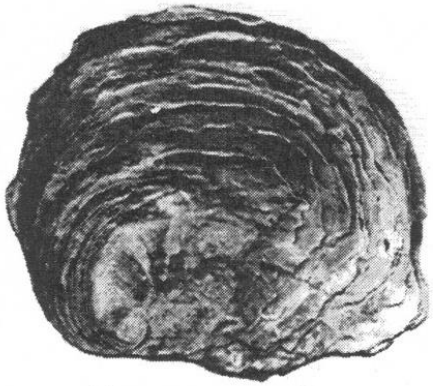

Exogyra costata **Say**
right valve, x1/2

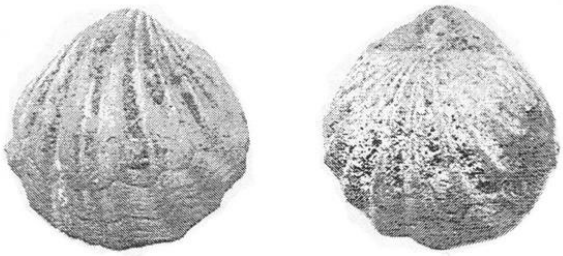

Choristothyris plicata **Say**
brachial (left) and pedicle (right) valves x2

Plate 1. Common Invertebrate Fossils of the Navesink Formation (modified from Rose 2000)

Enchodus ferox **Leidy**
mandibular tooth with jaw bone &
palatine tooth with jaw bone, x2

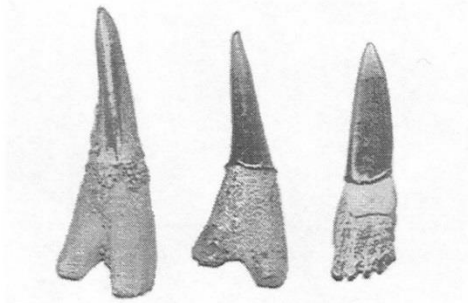

Ischyrhiza mira **Leidy**
2 lateral views and one occlusal view of the rostral spines of a sawfish, note the forked lateral profile, all x2

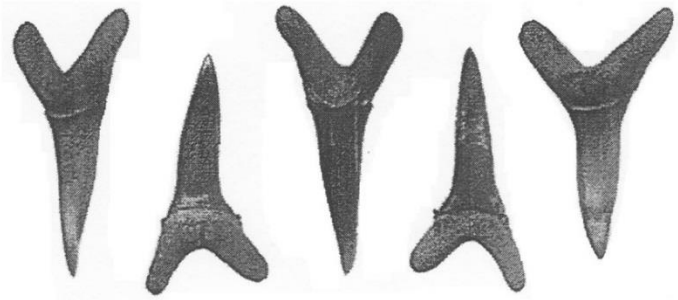

Scapanorhynchus texanus **(Roemer)**
lingual and labial views of the anterior teeth, all x1-1/2

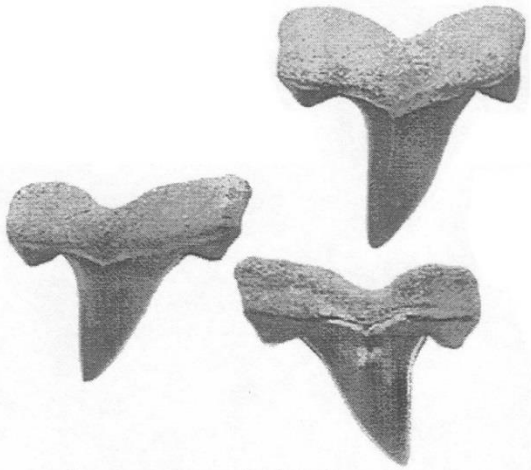

Cretolamna appendiculata **(Agassiz)**
lingual and labial views, all x2

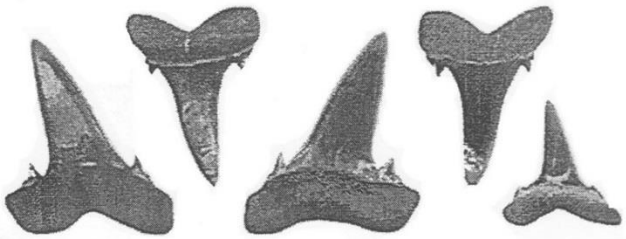

Scapanorhynchus texanus **(Roemer)**
lingual and labial views of the lateral teeth, all x1-1/2

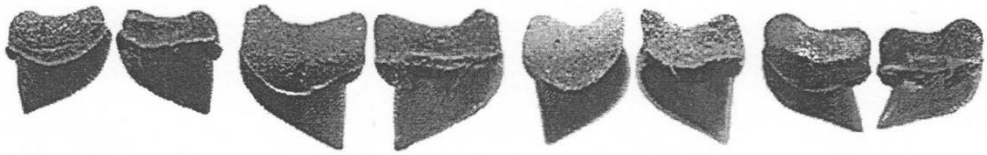

Squalicorax kaupi **(Agassiz)**
lingual and labial views of 4 different teeth, all x1-1/2

Plate 2. Common Vertebrate Fossils of the Navesink Formation (modified from Rose, 2000)

TRIP A2: HISTORICAL SEDIMENT CARBON ACCUMULATION RATES AND CURRENT ACCRETION PATTERNS IN THE MEADOWLANDS OF NEW JERSEY

FRANCISCO ARTIGAS, JOSEPH GRZYB and MICHAEL STEPOWYJ
Meadowlands Environmental Research Institute, One DeKorte Park Plaza
Lyndhurst, New Jersey 07071

ABSTRACT

Historical carbon accumulation rates are preserved in the sediment stratigraphy of temperate macrotidal salt marshes. Tidal wetlands will most likely play a role as a source of carbon credits for a global carbon market (blue carbon) so estimating their long term carbon storage potential (i.e. greater than 100 years) and the marsh ability to persist over time is a necessary first step. If accretion rates are not keeping up with rising sea level there is a chance that these ecosystems could be completely inundated and lose their ability to capture carbon in the future. We analyzed the remaining carbon content in sediments using core samples and measured accretion rates and elevation change of marsh surfaces by performing Surface Elevation Table (SET) readings and feldspar marker readings over a 6 year period. Sediment core analysis shows a sharp increase in carbon accumulation rate that started around 600 years ago and reaches a maximum of 192.2 gr/m^2/yr in the most recent layers. Measurement of surface and sub surface processes (i.e. accretion and subsidence) revealed that the average rate of marsh surface elevation change is approximately 4.6 mm/yr. The 60+ year rate of sea level rise established through tide gauge measurements in New York, Connecticut and Rhode Island average 2.6 mm yr-1. Based on these figures we conclude that under the current circumstances, marsh surfaces in the Meadowlands are out passing sea level rise or at least they are keeping up with sea level rise.

INTRODUCTION

Tidal marshes in glaciated northern New Jersey are connected with the retreat of the Wisconsin Ice sheet (15,000 yr. B.P), the creation of a post glacial lake Hackensack, the rise in sea level and entry of tidewater into the Hackensack valley which resulted in deposition of peat and muck over the glacier lake sediments (Heusser, 1949; Peteet, 1980). An apparent reduction in the rate of sea level rise from 3,000 to 2,000 yr B.P. (Stuiver and Daddario, 1963) is now linked to the earliest development of coastal peats (3.8 m deep) in the Hackensack valley. Evidence of this early colonization are the *Alnus* seeds and associated fresh water species dated to 2060 +-120 yr B.P. (Peteet, 1980) and basal peat formation over the same lake sediment dated to 2025+- 300 yr B.P. only a few Km away (Heusser, 1963). Palynology and peat stratigraphy evidence suggests marine transgressions and regressions, where established tidal marsh areas became sufficiently fresh water to support swamps containing alder and birch that later reverted back to marshland during marine transgressions (Heusser, 1963).

Tidal wetlands will most likely play a role as a source of carbon credits for a global carbon market so estimating their long term carbon storage potential (i.e. greater than 100 years) is a necessary first step (Freedman et al., 2009; Hansen, 2009). Moreover, solid baselines for accretion rates and quantifiable carbon flows would also be critical to any future CO_2 emission reduction program. On the other hand, if accretion rates are not keeping up with rising sea level there is danger that these ecosystems could be completely inundated and lose their ability to capture carbon. Furthermore, there is a need for standardized methods for quantifying carbon sequestration and carbon storage baselines as concluded by Chumra (2003), Rocha and Goulden (2009), Crooks et al. (2010) and Moffett et al. (2010).

Historical carbon accumulation rates are preserved in the sediment stratigraphy of temperate macrotidal salt marshes (Allen, 2000). The rates of vertical accumulation depend on the type of plant community, sediment inputs, flooding regime, micro topography and autocompaction of the peat (Pethick, 1979; Stumpf, 1983). Studies in Delaware Bay, the lower Hudson Valley and Connecticut (Bloom 1964; Fletcher et al., 1993; Pederson et al., 2005, respectively) show that around 6000 yr. ago palustrine wetlands occupied the coastal valleys of the north eastern shore and that by ~3000-2000 yr. B.P., the ongoing Holocene transgression created a variety of mud flats and subtidal environments and eventually the modern marsh, which is only a few hundred years old and holds the record of recent carbon sequestration rates (Pizzuto and Schwendt, 1997). The remaining carbon in the sediments not only accounts for carbon lost to the atmosphere through decomposition in the form of methane (CH_4), carbon monoxide (CO) and volatile organic carbon (VOC) but also accounts for leaching of dissolved inorganic and organic carbon and lateral particulate carbon transfers.

Due to sea level rise, surface and sub-surface processes (i.e. accretion and subsidence) of tidal marshes is an important factor in maintaining the ecosystems' ability to capture and store carbon. We analyze the accretion rate and elevation change of the meadowlands marsh ecosystems by performing Surface Elevation Table (SET) readings and feldspar marker readings. The SET is a leveling device measuring the relative elevation change of wetland sediments. These elevation readings allow us to see the buildup of the marsh in relation to rising seas. The shallow zone of subsidence contributes to the overall elevation of the marsh, as the subsurface processes in this zone counteract the increase in vertical accretion above the feldspar layer. Separating the vertical accretion surficial processes from the subsidence at depth is important in identifying different roles of the sediment column in marsh elevation dynamics. In this study we attempt to compare historical carbon accumulation rates by looking at carbon content in the sediment column and assess future carbon storage potential given local accretion rates and sea level rise forecasts.

METHODS

To explore the total organic carbon remaining in the sediments of a natural marsh, 50cm increment peat cores to a depth of 5.5 m were extracted from the nearby undisturbed Riverbend Wetland Preserve (RWP) tidal salt marsh (N 400 45' 11.37"; W 740 05' 36.62") (Figure 1). Only the upper 2.5 m of the core was used in this study. An important consideration to dating sediment profiles is the vertical stability of materials once they are deposited and minimizing disturbance while sampling. In our case, sediment cores were extracted with a Russian Peat Corer which minimizes compaction of the sample during extraction (Pitkanen et al., 2011). Core samples were saran wrapped, placed in a 50cm PVC pipe and transported in a cooler to the lab where they were stored in a 4°C refrigerator. Core segments were sampled from top to bottom every 6 cm with a 0.13 cm diameter brass auger. Total organic carbon (TOC) was determined using weight loss on ignition (LOI) method (500°C for 12 hrs) following Wang

(2011). Bulk density was determined by the sample ratio of mass over the volume. Total organic carbon (TOC) was determined as shown in Equation 5 following Dean's (1974) equation (1).

TOC (g/cc)=(LOI in decimal)/2 X bulk density **Equation 1.**

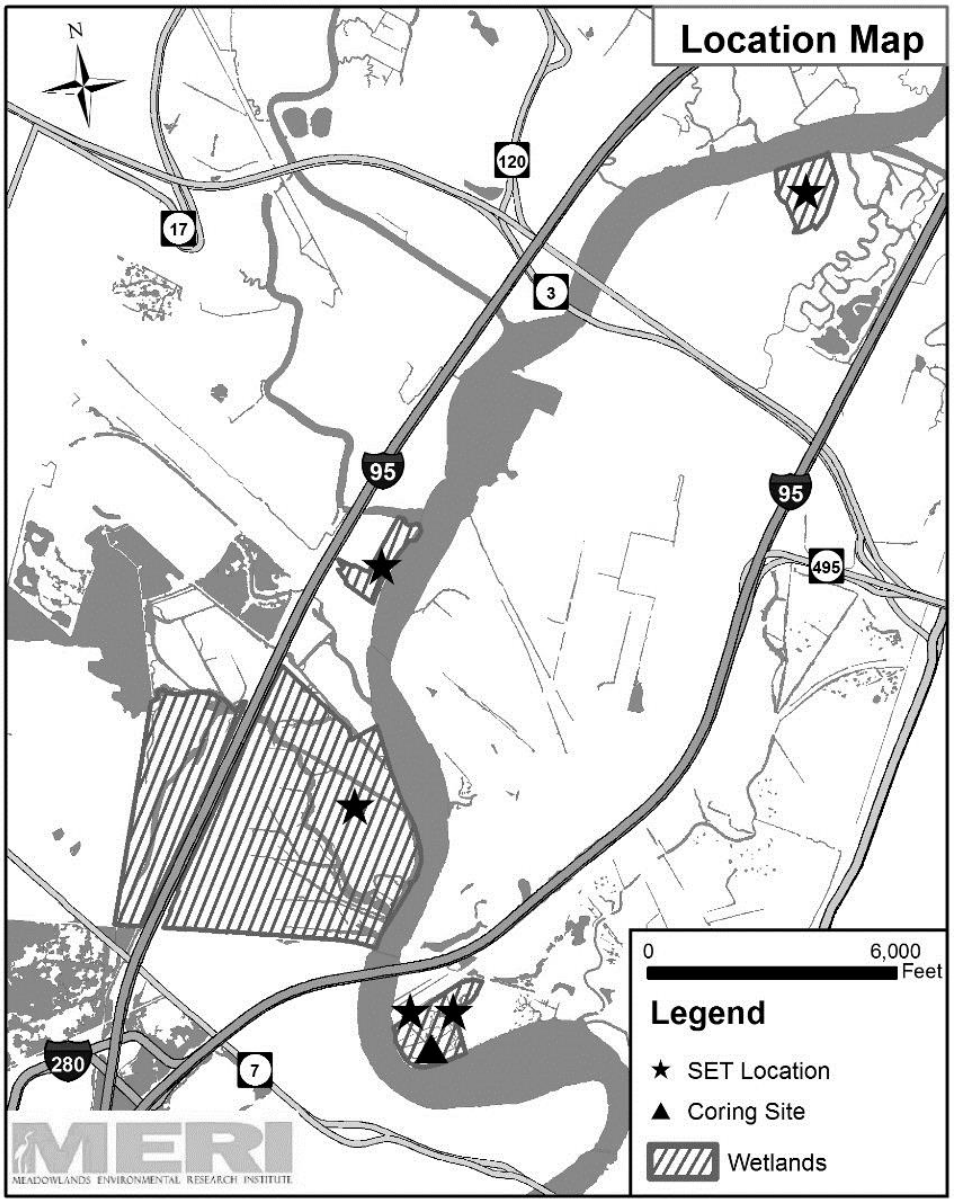

Figure 1. Location map of SET locations and coring site

The approximate time of recent carbon burial was determined by dating marsh sediment deposits using ^{137}Cs radioisotope. We applied this method, since ^{137}Cs has proven to be a reliable method for dating recent peat deposits in current studies (Orson et al., 1998; Jetter, 2000). Deeper stratigraphic

sequences on the other hand are distorted due to compaction involving a combination of physical and biochemical process that reduces the vertical thickness of the sediment column (Allen, 2000; Brain et al., 2012). Hence our age model is based on a combination of ^{137}Cs method for the most recent peat deposits, and for sediments deeper than 30 cm Heusser's (1963) and Peteet's (1980) age models were adopted. Fresh from the field, the first 30 cm of the core was cut into ten 3 cm segments, stored in air tight containers and shipped to a radioactive testing lab (University of Delaware, Department of Oceanography, Newark, DE) where ^{137}Cs isotope dating was performed according to Robbins and Edgington (1975) and Arnaud et al. (2006) using a high-purity Germanium well-type detector (Canberra Model GCW2523).

Both surface and subsurface process in the soil profile were measured to estimate marsh surface elevation. To measure changes in marsh elevation, five locations were chosen to span several miles of tidal wetlands and represent different vegetation and marsh regimes. To estimate subsurface process, three replicate plots with benchmark rods were measured at five sites with a soil elevation table (SET) apparatus (USGS, 2010). The SET apparatus is attached to the benchmark rod that gets permanently placed in the ground and extends several meters depth to the zone of deep subsidence. The rod attached to the benchmark pole acts as a constant plane in space and the distance from this plane down to the sediment surface is measured with pins. Over a period of 5.9 years and at each plot, nine pins are lowered from the benchmark rod plane to the marsh surface and readings taken in each of the four compass directions resulting in a total of 108 measurements for each of the 5 sites. Measurements obtained from each pin are compared to the previous sampling date reading, and the resulting differences become one data point that represents marsh surface elevation rate (mm/yr). The five sites measured include a restored *Spartina alterniflora* low marsh (Secaucus High School, SHS), a *Spartina alterniflora* low marsh (Saw Mill, SM), a *Spartina patens* dominated high marsh (Riverbend-Patens, RBP), a mixed *Spartina patens* and *Phragmites australis* high marsh (Riverbend Mixed, RBM) and a Phragmites australis dominated high marsh (Lyndhurst Riverside, LR) (Figure 1).

Vertical accretion or surface processes on the other hand, was measured using feldspar marker horizons at all three corners of each plot. Surface processes of deposition and erosion over time are measured from buildup of sediment from the feldspar horizon marker. Accretion was measured by taking readings at each of the three corners of each plot resulting in nine values for each site. The average of all readings for each site is shown in Table 1. Not all horizons produced recognizable accretion. Where negligible material accumulated above the horizon, "0.0 accretions" was designated. To obtain a yearly rate, the accretion value is divided by the number of days that have elapsed between establishment of the benchmark and the subsequent reading. Approximately five years and nine months elapsed between the readings. Table 1 provides the dates for each reading, accretion rate (mm/yr) and the time elapsed in days and years.

Marsh surface elevation change measured by the SET method captures both surface and subsurface processes occurring within the soil profile. The feldspar marker horizon reveals surfaces process only. We estimate the relative contribution of surface and subsurface process to marsh surface elevation by looking at the difference between shallow subsidence and accretion.

RESULTS

The variations in ^{137}Cs concentrations with depth show a well resolved peak at 5.5 cm depth (Figure 2), that coincides with maximum atmospheric fallout due to the testing of thermonuclear devices that started in 1954 and peaked in 1963/1964. We can infer that roughly 8 cm of sediments accumulated between 1954 and 2012, therefore – without accounting for compaction – on average, 1.4 mm of sediments accumulated per year since 1954.

Figure 3C shows a sharp increase in LOI values starting at 125 cm (~660 year BP) indicating a shift from subtidal environments dominated by mudflats to palustrine peats and finally to the modern emergent marsh (Holocene transgression in Allen, 2000). This change is corroborated by the marked decrease in bulk density for the same time period (Figure 3A).

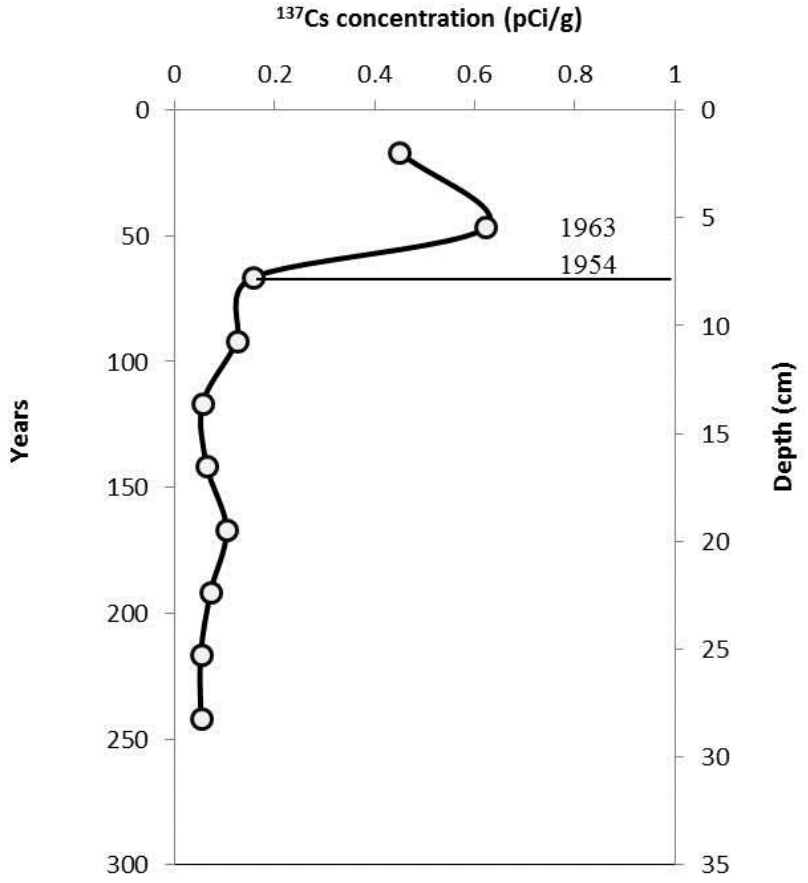

Figure 2. ^{137}Cs profile in sediment core of the Hackensack Meadowlands

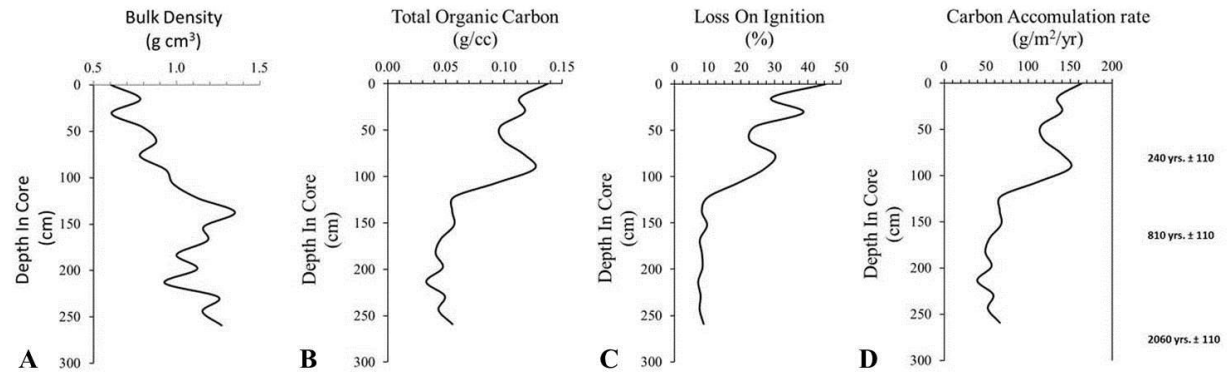

Figure 3. Bulk density (A), total organic carbon (B), loss on ignition (C) and carbon accumulation rate (D) in the sediment of the Hackensack Meadowlands over the course of approximately 1400 years

According to Artigas et al. (2015), after accounting for respiration, 22% of the carbon fixed by marsh vegetation on any given day is buried. The analysis of total organic carbon from the first 20 cm of the core shows that approximately 78% of the buried carbon remains stored 15 cm deep or at 134 years (^{137}Cs dating) and 50% of the carbon fixed by photosynthesis remains buried beyond 122 cm or 645 years B.P. Finally, Figure 3D shows a sharp increase in carbon accumulation rate around 600 years ago that reaches a maximum of 192.2 gr/m2/yr. in the most recent layers.

	Accretion (mm/yr)					Subsidence (mm/yr)				
Days	LN	RPP	RBM	SM	SHS	LN	RPP	RBM	SM	SHS
0	2.7	0	0	0	10	-6.05	-2.48	-5.96	4.66	0.03
181	4.6	5.3	5.4	7.7	5.26	-5.01	-0.78	-1.8	1.1	-1.51
349	3.9	5.7	7.8	13.8	4.4	-2.45	-0.33	0.22	8.29	-0.63
549	4.7	7.2	7.3	12	8.2	-1.55	0.32	-1.03	5.72	1.32
927	4.2	6.39	6.31	11.1	6.7	-3.33	0.47	-0.68	3.16	0.18
1434	3.4	5.03	5.05	9.9	8.9	-0.25	1.35	1.42	4.2	2.74
1799	4.4	5.67	7.18	9.7	7.9	1.22	1.5	2.02	4.96	2.06
2162	5	6.31	8.59	7.4	5.9	3.09	3.29	5.65	3.47	2.23

Table 1.- Accretion and subsidence rates in (mm/yr) for five different marsh surface type

Almost six years of accretion rate measurements from five different marsh surface types are presented in Figure 4. Each sampling date represents the average of nine measurements from the feldspar marker to the horizon. For the entire sampling period accretion rates remained above 4 mm/yr with an average of 6.6. mm/yr. The slopes of accretion rates over time were positive for all sites but were not significantly different from zero at $p<0.05$.

Subsurface process affecting marsh elevation (e.g. root growth, oxidation of organic matter, waterlogging, compaction, etc.) is captured by the SET measurement. The change in marsh surface elevation is expressed as the difference between shallow subsidence and accretion. All sites showed an

increase in elevation over time and this increase was significant for all sites ($p<0.05$) but for Mill Creek (Figure 5). On average, when all sites are combined and surface and subsurface processes taken into account, the average rate of marsh surface elevation change is 4.6 mm/yr.

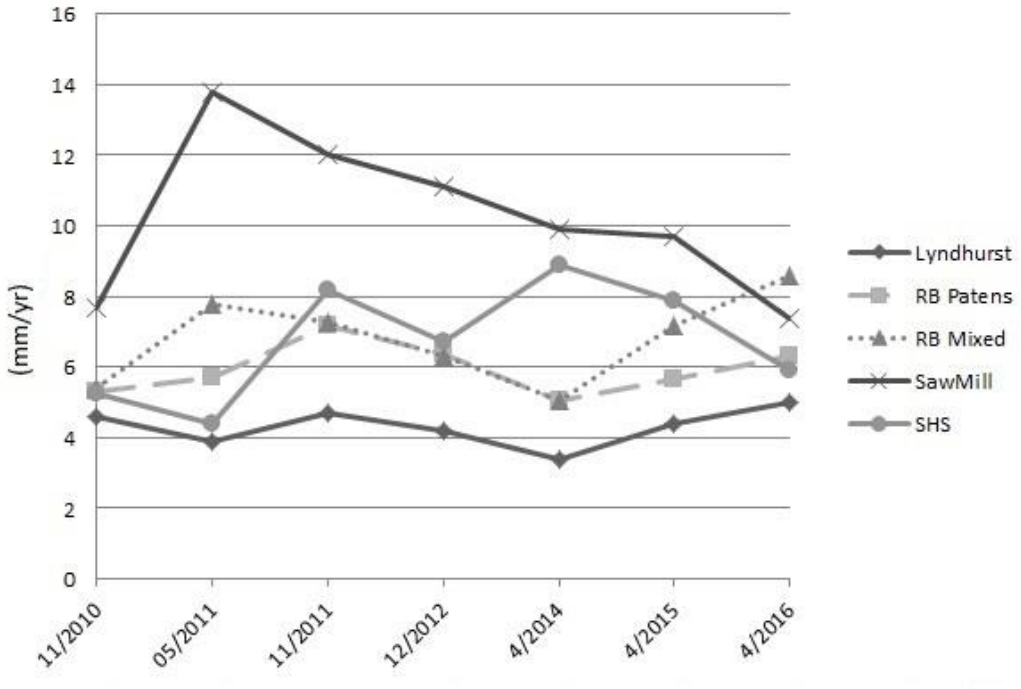

Figure 4. Accretion rates (mm/yr) from five different marsh surface types between 2010 and 2016

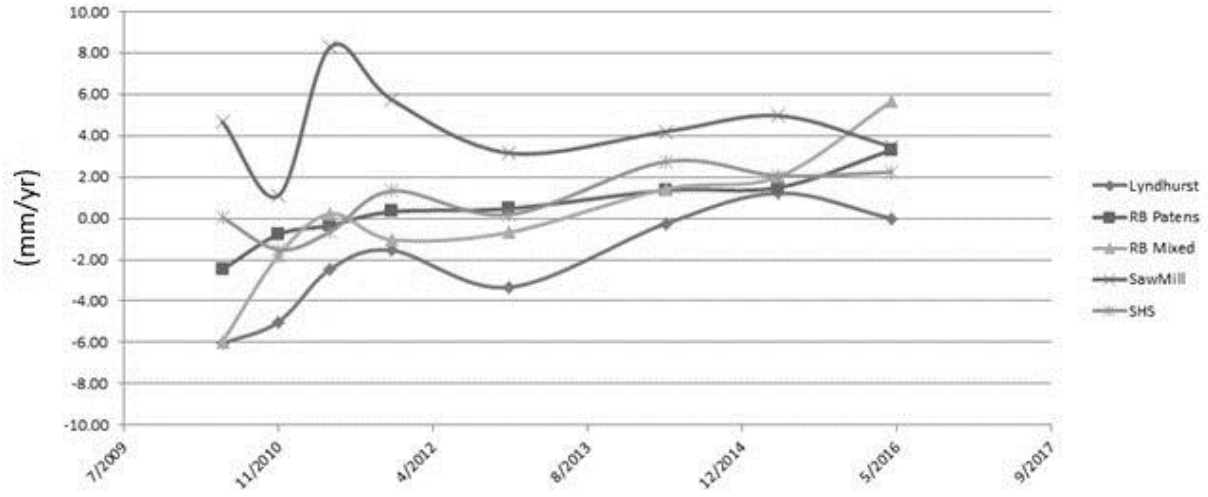

Figure 5. Shallow subsidence (accretion minus elevation) mm/yr.

DISCUSSION

Sediment core analysis shows that sharp increase in carbon accumulation rate that started around 600 years ago and reaches a maximum of 192.2 gr/m^2/yr in the most recent layers. These data confirm the

generalization that short-term (0-150 years) rates of carbon accumulation are consistently larger than long-term (>1000 years) rates (Glaser et al., 2012)

Current Eddy Covariance measurements of carbon dioxide fluxes in the Meadowlands between the canopy and the atmosphere Artigas (2014) show that after accounting for respiration, 22 % of the carbon fixed through photosynthesis remains as standing biomass or is buried in any given growing season making tidal wetlands in this case net carbon sinks. Analyses of the remaining carbon in dated sediment core samples show that of the buried carbon pool, 78% remained in the sediments 130 years later and only the most recalcitrant carbon (50%) remains buried in the sediments beyond 645 years.

The annual rate of accretion based on the 137Cs dating was estimated to be 1.4 mm. This is comparable with sedimentation rates of 1.8 mm yr-1 that have been reported for comparable *Spartina patens* communities in Connecticut (Orson et al., 1998). In this study, however, sedimentation rates on the order of 5-7 mm yr-1 were measured from feldspar horizons. Differences in sedimentation rates between what is observed from the core samples (1.4 mm/yr) and recent measurements from feldspar horizons (6.5 mm/yr) can be attributed to the age of the marsh (Pethick, 1979), distances from tidal creeks, availability of sediments, compaction and shallow subsidence (Cahoon et al., 1995). In this highly man modified environment, sediment loads from storm water outflows and sediment contributions from high capacity sewage treatment plants in the estuary suggests that true sedimentation rates may be more in line with values measured from the five permanent sediment elevation tables (i.e. 4.6 mm yr-1) than from the estimates from the 137CS dating (1.4 mm/yr).

Surface and sub surface processes contribute to the overall elevation of the marsh and will be affected by sea level rise. Subsurface processes in this zone counteract the increase in vertical accretion above the feldspar layer. Separating the surficial processes of vertical accretion from the subsurface processes is important in identifying different roles of the sediment column in marsh elevation dynamics. In this case, when both processes are taken into account the average rate of marsh surface elevation change is 4.6 mm/yr. Church and White (2011) reported the global rise in sea level from 1900 to 2009 to be on average 1.7±0.3 mm yr-1, which has accelerated to 3.3 mm yr-1 in recent years. Locally, however, the 60+ year rate of sea level rise established through tide gauge measurements in New York, Connecticut and Rhode Island average 2.6 mm yr-1 (Orson et al., 1998). Based on these figures, we can conclude that under the current circumstances, marsh surfaces in the Meadowlands are exceeding regional sea level rise or they are at least keeping up with it.

REFERENCES CITED

Allen, J.R.L. 2000. Morphodynamics of Holocene salt marshes: a review sketch from the Atlantic and Southern North Sea coasts of Europe. Quater. Sci. Rev. 19:1155-1231.

Arnaud, F., et al, 2006. Radionuclide dating (^{210}Pb, ^{137}Cs ^{241}Am) of recent lake sediments in a highly active geodynamic setting (Lakes Puyehue and Icalma-Chilean Lake District). Sci. Total Environ. 366(2-3), 837-850.

Artigas, Francisco, et al. "Long term carbon storage potential and CO 2 sink strength of a restored salt marsh in New Jersey." *Agricultural and Forest Meteorology* 200 (2015): 313-321.

Bloom, A.L. 1964 Peat accumulation and compaction in a Connecticut salt mars. J. Sed. Petrol. 34:599-603.

Brain, M.J. et al. 2012. Modelling the effects of sediment compaction on salt marsh reconstructions of recent sea-level rise. Ear. Plan. Sci. Let. 345-348:180-193.

Cahoon, Donald, et al., 2010, "Surface Elevation Table (SET)." *Patuxent Wildlife Research Center* US Department of the Interior, U.S. Geological Survey, Pwrc.usgs.gov/set/SET/original.html. Accessed 6 July 2016.

Chumra, G.L. et al., 2003 Global carbon sequestration in tidal, saline wetland soils. Global Biogeochem. Cycles, vol 17(4), 22-1-11.

Crooks, S., et al., 2010. Findings of the National Blue Ribbon Panel on the Development of a Greenhouse Gas Offset Protocol for Tidal Wetlands Restoration and Management: Action Plan to Guide Protocol Development. Restore America's Estuaries, Philip Williams & Associates, Ltd., and Science Applications International Corporation.

Dean, W.E., 1974, Determination of carbonate and organic matter in calcareous sediments and sedimentary rocks by loss on ignition: comparison with other methods. J. of Sed. Petrol. 44, 242-248.

Fletcher et al., 1993, Tidal wetland record of Holocene sea-level movements and climate history. Palaeogeog. Palaeoclim. Palaeoecol. 102:177-213.

Freedman, B., et al., 2009, Carbon credits and the conservation of natural areas. 2009 Environmental Reviews. 17: 1-19.

Hansen, L.T., 2009, The Viability of Creating Wetlands for the Sale of Carbon Offsets. J. Agr. Resour. Econ. 34, 350-365.

Hansen, L.T., 2009, The Viability of Creating Wetlands for the Sale of Carbon Offsets. J. Agr. Resour. Econ. 34, 350-365.

Heusser, C. J., 1949, "History of an estuarine bog at Secaucus, New Jersey."*Bulletin of the Torrey Botanical Club*: 385-406.

Heusser, C.J., 1963, Pollen diagrams from three former cedar bogs in the Hackensack tidal marsh, Northeastern New Jersey. Bull. Torrey Bot. Socitety. 90(1):16-28.

Jetter, H. W., 2000, Determining the ages of recent sediments using measurements of trace radioactivity. Terra et Aqua, 78: 21-28.

Meadowlands Environmental Research Institute. 'Measuring Elevation Change in Meadowlands Marshes Using Surface Elevation Tables (SETs) and Marker Horizons." meri.njmeadowlands.gov. Accessed 30 June 2016.

Moffett, K.B., et al., 2010, Salt marsh–atmosphere exchange of energy, water vapor, and carbon dioxide: Effects of tidal flooding and biophysical controls. Water Resour. Res. 46-10.

Orson, et al., 1998, Interpreting sea level rise and rates of vertical marsh accretion in a southern New England tidal salt marsh. Estu. Coast. Shelf Sci. 47:419-429.

Pederson et al., 2005, Medieval warming, little Ice Age, and European impact on the environment during the last millennium in the lower Hudson Valley, New York, USA. Quat. Res. 63:238-249.

Peteet, D., 1980, A Record of Environmental Change During Recent Millennia in the Hackensack Tidal Marsh, New Jersey. Bulletin of the Torrey Botanical Club 107 (4), 512-524.

Pethick, J.S., 1979, Long-term accretion rates on tidal marshes. J. Sed. Pterol. 51(2):571-577.

Pitkänen, A. et al., 2011, Comparison of different types of peat corers in volumetric sampling. Suo. 62(2):51-57.

Pizzuto, J.E. and Schwendt, A.E., 1997, Mathematical modelling of a Holocene transgressive valley-fill deposit, Wolfe Glade, Delaware. Geol. 258:57-60.

Robbins, J.A., Edgington, D.N., 1975. Determination of recent sedimentation rates in Lake Michigan using Pb-210 and Cs-137. Geochim. Cosmochim. Ac. 39, 285-304.

Rocha, A.V., Goulden, M.L., 2009. Why is marsh productivity so high? New insights from eddy covariance and biomass measurements in a Typha marsh. Agr. Forest Meteorol. 149, 159–168.

Stuiver, M. and Daddario, J.J., 1963. Submergence of the New Jersey Coast. Science, 142(3594):951.

Stumpf, R.P., 1983. The process of sedimentation on the surface of a salt marsh. Estuarine Coastal Shelf Sci. 17, 495-508.

Wang, et al., 2011. Optimizing the weight loss on-ignition methodology to quantify organic and carbonate carbon of sediments from diverse sources. Environ Monitoring Assess 174:241-257


Historical Sediment Carbon Accumulation Rates and Current Accretion Patterns in the Meadowlands of New Jersey
Field Guide
N
Metlife Stadium
#1
#2
120
17
3
95
495
7
1
MERI
MEADOWLANDS ENVIRONMENTAL RESEARCH INSTITUTE
0
2,500
Feet
Legend
SET Location
Coring Site

FIELD GUIDE AND ROAD LOG

Historical Sediment Carbon Accumulation Rates and Current Accretion Patterns in the Meadowlands of New Jersey

Authors: Francisco Artigas, Joseph Grzyb, and Michael Stepowyj

Directions from Nanuet to River Barge Park Marina

Get on Palisades Interstate Pkwy S
Continue to Fort Lee. Take the US 9W exit from Palisades Interstate Pkwy S
Get on I-95 in Ridgefield from US 46 W
Continue on I-95 S to N Connection Rd. Take the exit towards Sports Complex from I-95
Take Paterson Plank Rd to Outwater Ln, Carlstadt
End destination at River Barge Park. 269 Outwater Lane, Carlstadt 07072

Directions from River Barge Park Marina to Nanuet

Take Paterson Plank Rd and NJ-17 N to I-80 W
Take exit 62 toward Midland Ave/Saddle Brook. Continue to Garden State Pkwy
Exit 14-1 for I-87 S/I-287 E toward New York City, keep right and follow signs for Nanuet

Site 1: Secaucus High School Marsh

Secaucus High School Marsh is location where we collect Surface Elevation Table (SET) readings. The SET is a leveling device measuring the relative elevation change of wetland sediments. These elevation readings allow us to see the buildup of the marsh in relation to rising seas, referencing a fixed subsurface datum. This process evaluates the surface processes at hand such as sediment deposition and erosion. Below the feldspar horizon is the zone of shallow subsidence, a stratigraphic zone extending down to the bottom of the SET rod. The shallow zone of subsidence contributes to the overall elevation of the marsh, as the subsurface processes in this zone counteract the increase in vertical accretion above the feldspar layer. Separating the vertical accretion surficial processes from the subsidence at depth is important in identifying different roles of the stratigraphic column in marsh elevation dynamics.

Site 2: Riverbend Wetlands Preserve

To explore the total organic carbon remaining in the sediments of a natural marsh, 50cm increment peat cores to a depth of 5.5 m were extracted from the nearby undisturbed Riverbend Wetland Preserve (RWP) tidal salt marsh (N 400 45’ 11.37”; W 740 05’ 36.62”)

TRIP A2: ELECTRICAL GEOPHYSICAL METHODS FOR ENVIRONMENTAL APPLICATIONS

DIMITRIOS NTARLAGIANNIS

Department of Earth and Environmental Sciences, Rutgers University, Newark, NJ 07102.

ABSTRACT

Accurate and high resolution characterization and monitoring of the contaminant domain is needed to efficiently address environmental problems in the subsurface. Limited, or no direct access to the area of interest complicates characterization and remediation efforts. Advanced geophysical methods can be used to characterize the subsurface.

Electrical resistivity imaging (ERI), a widely used and well established geophysical method, is increasingly used in environmental investigations, especially for hydrocarbon plume characterization, and monitoring of degradation processes. The induced polarization (IP) method, an extension to common resistivity imaging, can provide additional insight in subsurface characterization utilizing the same network of electrodes and typically the same instrumentation. ERI and IP can offer a lot of advantages in environmental applications such as inexpensive data with high temporal and spatial resolution. Such data can be used quantitatively if constrained by a small number of direct (e.g. geochemical) data.

Implementation of ERI and IP is straightforward, requiring a network of electrodes on the ground surface or in boreholes. Advances in instrumentation allow for the efficient acquisition of large data-sets that can produce 2D and 3D images of the subsurface. Caution should be taken for correct data collection and processing to avoid erroneous interpretation of electrical geophysical data-sets.

INTRODUCTION

Environmental contamination is a worldwide problem directly affecting humans (e.g. health, property values) and ecosystems. Contamination can also impact valuable and often limited resources (e.g. groundwater, surface water, soils). The problem is exacerbated by the vast differences in impacted sites from a leaking underground storage tank to mega sites that stretch across several industrial facilities. Although contamination is primarily the result of anthropogenic activities such as manufacturing, mining and improper waste disposal, some natural processes can also contribute to environmental degradation. This can result in a wide variety of contaminants, across a range of concentrations and different media. Subsurface characterization for environmental purposes can be challenging since it can occur across a variety of depths, often with no surface footprint. To efficiently address environmental problems in the subsurface, accurate and high resolution characterization and monitoring of the contaminant domain is needed.

Subsurface characterization for environmental applications is an inherently difficult task due to:

- very large number of contaminants at varying concentrations,
- variety of host media,
- different depths and extend of impacted media.

Continuous advances in characterization methods and protocols, changes in regulatory standards, and

the update of existing and development of new remediation systems further complicate this task. In

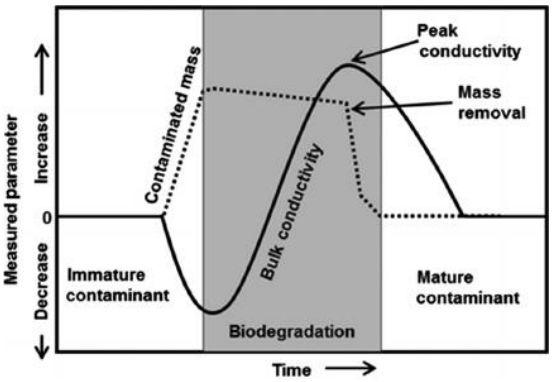

1: Figure 1: Conceptual model of the hydrocarbon electrical conductivity properties change with time. The electrical conductivity of the subsurface is dropping as a result of the contaminant release; when degradation processes become significant the conductivity starts to increase, until the contaminant mass has been largerly removed / re-mediated and the system returns to the original condition (adapted from [Heenan et al., 2015]).

recent years, novel applications of near surface geophysical methods has shown the potential that exists for enhancing subsurface characterization. Advances in technology and improved understanding of geophysical signals have allowed for geophysical methods, such as electrical resistivity, to be used for environmental applications such as hydrocarbon mapping and delineation [Atekwana and Atekwana, 2009; Flores Orozco et al., 2012], mapping and characterization of buried waste and engineered structures (e.g. landfill boundaries) [Soupios et al., 2007; Tsourlos et al., 2014], geological characterization [Robinson et al., 2015], contaminant leak detection and monitoring [Johnson and Wellman, 2015], monitoring enhanced remediation[Williams et al., 2009a; Flores Orozco et al., 2011] and monitoring natural attenuation [Heenan et al., 2015].

Electrical resistivity imaging (ERI), a widely used and well established geophysical method, has been successfully used to characterize hydrocarbon plumes, and in some instances to monitor degradation processes [Atekwana and Atekwana, 2009; Atekwana and Slater, 2009; Heenan et al., 2015]. Hydrocarbon contamination and related processes (e.g. degradation) appear to significantly alter the subsurface electrical properties due to the production of electrically conductive degradation end products such as organic acids, increased dissolved ion concentrations resulting from mineral weathering, hydrocarbon emulsification and solid phase precipitates [Atekwana and Slater, 2009]. In recent decades, the conductive layer model has been develop to describe the links between hydrocarbon contamination in the subsurface and ERI signals. This new conceptual model extends the traditional model that requires the hydrocarbon plumes to act strictly as insulators. It suggests that the conductivity of the contaminated area will increase as the plume ages, resulting in higher condutivities relative to the bulk formation [Sauck, 2000, p.200; Atekwana et al., 2004; Atekwana and Atekwana, 2009; Heenan et al., 2015] (Figure 1). The suggested change of electrical conductivity is visually described in Figure 1; the initial hydrocarbon contamination causes an increase in organic contaminated mass and a corresponding decrease in conductivity. As biodegradation intensifies, contaminant mass decreases resulting in increasing biodegradation byproducts (i.e. increased ionic concentration), that lead to the observed decrease of bulk conductivity. Upon completion of the degradation processes, the system is expected to return to the original state (as far as electrical properties is considered).

The induced polarization (IP) method is a natural extension of the resistivity method where not only the resistive, but also the capacitive properties of the earth are measured [Rubin and Hubbard, 2005; Reynolds, 2011]. Although the IP is a well-established geophysical method, especially in the mineral exploration field, it has seen limited use for environmental applications until very recently mainly due to instrumental and computational limitations [Kemna et al., 2012]. In certain cases, IP surveys can offer additional information about the subsurface conditions. For example, IP has been repeatedly shown to provide diagnostic information on organic contamination, including (bio)degradation processes [Atekwana and Slater, 2009; Schmutz et al., 2010; 2012; Revil et al., 2012; Heenan et al., 2013]. The majority of this work though is based on laboratory experiments under controlled conditions, allowing for the links between geophysical signals and biogeochemical processes to be assessed [Schmutz et al., 2010; 2012; Heenan et al., 2013; Personna et al., 2013]. Conceivably, IP measurements may offer more information on hydrocarbon plumes, and associated bio-geochemical processes during environmental characterization and monitoring. However, broad use of the method in environmental applications has been hindered due to issues with acquisition of IP data such as data quality, processing, survey time requirements, and data interpretation. Recent field applications have highlighted the benefits of the IP method vs ERI and/or conventional monitoring but also emphasized the need for high quality data acquisition and processing [Williams et al., 2009b; Flores Orozco et al., 2011; 2012; 2015; Ntarlagiannis et al., 2015]. It should be highlighted that during IP surveys ERI data are inherently collected.

The need for more sustainable remediation methods [U.S. Sustainable Remediation Forum, 2009] highlight the need for robust tools suitable for efficient long term monitoring. Geophysical methods offer the monitoring capabilities including cost efficiency, spatial and temporal resolution required for long term monitoring, but lacked the technological background (e.g. communication, power needs) for long term autonomous operation. Technology advances in the recent years effectively overcame such problems rendering ERI and IP methods prime candidates for long term monitoring operations. Heenan et al. [2015] for example, used an ERI system to monitor the evolution of the British Petroleum (BP) Macondo well oil spill on Louisiana beaches for a period of ~ 18 months. The system was operated remotely with periodic visits (every few months) for preventive maintenance (Figure 2).

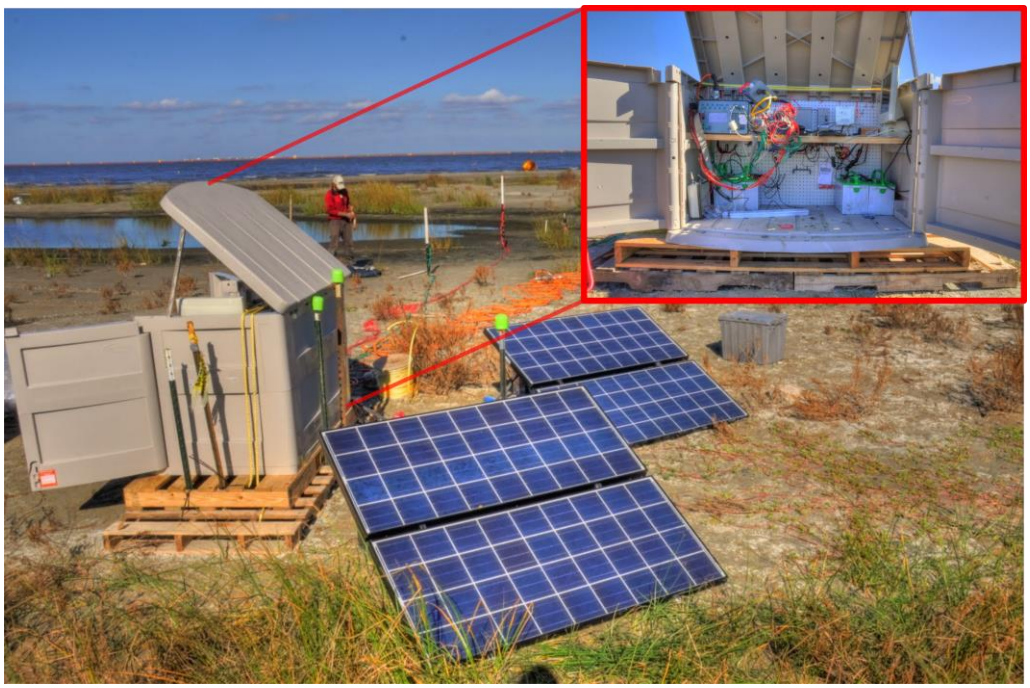

Figure 2: Long term ERI monitoring system built around standard off the shelf ERI instrumentation (Syscal Pro - Iris Instruments [IrisInstruments, 2016]). The system was anchored, secured in a weatherproof housing, powered by sun and remotely accessible through cellular connection. Modified from Heenan et al. [2015]

METHODS

Electrical properties of the subsurface

In the absence of metallic minerals, electrical current travels in the subsurface via electrolytic (σ_{ele}) and surface conduction (σ_{surf}). Both pathways involve ionic charge transport with σ_{ele} considering the fluids in the interconnected pore space, and σ_{surf} the electrical double layer at the mineral grain – fluid interface. Electrolytic conduction is directly related to fluid properties, ionic concentration, saturation and porosity [Binley and Kemna, 2005]. Surface conduction is a complex electrical property controlled by the surface area of the material, and the pore size or grain size distribution [Lesmes and Frye, 2001; Weller et al., 2010; 2013]. Surface conduction depends on fluid properties and mineralogy to a lesser degree [Lesmes and Frye, 2001; Weller et al., 2010]. Electrolytic and surface conduction pathways are commonly modeled to add in parallel [Waxman and Smits, 1968]

In terms of measurements, the real (σ') component of the measured complex conductivity (σ^*) represents electro-migration and the imaginary (σ'') parts represents charge polarization. These are related to the measured conductivity magnitude ($|\sigma|$) and phase (φ):

$$\sigma^* = |\sigma|e^{i\varphi} = \sigma' + i\sigma'', \qquad (1)$$

$$\sigma' = |\sigma|cos\varphi, \qquad (2)$$

$$\sigma'' = |\sigma|sin\varphi, \qquad (3)$$

where i = $\sqrt{-1}$. Based on the model of parallel conduction paths for electrolytic and surface conduction,

$\sigma' = \sigma'_{ele} + \sigma'_{surf}$, (4)

$\sigma'' = \sigma''_{surf}$ (5)

ERI is a widely used geophysical method that aims to model the subsurface conductivity ($|\sigma|$) structure of the area under investigation. ERI uses a network of electrodes to inject current *(I)* into the ground via two transmitting electrodes, and then measures the resulting potential drop *(ΔV)* among one, or more, pairs of receiving electrodes [Binley and Kemna, 2005]. The true subsurface conductivity distribution is estimated via inverse methods from a large number of measured transfer resistance (R) values,

$$R = \frac{\Delta V_p}{I} \quad (6)$$

where ΔV_p is the measured voltage, and *I* is the injected current.

The IP method measures the complex electrical properties (i.e. electromigration and polarization mechanisms) of the area under investigation [Binley and Kemna, 2005; Kemna et al., 2012; Revil et al., 2012]. Many modern instruments offer the option to acquire IP measurements in addition to ERI surveys, utilizing the same network of electrodes. Time domain IP measurements record the resistance magnitude (R) and an apparent chargeability m_a (mV/V),

$$m_a = \frac{V_s}{V_p}, \quad (7)$$

where V_p is the primary voltage, and V_s is the secondary voltage immediately after current shut off. The secondary voltage only exists when polarization mechanisms are significant. Since V_s is small relative to V_p and thus difficult to measure, an integral measure of m_a over a decay curve measured over a period of time (t) following current shut off is used:

$$m_a = \frac{1}{(t_2 - t_1)} \frac{1}{V_p} \int_{t_1}^{t_2} V(t) dt \quad (8)$$

The field IP parameters chargeability (m_a) and phase (φ) shift are both measures of the polarization strength relative to the electromigration strength (e.g. Slater and Lesmes, 2002). Consequently,

$m_a = -k \varphi$, (9)

where the constant of proportionality *k* can be experimentally derived in the laboratory (Mwakanyamale et al. 2012).

Field surveys

Electrical resistivity imaging (ERI) aims at determining the spatial distribution of resistivity ρ in the subsurface, typically with the use of four electrode measurements [Rubin and Hubbard, 2005]. ERI surveys utilize electrodes on the surface of the earth, in boreholes or a combination of the two. Surface surveys are typically categorized as either 'profiling' or 'sounding'. Profiling describes ERI surveys aiming at lateral variability (at a constant depth) while sounding (vertical electrical sounding – VES) is used to determine the change of electrical properties with depth at a single location. The development of modern multichannel ERI systems that are capable for simultaneous measurement of multiple pairs of electrodes and for the automated acquisition of a large number of measurements allows for efficient acquisition of large datasets. This effectively led to the wide adoption of imaging approaches where both VES and profiling are combined to produce 2D, and even 3D, images of the subsurface apparent

resistivity [Rubin and Hubbard, 2005; Slater et al., 2010; Johnson et al., 2012; Heenan et al., 2015; Robinson et al., 2015; Ntarlagiannis et al., 2016].

Surface electrical surveys can be extended by placing electrodes in a single, or multiple, boreholes [Rubin and Hubbard, 2005]. The electrodes can either be placed permanently, or downloaded for each use, in uncased boreholes, or in PVC lined boreholes with sufficient slotted/open intervals; in some cases electrodes can be permanently placed (wrapped) on the outside of pvc boreholes. When two or more boreholes are used for resistivity surveys, the suggested term is electrical resistivity tomography (ERT).

ERT offers certain advantages over ERI such as high resolution with depth, and does not require surface access (e.g. below buildings). The disadvantages are that boreholes are needed, survey area is constrained by the boreholes, and data acquisition and processing might be more complicated and challenging. Very often surface electrodes are combined with borehole electrodes to provide more accurate image of the subsurface.

Field application of the IP method is similar to the ERI method, where four electrodes are used (two for current injection, and two for potential/chargeability measurement). Additional care should be taken to utilize electrode configurations that provide high S/N ratio, and maintain good contact with the ground (e.g. [Mwakanyamale et al., 2012]). In addition to the voltage difference measured during ERI surveys, in an IP survey the voltage decay with time, after current injection has stopped, is measured. The recorded gradual voltage decrease is a complex function of charge polarization at the interfaces (e.g. fluid-grain) and charge conduction within the fluid and the along the grain [Binley and Kemna, 2005]. The IP method has its origins ore prospecting, specifically for disseminated metallic minerals [Telford et al., 1990; Kemna et al., 2012]. Advances in instrumentation, along with better understanding of the underlying processes, led to the resurrection of the IP method in recent decades. IP is now more routinely used in environmental, and other, near surface geophysical applications, due to the unique sensitivity in interfacial processes [Rubin and Hubbard, 2005; Kemna et al., 2012; Revil et al., 2012; Ntarlagiannis et al., 2016].

DATA ACQUISITION AND INTERPRETATION

A variety of standard electrode configurations have been developed over the years that offer different survey characteristics and can be suited for different applications (Figure 3). In addition, custom made sequences can be utilized that address the specific objectives of each project [Rubin and Hubbard, 2005; Reynolds, 2011; Tsourlos et al., 2014]. In a typical survey, multiple measurements are acquired along one transect (2D) or multiple transects (3D). Measurements are acquired using a variety of electrode combinations and electrode separations (Figure 4) to create the so called pseudo-section. For the pseudo-section, a lateral and vertical position of the measured point is assigned for each data acquisition (Figure 4). The lateral position of the measurement is usually the midpoint of the 4 electrodes and the vertical depends on electrode separation; the depth increases as the electrode separation increases. Using all the measurements, the pseudo-section can be created, which shows the subsurface resistivity – termed apparent resistivity (ρ_a)- distribution assuming homogenous half-space. The true resistivity is then calculated using inverse methods. Figure 4 also highlights some of the limitations of such surveys showing areas with limited numbers of measurements (towards the ends).

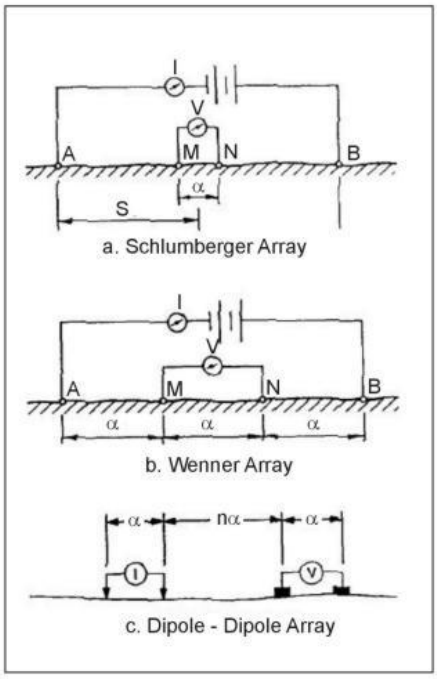

Figure 3: Common electrode configuration used for ERI/IP surveys. 'α' is the electrode (dipole) separation distance, and 'n' is the dipole separation factor (image from https://archive.epa.gov).

The apparent resistivity (ρ_a) is calculated from the measured resistance (equation 6) using the geometric factor *k* according to the following equation:

$$\rho = k * R \qquad (10)$$

The geometric factor depends on the electrode position and can be estimated using the general equation:

$$k = \frac{1}{AM} - \frac{1}{BM} + \frac{1}{BN} - \frac{1}{AN} \qquad (11)$$

where A is the location of electrode used currrent injection, B for current return, M is the electrode for the potential measurement and N is the potential measurement return (Figures 3, 4). For the most common surveys *k* is known (table 1).

Table 1: Geometric factor for common arrays. 'α' is the electrode separation distance, and 'n' is the dipole separation factor.

Array type	Geometric factor (*k*)
Wenner	$2\pi a$
Schlumberger	$\pi(n(n+a))/a$ $\pi(n^2/a)$, if a<<n
Dipole – dipole	$\pi an(n+1)(n+2)$
Pole-pole	$2\pi a$

The true distribution of subsurface resistivity, and chargeability, can be estimated using inverse methods. Since this is a non unique problem, the solution is typically the result of a regularized optimization problem involving the minimization of an objective function comprising both data misfit (measured vs. modeled) and a correction term accounting for deviations from the desired model attributes [Binley and Kemna, 2005].

An important, but often overlooked, parameter for accurate electrical data processing is the reliable quantification of measurement errors; the inversion then needs to be weighted by a model reflecting the measurement error. A common method for error

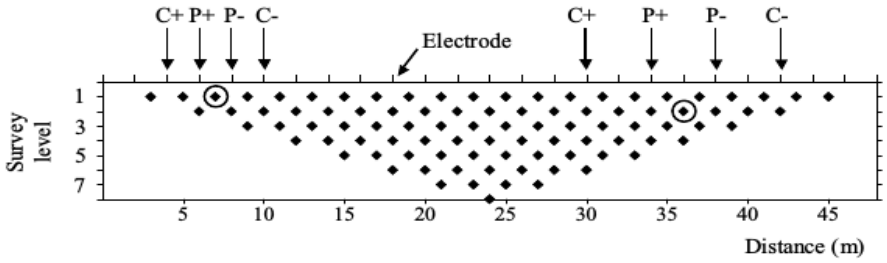

Figure 4: Typical ERI field survey. Circles identify the location assignment for the two measurement configurations shown. Each survey level corresponds to a different electrode spacing. (from [Binley and Kemna, 2005])

quantification is use of reciprocal measurements, whereby the potential and current electrodes are switched. As per the principle of reciprocity, differences between normal and reciprocal errors can be used to quantify the error in a measurement [Koestel et al., 2008].

An example of data acquisition, the resulting pseudo-section, and the inverted image can be seen in Figure 5. In this simulation exercise, we can see the true subsurface model (Figure 5a), and the resulting pseudo-section using the Wenner configuration (Figure 5b). Using inverse methods, an image of the subsurface resistivity can be reconstructed (Figure 5c). The inverted image appears to be closer to the real subsurface model, than then pseudo-section. The Wenner configuratin has poor lateral resolution, and is reflected in the inverted image (Figure 5c). A combination of multiple configurations could

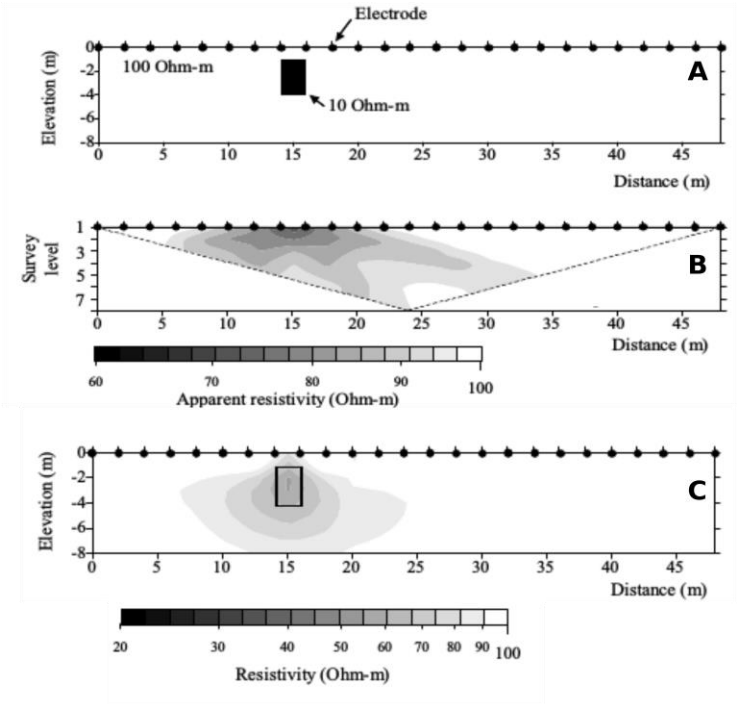

Figure 5: Example of electrical data acquisition and processing. A) the true model of subsurface, B) the pseudo-section of the acquired data, and C) the inverted image of 'real' resistivity distribution. (adapted from [Binley and Kemna, 2005])

provide a more accurate representation of the subsurface. Details and further information on data processing and inversion can be found in many textbooks [Telford et al., 1990; Rubin and Hubbard, 2005; Reynolds, 2011].

CASE STUDIES

Characterization of an organic contaminant plume.

The successful use of electrical methods for environmental applications has been demonstrated in many field projects. Ntarlagiannis et al. [2016] used ERI and IP to characterize, and monitor, the contaminant plume associated with an olive oil mill waste (OOMW) deposition pond (Figure 6). Data processing and inversion of the field ERI dataset revealed that the organic plume is characterized as a region of high electrical conductivity consistent with the conceptual model for the electrical structure of a biodegraded LNAPL contaminant plume. Furthermore, inverting of the IP dataset, they showed that the plume is also

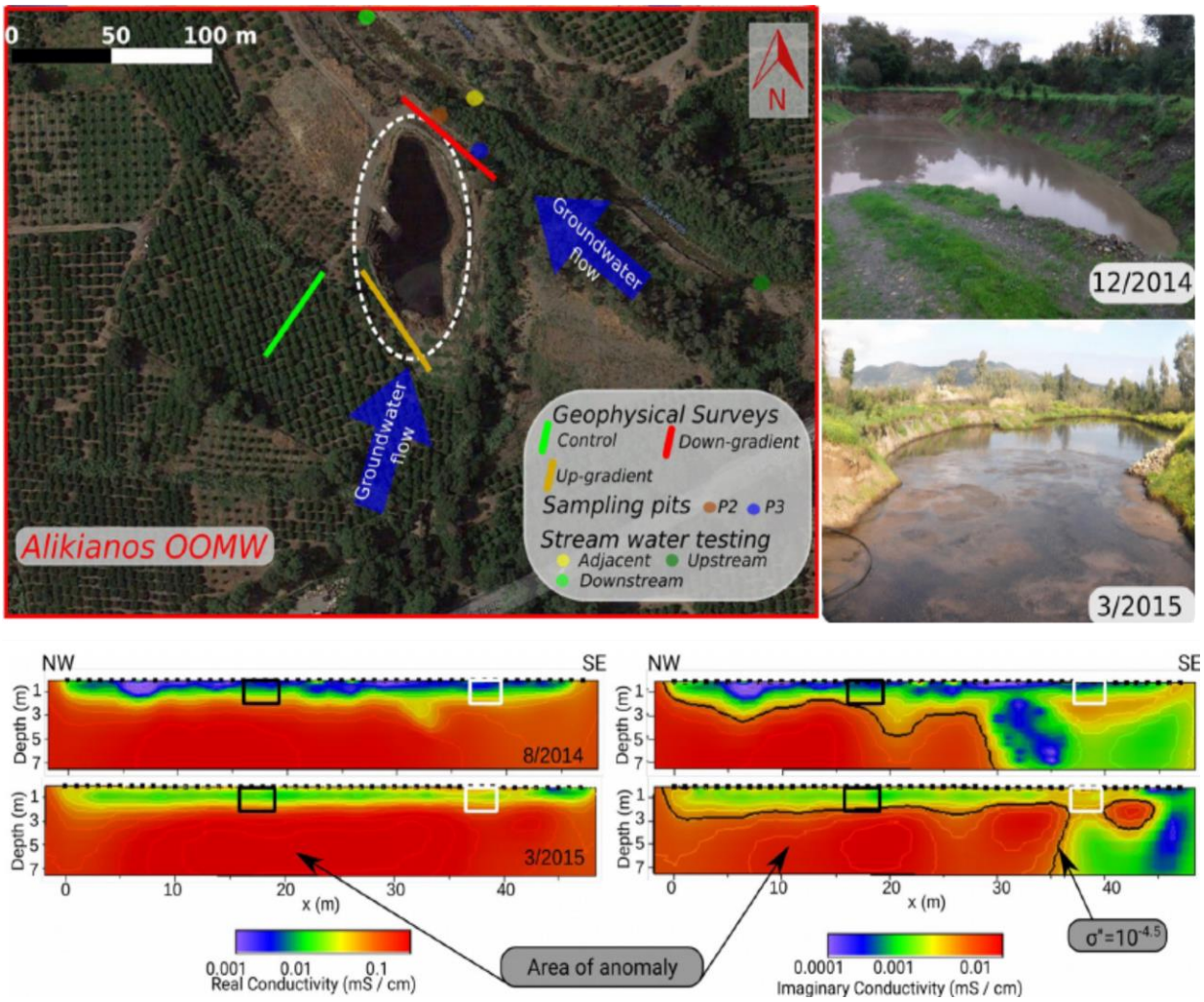

Figure 6: Map view of the Alikianos OOMW showing the areas where geophysical surveys have been performed, the geochemical sampling locations, and groundwater flow. On the upper right corner two images of the pond filled with increasing volume of organic waste. Characteristic imaging results from the down-gradient geophysical survey line are shown (bottom). ERI images (left) show the elevated conductivities as the result of organic contamination. IP (right) images delineate the plume more accurately, and are more sensitive to temporal changes. Adapted from [Ntarlagiannis et al. 2016].

characterized by a region of high polarizability that is more localized to the known plume location (based on conventional monitoring) relative to the high conductivity region in the electrical conductivity image. This observation is attributed to the fact that electrical conductivity is more strongly controlled by hydrogeological and geological characteristics of the site that mask the response from the biodegraded plume. This result encourages the use of field IP to improve the spatial delineation of organic contamination in the subsurface. However, more laborious field procedures are required to acquire reliable field IP data and the inversion of field IP data remains more challenging than resistivity data alone.

Long term monitoring of a young hydrocarbon plume in saline environment.

Geophysical methods are increasingly being used for detection/monitoring of microbial processes within earth media [Atekwana and Slater, 2009]. Although most of the previous work is on freshwater systems (mainly groundwater), the Deepwater Horizon (DH) oil spill into the Gulf of Mexico in 2010 allowed researchers to study an oil spill from it's early stages in a variety of brackish to saline environments. Heenan et al. [2015] deployed and autonomous resistivity monitoring system on Grand Terre, Louisiana, in an effort to monitor natural degradation processes in hydrocarbon-impacted beach sediments as a result of the DH accident (Figure 7). A 48-electrode surface array with a 0.5-m spacing was installed and was programmed to obtain twice-daily images of the resistivity structure of the shallow subsurface impacted by oil (Figure 2). Over the course of approximately 18 months, they observed a progressive decrease in the resistivity of the DH spill-impacted region, consistent with previous observations in fresh water environments (Figure 8). The observed change in conductivity is in agreement with the

Figure 7: The location of the autonomous ERI monitoring system on Grand Terre barrier island, LA. Oil observations from the BP response team are also shown. From [Heenan et al., 2015]

hydrocarbon conductive model, suggesting increase of conductivity as a hydrocarbon plume ages [Atekwana and Atekwana, 2009].

Detailed analysis of pixel/point resistivity variation within the imaged area showed that long-term

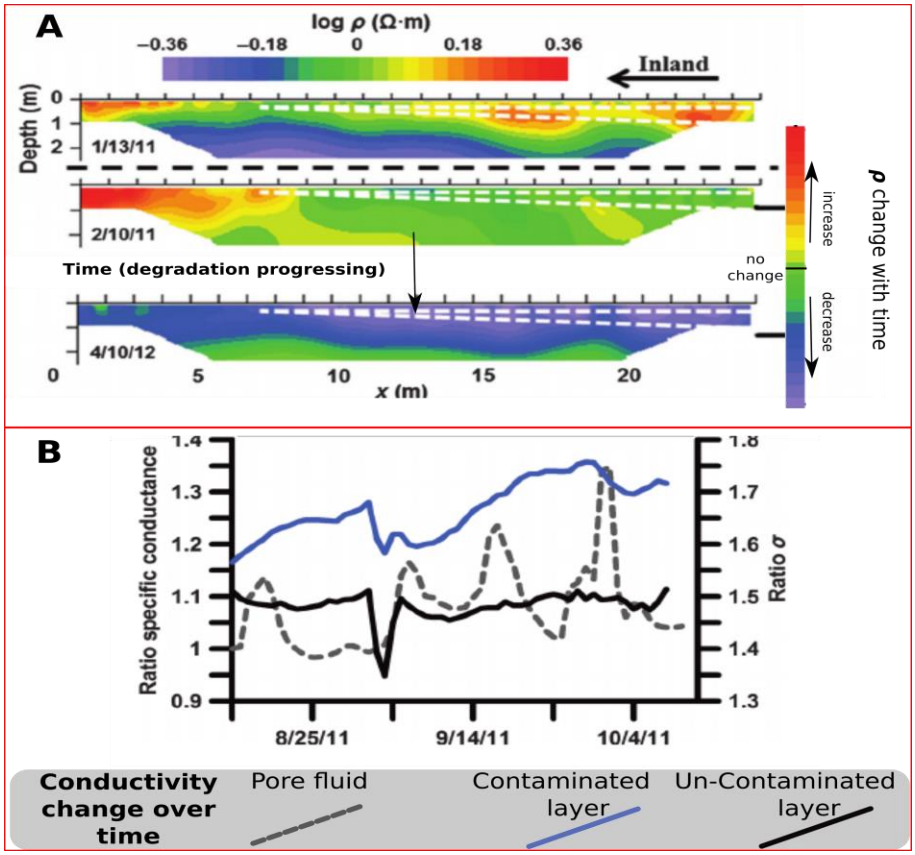

Figure 8: [A] Background resistivity (top) and ratio resistivity changes (bottom) from the ERI monitoring system. Overtime changes show resistivity decrease over time. The primary change is associated with the inferred location of the DH impacted oil layer. [B] Single pixel ratio conductivities change provide further evidence on the resistivity decrease of the DH oil impacted layer vs. the non impacted one. Modified from [Heenan et al., 2015]

decreases in resistivity were largely associated with the DH-impacted sediments (Figure 8). A microbial diversity survey revealed the presence of hydrocarbon-degrading organisms throughout the test site. This is consistent with the history of the site experiencing continuous hydrocarbon impacts (due to seeps and/or accidental spills). However, hydrocarbon degradation activity was much higher in the DH-impacted locations compared to non-impacted locations, suggesting the presence of active hydrocarbon degraders, supporting biodegradation processes. The results of this long-term monitoring experiment suggested that resistivity might be used to non-invasively monitor the long-term degradation of crude oil spills.

Electrical geophysical characterization for waterborne applications.

Electrical geophysical imaging can be used in waterborne configurations. Slater et al. [2010] used continuous waterborne electrical imaging (CWEI) to study hyporheic exchange at the Columbia River, at Hanford, WA. For over 40 years, starting in 1943, fluids containing radioisotopes and metals, generated during reactor fuel fabrication and chemical separation processes, were discharged to the shallow subsurface of the U.S. Department of Energy (DOE) Hanford 300 Area. Although studies in the 1990's predicted the decline of U in the groundwater, the concentrations remained largely unchanged. It was

imperative to better understand and characterize U discharge, from the plume to the Columbia River. To achieve this goal, it was necessary to capture the spatial distribution of the primary lithologic units along the river corridor as well as spatio-temporal complexity in surface water–groundwater exchange driven by variations in stage levels on the Columbia River [Slater et al., 2010].

The research involved a novel implementation of CWEI to accurately resolve lithologic variability along a major river corridor by determining the spatial variation in the electrochemical polarizability, a property closely related to lithology, in addition to the electrical resistivity as routinely captured in CWEI studies.

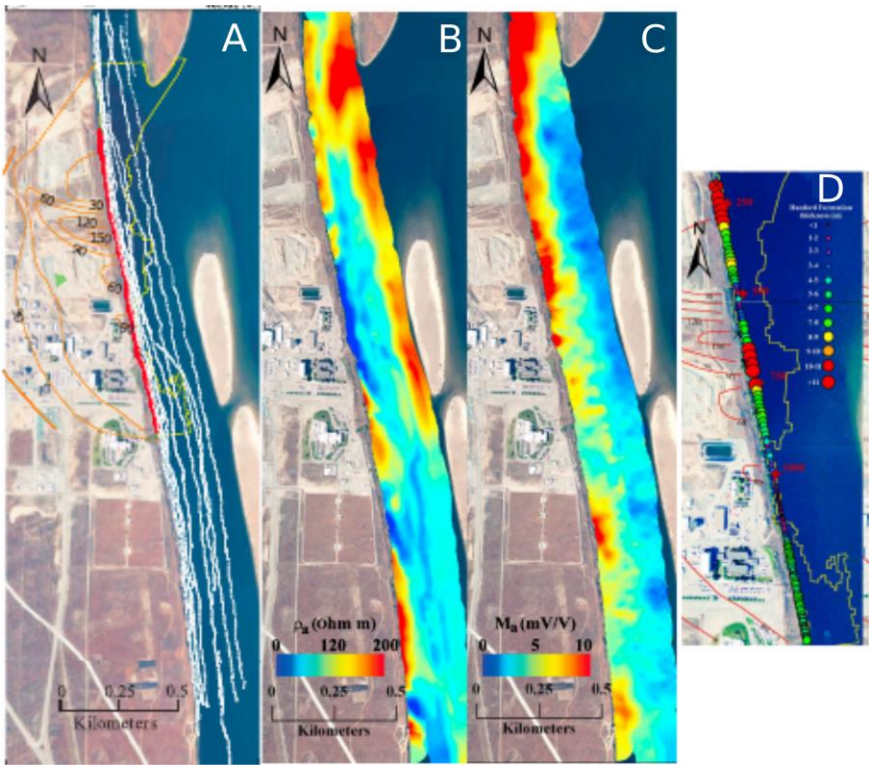

Figure 9: A) map of the CWEI tracks in the Columbia river. B) apparent resistivity and C) chargeability at the pseudodepth of 8.5m. D) Deteailed lithologic characterization of the surface / groundwater interface as estimated by the electrical data. Adapted from [Slater et al., 2010].

The raw CWEI data were processed and inverted to produce subsurface image of resistivity and changeability (measure of polarization) (Figure 9). The electrical data were used to estimate measures of lithologic variability with the use of established petrophysical relationships. Finally, the lithologic variation appeared to be the controling factor on hyporheic processes and U discharge in the river (Figure 9).

In another waterborne ERI implementation, Mansoor and Slater [2007] were successfully able to identify and characterize landfill contamination leaks into a wetland system. They were able to use conventional ERI survey in the brackish Kearny Freshwater Marsh, NJ by developing and utilizing a custom survey

configuration. The custom non-conventional electrode configuration ensured high S/N and good quality data collection even in the highly conductive brackish marsh. This research showed that ERI can be used to spatially and temporally monitor pore-fluid conductivity changes in a shallow-water wetland when constrained by common field data (e.g. surface water conductivity, depth T profiles). The study conclusively showed that water from marginal landfills will enter wetland soils as a result of intense rainfalls.

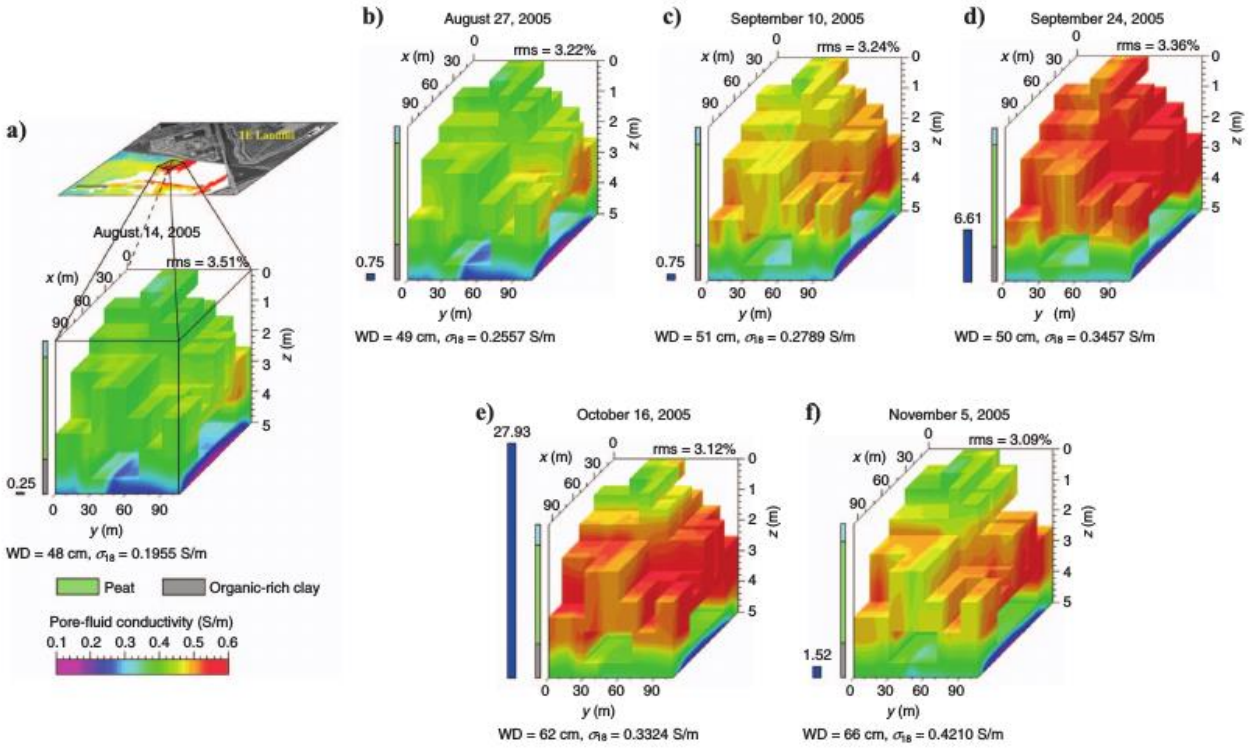

Figure 10: Subsurface pore-fluid conductivity models calculated from 3D inverted apparent resistivity data. Rainfall events are also shown to highlight the correlation between the event and marsh pore fluid conductivity changes. From [Mansoor and Slater, 2007]

CONCLUSIONS

Electrical geophysical methods such as ERI and IP offer unique advantages for subsurface characterization and monitoring related to environmental investigations. The current state of the art allows for efficient data acquisition and robust long term monitoring using ERI/IP. Geophysical methods can be used to delineate and monitor contaminant plumes. Additionally, ERI/IP are very well suited for monitoring long term remediation projects; the recent development of robust instruments with minimal power needs, and remote control capabilities, allow the autonomous operation in remote and sensitive environmetns. Better understanding of the signal source processes along with advances in processing and interpretation, could potentially allow the quantitative use of such tools. Implementation is not limited on land applications, with waterborne surveys becoming more common.

REFERENCES CITED

Atekwana, E. a., and E. a. Atekwana (2009), Geophysical Signatures of Microbial Activity at Hydrocarbon Contaminated Sites: A Review, *Surv. Geophys.*, *31*(2), 247–283, doi:10.1007/s10712-009-9089-8.

Atekwana, E. A., and L. D. Slater (2009), Biogeophysics: A new frontier in Earth science research, *Rev. Geophys.*, *47*(4), 1–30, doi:10.1029/2009RG000285.

Atekwana, E. A., D. D. Werkema, J. W. Duris, S. Rossbach, E. A. Atekwana, W. A. Sauck, D. P. Cassidy, J. Means, and F. D. Legall (2004), In-situ apparent conductivity measurements and microbial population distribution at a hydrocarbon-contaminated site, , *69*(1), 56–63.

Binley, A., and A. Kemna (2005), DC resistivity and induced polarization methods, in *Hydrogeophyiscs*, edited by Y. Rubin and S. S. Hubbard, Springer-Verlag.

Flores Orozco, A., K. H. Williams, P. E. Long, S. S. Hubbard, and A. Kemna (2011), Using complex resistivity imaging to infer biogeochemical processes associated with bioremediation of an uranium-contaminated aquifer, *J. Geophys. Res.*, *116*(G3), 1–17, doi:10.1029/2010JG001591.

Flores Orozco, A., A. Kemna, C. Oberdörster, L. Zschornack, C. Leven, P. Dietrich, and H. Weiss (2012), Delineation of subsurface hydrocarbon contamination at a former hydrogenation plant using spectral induced polarization imaging, *J. Contam. Hydrol.*, doi:10.1016/j.jconhyd.2012.06.001.

Flores Orozco, A., M. Velimirovic, T. Tosco, A. Kemna, H. Sapion, N. Klaas, R. Sethi, and L. Bastiaens (2015), Monitoring the Injection of Microscale Zerovalent Iron Particles for Groundwater Remediation by Means of Complex Electrical Conductivity Imaging, *Environ. Sci. Technol.*, *49*(9), 5593–5600, doi:10.1021/acs.est.5b00208.

Heenan, J., A. Porter, D. Ntarlagiannis, L. Y. Young, D. D. Werkema, and L. D. Slater (2013), Sensitivity of the spectral induced polarization method to microbial enhanced oil recovery processes, *GEOPHYSICS*, *78*(5), E261–E269, doi:10.1190/geo2013-0085.1.

Heenan, J., L. D. Slater, D. Ntarlagiannis, E. A. Atekwana, B. Z. Fathepure, S. Dalvi, C. Ross, D. D. Werkema, and E. A. Atekwana (2015), Electrical resistivity imaging for long-term autonomous monitoring of hydrocarbon degradation: Lessons from the Deepwater Horizon oil spill, *GEOPHYSICS*, *80*(1), B1–B11, doi:10.1190/geo2013-0468.1.

IrisInstruments (2016), Iris Instruments, Available from: http://www.iris-instruments.com/Product/Brochure/syscal.html (Accessed 1 April 2016)

Johnson, T. C., and D. Wellman (2015), Accurate modelling and inversion of electrical resistivity data in the presence of metallic infrastructure with known location and dimension, *Geophys. J. Int.*, *202*(2), 1096–1108, doi:10.1093/gji/ggv206.

Johnson, T. C., R. J. Versteeg, M. Rockhold, L. D. Slater, D. Ntarlagiannis, W. J. Greenwood, and J. Zachara (2012), Characterization of a contaminated wellfield using 3D electrical resistivity tomography implemented with geostatistical, discontinuous boundary, and known conductivity constraints,

GEOPHYSICS, *77*(6), EN85–EN96, doi:10.1190/geo2012-0121.1.

Kemna, A. et al. (2012), An overview of the spectral induced polarization method for near-surface applications, *Surf. Geophys.*, 453–468, doi:10.3997/1873-0604.2012027.

Koestel, J., A. Kemna, M. Javaux, A. Binley, and H. Vereecken (2008), Quantitative imaging of solute transport in an unsaturated and undisturbed soil monolith with 3-D ERT and TDR, *Water Resour. Res.*, *44*(12), 1–17, doi:10.1029/2007WR006755.

Lesmes, D. P., and K. M. Frye (2001), Influence of pore fluid chemistry on the complex conductivity and induced polarization responses of Berea sandstone, *J. Geophys. Res.*, *106*(B3), 4079–4090, doi:10.1029/2000JB900392.

Mansoor, N., and L. Slater (2007), Aquatic electrical resistivity imaging of shallow-water wetlands, *GEOPHYSICS*, *72*(5), F211–F221, doi:10.1190/1.2750667.

Mwakanyamale, K., L. Slater, A. Binley, and D. Ntarlagiannis (2012), Lithologic imaging using complex conductivity: Lessons learned from the Hanford 300 Area, *GEOPHYSICS*, *77*(6), E397–E409, doi:10.1190/geo2011-0407.1.

Ntarlagiannis, D., P. Kirmizakis, J. Robinson, P. Soupios, and L. Slater (2015), Electrical Geophysical Monitoring of Organic Waste Contamination, in *Near Surface Geoscience*, pp. 6–10, Turin, Italy.

Ntarlagiannis, D., J. Robinson, P. Soupios, and L. Slater (2016), Field-scale electrical geophysics over an olive oil mill waste deposition site: Evaluating the information content of resistivity versus induced polarization (IP) images for delineating the spatial extent of organic contamination, *J. Appl. Geophys.*, *62*, 51–60, doi:10.1016/j.jappgeo.2016.01.017.

Personna, Y. R., L. Slater, D. Ntarlagiannis, D. Werkema, and Z. Szabo (2013), Complex resistivity signatures of ethanol biodegradation in porous media, *J. Contam. Hydrol.*, *153*, 37–50, doi:10.1016/j.jconhyd.2013.07.005.

Revil, a., M. Karaoulis, T. Johnson, and a. Kemna (2012), Review: Some low-frequency electrical methods for subsurface characterization and monitoring in hydrogeology, *Hydrogeol. J.*, 617–658, doi:10.1007/s10040-011-0819-x.

Reynolds, J. (2011), *An Introduction to Applied and Environmental Geophysics*, 2nd ed.

Robinson, J. et al. (2015), Imaging Pathways in Fractured Rock Using Three-Dimensional Electrical Resistivity Tomography, *Groundwater*, 1–16, doi:10.1111/gwat.12356.

Rubin, Y., and S. S. Hubbard (Eds.) (2005), *Hydrogeophysics*, Water Science and Technology Library, Springer Netherlands, Dordrecht.

Sauck, W. a (2000), A model for the resistivity structure of LNAPL plumes and their environs in sandy sediments, *J. Appl. Geophys.*, *44*(2–3), 151–165, doi:10.1016/S0926-9851(99)00021-X.

Schmutz, M., A. Revil, P. Vaudelet, M. Batzle, P. F. Viñao, and D. D. Werkema (2010), Influence of oil

saturation upon spectral induced polarization of oil-bearing sands, *Geophys. J. Int.*, *183*(1), 211–224, doi:10.1111/j.1365-246X.2010.04751.x.

Schmutz, M., a. Blondel, and a. Revil (2012), Saturation dependence of the quadrature conductivity of oil-bearing sands, *Geophys. Res. Lett.*, *39*(3), 2–7, doi:10.1029/2011GL050474.

Slater, L. D., D. Ntarlagiannis, F. D. Day-Lewis, K. Mwakanyamale, R. J. Versteeg, A. Ward, C. Strickland, C. D. Johnson, and J. W. Lane (2010), Use of electrical imaging and distributed temperature sensing methods to characterize surface water–groundwater exchange regulating uranium transport at the Hanford 300 Area, Washington, *Water Resour. Res.*, *46*(10), 1–13, doi:10.1029/2010WR009110.

Soupios, P., N. Papadopoulos, I. Papadopoulos, M. Kouli, F. Vallianatos, A. Sarris, and T. Manios (2007), Application of integrated methods in mapping waste disposal areas, *Environ. Geol.*, *53*(3), 661–675, doi:10.1007/s00254-007-0681-2.

Telford, W., L. Geldart, and R. Sheriff (1990), Electrical Properties of Rocks and Minerals, *Appl. Geophys.*, 283–292.

Tsourlos, P., N. Papadopoulos, M.-J. Yi, J.-H. Kim, and G. Tsokas (2014), Comparison of measuring strategies for the 3-D electrical resistivity imaging of tumuli, *J. Appl. Geophys.*, *101*, 77–85, doi:10.1016/j.jappgeo.2013.11.003.

U.S. Sustainable Remediation Forum (2009), Sustainable remediation white paper-Integrating sustainable principles, practices, and metrics into remediation projects, *Remediat. J.*, *19*(3), 5–114, doi:10.1002/rem.20210.

Waxman, M. H., and L. J. M. Smits (1968), Electrical Conductivities in Oil-Bearing Shaly Sands, *Soc. Pet. Eng. J.*, *8*(2), 107–122, doi:10.2118/1863-A.

Weller, A., L. Slater, S. Nordsiek, and D. Ntarlagiannis (2010), On the estimation of specific surface per unit pore volume from induced polarization: A robust empirical relation fits multiple data sets, *GEOPHYSICS*, *75*(4), WA105–WA112, doi:10.1190/1.3471577.

Weller, A., L. Slater, and S. Nordsiek (2013), On the relationship between induced polarization and surface conductivity: Implications for petrophysical interpretation of electrical measurements, *Geophysics*, *78*(5), D315–D325, doi:10.1190/geo2013-0076.1.

Williams, K. H., A. Kemna, M. J. Wilkins, J. Druhan, E. Arntzen, a L. N'Guessan, P. E. Long, S. S. Hubbard, J. F. Banfield, and A. L. N. Guessan (2009a), Geophysical monitoring of coupled microbial and geochemical processes during stimulated subsurface bioremediation., *Environ. Sci. Technol.*, *43*(17), 6717–23.

Williams, K. H., A. Kemna, M. J. Wilkins, J. Druhan, E. Arntzen, a L. N'Guessan, P. E. Long, S. S. Hubbard, J. F. Banfield, and A. L. N. Guessan (2009b), Geophysical monitoring of coupled microbial and geochemical processes during stimulated subsurface bioremediation., *Environ. Sci. Technol.*, *43*(17), 6717–23.

TRIP A-3: CRYSTALLINE MEGABOUDINS ALONG THE LEADING EDGE OF THE TACONIC THRUST SHEET, ORANGE COUNTY, NY

ALEXANDER E. GATES
Department of Earth & Environmental Sciences, Rutgers University, Newark, NJ 07102

INTRODUCTION

As rocks are extended during deformation and break into fragments, they are termed boudins and the spaces between are gaps. However, in some geological settings, theses boudins can be quite large and are considered megaboudins or megalenses (Tricart and Lemoine, 1986). Typically, these terms were reserved for plate boundaries and highly active tectonic situations. However, large lenses of rock can form within actively deforming belts outboard of a plate boundary. This is the situation with the Monroe megaboudins of Orange County, southeastern New York which are the subject of this field trip.

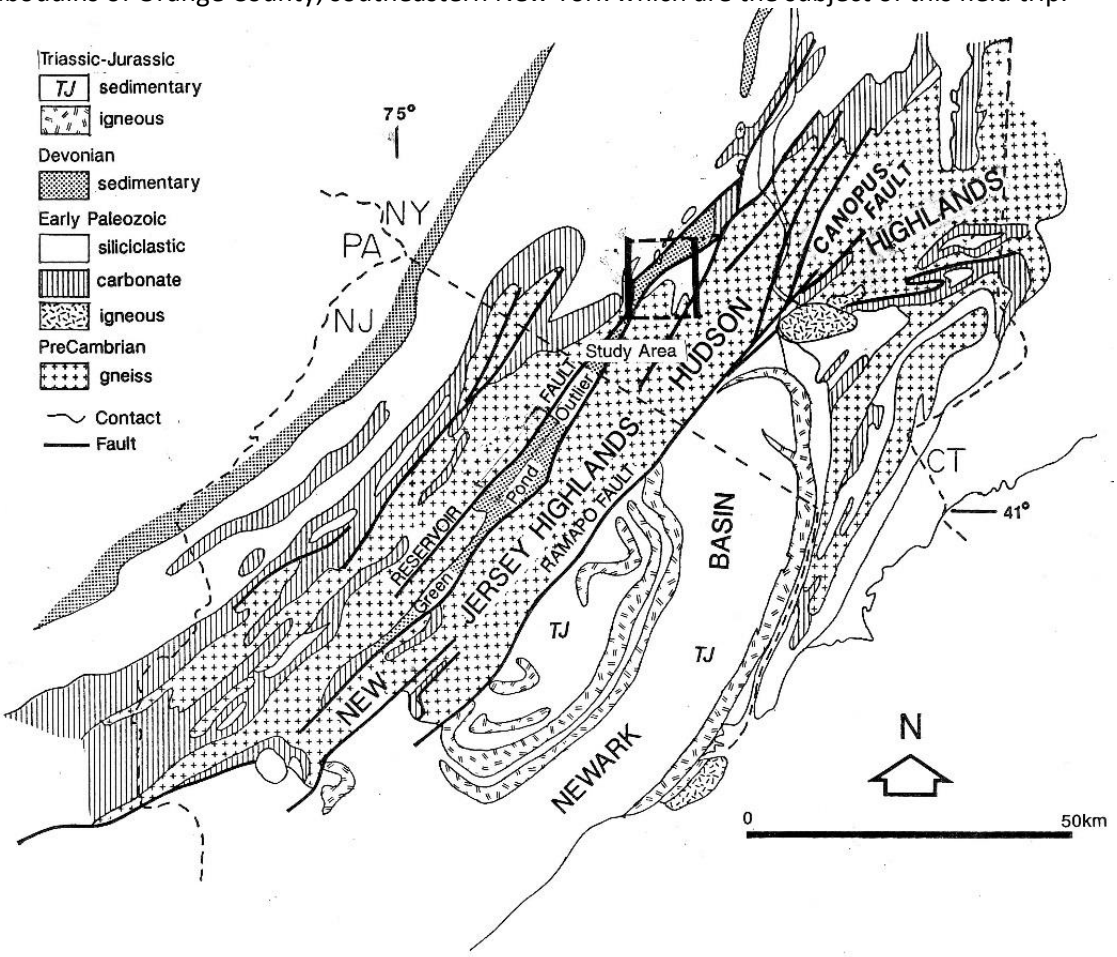

Figure 1. Geologic map of the NJ-NY border area. Box shows Monroe 7.5 minute quadrangle.

The Monroe area encompasses parts of the western Hudson Highlands, an extension of the Reading Prong, the Valley and Ridge province and the Green Pond Outlier (Figure 1) (Offield, 1967; Jaffee and Jaffee, 1973; Gates and Valentino, 2000; Gates and Kush, 2007; Gates and Valentino, 2014). The Hudson Highlands are composed of 1.0-1.3 Ga Grenville ridge forming igneous and high grade metamorphic rocks of the Rodinian tectonic cycle (Gates et al, 2001; Gates et al, 2006; Gates and Valentino, 2014). The Valley and Ridge rocks in southeastern New York are composed of Cambrian to Silurian unmetamorphosed sedimentary rocks of the Pangean cycle (Rodgers, 1970; Gates and Valentino, 2014). The Green Pond outlier is a belt of unmetamorphosed Silurian-Devonian sedimentary rocks that are equivalent to the Valley and Ridge units but which occur within the Grenville rocks of the Highlands (Herman and Mitchell, 1991).

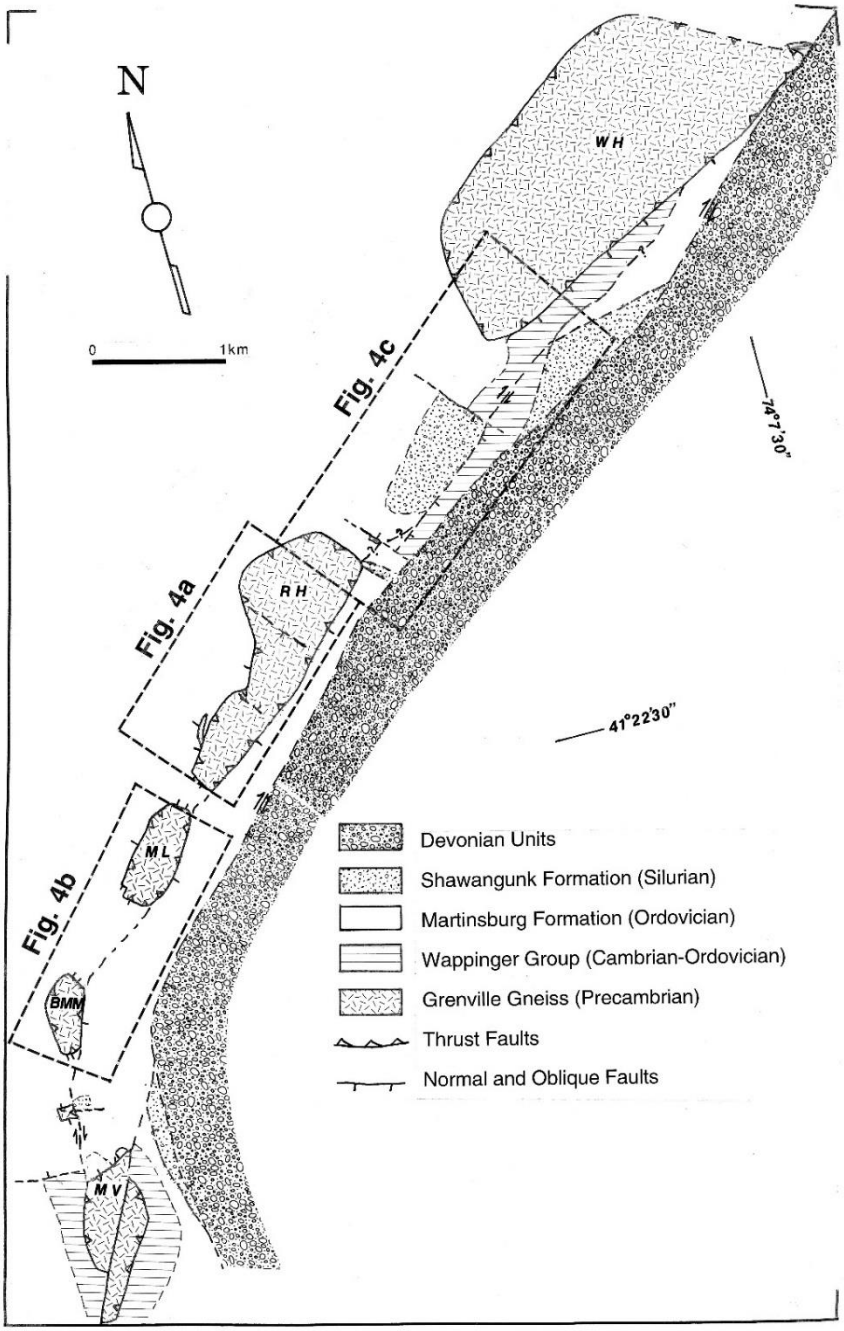

Figure 2. Geologic map of the Monroe megaboudin chain showing locations of figures. MV = Museum Village, BMM = Bull Mine Mountain, ML= Merriewold Lake, RH=Round Hill, WH=Woodcock Hill.

The Monroe megaboudins form a chain of small hills of 50-100 m elevation in an otherwise relatively flat terrain of ±20 m relief (Figure 2). The megaboudins range in size from 50 m on an edge to as large as 1.2 X 3 km with northeast trending long axes parallel to the regional structural grain and the chain. There is

no pattern to the size order. The gaps between the boudins are as large as 2 km but generally decrease towards the southwest. Jaffee and Jaffee (1973) interpreted the megaboudins to be klippe that were erosionally separated from the Highlands massif to the southeast but Gates (1996) showed that they are megaboudins. To the northwest, the area is completely underlain by shales of the Martinsburg Formation.

STRATIGRAPHY

Grenville Rocks

Metasedimentary Gneiss

The metasedimentary gneiss includes granulite facies rocks with protoliths that were likely sedimentary (Gundersen, 1986; Gates et al., 2001; Gates et al., 2006). This unit includes pelitic and semipelitic to psammitic gneiss, and calcsilicate with minor quartzite and marble. The metapelite-psammite consists of medium to coarse-grained biotite-garnet gneiss with quartz, plagioclase, K-feldspar and local sillimanite, and cordierite. Thin zones of graphite-pyrite-garnet gneiss with biotite, quartz, K-feldspar, plagioclase, and minor sillimanite occur locally. Some metapelites are migmatitic with biotite-garnet gneiss melanosomes and thin layers of medium-coarse granite. The pelitic gneiss is interlayered with semipelitic and psammitic gneiss and local discontinuous quartzite, diopside and diopside-garnet marble, and calcsilicate gneiss. The calcsilicate gneiss is commonly migmatitic and quartzofeldspathic with K-spar, salite, plagioclase and hornblende with minor apatite, titanite and scapolite. Most of these gneisses include intrafolial pegmatites that exhibit rootless isoclinal folding. The contacts with quartzofeldspathic and metavolcanic gneiss can be sharp or gradational.

Metavolcanic Gneiss

The metavolcanic gneiss that are made up of interlayered black metamafic and gray metaintermediate bands at centimeter to meter scale (Gundersen, 1986; Gates et al., 2001; Gates et al., 2006). The mafic gneiss is medium to coarse grained with well-developed foliation defined by aligned augite, hornblende, plagioclase, ortho and clinopyroxene, and local concentrations of magnetite. The intermediate gneiss consists of medium to coarse-grained plagioclase, quartz, and minor hornblende and/or biotite. These lithologies include minor layers of felsic gneiss consisting of quartz, K-feldspar, plagioclase with minor hornblende.

The gneissic banding ranges in thickness from 5 cm to 1.5 m. These rocks were interpreted to have a volcanic origin based on the diverse range of rock compositions that are dominated by mafic and intermediate lithologies, and supporting bulk and trace element geochemistry (Gates et al., 2006). Local interlayers of quartzite and calcsilicate gneiss also occur. The contact of the metavolcanic gneiss unit quartzofeldspathic gneiss and metasedimentary gneiss are generally gradational but can be sharp locally.

Metavolcaniclastic Lithofacies

Much of the western Hudson Highlands is underlain by medium to coarse grained gray quartzofeldspathic gneiss Gates et al. (2001). The gneiss is characterized by massive to layered quartz-plagioclase aggregates with minor amounts of biotite, and/or hornblende, and trace magnetite, K-

feldspar, or garnet locally. Compositional layering is defined by differences in the proportion of mafic minerals. Quartzofelspathic gneiss locally contains interlayers of amphibolite that are parallel to compositional layering and pervasive foliation. The gneiss is interlayered with quartzite and amphibolite layers near the contacts with the metavolcanic and metasedimentary gneiss, respectively in an interstratal gradational contact. Commonly small pockets of granite occur between foliation boudins in the gneiss and the unit hosts younger cross cutting pegmatites ranging from decimeter to several meters thick. Based on the mineral composition and the occurrence of compositional layers in the quartzofeldspatic gneiss, the unit is interpreted to represent a sequence of volcaniclastic metasedimentary rocks.

Paleozoic Rocks

Poquag Formation

The Poughquag Formation is a Cambrian fluvial to shallow marine sandstone to conglomerate deposit with trilobites and variably sized worm burrows that lies directly on Grenville basement rocks. This unit is called the Hardyston Formation in New Jersey. The rock ranges from feldspathic sandstone to arenite that can contain iron cementation. It commonly contains trough cross beds and forms channels into the basement rocks. Bed thickness ranges from about 20 cm to 1-2 m but is highly variable, thinning laterally in many areas. The thickness of the unit is variable and it is commonly missing in which case, the Wappinger Group rests directly on basement.

Wappinger Group

The Wappinger Group of limestone and dolomite units overlie the Poughquag Formation or lie directly on basement in many areas. The basal unit is dolomite that can be interlayered with Poughquag sandstone at the contact. It contains flaser and lenticular bedding with herringbone cross stratification near the base and nodular chert in much of the lower unit. Bed thickness in the lower part ranges from 10 cm to 50 cm in repeating cycles. The upper unit is a limestone that contains stromatolites, tempestites and oolitic packstones. Bedding thickness ranges from 10 to 30 cm and exhibits regular erosional surfaces filled with intraclast breccia. In New Jersey, this group also contains the Jacksonburg Formation of limey shale but the unit has not been identified in the field area. The Cambrian to Ordovician age Wappinger Group is equivalent to the Kittatiny Group in New Jersey.

Martinsburg Formation

The up to 3,000 m-thick, Ordovician age Martinsburg Formation overlies the Wappinger Group and exhibits a coarsening upward sequence. There are two members of the Martinsburg in the study area including the basal Bushkill shale member and the Ramseyburg sandstone member. The Bushkill member is primarily black shale with thin 1-10 cm silt and fine sand layers that occur in rhythmic cycles. The sand layers are thicker higher in the member and contain ripple and hummocky cross stratification. There is a gradational contact with the overlying Ramseyburg member which is composed of gray sandstone interlayered with shale grading into pure sandstone that is fossiliferous. Bedding ranges from 10 to 50 cm and is locally trough cross bedded.

Shawangunk Formation

There is an angular unconformity between the Martinsburg Formation and the overlying Silurian Schawangunk Formation so the contact is sharp. The unit is an interlayered quartz pebble to cobble conglomerate, quartzite and sandstone in a fining upward sequence. The rocks range in color from white

to tan and red. The upper unit contains thinly (10-20 cm) bedded sections of arenitic sandstone with trough cross bedding, shale rip-up clasts and pebble lags. The lower unit contains interlayered trough cross bedded lithic sandstone with lithic and quartz pebble-cobble conglomerate and conglomeratic sandstone. The conglomerate locally displays reverse grading and weathered rinds on cobbles. The Schawangunk is so resistant to weathering that it forms prominent ridges from New York to Alabama. An equivalent unit of the Schawangunk Formation is the Green Pond Formation which occurs in the Green Pond Outlier, a sequence of Paleozoic rocks that bisects the western Hudson and New Jersey Highlands.

Esopus Formation

The Devonian Esopus Formation is a gray to black shale that overlies both the Schawangunk Formation and the Green Pond Formation within the Green Pond Outlier. It displays a coarsening upward sequence. The lower section ranges from massive to rhythmically interlayered with 1-2 cm tan silt to fine sand laminae to beds. The upper part of the formation contains thicker gray sandstone beds of 10-20 cm and normally graded with local cross bedding. The shale locally contains large trilobites and other fossils.

Bellvale Formation

The Devonian Bellvale Formation is in gradational contact with the underlying Esopus Formation. It is a trough cross bedded to massive lithic greywacke sandstone with bedding thickness ranging from 20 cm to 2 m. The lower unit contains 5-25 cm-thick shale interbeds with sharp contacts. Some sandstone layers have local quartz pebble concentrations along the lower contacts. The unit can be locally fossiliferous including terrestrial fossils.

Schunemunk Formation

The top unit in the sequence is the Devonian Schunemunk Formation which is a red-purple conglomerate, quartzite and sandstone. This unit is gradational with the underlying Bellvale Formation and the transition is marked by the appearance of red in the otherwise gray sandstone. This is succeeded by red siltstone and minor shale. The lithic and quartz pebble to cobble conglomerate that characterizes the Schunemunk lies in sharp contact with the finer lithologies. The conglomerate and conglomeratic sandstone is trough cross bedded and contains imbricated clasts locally. It is interlayered with trough cross bedded sandstone. Beds in this section are about 1 m thick.

STRUCTURAL GEOLOGY OF THE MEGABOUDINS

The megaboudins of Grenville gneiss form a 35 km long, northeast trending chain along the northwest edge of the western Hudson Highlands massif (Figure 1). A 12 km long segment in the central part of this chain is relatively well-exposed and display complex structural relations (Figure 2). Northwest of the chain, the Martinsburg Formation contains two cleavages. The S_2 foliation is a spaced crenulation cleavage that is locally continuous in shale but absent in the sandier lithologies. Poles to S_2 are tightly clustered with an orientation of 044 73 SE. The earlier S_1 cleavage was folded during the formation of S_2 and defines a fold axis of 10/047 with a spread in orientations of 46^o. Similarly, the poles to S_0 bedding define a fold axis of 2/047. Locally, NE-trending tight to isoclinal folds of bedding are visible (Gates, 1996).

The bedding and cleavages in the Martinsburg Formation can be seen dipping beneath the crystalline basement in an overthrust contact. The fault contact exhibits extensive fracturing and multiple slicken-

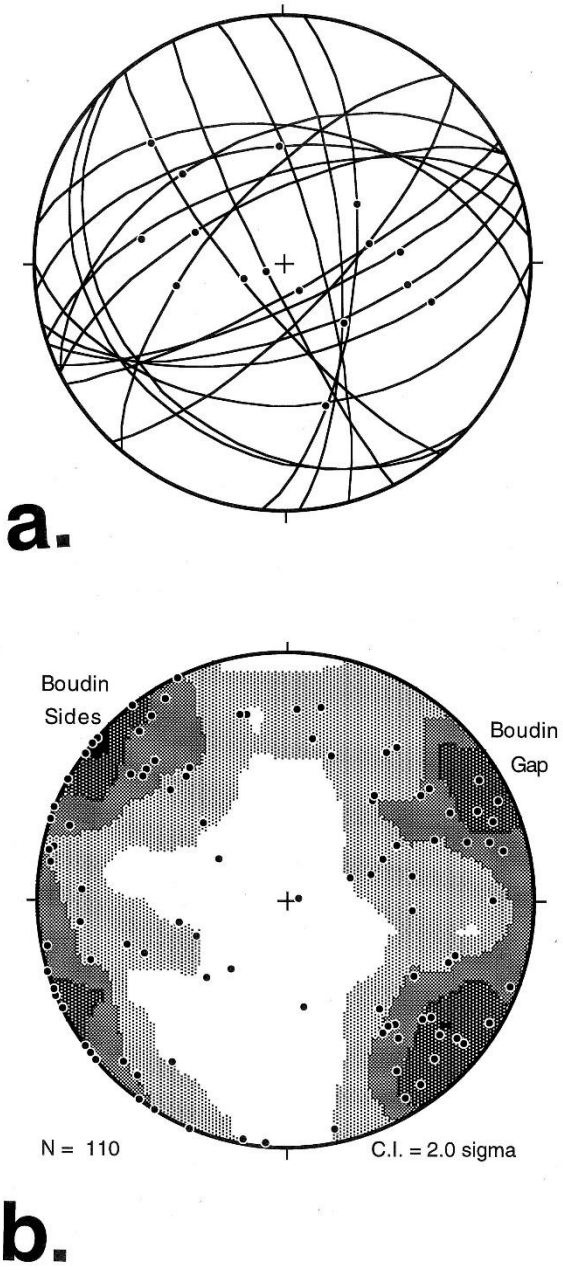

side surfaces primarily with thrust and reverse motion in both the gneiss and shale. The faults primarily dip shallowly to moderately southeast and less commonly to the northwest. The gneiss also contains epidote and quartz veins as well as pockets of chloritic breccia 5-15 cm long.

Figure 3. Equal area plot of a. Normal faults (great circles) with slickensides (dots) (n=19) and b. contour diagram of poles to joints.

The Round Hill megalens forms an hourglass map pattern with the thinned or necked area characterized by extensive normal faulting, jointing and epidote-chlorite alteration (Figure 3). Individual fractures cannot be assigned to a deformational even but fracture orientation maxima in the gneiss and cover rocks are consistent with lateral extension. Faults in the gneiss form individual planes with chlorite or epidote coating containing grooved slickensides with tapered prod marks (Means, 1987), R criteria of Petit (1987) and rare fibrous slickensides documenting kinematics. All crystalline blocks in the chain exhibit two sets of steeply dipping normal faults with northeast and northwest trends.

There are many orientations of joints in the area but there are two maxima with steep northwest and northeast orientations. The density of both the joints and normal faults is higher in the necked area of Round Hill (Figure 4a). This area also contains steep Northeast and Southwest dipping faults that offset the basement cover contact. Normal faults also occur along the northeast-trending margins of the megalens. Extensive jointing and steep slickensides are especially common along the northwest margins. At the southwest corner, Martinsburg Formation has been juxtaposed with gneiss creating a repeated succession of gneiss and shale separated by a normal fault.

The bedding and cleavage in the shale are parallel to the NE-trending block margins but are rotated towards the NW in the thinned and gap areas where they are small. In Round Hill, the rotation of the bedding into the gap area to the south is through 61^{o} and defines a fold axis of 37/064 (Figure 5a). Cleavage orientation spread defines a similar axis but there is less rotation. Slickensides and foliation drag defines strike slip shearing such that on the northwest side of the gap, the northern corner shows sinistral motion and the southern corner shows dextral motion.

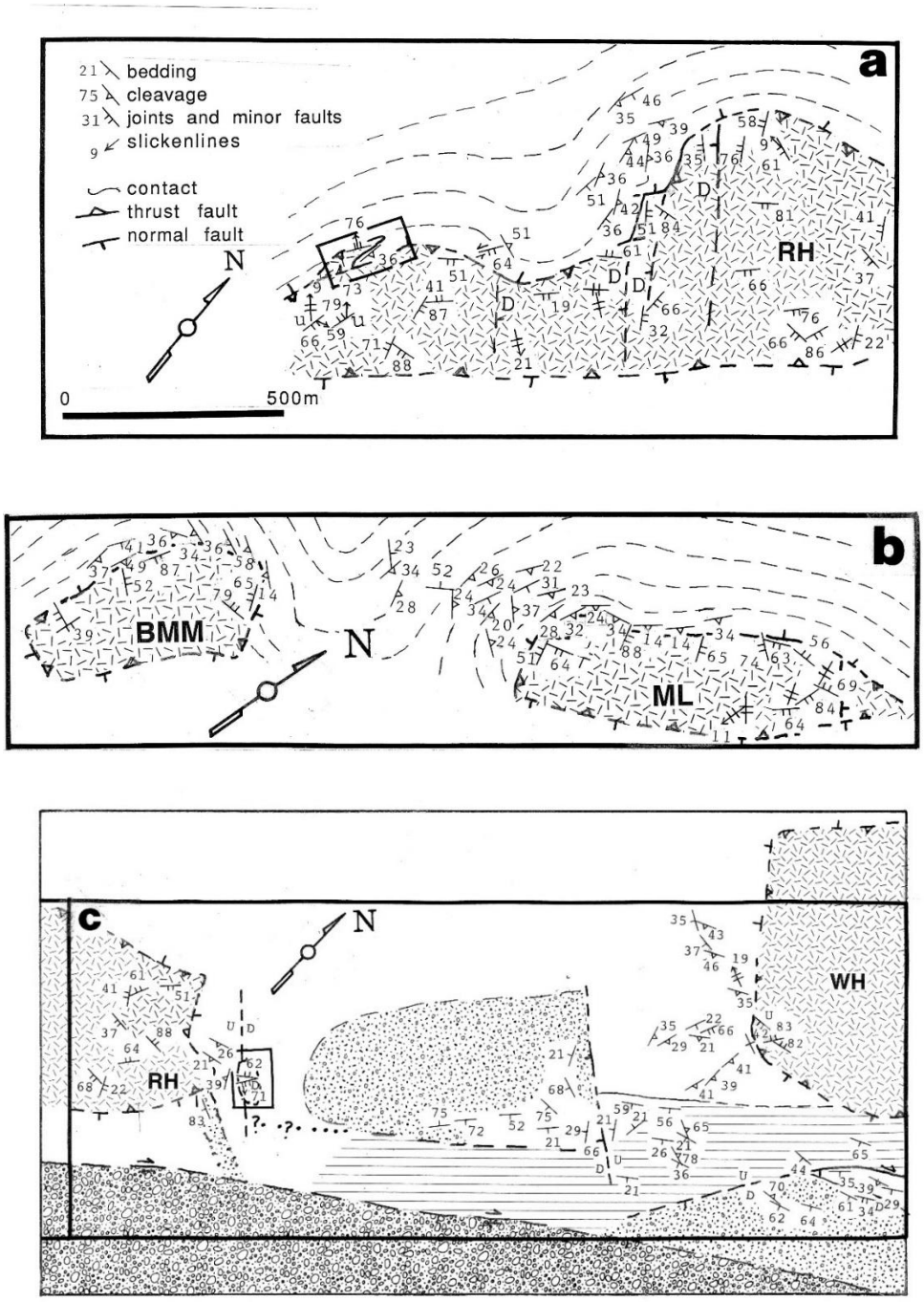

Figure 4. Geologic map of megaboudins and gaps between them. Boxed areas show normal fault offset fragments. a) Round Hill (RH), b. Bull Mine Mountain (BMM) and Merriewold Lake and gap and c. Woodcock Hill-Round Hill gap.

The gap between the Bull Mine Mountain and Merriewold Lake megaboudins is much larger (Figure 4b). The contacts between the gneiss of the megalenses and the Martinsburg shale in the gap is sharp along NW-striking, near vertical planes. Cleavage orientation swings about 77° from NE-striking along the

northwest margins of the Bull Mine megalens to NW-striking in the gap. The fold axis produced by this swing in orientation is 23/149 (Figure 5b). On the north side of the gap, cleavage swings 69° from NE-striking along the NW margin of the Merriewold Lake lens trhough N-S and towards the NW producing a fold axis oriented 16/052 (Figure 5c). Crenulation cleavage S_2 is well developed in this area and also swings through 74°, producing a fold axis of 14/052 (Figure 5d) similar to that of S_1 both in this gap and in the thinned area of Round Hill. This swing is in sharp contrast to the S_2 away from the megalenses which has a consistent orientation.

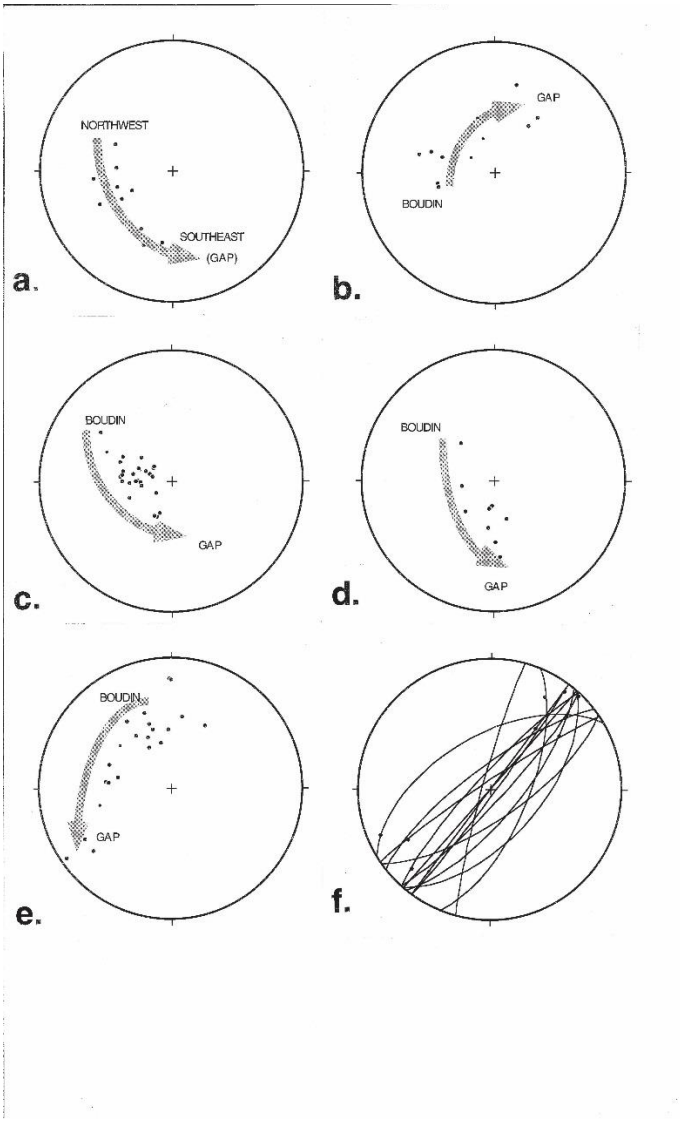

Figure 5Equal area plots of poles to cleavage in Martinsburg shale (dots) around megaboudins with arrows showing wrapping of cleavage from sides and into gaps. a. S1 in center of Round Hill. b. S1 on NW Bull Mine Mountain and N into gap. c. S1 on NW Merriewold Lake and S into gap. d. S2 on NW Merriewold Lake and S into gap. e. S1 around W and SW Woodcock Hill. f. dextral strike-slip faults along the SW side of the chain. Great circles=faults; dots=slickenside lineations

The area of deviation of cleavage from regional trend around the lenses is not symmetric across the gap (Figure 4b). The area of deflected cleavage southwest of the Merriewold Lake lens is much larger than the area of deflection to the northeast of the Bull Mine Mountain megalens. The geometric center of the cleavage deviation in the gap is significantly closer to the Bull Mine Mountain lens.

The widest gap in the chain occurs between the Round Hill and Woodcock Hill blocks (Figure 4c). Cleavage in the Martinsburg Formation shows a similar wrapping pattern around the blocks and into the gap area. The deviation in cleavage from NE regional trend through N-S and towards the NW in the gap to the southwest of Woodcock Hill indicates 115^{o} of rotation. It defines a fold axis of 35/122 (Figure 5e). There are only four appropriate outcrops of Martinsburg Formation on the north side of Round Hill and into the gap. The fold axis defined by this small amount of data is 22/186 but it is not considered representative. Unlike the other gaps, there is a block of Silurian Shawangunk Formation within the Round Hill-Woodcock Hill gap. The northeast contact of the Shawangunk quartzite and conglomerate is a steep, NW-striking, steeply SE-dipping normal fault that is visibly juxtaposes it against Cambrian Wappinger Group limestone. The fault surface is composed of weathered brecciated limestone with anastomosing fibrous and polished slickensides. The fault crosses a NE-striking conformable contact between Martinsburg shale and Wappinger limestone in the footwall to the northwest. The southwest edge of the fault block of Shawangunk Formation is not exposed but a moderately NE-dipping normal fault offsets a small block of brecciated gneiss from the Round Hill megalens and into the gap. A thin band of Martinsburg shale between Round Hill and the brecciated gneiss. The breccia is sericitized and sausseritized.

The cross-trend normal faults form a graben within the Round Hill-Woodcock Hill gap area. The Shawangunk Formation within the graben block exhibits folds that are truncated by the normal faults and therefore predate them. These shallowly SE-plunging folds resemble typical Alleghanian folds in the Green Pond outlier (Jaffee and Jaffee, 1973; Mitchell and Forsythe, 1988) and those in the Valley and Ridge in the area (Drake and Lyttle, 1981).

Wappinger Group and locally Martinsburg Formation rocks are juxtaposed against Precambrian gneiss on the SE-side of the Museum Village and Goose Pond megaboudins by normal faulting. Shawangunk Formation is also juxtaposed with gneiss along the southeast side of the small unnamed megaboudin between Museum Village and Bull Mine Mountain. There was certainly some normal movement along this contact but slickensides and drag folds in the Shawangunk Formation show right lateral strike-slip kinematics. A thin EW-trending band of Shawangunk quartzite extends from the southeast side of Round Hill and appears to have strike-slip offset. A similar EW-trending band of Shawangunk Formation is faulted against Wappinger carbonates and Martinsburg shale at the north end of Woodcock Hill. Slickensides and pockets of breccia along these contacts consistently show strike-slip movement though significant normal movement is also required to achieve the current geometry.

MEGABOUDIN FORMATION

The interpreted Taconic westward thrusting of the Highlands massif over the Martinsburg Formation (Offield, 1967; Rodgers, 1970; Jaffee and Jaffee, 1973; Drake and Lyttle, 1981) is well displayed by the rocks in the Monroe area. The band of gneiss that was stretched into the megaboudin chain may have been an erosionally separated klippe from the main sheet or an infold in the Martinsburg Formation. During Alleghanian compression, the shale of the Martinsburge Formation extended laterally along strike in pure shear deformation. The high competency contrast between the gneiss and shale resulted in ductile flowing of the shale matrix and brittle fracturing of the gneiss. The points where the gaps

developed experienced a higher degree of strain but the reason for the locations of the breaks is unclear. There could have been preexisting weaknesses but there could also have been some periodicity to the separations. As the megaboudins separated and the gaps widened, the shale was able to flow into the gaps and ultimately, cross-strike normal faults developed locally.

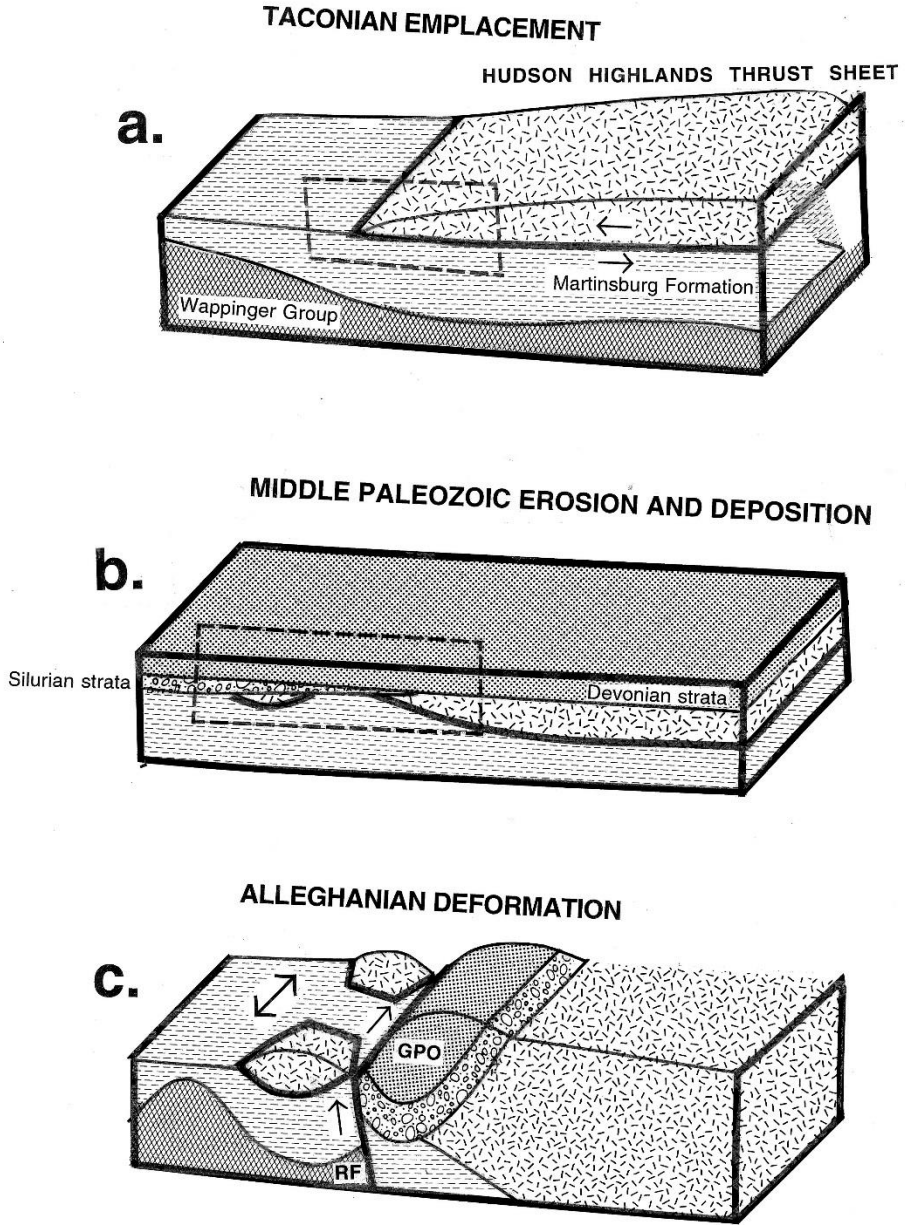

Figure 6. Model for megaboudin formation. a. Taconian emplacement of Hudson Highlands sheet. b. Silurian-Devonian erosion and deposition of sedimentary rocks. c. Alleghanian deformation and megaboudin formation. RF=Reservoir Fault; GPO=Green Pond Outlier.

The cleavage and bedding in the Martinsburg shale rotated from NE-striking to NW-striking as the rock flowed into the gaps. However, it rotated clockwise on the north side of the megaboudins and

counterclockwise on the south sides. This opposing direction of rotation produced contrasting fold axes on the north versus the south side of the gaps. The S_2 foliation is also reoriented into the gap whereas it is consistent on a regional scale. This means that the boudin formation post-dated the S_2 fabric to some degree.

The size of the megaboudins and their gaps vary considerably (Figure 2). The mapped area on the unnamed megaboudin (smallest) between Museum Village and Bull Mine Mountain is only 0.1 km^2 in contrast to Woodcock Hill which is 5 km^2. Others in the chain are even larger. The megaboudin gaps similarly vary considerably. Ferguson (1981) and Ferguson and Lloyd (1984) have shown that gap aperture in a boudin chain commonly reflects the duration of opening. Applying this theory to the megaboudin chain indicates that the gaps initiated at various times during the deformational event. The Woodcock Hill-Round Hill gap would be the earliest formed and the nascent separation of the two halves of Round Hill would be the youngest. Smith (1975) proposed that the gaps in boudin chains reflect points of weakness or stress nodes. Such an evaluation is not possible in the megaboudin chain.

The asymmetry of the cleavage-bedding flow patterns in Martinsburg shale within the Bull Mine Mountain-Merriewold Lake gap complicates a simple explanation of passive boudinage. A possible explanation for this asymmetry is that both megaboudins may have moved northeastward during separation. In pure shear fracture boudins (Cloos, 1947; Rast, 1956), all boudins separate in opposite directions as the chain elongates. Material is transported from the high stress sides of the boudins into the gaps which are low stress areas in the system (Ramberg, 1955; Stromberg, 1973). This produces a wrapping geometry in the transported material. As the gaps widen, the material in the gap is flattened perpendicular to the maximum stress direction as the shielding by the rigid boudin becomes less effective. However, if adjacent boudins move in the same direction, once initial opening takes place, the gap will only be filled behind the leading boudin and produce an asymmetric gap fill. In this scenario, the trailing boudin would compress the material in the gap area and may even overthrust it. Such a process could be considered extrusion boudinage (Gates, 1996). There is no definitive evidence to support this in the megaboudin chain though it cannot be ruled out. The staggered opening times of the gaps between the megaboudins may have created a complex pattern of deformation in the gap areas. A symmetric fill pattern could have become asymmetric if subsequent opening of a gap in an adjacent boudin created asymmetric motion and a leading-trailing boudin situation.

The opening of the gaps between the megaboudins is marked by extensive fracturing and normal faulting. In some cases, extension formed a saddle-like graben across the spine of the megaboudin producing a sag in the topography and normal fault offset of the gneiss-shale contact. In other gaps, the separation is abrupt along NW-striking, vertical fractures. Once the gaps opened, shale flowed into them. Fullagar (1980) describes the type of flow around the megaboudins in terms of vorticity. The strike-slip shearing around the megaboudins further documents this vorticity in the horizontal direction. However, the normal faulting around the megaboudins demonstrates vorticity in the vertical plane as well thus suggesting three-dimensional vorticity.

Vertical movements appear to have become more important in the wider gaps. In the wide Round Hill-Woodcock Hill gap, after the gap opened and the shale flowed in from the sides, cross-strike conjugate normal faults formed a graben that juxtaposed Shawangunk Formation rocks with older rocks in the gap.

The sequential progression of deformation dominated by horizontal flow of shale into the gap to that dominated by vertical displacement of conglomerate into the gap appears to be the result of deformation of a layered sequence with contrasting competencies (Figure 7) . In the early stages of boudin development, the weak and ductile shale quickly flowed into the gap. The overlying

conglomerate and quartzite may have deformed within its stratigraphic level but the rigidity of the rock prevented it from moving into another horizon. Only when the gap achieved a critical aperture was the rigid layer able to drop into the gap area. There are several instances of normal faulting juxtaposing rock from a higher horizon into the gap both by clipping off the leading edge of the crystalline boudin and by normal faulting of Shawangunk Formation.

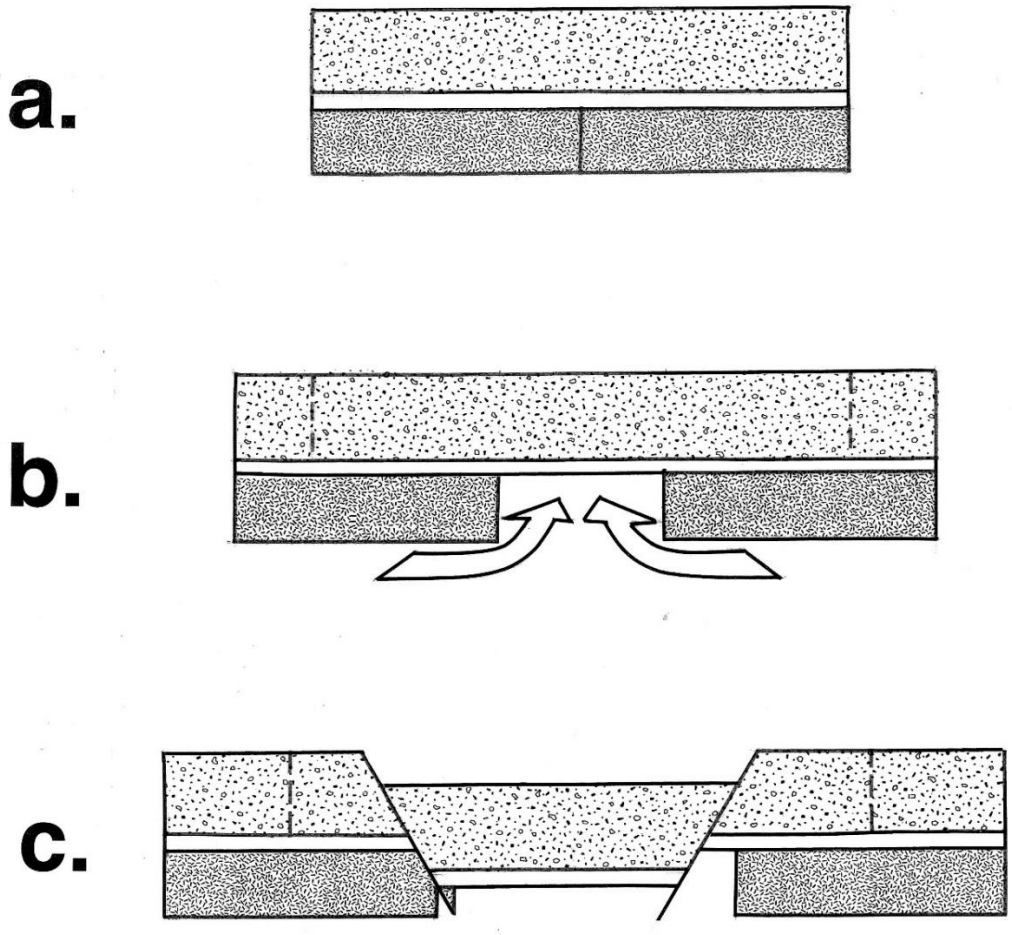

Figure 7. Model showing sequential development of boudin gaps in a rheologically layered sequence. a. Rigid block (stippled) with incipient break encased in incompetent material (white). b.Opening of gap and flow of incompetent material along horizontal plane into gap. c. Normal faulting and vertical displacement of overlying competent material into gap.

Map reconstruction of the crystalline megaboudins yields a gap length of 3.6 km along the 12 km-long chain. There may have been some internal brittle extension within the crystalline rock that cannot be accounted. The exposure along the chain is only fair and small pieces of crystalline rock may have been clipped by normal faults like on the north side of Round Hill but that are not exposed. Late vertical motion on the chain may further have shifted deformational horizons so that the current level of exposure may not reflect a single deformational horizon. All of these factors may result in some missing crystalline rock from the reconstruction and therefore introduce error into calculations. Nonetheless, a □ = 3.3 was calculated using the strain reversal method of Ferguson (1981). The Martinsburg Formation

had a much higher amount of strain because it undoubtedly extended laterally well before the crystalline body began to fracture into the megaboudins.

The right-lateral faulting along the southeast margin of the megaboudin chain could have resulted from variable lateral extension of the belts in response to compression. The thick sandstones and conglomerates of the Green Pond outlier (Herman and Mitchell, 1991) to the southeast of the megaboudins are likely more rigid and less prone to pure shear extrusion than the Martinsburg Formation. The difference in lateral expansion would account for the faulting between the two making it a stretching fault (Means, 1989; 1990). On the other hand, it may be part of the larger Alleghanian dextral strike-slip system in the Appalachians (Gates, 1996).

REFERENCES CITED

Cloos, E., 1947, Boudinage; Transactions of the American Geophysical Union, vol. 28, p. 626-632.

Drake, A.A., Jr., 1984, The Reading Prong of New Jersey and eastern Pennsylvania: An appraisal of rock relations and chemistry of a major Proterozoic terrane in the Appalachians, in Bartholemew, M. J. (ed) The Grenville Event in the Appalachians and Related Topics; Geological Society of America Special Paper 194, p. 75-109.

Drake, A.A., Jr. and Lyttle, P.T., 1981, Alleghanian thrust faults in the Kittatinny Valley, New Jersey, in Manspeizer, W., (ed) Field Studies of New Jersey Geology and Guide to Field Trips, New York State Geological Association vol. 52, p. 278-311.

Ferguson, C.C., 1981, A strain reversal method for estimating extension from fragmented rigid inclusions; Tectonophysics, vol. 79, p. T43-T52.

Ferguson, C.C. and Lloyd, G.E., 1984, Extension analysis of stretched belemnites: a comparison of methods; Tectonophysics, vol. 101, p. 199-206.

Fullagar, P.K., 1980, A description of nucleation of folds and boudins in terms of vorticity; Tectonophysics, vol. 65, p. 39-55.

Gates, A.E., 1996, Megaboudins and lateral extension along the leading edge of a crystalline thrust sheet, Hudson Highlands, New York, USA; Journal of Structural Geology, vol. 18, p. 1205-1216.

Gates, A.E., and Kush, E., 2007, Geologic map of the Maywood 7.5 minute quadrangle, NY; New York State Geological Survey Open-file Report, 2507.

Gates, A.E. and Valentino, D.W., 2000, Geologic map of the Monroe 7.5 minute quadrangle, NY; New York State Geological Survey Open-file Report No 1g1436,

Gates, A.E. and Valentino, D.W., 2011, Bedrock Geology of the Highlands Province, Connecticut, New York, New Jersey And Pennsylvania, in Lathrop, R. G. (ed), The Highlands: Treasured Landscapes, Critical Resources, Rutgers University Press, p. 9-25.

Gates, A.E., Valentino, D.W., Chiarenzelli, J., Gorring, M., and Hamilton, M., 2001, The Assembly of the Supercontinent Rodinia in the western Hudson Highlands, New York State Geological Association Field Trip Guidebook, vol. 73, p. 174-204.

Gates, A.E., Valentino, D.W., Gorring, M., Thern, E. and Chiarenzelli, J., 2006, Rodinian collisional and escape tectonics in the Hudson Highlands, New York, in Pazzaglia, F.J., ed., Excursions in Geology and History: Field Trips in the Middle Atlantic States: Geological Society of America Field Guide 8, p. 65-82.

Gundersen, L.C., 1986, Geology and geochemistry of the Precambrian rocks of the Reading Prong of New York and New Jersey – Implications for the genesis of iron-uranium-rare earth deposits, in Carter, L.M.H. (ed) USGS Research on Energy Resources; U.S. Geological Survey Circular 974.

Herman, G.C. and Mitchell, J.P., 1991, Geologic map of the Green Pond Mountain region from Dover to Greenwood Lake, New Jersey; N.J. Geological Survey, Geologic Map Series 91-92.

Jaffee, H.W. and Jaffee, E.B., 1973, Bedrock Geology of the Monroe Quadrangle, Orange County, New York; N.Y State Museum and Science Service, Map and Chart Series vol. 20, 74 p.

Jaffee, H.W. and Jaffee, E.B., 1989, Structure and petrology of the Precambriam allochthon, autochthon, and Paleozoic sediments of the Monroe area, New York. New York State Geological Association Guidebook, vol. 61, p. 29-50.

Means, W.D., 1987, A newly recognized type of slickenside striation; Journal of Structural Geology, vol. 9, p. 585-590.

Means, W.D., 1989, Stretching faults; Geology, vol. 17, p. 893-896.

Means, W.D., 1990, One dimensional kinematics of stretching faults; Journal of Structural Geology, vol. 12, p. 267-272.

Mitchell, J.P. and Forsythe, R., 1988, Late Paleozoic non-coaxial deformation in the Green Pond Outlier, New Jersey Highlands; Geological Society of America Bulletin, vol. 100, p. 45-59.

Offield, T.W., 1967, Bedrock Geology of the Goshen-Greenwood Lake area, N.Y., N.Y State Museum and Science Service, Map and Chart Series vol. 9, 78 p.

Petit, J.P., 1987, Criteria for the sense of movement on fault surfaces in brittle rocks; Journal of Structural Geology, vol. 9, p. 597-608.

Ramberg, H., 1955, Natural and experimental boudinage and pinch and swell structures; Journal of Geology, vol. 63, p. 512-526.

Rast, N., 1956, The origin and significance of boudinage; Geological Magazine, vol. 93, p. 401-408.

Rodgers, J., 1970, Tectonics of the Appalachians, J.W. Wiley and Sons, New York.

Smith, R.B., 1975, Unified theory of the onset of folding, boudinage and mullion structure; Geological Society of America Bulletin, vol. 86, p. 1601-1609.

Stromgard, K.E., 1973, Stress distribution during the formation of boudinage and pressure shadows; Tectonophysics, vol. 16, p. 215-248.

Tricart, P. and Lemoine, M., 1986, From faulted blocks to megamullions and megaboudins: Tethyan

heritage in the structure of the western Alps; Tectonics, vol. 5, p. 95-118.

FIELD GUIDE AND ROAD LOG

NOTE: Most of these exposures are on private property and the owners are protective of their privacy. Please respect their property both during this trip and in subsequent visits.

Meeting Point: West parking lot of the Double Tree Inn, located at 425 NY-59, Nanuet, NY, 10954.

Meeting Point Coordinates: 18T 0584372mE, 4549264mN

Meeting Time: 8:30 AM

Distance in Miles (km) Cumulative	Point to Point	Route Description
0.0 (0.0)	0.0 (0.0)	Assemble in the western parking lot of the Double Tree Inn in Nanuet, NY.
0.3 (0.5)	0.3 (0.5)	Head East on NY-59 E toward Rose Rd.
0.5 (0.8)	0.2 (0.3)	Use the right lane to take the ramp to Palisades County Rd N.
16 (25.6)	15.5 (24.8)	Merge onto Palisades Interstate Parkway N.
16.2 (25.9)	0.2 (0.3)	Take exit 18 toward US-6, NY-17, I-87.
26.7 (42.7)	10.5(16.8)	At circle, take 2nd exit onto US-6.
26.8 (42.9)	0.1 (0.2)	Take Exit 129 toward Museum Village and merge onto Curly Rd.
26.9 (43.0)	0.1 (0.2)	Turn left on Museum Village Rd.
		Park on the corner of Museum Village Rd. and Old Mansion Rd.

STOP 1: Traverse through the Museum Village megaboudin

Location Coordinates: 41°20’31”N 74°12’00.93”W

Quartzofeldspathic gneiss with intense fracturing and alteration. The entire span of the megaboudin can be observed on the transect exposed in the Rt 17/6 road cut. Rock types and structures are observed near the Museum Village Rd overpass. The gneiss shows chlorite and hematite alteration on most fracture faces and the rock is altered throughout. Fracturing is more intense along the edges of the megaboudin and is multidirectional. Many surfaces exhibit both fibrous and polished slickensides that primarily show reverse motion but locally show many directions.

Distance in Miles (km) Cumulative	Point to Point	Route Description
27.0 (43.2)	0.1 (0.2)	Continue on Museum Village Rd. across highway overpass to stop sign
27.1 (43.4)	0.1 (0.2)	Turn left on Orange & Rockland Rd. and turn into parking lot on right
		Park in the Heritage trail lot for hikers and walk west about 200 feet to the underpass outcrop is around the bridgeworks.

STOP 1a: Wappinger Group Limestone on the Museum Village megaboudin

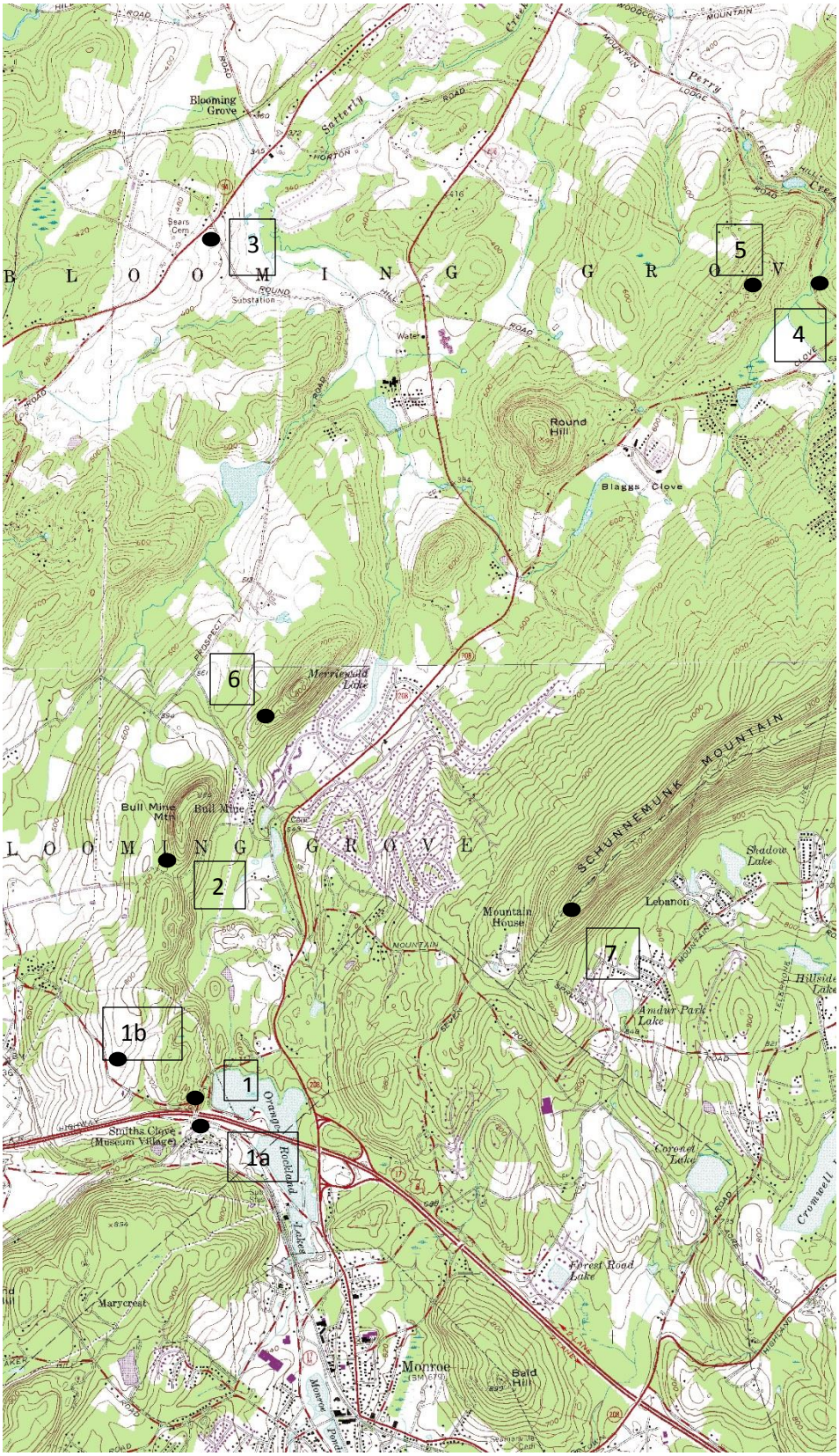
3
5
4
6
2
7
1b
1
1a
Blooming Grove
Round Hill
Blaggs Clove
Merriewold Lake
Bull Mine Mtn
Bull Mine
Mountain House
Lebanon
Shadow Lake
Hillside Lake
Amdur Park Lake
Smiths Clove (Museum Village)
Coronet Lake
Forest Road Lake
Marycrest
Monroe
Bald Hill
Schunnemunk Mountain

Location Coordinates: 41°20’48.19”N 74°12’01.42”W

Small outcrop of bedded Cambrian limestone with nodular chert layers. This rock lies unconformably above the gneiss. Note the lack of intense jointing seen in the gneiss and the gentle deformation. This is a small outcrop for reference. Limestone occurs both above and beneath the megaboudins because it is structurally repeated.

Distance in Miles (km)		Route Description
Cumulative	Point to Point	
27.2 (43.5)	0.1 (0.2)	Return to Station 1
27.5 (44.0)	0.3 (0.5)	Turn left on Old Mansion Rd.
		Stop at intersection of Old Mansion Rd. and Mediacom Way

STOP 1b: Martinsburg Formation and view of the Goose Pond megaboudin

Location Coordinates: 41°20’06.38”N 74°12’28.6”W

The Goose Pond megaboudin is the next south from the Museum Village megaboudin in the chain. It is located far to the west of the rest of the chain. This is because the E-W trending Monroe Fault offsets the megaboudin by approximately 1 mile in a dextral strike-slip sense. The Monroe Fault is interpreted as a Cretaceous fault but appears to be currently active with several recent epicenters located along its western extension. Several hundred feet west of the parking area are outcrops of Martinsburg shale. This shows the western contact of the Museum Village megaboudin is with lower Martinsburg Formation (Bushkill Member) and indicating a loss of section.

Distance in Miles (km)		Route Description
Cumulative	Point to Point	
28.2 (45.1)	0.7 (1.1)	Continue on Old Mansion Rd. to Craigville Rd.
28.5 (45.6)	0.3 (0.5)	Turn right on Craigville Rd.
29.0 (46.4)	0.5 (0.8)	Turn right on Bull Mine Rd. Park at circle
		Walk up road to right pass through gate and continue along dirt road to circle and crossing path. Follow path to left and visit mine and dump. NOTE: be careful of hidden adits in underbrush. Continue north along west face of hill to outcrops of gneiss overlying Martinsburg Shale. These slopes can be slippery.

STOP 2: Bull Mine Mountain megaboudin

Location Coordinates: 41°20’42.12”N 74°12’19.27”W

Bull Mine is a magnetite (iron) mine in the Bull Mine Mountain megaboudin. There are several adits and shafts within the mine complex and a tailings pile with large quantities of ore. The host gneiss for this iron deposit is largely metavolcanic gneiss but is also metasedimentary including calcsilicates. The mine is accessible and the dump contains a significant amount of ore. Farther along the western slope of the Bull Mine Mountain megaboudin, gneiss can be seen directly overlying Martinsburg shale in an overthrust contact. Both the gneiss and shale are highly fractured and contain slickensides showing thrust and reverse movement. The shale is highly cleaved and shows foliation and some bedding that dips beneath the gneiss.

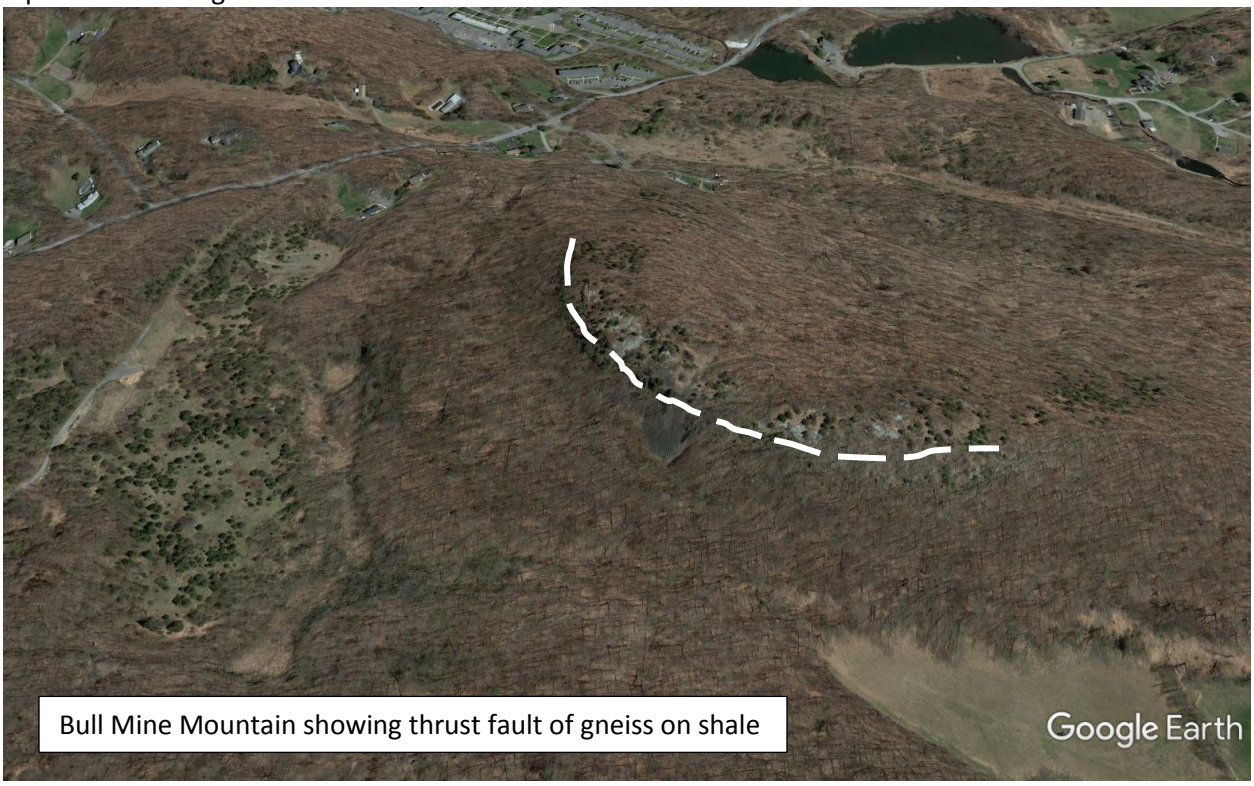

Bull Mine Mountain showing thrust fault of gneiss on shale

Distance in Miles (km) Cumulative	Point to Point	Route Description
29.5 (47.2)	0.5 (0.8)	Drive back down Bull Mine Rd. and turn right on Craigville Rd.
33.1 (53.0)	3.6 (5.8)	Drive northwest on Craigville Rd. and turn right on Rt. 94.
		Stop in the gravel area on the corner of Rt. 94 and Round Hill Rd.

STOP 3: View of Round Hill megaboudin

Location Coordinates: 41°24’7.8”N 74°11’53.75”W

The Round Hill megaboudin has a saddle in the middle where it began to separate but never developed a gap. The gneiss is continuous across the megaboudin but at a much lower elevation where intense fracturing made it subject to erosion. From this location, the abrupt hill of the weakly to unfractured gneiss in the northern part of the Round Hill megaboudin can be seen in the other low lying shale plain. To the south of Round Hill Rd. the southern elevated part of the Round Hill megaboudin can be seen.

There are outcrops of Martinsburg shale along Round Hill Rd. and an abrupt contact with gneiss at the megaboudin saddle.

Possible stop on Rt 94 (if time permits) to view Martinsburg Formation outside the influence of the megaboudins for comparison. Outcrop is beneath Railroad trestle.

Location Coordinates: 41°23'38.83"N 74°13'03.65"W

Distance in Miles (km)		Route Description
Cumulative	Point to Point	
33.8 (54.1)	0.7 (1.1)	Continue on Round Hill Rd. to Rt. 208
34.9 (55.8)	1.1 (1.8)	Turn right on Rt. 208 to Clove Rd.
35.8 (57.3)	0.9 (1.4)	Turn left on Clove Rd.
36.4 (58.2)	0.6 (1.0)	Turn Left on Mountain Lodge Rd.
		Park at bridge over stream. Outcrops of limestone occur along road and in stream to the southwest of the road. Walk up road to northwest to view outcrops of Martinsburg formation to quarry on the left side of the road.

STOP 4: Wappinger Group and Martinsburg Fm. In the Round Hill-Woodcock Hill gap

Location Coordinates: 41°23'54.78"N 74°08'55.1"W

At the stream is Wappinger Group limestone with nodular chert beds. Bedding is well developed but outcrops are weathered and difficult to see in many cases. Good cliff outcrops of limestone along stream bed to the southwest. Continue along the road to the west to observe a good section of the Martinsburg shale that is not excessively deformed near the carbonate but is progressively deformed up the hill and towards the quarry. Just 200 feet northwest of this entire section, are the rugged slopes and gneiss of the Woodcock Hill megaboudin.

Distance in Miles (km)		Route Description
Cumulative	Point to Point	
36.9 (59.0)	0.5 (0.8)	Continue on Mountain Lodge Rd. to Helms Hill Rd.
37.5 (60.0)	0.6 (1.0)	Turn left on Helms Hill Rd.
37.6 (60.2)	0.1 (0.2)	Turn left on Calvert Dr.
37.6 (60.2)	0.05 (0.1)	Quick turn on Mandy Dr.
		Park at cul-de-sac. Outcrop is on the road leading up on north side.

STOP 5: Shawangunk Formation infilling the gap

Location Coordinates: 41°23'57.57"N 74°09'11.43"W

Large exposure of classic Shawangunk Formation conglomerate and quartzite. Thick bedded quartz pebble to cobble conglomerate with lithic sparse clasts. Some imbrication of cobbles and reverse graded beds. Sandstone is arenitic and locally cross bedded. Minor slickensides show strike-slip and normal offset. This rock is juxtaposed directly against the carbonate of Stop 4 along a visible normal fault in the stream below this point.

Distance in Miles (km)		Route Description
Cumulative	Point to Point	
37.8 (60.4)	0.1 (0.2)	Return to Calvert Dr. and turn right
38.3 (61.2)	0.5 (0.8)	Return to Helms Hill Rd. and turn left to the end
38.3 (61.3)	0.05 (0.1)	Turn left on Round Hill Rd.
40.7 (65.1)	2.4 (3.8)	Turn right on Clove Rd
41.6 (66.6)	0.9 (1.4)	Turn right on Rt. 208
42.2 (67.5)	0.6 (1.0)	Turn right on Peddler Hill Rd.
		Turn right into private driveway and park Hike up the hill through the woods to the east to rock exposures.

STOP 6: Northern contact of the Merriewold Lake megaboudin

Location Coordinates: 41°22’27.26”N 74°11’40.5”W

This exposure shows the sharp contact of the gneiss with mobilized Martinsburg shale. Blocks of quartzofeldspathic gneiss of the Merriewold Lake megaboudin have sharp southern terminations along NW-striking planes. Martinsburg shale shows progressive strikes from NE along the northwest side of the megaboudin towards the NW in the gap to the southwest. It has well-developed cleavage and crenulation cleavage that demonstrate this swing in orientation. This stop may not be available or it may be too late in the day. There are two other exposures that clearly demonstrate the swing in orientation of fabric in the Martinsburg Formation from deformation.

This exposure on Prospect Rd. shows very shallowly southeast dipping fabric in Martinsburg shale reflecting the overthrusting of the Highlands massif and subsequent deformation.

Location Coordinates: 41°22’15”N 74°11’49.83”W

This exposure is on Peddler Hill Rd. and shows Martinsburg Formation with a clear northwest strike. This rock demonstrates the reorientation of the fabric from NE-striking to NW-striking through nearly 90° as a result of flow into the gap between the Merriewold Lake and Bull Mine Mountain megaboudins.

Location Coordinates: 41°22’20.47”N 74°12’16.64”W

Distance in Miles (km)		Route Description
Cumulative	Point to Point	
42.8 (68.5)	0.6 (1.0)	Return to Peddler Hill Rd and drive east to Rt 208

43.3 (69.3)	0.5 (0.8)	Turn left (south) on Rt. 208
43.8 (70.1)	0.5 (0.8)	Turn left on Mountain Rd.
44.1 (70.6)	0.3 (0.5)	Turn left on Seven Springs Rd.
		Park at trailhead for Skunnemunk Mountain. Hike up trail about ¼ mile until the megaboudin chain can be clearly seen to the west at the base of the hill.

<u>STOP 7: View of the megaboudin chain</u>

Location Coordinates: 41°21'36.01"N 74°10'37.39"W

The walk to the vantage point is on Bellvale Sandstone up Skunnemunk Mountain. Look to west to see the entire observed megaboudin chain sitting in the plain underlain by Martinsburg shale.

Distance in Miles (km)		
Cumulative	Point to Point	Route Description
44.4 (71.0)	0.3 (0.5)	Take Seven Springs Rd. to Mountain Road
45.0 (72.0)	0.6 (1.0)	Turn right on Mountain Springs Rd. towards Rt. 208
45.9 (73.4)	0.9 (1.4)	Turn left on Rt 208 (south).
56.4 (90.2)	10.5 (16.8)	Take ramp onto Rt. 17/6 East.
71.9 (115.0)	15.5 (24.8)	At traffic circle, take second right to Palisades Interstate Parkway South
72.2 (115.5)	0.3 (0.5)	Exit 8W at Rt 59 West in Nanuet towards Spring Valley.
72.4 (115.8)	0.2 (0.3)	Reverse direction on Rt. 59 at Smith Rd. to the left
		Return to Double Tree Inn at 425 New York 59, Nanuet, NY, 10954. Destination will be on the right.
		END OF TRIP

TRIP A4: PETROGENESIS AND TECTONICS OF PRE-, SYN-, AND POST-OTTAWAN GRANITOIDS OF THE WESTERN HUDSON HIGHLANDS, NY

Matthew L. Gorring
Department of Earth & Env. Studies, Montclair State University, Montclair, NJ 07043

Alexander E. Gates
Department of Geology, Rutgers University, Newark, NJ 07102

David W. Valentino
Department of Earth Sciences, SUNY-Oswego, Oswego, NY 13126

INTRODUCTION AND GEOLOGIC SETTING

The purpose of this field trip will be to examine the field relations, geochemistry, and geochronology of a diverse suite of pre-, syn-, and post-Ottawan (1090-1030 Ma) granitoid rocks exposed in the western Hudson Highlands, NY. These rocks are critically important for constraining petrogenetic processes and the tectonic history of the Grenville Orogen (1350-960 Ma) in the north central Appalachians. The Hudson Highlands, along with the physically contiguous New Jersey Highlands and similar rocks extending into eastern Pennsylvania, are collectively called the Reading Prong, one of the largest of several Grenville-age (~1350 to 1000 Ma) basement massifs within the core of the Appalachian orogenic belt of eastern North America (Figs. 1 and 2; Rankin, 1975). These basement massifs lie outboard (east) of the main Grenville Province in eastern Canada and record variable amounts of post-Mesoproterozoic metamorphic and deformational overprint (e.g., Rankin et al., 1989; Gates and Costa, 1998). The Reading Prong displays evidence of only brittle deformation concentrated along narrow, reactivated Mesoproterozoic shear zones due to late Paleozoic compression and Mesozoic rifting (Gates, 1995; 1998) and thus, have a well preserved record of Grenville-age metamorphism and deformation. Rocks of the Hudson Highlands consist of a complex assemblage of metasedimentary, metavolcanic, and quartzofeldspathic ("granitic") gneiss, and intrusive granitoid rocks that were variably deformed and metamorphosed at upper amphibolite to hornblende-granulite facies conditions during at Grenville orogenesis (Dallmeyer and Dodd, 1971; Dallmeyer, 1974; Helenek and Mose, 1984). Based on field relations and recent SHRIMP U-Pb zircon ages (Ratcliffe and Aleinikoff, 2001; Gates et al. 2004; Volkert et al., 2005; Volkert et al., 2010; Aleinikoff et al., 2012), rocks of the Hudson Highlands, and the contiguous New Jersey Highlands can be roughly divided into two groups: (1) pre-Ottawan (>1060 Ma) and (2) syn- to post-Ottawan (<1060 Ma). Pre-Ottawan rocks all have strong, penetrative, high-grade metamorphic fabrics related to the Ottawan orogeny. Syn- to post-Ottawan rocks are variably deformed, ranging from undeformed to those that locally have strong, highgrade, ductile fabrics but lack the regional-scale, penetrative fabrics that characterize the pre-Ottawan rocks. Locally, syn- to post-Ottawan rocks truncate fabric elements in pre-Ottawan rocks. The area of the field trip is located in parts of the Sloatsburg and Popolopen Lake quadrangles west of the Hudson River within the west central Hudson Highlands, New York (Figs. 2 and 3). Previous mapping in this area, divided the units by rock types (Dodd, 1965; Jaffe and Jaffe, 1973; Dallmeyer, 1974; Helenek and Mose, 1984).

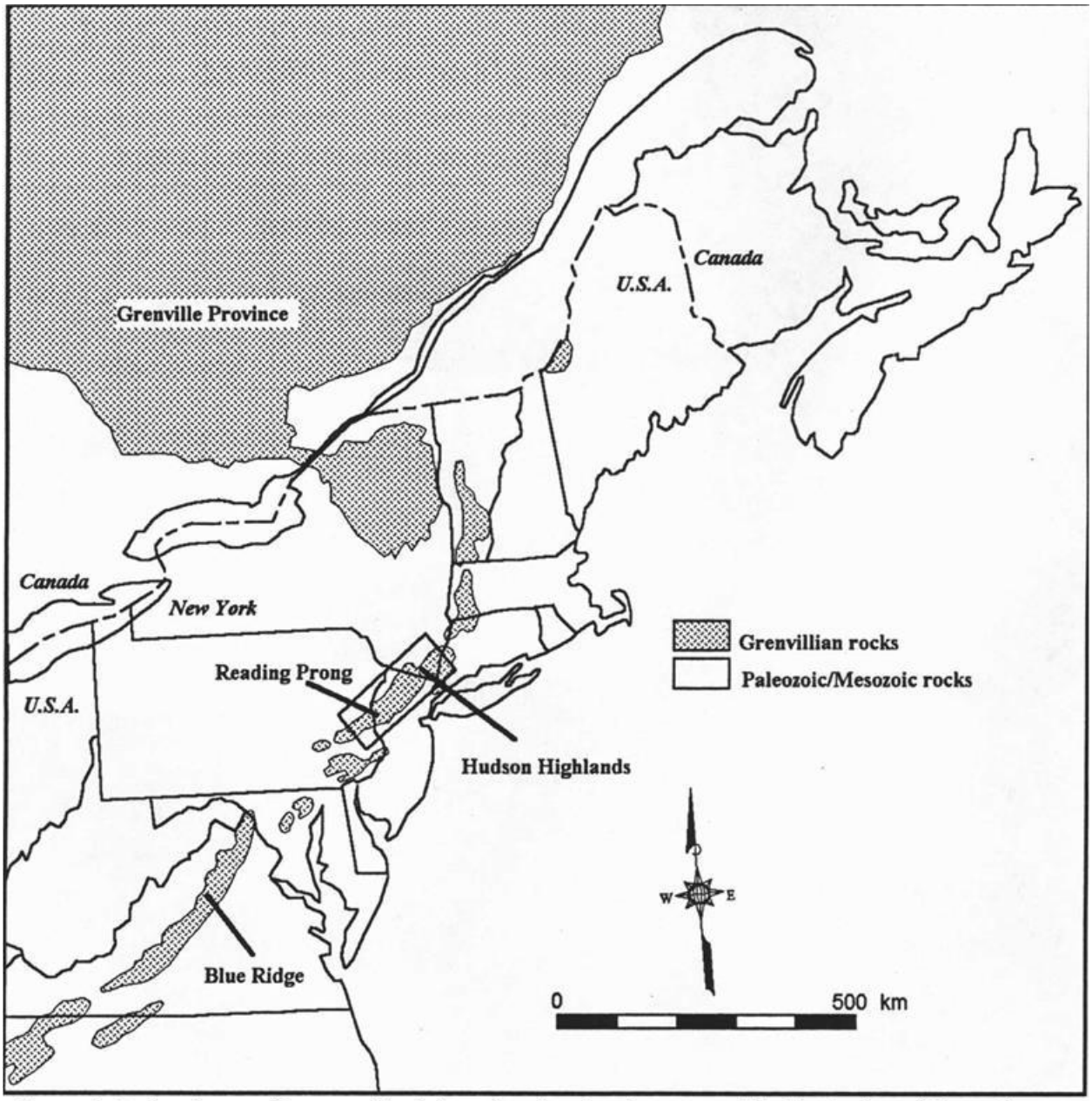

Figure 1. Regional map of eastern North America showing the geographic distribution of Grenville rocks. The area of Figure 2 is outlined by a rectangle. Map modified from Gates et al. (2001).

PRE-OTTAWAN ROCKS

Metavolcanic Lithofacies (~1350-1250 Ma)

The oldest rocks in the region are a suite of quartzofeldspathic orthogneiss which include strongly banded, interlayered, very light colored, biotite- and/or hornblende-quartz-plagioclase gneiss, charnockitic (orthopyroxene-bearing) quartz-plagioclase gneiss, and amphibolites of mafic to intermediate compositions. Mafic, intermediate, and felsic compositional banding ranges in thickness from 5 cm to 5 m with varying proportions of each rock type. There are local interlayers of quartzite and

calc-silicate gneiss. Migmatites also occur locally in this unit. These rocks are interpreted to represent a

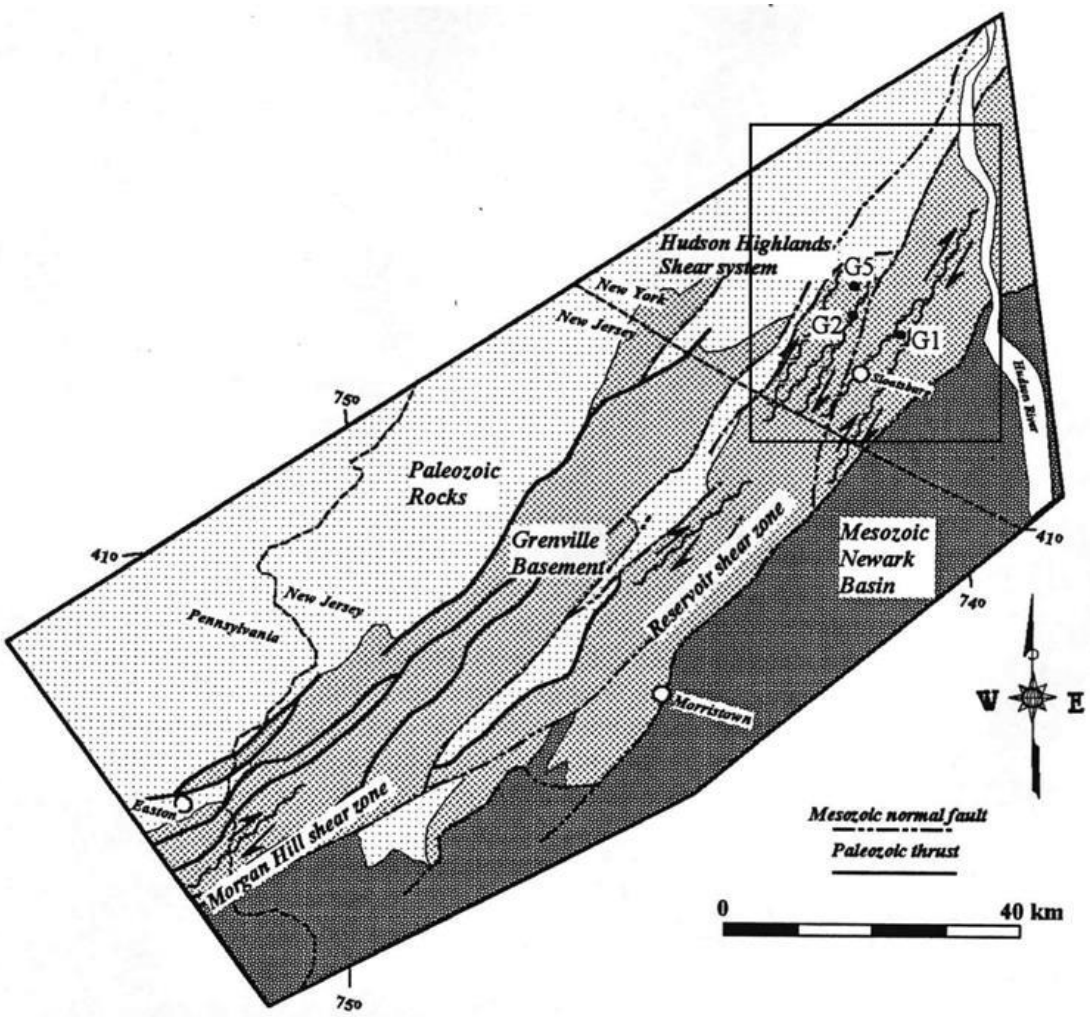

Figure 2. General geologic map of the Reading Prong and Hudson Highlands. The inset box shows the approximate area shown in Figure 3. G1, G2, and G5 are sample localities where Gates et al. (2001b; 2004) obtained SHRIMP U-Pb zircon ages. G1 is the Lake Tiorati Diorite at Stop #2 (see Fig. 6) and G2 is the sheared quartzofeldspathic gneiss at Stop #3. Map modified from Gates et al. (2001).

continental volcanic-plutonic arc suite of calc-alkaline rocks mixed with minor sediments (Ratcliffe, 1992; Gates et al., 2001c). Rocks equivalent to the metavolcanic lithofacies extends southwestward into the New Jersey Highlands where it is called the Losee Metamorphic Suite (Volkert and Drake, 1999) and northeastward into the eastern Hudson Highlands (Ratcliffe, 1992) where SHRIMP U-Pb zircon ages for these areas range from ~1.36 to ~1.25 Ga (Walsh et al., 2004; Volkert et al, 2010). Rocks of the metavolcanic lithofacies are lithologically and chemically very similar to tonalitic and charnockitic gneisses found in the southern Adirondacks (McLelland and Chiarenzelli, 1990) and to the Mount Holly Complex in the Green Mountain Massif in Vermont (Ratcliffe et al., 1991), which are dated at ~1.35 to 1.3 Ga. Overall, these rocks are interpreted to represent an Andean-type, continental arc system with northwestward-dipping subduction that existed along the entire eastern margin of the Laurentia from ~1.4 to ~1.2 Ga (see discussion in Volkert et al., 2010).

Metasedimentary Lithofacies (~1300-1200 Ma)

Throughout the western Hudson Higlands there are belts of rock considered to have sedimentary protoliths including pelitic-, psammitic-, calcsilicate-gneisses, quartzite, and marble. Belts of rock upward of a few kilometers wide may contain all or some of these rock types, interlayered at the scale of meters to 100's of meters. These rocks have been included in the metasedimentary lithofacies that is portrayed on the geologic map (Fig. 3). The metapelite consists of interlayered biotite-garnet gneiss with medium to coarse quartz, plagioclase, K-feldspar and local sillimanite, and cordierite with quartzofeldspathic layers. Within the metapelite are zones of graphite-pyrite-garnet gneiss with biotite, quartz, K-feldspar, plagioclase, and sillimanite locally. Quartzite layers of 10-50 cm thickness also occur within this unit as do rare and discontinuous layers of diopside and diopside-garnet marble to calcsilicate of 10 cm to 2 m thickness. The calc-silicate is quartzofeldspathic with salite, apatite, sphene, scapolite, and hornblende, and is commonly migmatitic. Based on the abundance of graphite-sulfide rocks and the presence of minor interlayers of amphibolite of probably volcanic origin, Gates et al. (2001c) interprets this sequence as most likely a suite of continental- to oceanic-arc extensional basin deposits. Volkert and Drake (1999) came to a similar conclusion based on field relations and whole-rock geochemical data on correlative rocks in New Jersey Highlands. Similar packages of metasedimentary rocks are common in the Adirondacks (e.g., McLelland et al., 1996) and in the Central Metasedimentary Belt in Canadian Grenville (e.g., Rivers, 1997; Carr et al., 2000).

The contacts with the quartzofeldspathic gneiss and rocks of the metavolcanic lithofacies are usually gradational such that age relations based on field relations are ambiguous due to transposition of original stratigraphic and/or cross-cutting relations. However, in the New Jersey Highlands, Volkert and Drake (1999) have recognized field evidence that indicates that the correlative metasedimentary sequence unconformably overlies the equivalent of the metavolcanic lithofacies (Losee Metamorphic Suite). Demonstrably unconformable relations between these units in the Hudson Highlands has yet to be recognized in the study area of this field trip, however, Ratcliffe (1992) also places the equivalent of the metavolcanic lithofacies in the eastern Hudson Highlands at the base of the "stratigraphy", below metasedimentary rocks. Dodd (1965) and Helenek and Mose (1984) document a few localities where metasedimentary lithofacies rocks are crosscut by metaplutonic quartzofeldspathic gneisses (e.g. Storm King granite gneiss) in the Popolopen Lake quadrangle near Bear Mountain. Thus, the age of the metasedimentary lithofacies rocks is roughly constrained to be younger (or at least contemporaneous with) than the metavolcanic lithofacies (<1300 Ma), but clearly older than quartzofeldapthic gneiss unit (see below) which has been dated ato be in the range of 1230-1160 Ma (see below; Ratcliffe and Aleinikoff, 2001; Gates et al, 2004; Volkert et al., 2010). This interpretation is also supported by SHRIMP U-Pb zircon ages of (1) detrital grains from a semi-pelite from the western Hudson Highlands (G5 in Fig. 2) which yielded a wide range of ages from 2000-1200 Ma (Gates et al., 2004) and (2) interlayered rhyolitic gneisses within the metasedimentary sequence from the New Jersey Highlands that yield ages of 1300 to 1240 Ma and thus roughly bracket the upper and lower age limit of the as well as inherited cores that range from 1390 to 1300 Ma (Volkert et al., 2010).

Quartzofeldspathic Gneiss (~1230-1160 Ma)

The quartzofeldspathic gneiss ranges from massive to layered quartz-plagioclase gneiss and quartz-K-feldspar-plagioclase gneiss with minor amounts of clinopyroxene, hypersthene, hornblende and/or biotite. Locally, this unit contains magnetite or garnet in trace amounts. Compositional layers are defined by the proportion and type of the ferromagnesian mineral component. Locally, this unit contains apparent textural gradation across the fabrics by an increase in the amount of mica and

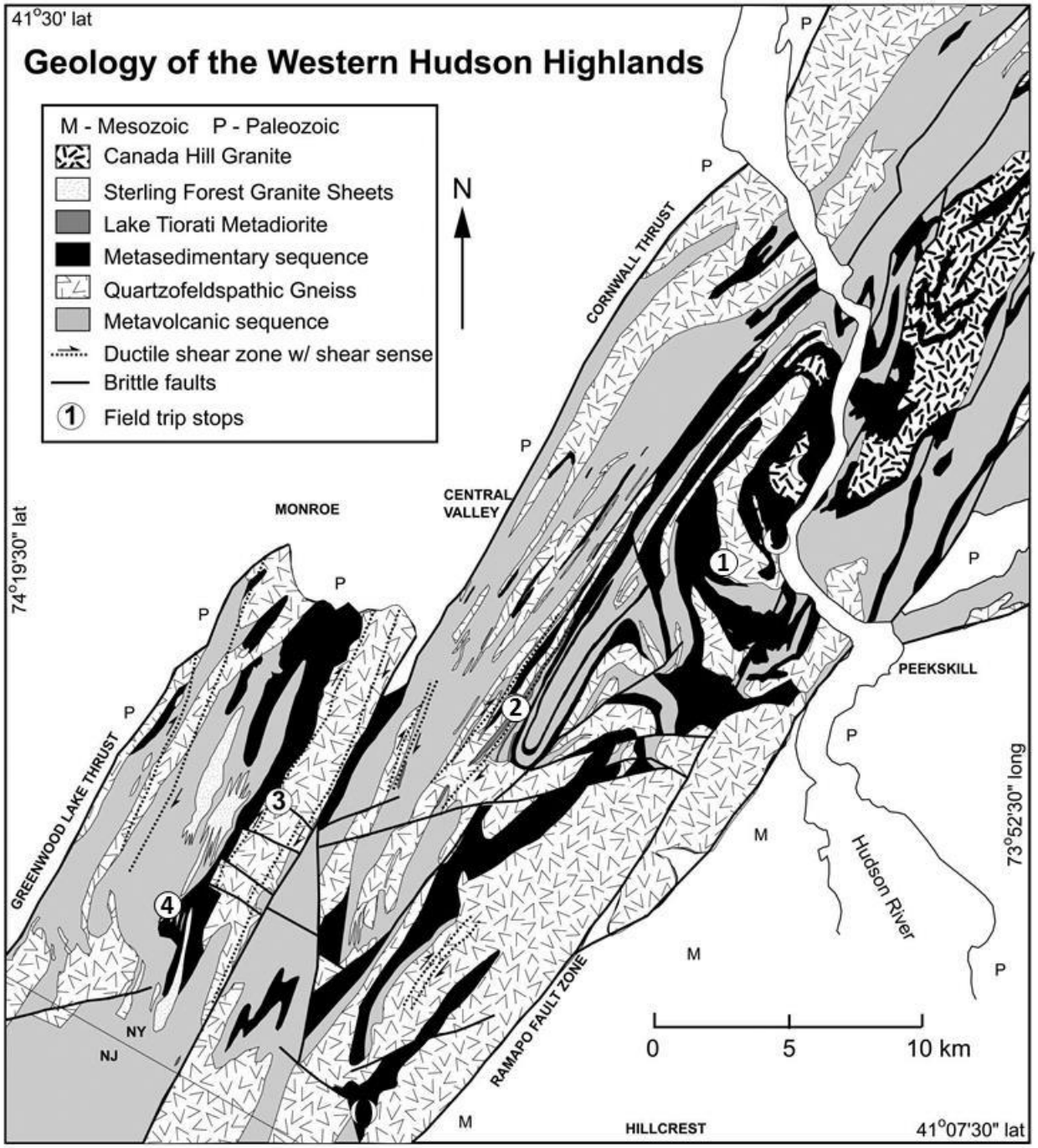

Figure 3. Generalized geologic map of the west central Hudson Highlands showing field trips stops 1-4. Based on geologic mapping of Dodd (1965), Offield (1967), Helenek (1971), Ratcliffe (1992), Valentino et al. (2001); Gates et al. (2001).

decrease in layer spacing with sharp contacts between, suggesting a relict sequence. However, such relict sequences in granulite terranes are difficult to interpret. Quartzofeldspathic gneiss is locally interlayered with quartzite and with mafic gneiss at the contact with the metavolcanic lithofacies. The gradational contacts with the metavocanic and metasedimentary lithofacies, and the internal compositional layers suggest that parts of the quartzofeldspathic units could represent a volcaniclastic

sequence. However, in the more massive rocks, this unit is strongly lineated (L>S) defined by stretched hornblende prisms and rodded quartz-feldspar aggregates interspersed with large (2-4 cm) plagioclase and/or K-feldspar augen and locally contains mafic gneiss xenoliths. These features clearly support a metaplutonic origin for at least part of quartzofeldspathic gneiss. These more massive textured rocks are interpreted here to be correlative to hornblende granite gneiss mapped in the Popolopen Lake (Dodd, 1965) and West Point quadrangles (Helenek and Mose, 1984), and Oscawana Lake quadrangles (Ratcliffe, 1992) which has been historically referred to as the "Storm King Granite" (Berkey, 1907; Lowe, 1950). These rocks also correlate with similar metaplutonic hornblende granite gneiss lithologies within the Byram Intrusive Suite in the New Jersey Highlands (Volkert et al., 2000; Volkert, 2004).

Geochemical data shows that massive-textured quartzofeldspathic gneiss, Storm King granite gneiss, and the Byram Intrusive Suite all have nearly identical chemistry characterized by metaluminous A/CNK ratios (<1.0) and A-type compositionally affinity defined by high Fe/(Fe+Mg) (~0.9), K_2O/Na_2O (1.5-2), high Ba (500-1800 ppm), Nb (20-50 ppm), Y (60-180 ppm), total REE (300-800 ppm) and low MgO (<0.7%), CaO (<2%), and Sr (80-180 ppm). REE patterns are LREE-enriched (La/Yb_n = 5-15), but have flat MREE and HREE and relatively high HREE concentrations (~20-40x chondrite) with moderately deep negative europium anomalies (Eu/Eu* = 0.20-0.50) (Figs. 4A and B). All three suites largely overlap in the "within plate granitoid" (WPG) field on tectonic discrimination diagrams (Figs. 4C and D). Similar

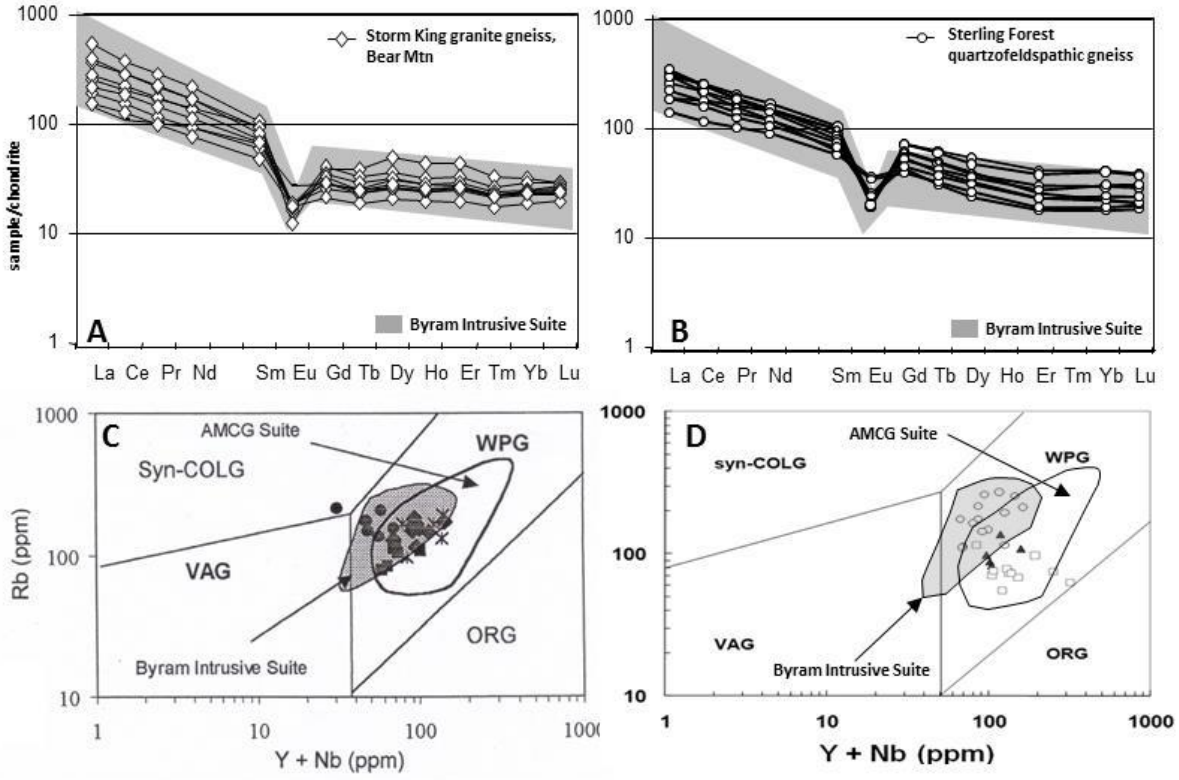

Figure 4. Geochemical plots (A) and (C) for the Storm King granite gneiss from the Bear Mountain area (including Stop #1), and plots (B) and (D) for massive quartzofeldspathic gneiss from the Sterling Forest area (including Stop #3) showing their striking geochemical similarity with each other and with correlative granite gneisses of the Byram Intrusive Suite, NJ (Volkert et al., 2000). These are rocks also similar to AMCG granitic gneisses from the Adirondacks, NY (McLelland et al., 1996). A) and (B) are REE plots and (C) and (D) are tectonic discrimination diagrams modified from Pearce et al. (1984); fields are for syn-collision (syn-COLG), volcanic arc (VAG), within plate (WPG), and ocean ridge (ORG) granitoids.

field relations and geochemical characteristics, that spans more than 150 km through the NJ Highlands northeastward into the Hudson Highland strongly supports a regional correlation and is consistent with a relatively uniform A-type granitoid protolith (Verrengia and Gorring, 2002; Peterson et al., 2011).

Current radiometric constraints on the crystallization age of these granitic metaplutonic rocks are based on SHRIMP U-Pb zircon ages that have been obtained over the last 10-15 years. Ratcliffe and Alenikoff (2001) reported a SHRIMP zircon age of 1174 ±8 Ma for the Storm King granite gneiss at Dunderberg Mountain (~10 km SE of Bear Mountain). Gates et al. (2004) obtained a broad crystallization age range of ~1160-1230 Ma by SHRIMP zircon analysis on one sample of quartzofeldspathic gneiss from within the Indian Hill Shear Zone in the Sterling Forest area (Stop #3). More recently, Volkert et al. (2010) reported SHRIMP zircon crystallization ages of 1182 ±11 and 1184 ±8 Ma from two samples of hornblende granite gneiss from the Byram Intrusive Suite. As noted by Volkert et al. (2010), the timing of this magmatism (~1180 Ma) correlates with the early stages of the Shawinigan Orogeny (1190-1140 Ma) in the Canadian Grenville Province (see Rivers, 1997 and refs. therein). Quartzofeldspathic gneisses from the New Jersey and western Hudson Highlands are chemically similar to other metaplutonic rocks of A-type chemical affinity with ages of 1210-1170 Ma from other parts of the Grenville Orogen including southeastern Canada (Easton, 1986; Lumbers et al., 1990; Davidson 1995) and the Adirondack Lowlands (Wasteneys et al., 1999; Hamilton et al., 2004; Peck et al., 2004; Heumann et. al, 2006) as well as granitic gneisses from the slightly younger AMCG suite (~1155 Ma) in the Adirondack Highlands (McLelland and Whitney, 1990; McLelland et al., 2001; 2004). The consistent A-type geochemical affinity and the large volumes of magma generated to form the protolith of the massive-textured quartzofeldspathic gneiss, Storm King granite gneiss, and the Byram Intrusive Suite supports a tectonic model that involves a major heat source to the crust. Verrengia and Gorring (2002) proposed that the Storm King granite gneiss formed from partial melting of mafic to intermediate calc-alkaline sources at mid-crustal depths with the heat source coming from asthenospheric upwelling due to gravitational collapse and delamination of an overthickened continental lithosphere produced during the final stages of Elzevirian Orogeny. Volkert et al (2010) proposed a model for Byram Intrusive Suite granitic gneisses where asthenospheric upwelling occurs by a combination of lithospheric delamination and/or slab rollback after the closure of a backarc basin that occurred post-Elzevirian (e.g <1.2 Ga).

PRE- TO SYN-OTTAWAN METAMORPHISM AND DEFORMATION

There are at least two (and perhaps three) major deformational events recorded in the crystalline rocks of the Hudson Highlands. The dominant deformational structure of the older event(s) is a penetrative gneissosity that occurs in every unit except the Lake Tiorati Diorite, Sterling Forest Granite Sheets, Canada Hill Granite, and late pegmatites (see below). This gneissosity is defined by virtually all minerals but especially by platy and elongate minerals. Biotite, amphibole, sillimanite, and pyroxene are aligned in the strongly foliated quartz-feldspar matrix. Additionally, aggregates of quartz and feldspar define layering in some lithologies. Amphibole and pyroxene clots show similar rotation textures forming sigma-porphyroclasts (Passchier and Simpson, 1986). Some pelitic rocks contain garnet-fish structures, and locally, some rocks contain intrafolial asymmetric isoclinal folds 5 to 20 cm thick. The vergence of these folds is consistent in some areas and appears to indicate westward transport. Mesoscopic and megascopic folds produced during this event are recumbent to shallowly reclined. They are tight to isoclinal and commonly asymmetric with the lower limbs sheared out. This asymmetry consistently indicates northwestward transport. The weak and sparse kinematic indicators described above support this shear sense. Thinner layers in these folds contain mesoscopic parasitic folds that are especially well developed on the upper limb. Metamorphism associated with these structures is of hornblende

granulite facies and maximum P-T estimates are on the order of 700-750ºC and 4±1 kilobar based on mineral assemblages in metapelitic and mafic metavolcanic units (Dallmeyer and Dodd, 1971). Deformation and metamorphism associated with this event is most likely of Ottawan age and is interpreted to have been the result of a Himalayan-type continent-continent collision (Gates et al., 2004). However, this does not preclude the possibility of pre-Ottawan deformation events (e.g., Elzeverian, Shawinigan as defined by Rivers, 1997) that could have been obliterated by the Ottawan event. In fact, this is likely the case. Dallmeyer (1972), Helenek and Mose (1984) and Ratcliffe (1992) report structural evidence (e.g. refolded foliation) for multiple deformation events (e.g. refolded foliation) in the Bear Mountain area and in the eastern Hudson Highlands. Further evidence for a pre-Ottawan deformational history comes from U-Pb SHRIMP zircon crystallization age of 1144 ±13 Ma on the Canopus Pluton in the eastern Highlands that lacks the older fabric elements (Ratcliffe and Aleinikoff, 2001). Structural and geochronologic evidence for multiple, penetrative fabric elements that can be assigned to distinct pre- and syn-Ottawan deformation events has yet to be recognized in the western Hudson Highlands.

EMPLACEMENT AND GEOCHEMISTRY OF SYN- AND POST-OTTAWAN GRANITOIDS

Granitoids of syn- to post-Ottawan age (1060 to 960 Ma) are volumetrically minor in the Hudson Highlands compared to pre-Ottawan rocks, but are important for constraining the late geologic history of the area. Syn-Ottawan granitoids consist of two suites of leucogranites; (1) the Sterling Forest granite sheets (Gorring et al., 2002), and (2) the Canada Hill Granite (1058 ±14 Ma; Helenk and Mose, 1984; Aleinikoff et al., 2012). Post-Ottawan granitoids consist of the Lake Tiorati Diorite (1008 ±4 Ma; Gates et al., 2004) and a suite of late, crosscutting pegmatitic granite dikes. The Mount Eve Granite (1019 ±5 Ma; Drake et al., 1991; Gorring et al., 2004; Volkert et al., 2010), located in the far western New Jersey and Hudson Highlands, is also part of the post-Ottawan suite granitoids, but will not be visited on this field trip. Similar plutonic granitoid activity of syn- to post-Ottawan age has been documented elsewhere in the Adirondacks (1060-1045 Ma; Lyon Mountain granitic gneiss; 1035 Ma; Lyonsdale Bridge pegmatite; 935 Ma Cathead Mt leucogranite; McLelland et al., 2001) and in the Green Mountain Massif (ca. 960 Ma; Stamford Hill rapakivi granite; Ratcliffe et al., 1991).

Sterling Forest Granite Sheets (syn-Ottawan)

Mapping in the Monroe and Sloatsburg quadrangles by Valentino et al. (2001) and Linguanti et al. (2011) have identified a series of leucocratic granite sheets, primarily occurring west of the NY Thruway in the Sterling Forest section of Harriman State Park, that intrude pre-Ottawan rocks of the metavolanic and metasedimentary lithofacies and the quartzofeldspathic gneiss unit. Jaffe and Jaffe (1973) recognized these rocks in the Monroe quradrangle and mapped them as alaskite bodies. Offield (1967) also mapped isolated occurrences of this lithology immediately to the east in the Greenwood Lake quadrangle. The granite sheets are typically medium to coarse-grained, locally megacrystic (K-feldspar and plagioclase), lack penetrative deformational fabrics, and have concordant intrusive contacts with the surrounding gneisses. Currently there are no radiometric age constraints on this important unit. The granite sheets are leucocratic, with K-feldspar, quartz, plagioclase, only minor (<5%) hornblende and/or biotite, and accessory apatite, zircon, and titanite. The texture is equigranular with subhedral to anhedral interlocking grains, and locally they contain xenoliths of metasedimentary and metavolcanic lithofacies rocks. The interior of the granite sheets are not foliated, however the margins typically show high-grade ductile foliation textures that are parallel to the enclosing gneisses. The sheets range in thickness from 10’ s to 100’s of meters thick and typically strike northeast-southwest and dip

moderately to steeply to the southeast parallel to foliation in the surrounding gneiss. Most are laterally continuous for several kilometers and parallel the hinge zone of fold nappes in the metavolcanic and metasedimentary sequences. In the central part of Sterling Forest, the granite sheets extend out from two large tabular shaped bodies of granite. These two bodies of granite and sheet appendages occur within core of shallowly plunging, northeast trending, parallel, open antiformal structures that can be traced from the Monroe quadrangle southward. These field relations, along with the ductile deformation textures at the sheet margins, strongly suggest a genetic relationship between granite emplacement and fold development indicating that the granite sheets were emplaced during deformation (e.g. syn-Ottawan).

The Sterling Forest granite sheets are high SiO_2 (~75%), leucocratic granites with <5% modal mafic minerals (Appendix Table 2; Fig. 5A). They are metaluminous to slightly peraluminous (ASI = 0.95 to 1.1) and have highly variable K_2O/Na_2O (0.3 to 3.3) reflecting variability in the modal abundance of K-feldspar or Na-plagioclase as the dominant feldspar. These rocks are divided into three chemically distinct groups based on REE patterns (Fig. 5C). The first group is characterized by LREE-enriched, HREE-depleted patterns with moderately negative Eu anomalies (Eu/Eu* = 0.50 to 0.7). The second group has a distinctive concave upward, "dished" MREE-depleted, HREE-enriched pattern with moderately negative to neglible Eu anomalies (Eu/Eu* = 0.35 to 1). The third group is defined by very low total REE's, strong LREE enrichment, depleted and flat MREE to HREE, extremely positive Eu anomalies (Eu/Eu* up to 3.5), and relatively high Sr and Ba concentrations (Appendix Table 2) relative to the other two groups. Group 1 granite sheets are best interpreted as partial melts of plagioclase-free source rocks with abundant residual amphibole ± garnet coupled with fractional crystallization of quartz + feldspars ± trace element-rich accessory phases (e.g., zircon, apatite, monazite, allanite). The garnet-bearing, plagioclase-free source mineralogy implies melt generation probably occurred at deep crustal levels probably involving source rocks of mafic to intermediate compositions. In comparison, Group 2 granite sheets clearly were generated by partial melting of garnet-free source rocks and hence melt generation probably occurred at shallower crustal levels. Group 3 granite sheets most likely represent rocks that accumulated feldspar, perhaps by some sort of filter pressing mechanism that extracted granitic melts during emplacement. These chemically distinctive groups of granite sheets have similar field relations and appear to be part of the same magmatic event, thus crustal melting apparently occurred at various crustal levels. On tectonic discrimination diagrams, the Sterling Forest granite sheets plot scattered along the boundary between fields for syn-collisional and volcanic arc granitoids (Figs. 5D-E).

Canada Hill Granite (syn-Ottawan; ~1060 Ma)

The Canada Hill Granite (Berkey and Rice, 1919; Lowe, 1950; Helenek and Mose, 1984) is a distinctively white to blue-gray, coarse-grained leucogranite that occurs as small plutons, sheets, pods, and stringers almost exclusively within metapelitic gneisses of the metasedimentary lithofacies in the northeastern part of the Hudson Highlands (Fig. 3). The largest masses of this unit occur on the eastern side of the Hudson River in the vicinity of Canada Hill in the West Point quadrangle, where it was originally mapped and defined by Berkey and Rice (1919) and again formalized as a distinct, mappable unit by Helenek (1971). Lowe (1950) and Dodd (1965) also recognized this unit to the southwest in the Popolopen Lake quadrangle as well as by Ratcliffe (1992) to the east in the Oscawana Lake quadrangle. The Canada Hill granite is almost always associated with migmatitic host rocks. The Canada Hill Granite is composed of quartz, white K-feldspar, and white to gray plagioclase in roughly equal proportions. Biotite is ubiquitous as the mafic phase with accessory amounts of sphene, apatite, and zircon. Garnet is locally abundant, especially near contacts with the enclosing migmatitic metapelite and is interpreted to represent undigested xenocrysts derived from the metapelites. It is predominantly massive textured

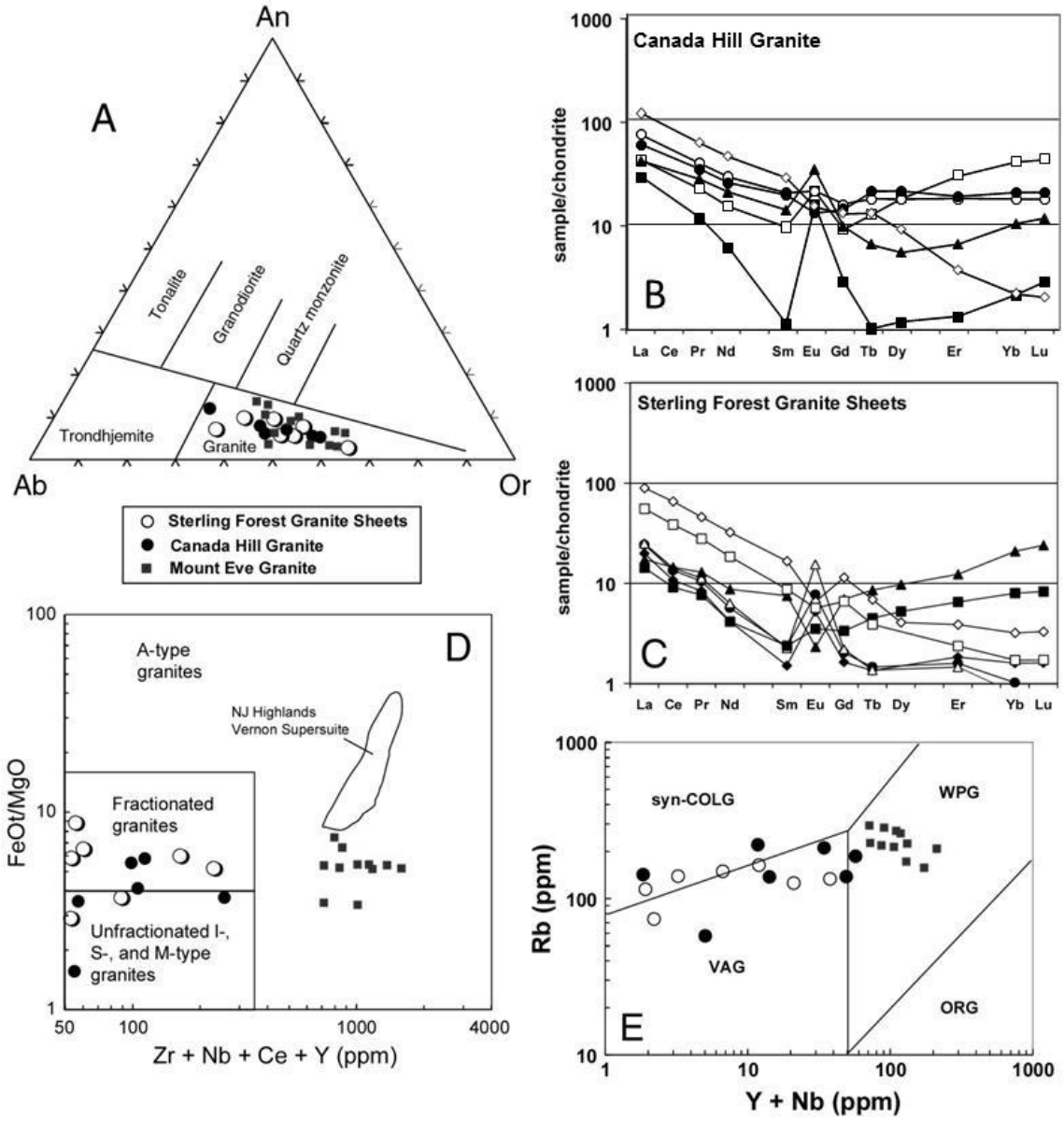

Figure 5. Geochemical plots for Sterling Forest granite sheets, the Canada Hill Granite, and the Mount Eve Granite for comparison. (A) Normative Ab-An-Or classification diagram. REE plots for (B) Canada Hill Granite and (C) Sterling Forest Granite Sheets. (D) and (E) are tectonic discrimination diagram; VAG = volcanic arc; syn-COLG = syn-collisional; WPG = within-plate; and ORG = ocean ridge granitoids.

with only local development of a weak foliation. The orientation of the sheets and pods of Canada Hill Granite parallel the foliation in the surrounding gneisses and contacts are generally gradational and migmatitic, except locally where the granite clearly truncates enclosing gneissic foliation.

Recent U-Pb SHRIMP zircon age dating by Aleinikoff et.al. (2012) indicate a crystallization age of 1058 ±14 Ma from one sample collected from roadcut exposures on NY Rte 9W located ~5 km north of Bear Mountain. The Canada Hill Granite has long been interpreted as a late, syn-metamorphic (anatectic) granite derived from partial melting of the surrounding metapelitic layers within the Metasedimentary Lithofacies (Lowe, 1950; Helenek and Mose, 1984; Ratcliffe, 1992). The intimate association of Canada

Hill Granite and the migmatites on a regional scale and the similarity of leucosome compositions and U-Pb zircon ages in migmatites with the Canada Hill support a petrogenetic link between them. The Canada Hill Granite is a high SiO_2 (71 to 75 wt%), very low FeO_T (generally <1 wt%), strongly peraluminous (ASI > 1.4) and have highly variable K_2O/Na_2O (0.3 to 3.3) reflecting variability in the modal abundance of K-feldspar or Na-plagioclase as the dominant feldspar (Appendix Table 2). REE patterns and other trace element systematics are striking similar to Sterling Forest granite sheets indicating a common petrogenetic origin for both suites (Fig. 5B). These major-element and trace element characteristics, along with a high initial $^{87}Sr/^{86}Sr$ ratio of 0.7186±0.0017 reported by Helenek and Mose (1984), provides strong support for partial melting of metapelitic sources to form the Canada Hill Granite (e.g., S-type granitoid).

Lake Tiorati Diorite (post-Ottawan; ~1010 Ma)

The Lake Tiorati Diorite is a coarse- to very coarse-grained black and white speckled rock composed of sodic-plagioclase, pyroxene (both clinopyroxene and orthopyroxene), hornblende, and biotite locally. The type locality and location of the largest body (~0.5 km wide and ~5 km long) is along the western shores of Lake Tiorati in the central part of Harriman State Park within the Popolopen Lake quadrangle (Fig. 3) and was originally described by Lowe (1950) and mapped by Dodd (1965) as a coarse grained amphibolite ("Amphibolite II"). A few smaller, lens-shaped bodies occur a few kilometers to the southwest in the northeast corner of the Sloatsburg quadrangle recently mapped by Valentino et al. (2001). The diorite grades to lower pyroxene, gabbroic anorthosite compositions locally. Texture ranges from granoblastic to foliated and mylonitic with S-C fabric and rotated porphyroclasts. The diorite also locally contains xenoliths of mostly mestasedimentary lithofacies rocks. SHRIMP U-Pb zircon dating of small, subhedral zircons with minimal zoning obtained from undeformed diorite from the type locality (Stop #2) yielded a cluster of concordant ages averaging 1008 ±4 Ma (Fig. 6). This is interpreted to be the crystallization age of the Lake Tiroati Diorite.

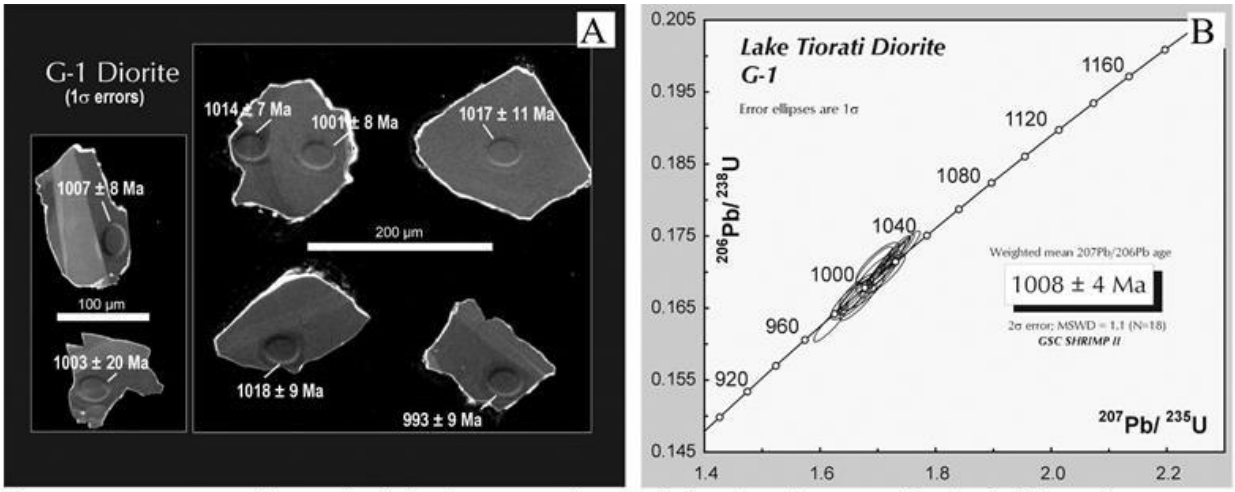

Figure 6. Representative cathodoluminescence images (A) and U-Pb concordia plot (B) from zircons extracted from the Lake Tiorati Diorite from Stop 2 analyzed using the SHRIMP II instrument at the Geological Survey of Canada (Gates et al., 2004).

Major element chemistry of coarse-grained, relatively undeformed samples of the Lake Tiorati Diorite indicate they are uniformly mafic plutonic rocks that have moderate to strong calc-alkaline geochemical signatures (Table 1; Fig. 7A). REE patterns of most samples are weak to moderately LREE-enriched

(La/Yb_N = 1.5 to 5) and slightly concave upward or "dished", MREE-depleted patterns with little to no HREE-depletion (Fig. 7B). They also have variable negative Eu anomalies (Eu/Eu* = 0.6 to 1.0). The mafic, calc-alkaline composition, relative strong negative Eu anomalies and slight MREE depletions in some samples suggests that significant plagioclase ± hornblende crystallization was important in the petrogenesis of these rocks before final emplacement. The lack of strong HREE and Y depletions relative to other trace elements indicates mantle melting occurred at relatively shallow depths above the garnet stability field (e.g. <65 km). All samples have very strong HFSE depletions and on plot well within volcanic arc fields on tectonic discrimination diagrams characteristic of calc-alkaline rocks associated with subduction zones (Figs. 7C). We interpret the arc signature in these rocks to have been inherited from lithospheric mantle sources that had been metasomatized by prior subduction events and/or

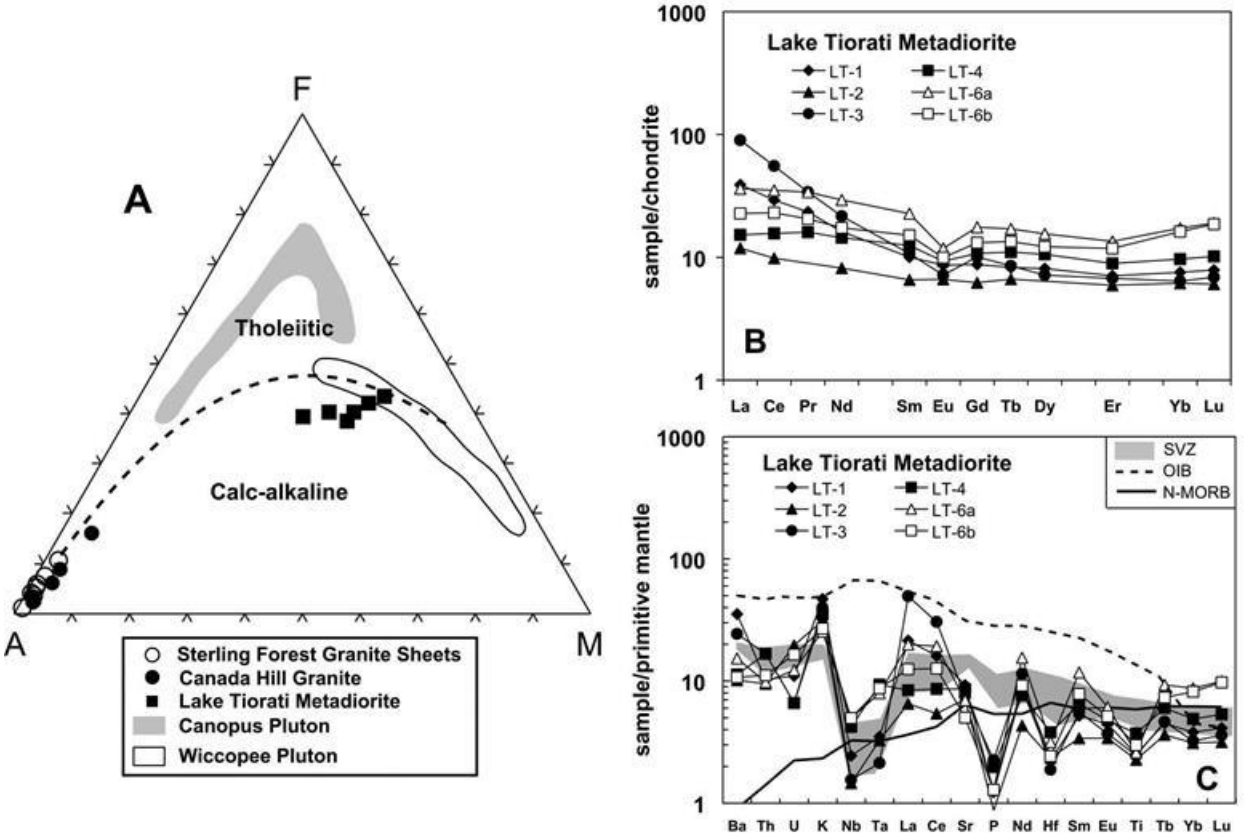

Figure 7. (A) AFM diagram showing the calc-alkaline affinity of the Lake Tiorati Metadiorite in comparison with other Mesoproterozoic mafic plutonic rocks (Canopus and Wiccopee Plutons) from the eastern Hudson Highlands (Ratcliffe, 1992). (B) REE patterns and (C) multi-element diagrams showing the strong volcanic arc chemical signature (LREE-enriched, HFSE-depleted) of the Lake Tiorati Metadiorite. OIB is average oceanic island basalt; N-MORB is average normal mid-ocean ridge basalt; and SVZ is field for Quaternary mafic lavas from the Andean Southern Volcanic Zone (Hickey et al., 1986; López-Escobar et al., 1993). OIB, N-MORB, and normalizing factors are from Sun and McDonough (1989) and Masuda et al., (1973).

extensive crustal contamination during emplacement in the crust.

Late Pegmatite Dikes (post-Ottawan)

The late pegmatitic dikes are pink, and very coarse grained with K-spar, quartz, and locally muscovite, hornblende, magnetite, pyroxene, titanite, and/or garnet depending upon the rock intruded. They are

highly discordant, commonly within brittle faults, and contain xenoliths of fault rocks. They exhibit no deformational fabric. Thickness ranges from 1m to 10m. They are locally associated with small granite bodies. Dodd (1965), Offield (1967), Jaffe and Jaffe (1973), Ratcliffe (1992), and Volkert et al. (2005) have also described similar late, cross-cutting granite pegmatites throughout the New Jersey and Hudson Highlands. Existing radiometric age dates for these late pegmatite dikes include a hornblende $^{40}Ar/^{39}Ar$ ages of 923 ± 2.8 Ma reported by Gates and Krol (1998), and conventional TIMS U-Pb zircon ages of 965 ±10 Ma by Grauch and Aleinikoff (1985) and 986 ±4 Ma and 1004 ±3 Ma by Volkert et al. (2005). Based on limited geochemical information, Volkert et al. (2005) reported that NJ Highlands late pegmatite dikes are dominantly metaluminous, have fractionated A-type geochemical affinities, and share characteristics of the niobium–yttrium–fluorine (NYF) class of pegmatites of Cerny (1992). Based on the available geochronology and field relations, these late pegmatite dikes are interpreted to have been emplaced during a period of postorogenic extension that significantly postdates the gravitational collapse of the Ottawan Orogeny and the late- to post-Ottawan, high-grade, ductile transpressional events (e.g. Indian Hill Shear Zone).

IMPLICATIONS FOR GRENVILLE TECTONICS

The pre-Ottawan history of the western Hudson Highlands spans a ~200 Ma period of the Mesoproterozoic between ~1350 to ~1160 Ma that is strikingly similar to many events recorded in the Canadian Grenville Province, the Adirondacks, and the northern Appalachians. Important tectonomagmatic events include: (1) continental margin arc magmatism (metavolcanic unit; ~1350-1250 Ma); (2) backarc magmatism and sedimentation (metasedimentary unit; ~1300-1230 Ma) , and (3) post-orogenic lithospheric thinning and asthenospheric upwelling (quartzofeldspathic unit, ~1230-1160 Ma). The first two events correspond to the Elzevirian Orogeny in the Grenville Province which is interpreted to have been an Andean-type, continental arc-back arc system with northwestward-dipping subduction that existed along the entire eastern margin of the Laurentia between ~1400 to 1200 Ma (McLelland et al., 1996; Rivers, 1997) (Fig. 8A). The third event corresponds to post-Elzevirian magmatic processes that occurred in other parts of the Grenville Orogen between ~1210-1155 Ma that produced similar A-type metaplutonic rocks by mechanisms that involve crustal melting caused by post-orogenic lithospheric thinning and asthenospheric upwelling (Fig 8B).

One of the principal tectonomagmatic events in the Grenville orogen during the late Mesoproterozoic was the Ottawan Orogeny (~1090–1030 Ma; e.g., McLelland et al., 1996; 2001). The Ottawan Orogeny is thought to have been a Himalayan-style continental collision event with associated crustal thickening, high-grade metamorphism, ductile nappe-style folding in the southeast (e.g., in the Central Granulite Terrane, Adirondack Highlands, and Appalachian massifs) and brittle northwest-directed thrusting farther west (e.g., Grenville Front Tectonic Zone and Central Metasedimentary Belt) in the orogen. This collisional event is thought to be related to the acrretion of various continental masses to form the supercontinent Rodinia (Hoffman, 1988; Dalziel, 1991; Borg and DePaolo, 1994). Although the timing of peak Ottawan orogenesis varies spatially, this event severely affected most rocks older than ~1060 Ma throughout much of the Grenville orogen (e.g., McLelland et al., 1996, 2001; Aleinikoff et al., 2000). Partial melting and migmatization of a variety of source rocks (e.g. metapelites and mafic/intermediate rocks) due to crustal thickening during peak Ottawan metamorphic conditions could explain the petrogenesis of the S-type Canada Hill granite and I-type Sterling Forest granite sheets (Figs. 5 and 8C). These magmatic events would be approximately coeval with events in the Adirondacks that produced the Lyon Mountain granite gneiss at ~1060 Ma. The age and field relations of the Lake Tiorati Diorite

suggests that penetrative deformation assigned to the Ottawan Orogeny as classically defined was finished prior to ~1010 Ma in the Hudson Highlands. Supporting evidence for this statement also comes from the undeformed Mount Eve Granite suite which places a lower limit of ~1020 Ma for penetrative Ottawan metamorphism and deformation in the far western portion of the New Jersey/Hudson

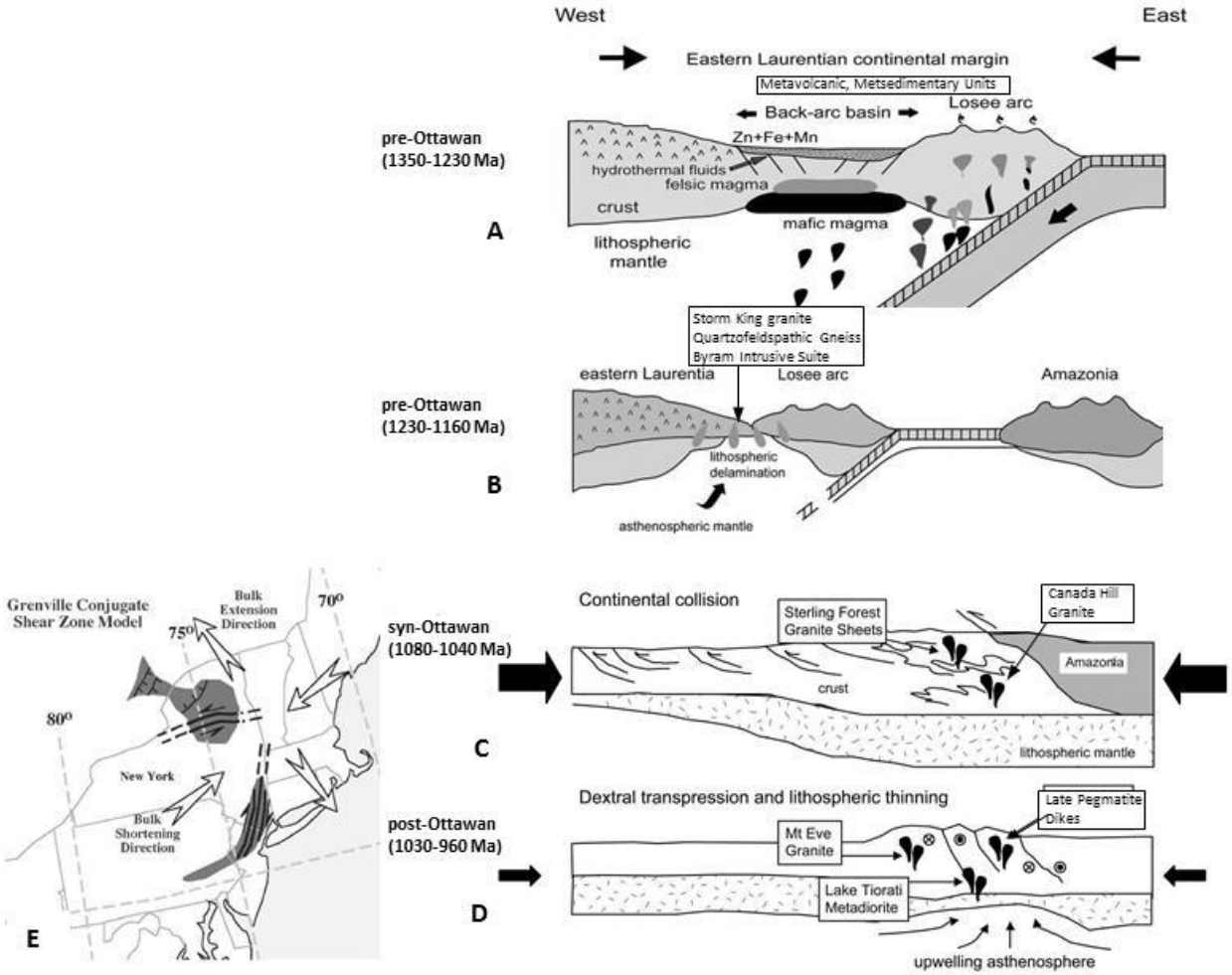

Figure 8. (A – D) Schematic cross-sectional view of model of the pre-Ottawan, syn-Ottawan, and post-Ottawan tectonics in the NJ/Hudson Highlands Diagrams modified from McLelland et al., 1996; Volkert et al., 2010). (E) Regional map view of the NE United States showing the syntaxis tectonic model for the post-Ottawan ductile shearing event that affected the NJ/Hudson Highlands and the Adirondacks (Gates et al., 2004).

Highlands. More recently, Volkert et al (2010) obtained a U-Pb SHRIMP zircon crystallization age of an undeformed granite from the NJ Highlands of 1027 ±6 Ma which pushes the lower limit of Ottawan deformation further back to ~1030 Ma.

The presence of large-scale, vertical strike-slip ductile shear zones that cross-cut rocks of ~1010 Ma indicates that the late- to post-Ottawan history in the Hudson Highlands is characterized by a high-grade, dextral transpressional shearing event that occurred between ~1010 to 925 Ma (Gates et al., 2004) (Fig. 8D). This event likely represents final adjustments of the amalgamated Rodinian supercontintent and/or another accretionary event that must have occurred far to the north of the Hudson Highlands. A collision in the area of the Canadian Appalachians and Scandinavia may have generated tectonic escape (e.g., Tapponnier et al., 1982; Burke and Sengor, 1986) of eastern Laurentia

to the south along large dextral strike-slip faults (Fig. 8E). The strike-slip environment could explain the temporal association of the late- to post Ottawan granitoid suite described here (Lake Tiorati Diorite, Late Pegmatite Dikes, Mount Eve Granite). Collectively, these granitioids consist of small, dispersed plutonic bodies that form a volumetrically minor, chemically diverse group. Localized crustal heating due to upwelling asthenosphere associated with localized extension and/or transtension in the overall dextral transpressional regime could explain the small volumes and limited areal extent of these granitoids (Fig. 8D). A similar transpressional tectonic model has been proposed by Speer et al. (1994) to explain the occurrence of small volume, chemically diverse plutonic suites of Alleghenian age in the southern Appalachians. This type of model may explain similar small volume occurrences of late- to post-Ottawan (ca 1030–930 Ma) granitoids elsewhere in the Grenville orogen, particularly in the Adirondacks (e.g., Lyonsdale Bridge and Cathead Mountain pegmatites; McLelland et al., 2001) and the Green Mountain massif (e.g., Stamford Hill rapakivi granite; Ratcliffe et al., 1991). Although additional data is needed, the late pegmatite dikes in the western Hudson Highlands are interpreted to have been emplaced during a period of postorogenic extension that significantly postdates the gravitational collapse of the Ottawan Orogeny and the late- to post-Ottawan, high-grade, ductile transpressional events (e.g. Indian Hill Shear Zone).

REFERENCES

Aleinikoff, J.N., Burton, W.C., Lyttle, P.T., Nelson, A.E., and Southworth, C.S., 2000, U-Pb geochronology of zircon and monazite from Mesoproterozoic granitic gneisses of the northern Blue Ridge, Virginia and Maryland, USA: Precambrian Research, v. 99, p. 113-146.

Aleinikoff, J.N., Grauch, R.I., Mazdab, F.K., Kwak, L., Fanning, C.M., and Kamo, S.L., 2012, Origin of an unusual monazite-xenotime gneiss, Hudson Highlands, New York: SHRIMP U-Pb geochronology and trace element geochemistry: American Journal of Science, Vol. 312, September, p. 723–765, DOI 10.2475/07.2012.02.

Berkey, C.P., 1907, Structural and stratigraphic features of the basal gneisses of the Highlands: New York State Museum Bulletin, v. 107, p. 361-378.

Berkey, C.P. and Rice, M., 1919, Geology of the West Point quadrangle, New York: New York State Museum Bulletin, v. 225-226, 152 p.

Borg, S.C., and DePaolo, D.J., 1994, Laurentia, Australia, and Antarctica as a Late Proterozoic supercontinent: Constraints from isotopic mapping: Geology, v. 22, p. 307-310.

Burke, K., and Sengor, C., 1986, Tectonic escape in the evolution of the continental crust, In Barazangi, M., and Brown, L., (eds.), Reflection Seismology: The Continental Crust, American Geophysical Union Geodynamics Series, v. 14, p. 41-53.

Carr, S.D., Easton, R.M., Jamieson, R.A., and Culshaw, N.G., 2000, Geologic transect across the Grenville orogen of Ontario and New York: Canadian Journal of Earth Sciences, v. 37, p. 193-216.

Cerny, P., 1992, Geochemical and petrogenetic features of mineralization in rare-element granitic pegmatites in light of current research, Appl. Geochem. 7, 393–416.

Dallmeyer, R.D., 1972, Precambrian structural history of the Hudson Highlands near Bear Mountain, New York: Geological Society of America Bulletin, v. 83, p. 895-904.

Dallmeyer, R.D., 1974, Metamorphic history of the northeastern Reading Prong, New York and northern New Jersey: Journal of Petrology, v. 15, p. 325-359.

Dallmeyer, R.D., and Dodd, R.T., 1971, Distribution and significance of cordierite in paragniesses of the Hudson Highlands, southeastern New York: Contributions to Mineralogy and Petrology, v. 33, p. 289-308.

Dalziel, I.W.D., 1991, Pacific margins of Laurentia and East Antarctica-Australia as a conjugate rift pair: Evidence and implications for an Eocambrian supercontinent: Geology, v. 19, p. 598-601.

Davidson, A., 1995, A review of the Grenville orogen in its North American type area: Journal of Australian Geology and Geophysics, v. 16, p. 3-24.

Dodd, R.T., 1965, Precambrian geology of the Popolopen Lake quadrangle, southeastern New York: New York State Musuem Map and Chart Series, v. 6.

Drake, A.A., Jr., Aleinikoff, J.N., and Volkert, R.A., 1991, The Mount Eve Granite (Middle Proterozoic) of northern New Jersey and southeastern New York, in Drake, A.A., Jr., ed., Contributions to New Jersey Geology: U.S. Geological Survey Bulletin, 1952, p. C1-C10.

Easton, R.M., 1986, Geochronology of the Grenville Province: in Moore, J.M. Moore, Davidson, A., and Baer, A.J., eds., The Grenville Province: Geological Association of Canada Special Paper 31, p. 127-173.

Gates, A.E., 1995, Middle Proterozoic dextral strike-slip event in the central Appalachians: Evidence from the Reservoir fault, New Jersey: Journal of Geodynamics, v. 19, p. 195-212.

Gates, A.E., 1998, Early compression and late dextral transpression within the Grenvillian Event of the Hudson Highlands, NY, USA: in Sinha, A.K., ed., Basement Tectonics 13; Dordrecht, The Netherlands, Kluwer Academic Publishers, p. 85-98.

Gates, A.E., and Costa, R.E., 1998, Multiple reactivations of rigid basement block margins: Examples in the northern Reading Prong, USA, in Gilbert, M. C. and Hogan, J.P., eds., Basement Tectonics 12: Central North America and Other Regions; Dordrecht, The Netherlands, Kluwer Academic Publishers, p. 123-153.

Gates, A.E., and Krol, M.A., 1998, Kinematics and thermochronology of late Grenville escape tectonics from the central Appalachians: Geological Society of America Abstracts with Programs, v. 30-7, p. A-124.

Gates A.E., Valentino, D.W., Gorring, M.L., Chiarenzelli, J.R., and Hamilton, M.A., 2001, Bedrock geology, geochemistry, and geochronology of the Grenville Province in the western Hudson Highlands, New York: In Gates, A.E., ed., 73rd New York State Geological Association Guidebook, p. 176-203.

Gates, A.E., Valentino, D.W., Chiarenzelli, J.R., Solar, G.S., and Hamilton, M.A., 2004, Exhumed Himalayan-type syntaxis in the Grenville orogen, northeastern Laurentia: Journal of Geodynamics, v. 37, p. 337-359, doi:10.106/j.jog.2004.02.011

Gorring, M.L., Gates, A., Valentino, D., and Chiarenzelli, J., 2001, Magmatic history and geochemistry of meta-igneous rocks from the SW Hudson Highlands, NY: Tectonic implications and regional correlations, Geological Society of America Annual Meeting, 33-6, A-91.

Gorring, M.L., Gates, A., Valentino, D., and Chiarenzelli, J., 2002, Post-Ottawan magmatic history and geochemistry of intrusive rocks from southwestern Hudson Highlands, NY: plutonism related to ductile transpressional deformation?: Geological Society of America Abstracts with Programs, v. 34-1.

Gorring, M.L., Estelle, T.C., and Volkert, R.A., 2004, Geochemistry of the late Mesoproterozoic Mount Eve Granite suite: Implications for late to post-Ottawan tectonics in the New Jersey–Hudson Highlands, *in* Tollo, R.P., Corriveau, L., McLelland, J.M., and Bartholomew, M.J., eds., ProterozoicTectonic Evolution of the Grenville Orogen in North America: Geological Society of America Memoir 197, p. 505–523.

Grauch, R. I., and Aleinikoff, J. N., 1985, Multiple thermal events in the Grenvillian orogenic cycle, Origin of an unusual monazite-xenotime gneiss, Hudson: Geochronologic evidence from the northern Reading Prong, New York–New Jersey, Geological Society of America Abstracts with Programs, v. 17, p. 596.

Hamilton, M.A., McLelland, J., and Selleck, B., 2004, SHRIMP U-Pb zircongeochronology of the anorthosite-mangerite-charnockite-granite suite, Adirondack Mountains, New York, *in* Tollo, R.P., Corriveau, L., McLelland , J.M., and Bartholomew, M.J., eds., Proterozoic Tectonic Evolution of the Grenville Orogen in North America: Geological Society of America Memoir 197, p. 337–355.

Helenek, H.L., 1971, An investigation of the origin, structure, and metamorphic evolution of major rock units in the Hudson Highlands: Providence, R.I., Brown University, unpublished Ph.D. thesis, 244 p.

Helenek, H.L., and Mose, D.G., 1984, Geology and geochronology of Canada Hill Granite and its bearing on the timing of Grenvillian events in the Hudson Highlands, New York: in Bartholomew, M.J., ed., Grenville Events and Related Topics in the Appalachians: Geological Society of America Special Paper 194, p. 57-73.

Heumann, M.J., Bickford, M.E., Hill, B.M., McLelland, J.M., Selleck, B.W., and Jercinovic, M.J., 2006, Timing of anatexis in metapelites from the Adirondack lowlands and southern highlands: A manifestation of the Shawinigan orogeny and subsequent anorthosite-mangerite-charnockite-granite magmatism: Geological Society of America Bulletin, v. 118, p. 1283–1298, doi:10.1130/B25927.1.

Hickey, R.L., Frey, F.A, Gerlach, D.C., and López-Escobar, L., 1986, Multiple sources for basaltic arc rocks from the Southern Volcanic Zone of the Andes (34-41°S): Trace element and isotopic evidence for contributions from subducted oceanic crust, mantle, and continental crust: Journal of Geophysical Research, v. 91, p. 5963-5983.

Hoffman, P.F., 1988, United plates of America, the birth of a craton: Early Proterozoic assembly and growth of Laurentia: Annual Review Earth and Planetary Sciences, v. 16, p. 543-604.

Jaffe, W.H, and Jaffe, E.B., 1973, Bedrock geology of the Monroe quadrangle, Orange County, New York: New York State Musuem Map and Chart Series, v. 20.

Linguanti, C., Valentino, D.W., Gorring, M.L., and Gates, A.E., 2011, Synorogenic emplacement of granite sheets, Hudson Highlands, New York: Geological Society of America Abstracts with Programs, v. 43-1, p.149, abstract #61-13.

López-Escobar, L., Kilian, R., Kempton, P.D. and Tagiri, M., 1993, Petrography and geochemistry of Quaternary rocks from the Southern Volcanic Zone of the Andes between 41°30' and 46°00'S: Revista Geologico de Chile, v. 20, p. 33-55.

Lowe, K.E., 1950, Storm King granite at Bear Mountain, New York: Geological Society of America Bulletin, v. 61, p.137-190.

Lumbers, S.B., Heaman, L.M., Vertoli, V.M., and Wu, T.-W., 1990, Nature and timing of Middle Proterozoic magmatism in the Central Metasedimentary Belt, Ontario, in Gowers, C., Rivers, T., and Ryan, C., eds., Mid-Preoterozoic Laurentia-Baltica: Geological Association of Canada Special Paper, v. 38, p. 243-276.

Masuda, A., Nakamura, N., and Tanaka, T., 1973, Fine structures of mutually normalized rare-earth patterns of chondrites: Geochimica et Cosmochimica Acta, v. 37, p. 239-248.

McLelland, J.M, and Chiarenzelli, J., 1990, Geochronological studies in the Adirondack Mts. and the implications of a Middle Proterozoic tonalitic suite, in Gowers, C., Rivers, T., and Ryan, C., eds., Mid-Preoterozoic Laurentia-Baltica: Geological Association of Canada Special Paper, v. 38, p. 175-194.

McLelland, J.M, and Whitney, P., 1990, Anorogenic, bimodal emplacement of anorthositic, charnockitic, and related rocks in the Adirondack Mountains, New York, in Stein, H.J., and Hannah, J.L., eds., Ore-bearing Granite Systems, Petrogenesis, and Mineralizing Processes: Geological Society of America Special Paper 246, p. 301-315.

McLelland, J.M, Daly, S., and McLelland, J.M., 1996, The Grenville Orogenic Cycle (ca 1350-1000 Ma): an Adirondack perspective: Tectonophysics, v. 265, p. 1-28.

McLelland, J.M, Hamilton, M., Selleck, B., McLelland, J., Walker, D., and Orrell, S., 2001, Zircon U-Pb geochronology of the Ottawan Orogeny, Adirondack Highlands, New York: regional and tectonic implications: Precambrian Research, v. 109, p. 39-72.

McLelland, J.M, Bickford, M.E., Hill, B., Clechenko, C. C., Valley, J.W., and Hamilton, M.A., 2004, Direct dating of Adirondack massif anorthosite by U-Pb SHRIMP analysis of igneous zircon: Implications for AMCG complexes: Geological Society of America Bulletin, 116; no. 11/12; p. 1299–1317; doi: 10.1130/B25482.1.

Offield, T.W., 1967, Bedrock geology of the Goshen-Greenwood Lake area, New York: New York State Museum and Science Service Map and Chart Series, v. 9, 78 p.

Passchier, C.W., and Simpson, C., 1986, Porphyroclast systems as kinematic indicators: Journal of Structural Geology, v. 8, p. 31-843.

Pearce, J.A., Harris, N.B.W., and Tindle, A.G., 1984, Trace element discrimination diagrams for the tectonic interpretation of granitic rocks: Journal of Petrology, v. 25, p. 956-983.

Peck, W.H., Valley, J.W., Corriveau, L., Davidson, A., McLelland, J., and Farber, D.A., 2004, Oxygen-isotope constraints on terrane boundaries and origin of 1.19–1.13 Ga granitoids in the southern Grenville Province, *in* Tollo, R.P., Corriveau, L., McLelland, J.M., and Bartholomew, M.J., eds., Proterozoic Tectonic Evolution of the Grenville Orogen in North America: Geological Society of America Memoir 197, p. 163–182.

Peterson, E.K., Gorring, M.L., Valentino, D.W., and Gates, A.E., 2011, Geochemical analysis and regional correlation between granitic gneisses of the western Hudson Highlands, NY: Geological Society of America Abstracts with Programs, v. 43-1, p.64. abstract #9-13

Rankin, D.W., 1975, The continental margin of eastern North America in the southern Appalachians: the opening and closing of the proto-Atlantic Ocean: American Journal of Science, v. 275-A, p. 298-336.

Rankin, D.W., Drake, A.A., Jr., Glover, L., III, Goldsmith, R., Hall, L.M., Murray, D.P., Ratcliffe, N.M., Read, J.F., Secor, D.T. Jr., and Stanley, R.S., 1989, Pre-orogenic terranes, in Hatcher, R.D., Jr., Thomas, W.A., and Vield, G.W., eds., The Appalachian-Ouachita orogen in the United States: Boulder, Colorado, Geological Society of America, The Geology of North America, v. F-2, p. 7-100.

Ratcliffe, N.M., 1992, Bedrock geology and seismotectonics of the Oscawana Lake quadrangle, New York: United States Geological Survey Bulletin 1941-B, 38 p.

Ratcliffe, N.M., and Aleinikoff, J.N., 2001, Pre-Ottawan deformation and transpressional faulting in the Hudson Highlands of New York based on SHRIMP zircon ages of the Storm King Granite and the syntectonic Canopus pluton: Geological Society of America Abstracts with Programs, v. 33-1, p. A-5.

Ratcliffe, N.M., Aleinikoff, J.N., Burton, W.C., and Karabinos, P., 1991, Trondhjemitic, 1.35-1.31 Ga gneisses of the Mount Holly Complex of Vermont: evidence for an Elzeverian event in the Grenville basement of the United States Appalachians: Canadian Journal of Earth Sciences, v. 28, p. 77-93.

Rivers, T., 1997, Lithotectonic elements of the Grenville Province: review and tectonic implications: Precambrian Research, v. 86, p. 117-154.

Speer, J.A., McSween, H.Y., and Gates, A.E., 1994, Generation, segregation, ascent, and emplacement of Alleghenian plutons in the southern Appalachians: Journal of Geology, v. 102, p. 249-267.

Sun, S-s., and McDonough, W.F., 1989, Chemical and isotopic systematics of oceanic basalts; implications for mantle composition and processes: In Saunders, A.D. and Norry, M.J., (eds.), Magmatism in the Ocean Basins, Geological Society Special Publication, v. 42, p. 313-345.

Tapponier, P., Peltzer, G., Le Dain, A.Y., Armigo, R., and Cobbold, P., 1982, Propogating extrusion tectonics in Asia: new insights from simple experiments with plasticine: Geology, v. 10, p. 611-616.

Valentino, D., Gates, A., and Chiarenzelli, J., 2001, Geologic history of the Hudson Highlands basement massif: results from new geologic mapping in the Monroe and Sloatsburg Quads: Geological Society of America Abstracts with Programs, v. 33-1, p. A-31.

Verrengia, P., and Gorring, M.L., 2002, Geochemistry and tectonic implications of the Storm King Granite, Hudson Highlands, NY: Geological Society of America Abstracts with Programs, v. 34-1.

Volkert, R.A., and Drake, A.A., Jr., 1999, Geochemistry and stratigraphic relations of Middle Proterozoic rocks of the New Jersey Highlands, in Drake, A.A., Jr., ed., Geologic Studies in New Jersey and Eastern Pennsylvania: U.S. Geological Survey Professional Paper 1565-C, 77 p.

Volkert, R.A., Feigenson, M.D., Patino, L.C., Delaney, J.S., and Drake, A.A., Jr., 2000, Sr and Nd isotopic composition, age and petrogenesis of A-type granitoids of the Vernon Supersuite, New Jersey Highlands, USA: Lithos, v. 50, p. 325-347.

Volkert, R.A., 2004, Mesoproterozoic rocks of the New Jersey Highlands, northcentral Appalachians: Petrogenesis and tectonic history, *in* Tollo, R.P., Corriveau, L., McLelland, J.M., and Bartholomew, M.J., eds., Protero zoic Tectonic Evolution of the Grenville Orogen in North America: Geological Society of America Memoir 197, p. 697–728.

Volkert, R.A., Zartman, R.E., and Moore, P.B., 2005, U–Pb zircon geochronology of Mesoproterozoic postorogenic rocks and implications for post-Ottawan magmatism and metallogenesis, New Jersey Highlands and contiguous areas, USA: Precambrian Research, v. 139, p. 1-19, doi:10.1016/j.precamres.2005.06.003

Volkert, R.A, Aleinikoff, J.N., and Fanning, C.M., 2010, Tectonic, magmatic, and metamorphic history of the New Jersey Highlands: New insights from SHRIMP U-Pb geochronology, *in* Tollo, R.P., Bartholomew, M.J., Hibbard, J.P., and Karabinos, P.M., eds., From Rodinia to Pangea: The Lithotectonic Record of the AppalachianRegion: Geological Society of America Memoir 206, p. 307–346, doi: 10.1130/2010.1206(14).

Walsh, G. J., Aleinikoff, J. N., and Fanning, C. M., 2004, U-Pb geochronology and evolution of Mesoproterozoic basement rocks, western Connecticut, *in* Tollo, R. P., Corriveau, L., McLelland, J. M., and Bartholomew, M. J., editors, Proterozoic Tectonic Evolution of the Grenville Orogen in North America: Boulder, Colorado, Geological Society of America Memoirs, v. 197, p. 729–754, http://dx.doi.org/10.1130/0-8137-1197-5.729

Wasteneys, H., McLelland, J., and Lumbers, S., 1999, Precise zircon geochronology in the Adirondack Lowlands and implications for revising plate tectonic models of the Central Metasedimentary Belt and Adirondack Mountains, Grenville Province, Ontario and New York: Canadian Journal of Earth Science, v. 36, p. 967-984.

APPENDIX

Table 1: Representative analyses of pre-Ottawan Highland granitoids

Unit	Sterling Forest quartzofeldspathic gneiss					Storm King granite gneiss					
Sample	SF-41	SF-47	SF-48	SF-49	SF-50	SK-1	SK-2	SK-3	SK-6	SK-8	SK-9
SiO_2 (wt%)	72.17	72.60	72.69	72.75	72.29	70.19	71.77	70.77	74.03	72.44	72.83
TiO_2	0.42	0.29	0.31	0.30	0.29	0.35	0.18	0.23	0.22	0.28	0.35
Al_2O_3	13.63	12.32	12.82	12.53	12.78	13.80	12.69	11.60	11.82	11.39	11.76
$Fe_2O_{3\ (T)}$	3.50	3.20	3.54	3.47	3.36	5.06	3.19	4.43	3.61	4.21	4.39
MnO	0.04	0.02	0.04	0.05	0.04	0.05	0.04	0.05	0.04	0.05	0.05
MgO	0.20	0.69	0.23	0.18	0.20	0.11	0.09	0.08	0.09	0.12	0.20
CaO	1.41	0.72	1.29	1.25	1.06	1.69	1.42	1.11	0.96	1.05	1.19
Na_2O	3.53	2.76	2.76	3.21	3.10	3.33	3.27	3.39	3.55	3.41	3.60
K_2O	5.97	5.33	5.69	5.60	5.52	5.61	5.61	5.21	5.36	5.45	5.32
P_2O_5	0.08	0.04	0.04	0.04	0.04	0.04	0.04	0.04	0.03	0.03	0.06
Total	100.96	97.99	99.41	99.38	98.68	100.23	98.30	96.91	99.71	98.43	99.75
La (ppm)	51	68	123	80	67	55	97	208	58	154	84
Ce	108	168	233	168	148	108	201	367	123	283	180
Pr	14.7	23.1	26.5	20.4	18.0	15.6	25.6	43.2	15.0	33.7	21.9
Nd	62	99	98	83	73	66	102	154	57	121	82
Sm	12.9	21.8	17.7	16.8	14.9	15.4	22.3	24.4	11.1	19.3	15.9
Eu	2.93	1.99	2.06	2.18	2.09	2.38	1.07	1.41	1.52	1.50	1.58
Gd	12.1	18.7	16.5	15.9	13.7	8.8	12.4	12.8	6.8	10.5	9.1
Tb	1.88	2.85	2.35	2.47	2.14	1.56	2.34	1.96	1.14	1.50	1.48
Dy	10.3	15.2	12.6	14.0	12.0	12.3	19.5	14.1	8.2	10.4	11.2
Ho	2.03	2.86	2.43	2.85	2.38	2.48	3.87	2.81	1.68	2.17	2.25
Er	4.86	6.45	5.89	6.96	5.85	7.09	11.02	8.56	5.03	6.80	6.70
Tm	0.73	0.92	0.87	1.09	0.91	0.90	1.30	1.06	0.69	0.89	0.86
Yb	4.74	5.51	5.48	7.52	5.99	5.92	8.05	7.29	4.79	6.16	5.95
Lu	0.77	0.80	0.81	1.19	0.92	0.94	1.15	1.14	0.77	1.00	0.96
Sr	134	82	95	88	95	38	25	16	16	17	34
Ba	1189	634	656	772	833	439	147	129	186	174	254
Cs	0.32	0.35	0.34	1.13	1.61	0.61	0.57	0.56	0.51	0.57	0.63
Rb	125	177	214	154	177	115	171	148	130	181	166
U	0.98	1.04	2.62	3.10	1.27	2.97	6.52	4.00	1.63	4.44	3.16
Th	2.3	3.0	54	9.4	3.7	3.1	19	31	3.9	27	9.9
Y	53.6	76.0	70.6	80.1	66.0	69.2	109	78.4	47.1	61.4	62.9
Zr	550	329	344	446	440						
Hf	13.9	9.2	9.7	11.8	11.6	14.6	8.4	13.1	13.5	11.9	12.4
Nb	20.8	18.1	16.9	21.9	18.4	27.1	34.3	36.5	22.0	31.3	34.1
Ta	1.21	0.59	0.58	1.53	1.18	1.27	1.45	1.52	1.12	1.88	1.92
Sc	5.7	7.5	5.7	4.4	3.8		3.4		2.2		0.4
Cr	3.2	2.0	3.0	2.3	3.4	6.0	4.4	5.3	3.7	3.7	3.7
Ni	8.6	4.4	5.1	4.3	5.0						
Co	2.0	3.8	2.4	2.8	2.0	1.3	1.3	1.5	1.3	1.7	2.5
V	9.8	6.2	6.1	5.9	5.7	16.2	16.8	31	5.1	8.7	10.3

Major elements, Sr, Ba, Zr, Y, and Sc by ICP-OES; all other elements by ICP-MS
All analyses carried out at Montclair State University

Table 2: Representative geochemical analyses of syn- and post-Ottawan W. Hudson Highlands granitoids

Unit	Sterling Forest granite sheets					Lake Tiorati Metadiorite						Canada Hill Granite					
Sample	SF-28	SF-29	SF-31	SF-35	SF-36	LT-1	LT-2	LT-3	LT-4	LT-6a	LT-6b	CH-14	CH-16	CH-23	CH-37	CH-40	CH-42
SiO_2 (wt%)	75.57	76.01	74.97	75.25	74.83	50.66	51.02	49.71	50.94	51.78	49.09	71.66	71.18	71.06	74.38	72.62	71.64
TiO_2	0.04	0.03	0.02	0.05	0.10	0.54	0.49	0.53	0.80	0.57	0.64	0.03	0.04	0.06	0.07	0.45	0.03
Al_2O_3	14.18	13.73	13.41	13.55	13.57	15.63	15.34	14.63	18.54	13.74	12.92	15.00	14.23	15.02	15.83	14.29	15.08
$Fe_2O_{3\,(T)}$	0.41	0.51	0.17	0.47	1.18	9.09	8.36	9.34	7.99	10.12	11.48	1.64	0.77	0.38	0.51	2.35	0.17
MnO	0.02				0.02	0.14	0.16	0.15	0.10	0.16	0.18	0.05	0.02	0.00	0.00	0.01	0.00
MgO	0.10	0.07	0.05	0.07	0.20	6.90	7.40	7.91	5.42	8.59	9.90	0.29	0.19	0.26	0.20	0.69	0.06
CaO	1.06	1.32	0.80	0.87	1.39	10.61	12.27	12.41	10.00	11.77	11.86	1.20	0.99	0.47	3.90	1.16	1.64
Na_2O	4.61	3.64	2.73	3.53	3.43	3.66	3.52	3.09	4.38	2.96	2.48	3.37	2.98	1.44	3.06	3.58	4.83
K_2O	3.85	3.94	7.48	5.34	4.89	1.39	0.93	1.19	1.05	0.77	0.80	6.18	6.74	9.73	2.51	4.43	2.76
P_2O_5	0.01	0.01	0.02	0.02	0.02	0.03	0.02	0.05	0.04	0.03	0.03	0.07	0.09	0.09	0.01	0.07	0.07
Total	99.86	99.26	99.65	99.15	99.63	98.65	99.51	99.01	99.26	100.48	99.38	99.49	97.23	98.50	100.47	99.65	96.29
La (ppm)	7.2	7.5	9.2	5.9	35.0	14.7	4.5	34.0	5.8	13.7	8.6	15.6	27.2	15.2	10.5	21.7	43.5
Ce	15.5	10.5	13.2	9.9	67.1	28.6	9.6	54.1	15.3	34.3	22.5	27.2	57.6	28.6	11.3	81.4	114.2
Pr	2.1	1.3	1.6	1.3	7.3	3.5	1.7	5.1	2.4	5.1	3.1	3.3	5.8	4.1	1.7	5.1	9.1
Nd	7.0	3.0	4.1	3.4	24.8	11.6	5.8	15.5	10.3	21.0	12.4	10.7	20.4	14.7	4.3	18.0	32.1
Sm	1.94	0.35	0.54	0.64	4.19	2.31	1.51	2.47	2.87	5.22	3.48	2.18	4.60	3.20	0.26	4.44	6.51
Eu	0.23	0.45	0.67	0.35	0.64	0.75	0.57	0.62	0.81	1.03	0.86	1.82	1.80	2.87	1.33	1.12	1.29
Gd	2.43	0.51	0.63	1.20	3.94	2.72	1.93	3.14	3.35	5.47	4.09	2.80	4.87	3.01	0.89	4.37	3.98
Tb	0.56	0.08	0.09	0.30	0.46	0.49	0.39	0.50	0.65	1.00	0.79	0.74	1.03	0.38	0.06	1.23	0.77
Dy	4.22			2.32	1.82	3.16	3.04	2.79	4.13	6.06	4.75	6.94	6.77	2.15	0.46	8.18	3.50
Ho	1.08	0.06	0.06	0.61	0.36	0.64	0.54	0.60	0.89	1.40	1.19	2.06	1.54	0.49	0.11	1.69	0.51
Er	3.48	0.47	0.41	1.87	1.13	1.80	1.51	1.72	2.28	3.44	3.02	7.49	4.50	1.69	0.34	4.76	0.94
Tm	0.67	0.07	0.05	0.33	0.15	0.27	0.24	0.26	0.42	0.70	0.62	1.40	0.70	0.34	0.07	0.77	0.11
Yb	5.66	0.40	0.25	2.22	0.92	1.88	1.53	1.59	2.41	4.30	4.03	9.98	4.33	2.57	0.53	5.07	0.55
Lu	1.00	0.06	0.03	0.36	0.15	0.30	0.23	0.27	0.39	0.74	0.72	1.63	0.67	0.45	0.11	0.79	0.08
Sr	21	53	74	30	60	195	150	158	181	147	106	168	161	195	177	176	178
Ba	22	113	334	97	224	247	71	170	79	107	75	626	638	488	145	377	366
Cs	0.15	0.20	0.71	0.38	0.36	0.17	0.15	0.22	0.09	0.04							
Rb	133	74	139	125	163	27.5	10.6	22.6	13.9	8.8	8.0	175	191	220	63	161	77
U	4.88	0.96	0.67	2.45	6.42	0.23	0.41	0.14	0.14	0.26	0.35	1.57	4.06	1.73	1.87	11.9	3.42
Th	3.12	1.06	2.20	7.99	30.3	0.88	0.81	1.42	1.42	0.83	0.95	4.5	11.7	7.0	0.3	19.0	21.4
Y	33.7	1.6	3.0	20.6	11.6	18.2	14.4	16.5	24	40.2	34.7	62.5	47.7	15.0	3.3	53.9	14.0
Zr	22	50	19		134	29	22	25	43	40	28	24.1	77.1	3.7	134.7	130.1	38.2
Hf	0.29	1.72	0.19	1.14	3.67	0.69	0.73	0.58	1.17	0.98	0.75	0.94	2.76	0.26	5.48	4.32	1.35
Nb	15.1	0.6	0.2	0.5	0.4	1.7	1.0	1.1	3.0	3.5	3.5		1.3		1.3	30.8	
Ta	0.98	0.19	0.06	0.01	0.01	0.14	0.13	0.09	0.38	0.33	0.36	0.04	0.17	0.07	0.18	1.29	0.05
Sc	3.6	0.4	2.2	5.4	1.9	45.0	50.6	51.7	32.1	52.4	53.6						
Cr	1.8	1.9	2.1	2.2	3.2	41	91	135	198	137	133	1.8	3.1	1.6	8.4	16.5	5.8
Ni	4.4	2.5	2.2	1.4	2.3	56	65	160	64	73	99		5.8		7.3	0.8	0.1
Co	1.4	1.2	0.4	0.8	1.2	34	36	49	31	40	50	1.7	1.6	2.2	1.8	5.9	1.6
V	5.3	7.5	5.2	5.1	9.4	136		220	271	190	208	4.2	25.6	4.7	12.9	26.6	8.1

Major elements, Sr, Ba, Zr, Y, and Sc by ICP-OES at Montclair State University; all other elements by ICP-MS at Montclair State University

FIELD GUIDE AND ROAD LOG

Meeting Point: Lobby parking lot of DoubleTree by Hilton Hotel Nanuet. Turn right off of NYS 59 eastbound onto Rose Rd and then quick right into parking lot.

Meeting Point Coordinates: 41° 5'24.84"N, 73°59'43.90"W; address = 425 State Route 59; Nanuet, New York 10954

Meeting Time: 8:00 AM

Distance in miles (km)

Cumu-lative	Point to Point	Route Description
0.0 (0.0)	0.0 (0.0)	Assemble in the lobby parking lot of DoubleTree by Hilton Hotel Nanuet. Leave parking lot and turn left onto Rose Rd. and immediately right onto NY-59 and proceed east.
0.5 (0.8)	0.5 (0.8)	Use the right lane to the ramp for Palisades Interstate Pkwy North and then merge and proceed north the Palisades Interstate Pkwy.
17.1 (27.4)	16.6 (26.6)	Use the right lane to the ramp for Palisades Interstate Pkwy North and then merge onto Palisades Interstate Pkwy North.
17.4 (27.8)	0.3 (0.5)	Bear slightly right at Exit 18 continue northeastward on US-6 East/ Palisades Interstate Pkwy North and then take Exit 19 Sevens Lakes Drive and merge onto Seven Lakes Drive.
17.9 (28.6)	0.5 (0.8)	Proceed southeastward on Seven Lakes Drive. At 0.5 miles, turn right at unmarked dirt road and pull into small informal parking lot (Stop 1). If you drive by the AT crossing or intersection of with Perkins Memorial Drive (on left), you have gone too far east and need to turn around and go west 0.25 mi on Seven Lakes Drive.

STOP 1: Bear Mountain, NY

Location Coordinates: (41°18'16.37"N, 74° 0'54.94"W)

The next series of substops will require a moderately strenous hike (~5-6 miles roundtrip; 600 vertical feet of elevation change) mostly along the Appalachian Trail and the Perkins Memorial Drive (paved) to the summit of Bear Mountain. On the way, we will examine very nice exposures of not only the Canada Hill granite and Storm King granite gneiss, but also take the opportunity to look at outcrops of the "rusty" metapelitic gneisses of the Metasedimentary Lithofacies and the quartz-plagioclase-biotite-Opx ("charnockitic") gneiss of the Metavolcanic Lithofacies. We will examine the field relations between these units and discuss the current U-Pb zircon age constraints and whole-rock geochemical data to understand the petrogenesis and implications for Grenville tectonics in the region. Bring food and water. We will be out all morning and will have lunch at the summit of Bear Mountain.

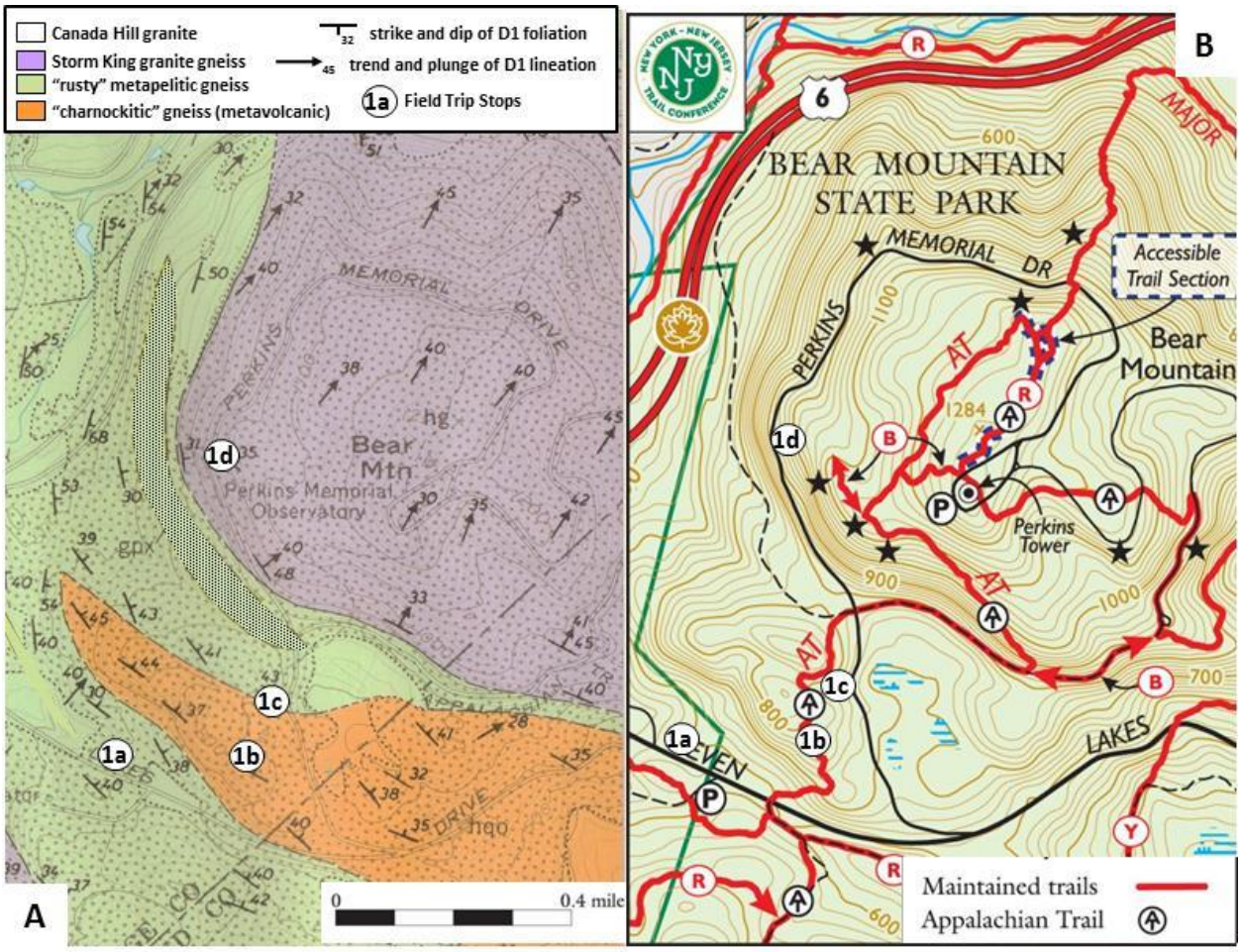

Figure 9. (A) Geologic and (B) topographic map showing the location of Stops 1a-1d at Bear Mountain, NY. Geologic map modified from Dodd (1965).

Stop 1a: The first of several stops during our hike is a very nice roadcut exposure of the "rusty" metapelitic gneiss unit of the Metasedimentary Lithofacies. The distinctive "rusty" weathering of this unit is from the alteration and breakdown of accessory Fe-sulfides (pyrite and/or marcasite?). At this locality, the metapelite has a fairly common assemblage of garnet-biotite-quartz-K-feldspar ± plagioclase ± sillimanite and has a strong foliation that is moderately NE-dipping. Metamorphism is of hornblende granulite facies and maximum P-T estimates are on the order of 700-750ºC and 4±1 kilobar based on mineral assemblages in metapelitic and mafic metavolcanic units (Dallmeyer and Dodd, 1971). Deformation and metamorphism associated with this event is most likely of Ottawan age.

Stop 1b: On the southwest flanks of Bear Mountain along the Appalachian Trail there are a series of excellent natural outcrops of the quartz-plagioclase-biotite-Opx ("charnockitic") gneiss of the Metavolcanic Lithofacies with a strong foliation that is moderately NE-dipping. We will make a quick stop to examine one of these outcrops. These rocks are significant because they presumably the oldest rocks in Hudson Highlands. Based on a U-Pb SHRIMP zircon core ages ranging from ~1360-1250 Ma (Volkert et al., 2010) on the correlative Losee Metamorphic Suite rocks in the NJ Highlands and whole-rock geochemical analysis (Volkert and Drake, 1999; Gorring et al., 2001; Volkert et al. 2004) these rocks

represent a calc-alkaline, continental arc suite related to subduction off the eastern margin of Laurentia during the Elzevirian Orogeny.

Stop 1c: At this locality, there is a spectacular, glacially plucked outcrop of the distinctively blue-gray to white, leucocratic Canada Hill granite that is commonly found in the Bear Mountain area and extending northeastward into the West Point and eastern Hudson Highlands region. The Canada Hill granite at this locality is a coarse- to very coarse-grained equigranular rock composed of quartz, K-feldspar, plagioclase, and biotite ± garnet. It forms a sheet-like body ~15-20 m thick and ~300-400m in length that has concordant contacts with the surrounding metavolcanic "charnockitic" quartz-plagioclase-biotite-Opx and "rusty" metapelitic gneisses (Fig. 10). Foliation in the surrounding gneisses is moderately NE-dipping (~N45W, 40NE). The contact between the Canada Hill granite and the "charnockitic" gneiss is well exposed for about ~100m along strike where small rafts and xenoliths of "charnockitic" gneiss are observed within the Canada Hill granite. Similar crosscutting relations have been documented elsewhere in the Hudson Highlands. For example, Helenek and Mose (1984) and Ratcliffe (1992) observed the Canada Hill granite cutting gneissic fabric elements within the Storm King granite gneiss, metapelitic, and metavolcanic rocks in the Popolopen Lake and Oscawana Lake quadrangles to the south and east. In the Bear Mountain area, Helenek and Mose (1984) found xenoliths of Storm King granite gneiss enclosed in Canada Hill granite along the southern margin of the Brooks Lake Pluton. Helenek and Mose (1984) also noted a weak axial planar foliation and the location of Canada Hill granite in the hinges of large-scale, broad, open, upright, plunging folds (e.g., Bear Mountain synform) and interpreted this to indicate that the Canada Hill Granite was syntectonic to and slightly deformed during a late-stage Grenville orogenic event. Based on a recent U-Pb SHRIMP zircon core age of 1058 ±14 Ma (Aleinikoff et.al., 2012) and whole-rock geochemical analysis (Kulick and Gorring, 2004), the Canada Hill Granite represents a syn-tectonic, S-type granitoid produced by partial melting of metapelitic gneisses and emplaced during the Ottawan Orogeny (Fig. 5 and 8C).

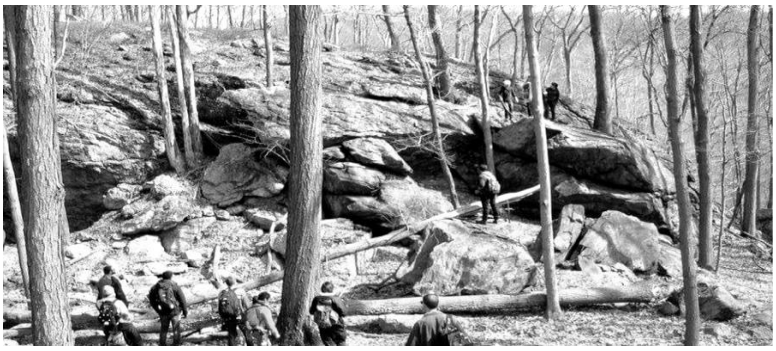

Figure 10. Canada Hill granite outcrop at Stop 1c

Stop 1d: Roadcuts along Perking Memorial Drive on the southwest side of Bear Mountain expose excellent examples of the Storm King granite gneiss. Here, the Storm King is a coarse-grained, quartz-K-feldspar-plagioclase-hornblende gneiss that is strongly lineated (L>S) rock (Fig. 11). The fabric is defined by stretched hornblende prisms and rodded quartz-feldspar aggregates interspersed with large (2-4 cm) plagioclase and/or K-feldspar augen. Based on U-Pb SHRIMP zircon age of 1174 ±8 Ma (Ratcliffe and Aleinikoff, 2001) and whole-rock geochemical analysis (Verrengia and Gorring, 2002), the Storm King granite gneiss is interpreted to represent a pre-Ottawan., A-type granitoid produced by partial melting of intermediate igneous source rocks during an early

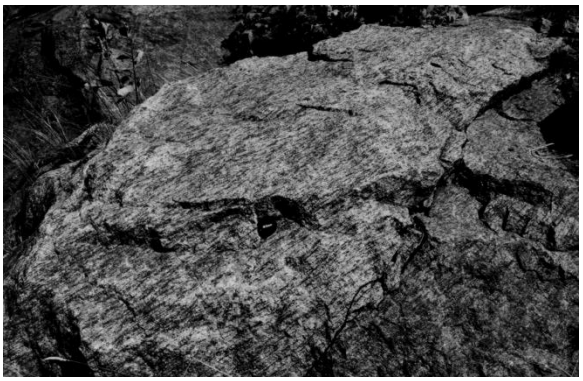

Figure 11. Lineated Storm King granite gneiss outcrop at Stop 1d

stage of AMCG-related lithospheric thinning that affected this part of the Grenville Orogen (Fig. 4A, C and Fig 8B).

Distance in miles (km)

Cumu-lative	Point to Point	Route Description
17.9 (28.6)	0.0 (0.0)	Leave informal parking lot and immediately turn left onto Seven Lakes Drive and proceed northwest.
18.4 (29.4)	0.5 (0.8)	Keep left and follow signs for Seven Lakes Drive and merge onto US-6 West.
18.8 (30.1)	0.4 (0.6)	Use the right 2 lanes to take Exit 18 for US-6 toward NY17/I-87/Central Valley/Seven Lakes Drive.
19.1 (30.6)	0.3 (0.5)	At the traffic circle, stay in right lane and take the 2nd exit (right) onto Seven Lakes Drive.
23.4 (37.4)	3.7 (5.9)	Proceed southwest on Seven Lakes Drive.
23.5 (37.6)	0.1 (0.2)	At the Lake Tiorati circle, take first exit (right) onto Arden Road and then an immediate left into the public park/picnic area (Stop 2). This stop requires an additional ~1 km walk south on Seven Lakes Drive to the first set of low road cuts on the west side of the road.

STOP 2: Lake Tiorati, NY

Location Coordinates: (41°16'31.34"N, 74° 5'18.73"W)

We will examine the field relations and chemistry of a sheared mafic granitoid, referred to as the Lake Tiorati Diorite at its type locality near the eastern margin of the Fingerboard Mountain Shear Zone (Gates et al., 2001c; 2004). This particular outcrop is part of a relatively large body of Lake Tiorati Diorite that is ~200-300 m thick and is ~5-6 km in length located on the west side of Lake Tiorati (Fig. 12A). At the southern end of the outcrop, the rock is essentially undeformed with igneous texture (Fig. 12C). The diorite is composed mostly of plagioclase, hornblende, and clinopyroxene with minor orthopyroxene, magnetite and ilmenite. The orthopyroxene occurs as brown cores surrounded by coronas of clinopyroxene and/or hornblende. There is also a large xenolith of well-foliated biotite-plagioclase-quartz (metasedimentary) gneiss in the upper part of the outcrop. In the central and northern parts of the exposure, the diorite is cut by several anastomosing mylonite bands (Fig. 12 B). The mylonite here is part of the Fingerboard Mountain Shear Zone which is one of several late- to- post-Ottawan ductile shear zones that occur in the western Hudson Highlands (Figs. 3 and 13A) that were mapped and described by Gates et al. (2004); the details of which will be the subject of trip B-3 on Sunday, October 2, 2016, led by Michael Kalczynski and Alexander Gates. U-Pb SHRIMP dating of small, subhedral zircons with minimal zoning from the undeformed diorite from this outcrop yielded a cluster of concordant ages averaging 1008 ±4 Ma (Fig. 6). Since this body is clearly cut by ductile shear zones, this age provides an upper limit on the ductile deformation event that produced the mylonitic fabric. Whole-rock major and trace element chemistry of samples from this outcrop indicate a mafic (~50% SiO_2, see Table 1) calc-alkaline, arc-like affinity for these rocks (Figs. 7A and C). We interpret the arc signature in these rocks to have been inherited from the continental lithosphere during magma generation and emplacement, and thus they do not indicate that there was active subduction zone in

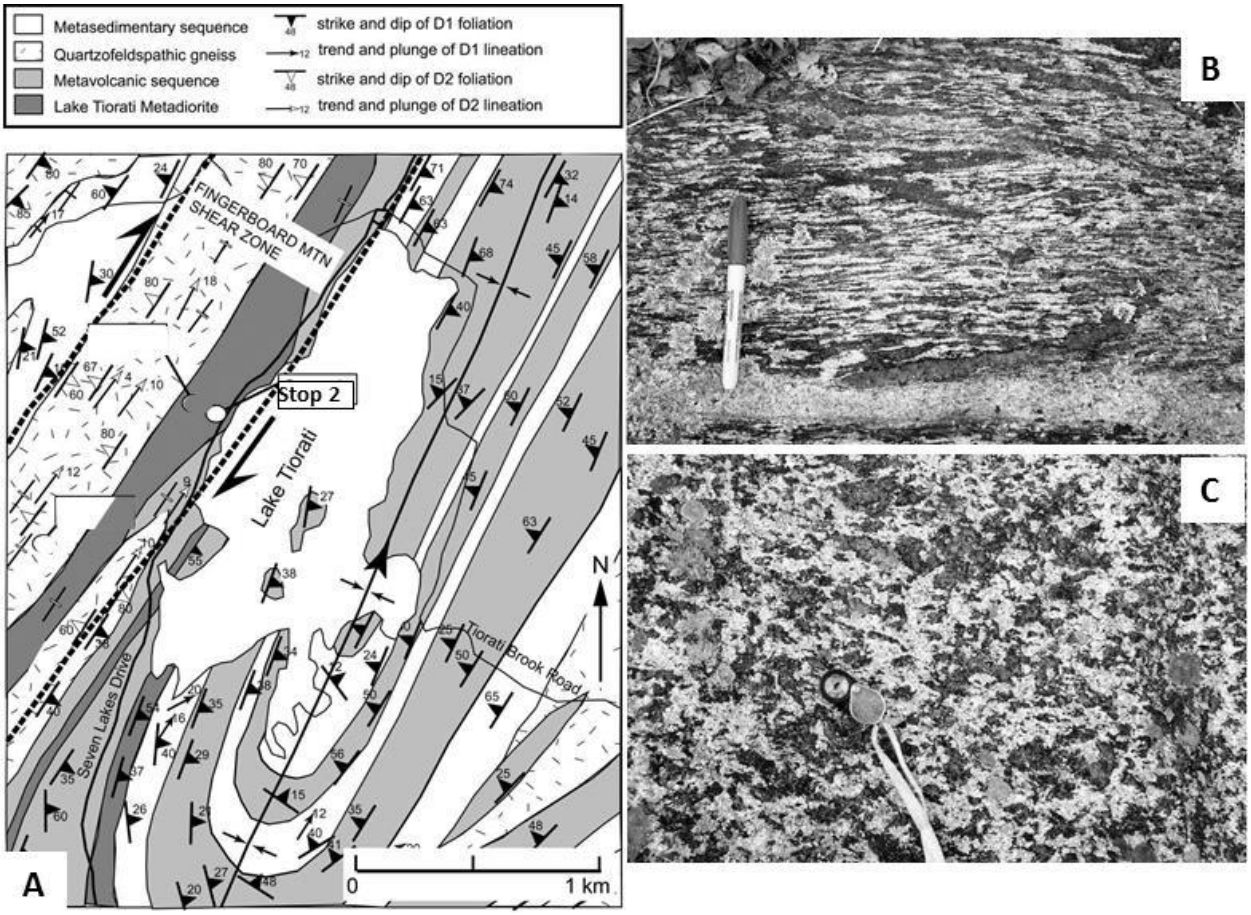

Figure 12. (A) Geologic map (modified from Dodd, 1965) showing the location of Stop 2. (B) Pavement surface of sheared Lake Tiorati Diorite from the summit of Blackrock Mountain ~5 km southeast of Stop 2. Pen is oriented NW-SE. (C) Undeformed diorite from Stop 2; hand lens for scale.

this part of the Grenville at the time. Based on field relations, geochronology, and geochemistry, the Lake Tiorati Diorite is best interpreted as a post-Ottawan mafic plutonic rock that was emplaced just prior to or synchronously with a major ductile shearing event that occurred ~1000 Ma (Fig. 8D).

Distance in miles (km)

Cumu-lative	Point to Point	Route Description

23.5 (37.6) 0.0 (0.0) Leave Lake Tiorati parking lot and immediately turn left onto Arden Road and proceed west.

28.5 (45.6) 5.0 (8.0) Turn left onto NY17 South.

31.4 (50.2) 2.9 (3.2) Bear right to take the NY-17A/CR-106 Exit..

31.6 (50.6) 0.2 (0.3) Turn right onto NY-17A West and proceed westward.

33.0 (52.8) 1.4 (2.2) Turn right onto Clinton Road and immediately park on the right shoulder (Stop 3). This stop requires an additional ~0.5 km walk east on NY-17A to the first set of road cuts that includes rock in the median strip.

STOP

3: Indian Hill Shear Zone, road cuts on NYS 17A

Location Coordinates: (41°14'15.29"N, 74°12'6.32"W)

Road cuts on north side and in median of NY Rte 17A afford an excellent view of a post-Ottawan pegmatitic granite dike that cuts mylonitc quartzfeldspathic gneiss (correlative to Storm King granite gneiss). The mylonite here is part of the Indian Hill Shear Zone which is one of several late- to- post-Ottawan ductile shear zones that occur in the western Hudson Highlands (Fig. 3 and 13A) that were mapped and described by Gates et al. (2004) and the details of which will be the subject of trip B-3 on Sunday, October 2, 2016, led by Michael Kalczynski and Alexander Gates. The pegmatitic dike is ~2-3 m thick, vertical dike that is composed of coarse-grained granite with large crystals of hornblende that

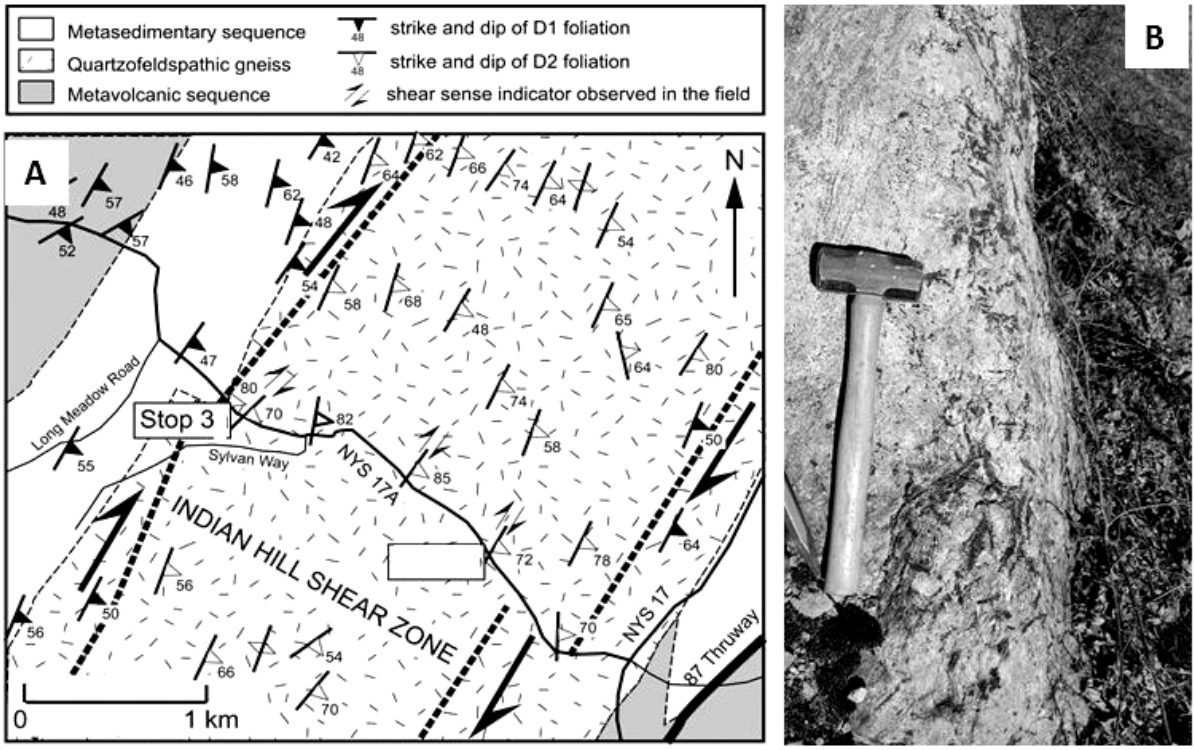

Figure 13. (A) Geologic map modified from Valentino et al., (2001) showing the location of Stop 3. (B) Pavement surface showing sharply discordant contact of pegmatitic granite dike with large sprays of hornblende (right) with mylonitic quartzofeldpathic gneiss (left). Hammer oriented NNW-SSE.

form radiating and linear aggregates. It is exhibits no deformation fabric and cross-cuts the mylonite at a high angle, and thus clearly postdates the ductile deformation of the quarztofeldspathic gneiss (Fig. 13B). Unfortunately, there are no radiometric age constraints or geochemical data for this particularly pegmatite dike, but field relations, texture, and mineralogy of this dike are very similar to pegmatitic granite dikes from the NJ Highlands (Volkert at al., 2005) and elsewhere in the Hudson Highlands (Grauch and Aleinikoff, 1985) that have U-Pb zircon ages in the range of ~1000 to ~960 Ma. Volkert et al. (2005) reported that NJ Highlands pegmatites are dominantly metaluminous, have fractionated A-type geochemical affinities, and share characteristics of the niobium–yttrium–fluorine (NYF) class of pegmatites of Cerny (1992). These late pegmatite dikes are interpreted to have been emplaced during a period of postorogenic extension that significantly postdates the gravitational collapse of the Ottawan Orogeny and the late- to post-Ottawan, high-grade, ductile transpressional events (Fig. 8D).

Distance in miles (km)

Cumu-lative	Point to Point	Route Description
33.0 (52.8)	0.0 (0.0)	Turn around on Clinton Road and immediately cross over NY-17A and proceed south on Long Meadow Road (CR-84).
36.6 (58.6)	3.6 (5.8)	Noticeable pink granite outcrop on the right (west) side of road (Stop 4). Park on the other side (east) of road where there is more gravel shoulder. If you come to Old Forge Road, you have gone past the locality by ~200m.

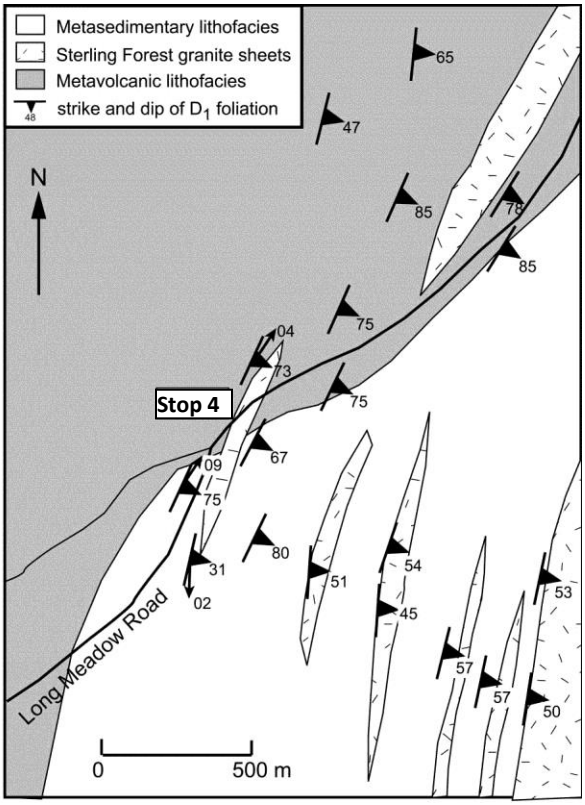

Figure 14. Geologic map showing the location of Stop 4.

STOP 4: Sterling Forest Granite Sheets, road cuts on Long Meadow Road (CR 84)

Location Coordinates: (41°12'9.28"N, 74°14'52.67"W)

This roadcut along northwest side of Long Meadow Road exposes a fine example of the syn-Ottawan Sterling Forest granite sheets found in the western Hudson Highlands (Fig. 14). These pink granite sheets are very leucrocratic (~75 wt% SiO_2) (Appendix Table 2), composed of almost entirely quartz, K-feldspar, and plagioclase, with only small amounts (<5%) of hornblende ± biotite with accessory apatite, titanite, and zircon. At this locality, the sheet has a medium-grained, equigranular igneous texture and shows no evidence of deformational fabric. However, locally these granite sheets are foliated where intersected by late-stage, ductile shear zones and thus, are clearly pre- or syntectonic with the shearing event. This particular sheet is one of several, 10-100 m thick, finger-like bodies that extend both southward and northward several

kilometers from the main plutonic masses at Hogback Mountain (to the north) and Bill White Mountain (to the south). Here, the sheet is about 20 m thick, strikes N20E and dips ~65° to the southeast and has intruded parallel to foliation in the surrounding gneisses. It intrudes amphibolites and intermediate gneisses of the metavolcanic unit (contact observed at the north end of the outcrop) and metapelitic gneisses of the metasedimentary lithofacies. The granite sheet exposed here (sample SF-28) has a distinctly "dished" MREE pattern, a moderately strong negative Eu anomaly (Eu/Eu* = 0.35), high HREE contents (~20x chondritic) and very low Ba and Sr concentrations (~20 ppm) (Fig. 5C and Appendix Table 2). These chemical characteristics indicate that amphiboles and feldspars were important phases in the petrogenesis of this particular granite. The data is consistent with partial melting of garnet-free, mafic amphibolitic source rocks and/or fractional crystallization of amphibole + plagioclase ± K-feldspar at shallower crustal levels. The Sterling Forest granite sheets represents a syn-tectonic, I-type granitoid produced by partial melting of mafic/intermediate igneous sources and were emplaced during the Ottawan Orogeny (Fig. 5 and 8C).

Distance in miles (km)

Cumu-lative	Point to Point	Route Description
36.6 (58.6)	0.0 (0.0)	Proceed southwest (turn around, if necessary) on Long Meadow Road (CR-84).
40.9 (65.4)	4.3 (6.9)	Turn left on Sterling Mine Road.
43.6 (69.8)	2.7 (4.3)	Use the right lane to take the ramp for NY-17 South, then merge onto NY-17 South and proceed southeast.
45.0 (72.0)	1.4 (2.2)	Use the right lane to take the ramp for NY-17 S/I-87 S/New York Thruway ramp to I-287, then merge onto I-87 South/NY-17 South and proceed south..
53.0 (84.8)	8.0 (12.8)	Keep left to continue on I-87 South.
54.9 (87.8)	1.9 (3.0)	Take Exit 14 for NY-59 toward Spring Valley/Nanuet. Use the left 2 lanes to turn left onto NY-59 and proceed southeast on NY-59.
54.9 (87.8)	0.1 (0.2)	Turn right onto Rose Road and then immediate right into parking lot of DoubleTree by Hilton Hotel Nanuet. (End of trip)

TRIP A5: STRATIGRAPHY, STRUCTURE, AND TECTONICS OF NEW YORK CITY AS VIEWED THROUGH ITS PARKS

CHARLES MERGUERIAN
Professor Emeritus, Geology Department, Hofstra University, Hempstead, NY 11549, Research Fellow, Yale University, New Haven CT 06520 and Principal, Duke Geological Laboratory, Stone Ridge, NY 12484

J. MICKEY MERGUERIAN
Geologist, Duke Geological Laboratory, Stone Ridge, NY 12484

INTRODUCTION

Geological Setting

NYC is situated at the extreme southern end of the Manhattan Prong (Figure 1), a northeast-trending, deeply eroded sequence of metamorphosed Proterozoic to Lower Paleozoic rocks that widen northeastward into the crystalline terrains of New England. Southward from NYC, the rocks of the Manhattan Prong plunge nonconformably beneath predominately buried Mesozoic rocks, younger Cretaceous strata, and the overlying Pleistocene drift found capping much of the region including all of Long Island and much of Staten Island. This NYSGA paper and allied Trip A-5 field guide are intended to prepare and expose participants to our subdivisions of the venerable Manhattan Schist into three separable units by utilizing exposures in NYC parks including Isham, Inwood Hill and Central parks.

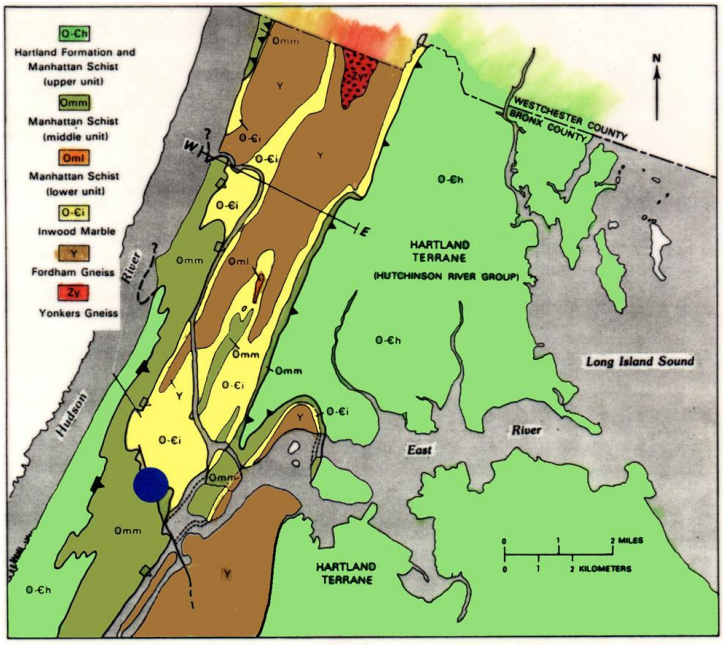

Figure 1 – Geological map of New York City showing the generalized structural geology of the region using older terminology of upper, middle, and lower units of the Manhattan Schist of Merguerian and Baskerville (1987) and Merguerian and Merguerian (2004). Triangles show the dip of Cameron's Line (solid) and the St. Nicholas thrust (open) and the flagged triangles indicate overturned thrusts. Most faults and intrusive rocks have been omitted. Blue dot is epicenter of 21 January 2001 magnitude 2.4 earthquake that occurred along Manhattanville fault.

Previous Investigations

A detailed history of NYC bedrock investigations appears elsewhere (Merguerian and Sanders 1991) so the following is simply a brief excerpt and overview. In 1890 (p. 390), Merrill named the Manhattan Schist for the micaceous metamorphic rocks found on Manhattan Island and suggested, following the views of Professors W. W. Mather (1843) and J. D. Dana (1880), that they represent metamorphosed equivalents of the lower Paleozoic strata of southern Dutchess County, New York. Merrill (1890) confides that "the name Manhattan Group was proposed by naturalist R. P. Stevens, Esq., to include the rocks of New York Island".

Despite this acknowledgement, Merrill and others (1902) produced the United States Geological Survey New York City Folio (#83) and following Dana chose to use the name Hudson Schist (rather than Manhattan Schist) for the schistose rocks of NYC. This pioneering work by Merrill and coworkers set the stage for a series of detailed investigations by many geologists in the 1900's that helped define the details of NYC bedrock units and use of the term Manhattan Schist as the name locality for the unit. Merrill also extended "Group" status to include the Manhattan Schist, the Inwood "limestone" and the Fordham and Yonkers gneisses and correctly correlated the Fordham with Proterozoic sequences of the Hudson Highlands. Formal removal of the significantly older Fordham and Yonkers gneisses from the "Manhattan Group" had to await the refinement and application of radiometric dating techniques and detailed mapping in the 1960's by Leo M. Hall (1968a; b). Formal "de-Grouping" of the "Manhattan Group" took place after spirited debate at a Symposium on the New York City Group of Formations at the 1968 meeting of the New York State Geological Association at Queens College, Queens, New York. Our studies of the metamorphic rocks of NYC since 1972 have benefited from these early works and access to surface and subsurface construction sites.

NYC BEDROCK STRATIGRAPHY

Based on study of over 1,000 natural exposures and a multitude of drill core and construction excavation geotechnical analyses our joint investigations of the bedrock geology of NYC have portrayed a complex structural history and suggests that the Manhattan Schist formation exposed in Manhattan and the Bronx is a lithically variable sequence consisting of three separable map units now known as the **Hartland, Manhattan, and Walloomsac** formations (Figure 1). These subdivisions agree with designations proposed by Hall (1976; 1980) but suggest the presence of a hitherto unrecognized structurally higher unit that is a direct correlative of the Hartland Formation (= Rowe and Ratlum Mountain schists) of western Connecticut (Merguerian 1983a; 1987; 2016). The three schistose units are juxtaposed along imbricate ductile faults known as the St. Nicholas thrust and Cameron's Line (Merguerian 1994; 1996a) as indicated in a simplified cross section across the northern tip of Manhattan into the Bronx (Figure 2).

Keyed to Figure 1, the W-E section of Figure 2 shows the general structure of NYC and how the St. Nicholas thrust and Cameron's Line overthrusts position the Manhattan and Hartland formations above the Walloomsac formation and the underlying Inwood- Fordham cover+basement sequence. Late stage regional F_3 folds produce digitations of the structural- and stratigraphic contacts that dip gently south, downward out of the page toward the viewer. The N-S section illustrates the southward topping of tectonostratigraphic units exposed in central Manhattan and the effects of the yet younger NW-trending

asymmetric folds. The structural geology of NYC is detailed in a later section and the proposed new stratigraphic interpretation is diagrammed in Figure 3.

Hartland Formation. The structurally high Hartland formation (O€h) is dominantly gray-weathering, fine- to coarse-textured, well-layered (cm- and m-scale) muscovite-quartz-biotite-plagioclase-kyanite-garnet-staurolite schist, gneiss, and migmatite with layers of gray quartzose granofels, greenish amphibolite±garnet and scarce coticule. *(Note: Minerals listed in descriptions are in decreasing order of abundance.)* The schistose facies is lustrous and consists of dense, aligned fine- to coarse-textured muscovite and lesser biotite that splits readily along the foliation (Figure 4). The gneiss and granofels lithotypes are massive, commonly more feldspathic, migmatitic and may or may not show pronounced foliation. Gray quartzites are also found as discrete interlayers up to 0.5 m thick. Although typically not exposed at the surface, the Hartland underlies most of the central and southern portions of Manhattan and the eastern half of the Bronx. Because it is lithologically identical to the Cambrian (?) to Ordovician Hartland Formation of western Connecticut and Massachusetts, the Hartland name has been extended into NYC (Merguerian 1983b) where it is considered part of the allochthonous **Taconic Sequence**.

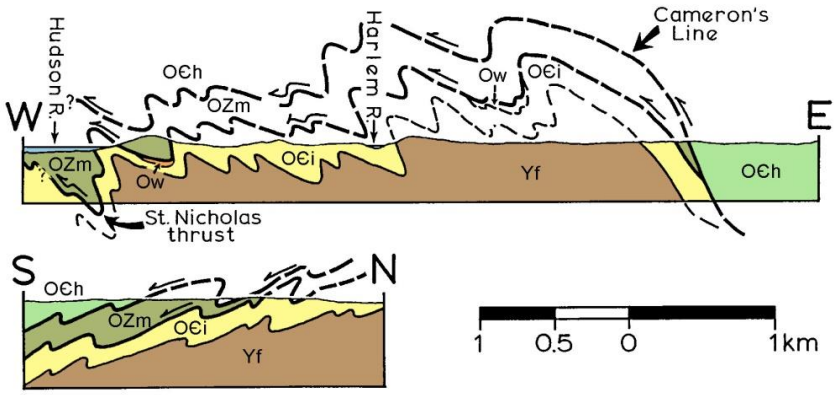

Figure 2 - Geologic cross sections across Manhattan and the Bronx showing the distribution of various tectonostratigraphic units in New York City and folded ductile faults (Cameron's Line and the St. Nicholas thrust). See Figure 1 for the line of the W-E section. The N-S section runs through the east edge of Central Park.

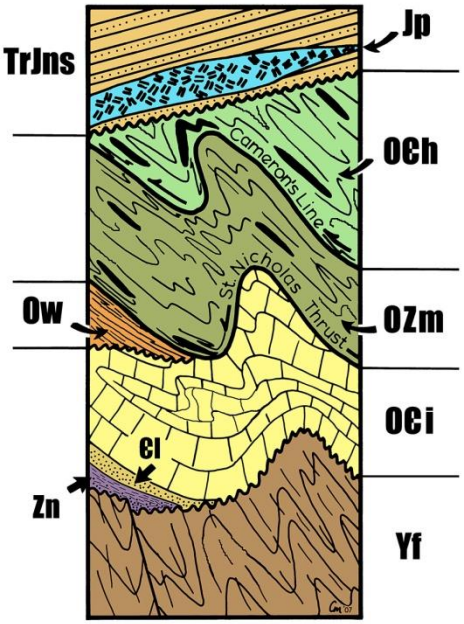

Figure 3 - Bedrock stratigraphy of New York City as described in text and noted in figures. Note that the polydeformed bedrock units are nonconformably overlain by west-dipping Triassic and younger strata (TrJns) and the Palisades intrusive (Jp).

Manhattan Formation. The Manhattan formation (OZm) consists of very massive rusty- to sometimes maroon-weathering, medium- to coarse-textured, biotite-muscovite-plagioclase-quartz-garnet-kyanite-sillimanite-magnetite-tourmaline gneiss, migmatite, and to a lesser degree, schist (Figure 5). The unit is characterized by a lack of internal layering except for the presence of kyanite+sillimanite+quartz+ magnetite layers and lenses up to 10 cm thick, cm- to m-scale layers of black amphibolite, and scarce thin, quartzose granofels. The unit is a major ridge former in northern Manhattan, a testament to its durability to weathering owing to the lack of layering and presence of resistant minerals quartz, garnet, kyanite, and sillimanite. Owing to the localized concentration of individual crystals and zones of disseminated magnetite some parts of the formation are strongly magnetic.

The Manhattan Formation forms the bulk of the “exposed" Paleozoic metamorphic rocks of northern Manhattan including most northern Central Park exposures and the bulk of the highlands of Inwood Park. The Manhattan is lithologically identical to Hall's Manhattan B and C and the Waramaug and Hoosac formations of Late Proterozoic (?) to Ordovician age in New England (Hall, 1976; Merguerian, 1977; 1983a; 1985; 2016). These rocks, which contain calc-silicate and quartzose interlayers in western Connecticut are inferred to represent metamorphosed sedimentary- and minor volcanic rocks deposited in the transitional slope- and rise environment of the Early Paleozoic continental margin of ancestral North America. As such, they are considered, along with the Hartland Formation, a part of the allochthonous **Taconic Sequence**.

Walloomsac Formation. Found interlayered at the top of the Inwood Marble in New York City, this discontinuous unit (Ow) is composed of fissile brown- to rusty-weathering, fine- to medium-textured, biotite-muscovite-quartz-plagioclase-kyanite-sillimanite-garnet-pyrite-graphite schist and migmatite. The formation contains interlayers centimeters to meters thick of plagioclase-quartz-muscovite granofels, layers of (“Balmville”) calcite marble, and hard diopside±tremolite±phlogopite calc-silicate rock. Pinkish garnet occurs as porphyroblasts up to 1 cm in size and amphibolite is absent. As shown in the photomicrograph of Figure 6, strongly pleochroic reddish biotite, pinkish garnet, graphite, and pyrite are diagnostic mineralogical features of the former pelitic portions of the formation.

Exposed Walloomsac Formation can be found interlayered with the underlying Inwood at five localities in Manhattan - (1) at the northern edge of Inwood Hill Park in Manhattan, (2) beneath the St. Nicholas thrust on the north and east sides of Mt. Morris Park (Merguerian and Sanders, 1991), and (3) in the northern edge of Central Park (Merguerian and Merguerian, 2004). The Walloomsac has also been detected sheared against Hartland rocks in numerous borings and building excavations from (4) northern and (5) southern Manhattan (Merguerian and Moss, 2006; 2007) including the World Trade Center site (Merguerian, 2010).

In the Bronx, four areas of Walloomsac rocks have been found; (1) on the Grand Concourse and I-95 overpass (Merguerian and Baskerville, 1987), (2) beneath the St. Nicholas thrust in the western part of Boro Hall Park (Fuller et al., 1999), (3) below the St. Nicholas thrust in the northwest and southeastern part of the New York Botanical Garden (Merguerian and Sanders, 1998 and unpublished data), and (4) in the western and northeastern part of Crotona Park (unpublished data). Because it is interpreted as being autochthonous (depositionally above the Inwood Marble and underlying Fordham Gneiss) it is assigned a middle Ordovician age. The lack of amphibolite and the presence of graphitic schist and quartz-feldspar granofels and calc-silicate layers enables the interpretation that the Walloomsac Schist is the metamorphosed equivalent of middle Ordovician carbonaceous shale and interlayered greywacke and calcareous strata of the Tippecanoe Sequence and is therefore considered correlative with parts of

the Annsville and Normanskill formations of SE New York and the Martinsburg formation of eastern Pennsylvania.

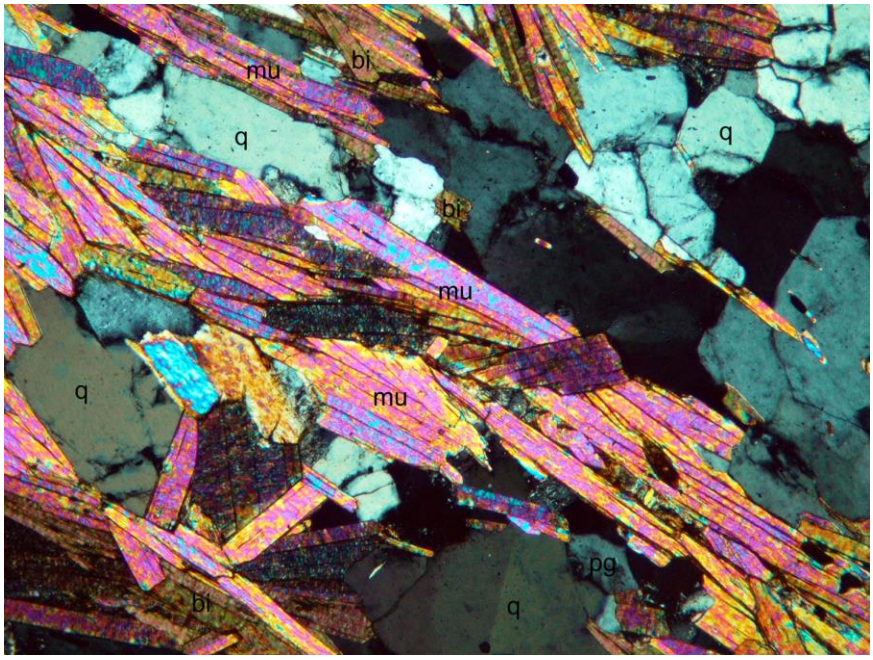

Figure 4 - Photomicrograph in cross-polarized light of Hartland schist (~~C~~Oh) showing a penetrative mica foliation consisting of intergrown and oriented muscovite (mu), biotite (bi), in a matrix of flattened quartz (q), and minor plagioclase feldspar (pg). Note the high mica content and prevalence of muscovite and quartz, diagnostic mineralogical characteristics of the Hartland. (CM Sample N125; 112th Street and Riverside Drive, Manhattan; 2 mm field of view.)

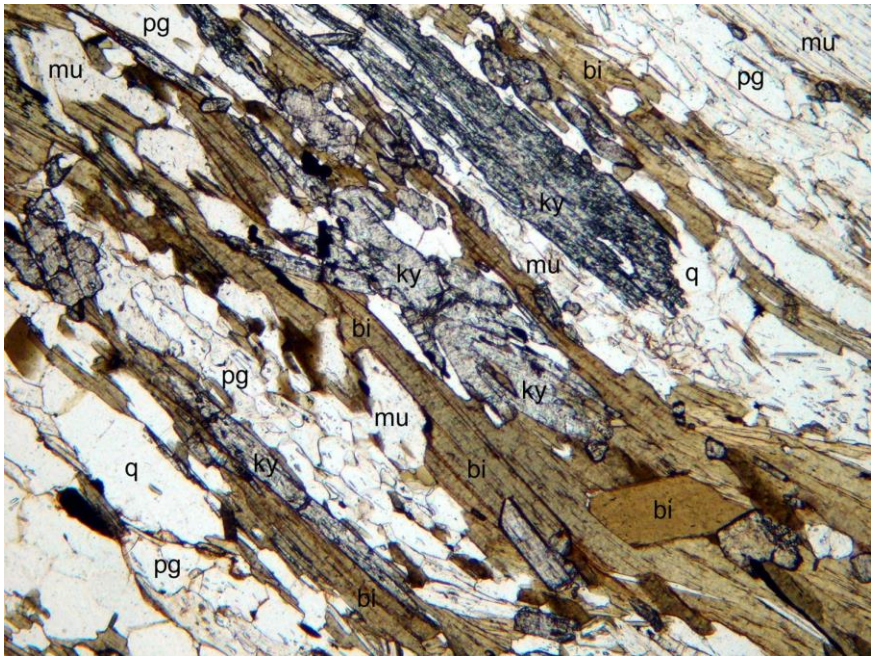

Figure 5 - Photomicrograph in plane-polarized light of the Manhattan Schist (OZm) showing an aligned intergrowth of biotite (bi), kyanite (ky), and muscovite (mu) in a fine-textured matrix of intergrown plagioclase (pg) and quartz

(q). The penetrative foliation in this view, which consists of aligned micas and kyanite as well as flattened quartz and feldspar, is diagonal across the image and marks a structural discontinuity that may split readily. (CM Sample N217; South of George Washington Bridge approach, Manhattan; 2 mm field of view.)

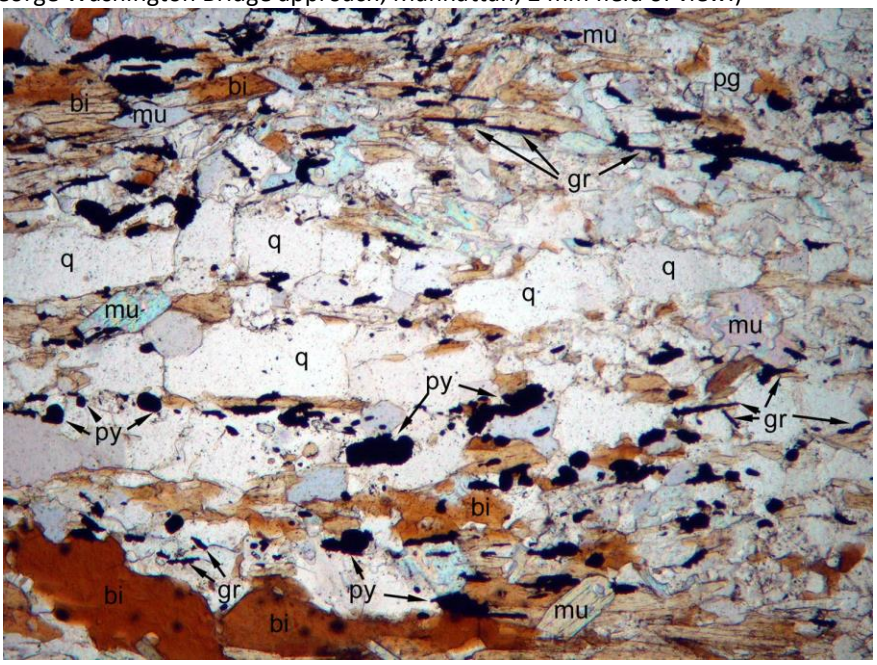

Figure 6 - Photomicrograph in plane-polarized light of the Walloomsac Schist (Ow) displaying a penetrative foliation (subhorizontal) defined by aligned biotite (bi), muscovite (mu), lenticular quartz (q), graphite (gr), and pyrite (py). Late idioblastic muscovite crystals overgrow the foliation. Diagnostic petrographic characteristics of the Walloomsac include the presence of graphite and pyrite and strongly pleochroic red-brown biotite. (CM Sample N113-3L; Inwood Hill Park, at south footing of Henry Hudson Bridge, Manhattan; 2 mm field of view.)

Origins of the Hartland, Manhattan, and Walloomsac Formations

Metamorphosed to amphibolite facies grade and then retrograded to biotite facies grade the exposed metamorphic cover rocks of NYC (Hartland, Manhattan, and Walloomsac Formations) were originally deposited as sediment and intercalated clastic, volcanic and volcaniclastic materials, though in vastly different depositional environments (Figure 7). The Hartland Formation was originally deposited in a deep ocean basin floored by oceanic lithosphere and fringed by offshore volcanic islands. The marginal ocean basin was the receptor of a huge influx of terrigenous and volcanogenic material. This produced a thick well-layered sequence of clay, silt, sand, and interlayered volcanogenic strata which resulted in a variable lithologic sequence. Even after protracted Paleozoic deformation and metamorphism, compositional layering was preserved in the Hartland, forming a dominantly well-layered metamorphic rock mass consisting of interlayered and locally migmatitic schist, gneiss, granofels, and amphibolite.

The Manhattan Formation originated along the edge of the former North American continental margin as thick clay-rich sediment with occasional sand interlayers and mafic igneous injection or flows. (See Figure 7.) As a result, the Manhattan is often more massive in character than the Hartland although some subunits appear similar. By contrast, the Walloomsac Formation is mineralogically unique since it originated under restricted oceanic conditions and consisted of thick accumulations of carbonaceous, sulphidic, and clay-rich sediment with occasional sandy and calcareous interlayers. This has resulted in a mineralogically distinct schistose rock enriched in biotite, graphite, garnet and pyrite together with

layers of calcite marble and calc-silicate rock. The contrast in internal compositional layering and mineralogy allows for separation of the three units in the field and also during routine core examination and petrographic analysis.

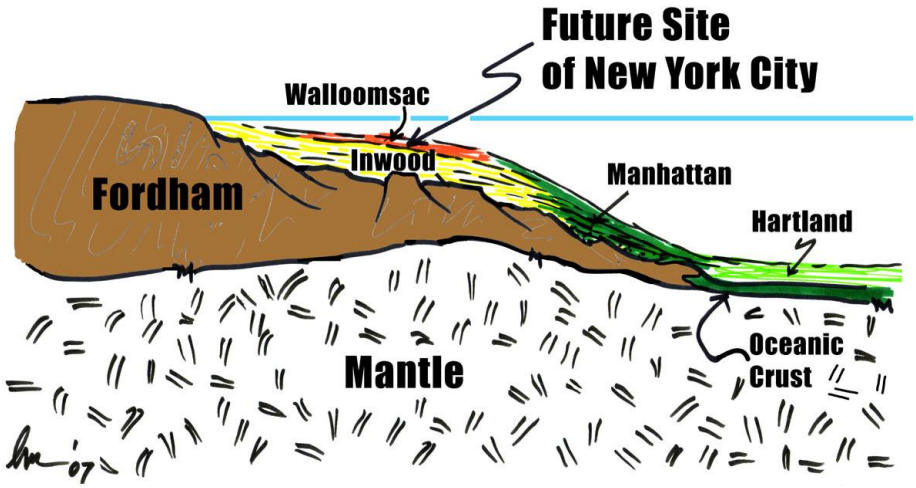

Figure 7 - Diagrammatic cartoon of eastern North America after rifting from Rodinia and during deposition of the Paleozoic strata that are to become the Hartland, Manhattan, and Walloomsac formations. Note the correlation of units and their relationships to the underlying units of the partly coeval Inwood and older Fordham.

NYC Bedrock Formations Found Beneath the Hartland, Manhattan, and Walloomsac Formations

The metamorphic rocks described above are in structural or unconformable contact with the predominately older units as described below.

Inwood Marble. The Inwood Marble (O~~C~~i in Figures 1-3) consists of white to bluish-gray fine- to coarse-textured dolomitic and lesser calcitic marble locally with siliceous interlayers containing diopside, tremolite, phlogopite, muscovite (white mica) and quartz (Figure 8) together with accessory graphite, pyrite, tourmaline (dravite-uvite), chlorite and zoisite according to our investigations (Merguerian, et al., 2011). Layers of calc-schist, calc-silicate rock and fine grained gray quartzite with a cherty appearance are also locally present. The unit is exposed in the Inwood section of northern Manhattan, the Harlem lowland NE of Central Park, in thin belts in the East River channel, in the subsurface of southeastern Manhattan, and also crops out in the Bronx and Westchester County. The Inwood is correlative with a continuous outcrop belt of non-metamorphosed Cambro-Ordovician carbonate rocks (Sauk Sequence) found along the entire Appalachian chain of North America.

Fordham Gneiss. The Fordham Gneiss (Yf in Figures 1-3) constitutes the oldest underpinning of rock formations in NYC and consists of a complex assemblage of Proterozoic Y ortho- and paragneiss, granitoid rocks, metavolcanic- and metasedimentary rocks. In NYC, only a few attempts have been made to decipher the internal stratigraphic relationships, hence, the three-dimensional structural relationships remain obscure. Based on detailed studies in the Queens and Brooklyn NYC water tunnels (Merguerian, 2000; Merguerian et al., 2001; Brock et al., 2001), the Fordham consists of predominately massive mesocratic, leucocratic, and melanocratic orthogneiss with subordinate schistose rocks. They are Grenvillian in age (1.1 Ga) and were metamorphosed to the high pressure granulite facies which has produced a tough, anhydrous interlocking mineral texture consisting of primary clino- and lesser orthopyroxene, plagioclase, and garnet that has partially resisted Paleozoic hornblende and biotite grade retrograde regional metamorphism (Figure 9).

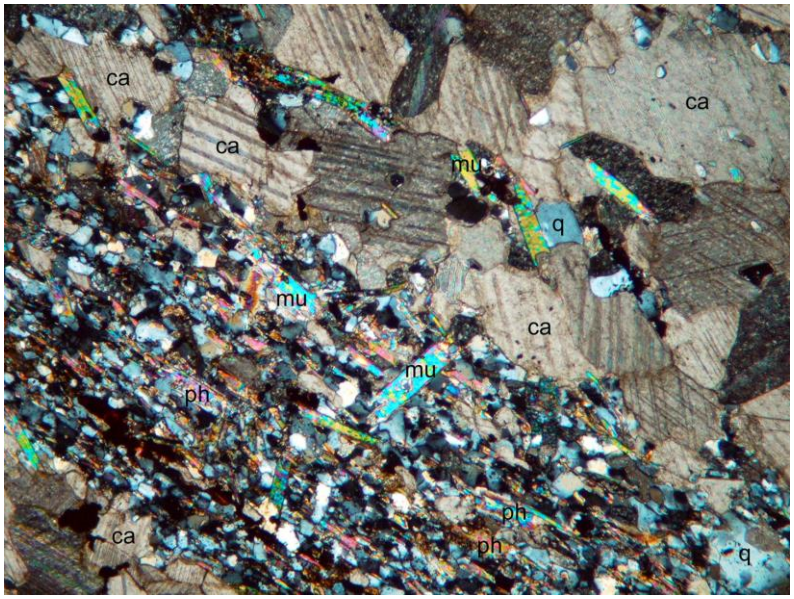

Figure 8 - Photomicrograph in cross-polarized light of the Inwood Marble near the contact with the Walloomsac showing the granoblastic texture produced by recrystallized twinned calcite (ca). A fine-textured mica-rich zone cutting diagonally across the slide defines a foliation which here consists of aligned muscovite (mu) and phlogopite (ph) in a matrix of recrystallized quartz (q), calcite, and biotite (bi). Normally the Inwood is quite pure and consists of coarse textured granoblastic calcite or dolomite. (CM Sample N113-4; Inwood Hill Park, at south footing of Henry Hudson Bridge, Manhattan; 2 mm field of view.)

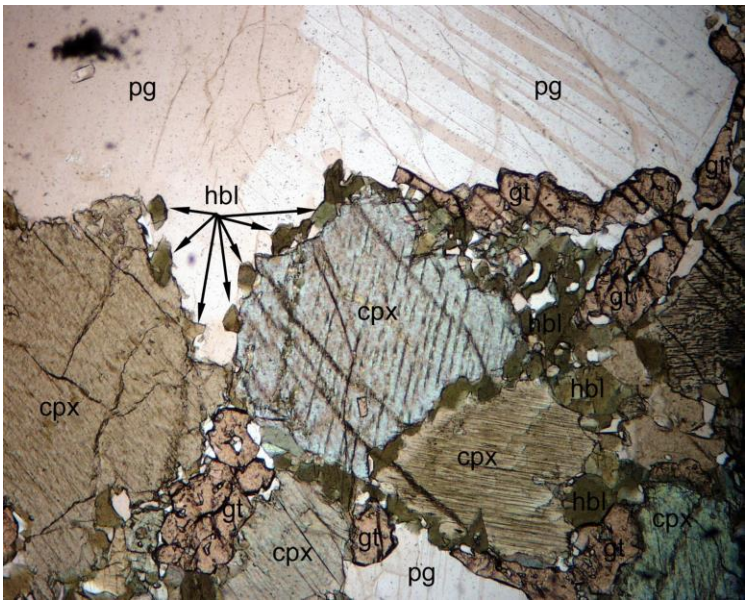

Figure 9 - Photomicrograph in plane-polarized light of Proterozoic mafic orthogneiss showing a coarse-textured granular intergrowth of clinopyroxene (cpx), plagioclase (pg), and garnet (gt) produced during Grenvillian metamorphic recrystallization of a former mafic igneous rock. Granular hornblende (hbl) was produced during a secondary Paleozoic metamorphism but the older interlocking granoblastic metamorphic texture has prevailed. (CM Sample Q114; Queens Tunnel Station 015+90; 2 mm field of view.)

The Fordham is exposed in the Bronx, in the subsurface of SE Manhattan, the East River channel, and western Queens and Brooklyn (City Water Tunnel #3, Stage 2) and presumably underlies most the region at greater depth (Figure 7). Occurring locally between the Inwood and Fordham, are two minor units that are poorly understood and somewhat controversial. One is the very local Lowerre Quartzite (unit Ꞓl in Figure 3) of Norton (1959) and the other a late Proterozoic unit known as the Ned Mountain Formation (unit Zn in Figure 3) of Brock (1989; 1993). The Ned Mountain is correlative with Proterozoic Z rocks mapped as the Yonkers Gneiss (Scotford, 1956) and the Ravenswood Granodiorite Gneiss (Ziegler, 1911) found in Westchester County and in western Queens, respectively. They have little bearing on the primary focus of this paper and field trip and are here referenced for sake of completion.

Other Rocks Associated with the Bedrock Series

Serpentinite. In addition to the famous Staten Island serpentinite, many scattered bodies of serpentine rock have been encountered in NYC (Figure 10). In addition to a few bodies known in Manhattan near 59th Street and 10th Avenue, the Bruckner Boulevard/Cross Bronx Expressway/Hutchinson River Parkway interchange at the north end of the Bronx-Whitestone Bridge approach in the Bronx, and a few bodies that were penetrated during construction of the Brooklyn Water Tunnel (Schnock, 1999) and the Manhattan Water Tunnel, serpentinite has also been found in a building construction site at 43rd Street and Sixth Avenue in midtown Manhattan (Merguerian and Moss, 2005) and in northern Manhattan (Merguerian and Moss, 2007). These sheared masses are interpreted as ophiolitic scraps and are commonly found in ductile fault contact with enclosing Hartland rocks or near the Manhattan-Hartland contact (Merguerian, 1979). The serpentinites are black to greenish fine-textured rocks containing serpentine group minerals including chrysotile, chromite, magnetite, orthoamphibole, magnesite, talc, calcite, chlorite together with relict olivine and pyroxene.

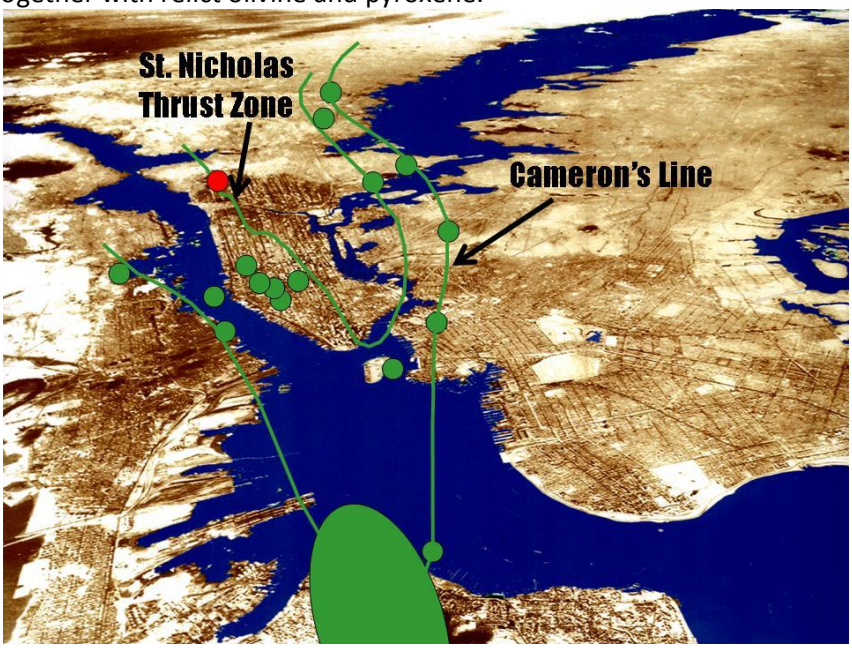

Figure 10 - Cartoon showing distribution of 18 known areas of serpentinite in the New York City area. The green lines surround areas of serpentinite defining a zone of sheared rock broadly coincident with the St. Nicholas thrust and Cameron's Line, two important elements of the Taconian suture zone in New York City. The red dot shows the location of a serpentinite in northern Manhattan described by Merguerian and Moss (2007).

Granitoid. All units of the NYC bedrock described above have been intruded by granitoids that range from foliated and internally sheared pre- and syn-tectonic intrusives to post-tectonic bodies. They range from fine-textured to pegmatitic and occur as dikes, sills, stocks, and small plutons consisting of essential K-feldspar, quartz, plagioclase, biotite, hornblende, muscovite, and subordinate garnet. Minor tourmaline and beryl are also locally found.

Rhyodacite. Found exclusively beneath the area of Woodside, Queens a swarm of five thin sub-parallel rhyodacite dikes, all displaying pristine igneous textures, were penetrated during construction of the Queens Tunnel (Merguerian, 2000; 2001). They occur as tabular, discordant injections roughly oriented N53°W and average roughly 3 m in thickness. The larger dikes vary from 5.3 m down to 1 m and taper off to thinner dikelets. The rhyodacites are reddish, glassy to aphanitic igneous rocks with no metamorphic fabric and low average density (2.58 g/cm^3).

The unique devitrified texture of the groundmass and the presence of vesicles unequivocally identify the Queens Tunnel rhyodacite as a hypabyssal rock. The dikes are Permian in age (~295 Ma) and crosscut folded Proterozoic Y granulite facies rocks of the Queens Tunnel Complex with which they are genetically and temporally unrelated. The injection of a suite of Permian rhyodacite dikes that are chemically, texturally, and temporally unrelated to their bedrock hosts, mark an anomalous geological formation that adds a new chapter to the evolution of the NYC area.

Alkalic and Mafic Dike Rocks. Mapping in conjunction with construction of NYC Water Tunnels # 1 and 2 also defined alkalic and mafic dike rocks (Berkey; 1911; 1933; 1948) and I have seen mafic dikes in the Queens Tunnel and elsewhere in NYC. Some of them are foliated and of presumable middle Ordovician age and others contain pristine igneous textures and are most likely associated with the early Jurassic Palisades intrusive epoch.

STRUCTURAL GEOLOGY

Deformational Episodes

All bedrock units in NYC have shared a complex Paleozoic structural history which involved three superposed phases of deep-seated deformation (D_1-D_3) followed by three or more episodes of open- to crenulate folds (D_4-D_6). The synmetamorphic juxtaposition of the various units occurred very early in their structural history ($D_1 + D_2$) based upon crosscutting relationships. The Fordham harbors a more complex history as a result of its great age. It has experienced deformation and metamorphism during the Grenville orogeny (~1.1 Ga) in addition to the three Paleozoic orogenies (Taconian, Acadian, and Allegenian) experienced by the overlying Inwood, Walloomsac, Manhattan, and Hartland rocks. Below, we will restrict our discussion to the Paleozoic deformation.

The obvious map scale folds in NYC are those with steep N- to NE-trending axial surfaces (S_3) and variable but typically shallow plunges toward the S and SW (Figures 1 and 2). The folds are typically overturned to the NW with a steep SE-dipping schistosity (Figure 11). Shearing along S_3 axial surfaces typically creates a transposition foliation of S_1, S_2, and S_3 that is commonly invaded by granitoids to produce migmatite both during the D_2 and subsequent D_3 events. The third-generation structures deform two earlier structural fabrics (S_1 and S_2). The older fabrics trend roughly N50°W and dip gently

toward the SW (except along the limbs of overturned F_3 folds). We suspect that all of these structures (D_1, D_2, and D_3) are products of the protracted middle Ordovician Taconic orogeny.
During D_2, the rocks acquired a penetrative S_2 foliation consisting of oriented mica and intergrown sillimanite and kyanite with flattened quartz together with staurolite and garnet porphyroblasts. Distinctive layers and lenses of kyanite+quartz+magnetite developed in the Manhattan formation and very locally in the Hartland during D_2. Near ductile fault contacts the S_2 fabric is highly laminated with frayed and rotated mica and feldspar porphyroclasts with and without fine-textured tails, ribboned and locally polygonized quartz, lit-par-lit granitization, and quartz veins all developed parallel to the axial surfaces of F_2 folds. The D_3 folding event, a period of dominantly L-tectonism, smeared the previously flattened kyanite+quartz layers and lenses into elongate shapes stretched parallel to F_3 axes. In addition, porphyroblasts of tremolite pseudomorphic after diopside also show alignment parallel to F_3 hingelines in the bounding Inwood Marble (Merguerian and Merguerian, 2012).

Although the regional S_2 metamorphic grain of the NYC bedrock trends N50˚W, the appearances of map contacts are regulated by F_3 isoclinal- to tight folds overturned toward the west and plunging SSE to SW at 25˚. (See Figure 11.) S_3 is oriented N30˚E and dips 75˚SE and varies from a spaced schistosity to a transposition foliation often with shearing near F_3 hinges. The F_3 folds and related L_3 lineations mark a period of L-tectonite ductile flow that smeared the previously flattened quartz and kyanite lenses and layers into elongate shapes. Metamorphism was of identical grade with D_2 which resulted in kyanite overgrowths and annealing of former mylonitic textures (Merguerian 1988).

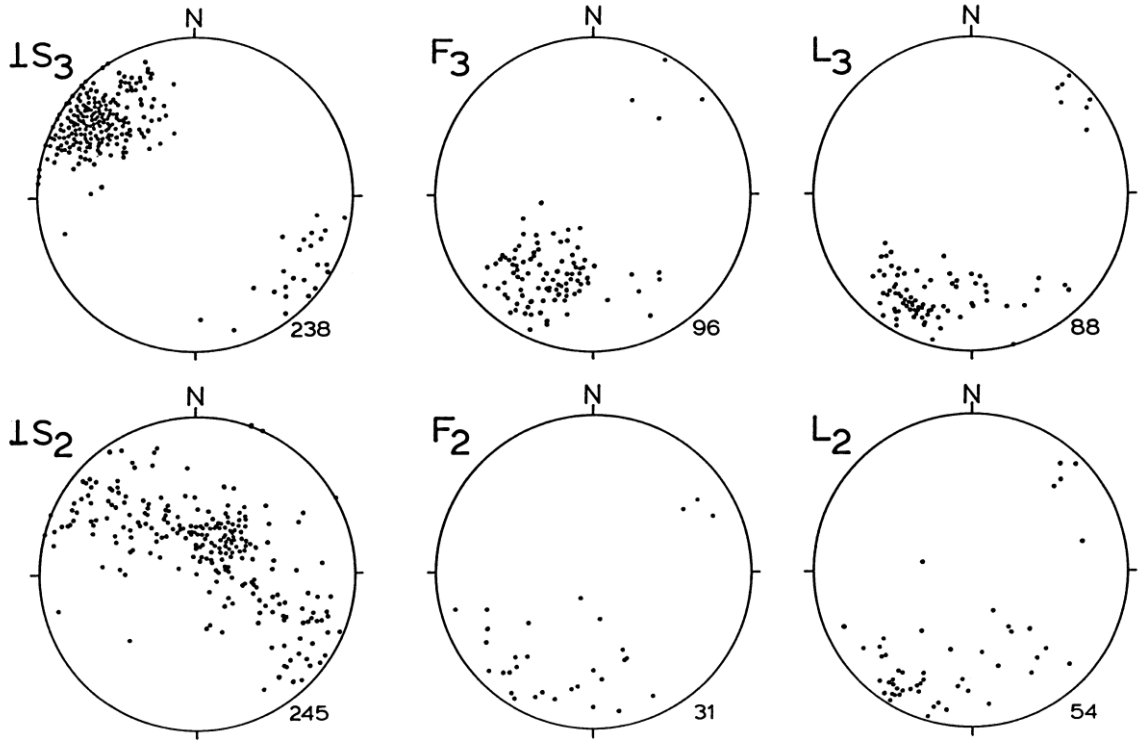

Figure 11 - Equal area stereograms showing the distribution of poles to S_2 and S_3, the orientation of F_2 and F_3 fold hingelines, and the orientation of L_2 and L_3 lineations. The number of plotted points indicated to the bottom right of each stereogram. (Adapted from Merguerian and Sanders, 1991, Figure 26, p. 113.)

Second Ave Subway Mapping

The long-delayed Second Avenue Subway project in NYC has provided us an opportunity for a thorough three-dimensional study of the stratigraphy, structure, and metamorphism of the Hartland formation in NYC. Between 83rd and 87th streets on Second Avenue twin TBM-bored tunnels and ground-down ancillary station complex excavations indicate that the Hartland in this part of NYC is a migmatitic amphibolite facies rock mass that is well-layered at the scale of 0.5 cm to 1.0 m. The project exposes a schistose to gneissic rock consisting of the assemblage muscovite-quartz-plagioclase-biotite±kyanite± staurolite±garnet with interlayers of quartz-plagioclase-mica granofels, greenish amphibolite±biotite± garnet, subordinate gray quartzite and coticule. The schistose facies is lustrous and consists primarily of aligned fine- to coarse-textured muscovite and thus splits readily along the foliation and lithologic contacts. The mica gneiss, granofels, amphibolite, and quartzite interlayers are typically massive and hard, contain much less mica than the schist and may not show pronounced foliation.

In 2012-13, we had the opportunity to observe and record the F_2 recumbent fold phase in large-scale fresh exposures during our site inspections and mapping of the 86th street station complex of the Second Avenue subway excavation (Merguerian and Merguerian, 2014). Figure 12 provides a south facing view of the main station cavern excavated below 86th street in NYC. The cavern was advanced by traditional drill and blast technology using access shafts at 87th and 83rd streets and by excavating in a series of top down slashes to open the cavern down to the level of existing TBM-bored north and southbound tunnels mined earlier.

Figure 12 - View from north of west (R) and center (L) slashes of North Cavern excavation at 86th Street Station for Second Avenue Subway. West (southbound) TBM tunnel crown at +77.2' exposed in right center of image below area of intersecting joints, faults and resulting overbreak. The center (wet. blackish area) and western (right of center) slashes are discussed in text. (Digital image taken 19 December 2012.)

Center Slash. Exposed in late 2012, the center slash of the 86th street north main station cavern for the Second Avenue Subway project in the vicinity of Station 1205+00 (below 85th street) exposed highly fractured and jointed Harland schist, granofels, and amphibolite in a series of top down excavations that ultimately breached through existing TBM-bored tunnels. The map and image of the center slash (Figure 13) shows SE-plunging F_2 reclined isoclinal recumbent folds of early SE-dipping gently inclined penetrative foliation and deformed grantoid sill (g). Another foliated granitoid is injected along a moderately inclined reverse shear showing 0.5 m of offset. Recrystallization during folding and shearing produces penetrative mica foliation (Feature 10.) that has formed parallel to compositional layering and the S_2 axial surface. Gently inclined foliation joints are prominent discontinuities (J_1) that formed parallel to the foliation and parallel compositional layering. Listed below Figure 13, these are intersected by steep NNE-trending (J_2) and NW-trending (J_3) joints and faults producing overbreak seen at top of image.

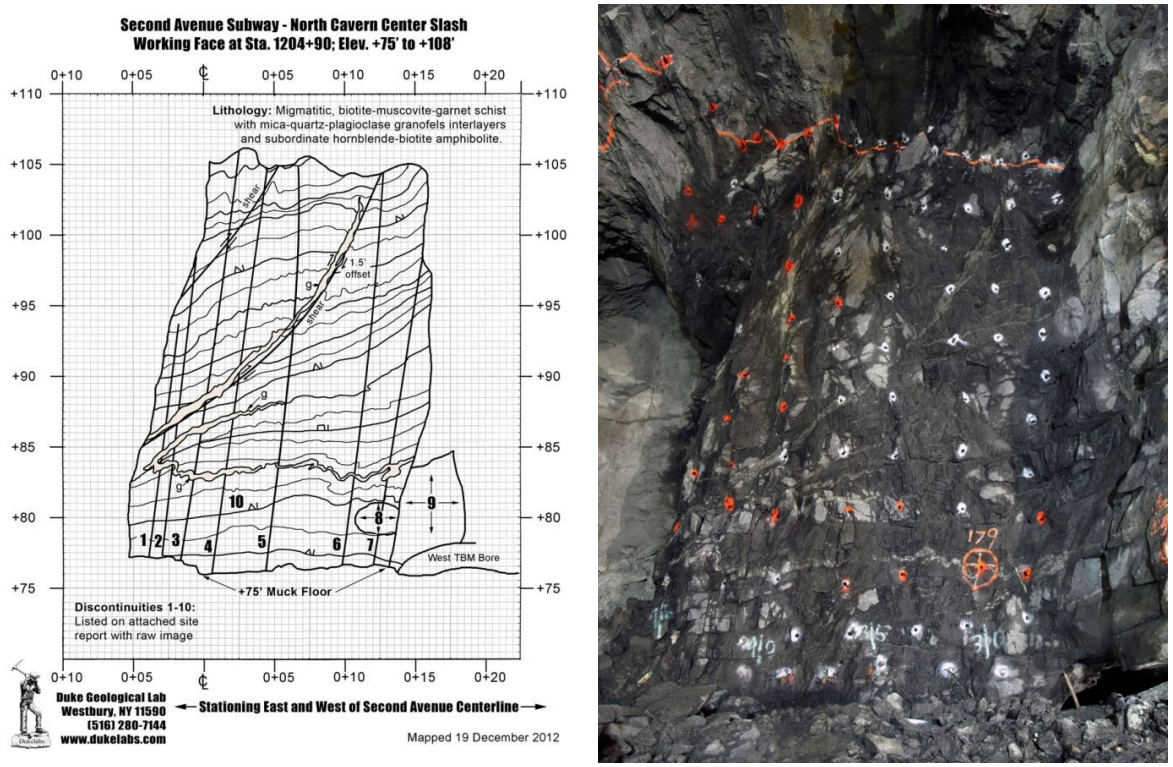

Figure 13 - Isoclinal recumbent folds of early SE-dipping foliation in Hartland formation (O~~C~~h) outlined by grantoid sills (g) with gently inclined penetrative foliation. Recrystallization during folding and shearing produces penetrative mica foliation (Feature 10.) that has formed parallel to compositional layering. Gently inclined foliation joints are prominent discontinuities (J_1) and have formed parallel to the foliation and parallel compositional layering. These are intersected by steep NE-trending (J_2) and NW-trending (J_3) joints and faults producing overbreak seen at top of image. (Digital image taken 19 December 2012.)

Discontinuities of Center Slash

NNE-trending Set (J_2) – Associated with NNE-trending fault system
1 – N32°E, 76°SE, planar, rough joint (one of 11 joints measured in easternmost 5' of rock face)
2 – N34°E, 82°SE, planar, rough joint (one of 11 joints measured in easternmost 5' of rock face)
3 – N30°E, 81°SE, planar, rough joint (one of 11 joints measured in easternmost 5' of rock face)

4 – N30°E, 78°SE, planar, rough joint (one of 15 joints measured in easternmost 10' of rock face)
5 – N19°E, 84°SE to N23°E, 86°NW planar, smooth joints
6 – N31°E, 90° planar, smooth joint
7 – N37°E, 77°SE planar, rough joint

NW-trending Set (J_3) – Associated with NW-trending fault system
8 – N41°W, 51°NE undulating, rough joint
9 – N29°W, 82°NE planar, smooth joint face with trace of K-feldspar and microcrystalline epidote

Foliation and Layering Joints (J_1)
10 – Foliation, layering and parallel J_1 joints are ~ N70°E, 20°SE

West Slash. Also exposed in late 2012, the west slash of the 86th street north main station cavern exposed highly fractured and jointed Harland schist, granofels, and amphibolite. The map and image of the west slash (Figure 14) shows SE-plunging F_2 isoclinal reclined recumbent folds of early SE-dipping gently inclined penetrative foliation. Recrystallization during folding and shearing produces penetrative mica foliation (Feature 13.) that has formed parallel to compositional layering and the S_2 axial surface.

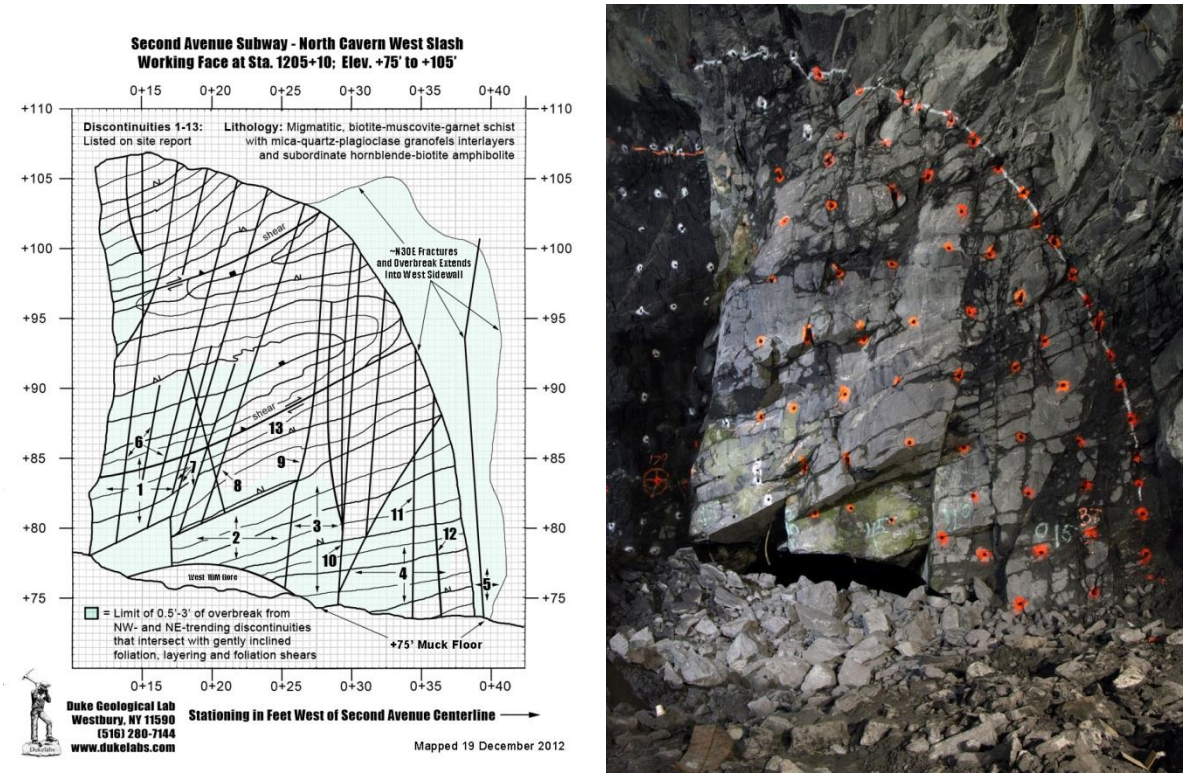

Figure 14 - Geological map and southward view digital image of west slash of North Cavern below 85th street in NYC. Note the internal structure dominated by internally sheared gentle SE-plunging isoclinal recumbent folds of early SE-dipping gently inclined foliation in Hartland formation (O~~€~~h). Recrystallization during folding and shearing produced penetrative mica foliation (Feature 13.) that formed parallel to transposed compositional layering. Gently inclined foliation joints are prominent discontinuities (J_1) and have formed parallel to the foliation and parallel compositional layering. These are intersected by steep NNE-trending (J_2) and NW-trending (J_3) joints and faults producing overbreak (light green shading). (Digital image taken 19 December 2012.)

Gently inclined foliation joints are prominent discontinuities (J_1) that formed parallel to the foliation and parallel compositional layering. Listed below Figure 14, these are intersected by steep NNE-trending (J_2) and NW-trending (J_3) joints and faults producing overbreak (green shading in Figure 14). Figure 15 shows the mineralized coatings on the prominent NW-trending J_3 joints.

Discontinuities of West Slash

NW-trending Set (J_3) – Associated with NW fault system
1 – N37°W, 81°SW, planar, smooth joint filled with K-feldspar and microcrystalline epidote
2 – N50°W, 77°SW, planar, smooth fault filled with K-feldspar and microcrystalline epidote
3 – N40°W, 88°NE, undulating, smooth joint filled with K-feldspar and microcrystalline epidote
4 – N27°W, 88°NE, planar, smooth joint filled with K-feldspar and microcrystalline epidote
5 – N20°W, 87°NE planar, smooth joint filled with K-feldspar and microcrystalline epidote

NNE-trending Set (J_2) – Associated with NNE fault system
6 – N35°E, 86°SE, planar, rough joints (3)
7 – Same as 6 (3 joints)
8 – N41°E, 77°SE, undulating, rough joint
9 – N25°E, 87°SE, slickensides of clay, steep down-dip slicks, planar, rough dip-slip fault
10 – N41°E, 62°SE to 90° at base of wall, undulating, rough reverse fault, seamy with 1.5” stilbite infilling and associated splays/joints (3)
11 – N37°E, 87°SE, undulating, stepped joint
12 – Same as 11

Foliation and Layering Joints (J_1)
13 – Foliation, layering and parallel J_1 joints vary from N66°E, 17°SE to N71°E, 20°SE

Figure 15 - View of microcrystalline epidote (green) and overgrown K-feldspar mineral coating on NW-trending joints cutting Hartland rocks above southbound TBM tunnel. (Digital image taken 19 December 2012.)

To summarize, field studies prior to 1983 (See Figure 11.) and the new views provided by the Second Avenue Subway excavation prove that the internal structure of NYC is dominated by gentle SSW- to SE-plunging recumbent isoclinal long-limbed reclined F_2 folds of an earlier S_1 foliation. This has resulted in a gently inclined (<30°) southward dipping composite penetrative regional foliation (S_1 x S_2) striking NW to ENE that formed mostly parallel to compositional layering (S_0) and includes sill-like masses and thin veins of foliated granitoid. Steeper dips are found in F_2 hinge areas and along the transposed limbs of upright southward plunging F_3 folds where the earlier S_1 x S_2 regional foliation and compositional layering are locally oversteepened. In NYC, the superposed ductile structures are cut by foliation joints (J_1) produced parallel to the regional foliation and by steep NNE- to NE-trending (J_2) joints and dip-slip faults infilled by stilbite+calcite, by younger steep NW-trending (J_3) joints and strike-slip faults infilled by K-feldspar, microcrystalline epidote, quartz and pyrite, and by moderately dipping J_4 joints.

Younger Folds

A geological map of Central Park (Merguerian and Merguerian, 2004 and Figure 18 in our allied 2016 NYSGA field guide) shows the F_4 folds as a series of warps and open folds with axial traces that strike roughly N30°W and exhibit dominantly steep dips to the SW. The effects on map contacts of these late features is negligible but the scatter of poles to S_3 and localized northward plunges of F_3 fold axes and L_3 lineations are the result of post-D_3 deformation. (See Figure 11.) Brittle S_4 cleavages in the bedrock may have helped localize the late stage brittle NW-trending faults that cut the region. Idioblastic muscovite pseudomorphs after D_3 kyanite are common throughout Central Park and many other places throughout NYC. Their abundance suggests a major post-Taconian retrograde metamorphism, presumably coincident with the intrusion of wet granitoids throughout the Manhattan Prong (Brock and Brock, 2001).

Brittle Faults and Joints

Five generations of brittle faults and joints cut polydeformed bedrock units of the NYC area (Merguerian, 2002; 2015). The brittle faults include NW-trending gently SW-dipping faults **(Group A)**, younger ENE-trending faults with moderate to steep dips **(Group B)**, subhorizontal faults and fractures **(Group C)**, and a steep dip-slip NNE-trending fault set **(Group D)** with thick clay- and zeolite-rich gouge zones. These are cut by NW- to NNW-trending strike-slip faults of the "Manhattanville" fault set **(Group E)**. Reactivation of older faults is quite common. The two youngest brittle fault sets (Groups D and E) cross cut all metamorphic structures in NYC and cut the Permian (295 Ma) glassy rhyodacite dikes.

The NYC Water Tunnel #3 cuts through the 125th Street "Manhattanville" fault beneath Amsterdam Avenue in Manhattan. Here, in an abrupt zone of highly fractured Manhattan Schist 40 m wide, the Manhattanville fault dips 55˚ to 75˚ SW and cuts orthogonally across the tunnel line and the steeply dipping foliation in the schist. In the crown of the tunnel, 2 to 3 m blocks of the Manhattan schist, which remained internally coherent within the broad zone of cataclastic rock, showed a minimum of 90˚ rotation about a vertical axis. Clearly, this observation indicates that along the Manhattanville fault, much of the motion has been strike-slip. Indeed, slickensides indicate that right-lateral, normal, oblique slip was the most recent offset sense. Cross-fault offset of the prominent Manhattan ridge indicates over 200 m of composite right-lateral slip.

Joint Orientations. Protracted brittle faulting in the NYC area has developed three mutually intersecting fracture orientations (NW, NNW, and NNE) that together produce a pattern of crustal weakness. Five joint sets, which are parallel to the brittle faults, are found in the NYC area. These include:

1) NW-trending, NE-dipping joints and their conjugates. The NW-trending joints are A-C joints related to southward-plunging F_3 folds.

2) NNE-trending joints with steep dips related to Group D faults. Also includes foliation parting joints and conjugate joint surfaces. Typically with a NE trend these are found more commonly in areas of regional F_3 fold limbs where parallelism of axial surfaces of folds, compositional layering, and foliation occur.

3) Gentle SW-dipping foliation joints developed parallel to SW-dipping foliation and original compositional layering at F_3 fold hinges.

4) Subhorizontal unloading joints and joints related to subhorizontal shear zones, and,

5) Steep ENE joints related to the oldest brittle fault set.

TECTONICS

Modern studies of the Appalachian orogen indicate that an arc-continent collision during the Taconic orogeny produced the imbrication of the oceanward facing passive continental margin of proto North America, development of primary penetrative metamorphic fabrics, F_1 though F_3 folding and the D_2 development of the St. Nicholas and Cameron's Line thrusts. Thus, the deformed Paleozoic bedrock of NYC may have originated within the deep-seated convergent walls of a subduction zone formerly situated off shore from proto-North America. The D_1 to D_3 folds and crosscutting fabrics that presumably formed during the Taconic orogeny are overprinted by two- and possibly three fold phases that, based on their style and general lack of attendant foliation, undoubtedly took place at much-higher crustal levels than did the three Taconian fabrics and are responsible for retrograde fabrics and mica growth. As such, the younger fold phases record the effects of the Acadian- and terminal-stage Appalachian (Alleghenian) orogenesis.

FIELD TRIP GUIDE

In the associated field guide, participants will find more specific details on the trip to Isham, Inwood, and Central parks with individual stop descriptions for each stop. We will try to visit all of the intended stops and will endeavor to fit in additional stops. So pay attention, get your digital cameras ready and for heaven's sake leave the iPods, iPhones, and other distractions in your bags as they are strictly forbidden during the day on our trip! Public humiliation and post-trip drive-by insults at your homes will be a deterrent. Remember that hammering and rock collecting in NYC parks is strictly forbidden.

REFERENCES CITED

Baskerville, C. A., 1994, Bedrock and engineering geology maps of New York County and parts of Kings and Queens counties, New York and parts of Bergen and Hudson counties, New Jersey: U. S. Geological Survey Miscellaneous Investigations Series Map I-2306 (2 sheets; colored maps on scale of 1/24,000).

Berkey, C. P., 1911, Geology of the New York City (Catskill) aqueduct: New York State Museum Bulletin 146, 283 p.

Berkey, C. P., 1933, Engineering geology of the City of New York, p. 77-123 *in* Berkey, C. P., *ed.*, Guidebook 9, New York Excursions, New York City and vicinity: International Geological

Congress, 16th, United States, 1933, Washington, D. C., United States Government Printing Office, 151 p.

Berkey, C. P., 1948, Engineering geology in New York City, Excursion No. 4, p. 51-66 *in* Creagh, Agnes, *ed*., Guidebook of Excursions: Geological Society of America Annual Meeting, 61st, New York City, 135 p.

Brock, P. J. C., 1989, Stratigraphy of the northeastern Manhattan Prong, Peach Lake quadrangle, New York-Connecticut, p. 1-27 in Weiss, Dennis, ed., New York State Geological Association Annual Meeting, 61st, Field trip guidebook: Middletown, NY, Orange County Community College, Department of Science and Engineering, 302 p.

Brock, P. J. C., 1993 ms., Geology of parts of the Peach Lake and Brewster quadrangle, southeastern New York and adjacent Connecticut, and basement blocks of the north-central Appalachians: New York, NY, City University of New York Graduate Faculty in Earth and Environmental Sciences, Ph. D. Dissertation, 494 p., 6 plates.

Brock, P. J. C., and Brock, P.W.G., 2001, Bedrock geology of New York City: More than 600 m.y. of geologic history: http://pbisotopes.ess.sunysb.edu/reports/NYCity/index.html, 11 p.

Brock, Pamela Chase; Brock, Patrick W. G.; and Merguerian, Charles, 2001, The Queens Tunnel Complex: a newly discovered granulite facies Fordham orthogneiss complex that dominates the subsurface of western Queens: p. 1-8 *in* Hanson, G. N., *chm*., Eighth Annual Conference on Geology of Long Island and Metropolitan New York, 21 April 2001, State University of New York at Stony Brook, NY, Long Island Geologists Program with Abstracts, 128 p. http://www.geo.sunysb.edu/lig/Conferences/abstracts-01/brock-3/PCBetal2001.htm

Dana, J. D., 1880, On the geological relations of the limestone belts of Westchester Co., N. Y.: American Journal of Science, 3rd series, v. 20, p. 21-32, 194-220, 359-375, 450-456 (1880); v. 21, p. 425-443; v. 22, p. 103-119, 313-315, 327-335, maps (1881).

Fuller, Tyrand; Short, Lesley; and Merguerian, Charles, 1999, Tracing the St. Nicholas thrust and Cameron's Line through the Bronx, NYC, p. 16-23 *in* Hanson, G. N., *chm*., Sixth Annual Conference on Geology of Long Island and metropolitan New York, 24 April 1999, State University of New York at Stony Brook, NY, Long Island Geologists Program with Abstracts, 143 p.

Hall, L. M., 1968a, Times of origin and deformation of bedrock in the Manhattan Prong, p. 117-127 *in* Zen, E-an; White, W. S.; Hadley, J. B.; and Thompson, J. B., Jr., *eds*., Studies of Appalachian geology, northern and maritime: New York, Wiley-Interscience Publishers, 475 p.

Hall, L. M., 1968b, Bedrock geology in the vicinity of White Plains, New York, Trip A, p. 7-31 *in* Finks, R. M., *ed*., Guidebook to Field Excursions: New York State Geological Association Annual Meeting, 40th, Queens College, Flushing, New York: Flushing, NY, Queens College Department of Geology, 253 p.

Hall, L. M., 1976, Preliminary correlation of rocks in southwestern Connecticut, p. 337-349 in Page, L. R., ed., Contributions to the stratigraphy of New England: Geological Society of America Memoir 148, 445 p.

Hall, L. M., 1980, Basement-cover relations in western Connecticut and southeastern New York, p. 299-306 *in* Wones, D. R., *ed*., International Geological Correlation Project, Proceedings, Project 27: The Caledonides in the U. S. A.: Blacksburg, VA, Virginia Polytechnic Institute and State University Department of Geological Sciences Memoir 2, 329 p.

Merguerian, Charles, 1977, Contact metamorphism and intrusive relations of the Hodges Complex along Cameron's Line, West Torrington, Connecticut: New York, NY, The City College of New York Department of Earth and Planetary Sciences Master's thesis, 89 p. with maps (also on open-file Connecticut Geological Survey, Hartford, Connecticut).

Merguerian, Charles, 1979, Dismembered ophiolite along Cameron's Line, West Torrington, Connecticut (abs.): Geological Society of America Abstracts with Programs, v. 11, p. 45.

Merguerian, Charles, 1981, Tectonic history of the New York City area (abstract): Empire State Geogram, v. 17, p. 28 (only).

Merguerian, Charles, 1983a, Tectonic significance of Cameron's Line in the vicinity of the Hodges Complex--an imbricate thrust (sic) model for Western Connecticut: American Journal of Science, v. 283, p. 341-368.

Merguerian, Charles, 1983b, The structural geology of Manhattan Island, New York City (NYC), New York (abstract): Geological Society of America Abstracts with Programs, v. 15, p. 169 (only).

Merguerian, Charles, 1987, The geology of Cameron's Line, West Torrington, Connecticut: in Roy, D.C., ed., Northeastern Section of the Geological Society of America, Centennial Fieldguide, p. 159-164.

Merguerian, Charles, 1988, Annealed mylonitic textures in polyphase deformed metamorphic terrains (abs.): Geological Society of America, Abstracts with Programs, v. 20, p. A214.

Merguerian, Charles, 1994, Stratigraphy, structural geology, and ductile- and brittle faults of the New York City area, p. 49-56 *in* Hanson, G. N., *chm*., Geology of Long Island and metropolitan New York, 23 April 1994, State University of New York at Stony Brook, NY, Long Island Geologists Program with Abstracts, 165 p.

Merguerian, Charles, 1996a, Stratigraphy, structural geology, and ductile- and brittle faults of New York City, p. 53-77 *in* Benimoff, A. I. and Ohan A. A., *chm.*, The Geology of New York City and Vicinity, Field guide and Proceedings, New York State Geological Association, 68th Annual Meeting, Staten Island, NY, 178 p.

Merguerian, Charles, 1996b, Evidence for post-glacial surface faulting in New York City (abs.): Geological Society of America Abstracts with Programs, v. 28, no. 3, p. 81.

Merguerian, Charles, 2000, Rock mass properties of the Queens Tunnel Complex: Duke Geological Laboratory Report QT0010, 257 p. + Geological Field Map Album, Scale 1"=10' (Stations 3+65 to 254+00).

Merguerian, Charles, 2001, Young rhyodacite dikes found in the Queens Tunnel, beneath Woodside, Queens: p. 9-19 *in* Hanson, G. N., *chm*., Eighth Annual Conference on Geology of Long Island

and metropolitan New York, 21 April 2001, State University of New York at Stony Brook, NY, Long Island Geologists Program with Abstracts, 128 p.

Merguerian, Charles, 2002, Brittle faults of the Queens Tunnel Complex, NYC Water Tunnel #3: p. 63-73 *in* Hanson, G. N., *chm*., Ninth Annual Conference on Geology of Long Island and metropolitan New York, 20 April 2002, State University of New York at Stony Brook, NY, Long Island Geologists Program with Abstracts, 116 p.

Merguerian, Charles, 2010, Tectonics implications of bedrock studies at the World Trade Center Site (WTC), NYC: Geological Society of America Abstracts with Programs, v. 42, no. 1, p. 171.

Merguerian, Charles, 2015, Review of New York City bedrock with a focus on brittle structures; *p. 17-67 in Herman, G. C. and Macaoay Ferguson, S., eds.*, Geological Association of New Jersey Guidebook, Neotectonics of the New York Recess, 32nd Annual Conference and Field Trip, Lafayette College, Easton, PA, 214 p.

Merguerian, Charles, 2016, Wallrocks of the Hodges Complex and Tyler Lake Granite, West Torrington, Connecticut: Geological Society of Connecticut Fieldguide No. 7, 16 April 2016, 46 p.

Merguerian, Charles; and Baskerville, C. A., 1987, The geology of Manhattan Island and the Bronx, New York City, New York, p. 137-140 in Roy, D. C., ed., Northeastern Section of the Geological Society of America, Centennial Fieldguide, Volume 5, 481 p.

Merguerian, Charles; and Merguerian, Mickey, 2004, Geology of Central Park – From rocks to ice: *in* Hanson, G. N., *chm*., Eleventh Annual Conference on Geology of Long Island and Metropolitan New York, 17 April 2004, State University of New York at Stony Brook, NY, Long Island Geologists Program with Abstracts, 24 p.
http://www.geo.sunysb.edu/lig/Conferences/abstracts-04/merguerian/Merguerians2004.htm

Merguerian, Charles; and Merguerian, J. Mickey, 2012, Structural geology and metamorphism of the Inwood Marble, NYC, NY: Geological Society of America Abstract # 199974, Abstracts with Programs, v. 44, no. 2, p. 73.

Merguerian, Charles; and Merguerian, J. Mickey, 2014, Stratigraphy, structural geology and rock mass properties of the Hartland Formation, Second Avenue Subway, NYC, NY: Geological Society of America Abstract # 235972, Abstracts with Programs, v. 46, no. 2, p. 90.

Merguerian, Charles; Merguerian, J. Mickey; and Cherukupalli, Nehru, E., 2011, Stratigraphy, structural geology and metamorphism of the Inwood Marble Formation, northern Manhattan, NYC, NY: *in* Hanson, G. N., *chm*., Eighteenth Annual Conference on Geology of Long Island and Metropolitan New York, 09 April 2011, State University of New York at Stony Brook, NY, Long Island Geologists Program with Abstracts, 19 p.
http://www.geo.sunysb.edu/lig/Conferences/abstracts11/merguerian-2011.pdf

Merguerian, Charles; and Moss, C. J., 2005, Newly discovered ophiolite scrap in the Hartland Formation of midtown Manhattan: *in* Hanson, G. N., *chm*., Twelfth Annual Conference on Geology of Long Island and Metropolitan New York, 16 April 2005, State University of New York at Stony Brook, NY, Long Island Geologists Program with Abstracts, 8 p.
http://www.geo.sunysb.edu/lig/Conferences/abstracts-05/merguerian-moss.htm

Merguerian, Charles; and Moss, C. J., 2006**,** Structural implications of Walloomsac and Hartland rocks displayed by borings in southern Manhattan: *in* Hanson, G. N., *chm*., Thirteenth Annual Conference on Geology of Long Island and Metropolitan New York, 22 April 2006, State University of New York at Stony Brook, NY, Long Island Geologists Program with Abstracts, 12 p.
http://www.geo.sunysb.edu/lig/Conferences/abstracts06/merguerian-06.pdf

Merguerian, Charles; and Moss, C. J., 2007, Newly discovered serpentinite bodies associated with the St. Nicholas thrust zone in northern Manhattan: *in* Hanson, G. N., *chm*., Fourteenth Annual Conference on Geology of Long Island and Metropolitan New York, 14 April 2007, State University of New York at Stony Brook, NY, Long Island Geologists Program with Abstracts, 13 p.
http://www.geo.sunysb.edu/lig/Conferences/abstracts07/abstracts/merguerian-07.pdf

Merguerian, Charles; and Sanders, J. E., 1991, Trip 16: Geology of Manhattan and the Bronx, 21 April 1991: New York Academy of Sciences Section of Geological Sciences Trips on the Rocks Guidebook, 141 p.

Merguerian, Charles; and Sanders, John E., 1998, Annealed mylonites of the Saint Nicholas thrust (SNT) from a new excavation at the New York Botanical Gardens, The Bronx, New York: p. 71-82 *in* Hanson, G. N., *chm*., Geology of Long Island and metropolitan New York, 18 April 1998, State University of New York at Stony Brook, NY, Long Island Geologists Program with Abstracts, 161 p.

Merrill, F. J. H., 1890, On the metamorphic strata of southeastern New York: American Journal of Science, 3rd series, v. 39, p. 383-392.

Merrill, F. J. H., and others, 1902, Metamorphic crystalline rocks of the New York City quadrangle, *in* Merrill, F. J. H.; Darton, N. H.; Hollick, Arthur; Salisbury, R. D.; Dodge, R. E.; Willis, Bailey; and Pressey, H. A., Description of the New York City district: United States Geological Survey Geologic Atlas of the United States, New York City Folio, No. 83, 19 p. (Includes colored geologic map on a scale of 1:62,500).

Mather, W. W., 1843, Geology of New York. Part I. Comprising the geology of the First Geological District: Albany, NY, Carroll & Cook, Printers to the Assembly, 653 p., 46 pl. (Includes report of Prof. L. D. Gale on New York Island based on survey of 1828 and 1829.)

Norton, M. F., 1959, Stratigraphic position of the Lowerre Quartzite: p. 1148-1158 *in* Lowe, K. E., *chm. and consulting ed*., Modern aspects of the Geology of New York City and environs: New York Academy of Sciences Annals, v. 80, art. 4, p. 1047-1169.

Schnock, E. M., 1999, Construction of the Brooklyn Tunnel: p. 91-100 *in* Mega Projects – Means, methods and other construction issues, American Society of Civil Engineers, Metropolitan Section, Annual Seminar Proceedings, Cooper Union, NY, February 1999, 140 p.

Scotford, D. M., 1956, Metamorphism and axial-plane folding in the Pound Ridge area, New York: Geological Society of America Bulletin, v. 67, p. 1155-1198.

Ziegler, Victor, 1911, The Ravenswood granodiorite: New York Academy of Sciences Annals, v. 21, p. 1-10.

TRIP A-5 - FIELD GUIDE TO ISHAM, INWOOD, and CENTRAL PARKS, NYC, NY

CHARLES MERGUERIAN
Professor Emeritus, Geology Department, Hofstra University, Hempstead, NY 11549, Research Fellow, Yale University, New Haven CT 06520 and Principal, Duke Geological Laboratory, Stone Ridge, NY 12484

J. MICKEY MERGUERIAN
Geologist, Duke Geological Laboratory, Stone Ridge, NY 12484

The following field guide and road log is intended to provide participants with keys to understanding our subdivisions of the venerable Manhattan Schist into three separable units by utilizing exposures in New York City including Isham, Inwood Hill and Central parks and to show in the bedrock structural evidence for our tectonic interpretations. The field guide is split into two major field localities, each with individual stops. Locality 1 is Isham and Inwood Hill parks in northern Manhattan and Locality 2 is the south part of Central Park in midtown Manhattan.

Meeting Points: NE corner of Isham Street and Seaman Avenue, NYC, NY. Parking is available in the streets to the north, south and east of meeting point. Parking is typically good on weekends but be sure to read posted parking signs to avoid ticketing. We plan to use public transportation (A-Train at 207th Street and Broadway downtown to Columbus Circle) to travel between Locality 1 and Locality 2. Those planning to drive to Locality 2 should leave ample time for parking on midtown Manhattan.

*****Maximum of 20 participants - Bring lunch and drinking water!*****

Locality 1 - Isham Park and Inwood Hill Park entrances (Isham Street and Seaman Avenue).
Locality 2 - Central Park at the SW entrance (59th Street and Eighth Avenue).

Meeting Point Coordinates: Locality 1 - 40.869°N; 73.921°W; Locality 2 - 40.768°N; 73.981°W

Meeting Times: Locality 1 - 9:00 AM sharp; Locality 2 - about 1:30 PM (01 October 2016).

Distance in miles

Cumulative	Point to Point	Route Description
0.0	0.00	Start out at Hilton Hotel in Nanuet (425 State Route 59, Nanuet, NY).
0.06	0.06	Drive east on NY-59/Route 59 then stay straight to ramp for Palisades Interstate Parkway.
0.33	0.27	Merge onto Palisades Interstate Pkwy S (Crossing into NJ).
18.63	18.30	Drive S on PIP, then take I-95 N/US-1 N/US-9 N (Crossing into NY).
19.67	1.04	Take the NY-9A/Henry Hudson Pkwy exit (EXIT 1).
20.08	0.41	Keep right to take the ramp toward NY-9A N.
20.28	0.20	Merge onto NY-9A N/Henry Hudson Pkwy N via the ramp on left toward Pkwy N/Upstate.
21.79	1.51	Take EXIT 17 toward Dyckman Street.
21.91	0.12	Turn slight right onto Riverside Drive.
22.10	0.19	Turn slight left onto Broadway/US-9 N.
22.53	0.43	Destination = Isham Street and Broadway, just beyond W. 207th Street. Isham Park is upslope, west of Broadway on Isham Street just before Seaman Avenue.

Locality 1 – Isham and Inwood Hill Parks

Today's field trip will start where bedrock is exposed in northernmost Manhattan in Isham and Inwood Hill parks (Figure 1). Northern Manhattan boasts the highest natural point of elevation at +265.5' achieved atop rocky ridges in Bennett Park. The rocky ridges rise abruptly above the lowland plain to the east underlain by Inwood Marble. The adjacent prominent ridges are underlain by the venerable Manhattan Schist (OZm). Our analysis of the area departs a bit from published work in that we recognize schistose rocks in Manhattan aside from the Manhattan Schist. Indeed, in Inwood Hill Park representatives of all three ductile fault bounded schistose units can be found (Walloomsac [Ow], Manhattan [OZm] and Hartland [O€h] formations).

A cut-away cross-sectional view of northern Manhattan appears on a Google Earth basemap in Figure 2. Note the interpretation of the structure suggesting that the rocky ridges of northern Manhattan are controlled by overturned synforms of Manhattan Schist rooted by a major shear zone known as the St. Nicholas thrust which cuts both the Inwood Marble (O€i) and locally, the Walloomsac Schist (Ow). Below the flat plains of northeastern Manhattan, the Inwood is folded upward to the earth's surface and beveled above two eroded F_3 antiforms cored by Fordham Gneiss and an intervening F_3 synform with all folds and most associated fabrics overturned toward the NW.

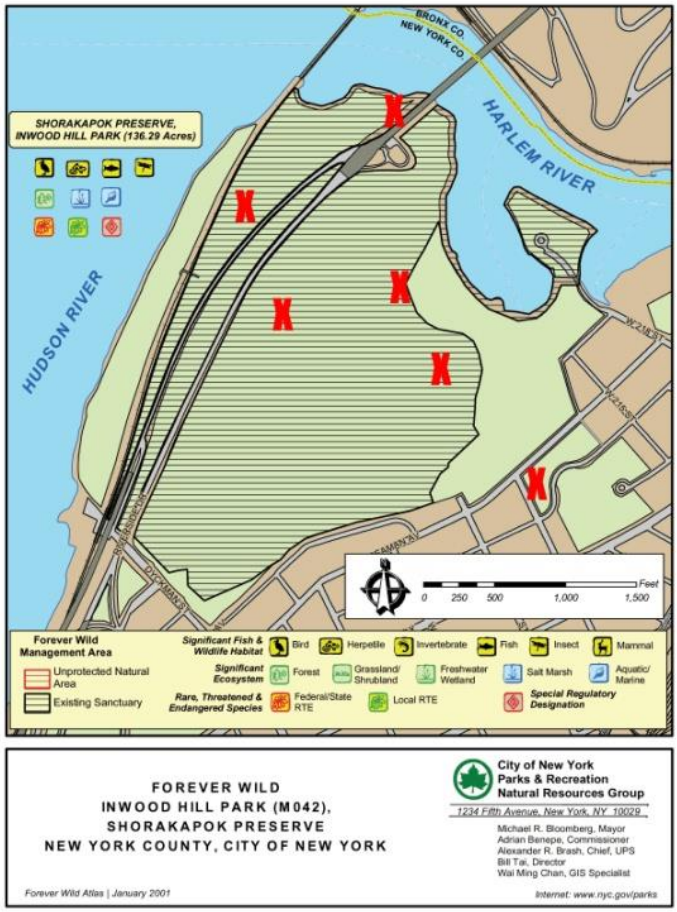

Figure 1 - Index map of Isham and Inwood Hill Parks showing the location of our intended sub-stops.

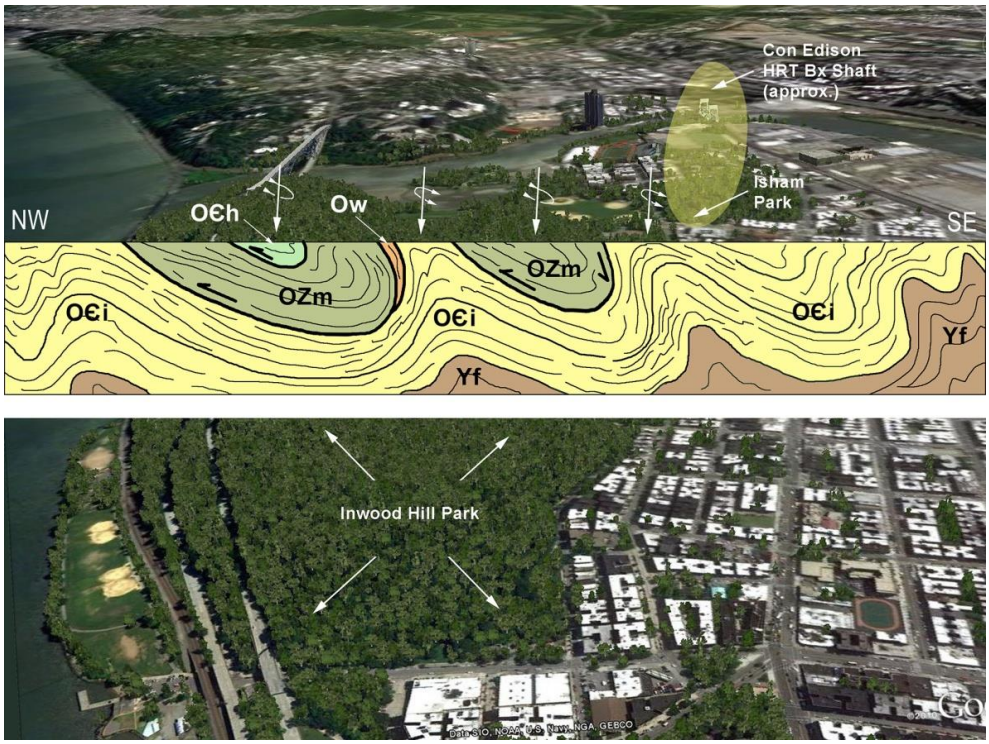

Figure 2 - Oblique northeastward Google Earth terrain view of northern Manhattan and the Bronx with Dyckman Street near the edge of the lower section. Interpretive geological section in cut-away slice roughly across Isham Street in Manhattan. Proposed along-strike correlation between Isham Park and the Bronx Shaft of a utility tunnel (approximately located for security reasons) shown in yellow shading marks the along strike extension of the SE-dipping limb of an overturned SW-plunging F_3 antiform. Note the positions of major overturned F_3 antiforms and synforms (shown in white), the folding of sheared lithologic contacts, and the position of a thin slice of Waloomsac Schist (Ow) exposed beneath the south footing of the Henry Hudson Bridge in Inwood Hill Park.

Isham Park contains near continuous exposure of white to blue-white Inwood Marble cut by high-angle conjugate joints which have facilitated the weathering process by allowing aqueous solutions to permeate the rocks (Figure 3). Several lithologies occur such as dolomitic marble, calcite marble, amd foliated calc-schist, units that contain siliceous layers and calc-silicate aggregates that stand in relief on the weathered surface (Figure 4).

Depending on the amount of impurities the Inwood Marble weathers gray or tan and produces a sugary-textured surface on outcrops that ultimately develops into residual calcareous sand. Overall, the outcrops illustrate profound differential weathering with dolomite-silicate units standing in higher relief and calcite marble forming local depressions. With a bit of imagination, an overview of the entire outcrop at Isham Park allows a vision of mini-karst-like topography. Perched on this eroded surface are a number of Palisades diabase erratics and red-colored till, products of glacial advance from the NW.

A preliminary geological map of Isham Park is shown as Figure 5. Four major lithotypes are shown – white, coarse-textured calcite marble, white to gray dolomitic and calcite marble, marble, schist and calc-silicate rock and well-layered white to gray dolomitic marble. Although variable, the Inwood trends roughly N55°E, 73° SE in Isham Park and forms the eastern overturned limb of a large F_3 synform which is cored to the west in Inwood Hill Park by the Manhattan Schist.

Figure 3 - Northward view of highly jointed east-dipping Inwood Marble exposed in Isham Park in Manhattan. Although well-foliated, the obvious compositional layering preserves ancient bedding in the rock mass. (Digital image taken 19 August 2007.)

Figure 4 - View of a cluster of aligned 6-12 cm tremolite porphyroblasts found to overgrow the S_1 x S_2 composite foliation in dark gray marble with interlayered calc-schist. We are convinced that these are pseudomorphs after diopside. Exposed portion of knife is 6 cm long. (From Merguerian et al., 2001.)

The marble, schist, and calc-silicate unit is intensely sheared and internally deformed by F_2 tight- to isoclinal and F_3 asymmetric folds producing complex interference patterns, boudinage and internal shearing of schistose boudins over a meter in dimension (Figure 6). Clearly, the marble + schist + calc-silicate sub-unit shows overthickening and repetition of layers however most of the remaining carbonate sequence exposed in Isham Park appears to be homoclinal. Perhaps the overthickening of the calc-schist unit is the result of the buttressing effect of the massive, well-layered marble that surrounds it. Asymmetric south-plunging F_3 folds are locally developed in the Inwood of Isham Park (Figure 7). Abundant examples of boudinage of the quartzite and calc-silicate layers into lenses occur presumably the result of ductility contrast between the more competent siliceous rocks and the surrounding marble (Figure 8).

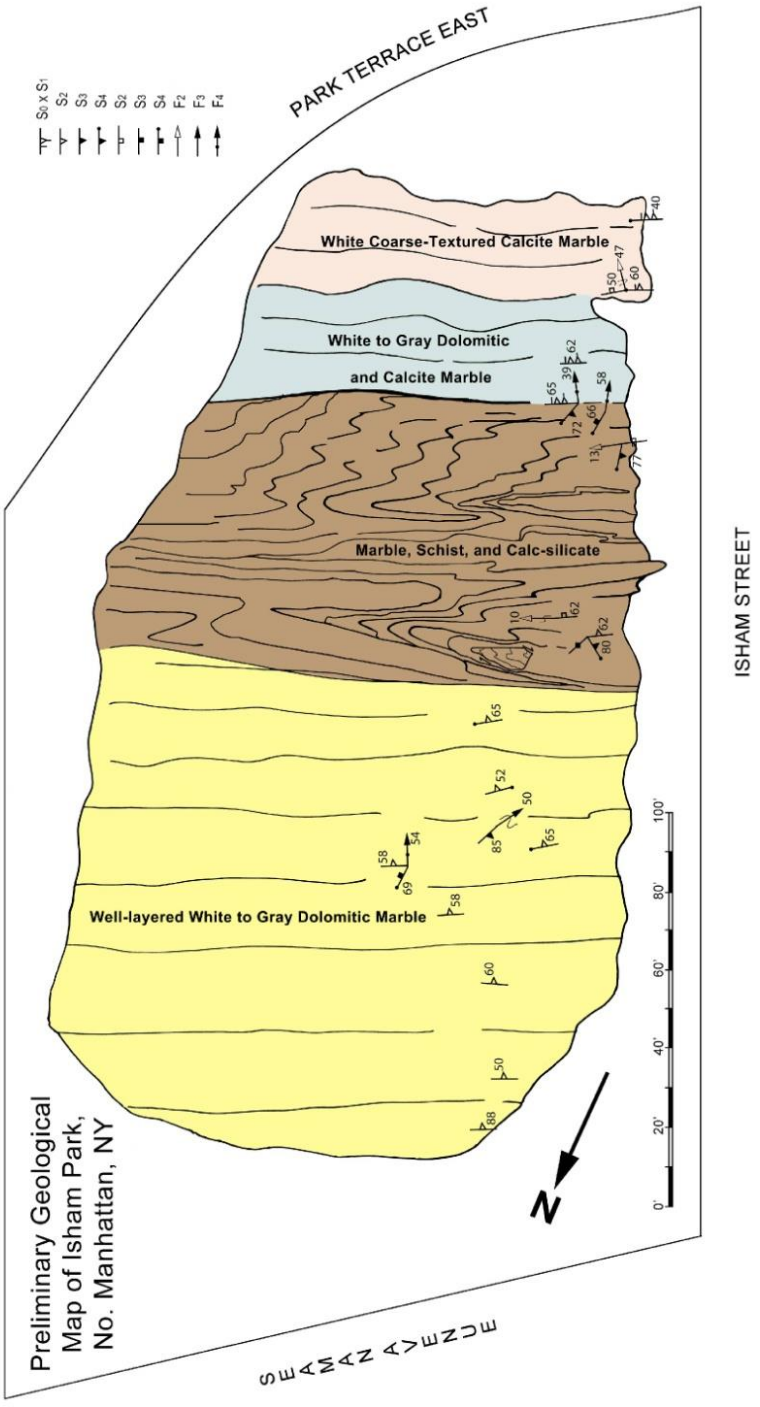

Figure 5 - Preliminary geological map of Isham Park showing the four major lithologic varieties and the form lines of the composite S_1 x S_2 foliation and parallel compositional layering. (From Merguerian et al., 2011.)

The broad outcrop-scale folding and warping of the S_1 x S_2 fabric is controlled not only by regional F_3 folds but also are affected by open 2 m-wavelength SE-plunging F_4 crenulate folds and open warps (~ 55° plunge) with axial planar slip cleavage (S_4), solution cleavage and joints trending ~ N-S bearing moderate to steep dips.

Figure 6 - View on internal deformation in the Inwood Marble of Isham Park in Manhattan showing shearing and disarticulation of resistant quartzite and calc-silicate interlayers and meter-scale blocks of calc-marble and the overall complex patterns produced by gently plunging upright F_2 isoclinal folds. (Digital image taken 08 Sept 2007.)

Figure 7 - View of a south-plunging asymmetric F_3 z-fold of layering and foliation in the Inwood Marble of Isham Park in northern Manhattan. Pen points in plunge direction. (Digital image taken 08 Sept 2007.)

Figure 8 - View of disarticulated boudin of quartzite (former chert?) in differentially weathered Inwood Marble exposed in Isham Park in northern Manhattan. Such features result from the mechanical differences between the competent quartzite and the less competent marble which undoubtedly flowed around the resilient quartzite layers and lenses. Note 9-cm long black pocket knife to left of boudin for scale. (Digital image taken 19 August 2007.)

Inwood Hill Park

The area of Manhattan north of Dyckman Street is known as the Inwood section. Except for Inwood Hill Park most of the region is underlain by the Inwood Marble marking the type-locality for that particular unit of NYC bedrock. This unit was originally called the Inwood Limestone by Merrill (1890). The geology of Inwood Hill Park is published elsewhere (Merguerian and Sanders 1991; Merguerian et al., 2011) but a brief summary is in order. Inwood Hill Park is located in the extreme northwest corner of Manhattan Island (Figure 22). The park is bordered by Dyckman Street on the south, the Hudson River on the west, Spuyten Duyvil (Harlem Ship Canal) on the north, and Payson and Seaman Avenues on the east. Isham Park occupies the flat area northeast of Inwood Hill Park extending eastward to Broadway between Isham and West 214th Streets.

We enter Inwood Park by following the path past the playground. The first prominent ridge to your left is composed of Manhattan Schist (OZm) which also dips steeply toward the SE, essentially parallel to the orientation of the Inwood Marble exposed in Isham Park. The S_3 foliation in the schist is related to F_3 folds with axial surfaces oriented N4l°E, 75°SE and south-plunging hingelines. The F_3 structures are superimposed on an older gently inclined S_2 metamorphic layering which trends across Manhattan at roughly N50°W, 25°SW (Merguerian, 1983; 1996a). Both units are in contact but the contact is covered with soil. They form part of a huge south-plunging syncline with the Manhattan Schist preserved in the central core of the structure (Figure 10).

Strangely, the downfolds (synclines) hold up ridges and the upfolds (anticlines) underlie the flat valleys in northern Manhattan. Such inverted topography results from the marked contrast in weathering

susceptibility afforded by the marble and schist. In the overall wet temperate climates such as we experience in this region, carbonate rocks (such as the Inwood Marble) weather and dissolve much more readily than do silica-rich rocks of the Manhattan Schist. As a result, structural synclines tend to be preserved to form topographically high ridges and structural anticlines are breached by weathering and erosion and commonly underlie the low valleys. (See Figure 2.) Such topographic inversions are well known in the folded central and northern Appalachians.

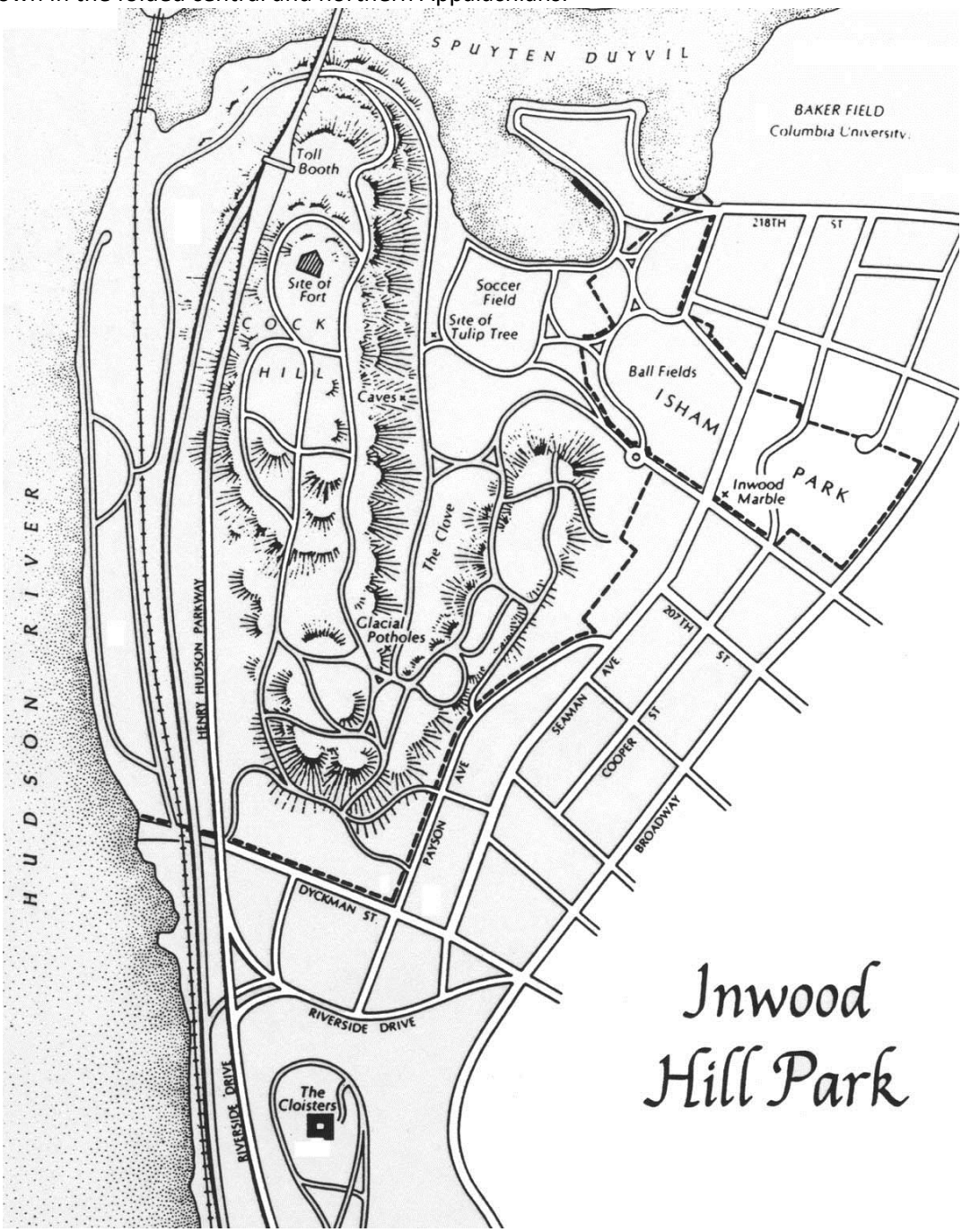

Figure 9 - Index map showing the location of our field trip area in Isham and Inwood Hill parks in northern Manhattan. You can use this map to put in the ad-hoc field stops for today's trip to Locality 1.

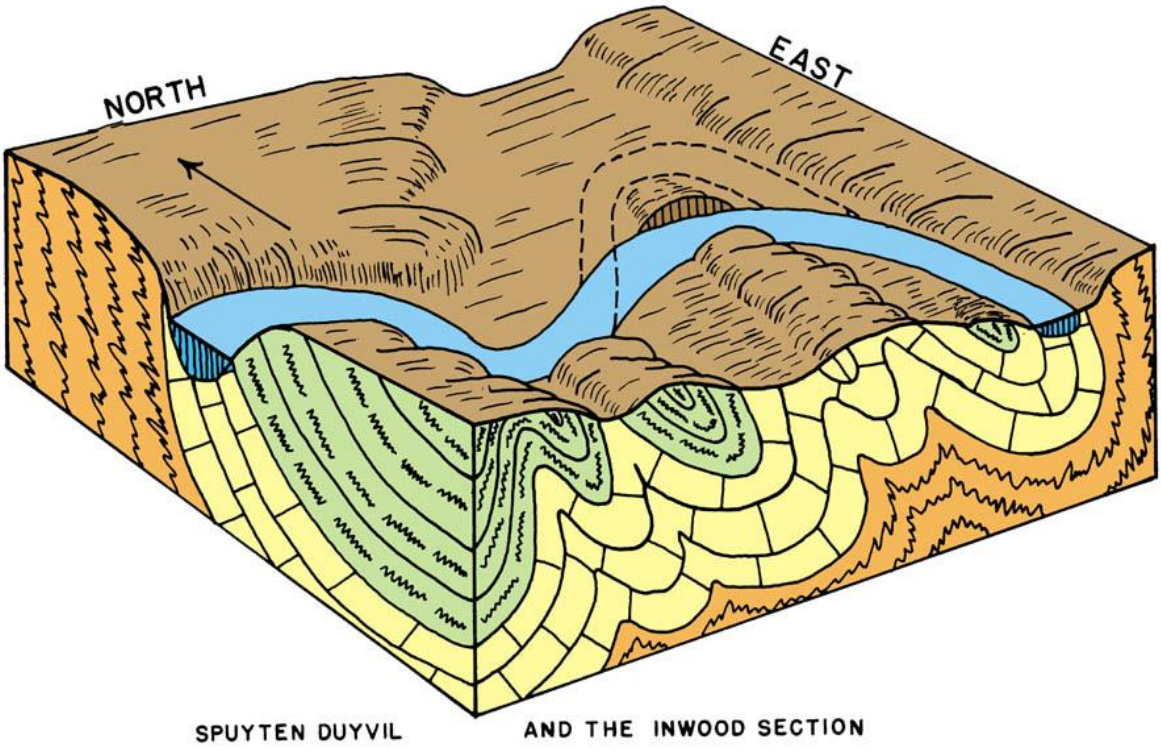

Figure 10 - Block diagram illustrating the structural geology of Inwood and Isham parks. Note that the topographically higher portions of Inwood Park are underlain by the Manhattan Schist (green) and that the topographically lower portions are underlain by the Inwood Marble (yellow). This is the result of the difference in weathering susceptibility of the Inwood and Manhattan. In overall humid, wet climates such as we experience in this region, carbonate rocks (such as the Inwood) weather much more readily than do silica-rich rocks of the Manhattan Schist. Note how the topographically higher ridges are structural synforms (downfolds) yet the valleys are underlain by structural upfolds (antiforms). Such "inverted" topographic relationships are common in the folded Appalachians. (Legacy diagram from CCNY Geology Department.)

Take the “high-road” path going southward to examine the dual potholes drilled into the east-facing slope of the westernmost synclinal ridge. The structure of the westernmost ridge is another south-plunging syncline overturned toward the northwest. (See Figure 10.) The S_3 foliation in the Manhattan schist has transposed earlier fabrics and is associated with tight isoclinal F_3 folds south-plunging hingelines and axial surfaces oriented N41°E, 75°SE. At the north end of this ridge, we'll see the S_2 foliation change trend from NE to NW to wrap around the synformal trough.

At the top of the trail, a bonus for glacial enthusiasts, two circular potholes produced by torrents of meltwater during the Pleistocene deglaciation are found (Figure 11). Clearly the potholes are cut into an already glacially polished rock outcrop. Here, we assume that resistant glacial drift boulders settled into a small depression (perhaps in ridge hugging drift) and then began to drill downward in response to vortices produced during turbulent flow from liberated glacial melt waters. A self-fulfilling prophesy, once the drilling begins the resistant boulders are trapped and constantly replenished by new boulders moved by water. In this case (Figure 11) the upper pothole merged to drill a second adjacent pothole. Since the potholes are developed on a sloping glaciated surface (pre-Woodfordian?), it may be tempting to envision that the potholes formed during a younger glaciation (Woodfordian?).

Figure 11 - View of dual potholes "drilled" by resistant boulders driven by glacial meltwater torrents. (Digital image taken 13 Nov 2004.)

Farther up at the top of the trail past the potholes but before the trail bends into a hairpin turn to the right, note the highly polished outcrop of Manhattan Schist (Figure 12). The glacial striae and grooves are oriented N35°W to S35°E indicating the same glaciation that brought Palisades boulders from New Jersey. Sanders and Merguerian (1998) suggest this glaciation (from the NW to SE) was responsible for most of the deep glacial erosion in the NYC area and produced the prominent Harbor Hill moraine that extends across Staten Island, Brooklyn, Queens, and Long Island.

Figure 12 - View from the NNW of a glacially polished outcrop of Manhattan Schist in Inwood Hill Park showing a smooth up-glacier side (foreground) and steep, rough down-glacier side (behind White Fang). The glacial striae and grooves are oriented N35°W to S35°E, a product of the pre-Woodfordian glaciation. (Digital image taken November 2007.)

To Scenic Overlook of Hudson River and Palisades Intrusive Sheet

Continue up the trail on top of the westernmost ridge and jog left after awhile to get to the fine overlook across the Hudson to the Palisades ridge of New Jersey (Figure 13). Here, the columnar joints of the Palisades ridge are quite visible forming a steep wall of mafic rock that was intruded at shallow depth during the late Triassic-Early Jurassic split up of Pangea. Thus, we view across the Hudson, the products of a totally different type of tectonic activity than we have been viewing today. The metamorphic rocks of New York City were produced during deep-seated compressive deformation while the sedimentary and igneous rocks of New Jersey were produced by extensional tectonics associated with initial formation of the Altantic Ocean basin. A cross sectional view from Manhattan to central New Jersey (Figure 14) shows that the entire Newark Basin is a rotated block of the earth's crust with downward motion and westward tilting accommodated along the Ramapo fault. In this way the ancient Newark Basin is analogous to the modern rift basins of East Africa.

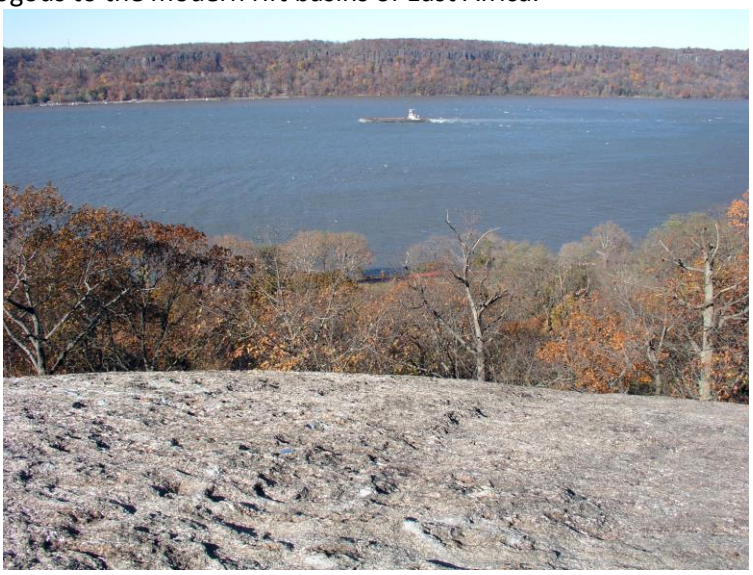

Figure 13 - View from the overlook atop the westernmost ridge of Inwood Hill Park westward across the Hudson River towards New Jersey. Note the glacially polished exposure of schist and the NW-SE trending grooves and striae pointing to the Palisades sheet of New Jersey. (Digital image taken November 2007.)

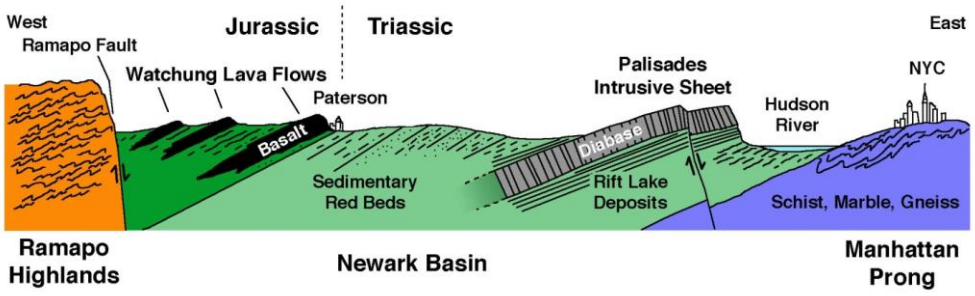

Figure 14 - Cross section showing the geology of the Newark Basin and its relationship to the basin marginal Ramapo fault. Note also the nonconformable contact with the deformed rocks of New York City. The nonconformity spans roughly 300 million years of missing time and thus project with regional tilt of about 12° NW above Manhattan Island. (From Bennington and Merguerian, 2007.)

From the scenic overlook walk northward along trail toward the Henry Hudson Bridge and note that the foliation in the schistose rocks is oriented northwesterly and dips southward at the end of the trail before it heads downward. As mentioned earlier, this is the result of the wrapping of the early S_1 x S_2 foliation in the schist about the southward-plunging keel of the overturned F_3 synform that holds up the westernmost ridge.

The contact between the middle and lower schist units (the St. Nicholas thrust) is exposed in a 20 m zone from beneath the Henry Hudson Bridge abutment to river level. Structurally beneath the Manhattan Schist, a 0.5 m layer of sheared (mylonitic) amphibolite is deformed by folds. Unlike the amphibolite in the schist unit above, which contains subidioblastic hornblende, this exposure of Manhattan amphibolite has been intensely sheared. Green hornblende porphyroclasts are set in a wavy, anastomosing foliation consisting of colorless amphibole, biotite, and quartz ribbons. The thrust zone is structurally complex consisting of intercalated lithologies of Walloomsac (Ow) and Manhattan Schist (OZm) together with mylonitic amphibolite. The Wallomsac is highly flattened and mylonitic at this location with a strong down-dip lineation, the result of localized shearing associated with the St. Nicholas thrust zone.

Directly beneath the bridge, where a dirt trail leads down to the river, a coarse-textured gray-white calcite marble with differentially eroded calc-silicate nodules is exposed at low tide. It is unknown whether the marble exposed at the low-tide mark is an interlayer in the Walloomsac schist (Ow) or the Inwood Marble (O~~Є~~i). Unquestionably, the Inwood Marble lurks nearby as it wraps around the westernmost ridge of Manhattan Schist and underlies the Spuyten Duyvil, Marble Hill in the Bronx, and the Hudson River and was penetrated by a utility tunnel found east of and parallel to the Broadway Bridge. As a geometric result of the southward plunge of the major folds, the oldest unit of the NYC bedrock (Fordham Gneiss) projects up to the surface in the Bronx in a huge vertical exposure immediately across the Harlem Ship Canal. Here, in the Bronx, the Fordham is painted blue with the Columbia University “C”.

Locality 2 - Central Park

The impressive natural rock exposures left in Central Park by implementation of Olmstead and Vaux's Greensward Plan stand as geologic sentinels that offer the geologist a glimpse into the past. Sculpted by glacial ice from at least two contrasting ice-flow directions during Pleistocene times, the rocky knolls expose at the earth’s present surface evidence of sedimentary- and volcanic protoliths that were folded and metamorphosed at depths originally exceeding 20 km. Uplift and erosion have elevated these former deep-seated rocks allowing analysis and interpretation by geologists.

J. F. Kemp (1887) produced the first detailed map of Manhattan, here colorized and reproduced as Figure 15. The map and closely spaced sections were made at a time when bedrock was well exposed in the city both naturally and as a result of active construction. Sections G-H and E-F especially show the dominant tightly-folded structure of Central Park. Detailed work throughout Manhattan by CM started in the early 1970s which ultimately indicated that all three of the units formerly lumped as the Manhattan Schist were present in Central Park. The bulk of the rocks are in tectonic contact with the underlying autochthonous Walloomsac-Inwood sequence. With few exceptions, the southern part of Central Park consists of rocks of the Hartland formation (O~~Є~~h). North of roughly 80th Street, the rocks are predominantly Manhattan Schist (OZm) and Wallomsac (Ow) and Inwood (O~~Є~~i) dominate from

105th Street northward. They crop out along the edges of Mt. Morris Park (near 123rd Street), a klippe that places Manhattan Schist structurally above Walloomsac and Inwood. Rocks found within Cameron's Line bear mylonitic fabrics recording a former deep-seated ductile shear zone. By 1983 a geological map of the south part of Central Park (Figure 16) showed the distribution of Hartland and Manhattan rocks and the position of Cameron's Line between them.

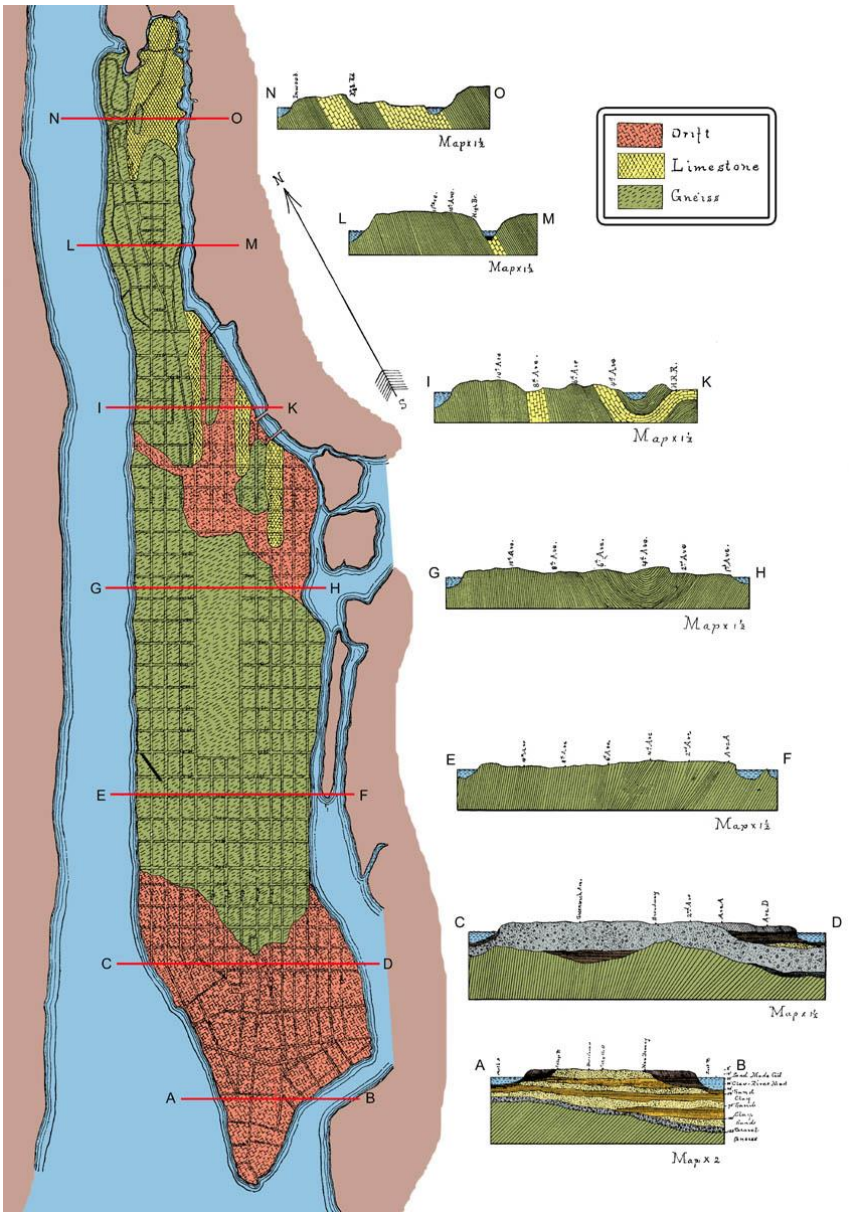

Figure 15 – Colorized version of the first geological map of Manhattan based on the work of J. F. Kemp (1887). The geological profile-sections were drawn parallel to streets in Manhattan with subsurface relationships in the southwestern part based on borings. Produced in an era when rocks were exposed in a rural setting in the north half of the island and when they were also being uncovered in excavations, Kemp's sections are detailed. For the purposes of illustration, we have colored the Manhattan "Gneiss" as a single unit as Kemp originally intended. Notice that the scale of the profile-sections does not match that of the map.

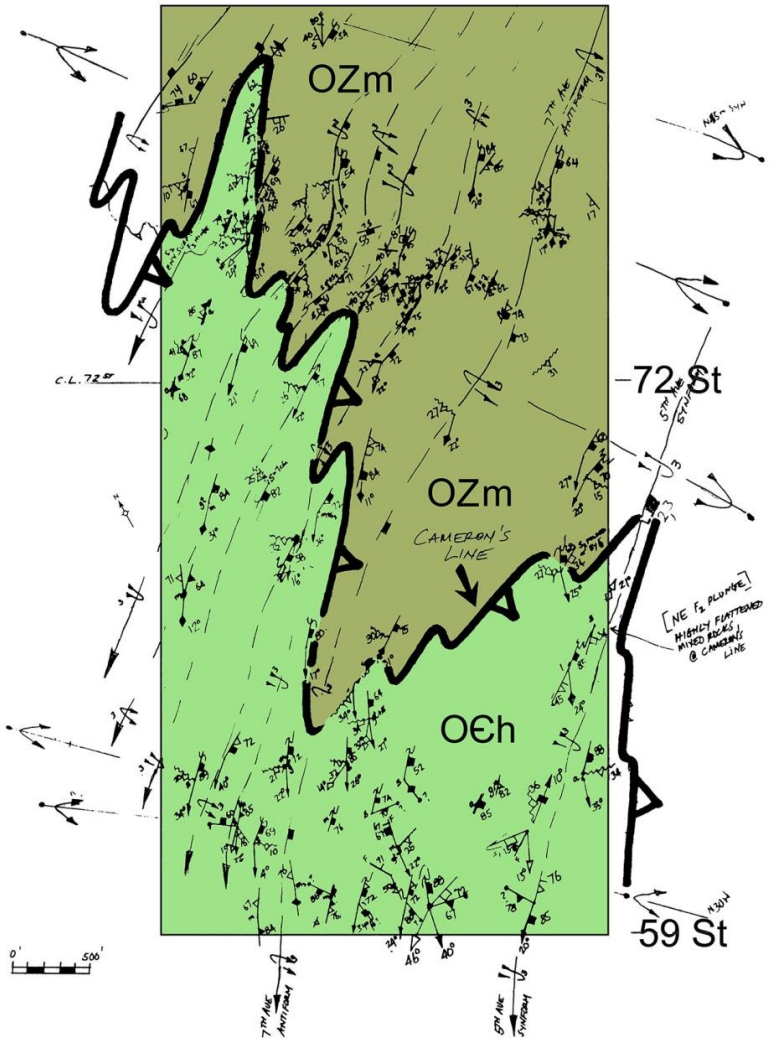

Figure 16 – Geological map of the southern part of Central Park showing the trace of Cameron's Line, axial surface traces of major folds, and structural details.

Taterka's (1987) work in Central Park agreed with earlier interpretations of the overall geologic relationships. Taterka placed the trace of Cameron's Line across an outcrop-free area of Central Park in the vicinity of the Great Lawn between 80th and 86th streets (Figure 17, left panel) and showed a relatively simplistic folded structure unlike the patterns actually found in the bedrock. He subdivided the Manhattan and was able to trace early structures across the park and provided important basic cartographic and petrographic information. Based on our new investigations and considering the degree of superposed F_1 and F_2 isoclinal folding and shearing observed in the field, we suggest that Taterka's interpretation of the geometry of Cameron's Line are too simple. Baskerville's (1994) placement of Cameron's Line across the extreme northern part of Central Park (Figure 17, right panel) simply does not agree with our mapping. Yet, he has identified the Walloomsac in the northern part of the park in an area mapped as the 110th Street member of the Manhattan by Taterka. We agree with the Manhattan call on the bulk of these rocks and have found Walloomsac in the northern part of Central Park during recent mapping.

New Geological Map of Central Park

Our new bedrock map of Central Park (Figure 18) is similar to earlier efforts (compare with Figures 16 and 17) but we have modified the position of Cameron's Line and have adjusted the position of bounding lithotypes. The major revision that we have made is that well-layered Hartland rocks occupy a broader area on the east-central side of the park and a refinement of the structural interpretation. Owing to a lack of exposure to the east of the park we are not sure whether the northern Hartland exposures constitute a separate allochthonous sheet that terminates against the 125th Street fault (along the NE corner of the park), whether the two strands of Cameron's Line are sheared against each other, or whether they merge into an F_2 fold hinge. In the third case, the development of the dislocation known as Cameron's Line would be very early in the structural sequence (D_1). If the exposed areas are indeed separate, Cameron's Line may be the product of the D_2 event. Clearly, Cameron's Line shows strong deformation by S-plunging F_3 major and minor folds.

The complex sequence of structural events established from other parts of New York City (Merguerian, 1996a; 2015) is identical to the structural sequence mapped in Central Park. The obvious map scale folds in Central Park (F_3) are those with steep N- to NE-trending axial surfaces (S_3) and variable but typically shallow plunges toward the S and SW. The folds are typically overturned to the NW with a steep SE-dipping schistosity. Shearing along S_3 axial surfaces typically creates a transposition foliation of S_1, S_2, and S_3 that is commonly invaded by granitoids to produce migmatite during both the D_2 and D_3 events. The third-generation structures deform two earlier structural fabrics (S_1 and S_2). The older fabrics trend roughly N50°W and dip gently toward the SW (except along the limbs of overturned F_3 folds). As explained in our accompanying 2016 NYSGA paper, we suspect that all of these structures (D_1, D_2, and D_3) are products of the Taconic orogeny (Figure 19).

During D_2, the rocks acquired a penetrative S_2 foliation consisting of intergrown and oriented kyanite with flattened quartz together with staurolite and garnet porphyroblasts. The distinctive layers and lenses of kyanite+quartz+magnetite developed in the Manhattan formation and very locally in the Hartland during D_2. Near ductile fault contacts the S_2 fabric is highly laminated with frayed and rotated mica and feldspar porphyroclasts, ribboned and locally polygonized quartz, lit-par-lit granitization, and quartz veins all developed parallel to the axial surfaces of F_2 folds. The D_3 event, a period of L-tectonism, smeared the previously flattened kyanite+quartz layers and lenses into elongate shapes parallel to F_3 axes.

The D_1 to D_3 folds and crosscutting fabrics formed during the Taconic orogeny are overprinted by two- and possibly three fold phases that, based on their style and general lack of attendant foliation, undoubtedly took place at much-higher crustal levels than did the three Taconian fabric elements. We suspect that the younger fold phases record the effects of the Acadian- and terminal-stage Appalachian orogenies. On the geological map (Figure 18) we show the F_4 folds as a series of warps and open folds with axial traces that strike roughly N30°W and exhibit dominantly steep dips to the SW. Their brittle cleavages in the bedrock may have helped localize the late stage brittle NW-trending faults that cut the region. Idioblastic muscovite pseudomorphs after D_3 kyanite are common throughout Central Park. Their abundance suggests a major post-Taconian retrograde metamorphism, presumably coincident with the intrusion of post-Taconian wet granitoids throughout the Manhattan Prong discussed by Brock and Brock (2001).

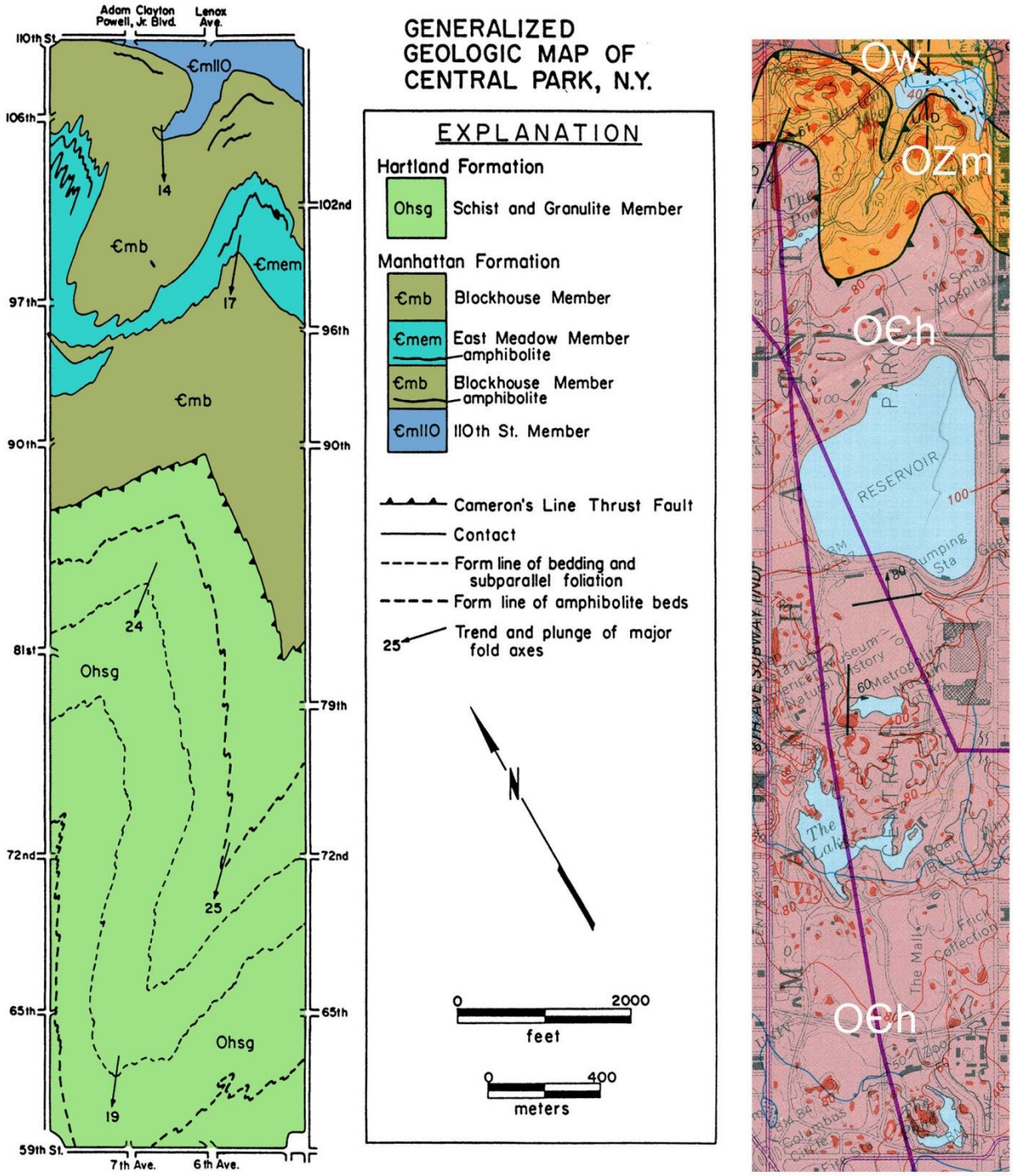

Figure 17 – Colorized and annotated bedrock maps of Central Park by Taterka (1987, left panel) and Baskerville (1994, right panel). See discussion in text.

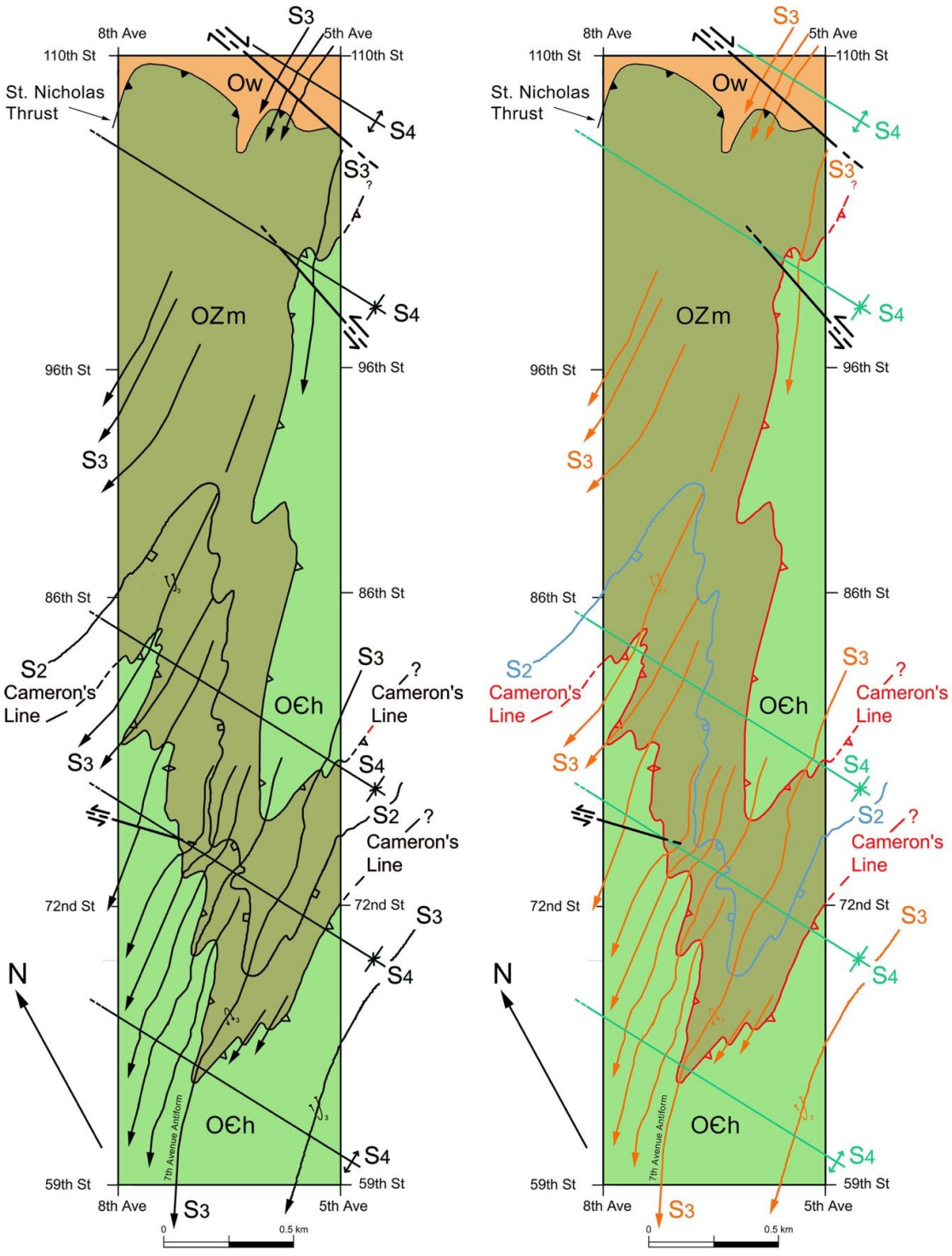

Figure 18 – Preliminary bedrock geological map of Central Park showing ductile and brittle faults and the axial traces of the major structural features, based on our current mapping program.

Figure 19 – Downplunge view of south-plunging F_3 fold in Hartland formation with green pencil aligned with the steep SE-dipping S_3 axial trace. Note how the F_3 synform folds an older F_2 long-limbed isocline in thin quartzose granofels. The similarity in metamorphic grade and style of the three superposed structures suggests they are genetically related; we suspect the Taconic Orogeny as the culprit (CM Stop N361.)

Brittle Faults

Two generations of brittle faults cut Central Park. They conform to the Group D and Group E faults found in the Queens Tunnel and elsewhere in NYC (Merguerian, 1996b; 2002a). Group D faults form a major system of NNE-trending dip-slip normal faults and related joints with an average N21°E trend and steep dips. Fault-associated mineralization takes the form of zeolite minerals (especially orange stilbite) and calcite. In the fault surface, dip-slip slickenlines show oblique-slip reactivation, the result of younger (Group E) faults. Both Group D and Group E faults cut Permian (295 Ma) rhyodacite dikes in the Queens Tunnel (Merguerian, 2001; 2002b; 2004). Regional joints mimic the brittle fault orientations and are characterized by their unique infilling mineralization.

The youngest group of brittle faults trend N20°W to N50°W, exhibit steep dips and show predominately strike-slip offset. These typically healed faults are steeply inclined with subhorizontal slickensides, flower structure, and mineralization that includes quartz, K-feldspar, and microcrystalline epidote veining. In the Queens Tunnel, areas cut by the Group E faults are typically highly fractured and show evidence of high internal strain in the form of overstress phenomenon including invert heave, spalled

rock slabs, rock popping, and other forms of overstress phenomenon within the excavated tunnel perimeter (Merguerian and Ozdemir, 2003).
Both left-lateral and right-lateral Group E faults cut the park in three places. Across the NE tip of the park right-lateral offset is indicated for the 125th Street or Manhattanville fault, based on regional map pattern. (See Figures 18 and 20) Two areas in Central Park show evidence for left-lateral strike slip faulting. The northern fault (N12°W) cuts vertical isoclinally folded gneiss and amphibolite of the Manhattan formation near 101st Street and the East Drive. Three main slip surfaces and many healed microfaults cut the glaciated exposure and show well over a meter of composite offset (Figure 20). The southern fault (N45°W, 90°) shows very minor left-lateral offset in highly jointed Hartland granofels near the Ladies Pavilion on the west side of The Lake.

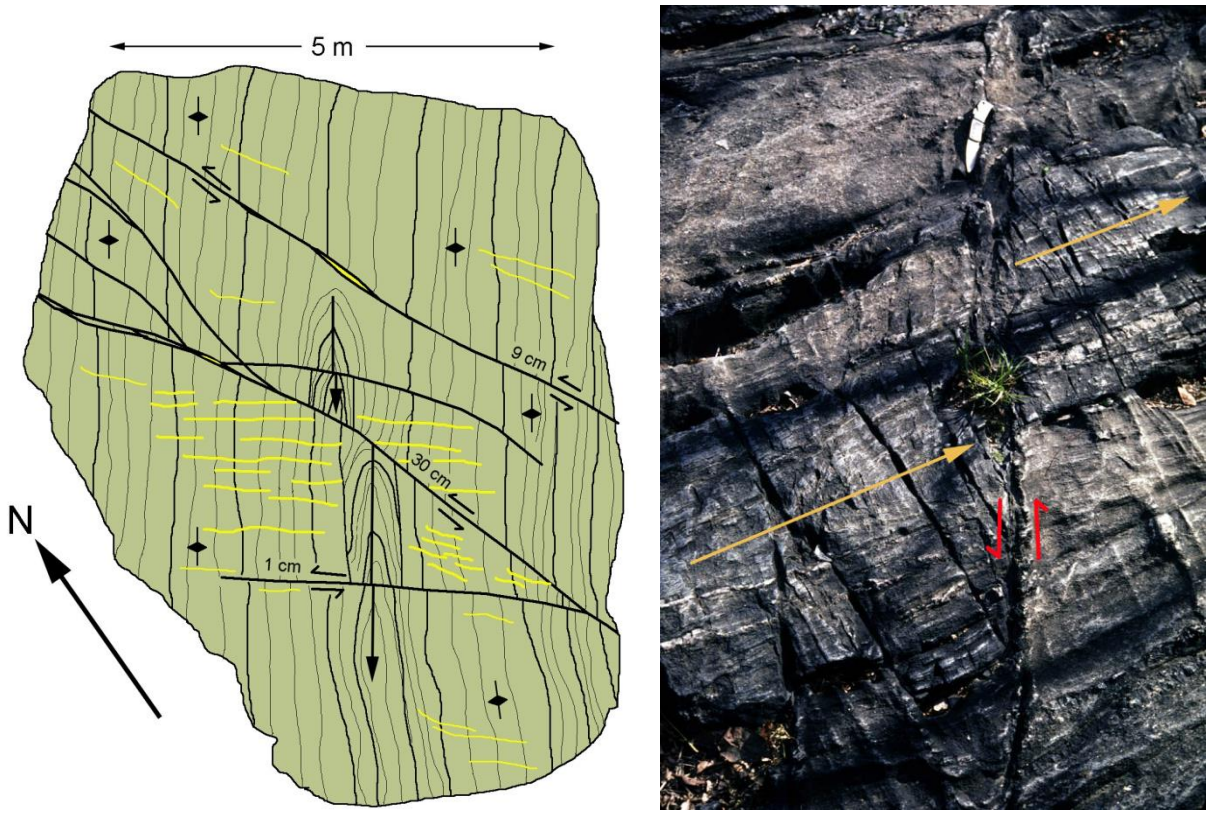

Figure 20 - Field sketchmap showing Group E fault in northern Central Park near intersection of 101st Street and the East Drive. Field image (R) shows 30 cm left-lateral offset of isoclinal folds and vertical fabrics in Manhattan Schist (OZm). (CM Stop N537.)

The famous McCoun map of 1609 shows the drainage systems before urbanization took hold in Manhattan. In Figure 21, we have shown the NW-trending Group E fault traces mapped in the park and suggest that other drainages outline faults not found in the field owing to poor exposure. The epicenter of a small earthquake (~2.4 Richter) localized in NYC on 17 January 2001 plots adjacent to the trace of the 125th Street fault near 102nd Street and Park Avenue in Manhattan. Later that year, on 27 October 2001, another similar earthquake (~2.6 Richter) struck NYC with an epicenter near 55th Street and Eighth Avenue. These epicenters have been plotted on Figure 7 to show that they are spatially coincident with NW-trending faults. North of NYC, seismicity along the NW-trending Dobbs Ferry fault in late October

1985 included two small (~4.0) tremors and many aftershocks. More robust earthquakes in and around the vicinity of NYC were recorded in 1884 (~5.0-5.5), 1783 (~4.9), and 1737 (~5.2). In The Bronx, field and geomorphic evidence suggests that right-lateral offset along the NNW-trending Mosholu fault was a post-glacial phenomenon with demonstrable offset of surface drainage (Merguerian, 1996b; Merguerian and Sanders, 1996; 1997). Because the contemporary stress regime in the lithosphere is oriented NE-SW, left-lateral offset should be expected in W- to NW-trending faults but NNW-trending faults might exhibit contemporary right-lateral offset. Given the modern stress regime, the presence of Group E NNW- and NW-trending faults in the NYC area portend seismic risk.

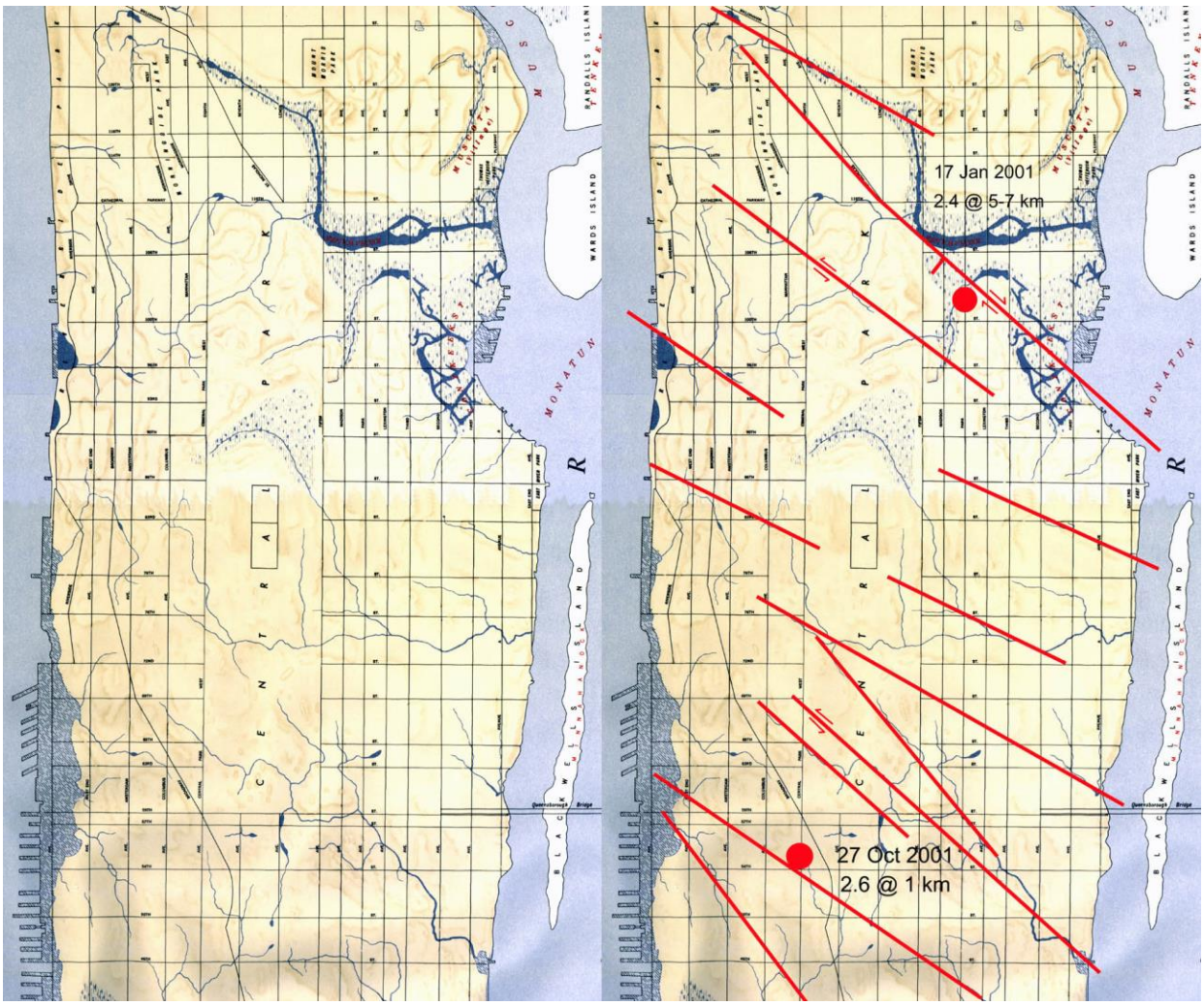

Figure 21 – Topographic map of Manhattan by McCoun (1609) showing the pre-industrial era drainage patterns. Drainages follow zones of structural weakness in crystalline rocks, typically faults. The pronounced NNW-SSE alignment of creek and stream valleys is striking. The right panel shows the traces of three mapped faults in Central Park (faults showing offset symbols), other inferred faults based on stream patterns and topography, and epicenters of two small tremors that struck Manhattan Island in 2001. Note that the vertical edge of the figure is oriented ~N30°E.

CENTRAL PARK FIELD STOPS

Field trip stops for the southern part of Central Park (Figure 22) illustrate the geology of critical exposures in the park. We will undoubtedly go visit other exposures as well.

Figure 22 – Index map showing locations of Central Park field trip stops described below.

STOP 1 - SE of Zoo work shed, Hartland formation. *[UTM Coordinates: 586.75E / 4513.10N, Central Park quadrangle.]*

The exposure consists of gray- and locally brown-weathering muscovite-biotite schist and thin interlayers of biotite granofels, rocks typical of the Hartland formation (O€h) in New York City. The S_2 foliation, which predominates at this exposure, consists of parallel thin laminae and local syntectonic granitoid veins oriented N80°W, 34°SW. F_3 z-folds are also obvious with traces of axial surfaces oriented N42°E, 88°SE and F_3 axes plunging 35° into S17°W. Abundant pegmatite veins (some with large books of muscovite) and veinlets create a nubby weathering appearance, but should not be confused with the aluminosilicate-induced nubby weathering of the OZm unit of the Manhattan Schist. Some of the pegmatite veins have been folded by the F_3 folds. Local 10-cm thick quartzose segregations are present. An amphibolite, 15 cm thick, can be found at the south end of the exposure near 63rd Street.

Evidence for SE-directed glacial flow is obvious in the glacially sculpted exposure in the form of large- and small grooves oriented N30°W to N35°W wrapping around the south end of the exposure and at an azimuth of N40°W on top of the exposure.

STOP 2 - E of walkway just N of 65th Street Transverse Road; mylonitic Hartland formation cut by glacial grooves. *[UTM Coordinates: 586.85E / 4513.32N, Central Park quadrangle.]*
The exposures of Hartland here consist of slabby, gray-weathering vitreous quartzite layers (thicknesses usually 4 to 5 cm, but locally up to 30 cm), granofels, minor schist and amphibolite with a laminated fabric developed parallel to a composite S_2 foliation. S_2, subparallel S_1 and bedding (S_0), are strongly transposed (oriented N56°E, 45°SE) because of the effects of F_3 z-folds with axial surfaces trending N50°E, 85°SE. The F_3 folds and associated lineations plunge 24° into S21°W. Away from the limbs of minor F_3 folds, at the NE corner of the first exposure, the S_2 fabric returns to its typical orientation, roughly N53°W, 28°SW. Pegmatites, up to 2 m thick, containing K-feldspar megacrysts up to 30 cm in size, have been intruded parallel to S_3. Vertical healed joints cut the exposures at a high angle (N42°W) and show positive relief producing a reticulate pattern with the dominant lithologic layering and parallel metamorphic fabrics.

All of the scattered outcrops show the effects of glacial rounding and -polish. Glacial grooves are oriented N47°W to S47°E; they resulted from ice flowing toward the SE.

STOP 3 - E of walkway near "X" crossing of paths S of "The Dene;" mylonitic Hartland formation and glacial grooves. *[UTM Coordinates: 586.90E / 4513.40N, Central Park quadrangle.]*

Similar to the last exposure (still in view toward the S), here the Hartland possesses a pronounced mylonitic fabric because we are approaching Cameron's Line. The composite $S_2 + S_3$ foliation is oriented N70°E, 49°SE (the combined effect of transposition by F_3 fold and late warps) and has been intruded by numerous foliated lit-par-lit granitoids. In fact, two generations of granitoids cut the bedrock: 1) an older foliated generation, as mentioned above, and 2) a younger sinuous granitoid that cuts across the metamorphic layers.

Glacial grooves are here oriented N25°W to N32°W; they are products of a glacier that flowed SE.

STOP 4 - Outcrop W of "The Dene"; two sets of cross-cutting glacial features on polydeformed Hartland formation. *[UTM Coordinates: 586.83E / 4513.40N, Central Park quadrangle.]*

This large polished exposure contains rocks similar to the last three stops and shows the effects of superposed F_2 and F_3 folds. The composite $S_2 + S_3$ foliation is oriented N53°E, and is vertical (90°) or dips steeply SE. The bedrock has been cut by two generations of healed fractures, an older one trending N40°W and a younger one, N-S.

Obscured by post-glacial weathering on the E end of the exposure a partial pothole greets the observant student of geology. Nearby, glacial grooves are oriented N35°W again, supporting our earlier observations, indicating a SE-directed glacial ice-flow direction. At the NE end of the exposure a glacial treat awaits our eyes. Here, a subdued roche-moutonnée structure oriented N37°E is cut by N36°W-trending glacial grooves. Thus, one of our older glacial advances has left its indelible mark on the bedrock. (See Table 1.)

STOP 5 - By "Platform" (outcrop E of "The Dene" and N of playground); beginning of the Cameron's Line shear zone, and glacial features. *[UTM Coordinates: 586.92E / 4513.43N, Central Park quadrangle.]*

At this exposure, we will try to convince you that deep-seated mylonitic faults such as Cameron's Line are not unique single surfaces of dislocation but rather zones of imbricated lithologies (termed mélange) bearing mylonitic fabrics. Here, we see comingled gray-weathering quartzite- and granofels-bearing schist of the Hartland (O€h) and rusty-weathering schist and gneiss of the Manhattan (OZm) formations in fault rocks bearing a highly penetrative $S_1 + S_2$ mylonitic foliation. Lithologies typical of unit OZm are mostly found near the north end of the exposure. Although variable because of F_3 folding, at the south end of the exposure, the $S_1 + S_2$ mylonitic foliation strikes N68°E and dips 22°SE and can be traced parallel to the axial surfaces of F_2 folds of the S_1 foliation in quartzites. The F_2 folds are reclined and plunge 25° into S10°W. Elsewhere, the enveloping S_2 mylonitic foliation is oriented N46°W, 27°SW.

At the north end of the large exposure, where rusty-weathering OZm predominates, O€h granofels layers, 30 to 50 cm thick, can be seen "floating" in a schistose matrix (Figure 23). Such intermixing is perhaps the product of shearing and imbrication related to the formation of mélange within the Cameron's Line thrust zone. Here the S_2 foliation swings to N75°W, 35°SW. The folds and fabrics related to the F_2 and older folds are strongly reoriented by F_3 folds. Tight- to isoclinal F_3 folds plunge 25° into S15°W with axial surfaces oriented N28°E, 68°SE. Beautiful examples of F_2 x F_3 interference patterns are found in this exposure.

Glacial plucking has here been facilitated by joints oriented N85°E, 70°NW. A broad roche-moutonnée structure oriented N10°E occurs at the north end of the exposure and glacial grooves and troughs are found elsewhere oriented N32°W but crosscutting relationships were not observed. Based on what we saw at Stop 4, we suspect that the NW-trending grooves are younger than the roche-moutonnée structure.

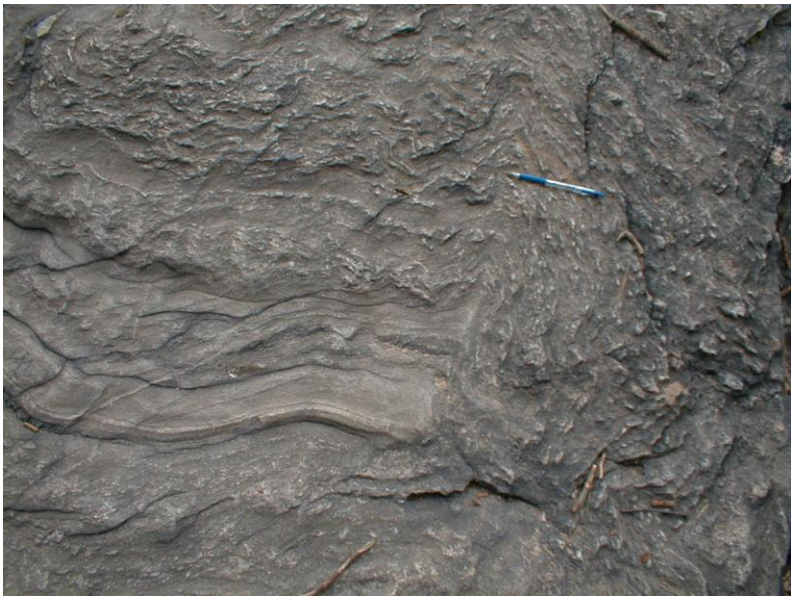

Figure 23 – Image of outcrop showing disarticulated Hartland granofels block in a tectonic mélange near Cameron's Line. (Digital image taken March 1998.)

STOP 6 - At USGS bench mark S of The Pond; typical Hartland Formation away from the Cameron's Line thrust zone. *[UTM Coordinates: 586.58E / 4512.93N, Central Park quadrangle.]*

Rocks of the Hartland formation here consist of typical gray-weathering, highly muscovitic schist and massive, structureless granofels in an exposure at the SE corner of "The Pond", across from the Plaza Hotel. The granofels layers are quite numerous; their thickness varies from 3 cm to 50 cm and they are separated by schistose layers, 3 cm to 4 cm thick, exceedingly rich in muscovite (only about 5% biotite). Bedding is thus preserved and our interpretation is that the protoliths of the granofels layers were turbidites. With a little imagination, relict grading indicates that bedding tops toward the NW with S_0 and parallel S_2 and S_3 oriented N48°E, 70° to 80°NW.

Upright F_3 synformal folds of S_0 and S_2 plunge 20° into S45°W with axial surfaces oriented N45°E, 85°SE. A marked difference in mechanical behavior is indicated as the granofels layers show only large-scale warping at the hands of F_3 folds yet the schistose interlayers are strongly folded and crenulated. Glacial grooves are oriented N32°W indicating SE-directed glacial-ice flow.

STOP 7 - W of the Pond, opposite the Avenue of the Americas access to Park; folded and glacially polished Hartland formation. *[UTM Coordinates: 586.39E / 4513.05N, Central Park quadrangle.]*

Muscovite schist and interlayered granofels of the Hartland are cut by open warps of the composite S_2 + S_3 foliation. These folds, which must postdate the F_3 folds, plunge southward at 51° with NE-trending axial surfaces. A minor shear zone in the center of the exposure cuts through a 10-cm-thick layer of amphibolite and an F_2 reclined fold refolded by F_3 occurs on the south end of the exposure.

STOP 8 - On S side of West Drive, near SW boundary of Park; Hartland rocks sheared along F_3 limbs and glacial features. *[UTM Coordinates: 586.32E / 4513.04N, Central Park quadrangle.]*

The effects of shearing along the limbs of F_3 folds here produce a penetrative foliation oriented N32°E, 90° in highly muscovitic rocks of the Hartland formation. The effects of rounding and smoothing of the bedrock surface here are quite obvious as are glacial grooves oriented N38°W.

STOP 9 - On N side of West Drive near bridge over walkway from 7th Avenue; Hartland rocks exhibiting bedding. *[UTM Coordinates: 586.27E / 4513.20N, Central Park quadrangle.]*

Pronounced interlayering of granofels and muscovite schist here typify the Hartland formation. Bedding (S_0) and the S_2 foliation are oriented N43°W, 30°SW near the vicinity of an F_3 antiformal hinge area (7th Avenue Antiform of Figures 16 and 18). The F_2 folds here show z-fold symmetry indicating we are on the eastern side of the south-plunging antiform.

STOP 10 - Umpire Rock; Hartland rocks "safe at home". *[UTM Coordinates: 586.27E / 4513.37N, Central Park quadrangle.]*

Umpire Rock is the most-spectacular natural exposure in the southern part of Central Park. Here, rocks of the Hartland formation show the superposed effects of F_2 and F_3 folds, abundant syn- and post-tectonic pegmatite intrusives, brittle faults, and numerous glacial features. The rocks consist of interlayered muscovite schist and granofels that have been cut by numerous granitoids. F_2 fold hinges are locally preserved but the glacial smoothing of the outcrop surface inhibits direct measurement of plunge orientation. The S_2 axial-planar foliation is strongly folded here but displays an average enveloping surface of N77°W, 21°SW.

F_3 z-folds vary from open- to tight- to isoclinal in profile and plunge 22° into S25°W with axial surfaces oriented N35°E, 72°SE. Beautiful interference patterns result from the superposition of F_2 and F_3 folds. Late-stage open warps with southward plunges are locally developed. Some pegmatites are syntectonic (foliated) and were intruded parallel to S_2. Other granitoids are thin aplites oriented N50°E and crosscut all structural fabrics. Yet younger micaceous pegmatites cut the aplites. At least two brittle faults oriented N32°E cut the exposure; the one on the eastern edge of the outcrop shows a crumbly gouge zone roughly 3 m thick.

Perhaps the most-obvious geologic features here are of glacial origin. At the NW edge of the exposure, glacial meltwaters have modified spectacular glacial troughs oriented N28°W. These troughs are related to the overall SE-directed roche-moutonnée shape of the exposure with its steep drop off toward the playground area. A potpourri of glacial erratics can be found on this outcrop. We identified erratics of Palisades diabase and hornfelsic Lockatong Formation from the Newark basin W of the Hudson River, granite, and diorite.

Around the steep, north-facing wall of the exposure, note the glacial grooves oriented N46°W and the grooves oriented N35°W on the eroded outcrops immediately north of the north-facing wall. Of additional structural interest, the north-facing wall offers a rare glimpse at the shallow dip of the S_2 foliation and a sub-parallel granitoid sill, all folded by F_3? or younger open warps.

STOP 11 - E side of walk E of Heckshcer Playground; pegmatite erratic on glacially polished Hartland rocks. *[UTM Coordinates: 586.39E / 4513.38N, Central Park quadrangle.]*

The most-obvious feature of this stop is the 2m-high K-feldspar megacrystic pegmatite erratic but we can not be sure whether the erratic has been placed there during park construction or renovation. The “erratic” rests on rocks of the Hartland that have been scored by N38°W glacial grooves. F_3 s-folds are locally found in the exposure.

STOP 12 - E of junction of walks N of Stop 11; mylonitic Hartland rocks. *[UTM Coordinates: 586.39E / 4513.39N, Central Park quadrangle.]*

The Hartland formation here shows some evidence for lithologic mixing; rocks of the Manhattan formation are present in the form of tectonic inclusions consisting of wisps- and shreds of aluminosilicate-bearing, rusty- to maroon-weathering schist. The outlines of the wisps and shreds are masked by shearing along S_2 and S_3. S_2 is well developed here and is oriented N68°W, 42°SW. F_3 folds are not hard to spot with their typical southward plunges and steep NE-trending axial surfaces.

STOP 13 - By the Carousel; the Manhattan formation. *[UTM Coordinates: 586.45E / 4513.43N, Central Park quadrangle.]*

The exposure of rocks immediately west of The Carousel show the rusty- to maroon-weathering typical of the Manhattan Formation (OZm). Layers and lenses of kyanite+quartz+magnetite weather in positive relief and outline the S_2 foliation which is largely mylonitic. Here, S_2 is variable but oriented N70°E, 25°SE because of pervasive F_3 folds plunging 34° into S25°W. The F_3 axial surfaces trend N42°E, 68°SE. We map this area as the beginning of the Cameron's Line thrust zone and links these exposures to those found at our earlier Stop 5.

REFERENCES CITED

Bennington, J Bret, and Merguerian, Charles, 2007, Geology of New York and New Jersey: Physical Geology Textbook Supplement: Thomson Brooks/Cole Company, 24 p.

Baskerville, C. A., 1994, Bedrock and engineering geology maps of New York County and parts of Kings and Queens counties, New York and parts of Bergen and Hudson counties, New Jersey: U. S. Geological Survey Miscellaneous Investigations Series Map I-2306 (2 sheets; colored maps on scale of 1/24,000).

Brock, P. J. C., and Brock, P.W.G., 2001, Bedrock geology of New York City: More than 600 m.y. of geologic history: http://pbisotopes.ess.sunysb.edu/reports/NYCity/index.html, 11 p.

Kemp, J. F., 1887, The geology of Manhattan Island [N. Y.]: New York Academy of Sciences Transactions, v. 7, p. 49-64.

Merguerian, Charles, 1983, The structural geology of Manhattan Island, New York City (NYC), New York (abstract): Geological Society of America Abstracts with Programs, v. 15, p. 169 (only).

Merguerian, Charles, 1996a, Stratigraphy, structural geology, and ductile- and brittle faults of New York City, p. 53-77 *in* Benimoff, A. I. and Ohan A. A., *chm.*, The Geology of New York City and Vicinity, Field guide and Proceedings, New York State Geological Association, 68th Annual Meeting, Staten Island, NY, 178 p.

Merguerian, Charles, 1996b, Evidence for post-glacial surface faulting in New York City (abs.): Geological Society of America Abstracts with Programs, v. 28, no. 3, p. 81.

Merguerian, Charles, 2001, Young rhyodacite dikes found in the Queens Tunnel, beneath Woodside, Queens: p. 9-19 *in* Hanson, G. N., *chm*., Eighth Annual Conference on Geology of Long Island and metropolitan New York, 21 April 2001, State University of New York at Stony Brook, NY, Long Island Geologists Program with Abstracts, 128 p.

Merguerian, Charles, 2002a, Brittle faults of the Queens Tunnel Complex, NYC Water Tunnel #3: p. 63-73 *in* Hanson, G. N., *chm*., Ninth Annual Conference on Geology of Long Island and metropolitan New York, 20 April 2002, State University of New York at Stony Brook, NY, Long Island Geologists Program with Abstracts, 116 p.

Merguerian, Charles, 2002b, Rhyodacite dikes of the Queens Tunnel Complex, NYC Water Tunnel #3 (abs.): Geological Society of America Abstracts with Programs, v. 34, no. 1, p. A75.

Merguerian, Charles, 2004, Brittle fault chronology of New York City (NYC): Geological Society of America Abstracts with Programs, v. 36, no. 2, p. 73.

Merguerian, Charles, 2015, Review of New York City bedrock with a focus on brittle structures; *p. 17-67 in Herman, G. C. and Macaoay Ferguson, S., eds.*, Geological Association of New Jersey Guidebook, Neotectonics of the New York Recess, 32nd Annual Conference and Field Trip, Lafayette College, Easton, PA, 214 p.

Merguerian, Charles; and Baskerville, C. A., 1987, The geology of Manhattan Island and the Bronx, New York City, New York, p. 137-140 in Roy, D. C., ed., Northeastern Section of the Geological Society of America, Centennial Fieldguide, Volume 5, 481 p.

Merguerian, Charles; Merguerian, J. Mickey; and Cherukupalli, Nehru, E., 2011, Stratigraphy, structural geology and metamorphism of the Inwood Marble Formation, northern Manhattan, NYC, NY: *in* Hanson, G. N., *chm*., Eighteenth Annual Conference on Geology of Long Island and Metropolitan New York, 09 April 2011, State University of New York at Stony Brook, NY, Long Island Geologists Program with Abstracts, 19 p.
http://www.geo.sunysb.edu/lig/Conferences/abstracts11/merguerian-2011.pdf

Merguerian, Charles; and Ozdemir, Levent, 2003, Rock Mass Properties and Hard Rock TBM Penetration Rate Investigations, Queens Tunnel Complex, NYC Water Tunnel #3, Stage 2: p. 1019-1036 *in* Robinson, R.A. and Marquardt, J.M., *eds.,* Rapid Excavation and Tunneling Conference, 2003 Proceedings, 1334 p.

Merguerian, Charles; and Sanders, John E., 1998, Annealed mylonites of the Saint Nicholas thrust (SNT) from a new excavation at the New York Botanical Gardens, The Bronx, New York: p. 71-82 *in* Hanson, G. N., *chm*., Geology of Long Island and metropolitan New York, 18 April 1998, State University of New York at Stony Brook, NY, Long Island Geologists Program with Abstracts,161 p.

Merguerian, Charles; and Sanders, J. E., 1991, Trip 16: Geology of Manhattan and the Bronx, 21 April 1991: New York Academy of Sciences Section of Geological Sciences Trips on the Rocks Guidebook, 141 p.

Merguerian, Charles; and Sanders, J. E., 1996, Diversion of the Bronx River in New York City - evidence for postglacial surface faulting?, p. 131-145 *in* Hanson, G. N., *chm*., Geology of Long Island and metropolitan New York, 20 April 1996, State University of New York at Stony Brook, NY, Long Island Geologists Program with Abstracts, 177 p.

Merguerian, Charles; and Sanders, J. E., 1997, Bronx River diversion: neotectonic implications (abs.): Paper No. 198, p. 710 *in* Hudson, J. A. and Kim, Kunsoo, *eds.*, International Journal of Rock Mechanics and Mining Sciences, Special Issue, 36th U.S. Rock Mechanics Symposium, Columbia University, New York, June 29-July 02, 1997, v. 34, no. 3/4, 714 p. Full version on CD-ROM, 10 p.

Merrill, F. J. H., 1890, On the metamorphic strata of southeastern New York: American Journal of Science, 3rd series, v. 39, p. 383-392.

Sanders, John E., and Merguerian, Charles, 1998, Classification of Pleistocene deposits, New York City and vicinity – Fuller (1914) revived and revised: p. 130-143 *in* Hanson, G. N., *chm*., Geology of Long Island and Metropolitan New York, 18 April 1998, State University of New York at Stony Brook, NY, Long Island Geologists Program with Abstracts, 161 p.

Taterka, B. D., 1987, Bedrock geology of Central Park, New York City: Amherst, MA, University of Massachusetts Department of Geology and Geography M. S. Thesis, (Contribution 61), 84 p. with maps.

TRIP A6 AND B5: NEW INSIGHTS ON RIFT BASIN DEVELOPMENT AND THE GEOLOGICAL CARBON CYCLE, MASS EXTINCTION, AND CARBON SEQUESTRATION FROM OUTCROPS, AND NEW CORE, DRILL HOLES AND SEISMIC LINES FROM THE NORTHERN NEWARK BASIN (NEW YORK AND NEW JERSEY)

PAUL E. OLSEN, SEAN T. KINNEY, NATALIA V. ZAKHAROVA
Lamont-Doherty Earth Observatory of Columbia University, Palisades, NY 10968

ROY W. SCHLISCHE, MARTHA O. WITHJACK
Department of Earth and Planetary Sciences, Rutgers University, Piscataway, NJ 08854

DENNIS V. KENT
Department of Earth and Planetary Sciences, Rutgers University, Piscataway, NJ 08854
and Lamont-Doherty Earth Observatory of Columbia University, Palisades, NY 10968

DAVID S. GOLDBERG
Lamont-Doherty Earth Observatory of Columbia University, Palisades, NY 10968

BRIAN E. SLATER
New York State Museum, Albany, NY 12230.

INTRODUCTION

The Carbon Cycle, Global Environments, and the Sedimentary Record

It is a viable theory that in the big picture, much of Earth's geological record of is, in one way or another, a reflection of changes in the carbon cycle, itself uniquely (as far as we know in THIS solar system) and profoundly a reflection of life. Plausibly, because of the interplay between photosynthesis, weathering, CO_2, radiative balance, and the thermal gradient of the crust and mantle, the Earth is the only body around our Sun with granite and plate tectonics (Sleep, 2012) and the only body with an atmosphere with significant O_2 (Sleep, 2012). This field trip will view the Newark Basin (Fig. 1) and its sedimentary and biotic record though this lens of the carbon cycle. The fact that there is a Newark rift valley at all and that it is filled with largely red beds reflects this profound difference of our planet compared to our companions. Even the packaging of the Newark Basin sedimentary sequence, which is so profoundly cyclical and clearly paced by variations in the Earth's orbit, seemingly entirely extrinsic to the intrinsic Earth system, must reflect a very strong, nonlinear amplification by feedbacks between the carbon cycle and climate. Finally, the end-Triassic mass extinction (ETE) appears to be an example of a carbon cycle perturbation caused by tectonics – the eruption of the giant Central Atlantic Magmatic Province (CAMP) pumping CO_2 and SO_2 into the atmosphere. These same rocks may be part of our effort to sequester anthropogenic CO_2, itself a product of combustion of a half a billion years of photosynthetic natural carbon sequestration. The fact that the eruptions could occur at all may be a function of the same thermal gradient reflecting the radiative balance that makes our planet hospitable. Much of the theory of the Earth as it relates to life and the carbon cycle is on the fringe of knowledge, but it is useful to ponder how these things might work in order to frame testable hypotheses that may not only help us understand the Earth system from the seemingly arcane vantage of the Newark basin, but also frame hypotheses that have practical consequence for our future.

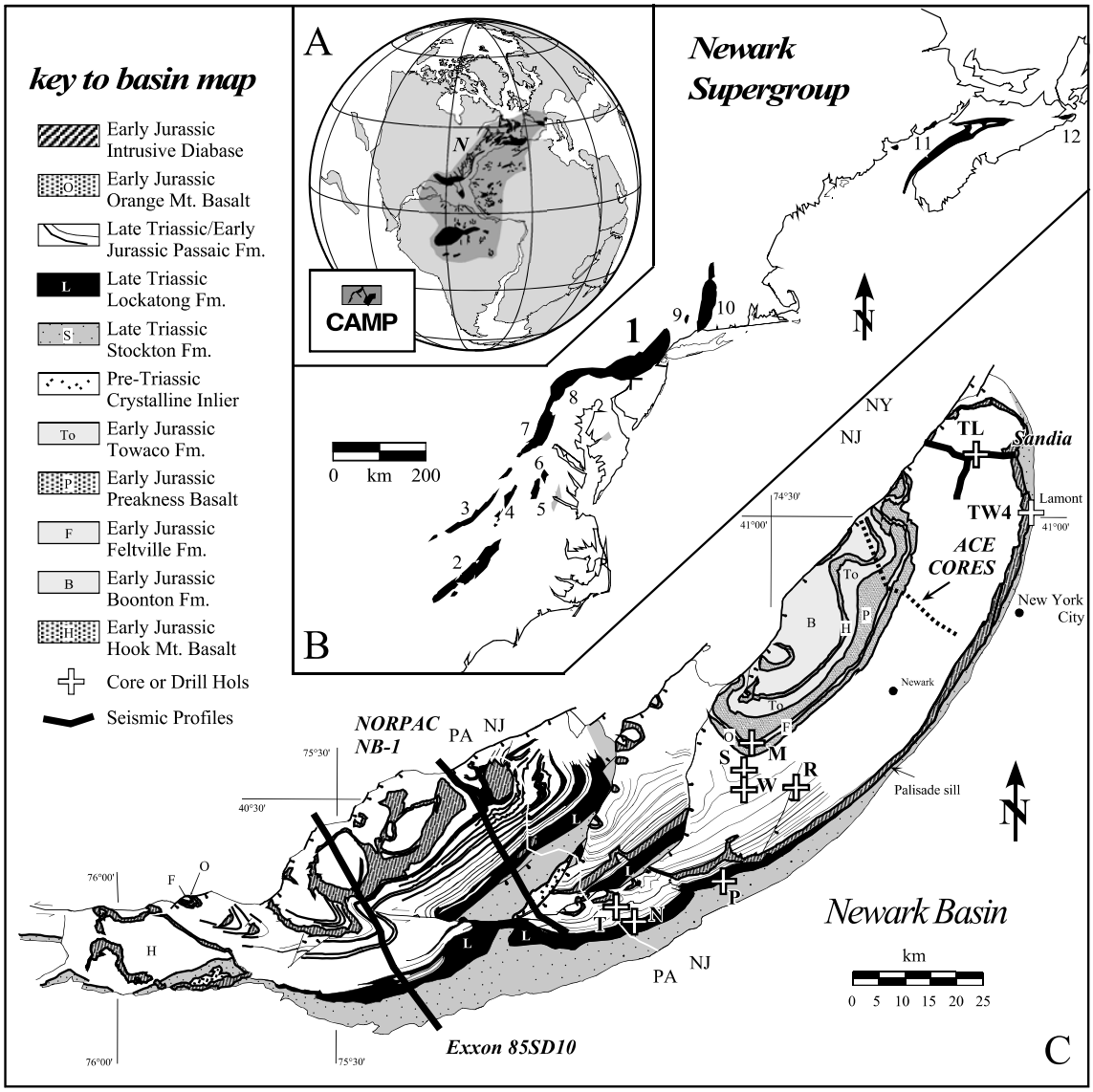

Figure 1: Location Map. **A**, Earth at 201 Ma showing the distribution of CAMP igneous rocks: A, Newark Basin. **B**, Newark Supergroup basins of eastern North America: 1, Newark; 2, Deep River, 3, Dan River; 4) Farmville; 5, Richmnd; 6, Taylorsville; 7, Culpepr; 8, Gettysburg; 9, Pomperaug; 10, Hartford/Deerfield; 11, Fundy; 12 Chebucto. **C**, Newark Basin with positions of core and drill holes and seismic profiles: M, Martinsville; N, Nursery; P, Princeton; R, Rutgers; S, Somerset; T, Titusville; TL, Tandem Lot; TW4, Test Well 4 (LDEO); W, Weston Canal.

The Newark Basin is a continental, compound, half graben rift basin (Fig. 2). While large compared to modern continental half grabens, it is a small part of very broad, still incompletely delineated rift zone that minimally stretched from the parts of central Pangea that would become northern Europe through western Africa, and eastern North America (Fig. 1). It is plausible that it extended all the way through to Panthalassa on the southwest, to the Tethyan rifts on the northeast, and between Greenland and Norway to the north. It is the largest continental rift complex we know to have existed, dwarfing those existing today, and formed as the African and north American plates began to pull apart from one another, plausibly as early as 260 Ma.

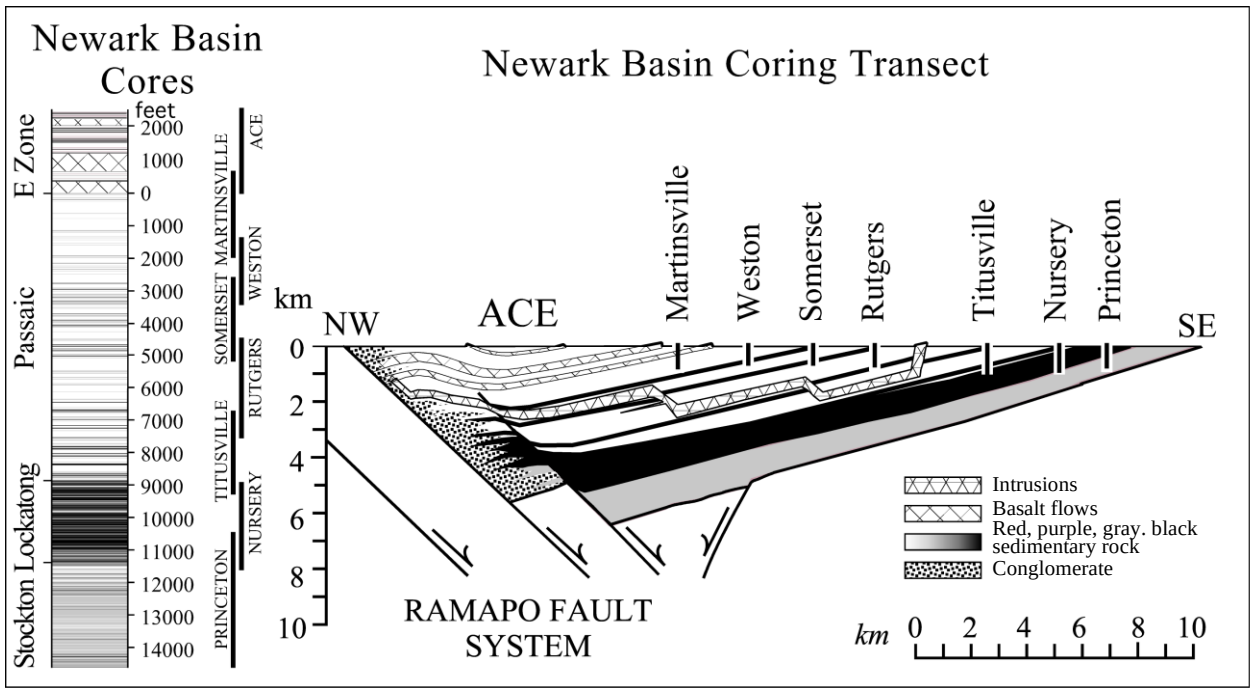

Figure 2: Diagrammatic cross section of the Newark Basin half graben showing the offset coring method. All the cores are projected onto one cross-section with no vertical exaggeration. Feet are shown because that was the orginal driller's units.

Continental rifting and basin filling seems to have begun in the latest Permian, ~40 Myr after the termination (~300 Ma) of the Permo-Carboniferous docking of North America and Africa, the last eastern North American Orogeny that completed the supercontinent of Pangea. The later orogeny temporally overlaps the Permo-Carboniferous Ice Ages. Multiple theories have been proposed for cause of the glaciations, but proxies (e.g., leaf stomata) indicating low CO_2 are roughly temporally correlated with the physical evidence of glaciation (Fig. 3). Current thinking is that in the long-term, or geological carbon cycle, variations in CO_2 are a function of the balance between the magnitude of carbon input, volcanic and metamorphic outgassing, and the removal of this carbon by carbon burial of organic photosynthetic products and chemical weathering of mineral silicates followed by precipitation and burial of carbonates. Because the proxy data for low CO_2 is correlated with high ^{13}C values in the Late Paleozoic, enhanced organic carbon sequestration resulting from the spread of vascular plants in wetlands and over the continents has been a leading hypothesis for the glaciations (Berner, 1997) – and thus plant evolution drove the Late Paleozoic Ice Ages. However, both orogeny-driven increased chemical weathering sequestration of CO_2, (Raymo, 1991) and a reduction of arc volcanism lowering CO_2 input (McKenzie et al., 2016) have also been offered as explanations, as well as a plethora of other explanations including continental position, ocean gateway changes, and elevation (Montañez & Poulsen, 2013).

The oldest putative rift strata found so far is present in Morocco and Atlantic Canada, the former based on diagnostic skeletal, tetrapod remains, the latter on as yet unpublished paleomagnetic data (Olsen & Et-Touhami, 2008; Sues & Olsen, 2015). Because the oldest strata in most of the rift basins in the US are undated, a geographic progression of rifting cannot be assumed on the basis of this information. In addition the plate configuration at this time is still poorly constrained (Domeier et al., 2012). Angular

unconformities separate these Permian strata from definitive Triassic strata, but it unknown if the Permo-Triassic boundary (252 Ma) is recorded in any of these strata. This boundary (more correctly the end-Permian) marks what is supposed to be the largest mass extinction of the Phanerozoic, including on the continents, but low latitude, continental records of this extinction are extremely scarce, and therefore it is hard to assess its global magnitude. That said, at least the marine extinction was profound and seems to overlap the emplacement of the Siberian Traps and related pyroclastics and intrusions. Both a super-greenhouse effect from volcanogenic and metamorphic CO_2 and CH_4 (methane) and cooling from similarly derived sulphur aerosols have been proposed as drivers of this extinction (Svensen et al., 2009; Jones et al., 2016). These concepts have very strong parallels for the end-Triassic extinction, for which an excellent record exists in the Newark and other Central Atlantic rift basins (see Stops 1.1, 1.3, 1.5 and below).

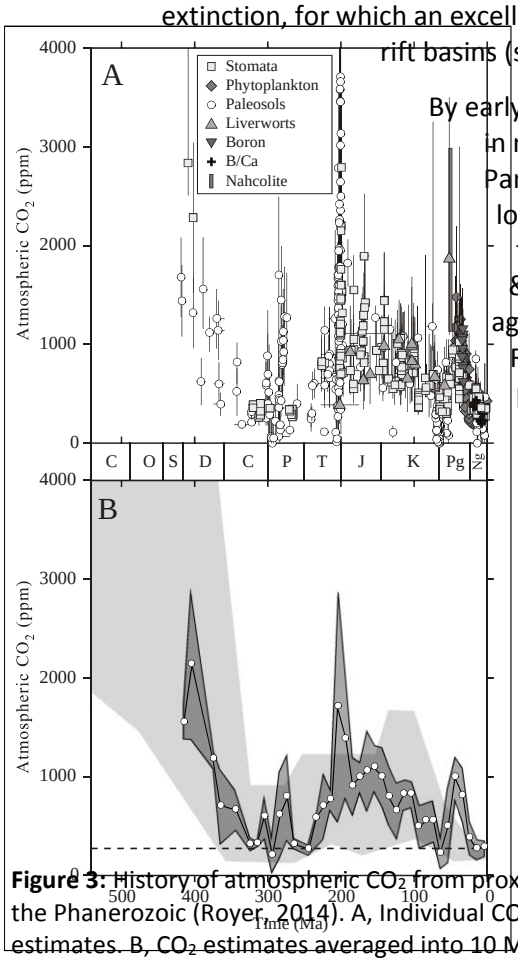

Figure 3: History of atmospheric CO_2 from proxies for the Phanerozoic (Royer, 2014). A, Individual CO_2 estimates. B, CO_2 estimates averaged into 10 My bins (white circles). Bins represented by single estimates are excluded; darker gray band captures ±1σ of the binned data set. Lighter gray band is GEOCARB model.

By early Late Triassic time (Carnian, ~230 Ma) definitive deposition in many rift basins, including the Newark Basin, in Central Pangea had begun. Although a case can be made that at least locally strata of minimally Middle Triassic age are present at the base of the sequences (Olsen & Et-Touhami, 2008; Sues & Olsen, 2015). Although it is possible that Middle Triassic age strata occur in the basal part of the Newark basin (Olsen & Rainforth, 2003), definitive geochronological or paleontological data are lacking (Kent et al., 2016) (Fig. 4).

From Carnian (~232 Ma) through early Early Jurassic (~199 Ma) time, the record of the Newark Basin is dominated by lacustrine deposition with very good geochronological control from Milankovitch lake-level cycles (astrochronology) based on continuous coring and U-Pb dates (zircon geochronology) from lava flows and associated intrusions (Fig. 4) and is the foundation for the Newark-Hartford Astrochronostratigraphic Polarity Time Scale (APTS) (Kent et al., 1995, 2016; Kent & Olsen, 1999; Olsen and Kent, 1999; Olsen et al., 2011). This timescale uses the large-scale lithological sequences, termed McLaughlin cycles, paced by the 405 kyr long-eccentricity-cycle of the Earth's orbit as its metronome, but a full hierarchy of precession-related Milankovitch cycles are represented from 20 kyr to 1.8 Myr (Olsen, 1986; Olsen and Kent, 1996; 1999; Olsen, 2010) (see Stops 1.1, 1.3, 1.5).

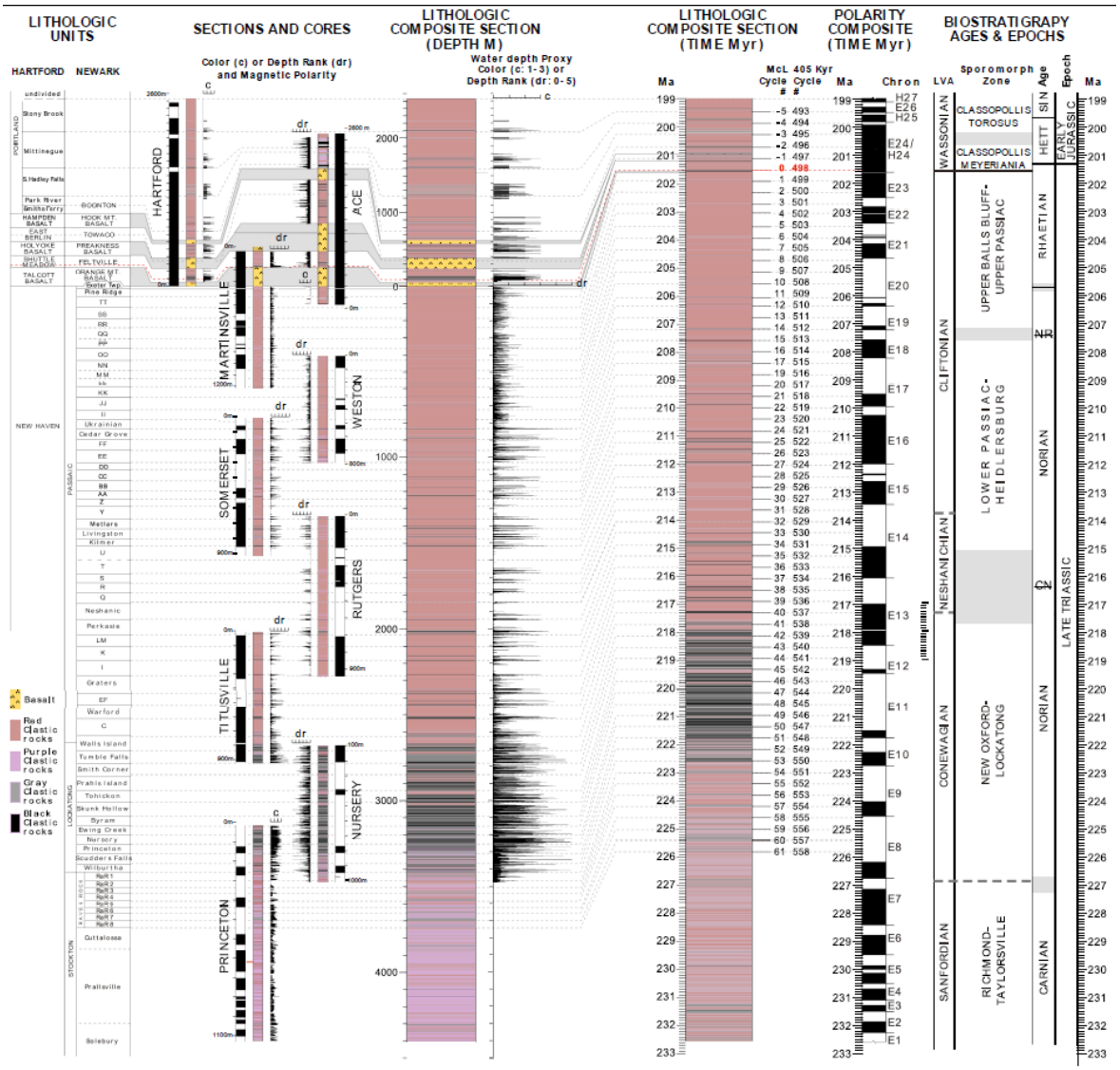

Figure 4: Newark Hartford APTS (from Kent et al., 2016). Stratigraphic framework for the Newark-Hartford APTS. Geologic columns show subdivisions of Hartford and Newark basin sections into formations and members (Olsen et al., 1996a). Magnetostratigraphy and lithostratigraphy are based on outcrop studies and short geotechnical cores from the Hartford Basin (Kent & Olsen, 2008) and in the Newark Basin, outcrop studies and numerous short Army Corps of Engineers (ACE) cores (Olsen et al., 1996b; Witte & Kent, 1990) plus seven long scientific drilling cores from the Newark Basin Coring Project (NBCP) (Kent et al., 1995; Olsen et al., 1996). Magnetic polarity is indicated by black and open bars for normal and reverse polarity. As seen in the cores, dominant Stockton lithologies are sandstones and minor mudstones and strata above that are are lacustrine mudstones and fine sandstones with colors indicative of their actual hues. (Olsen et al., 1996a; b). The composite section is scaled from depth to time by assigning each if the 66 McLaughlin cycles to the 405 kyr eccentricity climate cycle anchored to 201.5 Ma at the base of the Washington Valley Member, corresponding to 201.6 Ma for the onset Chron E23r (= base of the Exeter Twp. Mb). Column labelled Ecc405 is the number of 405 kyr cycles counting back from the present to match peak eccentricity at the base of the Washington Valley Mb. at 201.5 Ma.

In the central parts of the Newark basin, based on outcrops near the Delaware River and cores, the basal part of the section (lower Stockton Formation) is fluvial and the upper Stockton Formation (Raven Rock Member) is marginal fluvio-lacustrine. Based on seismic profiles (Reynolds, 1994), the entire Stockton Formation may become lacustrine in the central deep, buried parts of the basin. The overlying Lockatong and succeeding sedimentary Formations of the basin are lacustrine, except along the northeastern and southeastern termini of the basin where they are replaced by largely fluvial strata (see Stops for Day 2). Sedimentary formations above the Passaic Formation are interbedded with three flood basalt formations of the CAMP that provide U-Pb zircon CA ID-TIMS dates. The continental record of the ETE begins in the uppermost tens of meters of the Passaic Formation of latest Triassic (Rhaetian) age (at 201.564±0.015 Ma: Blackburn et al., 2013) and the Triassic-Jurassic boundary projects from its marine, ammonite-based Global Boundary Stratotype Section and Point (GSSP) in Austria to the Middle Feltville Formation at 201.3 to 201.4 Ma (Wotzlaw et al., 2014; Sha et al., 2015). The youngest strata in the Newark Basin (Boonton Formation) for which there is time control is about 200.6 Ma, but the lacustrine record in the nearby Hartford Basin of Connecticut and Massachusetts extend to about 199 Ma and is mostly if not entirely fluvial above that. The Hettangian-Sinemurian boundary is recorded in those strata at 199.7 Ma in the Newark-Hartford APTS (Fig. 4).

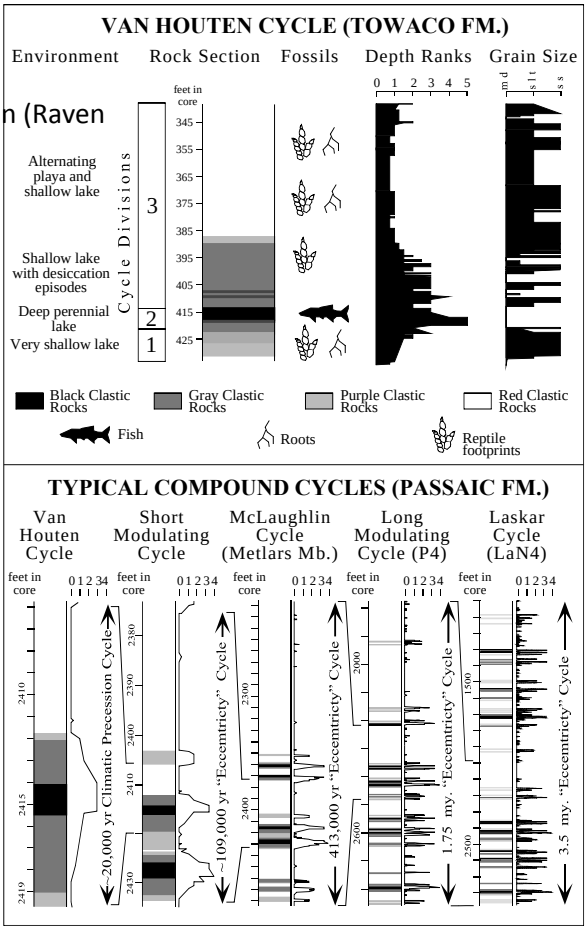

Figure 5: Van Houten and compound cycles (modified from Olsen and Kent, 1999).

Van Houten (1962; 1964; 1969) was the first to recognize the hierarchical cyclicity of the Newark lacustrine strata. Concentrating on the Lockatong and to a lesser extent Passaic formations, including the exposures at Stop 1.5, he correctly attributed the cyclicity to a celestial mechanical origin. Olsen (1986, 2010), Olsen & Kent (1996; 1999), Olsen et al. (1996a, 1996b), Kent and Olsen (2008), and elsewhere, showed that this astronomically paced cyclicity is characteristic of the entire lacustrine sequence (Fig. 5). Kent et al. (1995), Olsen et al. (1996), Kent and Olsen (1997), Kent and Olsen (2000; 2008), Deenen et al. (2011), Husing et al. (2014), Sha et al. (2015) and Kent et al. (2016) have shown that this cyclicity and associated paleomagnetic polarity zones are repeatable between different cores in the Newark basin and between basins on three continents. This cyclicity is remarkable, not so much because it influenced lake depth and sedimentary environments – it would be surprising if it did not, but rather because it is so extreme. The only Neogene cyclicity that is as obvious is in the Mediterranean sapropel record and related deposits (e.g., Rossignol-Strick, 1985; Grant et al., 2016) and those cover a much shorter period. Originally, it seemed that the extreme expression of cyclicity in the Newark (and other) Triassic-Jurassic basins might be due to the rifts forming in a particularly climatically sensitive tropical zone (Olsen, 1991); however, the intensity of that cyclicity changes dramatically through the section and

seems to correlate at the grossest level with pCO_2 (Fig. 6). Based on the soil carbonate proxy of atmospheric pCO_2 (Schaller, 2011; 2012; 2015) concentrations fluctuated about a mean of roughly 2500 ppmv during most of the Late Triassic (Fig. 6) (see Stop 2.2). However, from the late Norian (at about 210Ma) through nearly all of the Rhaetian, concentrations drop to about 1000 ppmv. During this time, the lacustrine cyclicity, so obvious previously, dropped in its apparent amplitude to barely discernable, but still there. The cyclicity then abruptly increased in amplitude during the emplacement of the CAMP and ETE when CO_2 reached nearly 6000 ppm and dropped down again afterward. This is especially remarkable in that not only is it seen in the Newark Basin, it is seen in every rift basin sequence in North America, Morocco, and even Europe – including in marine sequences (Olsen et al., 2015). While of much lower temporal resolution and with lower absolute values, the leaf stomatal record of pCO_2 agrees in outline (e.g., McElwain et al., 1999; Steinthorsdottir et al., 2011).

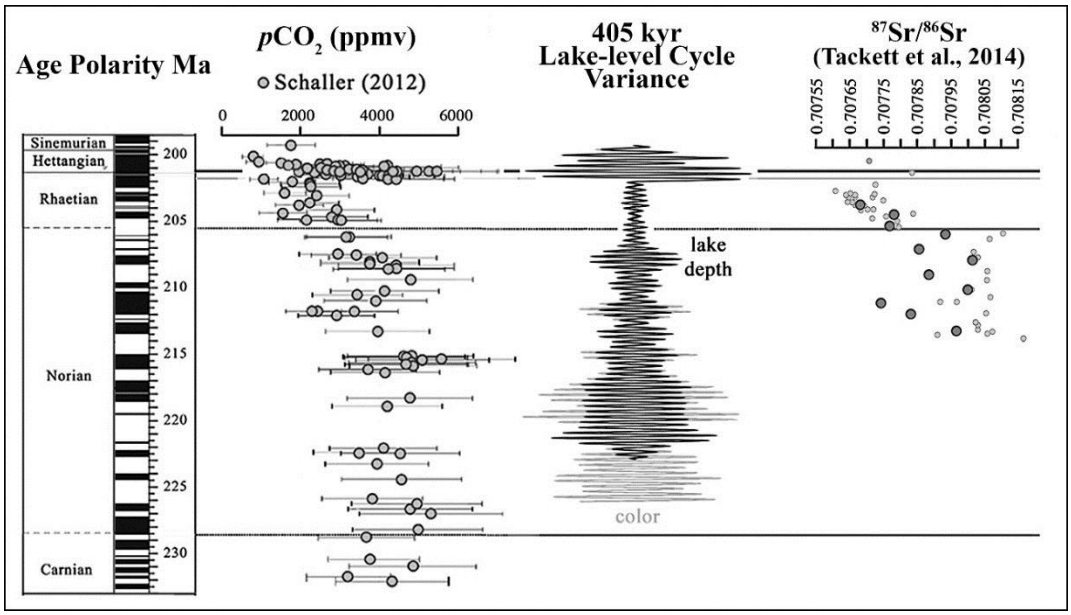

Figure 6: *p*CO2 estimates based on the soil carbonate proxy from (Schaller et al., 2012; 2015) compared to the envelope of variance at the 405 kyr level (Olsen et al., 1999) and the strontium isotope data of Tackett et al. (2014). Note the correlated drop in pCO_2, lake level variance, and $^{87}Sr/^{86}Sr$ during the Rhaetian and the rise during the CAMP episode at around 201.6 to 200 Ma.) compared to the envelop of variance at the 405 kyr level (Olsen et al., 1999) and the strontium isotope data of Tackett et al. (2014). Note the correlated drop in pCO_2, lake level variance, and $^{87}Sr/^{86}Sr$ during the Rhaetian and the rise during the CAMP episode at around 201.6 to 200 Ma.

Models of increasing atmospheric anthropogenic pCO_2 predict an intensification of the hydrological cycle, coupled with warming and an implied amplification of the effects of orbitally-forced precipitation fluctuations, with wet areas will growing wetter and dry areas drier (Stocker et al., 2013). There is also some evidence that higher CO_2 amplifies the effects of Milankovitch orbital forcing, including the effects on the monsoon (Araya-Melo et al., 2013). In addition, strontium isotopes ($^{87}Sr/^{86}Sr$) in marine strata apparently track the CO_2 proxy with a dramatic decrease from about 0.70795 to 0.70765 (Tackett et al., 2014) suggesting both a mechanistic link though weathering and that the relative changes in the soil carbonate and stomatal proxy data are meaningful, even if the absolute values of the two differ.

Viewed this way, one can argue that many of the primary features of the variability of these Triassic sequences are controlled by climate variations amplified by effect of background levels of atmospheric CO_2. High climate variability would be expected at precessional frequencies during very high CO_2 and low climate variability at times of low CO_2. This parallels the concept that the overall context of very low CO_2 during the Neogene greatly amplified climate variability in the obliquity (41 kyr) and later eccentricity range (~100 kyr) by allowing the development of glaciers at high latitudes. The Milankovitch cycles in insolation did not CAUSE the extreme variability, rather they PACED the variability of an unstable, non-linear climate system that tunes to different frequencies depending on pCO_2, ice or lack thereof, and plausibly other contexts (e.g., Huybers, 2004; Daruka & Ditlevsen, 2016), analogous to how a medical pacemaker stabilizes the rhythm of a chaotically beating heart. Such hypotheses require testing by more direct climate indicators over a broader geographic spread as well as more sophisticated modelling that can take advantage of the climate proxies. If indeed this view of the interplay between the quasiperiodic orbital cycles and a highly sensitive, non-linear system is correct, it does not bode well for forecasting the effects of pCO_2 outside present boundary conditions.

Generalizing a bit, the high CO_2 times of the Triassic (and Permian) are often referred to as arid times, supposedly indicated by the abundance of red beds. Although globally that certainly was not the case. The Late Triassic and earlier Early Jurassic (Hettangian-Sinemurian) are a time for which there is no evidence for ice at the poles – no dropstones, glendonites, or tills (Frakes et al., 1992). In fact, the North Pole was located in northeast Siberia within a few degrees of the present Lapdev Sea where there are Triassic-Jurassic gray, coaly beds, and abundant plant debris and macrofossil plants indicating a warm to cool temperate flora (Dobruskina, 1988; Ziegler et al., 1993; Ilyina & Egorov, 2008). Similarly, at 70° S latitude in what is now New Zealand similar gray deposits yield plant fragments of mesophytic (temperate) floral assemblages and relatively diverse sporomorph assemblages (Retallack, 1985; Zhang & Grant-Mackie, 2001). Evidently, both polar regions were temperate and relatively humid. In contrast, today's polar areas have extreme aridity with the two polar areas comprising the largest deserts on Earth (Loewe, 1974; Smiley & Zumberge, 1974; Doran et al., 2010; Callaghan et al., 2006), comprising about 28.6 million km^2 or 19 % of the area of land on Earth[1]. With the polar continental areas being relative humid during the Triassic-Early Jurassic, why the bias towards thinking the Triassic was an arid time? One important reason, is that many, maybe most, locations of post-graduate education were located in the tropics to subtropics of early Mesozoic Pangea, at one time or another. The second major reason is that central Pangea drifted northward during the Triassic-Jurassic, producing a highly diachronous swath of red beds and aeolianites (Kent & Tauxe, 2005), with the diachroneity not visible until non-biostratigraphic means of correlation became available (e.g., Kent & Tauxe, 2005; Irmis & Whiteside, 2010; Irmis et al., 2011; Olsen et al., 2011; Kent et al., 2014). In combination, it means that nearly every major location of higher learning, from Cape Town to New York, Berlin, to Stockholm has a nearby deposit from one part of the Triassic-Jurassic or the other, with red beds. A corollary to this is that the supposed aridification trend (Parrish, 1993) through the Triassic actually reflects the northward migration of central Pangea as well as southern high latitude sites from zonal more humid to arid climate belts. Thus, northern Europe and Greenland actually show the reverse trend, going from arid to humid though time, exactly what one would expect from a northward translation of those areas from the subtropics into the temperate latitudes. The null climatic hypothesis is that nothing changes, and it cannot be falsified until time and plate position are accounted for. When time and plate motion ARE accounted for there is no evidence of global aridification and no evidence that the arid belts were any wider in the Triassic-Early Jurassic, than at the present (Kent & Tauxe, 2005).

[1] Derived from http://geology.com/records/largest-desert.shtml

Thus, the famous red beds of the Newark Basin are NOT typical of the Triassic, anymore that the climate of Timbuktu is typical of the Earth today. We can go further and state quite the opposite of the usual bias for Triassic climate. It is actually, on the whole, wetter than today due to the lack of polar deserts. Once we account for plate position and time, there is a residuum of change that then may require special explanation, such as at the ETE (see below).

The Broad Terrane

Historically, the northern Newark basin has been a conceptual battleground area. It has been a locus of the "broad terrane" debate began by I. C. Russell in 1880 (although there were predecessor concepts, as he noted), which may be the most persistent controversy involving these basins and it melds into very substantive debates on not just the interconnectedness of the presently individual basins, but also on the area and volume of the CAMP, thereby bearing on the magnitude of CO_2 and SO_2 release and the cause of the ETE and other mass extinctions. Because the northeastern terminus of the Newark Basin is the closest part of the basin to the Hartford Basin, new data on its three dimensional geometry and the sedimentary and volcanic facies bear directly on the problem and we will examine that data on stops on Day 2.

Russell argued that the Newark and Hartford basin were once part of a much larger more symmetrical basin, now arched in the middle, and very deeply eroded. The basic evidence for this he listed in 1879, 1880, and 1892 (with later additions by others) paraphrased as follows:

1) The strata in the Newark Basin largely dip to the west and those of the Hartford Basin deep to east.
2) The distribution of marginal conglomeritic facies in the basins is highly asymmetrical and generally limited to one side.
3) There is a small basin in between – the Pomperaug Basin,
4) There are boundary faults[2] that determine the margins of opposing sides of the basins, and that on the west of the Newark Basin seems traceable up the Hudson River (for which there is no modern evidence).
5) The strata of the basins are very deeply eroded.

After Russell, many authors have discussed and debated the broad terrane hypothesis. Wheeler (1938) summarized Russell's arguments and cited evidence from a well boring that suggested that there is a continuation of the Hartford Basin in the subsurface to the south, below Long Island, and also provided a clear conceptual diagram to illustrate the overall concept (Fig. 7). The more recent proponents have been Sanders and colleagues (Sanders, 1960; 1963; 1974; Sanders et al., 1981; Friedman et al., 1982), and Hutchinson and Klitgord (1988). The basic 20th century concept is that the Newark and Hartford basins formed as a single large full graben within an extensional regime that was then arched and eroded, producing 2 asymmetric half-grabens (Fig. 7). The opposing concept has been termed the "isolated basin" model, which asserts that the strata of the various Newark Supergroup basins never extended much further than they are preserved today. Proponents of this model have included W. B. Rogers (1842; 1860, and elsewhere), Glaeser (1966), Savage (1968), Klein (1969), Abdel-Monem and Kulp (1968), and Faill (1973; 2003).

Because the strata and hanging wall onlap surfaces of the Newark and Hartford basins project into

[2] This was not clear in I. C. Russell's time but was introduced by Barrell (1915) and followed up on by W. L. Russell (1922) and Longwell (1922, 1937).

space, and are unquestionably deeply eroded, it is clear that the basins must have been to some extent larger than now, the questions are: 1) "how much bigger?", and 2) "did they connect by sedimentary or volcanic plains, or water?" However, it seems clear that the specific geometry expressed in the diagrams of Wheeler (1938) and Sanders (1963) (Fig. 7) cannot be correct, because the Pomperaug Basin section is very thin compared to counterparts in the Newark and Hartford basins, exactly where it should be thickest or at least intermediate in thickness between correlative strata in the Newark and Hartford basins. From the basal (East Hill Basalt), overlying sedimentary Cass Formation, to the top of the second basalt formation (Orenaug Basalt) only about 110 m of strata is present, and that is correlative to about 560 m in the Newark basin and 400 m in the Hartford Basin. Furthermore, the basal formation of the basin, the South Britain Formation underlying the East Hill Basalt comprises ~270 m of red beds while strata below the Orange Mountain Basalt (correlative to the East Hill) is ~3000 m in the northern Newark Basin (Olsen and Rainforth, 2003) and 2000 m below the Talcott Formation (correlative with the East Hill) in the Hartford Basin (Kent & Olsen, 2008) (thickness of Pomperaug strata from Huber and LeTourneau, 2006). Therefore, the geometry of the so-called Danbury anticline of Sanders (1960; 1963; 1974) must have been in existence during sedimentation or developed during sedimentation if it is an anticline at all.

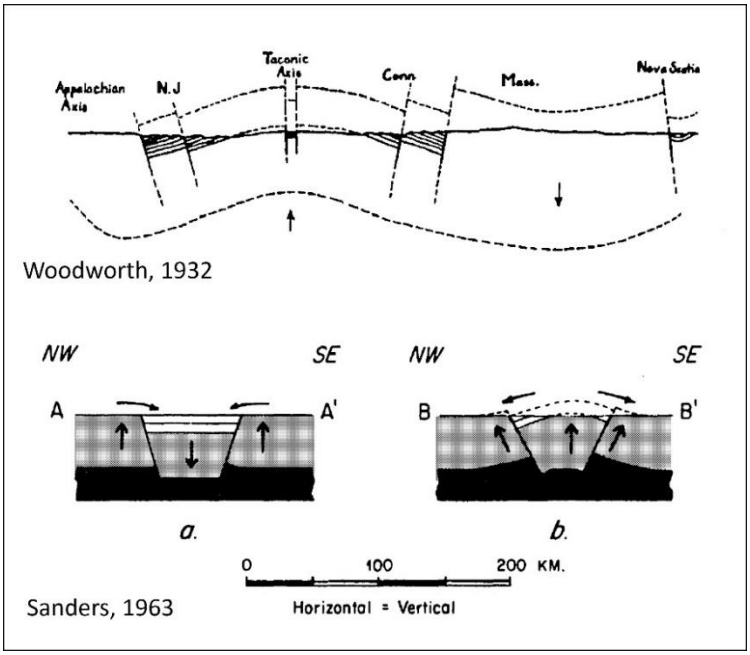

Figure 7: Broad Terrane hypothesis as expressed by Woodworth (1932) and Sanders (1963).

Olsen and Schlische (1987) proposed that the Pomperaug Basin was a crestal collapse graben (cf., McClay & Ellis, 1987), associated with rotation and extension on the conjoined hanging wall blocks of the Newark and Hartford basins. While the basic geometry is similar to what might be expected of a crestal collapse graben, we would argue that the length scale is inappropriately long compared to the thickness of the brittle crust. In this case, the Pomperaug Basin is more simply explained as just another of the many half grabens developed in the wide rifting zone of central Pangea, and has no special generative relationship with the Hartford and Newark basins.

That said, even if the strict geometrical construction of the Broad Terrane model is falsified by what is known now of the thicknesses of the strata in the Pomperaug Basin, that does not mean there was not a sedimentary connection between the Newark and Hartford basins, or between them and any of the other basins. Likewise, a local source for sediment or clasts from presumed highlands between the basins also does not obviate the possibility of sedimentary connections between those same basins.

McHone (1996) argued for a modified broad terrane model, in which the preserved basins formed more or less as half grabens and there was at least local relief between basins; however, the basins could have been interconnected by sediments. Additionally, the CAMP lavas covered vastly larger areas than today, with their former extent indicated by the numerous dikes of the CAMP intruded into basement rocks

now currently lying outside the areas of the preserved sedimentary basins.

Recently, Withjack et al. (2013) using a combination of seismic, field, core, borehole, and vitrinite-reflectance data have shown that the Newark basin was initially narrow and markedly asymmetric with significant thickening toward the basin-bounding faults. As the basin became wider though time the fanning towards the border fault became spread out over a longer distance and hence subtler. Projection of the cross-sectional geometry from the northern Newark Basin to the southeast, approximately perpendicular to the border fault system suggests that the Newark basin may have merged with the New York Bight Basin, which has a northwest-dipping border fault, producing a full-graben as much as 100 km wide and up to 10 km deep (along the border faults) by the cessation of rift sediment accumulation and before continued tilting and post-rift erosion. The New York Bight Basin (Hutchinson et al., 1986), lies along strike of the Hartford basin and may still be connected to it in the subsurface.

That the Newark basin was much wider than it is presently is consistent with studies of other Triassic-Jurassic basins in Eastern North America and Morocco (Withjack et al., 1995; 2009; 2010; 2012; 2013; Withjack & Schlische, 2005; Letourneau, 2003; Malinconico, 2003; 2010).

New data from the northern Newark basin

Four previous guidebooks have dealt with the Northern Newark basin in Rockland County, New York (Savage, 1968; Sanders, 1974; Olsen & Rainforth, 2003). All are based on scant surface information, and And all of them discuss the Broad Terrane model, at least to some extent. Acquisition of two seismic profiles, and drilling of a deep (6800 ft) test boring, and recovery of 352 m of core from a 550 m core in this area provides insights into the Broad Terrane issue.

Core TW4 and Surface Data

It has been apparent for over 30 years that the lower part of the Newark Basin section thins towards the east and the northeast (Manspeizer and Olsen, 1981; Olsen et al., 1996; Olsen & Rainforth, 2003; Withjack et al., 2013). This is most obvious in the thickness of the Stockton and Lockatong formations that thin by a factor of 6 from the central to the northeastern part (Bergen County) of the Newark Basin as well as in the thickness of lacustrine cycles in the Lockatong Formation that thin by of four towards the northeast (compare core at Stop 1.1 to exposures at Stop 1.5). It is also clear that the proportion of tan and gray arkose in the Lockatong increases in the same direction with the most northeastern outcrops of the Lockatong (northeastern Bergen County) being almost entirely composed of tan sandstone with only minor gray mudstone (Parker et al., 1988; Olsen and Rainforth, 2003; Monteverde, 2011). Rockland County outcrops have proved difficult to interpret in terms of the standard Stockton, Lockatong and Passaic formations and the same rock units have been variously labeled each of these names by various authors, with single authors such as PEO changing formational designations through time.

Core TW4 (Fig. 8) (41.002928, -73.910618) was acquired just north of the New Jersey-New York border on the campus of Lamont Doherty Earth Observatory (Zakharova, et al., 2016), funded by the TriCarb Consortium for Carbon Sequestration and EPA STAR grant 834503. It was spudded in the Palisade Sill and ended in gneiss basement. The sedimentary succession in the core consists mostly of white, tan and pinkish arkosic sandstone and red to purplish mudstone. The only candidate for Lockatong Formation is a few meters of gray massive mudstone and white arkose in contact with and as a xenolith within the sill. The most distinctive facies in the rest of the section (except at the bottom) is abundant purplish-red

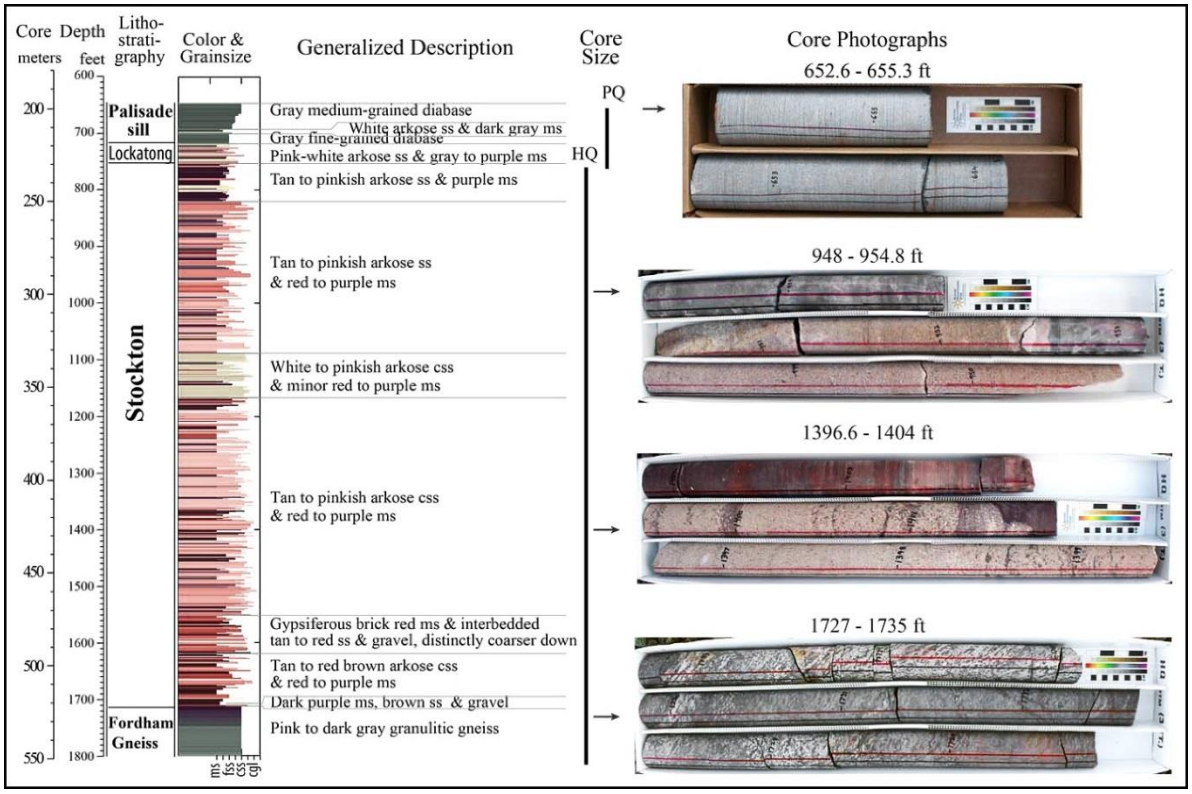

Figure 8: TW4 core from Zakharova et al. (2016).

massive mudstone with very large ptygmoidal dessication cracks filled with grayish coarse arkosic sandstone seen at Fort Lee and just to the north to Snedens Landing (Savage, 1968; Van Houten, 1969) and in the core, but never in the Passaic Formation. Associated sedimentary rocks include white, tan and pinkish arkosic sandstone and red to purplish mudstone. In total, this facies does not resemble coarser grained Passaic Formation but finds its closest match in what is identified as Stockton Formation below undoubted Lockatong Formation in Fort Lee, NJ (Stop 1.2) and Alpine, NJ on the upper surface of the sill (Fig. 9) (Monteverde, 2011). Prominent benches of tan arkosic sandstone are present and exposed near the level of the Hudson River, sporadically outcropping going north from Snedens Landing to Tallman Pool (41.032113°, -73.912819°) and in Piermont (41.041373°, -73.917571° and 41.041846°, -73.917116°), where the exposed section appears to be climbing stratigraphy as does the sill. Given that the sill jumps up section at Alpine, NJ (Monteverde, 2011), cutting through the tan, arkosic remnants of the Lockatong Formation, these tan sandstone at Tallman and Piermont may also pertain to that formation below the sill and its appearance before passing below the river. There are good exposures of red sandstones and mudstones closely resembling normal sandstone and mudstone facies of the Passaic Formation in northern Piermont in small stream gorges (41.051588°, -73.921605°, 41.056002°, -73.921888°), at Grand View-On-Hudson along a path (41.060802°, -73.921601°), and in several abandoned quarries (e.g., 41.071227°, -73.921185°). There are no significant tan sandstones and no hint of the purplish-red massive mudstone with the very large ptygmoidal dessication cracks, suggesting the sections are all above what is present in the TW4 core (as suggested by Van Houten, 1969). From South Nyack north to Upper Nyack, the sill dramatically rises and falls in stratigraphy making an arcuate outcrop pattern (Fig. 9), as stated by Kümmel (1900). Near the waters edge in Nyack (41.087859°, -73.917730°) the outcrops resemble normal Passaic Formation as do the low cuts for the New York State

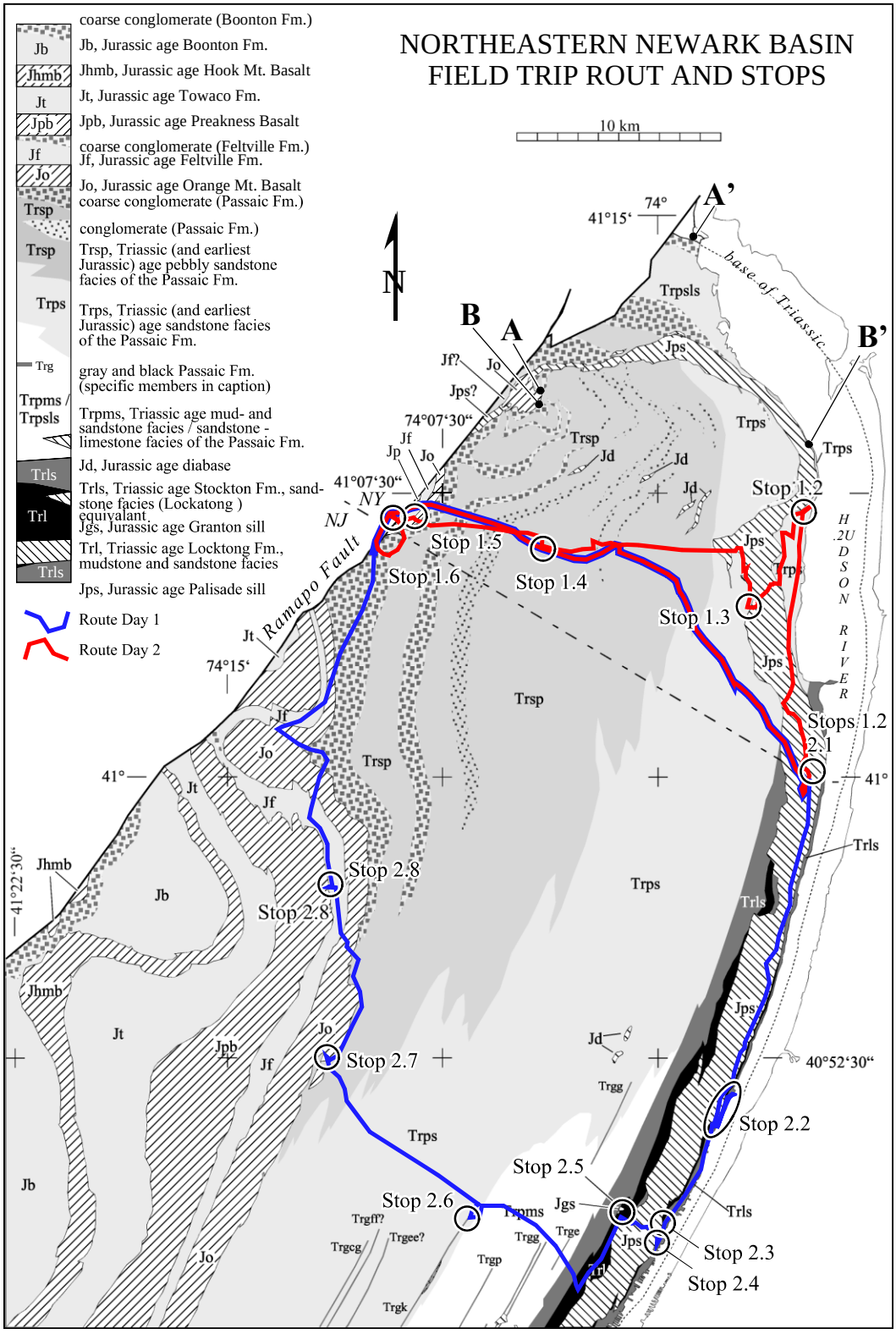

Figure 9: Geologic map of the northern Newark Basin with field stops. Modified from Olsen et al (2003).

Thruway. At Nyack Beach State Park (Stop 2.2) the long red bed section on the site of the former Manhattan Trap Rock Quarry looks like Passaic Formation and largely lacks tan arkosic sandstones. There is no hint of the purplish-red massive mudstone with the very large ptygmoidal dessication cracks typical of the section in most of the TW4 core. Near the very top of the section at Nyack Beach State Park there are purplish mudstones and tan sandstones, but these are difficult to separate from contact metamorphism due to the adjacent sill. More convincingly, at an exposure just to the north of 9W along the northwest terminus of Upper Nyack (41.112127°, -73.927668°), there are tan and gray strata consistent with coarser facies of gray portions of the Passaic Formation. These exposures have produced several small brontozooid (c.f. *Grallator*) (theropod dinosaur) footprints, possible *Atreipus* (non-dinosaurian, dinosauromorph) footprints, bone fragments, and fish scales. Savage (1968) documented that the arkose, interbedded with the unusual purplish-red massive mudstone seen at Snedens Landing, contains abundant zircon, rutile, and anatase, which consistent with TW4. Whereas, the Passaic Formation in Rockland has abundant tourmaline, garnet, and metamorphic rock fragments.

Going farther north along the Hudson, Kümmel (1900) documents the sill cutting up section progressively along Verdrietege Hook (Fig. 10) to the Rockland Lake trap rock quarry to north of Trough Hollow to Waldberg Landing in Haverstraw, the site of a small sandstone quarry that has produced many fossils over the last several decades (Olsen and Rainforth, 2003). According to Kümmel, who had good access to the exposures due to the quarrying activities and denudation at the time, the increase in height of the stratigraphic section exposed near waterline is about 56 to 170 m / km which means that from just north of Nyack Beach to Haverstraw, the section traversed is very roughly about 650 m. Some of this traverse has been described by the field guides of Savage (1968) and Sanders (1974). Along this traverse, now a lovely bike and pedestrian path in Hook Mountain State Park, there are several gray to buff sandstone and siltstone intervals separated by red beds that are most simply interpreted as coarser facies of gray sequences occurring at ~405 ky intervals in the Passaic Formation. Exposures and outcrops in Haverstraw near the level of the river (41.202875°, -73.973494°) and at higher elevation (41.200319°, -73.984453°) are of typical Passaic Formation facies.

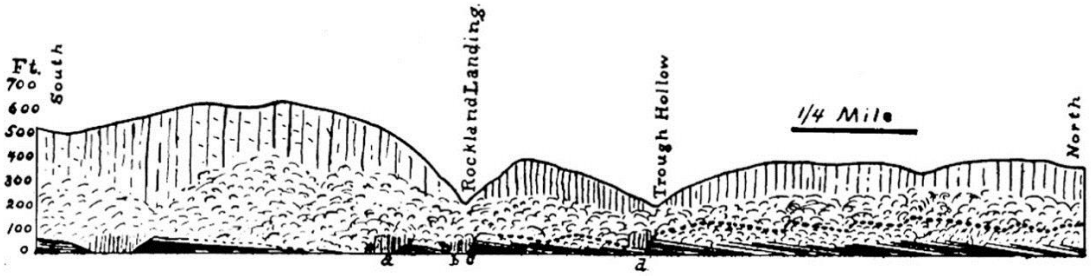

Figure 10: Section showing the step-wise climbing of stratigraphic level northward of the contact between Palisade Sill trap and Passaic Formation along the Hudson River near Rockland landing (from Kümmel, 1900).

Sanders (1974) provided a discussion of what he regarded as diametrically opposed models of how the stratigraphy of the northern terminus of the Newark basin relates to the former continuation of strata beyond the present limits of the basin and the Broad Terrane model (Fig. 11). He termed these the “shelving-basin school” (c.f., Savage, 1968) and the “transverse-anticline school” (Sanders, 1974). We are now in a position to evaluate these models with data, a goal Sanders explicitly desired.

According to Sanders' view of the "shelving-basin school," the strike of the sedimentary strata continues constant at about N 20° to 25°E striking directly into basement as the basement contact swings to the northwest at the basin's north end. In current parlance, we would call that onlap onto the hanging wall (Fig. 11A). According to Sanders, a corollary is that the Palisades sheet is a sill in southern Rockland County but becomes a dike cutting cut across Newark Basin strata as its outcrop expression swings to strike to the west (e.g., Lowe, 1959). Sanders viewed this concept as antithetical to the Broad Terrane model.

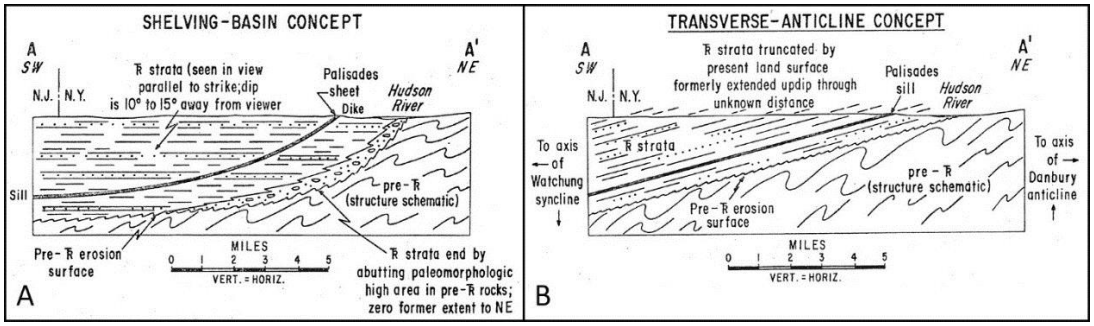

Figure 11: Sanders' (1974) two modles for the northern terminus of the Newark Basin.

According to Sanders' view of the "transverse-anticline school", for which he claimed to be the only proponent at the time, the strike of the sedimentary strata follows the course of the Hudson River and the outcrop attitude of the Palisade sheet reflects that it remains a sill as it curves towards the west and is folded. Thus the sedimentary strata, "…strike directly and perpendicularly into the Ramapo Fault and dip away from [the] major anticlinal axis lying to the northeast (named the Danbury anticline by Sanders, 1960)" (Sanders, 1974), consistent with the strict version of the Broad Terrane model.

Data on strike and dips and the mapped distribution of lithofacies in Rockland County, available before 1974 (Kümmel, 1899; Perlmutter, 1959; Savage, 1968) and accumulated since (Ratcliffe, 1980; 1988; Yager and Ratcliffe, 2010; Heisig, 2011), clearly show strike curving from the south to the east very roughly paralleling the river until Stony Point where the strike is east-southeast, perpendicular to the Ramapo fault system (Fig. 9). This is consistent with Sanders' "transverse-anticline school". However, it is also clear from the map relations of lithofacies (Ratcliffe, 1988; Yager and Ratcliffe, 2010) and compilations of strikes and dips (Heisig, 2011) that the Palisades Sill cuts dramatically up section though much of the Passaic Formation. In addition (Kodama, 1983) has shown that the Palisade sheet continues to the west of its last contiguous outcrop at Mount Ivy and connects to the Ladentown basalts, which is also consistent with the chemistry of the two units and Ratcliffe (1988) (a detailed discussion of the relationship is given in Blackburn et al., 2013, supplemental materials; DOI: 10.1126/science.1234204). These observations are consistent with the "shelving-basin school".

Outcrops at the northern terminus of the Newark Basin are mostly consistent with Passaic Formation. There is no sign at all of Lockatong Formation or Stockton facies (even as seen in core TW4), including near Stony Point, where section below the Hudson is present on land. In fact, along Cedar Pond Brook at Stony Point, there are outcrops of limestone and carbonate-rich sequences unlike any elsewhere in the Newark Basin, except in the Jacksonwald Syncline. The facies typical of the Newark Basin in Bergen County or the bulk of the basin do not project into the northern terminus of the basin, which is inconsistent with a simple version of the "transverse-anticline school".

From these observations, it is clear that if hanging wall onlap is present, it must be more subtle than Sanders' "shelving-basin school", but the geometry of the strata relative to the Palisades Sill is

incompatible with simple post-sill folding and the "transverse-anticline school". However, onlap does predict that there should be less thickness of strata present from the Ladentown basalts to the basement contact at Stony Point than between these basalts and the basement contact to the southeast in the Hudson River. Stratigraphic thicknesses estimates, based on published dip and strike data from two orthogonal transects of the northern Newark Basin (Fig. 9), show that the thickness along the transect from the Ladentown Basalt (= Orange Mountain Basalt) to basement parallel to the Ramapo Fault system (A-A') is projected to be significantly less than that perpendicular to the fault system (B-B'), consistent with a modified version of the "shelving-basin school" (Table 1). A model of dip change with distance along the transects is required to calculate stratigraphic depth and three simple models were used here (Table 1) to honor the field data or their dip-domain equivalents. A simple average of the field data is inappropriate because of the uneven spacing of the field data. The average of the three stratigraphic thickness models along traverse B-B' is 2986 m and for section A-A' it is 2266 m, which is an average difference of 302 m (Table 1. We regard the linear regression model (Table 1) as both the simplest and most reasonable and that predicts a difference of 269 m between the transects, but all three models produce reasonably similar results. However, these models are some kind of prediction of what the depth to basement near the middle of the transects might be. Simply projecting the 10.5° average dip (dip-domain data of Helsig, 2012) from the Ladentown Basalt to the basement contacts of each traverse gives us a difference of 798 m, still fully consistent with a modified version of the "shelving-basin school". Projecting from the Ladentown Basalt area is very sensitive to the specific dip value used and we really do not know what the appropriate value is within 10°. With all these caveats, however, all existing data are consistent with hanging wall onlap in exactly the directions there should be none according to the strict Broad Terrane model or Sanders' "transverse-anticline school".

Table 1

Stratigraphic Thickness Models[3]

Section	Linear interpolation Projection	Linear regression	4 degree polynomial	Average	Simple
Ladentown Basalt to Ossining Basement (Section B-B')[1]					
Average interpolated dip at 1 m	10.5°	10.6°	10.6°	10.5°	10.5°
Stratigraphic thickness	2953 m	3010 m	3005 m	2986 m	2983 m
Ladentown Basalt to Stony Point Basement (Section A-A')[2]					
Average interpolated dip at 1 m	12.6°	13.2°	13.2°	13.0°	10.5°
Stratigraphic thickness	2604 m	2740 m	2718 m	2688 m	2185 m
Difference between sections	349 m	269 m	287 m	302 m	798 m

[1] Traverse B-B' is 16369 m long with 10 dip values based on the dip-domain map of Heisig (2012) except for the two most two dips of 13.5° extrapolated from the most eastern dip-domain. Width of Palisade sheet has been removed from the traverse between the two dip points where it lies.

[2] Traverse is 11987 m long with 7 dip readings from Yager & Ratcliffe (2010) except for the two most southern dips of 10.5° which are from the dip-domain map of Heisig (2012). Width of Palisade sheet has been removed from the traverse between the two measured points where it lies.

[3] Stratigraphic thickness models were derived from dip models produced in Excel™ that are regressions of the original dip data against their projected linear distances along the traverses. The regression equations were then applied to a 1 m delta distance series of the transects from which a running sum of stratigraphic thickness was derived (in Excel™). The linear interpolation models were produced by interpolation of dip values between measured points along the traverses using Analyseries™ that were then applied to a 1 m delta distance series of the transects from which a running sum of stratigraphic thickness was derived (in Excel™).

It is worth noting that both transects B-B' and A-A' show an increase in dip down section, although it is more convincing for A-A' (r^2=0.55: ~10° to ~20°) than for B-B' (r^2= 0.34: ~10° to ~14°). Both sections also have a lower dip zone in the middle of ~8° and ~6°, respectively. Such an increase in dip is completely consistent with the Newark Basin half graben being a growth structure. That is, the basin developed through its history as a half graben with fanning of strata towards the boundary fault that was active during deposition. This can be more convincingly seen in the seismic profiles and Tandem Lot Well described below. The observations and interpretations are incompatible with the strict Broad Terrane model or the "transverse anticline school" of Sanders (1974). However, the surface data are compatible with some folding after deposition (e.g., the Passaic Formation in contact with the Ladentown Basalt is in a syncline) and with the Palisade sheet cutting up though the Passaic Formation to connect with the Ladentown Basalt.

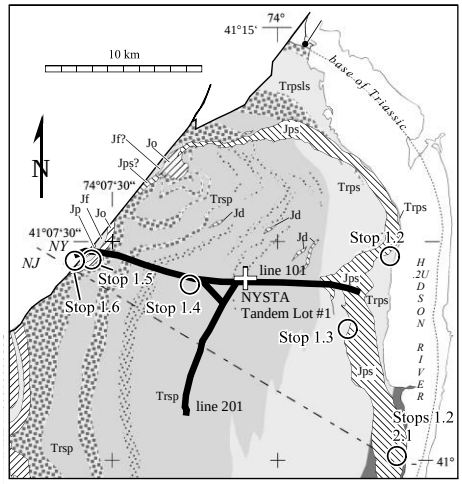

Figure 12: Left, Very early morning operation of Vibroseis truck on New York State Thruway) from Collins et al., 2011). Right, Geologic map of the northern Newark Basin with approximate location of the seismic profile, line 101 and line 102. Same key as Figure 9.

Seismic Profiles and the TriCarb Tandem Lot Well

Two high-resolution, roughly orthogonal seismic reflection profiles were surveyed in late March and early April, 2011 as part of the TriCarb Consortium for Carbon Sequestration Newark Basin characterization project (Slater et al., 2012; Tymchak et al., 2011; Olsen et al., 2011; Collins et al., 2014). One dip line (Sandia line 101) extends 21 km across almost all of the northern Newark Basin, east-west along the New York State Thruway. A shorter strike line (Sandia line 201) extends 8 km (north-south) along the Garden State Parkway, terminating in the north at the Thruway at Exit 14A, 1.3 km to the west-southwest of the location of the stratigraphic borehole (NYSTA Tandem Lot no. 1) drilled by the TriCarb consortium at exit 14 on the Thruway. Three vibroseis trucks comprised the source array (Fig. 12). Source points were spaced at 36.5 m (120-ft) intervals and geophone accelerometers collected data at 3.05 m (10 ft) intervals. The seismic profiles were processed by Conrad Geoscience Corp. (Tymchak et al., 2011) to obtain depth-migrated images of the basin's subsurface geometry (Fig. 13).

The NYSTA Tandem Lot no. 1 stratigraphic test well was spudded at (41.103782°, -74.027230°: Fig. 12) on August 17, 2011 and drilled by Union Drilling Inc. to a total depth of 2097.3 m (6881 ft) on October

15, 2011 (Fig. 14). About 150 ft of core was recovered along with cuttings, 50 sidewall cores, and an extensive suite of wireline geophysical logs. This hole, along with the surface data, ground truths the seismic line. The description of the seismic lines and the Tandem Lot drill hole will be superficial here; there is far more data available than can be covered, but the highlights are summarized. The most obvious features on the profiles are the pair of strong reflectors crossing the basin, making a trough- or scoop-shape (Fig. 14). Prior to drilling these were interpreted as demarcating the Palisade sheet, which proved to be correct. The hole was spudded in middle Passaic Formation. Visible metamorphism and metamorphic minerals (e.g., epidote) were encountered in reddish Passaic Formation gradationally at about 4500 ft, which is more intense downwards until the strata are drab reddish greenish gray. The Palisades Sill was encountered at (4992.25 ft) and the underlying metamorphosed Lockatong Formation was entered at (6567 ft). The drill hole reached total depth (T.D. = 6881 ft), still in the Lockatong. The border fault is not visible in the seismic profiles, but it can be projected from the surface on the seismic traverse to depth to the west of the faint bedding reflectors to the west of the Palisade sheet. At depth, strong discordant reflectors demarcate basement structures, plausibly Paleozoic thrust sheets incorporating Paleozoic carbonates, as are visible in other seismic lines across the basin (Fig. 15).

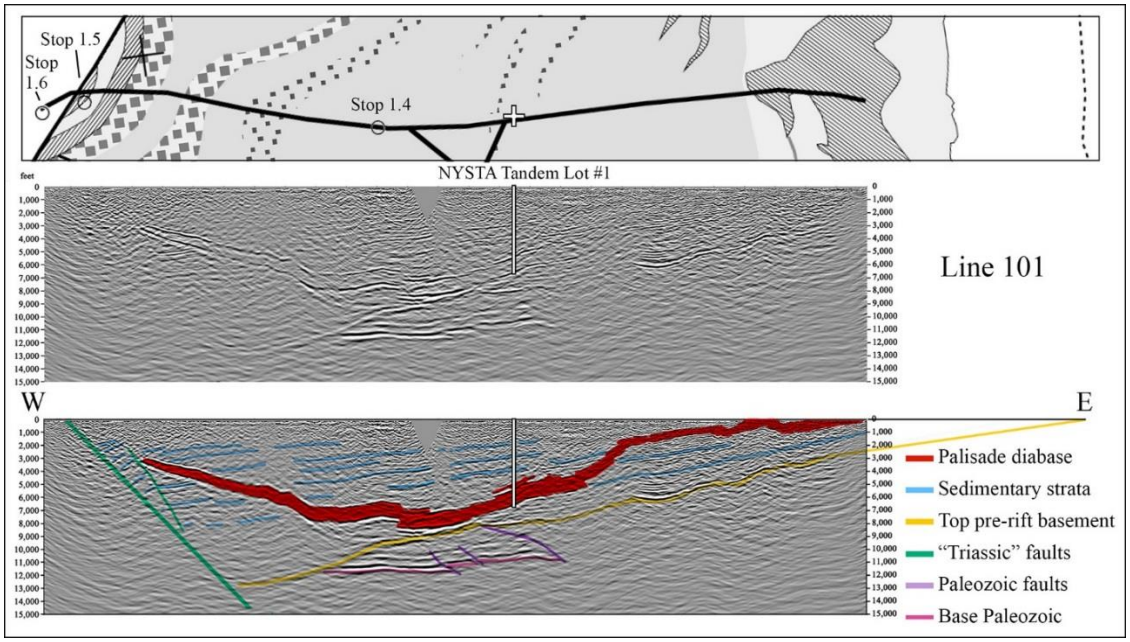

Figure 13: Sandia line 101, data and interepretation. Interpretation is consistent with drill hole and outcrop data.

Drilling cuttings and Schumberger's FMI (Fullbore Formation Microimager) and other geophysical wireline logs plus 150 ft of core near the base of the Passaic Formation allow the section encountered in the Tandem Lot core to be understood in some detail. The upper part of the section of Passaic Formation, made up of largely red interbedded conglomerate, sandstone, and mudstone is similar to what is exposed along the NYST between exits 14A and 15, although those exposures are higher stratigraphically. Many of the red muddy units have carbonate nodules of pedogenic origin. There is a largely white to tan sandstone sequence between 2230 and 2470 ft, a largely red sandstone sequences at 2790-3228 ft, and a cyclical appearing sandstone and mudstone unit at 3540-4250 ft. Peaks in natural

gamma radiation between 3228 ft and the Palisade Sill suggest the presence of cyclical red and some gray mudstone intervals in the lower Passaic Formation.

We can make a direct comparison of the gamma ray data between the lower Passaic of the Tandem Lot hole and the cores of the Newark basin coring project (NBCP) (Fig. 16). When this is done quantitatively, it appears as though the Lower Passaic section at the Tandem Lot is about 68% of the thickness of roughly correlative strata in the NBCP cores. The 405 kyr (58 m) and the double ~100ky eccentricity peaks (around 17 m) can be seen in the gamma ray data of the Tandem Lot hole. The ~20 kyr cycle is also present, but it is very smeared out in the gamma ray data of the Tandem Lot hole. However, that is true for gamma ray data of the NBCP cores examined here as well, even though it is evident in the depth rank data that when scaled to the Tandem Lot, it is about 3.4 m (11 ft) with broad dispersion.

The Palisades Sill exhibits much lower gamma values than the surrounding sediments. While the overlying Lower Passaic Formation averages 114 api-gamma-units, the sill averages 44 api-gamma-units. This is typical of basaltic rocks in general and the sharp upper and lower boundaries are typical of intrusions. The relatively higher values between 5100 and 5625 ft and especially between 5100 and 5375 ft, with peaks reaching nearly 100 api-gamma-units probably reflects enrichment in Uranium, plausibly in zircons, within a gabbroid (coarse grained) zone called the “sandwich horizon” (Shirley, 1987; Block et al., 2015) seen in outcrops. Zircons approximately from this level in outcrop have produced a very high precision zircon U-Pb CA-ID-TIMS date of 201.520±0.034 Ma (Blackburn et al., 2013). There is no indication in the geophysical logs of the famous olivine zone (Lewis, 1908; Walker, 1940), but they may not be diagnostic. The cuttings, still unstudied, should provide definitive data. In fact the olivine zone has been seen at Tallman Mountain State Park (Savage, 1968; Van Houten, 1969), so it should be present in TW4. We will see the lower part of the Palisades Sill at Stops 1.1-1.4, and an offshoot of it at Stop 1.5.

Theories on the origin of the various layers in the Palisade Sill are both contentious and important. Early ideas on the olivine zone regarded it a an early fractionation product following the Bowen Reaction Series (Lewis, 1908; Walker,

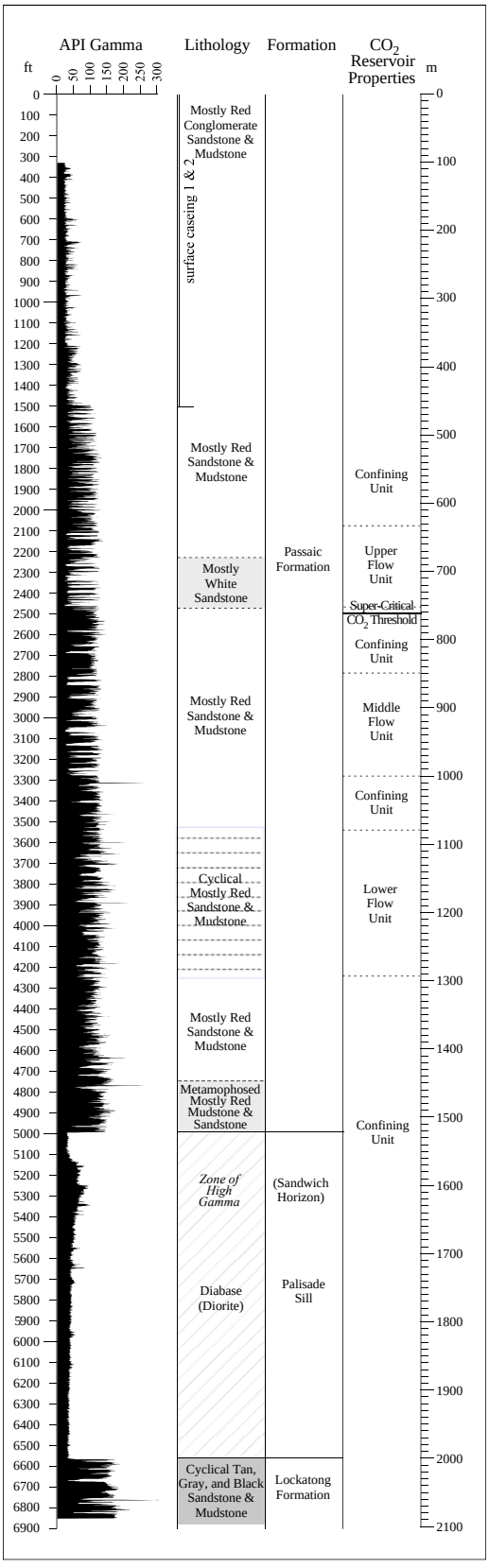

Figure 14: NYSTA Tandem Lot no. 1.

1940), but more recently it has been argued that it represents a separate injection (Husch, 1990) or the product of flow differentiation (Steiner et al., 1992; Gorring and Naslund, 1995). As mentioned, the Palisade sheet appears to have been a feeder and directly connected to the Orange Mountain Basalt (Ladentown Basalt). Most recently, Puffer et al. (2009) and Block et al. (2015) have made a case for multiple injection events within the sill spanning the ~600kyr duration of the CAMP in the Newark Basin and may have been a feeder to all of the flows. To have received multiple injections within the sill over ~600 kyr requires the interior of the sill to have been incompletely solidified over the duration, only possible if there was a continuous flow of magma within the sill to some extent over that period. There is some evidence for this in the form of scoria at multiple levels in the Towaco Formation.

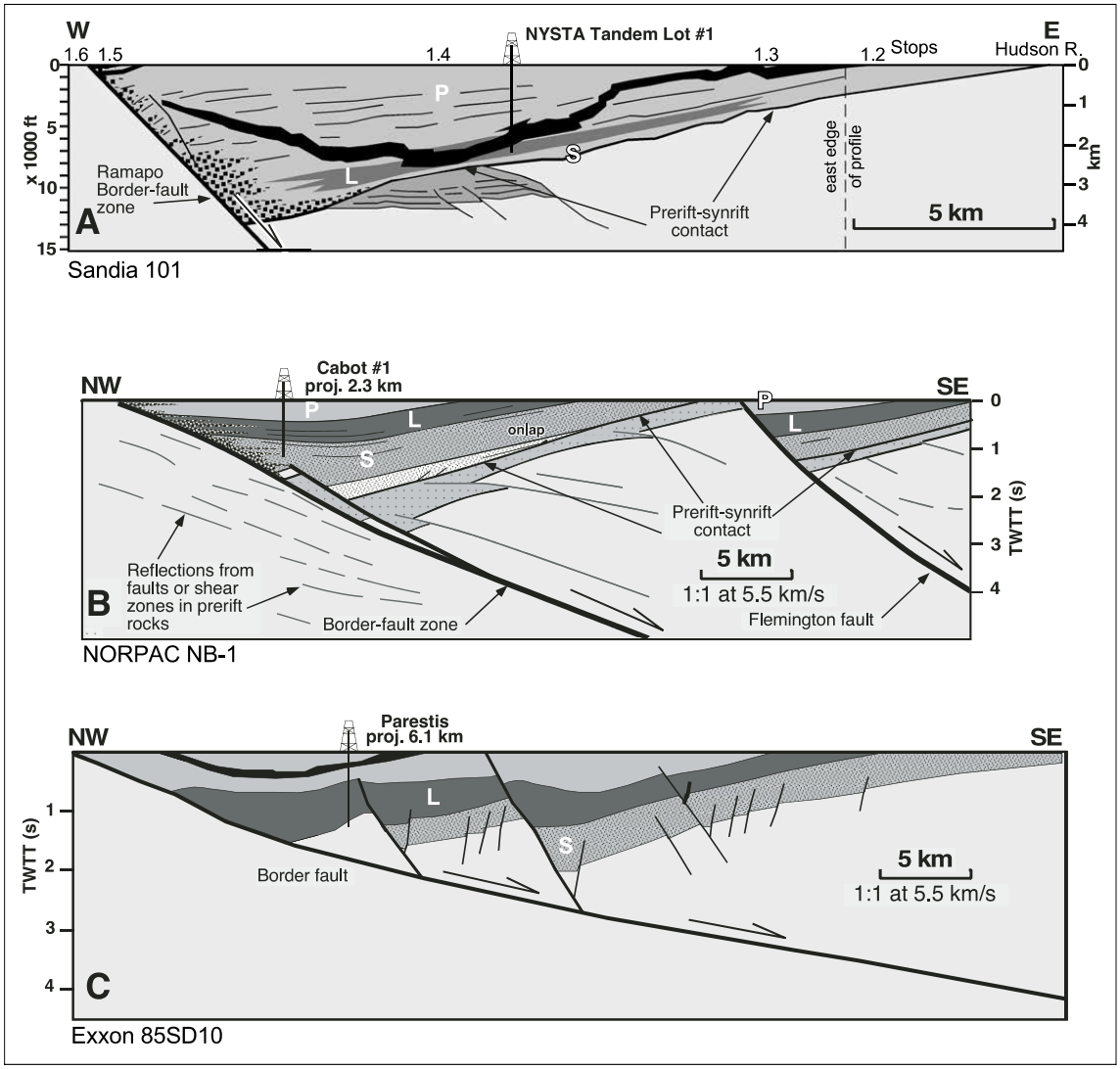

Figure 15: Interpretations of seismic profiles across the Newark Basin. A) Sandia Profile 101 with firldtrip stops shown; B) and C) are from Schlische & Withjack (2005). See Figs. 1 and 12B for locations.

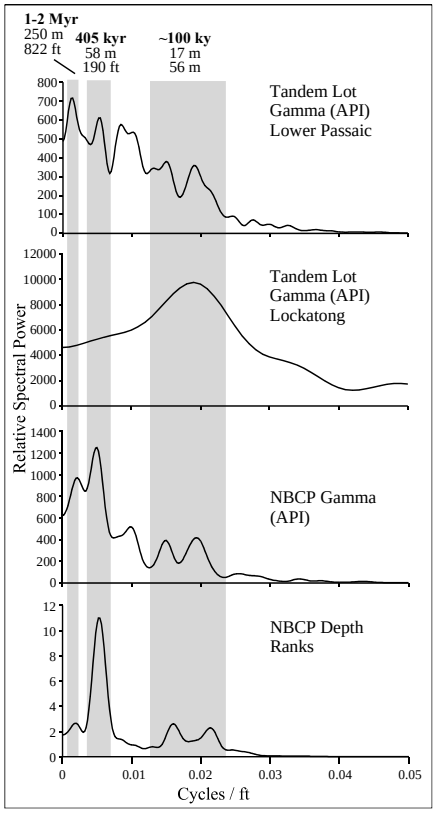

Figure 16: Blackman-Tukey spectral analysis of the NBCP cores (lower Passaic: Mb. C-Perkasie Mb.) and NYSTA Tandem Lot no. 1 natural gamma ray data. NBCP data has been scaled to the Tandem Lot section. Tandem Lot and NBCP data were filtered at the precessional cycle thickness based on previous analysis (Olsen & Kent, 1999) and them AM filtered (Hilbert Transform) and then subjected to Blackman-Tukey analysis. [3]

Strata below the Palisades Sill are drab in color to T.D. (based on cuttings and sidewall cores) and are metamorphosed. Based on the FMI images, they are cyclical alternations of laminated mudstone, massive mudstone, and arkosic sandstone and belong to the Lockatong Formation, similar to what we will see at Stops 1.2 and 1.4. Based on time series analysis of gamma logs from this interval, the periodicity of the cyclicity seen in this interval is similar to what is seen above the sill (Fig. 16) and the NBCP data scaled to the Tandem Lot. The short length of this data results in better resolution of the ~20kyr climatic precession cycle with two peaks around 3.1m (3.5 and 2.85), and there is a peak at 17m, as in the overlying Passaic Formation, consistent with the ~100ky eccentricity cycles. The section is too short to resolve the 405 ky cycle.[3]

With this "ground truth" in hand, it is relatively easy to interpret the Sandia seismic lines. While subtle, divergence of bedding is apparent in the seismic lines and agrees with the down-hole dipmeter logs and published surface measurements. The Palisade sheet clearly has a scoop shape in the seismic line, which

[3] Blackman-Tukey spectral analysis of the NBCP cores (lower Passaic: Mb. C-Perkasie Mb.) depth rank data shows a prominent spectral peak at 84.7m (277.8ft) that corresponds to the thickness of the 405 kyr orbital cycle. To compare with the much noisier gamma ray data from the same sequence the latter has to have the high values truncated (clipped) at 175api-gamma-units, because of the huge dynamic range of the high gamma peaks and their erratic positions. Blackman-Tukey spectral analysis of gamma over this interval also has a prominent peak at 84.7m (277.8ft) reflecting the lithological variations that covary with depth ranks and color corresponding to the same orbital cycle as well as an addional peak near infinity reflecting unremoved trend in the length of the data. The gamma ray data from the Tandem Lot, clipped at 115 api-gamma-units, has a prominent peak at 57.5m (188.7 ft) as well as another much longer period also reflecting the length of the data. Assuming the 84.7m and the 57.5m peaks represent the same lithological cyclicity, we can scale the NBCP data to the Tandem Lot data (NBCP thickness times 0.679245283) to make direct comparisons between spectra. An additional manipulation is needed however, because the gamma ray data in both the NBCP cores and the Tandem Lot are so noisy compared to the depth rank data in the NBCP cores, consisting of filtering the gamma ray data at 3.4m (11.1ft), and then using a Hilbert transform to recover the envelope of the data (AM filter in Analyseries™). When this is done to both the Tandem Lot and NBCP cores, the resulting spectra are remarkably similar showing the expected peaks around 58 m as well as two peaks centered around 17m. If the 58m peak is 405kyr, then the two peaks should correspond roughly to 136kyr and 104ky. In the depth rank an color data of the NBCP core, these twin cycles are identified as the double peak of the ~100ky orbital cycles.

agrees amazingly well with the cross-sections of Ratcliffe (in Yager and Ratcliffe, 2010) (Fig. 17), based almost totally on surface data. As it does in map view, on the west it cuts up through most of the Passaic Formation.

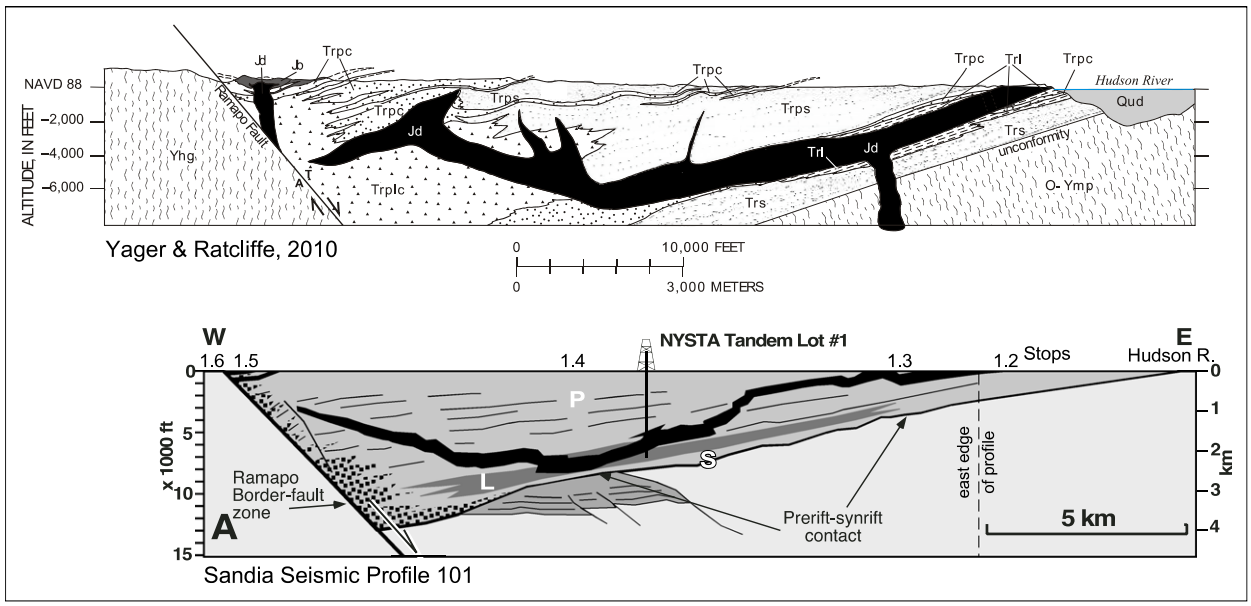

Figure 17: Comparison of Yager & Ratcliffe's (2010) crossection based on surface data with interpretation of the Sandia 101 Profile aquaired in 2012. The main features of the seismic profile were captured by the interpretive corss section.

All of the data from the Tandem Lot hole and the seismic lines indicate thinning towards the northeast, consistent with the Newark Basin being a growth structure, formed as a half graben. This does not mean, however, that the strata of the Newark Basin did not connect to the Hartford Basin; it just means that if they did connect it was via a much thinned veneer of strata. If they did connect, it also does not mean there could not have been basement highs (inselbergs) sticking out through the strata, shedding debris into the sediments around them. All this means that the actual argument about the Broad Terrane needs to be significantly more nuanced than it has been. This is especially clear when it comes to consideration of the original area covered by the CAMP lavas, described below.

Broad Terrane Triassic-Jurassic Flood Basalts

In the early formulation of the Broad Terrane model, especially as advocated by Sanders, lava flows of the CAMP were continuous between the Newark and Hartford basins prior to uplift of the Danbury anticline and subsequent erosion. McHone (1996) took this model one step further and argued the distribution of CAMP dikes was indicative of the distribution of the flows prior to erosion. That this is an oversimplification is clear from the distribution of dikes in Atlantic Canada, where dikes of chemistries of Preakness-Holyoke composition lie adjacent to the Fundy Basin, which appears to lack flows of similar composition (Pe-Piper et al., 1999). However, the Fundy Basin lies on the western edge of the entire rift system, and it is possible that it is not entirely representative of the very much larger rifting zone to the east.

It is clear that the present distribution of CAMP lavas is some fraction of the original eruptive volume because of the nearly pervasive erosion since the Early Jurassic. This makes it difficult to estimate the

possible environmental effects of the event. In order to address the hypothesis of Broad Terrane lavas, and perhaps get a handle on the distribution of lava shortly after the CAMP eruptions, an experiment was pursued in the late 1990s (Fairfield, 1998; Fairfield et al., 1999; Olsen et al., 1999) that looked for ghosts of the former extent of the lava. The experiment was predicated on the idea that if the lavas covered extensive areas outside the presently preserved basins, especially in the watersheds in higher elevations between basins, the basalts themselves should have contributed sediment to the basins beginning shortly after eruptions. A geochemical tracer of basaltic eruptions is needed because basalt debris would be very quickly weathered to clay in the tropical depositional climate of these basins. Because Nd, Sm/Nd, and Nd isotope ratios, particularly expressed as ε_{Nd} (epsilon Nd), differ so much between basement (~ -15 ± 5 ε_{Nd}) and CAMP rocks (~0 ± 6 ε_{Nd}) (Pegram, 1990; Dorais et al., 2005) they would make good tracers. Therefore, sediments derived from pre-rift basement should differ from those derived from the degradation of the CAMP flows. However, a preliminary assessment of a suite of Hartford basin mudstones (Fig. 18), from all of the exposed formations, shows no overall trend in the epsilon Nd or Sm/Nd isotopic ratios from pre-flow through syn-flow and post-flow units indicative of basalt input (y= -0.8161x-8.9683: r^2=0.24). Older pre-CAMP sediments have values of -10.0 ± 1.1 ε_{Nd} and younger syn- and post-CAMP sediments having values of -11 ± 1.9 ε_{Nd} (2σ error), indicating very little if any input from the basalts. We had included one sample of highly altered (paleo-weathered) Hampden Basalt to assure that a material we *knew* had a very high CAMP content would show it (which it did: Fig. 18). In retrospect, the Hartford Basin may have been a poor choice for the experiment, because it received most of its syn- and early post-CAMP input from the western, hanging wall, side of the basin, where there are no CAMP dikes. However, the data would seem to indicate that any flows emplaced between the Pomperaug Basin and the Hartford Basin could not have contributed significantly to the Hartford Basin strata, either because they were not there at all, or because they were quickly buried by a veneer of sediment and therefore not available for erosion into the basin.

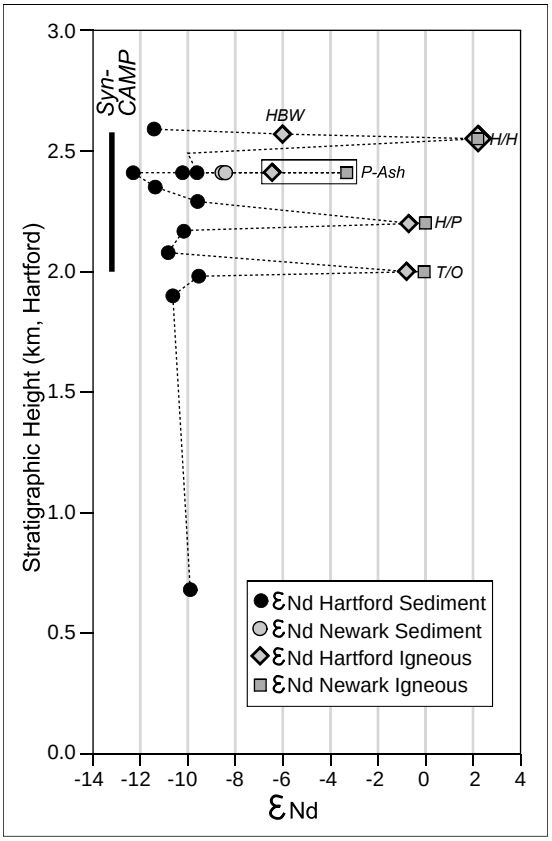

Figure 18: Epsilon Nd results for the Hartford and Newark Basin. Data for Hartford sedimets are from Fairfield (1998). Data for Basalts from Pegram (1990). Data for ashes courtesy of S. Jaret (pers comm., 2016).

Motivated by the negative results of the first experiment and by the question of whether completely weathered, essentially invisible, CAMP ashes could be identified at the Newarkian ETE (see below), we looked at a single small (~5 mm), definitive airfall ash in the middle Towaco and middle East Berlin Formation called the Pompton Ash (Olsen et al., 2012; 2016). The andesitic to basaltic ash occurs in microlaminated, fish-bearing units that are in the same 20kyr cycle in the two basins. The ash and about 1.5 cm of surrounding microlaminated strata were analyzed for ε_{Nd} to see if the ash showed a distinct igneous signature (Fig. 18). From the Hartford basin, the strata surrounding the ash are within the

range of the rest of the East Berlin Formation, and the ash is nearly 4 ε_{Nd} units closer to the CAMP basalts, although not as igneous-looking as anticipated. Clearly the ash as preserved is an admixture of igneous and non-igneous material and is very close to the altered Hampden Basalt previously mentioned. In contrast, the sediments around the Newark Basin sample of the ash is about 1 ε_{Nd} unit "more igneous looking" than exactly correlative Hartford sedimentary strata and isis shifted nearly 4 ε_{Nd} units towards CAMP basalts compared to its Hartford counterpart (Fig. 18). This may indicate a larger CAMP contribution to Newark Basin syn-CAMP sedimentary strata, consistent with it receiving much of sediment from the hanging wall side of the basin, which is in the direction of known CAMP on the conjugate margins of eastern North America and Morocco. Further work on Newark basin sediments should reveal how much contribution of CAMP there is from outside the basin to the preserved sediments.

A related issue is the size of the lakes that occupied the basins. It has been known for more than 30 years (e.g., Olsen et al, 1996b) that there is a very close correspondence between the cyclostratigraphy of the very latest Triassic age and Early Jurassic age lacustrine sequences in the Newark and Hartford basins and it is reasonable to ask if the lakes that made those sequence were connected by open water at least during highstands. The cyclicity was caused by variations in the hydrologic balance paced by variations in the Earth's orbit and axial orientation (Olsen, 1986; Olsen & Kent, 1996; 1999; Blackburn et al., 2013), and we know that the lacustrine cyclicity was synchronous in the two basins at the finest observable levels. The Pompton Ash is in the same position with cycles correlated long before the ash was known (e.g., Olsen, 1984 vs. Olsen, 2010), and additionally, there is a very close match of laminae around the ash between the two basins. Because both the cylicity and the laminae were paced by climate change (seasonal to millennial), it really is not surprising that the cycles and laminae match, but the match at multiple scales is close, much closer than anything documented in Pleistocene Great Basin lakes, for example. This raises the question of whether the lakes are one during high stands. Olsen (et al, 1982) originally thought that the lakes were not connected (or even correlated), because the fish assemblages seemed so different. Further collection proved that the differences were apparent, not real, and due to sampling biases (Olsen, 1983). The cyclcostratigraphy of what is known of syn-CAMP strata of the Culpeper Basin of Virginia and Maryland and the Deerfield Basin of Massachusetts, suggests a match with the Newark and Hartford basins and opens the possibility that during high stands, a single lake may have been present from northern Massachusetts to south central Virginia, a distance of nearly 700 km and significantly larger than Lake Tanganyika, and longer than Lake Superior, making it one of the largest lakes known. But testing this hypothesis is not easy and remains for future work. Perhaps comparison of the strontium isotopic composition of the carbonates in exactly contemporaneous laminae around the Pompton Ash could provide a test. They should differ if the lakes had different watersheds with different Sr isotopic compositions, and they should have the same Sr isotopic values if the lakes were connected by open water.

The Broad Terrane model thus survives in a modified form. The simplest interpretation of the existing data is that the presently preserved remnants of basins formed mostly as half graben growth structures that linked up through time with thinner and plausibly patchy cover of sediments and lavas covering intervening basement rocks. Water may have connected the basins by rivers, or open water with huge lakes, during lake highstands. However, there is no evidence supporting the strict Broad Terrane model. We can imagine a landscape comprised of a vast rifting zone with many depositional basins, many connected by flat plains, lakes or rivers, looking much like the Basin and Range does today. However, despite considerable progress, we are as yet unable to constrain the area occupied by CAMP lavas, within two orders of magnitude (0.3 – 10 Mkm^2: McHone, 2003) and thus constrain the volume and

direct volcanic output of volatiles and their environmental effects.

Record and Causes of the End-Triassic Mass Extinction

Formerly usually referred to as the Triassic-Jurassic boundary event, the end-Triassic mass extinction (ETE) is one of the "big-five" extinction events of the Phanerozoic, as first pointed out by literature reviews of the ranges of marine and continental animals (Raup and Sepkoski, 1982). The detailed review and update by Benton (1995) (Fig. 19) shows that, depending on the metric used, the ETE can be as large or larger in magnitude as the K-Pg (Cretaceous-Paleogene, or K-T) or even Permian-Triassic for continental organisms. The ETE was formerly often considered synonymous with the Triassic-Jurassic boundary. However, the recent establishment and ratification by the IUGS in 2010 (Morton, 2010) of the GSSP (Global boundary Stratotype Section and Point) of the base Hettangian at the marine section at Kuhjoch, Austria (Northern Calcareous Alps) at the first occurrence of the ammonite *Psiloceras spelae* (Morton, 2012; Hillebrandt et al., 2013) defines the ETE as a Late Triassic event. The Triassic-Jurassic boundary is thus part of the tenuous recovery identified in the marine realm occurring about 100-200kyr after the ETE (Schoene et al., 2010; Sha et al., 2015). Furthermore, because ammonites were cephalopods completely restricted to marine environments, recognizing the Triassic-Jurassic boundary in continental deposits is highly inferential, based on one or two provincial sporomorphs or extrapolation of astrochronologies from zircon U-Pb dates.

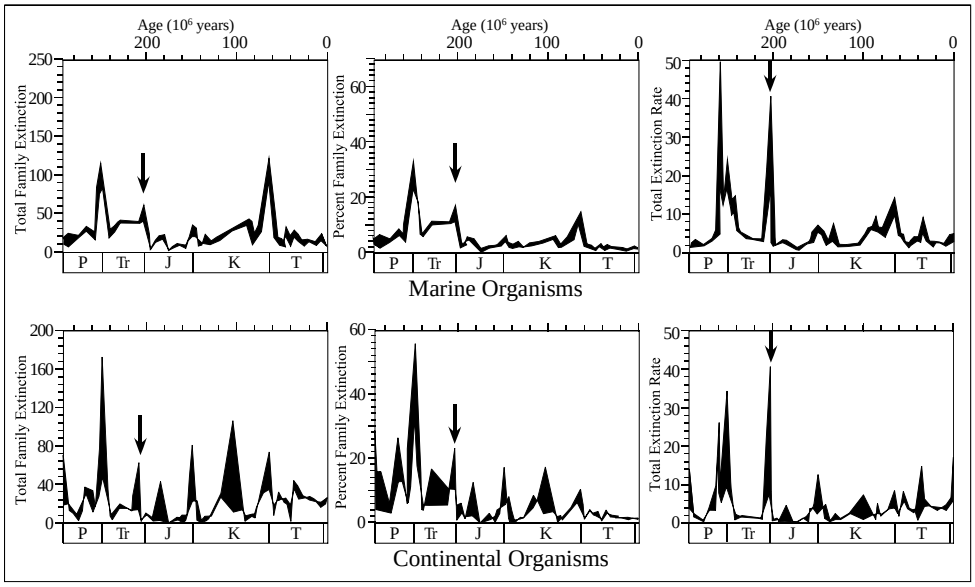

Figure 19: Various metrics of extinction for marine and just continental organisms (from Bention, 1995).

For those not intimately familiar with the literature, it is worth noting that this final (for now) definition of the Triassic-Jurassic boundary has produced considerable confusion in the literature because the meaning of the term Triassic-Jurassic boundary or Rhaetian-Hettangian boundary has changed since 2010 when it was equated with the ETE. Several relatively recent papers conflate the pre-2010 meaning of the Triassic-Jurassic boundary with its present GSSP meaning, arguing that pre-2010 correlations of the Newarkian continental to marine environments were incorrect (e.g., Cirilli et al., 2009; Lucas and Tanner, 2015), when in fact the correlations of the strata have not changed, only the definitions of the ages have.

In eastern North America, the most dramatic biotic change in the entire sedimentary record of the rifts

occurs very close to, but not at, the base of the oldest CAMP basalts (Fig. 20). This change involves the abrupt last appearances of all the Triassic-type footprint taxa (Fig. 21A) and nearly all Triassic-aspect pollen and spores, as documented by Olsen et al. (2002). Included are the previously abundant footprints *Brachychirotherium* that is representative of the non-crocodile, "crocodile-line" top terrestrial predator and possibly herbivore pseudosuchian, and *Apatopus*, a representative of the phytosaurs, the semi-aquatic, non-archosaur, crocodile-mimic pseudosuchians (see Stops 1.6 and 2.2). Amongst sporomorphs, the most prominent extinction includes the vessicate pollen forms, including previously very abundant *Patinasporites*, produced by an extinct, largely tropical conifer group. Many other pollen and spore taxa disappear as well. Above the level of the extinctions, the only representative of the pseudosuchians is *Batrachopus* (Fig. 21), a track that could have been made by small protosuchians or sphenosuchians, the only two crocodile-line lineages that survive the ETE, the former implicated in the origin of the modern crocodilians (see Stop 1.7). Below the extinction level, the only dinosaur footprints present are small brontozoids (*Grallator* and *Anchisauripus*), representing small carnivorous theropod dinosaurs, and *Evazoum* (e.g., Stop 1.6), made by a basal dinosaur (which is rare and disappears well below the ETE) (see Stop 1.6). Above the extinction level, the much larger theropod dinosaur brontozoid footprint *Eubrontes giganteus* abruptly appears and is abundant along with the smaller brontozoids. The dinosaurian herbivore tracks *Anomoepus* (made by small ornithischians) and *Otozoum* (made by basal sauropodomorphs = "prosauropods') appear at slightly higher levels (Olsen et al., 2002) (Figs. 21).

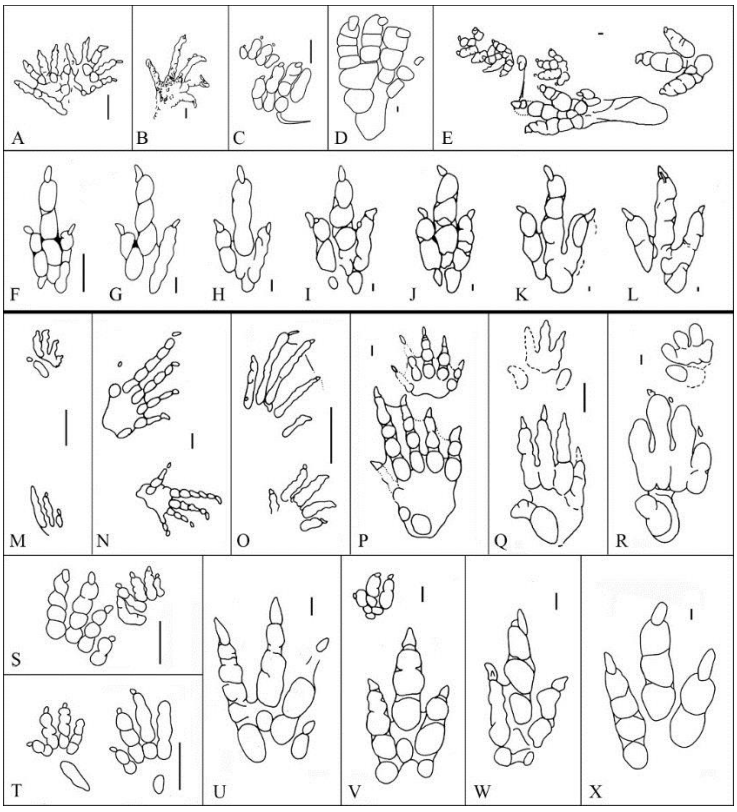

Figure 21: Post ETE taxa are A-L and pre-ETE fprms are M-X. Taxa are A, *Ameghinichnus* n,sp.; B, *Rhynchosauroides* n.sp.; C, *Batrachopus deweyii*; D, *Otozoum moodii*; E, *Anomoepus scambus*; F-G, different sizes of brontozoid with *Grallator* spp.. on the left, *Anchisauripus* in the middle and *Eubrontes giganteus* on the right; M, *Rhynchosauroides brunswickii*; N, *Rhynchosauroides hyperbates*; O, *Gwyneddichnium* sp.; P, *Apatopus lineatus*; , Q*, Chirotherium lulli*; R, *Brachichirotherium parvum*; S, "new taxon B"; T."*Batrachopus*" *gracilis*; U, *Evozoum* n.sp.; V, *Atreipus milforensis*; W, small brontozoid, *Grallator* sp.; X medium sized brontozoid *Anchisauripus* c.f. *tuberatus*. From Olsen and Rainforth (2003) and Rainforth (2003).

Lucas and Tanner (2015, and papers by the same authors cited within) argue that the ETE was not a major extinction event at all, pointing out the small number of tetrapod forms that go extinct at the Newarkian ETE. It is true that the skeletal material is relatively rare in Eastern North America, and that while tracks are very common, only 4 footprint taxa have their last appearances at the ETE in eastern North America. However, the footprint taxa may be representatives of several or even many biological species and as a proportion of what is present, the extinction level sees a 44% (4/9) diversity drop, much higher than documented anywhere else in the +30 Myr record of early Mesozoic faunal change in eastern North America. The change in the footprint diversity is also completely consistent with the global record of taxa represented by bones. One can argue that the footprint record in the Triassic-Jurassic is analogous to what one might see along the edges of a Serengeti (Tanzania and Kenya) lakeshore. Cohen et al. (1993) document that the abundant Serengeti animals leave the abundant footprints but not in proper proportion to their abundances. While it is possible to recognize the species that left these tracks, it is because we know what species are present and most have a more or less consistent adult body size – constraints not present for our Triassic-Jurassic assemblages. One footprint genus, for example, might be analogous to footprints of ALL feline and canine species or ALL artiodactyls (even-toed ungulates - antelope, wildebeest, giraffe, pigs, etc.) present in the Serengeti (Fig, 22). Thus, the footprint record sees biological diversity as, "through a glass darkly", surely massively underrepresenting the change in biological species diversity.

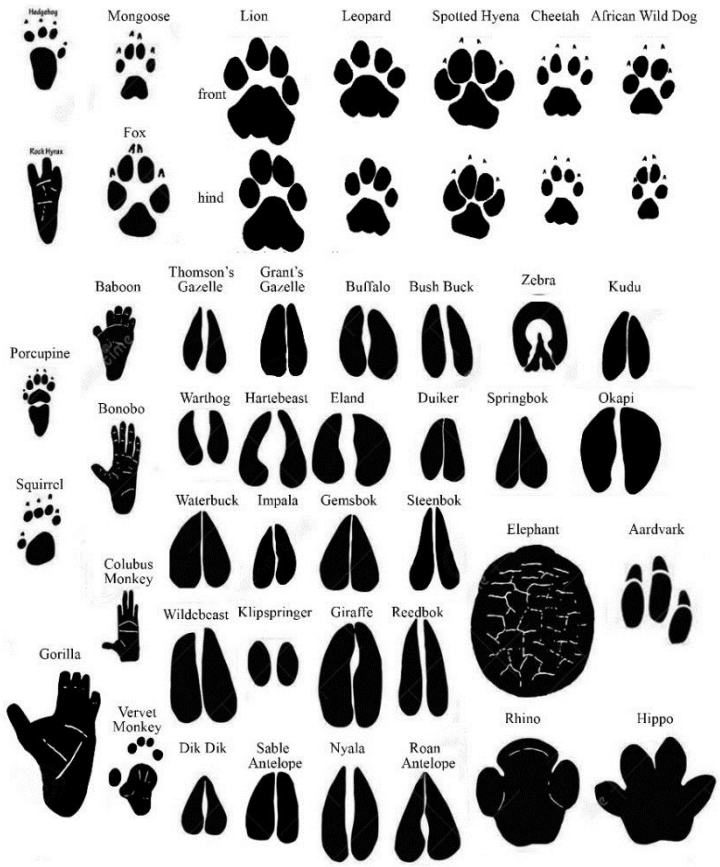

Figure 22: East African animals likely to leave footprints (ttps://www.dreamstime.com/royalty-free-stock-photography-african-animal-tracks-image7728337 and https://www.google.com/search?q=leopard+footprint&hl=en&biw=1436&bih=776&source=lnms&tbm=isch&sa=X&ved=0ahUKEwj7jvup0IPPAhVKdz4KHSRzBo0Q_AUICSgC#imgrc=5bfA6tSd

With plants, as seen via pollen and spores, the extinction level in eastern North America is dramatic and overlaps precisely with that of tetrapods, although with tighter stratigraphic and temporal precision. A high diversity assemblage dominated by the vessicate forms, especially *Patinasporites*, as well as bisaccate pollen, is replaced by an assemblage extremely strongly dominated (+90%) by the conifer pollen form *Classopollis meyeriana* with a net loss of 60% of the diversity (Fowell et al., 1994; Olsen et al., 2002). There is a laterally continuous "fern spike" exactly at the extinction level in the southwestern Newark Basin similar to that at the K-Pg boundary (Tschudy et al., 1984) in which fern spores constitute

50 to nearly 100% of the assemblage (Fowell, 1994; Olsen et al., 2002). While ferns might be expected to be dominant at any time locally, no other such level is known through the Newark Basin succession.

There is at least one major extinction event seen in the track record prior to ETE. The track taxon *Atreipus* is the most common three-toed form prior in much of the Triassic record (see Stops 1.6 and 2.2). *Atreipus* was originally interpreted as either a very "precocious" hadrosaur-like ornithischian dinosaur or a primitive dinosaurian belonging neither to ornithischians nor saurischians (Olsen & Baird, 1986). In modern context, the latter would be a non-dinosaurian dinosauromorph. The simplest interpretation of all the available evidence is that it was made by an herbivorous silesaurid, dinosauriform, dinosauromorph (c.f., *Silesaurus*; Dizk, 2003). The last known occurrence of this form is in member JJ in the Newark Basin (Olsen et al., 2002), which based on the newest version of the Newark APTS (Kent et al., 2016), is about 206 Ma. At the level of sampling of the Newark Basin section, this is indistinguishable from the 205.5-205.7 Ma age of the Norian-Rhaetian boundary (Wotzlow et al, 2015; Maron et al., 2015; Kent et al., 2016). Thus far, this is the only evidence in eastern North America of a tetrapod event correlating with that boundary.

The palynological transition seen between the Lower-Passaic-Heidlersburg and the Upper-Balls-Bluff-Upper-Passaic assemblages of Cornet (1977) was correlated to the marine Norian-Rhaetian boundary (Cornet, 1977; Fowell et al., 1994) and accepted as such by Kent and Olsen (1996) and Olsen et al. (1996) in the Newark APTS. This boundary was picked by Cornet (in Olsen et al., 1996a) at the first occurrence of *Classopollis torosus* and the last appearance of a few sporomorph taxa. This pick was criticized by Lucas & Tanner (2007) because *C. torosus* occurs in the Norian of Europe. However, there is a larger palynological extinction event identified by Fowell (1994), corresponding to about 206 Ma on the most recent Newark APTS. Based on the sampling density of palynological levels, it is indistinguishable from the the Norian-Rheatian boundary age (Wotzlaw et al, 2015; Maron et al., 2015). Because *Atreipus* was such an important component of Norian assemblages, and there is a significant correlative palynological event at current sampling density, the idea that Rhaetian-Norian boundary represents an important extinction or turnover event (Wotzlaw et al, 2015; Maron et al., 2015) is supported, although it is much smaller in magnitude than the ETE.

Identifying the cause of the ETE has been contentious. An iridium (Ir) anomaly occurs at the same level and sections as the fern spike (Olsen et al., 2002a; b), and the similarity to the K-Pg (K-T) extinctions, Ir anomaly, and fern spike was consistent with the idea that the ETE was the result of a major asteroid or comet impact (Olsen, 1999). A similar, perhaps correlative section with a fern spike in the Hartford basin (Olsen et al., 2003) has recently been shown also to have a significant Ir anomaly (Tanner & Kyte, 2016). Uncertainties in the age of the giant Manicouagan impact had earlier allowed it to be a candidate for the event (Olsen et al., 1987). However, the hypothesis that Manicouagan could be the cause was effectively tested and falsified by Hodych and Dunning (1995), who showed that the age of Manicouagan was far too old (214 +l.25/-1.03 Ma; corroborated by the ~215.5Ma date of Ramezani, 2005) to be implicated in the cause of the ETE, or the Norian-Rhaetian boundary, for that matter, although Manicouagan may have been involved in a lesser turnover event earlier in the middle Norian (Whiteside & Ward, 2011; Parker & Martz, 2011; Olsen et al., 2011; Onoue et al., 2016).

While shocked quartz has been reported from two marine sections at or near the ETE (Austria- Badjukov et al., 1987; Italy-Bice et al. 1992), these reports are uncorroborated by additional, more diagnostic, analyses (Olsen et al., 2002b). Furthermore, multiple Ir anomalies have been found at ETE sections since 2002, both above and below the extinction level (Tanner & Kyte, 2005; 2016; Tanner et al., 2008; Olsen, 2010), and a minor Ir anomaly has been identified in the GSSP section of the base Hettangian at

Kuhjoch, Austria above the base of the ETE (Tanner et al., 2016). Proposing multiple impacts based on Ir-alone seems unparsimonious.

Although there is thus no compelling evidence for the role of an impact at the ETE, there is nonetheless a small impact structure Rochecouart (pre-erosion diameter ~40-50km: Sapers et al., 2014), where if its date is accurate (201±2: Schmieder et al., 2010), it should have left some kind of record near the ETE level even if it was too small to have caused extinctions. Because impact rocks at Rochecouart are of reverse magnetic polarity (Eitel et al., 2014), it would have most likely hit during E23r, apparently before the extinction. Schmieder et al. (2009) has proposed that the Rochecouart impact produced a mega-seismic event that produced a well-known deformed unit present over a large part of the UK described as a mega-seismite by Simms (2007), present just below the ETE. The lack of impact debris (thus far) at these sections and the large uncertainties in the impact date make the association between Rochecouart and levels near the ETE only possible, not definitive. There is also no evidence of reverse polarity in strata in contact with upper surface of the seismite (Hounslow et al., 2004).

In contrast, Marzoli et al. (1999; 2004) argued that the close association of the ETE with the oldest lava flows of the CAMP (Marzoli et al. named the CAMP) indicated that the environmental effects of the emplacement of that large igneous province was the cause (Olsen et al., 1999). The two principle proposed triggers for the extinction are: 1) CO_2-induced global warming and ocean acidification, and/or methane release; and 2) H_2SO_4 (sulphuric acid) aerosols causing global dimming and cooling. These are not mutually exclusive, although their effects should operate on vastly different time scales and differ depending on the temporal concentration of the magmatism (mass CO_2 or SO_2 per unit time). Similar effects have been proposed as causes or contributors to the K-Pg (McLean, 1985; Caldeira & Rampino, 1990; Self et al., 2006) and the end-Permian (see reviews of Saunders & Reichow, 2009; van de Schootbrugge, 2016) mass extinctions, among others.

The CAMP could theoretically inject CO_2 through four main, not mutually exclusive, mechanisms: 1) direct outgassing (McHone, 2003); 2) thermogenic CO_2 and thermogenic methane (oxidizing to CO_2) (cf., Svensen et al., 2004; 2007); 3) triggering outgassing from methane clathrates in the oceans (Hesselbo et al., 2002); 4) destruction of the biological pump and turnover of the global oceans as a consequence of the mass-extinction (cf., McLean, 1985; Knoll et al., 1996). Each of these mechanisms is complex with complex predicted sequelae and a detailed exegesis of them is beyond this guidebook. However, there IS direct evidence of pulsed doublings to triplings of CO_2 in the Newark and Hartford basin section as seen in the soil carbonate proxy directly associated with CAMP eruptive events (Schaller et al., 2011, 2012; 2015). Carbonate proxy records of massive increases in CO_2 are consistent with plant leaf stomatal data from Greenland and Sweden (McEwain et al., 1999; 2009) and Germany (Bonis et al., 2010).

The killing mechanism for CO_2 would be expected to be different on land vs. the ocean. The ocean would see three possible effects: 1) ocean acidification; 2) warming with reduction of dissolved O2; and 3) nutrient increase by increase continental weathering. Ocean acidification would be expected to occur only if the CO_2 doubling occurred in less than 10kyr or so, in which case surface seawater aragonite saturation would drop and pH would drop as the oceans absorbed atmospheric CO_2, resulting in a bio-calcification crisis (Hönisch et al., 2012). While the entire CAMP episode took nearly 1 Ma, it was pulsed, and there is cyclostratigraphic and paleomagnetic evidence that at least some of the CO_2 doublings occurred within thousands of years with individual giant eruptions occurring in less than 100 years, so this is possible (Kent et al., 2009). This hypothesis is consistent with the preferential extinction of aragonitic and/or high-Mg calcitic marine organisms, such as virtually all ammonites, scleractinian corals, and sphinctozoid sponges (Hautmann et al., 2008; Martindale et al., 2012). If the CO_2 doublings take

longer, >50 ka, seawater aragonite saturation actually goes up as pH goes down and then both eventually go up and carbonate precipitation will increase. The decrease in greenhouse effects are not as sensitive to injection rate. CO_2 concentration and the temperature increase exponentially decrease for about 1Ma until background levels are reached with normal continental weathering. However, they would drop below background levels if weathering was enhanced by large areas of highly reactive exposed basalt flows in the tropics. Most of the CO_2 however would be consumed in about 300 ka or less depending on the acceleration of weathering.

The IPCC (AR5: Collins et al., 2013) consensus predicts about a 3°C (1.5°-4.5°) increase in global average temperature with each doubling of CO_2. But some models predict more than 6°C. Over geological time and with high initial pCO_2 (+1000 ppm), the temperature sensitivity is poorly constrained. The increase in temperature would be reached quickly and decrease slowly over many 10s to several 100s of ka. Multiple injections over tens of thousands of years would be additive in their effects on concentration and temperature effect, but not on acidification. Under higher ocean temperatures, O_2 concentration would decrease on the long term, which would also negatively impact pre-CAMP communities and add to any ocean acidification effects. On land, one would expect an amplification of the hydrological cycle, with drier areas becoming drier and wet areas becoming wetter (as discussed above), but some continental areas would become lethally hot with those zones greatly expanded compared to today. Increased heat (and associated fire) has been discussed both as a damper to dinosaur diversity in the tropics (Whiteside et al., 2015) and as major driver of plant extinctions during the ETE (e.g., McElwain et al., 1999). However, Late Triassic tropical areas were dominated by non-dinosaurian archosaurs and other reptiles, forms that would seem to be particularly resistant to additional heat, yet they were preferentially effected, while the pre-ETE dinosaurs at high latitudes, in presumably more temperate Triassic climes, were hardly effected.

On scales of millions of years, flood basalt eruptions such as the CAMP would be expected to produce huge continental areas that were more reactive to chemical weathering than normal continental crust, leading to long term cooling. The CAMP erupted primarily in the tropics where weathering (carbonation of basalt) would have been particularly intense, leading to a drawdown of CO_2 below pre-CAMP levels. Evidence for this is also seen in the Newark Supergoup carbonate proxy of CO_2 (Schaller et al., 2015), and a similar drawdown for the Cenozoic has been argued for the Deccan (Kent & Muttoni, 2008; 2013).

Sulfuric acid (H_2SO_4) aerosols, usually termed sulfate aerosols, the other main proposed CAMP effects on climate. In contrast to CO_2 (or methane), which are greenhouse gasses that cause warming, sulfate aerosols cause cooling by increasing planetary albedo. Most of the negative deviations from the CO_2 greenhouse warming over the past 2500 years have been due to volcanic sulfate aerosols (Sigl et al., 2015). Some spectacular examples include the historical eruptions of Laki in Iceland in 1783-1783, implicated in the death a huge number of people, 10,000 to millions globally by crop failures and social unrest (Thordaldson & Self, 2003); Tambora, Indonesia, in 1815 resulting in what was called in “The Year Without a Summer” and “Eighteen Hundred and Froze to Death” (Stothers, 1984); the eruption and explosion in 1883 of Krakatoa resulting in significant cooling and floods (Bradley,1988) as well as the Edvard Munch painting “The Scream” ten years later (Olson et al., 2007); and the 1991 eruption of Pinatubo in the Philippines that caused a 3-year, 0.5°C drop in global temperatures (Self et al., 1996), as well as major pandemics, famines, and socioeconomic disruptions in Eurasia and Mesoamerica in the 6th century. All of these eruptions are, however, at least two-orders-of-magnitude smaller than CAMP eruptions, and it seems parsimonious to hypothesize that the temperature decreases were at least an order of magnitude greater (McHone, 2003). Unlike the three major pulses of volcanism seen in outcrop and core and the consequent three or four CO_2 pulses, there were likely hundreds of brief (3 to 10 year)

volcanic winters, perhaps with freezing in the tropics, for which the tropical pre-ETE continental biota would have had no evolutionary adaptive experience. While the marine extinctions are consistent with the effects of increased CO_2, the continental biota pattern at the ETE seems more consistent with intense volcanic winters that the insulated (protofeathered) avemetatarsalians (Pterosauria + Dinosauromorpha) could survive (Olsen et al., 2013; Olsen, 2015).

Sedimentary and Igneous Facies and Carbon Sequestration

The Newark Rift Basin is the nearest best hope for carbon storage for the major CO_2 emission sources in New York, New Jersey and Pennsylvania. The TriCarb Consortium for Carbon Sequestration (Collins et al., 2014) was an organization of geologists and engineers from Sandia Technologies (Houston, TX) and LLC and Conrad Geoscience, Corp. (Poughkeepsie, NY) and academic advisors (LDEO, represented by DG, DVK, PEO) and the New York State Museum (BS) that undertook a basin characterization study that combined geophysical seismic profiling with data derived from a stratigraphic drilling, coring and logging program. American Recovery & Reinvestment Act (ARRA) funding was provided by a 2009 DOE Project Award co-funded with New York State Energy Research & Development Authority (NYSERDA) and DOE/NETL, with leveraged technical services partner, Schlumberger Carbon Services. This project was linked with a longer term set of projects at LDEO exploring CO_2 sequestering, including drilling, logging, and analysis of the TW4 core and hole, already described, funded by TriCarb and EPA STAR grant 834503 (Zakharova et al., 2016). Stops 1.1 and 2.2 will examine data derived from these projects and earlier drilling and logging projects on the LDEO campus (Yang et al., 2014).

The TriCarb project, core, and hole TW4 focused on characterizing conventional sandstone reservoirs for sequestering anthropogenic CO_2 in the northern Newark Basin. The basic concept is that CO_2 recovered from point sources such as power plants is injected into a porous sandstone reservoir sandwiched between much less permeable confining layers, such as mudstone or igneous rock. The CO_2 is generally injected in liquid form with low temperature and modest pressure, but at depth and increasing pressure, it transforms into a supercritical fluid and warms to the ambient temperature. A supercritical fluid has properties of both a liquid and a gas; it can diffuse through solids like a gas, but dissolves things or into things like a liquid. In non-saline waters at depth, supercritical CO_2 is denser than the water and thus tends not to ascend once it is pumped down. In the Newark Basin CO_2 would be supercritical deeper than 800m (2625ft) and would require thick sandstones with sufficient porosity for large volumes and permeable enough to permit injection at high flow rates without requiring overly high pressure. 800 m is also deep enough to protect drinking water resources.

Based on log analysis, but particularly side wall cores, several sandstone intervals were identified in the Passaic Formation in the Tandem Lot well with porosities exceeding 10% and permeabilities exceeding 100 millidarcys (Collins et al., 2014). Abundant low-permeability mudstones and the Palisades Sill are potential confining units. Specifically, Slater et al. (2013) reports over 300 m total of a potential sequestration zone, identified based on log data that was confirmed with core and thin section analyses. Additional laboratory measurements indicate porosity ranging from 3.6 to 15% (averaging 11.4%) and highly variable permeability values averaging 213 millidarcys but with a good correlation between porosity and permeability. Two relatively high porosity and permeable zones totaling 365 m were identified below the supercritical depth (Collins et. al., 2011). Below 1520 m (4990 ft), metamorphism and the Palisades Sill limited porosity and permeability. Measured porosities and permeabilities were not as high in sandstones in the nominal Stockton Formation in the TW4 core, all of which are relatively close to the Palisades Sill, and the correlation between measured porosity and permeability, although positive, is verging on non-existent (r^2=0.08).

Results from the Tandem Lot well suggest there are potential conventional sandstone sequestration zones and confining units below the supercritical level. However at the Tandem Lot site, these sequestration zones, if they are laterally continuous, tilt towards the surface, lack apparent structural closure, and are thus most simply interpreted as unsuitable for sequestration targets. However, they could be targets if more is known about their lateral distribution and if they intersect the discordant Palisades Sill in the up-dip direction.

Less conventional sequestration targets in the Newark basin are the mafic rocks of the CAMP, particularly lava flow units. The carbonation reaction of CO_2 (in water) is as follows in abstracted and abbreviated stoichiometric form:

$$CO_2 + CaSiO_3 = CaCO_3 + SiO_2$$

The CO2 as carbonic acid reacts with mafic mineral silicates (here as Wollastonite) to produce bicarbonate ions that react with Ca ions to precipitate limestone. Mg and Fe carbonates can also be produced from reaction with minerals (Takahashi et al., 2000). Once in the form of limestone, the CO_2 is effectively locked up on geological timescales of millions of years. This is part of the reaction series for chemical weathering that on geological time scales removes CO_2 from the atmosphere. But it also offers a fast way of sequestering CO_2 without the risk of long-term leakage Matter & Kelemen (2009).

Newark basin CAMP flows are obvious targets for sequestration (Goldberg et al., 2010). They can have porosity and permeability and are amongst the most reactive basaltic rocks. They were specifically examined for their potential for carbon sequestration Goldberg et al. (2010) using the NBCP cores and logs, specifically Martinsville no. 1 (Fig. 23). They showed that the density and porosity logs vary from 10% to 20% porosity over the 15-m (50-ft) thick flow-top boundary zone between the first and second flows of the Orange Mountain Basalt, which amounts to ~2.25×10^6 m^3 open pore volume per km^2. Results of direct carbonation experiments on various continental basalts by Schaef et al. (2009; 2010; 2010; 2014) show that the carbonation rates were highest for a sample of the upper (2^{nd}) flow of the Hartford Basin Holyoke basalt. This is particularly interesting because that particular flow has a characteristic and highly unusual joint pattern consisting of extremely abundant and dense vertical fractures that Faust (1978) termed platy-prismatic jointing that might represent a permeating anisotropy increasing mineral effective surface area. The platy-prismatic jointing is characteristic of the entablature of the second flow of the Holyoke basalt, nearly everywhere, from the southern to the northern Hartford Basin and it is also characteristic of that flow's apparent exact correlatives in other Newark Supergoup basins in the Deerfield (2^{nd} flow of the Deerfield Basalt), Newark (2^{nd} flow of the Preakness Basalt), and Culpeper Basin (1^{st} flow of the Sander Basalt). That this is the same eruptive unit is supported by both its chemistry (Puffer & Philpotts, 1989) and peculiar paleomagnetic directions (Prevot & McWilliams, 1989). If borne out by additional experiments this could represent a huge sequestration resource because the principle problem with basalts (or diabase for that matter) is the lack of dense permeable networks with reactive surface, which this basalt seems to have (Fig. 23). We will see this basalt and its platy-prismatic fracture at Stops 1.8 and 2.5.

While it has been recognized that in situ basalt carbonization could be a way of sequestering carbon safely for the long term, the speed of the reaction below the supercritical zone was very poorly constrained and there was concern it was slow (hundreds to thousands of years). However, the recent spectacular test described by Matter et al. (2016) at the CarbFix site in Iceland showed that the in situ carbonation reaction in basalt could be surprisingly fast. They found in their injection experiment that over 95% of the injected CO_2 was mineralized to carbonate minerals in less than 2 years. The experiment was terminated early because the sub surface pump became clogged with carbonate minerals. We do

not know how reactive basalts like the Preakness or Orange Mountain will be because they are much less fresh than those in Iceland, but the results thus far are promising. There is some irony in the promise of geological carbon sequestration in the Newark Basin in that the very source of CO_2 implicated in the ETE could be a viable sink for anthropogenic CO_2.

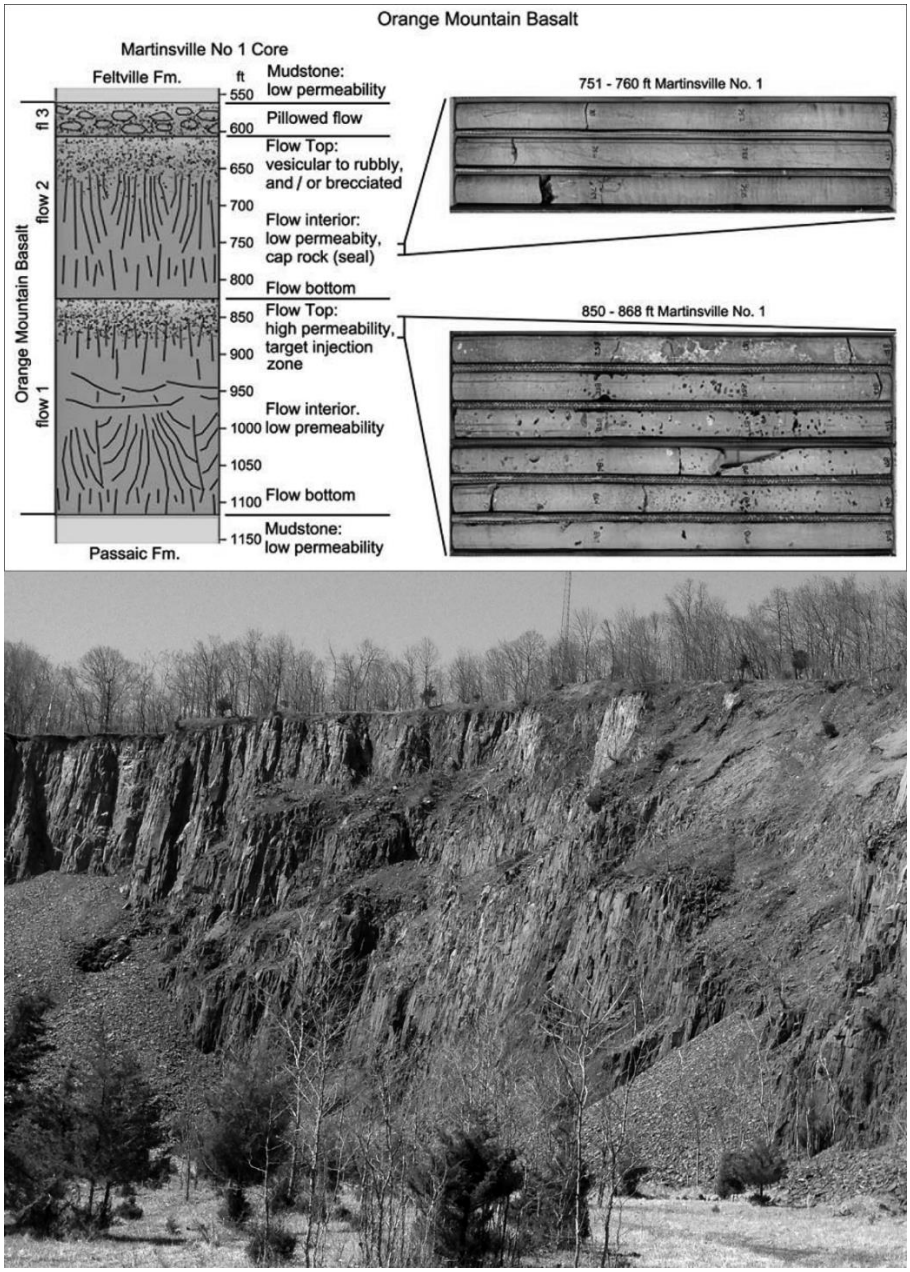

Figure 23: Above, schematic profile of multiple flow units and core photographs from the Orange Mountain basalt, modified from ref. 28. Flow-top boundary zones show considerable vesicular and rubbly pore space as compared to the dense, low-porosity flow interior. Scales are in feet). From Goldberg et al. (2009). Below, Preakness Basalt with platy-prisimatic jointing, at Dock Watch Hollow, Martinsville, NJ.

REFERENCES CITED

Abdel-Monem, A.A. & Kulp, J.L., 1968, Paleogeography and the source of sediments of the Triassic basin, New Jersey, by K-Ar dating. Geol. Soc. America Bull. 79:1231-1242.

Anonymous (Editorial Staff), 2011, http://newyorkhistoryblog.org/2011/04/09/hook-mountain-saved-100-years-ago/.

Araya-Melo, P.A., Crucifix, M., Bounceur, N., 2014, Global sensitivity analysis of Indian Monsoon during the Pleistocene. Climate of the Past Discussions, 10:1609-1651.

Baird, D., 1986, Some upper Triassic reptiles, footprints, and an amphibian from New Jersey. The Mosasaur 3:125-153.

Bradley, R.S., 1988, The Explosive Volcanic Eruption Signal in Northern Hemisphere Temperature Records. Climatic Change 12:221–243.

Barrell, J., 1915, Central Connecticut in the geologic past: Connecticut Geol. Nat. History Survey Bull. 23:44 p.

Benton, M.J., 1995, Diversification and Extinction in the History of Life. Science 268(5207):52-58

Berner, R.A., 1997, The rise of plants and their effect on weathering and atmospheric CO_2. Science 276 (5312): 544-546.

Bice, D.M., Newton, C.R., McCauley, S., Reiners, P.W., McRoberts, C.A., 1992, Shocked quartz at the Triassic-Jurassic boundary in Italy. Science 255:443-446.

Blackburn, T.J., Olsen, P.E., Bowring, S.A. , McLean, N.M., Kent, D.V., Puffer, J., McHone, G., Rasbury, E.T., Et-Touhami, M., 2013, Zircon U-Pb geochronology links the end-Triassic extinction with the Central Atlantic Magmatic Province. Science, v. 340 (6135), p. 941-945; DOI: 10.1126/science.1234204.

Block, K.A., Steiner, J.C., Puffer, J.H., Jones, K.M., Goldstein, S.L., 2015, Evolution of late stage differentiates in the Palisades Sill, New York and New Jersey. Lithos, 230:121-132.

Caldeira, K.G. & Rampino, M.R., 1990, Deccan volcanism, greenhouse warming, and the Cretaceous/Tertiary boundary. Geological Society of America Special Paper 247:117-124.

Callaghan, T.V., Björn, L.O., Chapin III, F.S., Chernov, Y., Christensen, T.R., Huntley, B., Ims, R., Johansson, M., Riedlinger, D.J., Jonasson, S., Matveyeva, N., 2006, Arctic tundra and polar desert ecosystems. Arctic climate impact assessment 1 (2005): 243-352.

Colbert, E.H. & Olsen, P.E., 2001, A new and unusual aquatic reptile from the Lockatong Formation of New Jersey (Late Triassic, Newark Supergroup). Novitates 3334:1-24.

Collins, D., Conrad, J.A., Goldberg, D., Kent., D.V., Olsen, P., Pasadena, P., Slater, B., 2014, Characterization of the Triassic-aged Newark rift basin in New York and New Jersey - assessment of CO_2 storage potential. Geological Society of America Abstracts with Programs 46(2):80.

Collins, M., Knutti, R., Arblaster, J., Dufresne, J.-L., Fichefet, T., Friedlingstein, P., Gao, X., Gutowski, W.J., Johns, T., Krinner, G., Shongwe, M., Tebaldi, C., Weaver A.J., Wehner, M., 2013, Long-term Climate Change: Projections, Commitments and Irreversibility. In: Climate Change 2013: The Physical Science Basis. Contribution of Working Group I to the Fifth Assessment Report of the Intergovernmental Panel on Climate Change [Stocker, T.F., D. Qin, G.-K. Plattner, M. Tignor, S.K. Allen, J. Boschung, A. Nauels, Y. Xia, V. Bex and P.M. Midgley (eds.)]. Cambridge University Press, Cambridge, United Kingdom and New York, NY, USA., p. 1029-1136.

Darton, N.H, 1890, The relations of the trap of the Newark System in the New Jersey region. U.S. Geological Survey Bulletin 67:1-82.

Deenen, M.H.L., Krijgsman, W. Ruhl, M., 2011, The quest for chron E23r at Partridge Island, Bay of Fundy, Canada: CAMP emplacement postdates the end-Triassic extinction event at the North American craton. Canadian Journal of Earth Sciences 48(8):1282-1291.

Deenen, M.H.L., Ruhl, M., Bonis, N.R., Krijgsman, W., Kuerschner, W.M., Reitsma, M. van Bergen, M.J., 2010, A new chronology for the end-Triassic mass extinction. Earth and Planetary Science Letters 291(1-4):113-125.

Dana, J. D., 1883, The origin of the Jura-Trias of eastern North America. Am. Jour. Sci., 3rd series 25:383-386.

Darton, N.H., 1890, Relations of the trap rocks of the Newark System in the New Jersey region. US Geol. Survey, Bull 67:70-74.

Daruka, I., & Ditlevsen, P.D., 2016, A conceptual model for glacial cycles and the middle Pleistocene transition. Climate Dynamics, 46(1-2):29-40.

Dzik, J., 2003, A beaked herbivorous archosaur with dinosaur affinities from the early Late Triassic of Poland. Journal of Vertebrate Paleontology, 23(3): 556-574.

Dobruskina, I. A., 1988, The history of land plants in the Northern Hemisphere during the Triassic with special reference to the floras of Eurasia. Geol. Paläont. Mitt. Innsbruck, ISSN 9378-6870, 15:1-12.

Domeier, M., Van der Voo, R., Torsvik, T.H., 2012, Paleomagnetism and Pangea: the road to reconciliation. Tectonophysics 514: 14-43.

Doran, P.T., Lyons, W.B., McKnight, D.M. (Eds.), 2010, Life in Antarctic deserts and other cold dry environments: astrobiological analogs (v 5). Cambridge University Press.

Eitel, M., Gilder, S.A., Kunzmann, T., Pohl, J., 2014, Rochechouart impact crater melt breccias record no geomagnetic field reversal. Earth and Planetary Science Letters 387:97-106.

Faill, R.T., 1973, Tectonic development of the Triassic Newark-Gettysburg basin in Pennsylvania: Geological Society of America Bulletin 84:725–740.

Faill, R.T., 2003, The early Mesozoic Birdsboro central Atlantic margin basin in the Mid-Atlantic region, eastern United States. Geological Society of America Bulletin 115(4):406-421.

Fairfield, H. 1998, Sm/Nd and Nd Isotopic Evidence for and Insignificant Basaltic Contribution to Shales in the Mesozoic Hartford Basin, U.S.A. M.A. Thesis, Columbia University.

Fairfield, H., Olsen, P.E., Hemming, S., 1999, Samarium and neodymium isotopic evidence for an isignificant basaltic contribution to shales in the Mesozoic Hartford Basin, U.S.A. Geological Society of America, Abstracts with Programs 31(2):A-14.

Faust, G.T., 1978, Joint systems in the Watchung basalt flows, New Jersey. US Geological Survey Professional Paper 864-B:B1-B46.

Fedosh, M.S. & Smoot, J.P., 1988, A cored stratigraphic section through the northern Newark basin, New Jersey. U.S. Geological Survey Bulletin 1776:19-24.

Fisher, D.W., 1981, The world of *Coelophysis*—a New York dinosaur of 200 Million years ago. New York State Museum Circular 49, 21 p.

Fowell, S.J., 1993, Palynology of Triassic/Jurassic boundary sections from the Newark Supergroup of Eastern North America: Implications for catastrophic extinction scenarios. [Ph. D. Thesis]: New York, New York, Columbia University, Department of Earth and Environmental Sciences, 133 p.

Fowell, S.J., Cornet, B., Olsen, P.E., 1994, Geologically rapid Late Triassic extinctions: Palynological evidence from the Newark Supergroup. In: Klein, G. D., (ed.) Pangaea: Paleoclimate, Tectonics and Sedimentation During Accretion, Zenith and Break-up of a Supercontinent. Geological Society of America Special Paper 288: 197-206.

Frakes, L.A., Francis, J.E., Sykyus, J.L., 1992, Climate Modes of the Phanerozoic, Cambridge Univ. Press, Cambridge, UK.

Friedman, G.M., Sanders, J.E., Martini, L.P., 1982, Excursion 17A; Sedimentary fades: products of sedimentary environments in a cross section of the classic Appalachian Mountains and adjoining Appalachian Basin in New York and Ontario, Field Excursion Guidebook, International Association of Sedimentologists. In 11th International Congress on Sedimentology, McMaster University, Field Excursion Guidebook, p. M1-M30.

Gallagher, W. & Hanczaryk, P., 2006, The West Patterson Quarry: An Early Jurassic Dinosaur track site in the Newark Basin of New Jersey, in Harris, J.D., Lucas, S.G., Spoelmannm J.A., Lockley, M.G., Milner,A.R.C., and Kirkland, J.I. (eds.),The Triassic-Jurassic Terrestrial Transition. New Mexico Museum of Natural History & Science Bulletin 37:238-240.

Glaeser, J.D., 1966, Provenance, dispersal and depositional environments of Triassic sediments in the Newark-Gettysburg basin. Pennsylvania Geol. Survey Rept. G-43, 168 p.

Goldberg, D.S., Kent, D.V. and Olsen, P.E., 2010, Potential on-shore and off-shore reservoirs for CO_2 sequestration in Central Atlantic magmatic province basalts. Proceedings of the National Academy of Sciences 107(4):1327-1332.

Grant, K.M., Grimm, R., Mikolajewicz, U., Marino, G., Ziegler, M., Rohling, E.J., 2016, The timing of Mediterranean sapropel deposition relative to insolation, sea-level and African monsoon changes. Quaternary Science Reviews, 140:125-141.

Hautmann, M., Benton, M. J., & Tomašových, A., 2008, Catastrophic ocean acidification at the Triassic-Jurassic boundary. Neues Jahrbuch für Geologie und Paläontologie-Abhandlungen, 249(1):119-127.

Heisig, P.M., 2011, Water resources of Rockland County, New York, 2005–07, with emphasis on the Newark basin bedrock aquifer: U.S. Geological Survey Scientific Investigations Report 2010–5245, 130 p.

Hesselbo, S.P., Robinson, S.A., Surlyk, F., Piasecki, S., 2002, Terrestrial and marine extinction at the Triassic-Jurassic boundary synchronized with major carbon-cycle perturbation: A link to initiation of massive volcanism? Geology 30(3):251-254.

Huene, F. von, 1913. A new phytosaur from the Palisades near New York. A new phytosaur from the Palisades near New York. Bulletin of the American Museum of Natural History 32(article 15):275-292.

Hillebrandt, A., Krystyn, L., Kürschner, W.M., Bonis, N.R., Ruhl, M., Richoz, S., Schobben, M.A.N., Urlichs, M., Bown, P.R., Kment, K. and McRoberts, C.A., 2013, The global stratotype sections and point (GSSP) for the base of the Jurassic system at Kuhjoch (Karwendel Mountains, Northern Calcareous Alps, Tyrol, Austria). Episodes, 36(3):162-198.

Hodych, J.P. & Dunning, G.R., 1992, Did the Manicouagan impact trigger end-of-Triassic mass extinction? Geology, 20(1):51-54.

Hönisch, B., Ridgwell, A., Schmidt, D.N., Thomas, E., Gibbs, S.J., Sluijs, A., Zeebe, R.E., Kump, L.R., Martindale, R.C., Greene, S.E., Kiessling, W., Ries, J.B., Zachos, J.C., Royer, D.L., Barker, S., Marchitto, T.M.J., Moyer, R.P., Pelejero, C., Ziveri, P., Foster, G., Williams, B., 2012, The geological record of ocean acidification. Science 335:1058–1063.

Hounslow, M.W., Posen, P.E. Warrington, G., 2004, Magnetostratigraphy and biostratigraphy of the Upper Triassic and lowermost Jurassic succession, St. Audrie's Bay, UK. Palaeogeography, Palaeoclimatology, Palaeoecology 213(3–4):331–358.

Huber, P., & LeTourneau, P.M., 2006, Revised lithostratigraphy of the Norian-Hettangian Pomperaug rift basin, western Connecticut: resolving a century-old conflict in geologic interpretation, in Harris, J.D., Lucas, S.G., Spoelmannm J.A., Lockley, M.G., Milner,A.R.C., and Kirkland, J.I. (eds.),The Triassic-Jurassic Terrestrial Transition. New Mexico Museum of Natural History & Science Bulletin 37:43-61.

Hubert, J.F., Reed, A.A., Dowdall, W.L. Gilchrist, J.M., 1978, Guide to the Mesozoic red beds of central Connecticut. Connecticut Geological and Natural History Survey, Guidebook 4, 129 p.

Husch, J.M., 1990. Palisades sill: origin of the olivine zone by separate magmatic injection rather than gravity settling. Geology 18:699–702.

Hutchinson, D.R. & Klitgord, K.D., 1988, Evolution of rift basins on the continental margin off southern New England. Triassic–Jurassic Rifting: Continental Breakup and the Origin of the Atlantic Ocean and Passive Margins, Part A, Amsterdam, Elsevier, p. 82-98.

Hutchinson, D.R., Klitgord, K.D., Detrick, R.S., 1986, Rift basins of the Long Island platform. Geological Society of America Bulletin 97(6):688-702.

Huybers, P., 2004, On the origins of the ice ages: insolation forcing, age models, and nonlinear climate change. Ph.D. Thesis, Massachusetts Institute of Technology.

Hyde, J.E., 1911, The Fort Lee phytosaur. Sixteenth Annual Report, 1911, of the American Scenic and Historic Preservation Society to the Legislature of the State of New York (Appendix. E): 357-363.

Ilyina, N.V. & Egorov, A.Y., 2008, The Upper Triassic of northern Middle Siberia: stratigraphy and palynology. Polar Research 27:372–392.

Irmis, R.A., Mundil, R., Martz, J.W., Parker, W.G., 2011, High-resolution U–Pb ages from the Upper Triassic Chinle Formation (New Mexico, USA) support a diachronous rise of dinosaurs. Earth and Planetary Science Letters 309:258–267.

Irmis, R.B., Whiteside, J.H., 2010. Newly integrated approaches to studying Late Triassic terrestrial ecosystems. Palaios 25:689–691.

Kent, D.V. & Muttoni, G., 2008, Equatorial convergence of India and early Cenozoic climate trends. Proceedings of the National Academy of Sciences 105(42):16065-16070.

Kent, D.V. & Muttoni, G., 2013, Modulation of Late Cretaceous and Cenozoic climate by variable drawdown of atmospheric pCO 2 from weathering of basaltic provinces on continents drifting through the equatorial humid belt. Climate of the Past 9(2):525-546.

Kent, D.V. & Olsen, P.E., 1997. Paleomagnetism of Upper Triassic continental sedimentary rocks from the Dan River-Danville rift basin (eastern North America). Geological Society of America Bulletin, 109: 366-377.

Kent, D.V. & Olsen, P.E., 1999. Astronomically tuned geomagnetic polarity time scale for the Late Triassic. Journal of Geophysical Research, 104(B6): 12831-12841.

Kent, D.V. & Olsen, P.E., 2000. Magnetic polarity stratigraphy and paleolatitude of the Triassic-Jurassic Blomidon Formation in the Fundy basin (Canada): implications for early Mesozoic tropical climate gradients. Earth and Planetary Science Letters, 179: 311-324.

Kent, D.V. & Olsen, P.E., 2008. Early Jurassic magnetostratigraphy and paleolatitudes from the Hartford continental rift basin (eastern North America): Testing for polarity bias and abrupt polar wander in association with the Central Atlantic Magmatic Province. Journal of Geophysical Research, 113: B06105, doi:10.1029/2007JB005407.

Kent, D.V., Olsen, P.E., Muttoni, G., 2016, Astrochronostratigraphic Polarity Time Scale (APTS) for the Late Triassic and Early Jurassic from Continental Sediments and Correlation with Standard Marine Stages. Earth Science Reviews, *in press*.

Kent, D.V., Olsen, P.E. Witte, W.K., 1995. Late Triassic-earliest Jurassic geomagnetic polarity sequence and paleolatitudes from drill cores in the Newark rift basin, eastern North America. Journal of Geophysical Research, 100: 14,965-14,998.

Kent, D.V., Santi Malnis, P., Colombi, C.E., Alcober, O.A. and Martínez, R.N., 2014. Age constraints on the dispersal of dinosaurs in the Late Triassic from magnetochronology of the Los Colorados Formation (Argentina). Proceedings of the National Academy of Sciences 111(22):7958-7963.

Kent, D.V. & Tauxe, L., 2005. Corrected Late Triassic latitudes for continents adjacent to the North Atlantic. Science 307:240–244.

Kent, D.V., Wang, H., Olsen, Paul E., 2009, Chron E23r, paleosecular variation, CAMP volcanism and the end-Triassic extinction event. Eos Trans. AGU, 90(52), Fall Meet. Suppl. GP22A-07 (http://www.agu.org/meetings/fm09/waisfm09.html).

Klein, G.deV., 1969, Deposition of Triassic sedimentary rocks in separate basins, eastern North America: Geol. Soc. America, Bull. 80:1825-1832.

Knoll, A.H., Bambach, R.K., Canfield, D.E., Grotzinger, J.P., 1996, Comparative Earth history and late Permain mass extinction. Science, 273(5274):452-457.

Kodama, K.P., 1983, Magnetic and gravity evidence for a subsurface connection between the Palisades sill and the Ladentown basalts. Geological Society of America Bulletin 94:51-158.

Kozur, H.W. & Weems, R.E., 2005, Conchostracan evidence for a late Rhaetian to early Hettangian age for the CAMP volcanic event in the Newark Supergroup, and a Sevatian (late Norian) age for the immediately underlying beds. Hallesches Jahrbuch für Geowissenschaften B 27:21-51.

Kozur, H.W. & Weems, R.E., 2010, The biostratigraphic importance of conchostracans in the continental Triassic of the northern hemisphere. in Lucas, S.G. (ed.), The Triassic Timescale, Geological Society, London, Special Publications, p. 315-417.

Kümmel, H.B., 1900, The Newark or New Red Sandstone rocks of Rockland County, N.Y. New York State Museum, 52nd Annual Report of the Regents 1998, vol. 2, 18th Report of the State Geologist and Paleontologist and Field Assistants. p. 8-50.

Letourneau, P.M., 2003, Stratigraphic architecture and paleomagnetic reversal stratigraphy of the Late Triassic Taylorsville Basin, Virginia and Maryland. In Letourneau, P.M. & Olsen, P.M. (eds.), The Great Rift Valleys of Pangea in Eastern North America, vol. 2, Sedimentology, Stratigraphy, and Paleontology, Columbia University Press, pp. 12-58 (ISBN 0-231-12676-X).

Lewis, J.V., 1908, The Palisades diabase of New Jersey. American Journal of Science 176:155–162.

Lockley, M.G. & Lucas, S.G., 2013, *Evazoum gatewayensis*, a new Late Triassic archosaurian ichnospecies from Colorado: implications for footprints in the ichnofamily Otozoidae. The Triassic System. Edited by LH Tanner, JA Spielmann, and SG Lucas. New Mexico Museum of Natural History & Science Bulletin, 61, pp.345-353.

Loewe, F., 1974, Polar dry deserts. In Klimatologische Forschung, Bonner Meteorologische Abahndlungen 17:195-208.

Longwell, C.R., 1922, Notes on the structure of the Triassic rocks in southern Connecticut: Am. Jour. Sci. (5th ser) 4:223·236.

Longwell, C.R., 1937, Sedimentation in relation to faulting: Geol. Soc. America Bull., 43:433-442.

Lucas, S.G., Klein, H., Lockley, M.G., Spielmann, J.A., Gierlinski, G.D., Hunt, A.P., Tanner, L.H., 2006, Triassic-Jurassic stratigraphic distribution of the theropod footprint ichnogenus Eubrontes. New Mexico Museum of Natural History and Science Bulletin 37:86-93.

Lucas, S.G. & Tanner, L., 2008, Reexamination of the end-Triassic mass extinction, in Elewa, M.T. (ed.), Mass Extinction, Springer Berlin Heidelberg, p. 65-102.

Malinconico, M.L., 2003, Paleo-maximum thermal structure of the Triassic Taylorsville (Virginia) basin: evidence for border fault convection and implications for duration of syn-rift sedimentation and long-term elevated heat flow, In Letourneau, P.M. & Olsen, P.M. (eds.), The Great Rift Valleys of Pangea in Eastern North America, vol. 2, Sedimentology, Stratigraphy, and Paleontology, Columbia University Press, pp. 80-103.

Malinconico, M.L., 2010, Synrift to early basin-scale groundwater history of the Newark basin based on surface and borehole vitrinite reflectance data, In Herman, G.C. & Serfes, M.E. (eds.),

Contributions to the Geology and Hydrogeology of the Newark Basin. New Jersey Geological Survey Bulletin 77, C1-C38.

Manspeizer, W., 1980, Rift tectonics inferred from volcanic and clastic structures, in Manspeizer, W. (ed.), Field Studies in New Jersey Geology and Guide to Field Trips, 52nd Ann. Mtg. New York State Geol. Assoc., Newark College of Arts and Sciences, Newark, Rutgers University, p. 314-350.

Manspeizer, W. and Olsen, P. E., 1981, Rift basins of the passive margin: tectonics, organic-rich lacustrine sediments, basin analysis. In W. Hobbs, III (ed.), Field Guide to the Geology of the Paleozoic, Mesozoic, and Tertiary rocks of New Jersey and the central Hudson Valley. New York, Petroleum Exploration Society of New York, p. 25-105.

Martindale, R.C., Berelson, W.M., Corsetti, F.A., Bottjer, D.J., West, A.J., 2012, Constraining carbonate chemistry at a potential ocean acidification event (the Triassic–Jurassic boundary) using the presence of corals and coral reefs in the fossil record. Palaeogeography, Palaeoclimatology, Palaeoecology 350:114-123.

Marzoli, A., Bertrand, H., Knight, K.B., Cirilli, S., Buratti, N., Vérati, C., Nomade, S., Renne, P.R., Youbi, N., Martini, R. and Allenbach, K., 2004, Synchrony of the Central Atlantic magmatic province and the Triassic-Jurassic boundary climatic and biotic crisis. Geology 32(11):973-976.

Marzoli, A., Renne, P. R., Piccirillo, E. M., Ernesto, M., Bellieni, G., De Min, A., 1999, Extensive 200-million-year-old continental flood basalts of the Central Atlantic magmatic province. Science 284:616–618.

Matter, J.M., Kelemen, P.B., 2009, Permanent storage of carbon dioxide in geologic reservoirs by mineral carbonation. Nat Geosci www.nature.com/naturegeoscience [online] doi: 10.1038/NGE0683.

Matter, J.M., Stute, M., Snæbjörnsdottir, S.Ó., Oelkers, E.H., Gislason, S.R., Aradottir, E.S., Sigfusson, B., Gunnarsson, I., Sigurdardottir, H., Gunnlaugsson, E. and Axelsson, G., 2016. Rapid carbon mineralization for permanent disposal of anthropogenic carbon dioxide emissions. Science 352(6291):1312-1314.

McClay, K.R. & Ellis, P.G.,1987, Geometries of extensional fault systems developed in model experiments. Geology 15(4):341-344.

McElwain, J.C., Beerling, D.J., Woodward, F.I., 1999, Fossil plants and global warming at the Triassic-Jurassic boundary. Science, 285(5432):1386-1390.

McHone, J.G., 1996, Broad-terrane Jurassic flood basalts across northeastern North America. Geology, 24(4):319-322.

McHone, J. G., 2003, Volatile emissions from Central Atlantic Magmatic Province basalts: mass assumptions and environmental consequences, in Hames, W.E., McHone, J.G., Renne, P.R, Ruppel, C. (eds.), The Central Atlantic Magmatic Province: Insights From Fragments of Pangea, Geophysical Monograph Series, v. 136, p. 241-254.

McKenzie, N. Ryan, et al., 2016, Continental arc volcanism as the principal driver of icehouse-greenhouse variability. Science 352(6284):444-447.

McLean, D.M., 1985, Deccan Traps mantle degassing in the terminal Cretaceous marine extinctions. Cretaceous Research 6:235–259.

McRoberts, C.A., Krysyn, L., Hautmann, M., 2012, Macrofaunal response to the end-Triassic mass extinction in the west-Tethyan Kössen Basin, Austria. Palaios 27:607–616.

Milani, E.J. & Zalán, P.V., 1999, An outline of the geology and petroleum systems of the Paleozoic interior basins of South America. Episodes 22(3):199-205.

Montañez, I.P & Poulsen, C.J., 2013, The Late Paleozoic ice age: An evolving paradigm Annual Review of Earth and Planetary Science 41:629-656.

Monteverde, D.H., 2011, Bedrock geological map of the Yonkers and Nyack Quadrangles, Bergen County, New Jersey. Department of Environmental Protection, New Jersey Geological Survey, Map GMS 11-1.

Morton, N., 2010, Progress in defining Jurassic stages – a learning process. Earth Science Frontiers 17(special edition):66-67.

Morton, N., 2012, Inauguration of the GSSP for the Jurassic System. Episodes, 35(2):328-332.

Naslund, H.R., 1998, The Palisade sill, New York and New Jersey, in Naslund, H.R. (ed.), Field Trip Guide for the 70th Annual Meeting of the New York State Geological Association, New York State Geological Association, New York State Geological Survey, Albany, p. 70-96.

Nesbitt, S., 2007, The anatomy of *Effigia okeeffeae* (Archosauria, Suchia), theropod-like convergance, and the distribution of related taxa. Bull. Amer. Mus. Nat. Hist. 302: 84 p.

Nicosia, U. & Loi, M., 2003, Triassic footprints from Lerici (La Spezia, northern Italy). Ichnos 10: 127-140.

Nyack Public Library, 2016 (date of download), Quarrying at Hook Mountain, Upper Nyack, NY. Hudson River Valley Heritage, http://www.hrvh.org/cdm/singleitem/collection/nyacklib/id/976/rec/64

Olsen, P.E., 1980a, The Latest Triassic and Early Jurassic Formations of the Newark Basin (Eastern North America, Newark Supergroup): Stratigraphy, Structure, and Correlation. New Jersey Academy of Science Bulletin 25:25-51.

Olsen, P.E., 1980b, Triassic and Jurassic formations of the Newark Basin, in Manspeizer, W. (ed.), Field Studies in New Jersey Geology and Guide to Field Trips, 52nd Ann. Mtg. New York State Geol. Assoc., Newark College of Arts and Sciences, Newark, Rutgers University, p. 2-39.

Olsen, P.E., 1980c, Fossil great: lakes of the Newark Supergroup in New Jersey: In W. Manspeizer (ed.), Field Studies in New Jersey Geology and Guide to Field Trips, 52nd Ann. Mtg. New York State Geol. Assoc., Newark College of Arts and Sciences, Newark, Rutgers University, p. 352-398.

Olsen, P.E., 1983, On the non-correlation of the Newark Supergroup by fossil fishes; biogeographic, structural, and sedimentological implications. Geological Society of America, Abstracts with Programs, v. 15, n. 3, p. 121.

Olsen, P.E., 1986. A 40-million-year lake record of early Mesozoic orbital climatic forcing. Science, 234: 842-848.

Olsen, P.E., 1999, Giant Lava Flows, Mass Extinctions, and Mantle Plumes. [perspective on Marzoli, et al.]. Science 284(5414):604-605.

Olsen, P.E., 2010, Fossil great lakes of the Newark Supergroup – 30 years later. In: Benimoff, A.I. (ed.), Field Trip Guidebook, New York State Geological Association, 83nd Annual Meeting, College of Staten Island, pp. 101–162.

Olsen, P.E., 2015, Fire and ice: super-eruptions, volcanic winters, the end-Triassic extinction, and the rise of dinosaur-dominance. Geological Society of America, Abstracts with Programs 47(7): https://gsa.confex.com/gsa/2015AM/webprogram/Paper264447.html.

Olsen, P.E. & Et-Touhami, M., 2008, Field Trip #1: Tropical to subtropical syntectonic sedimentation in the Permian to Jurassic Fundy rift basin, Atlantic Canada, in relation to the Moroccan conjugate margin. Central Atlantic Conjugate Margins Conference Halifax, Nova Scotia, Canada August 2008, 121 p. ISBN:0-9810595-3.

Olsen, P.E. & Kent, D.V., 1996. Milankovitch climate forcing in the tropics of Pangea during the Late Triassic. Paleogeography, Paleoclimatology, Paleoecology, 122: 1-26.

Olsen, P.E. & Kent, D.V., 1999. Long-period Milankovitch cycles from the Late Triassic and Early Jurassic of eastern North America and their implications for the calibration of the Early Mesozoic time-scale and the long-term behaviour of the planets. Philosophical Transactions of the Royal Society of London, Series A, 357: 1761-1786.

Olsen, P.E. & Kent, D.V., 2016, Falsification of hypotheses of a major hiatus in the Newark Supergroup Rhaetian (Late Triassic, US and CA) based on data from the Bristol Channel (UK) and North Germanic (DE) basins. Geological Society of America Abstracts with Programs 48(7): doi: 10.1130/abs/2016AM-287150.

Olsen, P.E., Kent, D.V., Whiteside, J.H., Schaller, M., 2013, Volcanic winter scenario for the selective nature of the Triassic-Jurassic transition on land. Geological Society of America Abstracts with Programs 46(3):20, https://gsa.confex.com/gsa/2013AM/finalprogram/abstract_228132.htm

Olsen, P.E., Kent, D.V., Whiteside, J.H., 2011. Implications of the Newark Supergroup-based astrochronology and geomagnetic polarity time scale (Newark-APTS) for the tempo and mode of the early diversification of the Dinosauria. Transactions of the Royal Society of Edinburgh, Earth Sciences, 101:201-229.

Olsen, P.E., Kent, D.V., Whiteside, J.H., 2004, The Newark Basin, The Central Atlantic Magmatic Province, and the Triassic-Jurassic Boundary. Field Trip for the 8th Annual DOSECC Workshop on Continental Scientific Drilling, May 22-25, 2004. Rutgers University New Brunswick, New Jersey, DOSECC, Salt Lake City, 45 p.

Olsen, P.E., McCune, A.R., Thomson, K.S., 1982, Correlation of the early Mesozoic Newark Supergroup by vertebrates, principally fishes. American Journal of Science 282:1-44.

Olsen, P.E., Philpotts, A.R., McDonald, N.G., Huber, P.G., 2012, Air-fall ashes of the CAMP from eastern North America and Morocco. Geological Society of America, *Abstracts with Programs* v. 44, no. 2, p. 56.

Olsen. P.E., Philpotts, A.R., McDonald, N.G., Steinen, R.P., Kinney, S.T., Jaret, S.J., Rasbury, E.T., 2016, Wild and wonderful implications of the 5 mm Pompton Ash of the Hartford and Newark basins (Early Jurassic, Eastern North America). Geological Society of America Abstracts with Programs, Northeastern Section, v. 48, No. 2, doi: 10.1130/abs/2016NE-272509

Olsen, P.E. & Rainforth, E.C., 2003, The "Age of Dinosaurs" in the Newark basin, with special reference to the lower Hudson Valley. in Gates, A.E., (ed.) and Olsen, P. E., (organizer), Geology of the Lower Hudson Valley, 2001 New York State Geological Association Field Trip Guide Book, New York State Geological Association, New York State Museum, Albany, 73 (2001):59-176.

Olsen, P.E. & Schlische, R.W., 1987, Paired half-graben, crestal collapse graben - examples from the Early Mesozoic of Eastern North America. Geological Society of America, Abstracts with Programs 19(7):794.

Olsen, P.E., Kent, D.V., Cornet, B., Witte, W.K., Schlische, R.W., 1996a, High-resolution stratigraphy of the Newark rift basin (Early Mesozoic, Eastern North America). Geological Society of America 108:40-77.

Olsen P.E, Schlische R.W, Fedosh M.S., 1996b, 580 ky duration of the Early Jurassic flood basalt event in eastern North America estimated using Milankovitch cyclostratigraphy. In Morales, M. (ed.) The Continental Jurassic, Museum of Northern Arizona Bulletin 60, p. 11-22.

Olsen, P.E., Shubin, N.H., Anders, M.E., 1987, New Early Jurassic tetrapod assemblages constrain Triassic-Jurassic tetrapod extinction event. Science 237:1025-1029.

Olson, M.S., Olson, D.W., Doescher, R.L., 2007, On the Blood-Red Sky of Munch's the Scream. Environmental History, 12(1);131-135.

Onoue, T., Sato, H., Yamashita, D., Ikehara, M., Yasukawa, K., Fujinaga, K., Kato, Y., Matsuoka, A., 2016, Bolide impact triggered the Late Triassic extinction event in equatorial Panthalassa. Scientific Reports 6, DOI: 10.1038/srep29609.

OPRHP (Office of Parks Recreation Historic Preservation of NY State), 2013, Final master plan for Rockland Lake, Hook Mountain, Nyack Beach and Haverstraw Beach State Parks. New York State

Parks, Recreation, and Historic Preservation, http://nysparks.com/inside-our-agency/master-plans.aspx

Osborn, H.F., 1911, Fort Lee dinosaur. The American Museum journal 11: 28-29.

Parker, R.A., Houghton, H.F., McDowell, R.C., 1988, Stratigraphic framework and distribution of early Mesozoic rocks of the northern Newark Basin, New Jersey and New York. U.S. Geological Survey Bulletin 1776:31-39.

Parker, W.G. & Martz, J.W., 2011, The Late Triassic (Norian) Adamanian–Revueltian tetrapod faunal transition in the Chinle Formation of Petrified Forest National Park, Arizona. Earth and Environmental Science Transactions of the Royal Society of Edinburgh 101:231–60.

Parrish, J.T., 1993, Climate of the supercontinent Pangea. The Journal of Geology 1993:215-233.

Pe-Piper, G. & Piper, D.J., 1999, Were Jurassic tholeiitic lavas originally widespread in southeastern Canada?: a test of the broad terrane hypothesis. Canadian Journal of Earth Sciences, 36(9):1509-1516.

Perlmutter, N.M., 1959, Geological and groundwater resources of Rockland County, New York, with special emphasis on the Newark Group. State of New York Ground Water Bulletin, GW-42, New York State Department of Conservation. Water Power Control Commission, 133 p.

Prevot, M. & McWilliams, M., 1989, Paleomagnetic correlation of the Newark Supergroup volcanics, Geology 17:1007-1010.

Puffer, J.H., 1987, The Palisades Sill and Watchung basalt flows, northern New Jersey. Northeastern Section of the Geological Society of America, Centennial Fieldguide, 5, pp.91-96.

Puffer, J.H., Block, K.A., Steiner, J.C., 2009, Transmission of flood basalts through a shallow crustal sill and the correlation of sill layers with extrusive flows: the Palisades intrusive system and the basalts of the Newark Basin, NewJersey, U.S.A. Journal of Geology 117:139–155.

Puffer, J.H. & Lechler, P., 1980, Geochemical cross sections through the Watchung basalt of New Jersey, part 2. Geological Society of America Bulletin 91:156-191.

Puffer, J.H. & Philpotts, A.R., 1988, Eastern North American quartz tholeiites: Geochemistry and petrology, in Manspeizer, W. (ed.), Triassic-Jurassic Rifting, Continental breakup and the Origin of the Atlantic Ocean and Passive Margins, Volume B, Developments in Geotectonics 22(A-B):579-605.

Puffer, J. H. & Volkert, R. A., 2001, Pegmatoid and gabbroid layers in Jurassic Preakness and Hook Mountain basalts, Newark Basin, New Jersey. The Journal of Geology 109:585-601.

Rainforth, E.C., 2003, Revision amd repevaluation of the Early Jurassic dinosaurian ichnogenus *Otozoum*. Palaeontolology 46(pt 4):803-838.

Ramezani, J., Fastovsky, D.E., Bowring, S.A., 2014, Revised chronostratigraphy of the lower Chinle Formation strata in Arizona and New Mexico (USA): high-precision U-Pb geochronological constraints on the Late Triassic evolution of dinosaurs. American Journal of Science 314(6):981-1008.

Ratcliffe, N.M., 1980, Brittle faults (Ramapo fault) and phyllonitic ductile shear zones in the basement rocks of the Ramapo seismic zone, New York and New Jersey, and their relationship to current seismicity, In Manspeizer, W. (ed.), Field studies of New Jersey geology and guide to field trips, 52d Annual meeting of the New York State Geological Association, Newark, New Jersey, Rutgers University, p. 278-813.

Ratcliffe, N.M., 1988, Reinterpretation of the relationship of the western extension of the Palisades Sill to the lava flows at Ladentown, New York, based on new core data. U.S. Geol. Surv. Bull. 1776: 113-135.

Raup, D.M & Sepkoski, J.J., 1982, Mass Extinctions in the Marine Fossil Record. Science 215(4539):1501-1503

Raymo, M.E., 1991, Geochemical evidence supporting TC Chamberlin's theory of glaciation. Geology 19 (4): 344-347.

Retallack, G.J., 1985, Triassic fossil plant fragments from shallow marine rocks of the Murihiku Supergroup, New Zealand. Journal of the Royal Society of New Zealand, 15(1):1-26.

Rogers, W.B., 1842, (On the prevailing dip in the various areas of New Red. Sandstone of the Atlantic slope, remarks on a paper by Edward Hitchcock). Am. Jour. Sci. 43:172-172.

Rogers, W.B., 1860, (On the stratigraphical relations of deposits formed in an ocean under conditions of stationary, subsiding, and rising portition of the sea bottom). Boston Soc. Nat. Hist., Proc. 7:246-249; 273-275.

Rossignol-Strick, M., 1985, Mediterranean Quaternary sapropels, an immediate response of the African monsoon to variation of insolation. Palaeogeography, palaeoclimatology, palaeoecology 49(3):237-263.

Ruhl, M., Kürschner, W.M., Krystyn, L., 2009, Triassic–Jurassic organic carbon isotope stratigraphy of key sections in the western Tethys realm (Austria). Earth and Planetary Science Letters 281:169–187.

Russell, I.C., 1880, On the former extent of the Triassic formation of the Atlantic states. American Naturalist 14:703–712.

Sanders, J.E., 1960, Sanders, J. E. , 1960, Structural history of Triassic rocks of the Connecticut Valley belt and its regional implications. New York Acad. Sci., Trans. (ser. 2), 23:119-132.

Sanders, J.E., 1963, Late Triassic tectonic history of northeastern United States. American Journal of Science 261:501–524.

Sanders, J.E., 1974. Guidbook to field trip in Rockland County, New York. New York: Petroleum Exploration Society of New York, 87 pp.

Sanders, J. E., Friedman, G. M., & Sternbach, C. A. (1981, October). Extinct and active continental margin deposits and their tectonicswitchover products: Appalachian orogen ("Eastern overthrust belt")-Catskill Plateau-Newark basin-Atlantic Coastal Plain. In Field guide to the geology of the Paleozoic, Mesozoic, and Tertiary rocks of New Jersey and the central Hudson Valley: American Association of Petroleum Geologists, 1981 Eastern Section Meeting, Atlantic Margin Energy Symposium, Atlantic City, New Jersey (pp. 4-6).

Sapers, H.M., Osinski, G.R., Banerjee, N.R., Ferrière, L., Lambert, P., Izawa, M.R.. 2014, Revisiting the Rochechouart impact structure, France. Meteoritics & Planetary Science 49(12):2152-2168.

Saunders, A. & Reichow, M., 2009, The Siberian Traps and the End-Permian mass extinction: a critical review. Chinese Science Bulletin, 54(1):20-37.

Savage, E.L., 1968, Trip C: The Triassic rocks of the northern Newark Basin, in Finks, R.M., (ed.) Guidebook to Field Excursions, New York State Geol. Assoc., Ann. Mtg., 40th, Queens College, Flushing, NY, p. 49-100.

Self, S., Widdowson, M., Thordarson, T., Jay, A.E., 2006 Volatile fluxes during flood basalt eruptions and potential effects on the global environment: A Deccan perspective." Earth and Planetary Science Letters 248(1): 518-532.

Sha, J., Olsen, P.E., Xu, D., Yao, X., Pan, Y., Wang, Y., Zhang, X., Vajda, V., 2015, Early Mesozoic, high-latitude continental Triassic–Jurassic climate in high-latitude Asia was dominated by obliquity-paced variations (Junggar Basin, Urumqi, China). PNAS 112(12):3624-3629.

Schaef, H.T. & McGrail, B.P., 2009, Dissolution of Columbia River Basalt under mildly acidic conditions as a function of temperature: Experimental results relevant to the geological sequestration of carbon dioxide. Applied Geochemistry 24(5):980-987.

Schaef, H.T., McGrail, B.P., Owen, A.T., 2010, Carbonate mineralization of volcanic province basalts. International Journal of Greenhouse Gas Control 4(2):249-261.

Schaef, H.T., McGrail, B.P., Owen, A.T., Arey, B.W., 2013. Mineralization of basalts in the CO_2–H_2O–H_2S system. International Journal of Greenhouse Gas Control, 16, pp.187-196.

Schaef, H.T., Horner, J.A., Owen, A.T., Thompson, C.J., Loring, J.S. McGrail, B.P., 2014, Mineralization of Basalts in the CO_2–H_2O–SO_2–O_2 System. Environmental Science & Technology 48(9):5298-5305.

Schaller, M.F., Wright, J.D., Kent, D.V., 2011, Atmospheric pCO_2 perturbations associated with the Central Atlantic magmatic province. Science, 331(6023):1404-1409.

Schaller, M.F., Wright, J.D., Kent, D.V., 2015, A 30 Myr record of Late Triassic atmospheric pCO_2 variation reflects a fundamental control of the carbon cycle by changes in continental weathering. Geological Society of America Bulletin, 127(5-6):661-671.

Schaller, M.F., Wright, J.D., Kent, D.V., Olsen, P.E., 2012, Rapid emplacement of the Central Atlantic Magmatic Province as a net sink for CO_2. Earth and Planetary Science Letters, 323:27-39.

Schlische, R.W. & Withjack, M.O., 2005. The early Mesozoic Birdsboro central Atlantic margin basin in the mid-Atlantic region, eastern United States: Discussion. Geological Society of America Bulletin 117(5-6):823-828.

Schmieder M., Buchner E., Schwarz W.H., Trieloff M., Lambert P., 2010, A Rhaetian $^{40}Ar/^{39}Ar$ age for the Rochechouart impact structure (France) and implications for the latest Triassic sedimentary record. Meteoritics & Planetary Science 45:1225–1242.

Schmieder M., Lambert P., and Buchner E., 2009, Did the Rochechouart impact (France) trigger an end-Triassic tsunami? (abstract #5140). Meteoritics & Planetary Science 44:A186.

Schoene, B., Guex, J., Bartolini, A., Schaltegger, U., Blackburn, T. J., 2010, Correlating the end Triassic mass extinction and flood basalt volcanism at the 100 ka level. Geology 38(5):387-390.

Shirley, D.N., 1987, Differentiation and compaction in the Palisades Sill. Journal of Petrology 28:835–865.

Simms, M.J., 2007, Uniquely extensive soft-sediment deformation in the Rhaetian of the UK: Evidence for earthquake or impact? Palaeogeography, Palaeoclimatology, Palaeoecology 244(1):407-423.

Self, S., Zhao, J.X., Holasek, R.E., Torres, R.C., King, A.J., 1996, The atmospheric impact of the 1991 Mount Pinatubo eruption, in Newhall, C.G. & Punongbayan, R. (eds.), 1996. Fire and Mud: Eruptions and Lahars of Mount Pinatubo, Philippines, Quezon City: Philippine Institute of Volcanology and Seismology, p. 1089-1115.

Sigl, M., Winstrup, M., McConnell, J.R., Welten, K.C., Plunkett, G., Ludlow, F., Büntgen, U., Caffee, M., Chellman, N., Dahl-Jensen, D. and Fischer, H., 2015, Timing and climate forcing of volcanic eruptions for the past 2,500 years. Nature 523:543-549.

Slater, B.E., Smith, L., Tymchak, M.P., Collins, D.J., 2012, Preliminary Results from the TriCarb Deep Stratigraphic Well drilled into the Newark Rift Basin, Rockland County, New York." American Association of Petroleum Geologists Search and Discovery Article #90154, 2012 AAPG Eastern Section Meeting, Cleveland, Ohio, 22-26 September 2012.

Sleep, N.H., Dennis K. Bird, D.K., Pope, E., 2012, Paleontology of Earth's mantle. Annu. Rev. Earth Planet. Sci. 40:277-300.

Smiley, T.L., & Zumberge, J.H. (Eds.), 1974, Polar Deserts and Modern Man. In Polar Deserts Symposium (1971: Philadelphia). University of Arizona Press, 173 pp.

Steiner, J.C., 1989, The Nyack section of the Palisades: Facies , contacts and lava domes. 64th Ann. Mtg. New York State Geol. Assoc., Orange County Community College, p. 269-282.

Steinthorsdottir, M., Jeram, A.J., McElwain, J.C., 2011, Extremely elevated CO_2 concentrations at the Triassic/Jurassic boundary. Palaeogeography, Palaeoclimatology, Palaeoecology, 308(3):418-432.

Stocker, T.F. and others, 2013, Climate Change 2013: The Physical Science Basis. IPCC, Cambridge.

Stothers, R.B., 1984, The Great Tambora Eruption in 1815 and Its Aftermath. Science 224(4654):1191–1198.

Sues, H-D. & Olsen, P.E., 2015, Stratigraphic and temporal context and faunal diversity of Permian-Jurassic continental tetrapod assemblages from the Fundy rift basin, eastern Canada. Atlantic Geology v. 51, p. 139-205.

Svensen, H., Planke, S., Chevallier, L., Malthe-Sørenssen, A., Corfu, F., & Jamtveit, B., 2007, Hydrothermal venting of greenhouse gases triggering Early Jurassic global warming. Earth and Planetary Science Letters 256(3):554-566.

Svensen, H., Planke, S., Malthe-Sørenssen, A., Jamtveit, B., Myklebust, R., Eidem, T. R., Rey, S. S., 2004, Release of methane from a volcanic basin as a mechanism for initial Eocene global warming. Nature 429(6991):542-545.

Tackett, L.S., Kaufman, A.J., Corsetti, F.A., Bottjer, D.J., 2014, Strontium isotope stratigraphy of the Gabbs Formation (Nevada): implications for global Norian–Rhaetian correlations and faunal turnover. Lethaia, 47(4):500-511.

Tanner, L.H. & Kyte, F.T., 2005, Anomalous iridium enrichment at the Triassic–Jurassic boundary, Blomidon Formation, Fundy basin, Canada. Earth and Planetary Science Letters 240(3):634-641.

Tanner, L.H. & Kyte, F.T., 2016, New report of elevated Ir in Upper Triassic-Lower Jurassic strata of the Newark Supergroup basins. Geological Society of America Abstracts with Programs 48(2):doi: 10.1130/abs/2016NE-271941

Tanner, L.H., Kyte, F.T., Walker, A.E., 2008, Multiple Ir anomalies in uppermost Triassic to Jurassic-age strata of the Blomidon Formation, Fundy basin, eastern Canada. Earth and Planetary Science Letters 274(1):103-111.

Tanner, L.H., Kyte, F.T., Richoz, S., Krystyn, L., 2016, Distribution of iridium and associated geochemistry across the Triassic–Jurassic boundary in sections at Kuhjoch and Kendlbach, Northern Calcareous Alps, Austria. Palaeogeography, Palaeoclimatology, Palaeoecology 449:13-26.

Tanner, L.H. & Lucas, S.G., 2015, The Triassic-Jurassic strata of the Newark Basin, USA: A complete and accurate astronomically-tuned timescale? Stratigraphy 12(1):47–65.

Takahashi, T., Goldberg, D., Mutter, J.C., 2000, Secure, long-term sequestration of CO_2 in deep saline aquifers associated with oceanic and continental basaltic rocks. Proc of the SRI Int Sympos, Deep Sea & CO_2 (The Ship Research Inst, Mitaka, Japan).

Thordaldson, T. & Self, S., 2003, Atmospheric and environmental effects of the 1783–1784 Laki eruption: A review and reassessment. Journal of Geophysical Research. 108 (D1 40111), 4011, doi:10.1029/2001JD002042, 2003.

Tolan T.L., Reidel, S.P. Beeson, M.H. Anderson, J.L. Fecht, K.R. Swanson, D.A., 1989, Revisions to the estimates of the area extent and volume of the Columbia River Basalt Group, in Reidel, S.P. & Hooper, P.R. (eds.), Volcanism and Tectonism in the Columbia River Flood-Basalt Province, Geological Society of America Special Paper 239, p. 1–20.

Tollo, R.P., Hawkins, D.P., Gottried, D., 1990, Petrographic and geochemical data for Jurassic basalt from eight cores, Newark basin, New Jersey. US Geological Survey, Open File Report No. 90-689:1-32.

Tollo, R.P. & Gottfried, D., 1992, Petrochemistry of Jurassic basalt from eight cores, Newark basin, New Jersey: Implications for the volcanic petrogenesis of the Newark Supergroup. Geological Society of America Special Paper 268:233-260.

Town of Orangetown (Ambrose, A.M., stenographer), 2009, Town of Orangetown Planning Board Meeting of May 13, 2009, http://www.orangetown.com/residents/planning_board_minutes/minutes_from_2009/may_13_2009.php

Thulborn, T., 2003, Comment on "Ascent of dinosaurs linked to an iridium anomaly at the Triassic-Jurassic boundary". Science 301:169b.

Tschudy, R.H., Pillmore, C.L., Orth, C.J., Gilmore, J.S., Knight, J.D., 1984, Disruption of the terrestrial plant ecosystem at the Cretaceous-Tertiary boundary, Western Interior. Science 225(4666):1030-1032.

van de Schootbrugge, B. & Wignall, P.B., 2016, A tale of two extinctions: converging end-Permian and end-Triassic scenarios. Geological Magazine, 153(02):332-354.

Volkert, R.A., 2011, Bedrock Geological Map of the Ramsey Quadrangle, Passaic and Bergen Counties, New Jersey and Rockland County, New York - Open File Map OFM 87. New Jersey Geological Survey, 2011.

Walker, F., 1940, The differentiation of the Palisades diabase, New Jersey. Bulletin of the Geological Society of America 51:1059–1106.

Walker, K.R., 1969, The Palisades Sill, New Jersey: a reinvestigation. Geological Society of America, Special Paper 111, 178 p.

Wheeler, G., 1938. Further evidence of broad-terrane Triassic. Jour. Geomorphology 1:140-142.

Whiteside, J.H., Lindström, S., Irmis, R.B., Glasspool, I.J., Schaller, M.F., Dunlavey, M., Nesbitt, S.J., Smith, N.D. and Turner, A.H., 2015, Extreme ecosystem instability suppressed tropical dinosaur dominance for 30 million years. Proceedings of the National Academy of Sciences 112(26):7909-7913.

Whiteside, J.H. & Ward, P.D., 2011, Ammonoid diversity and disparity track episodes of chaotic carbon cycling during the early Mesozoic. Geology 39, 99–102.

Withjack, M.O., Baum, M.S. Schlische, R.W., 2010, Influence of pre-existing fault fabric on inversion-related deformation: A case study of the inverted Fundy rift basin, southeastern Canada. Tectonics 29, TC6004, doi:10.1029/2010TC002744.

Withjack, M.O., Schlische, R.W., Malinconico, M.L., Olsen, P.E., 2013, Rift-basin development: lessons from the Triassic–Jurassic Newark Basin of eastern North America. Geological Society, London, Special Publications 369(1):301-321.

Withjack, M.O., Olsen, P. E. Schlische, R.W., 1995, Tectonic evolution of the Fundy basin, Canada: Evidence of extension and shortening during passive-margin development. Tectonics 14:390-405.

Withjack, M.O. & Schlische, R.W., 2005, A review of tectonic events on the passive margin of eastern North America. In: POST, P. (ed) Petroleum Systems of Divergent Continental Margin Basins. 25th Bob S. Perkins Research Conference, Gulf Coast Section of SEPM, p. 203-235.

Withjack, M.O., Schlische, R.W., Baum, M. S. 2009. The extensional development of the Fundy rift basin, southeastern Canada. Geological Journal 44:631-651.

Withjack, M.O., Schlische, R.W., Olsen, P.E., 1998, Diachronous rifting, drifting, and inversion on the passive margin of central eastern North America: An analog for other passive margins. American Association of Petroleum Geologists Bulletin 82:817-835.

Withjack, M.O., Schlische, R.W., Olsen, P.E., 2012, Development of the passive margin of eastern North America: Mesozoic rifting, igneous activity, and breakup. In: Roberts, D.G. & Bally, A.W. (eds) Regional Geology and Tectonics, Volume 1B—Phanerozoic Rift Systems and Sedimentary Basins: New York, Elsevier, 301-335.

Wotzlaw, J-F., Guex, J., Bartolini, A., Gallet, Y., Krystyn, L., McRoberts, C.A., Taylor, D., Schoene, B. Schaltegger, U., 2014. Towards accurate numerical calibration of the Late Triassic: High-precision U-Pb geochronology constraints on the duration of the Rhaetian. Geology, doi:10.1130/G35612.1.

Yager, R.M. & Ratcliffe, N.M., 2010, Hydrogeology and simulation of groundwater flow in fractured rock in the Newark basin, Rockland County, New York: U.S. Geological Survey Scientific Investigations Report 2010–5250, 139 p.

Yang, Q., Matter, J., Stute, M., Takahashi, T., O'Mullan, G., Umemoto, K., Clauson, K., Dueker, M.E., Zakharova, N., Goddard, J. and Goldberg, D., 2014, Groundwater hydrogeochemistry in injection experiments simulating CO_2 leakage from geological storage reservoir. International Journal of Greenhouse Gas Control 26:193-203.

Zhang W. & Grant-Mackie, J.A., 2001, Late Triassic-Early Jurassic palynofloral assemblages from Murihiku strata of New Zealand, and comparisons with China, Journal of the Royal Society of New Zealand 31(3):575-683, DOI:10.1080/03014223.2001.9517668

Ziegler, A.M. and others, 1993, Early Mesozoic phytogeography and climate. Philosophical Transactions of the Royal Society of London B: Biological Sciences, 341(1297):297-305.

Zakharova, N.V., Goldberg, D.S., Olsen, P.E., Kent, D.V., Morgan, S., Yang, Q., Stute, M., J. Matter, J., 2016, New insights into lithology and hydrogeology of the northern Newark Rift Basin, Geochemistry, Geophysics, Geosystems 17:2070–2094, doi: 10.1002/2015GC006240.

FIELD GUIDE AND ROAD LOG

DAY 1

Meeting Point: Parking Lot of DoubleTree by Hilton Hotel, 425 State Route 59, Nanuet, New York, 10954. Access is from the east-bound lanes of State Route 59.

Meeting Point Coordinates: 41.090694°N, 73.995438°W

Meeting Time: 8:00 AM (Both Days)

Distance in miles (km)		
Cumu-Lative	Point to Point	Route Description
0.0 (0.0)	0.0 (0.0)	Assemble in the parking lot of the DoubleTree, Nanuet. Leave Parking lot, turning right at entrance on to eastbound State Route 59, keep in right lane.
0.1 (0.2)	0.1 (0.2)	Get on entrance ramp to Palisades Interstate Parkway South from NY-59 E.
0.3 (0.5)	0.2 (0.3)	Merge onto Palisades Interstate Parkway South.
8.4 (13.5)	8.1 (13.0)	Follow Palisades Interstate Parkway South to US-9W N/N Rte 9W N in Alpine. Take exit 4 from Palisades Interstate Parkway South.
8.5 (13.7)	0.1 (0.2)	Turn right onto US-9W northbound.
9.4 (15.1)	0.9 (1.5)	Pass traffic light and turn right into campus of Lamont-Doherty Earth Observatory of Columbia University just before New York-New Jersey State line (Ludlow Lane).
9.7 (15.6)	0.3 (0.5)	Proceed to the front of the Geoscience building. Park and you will be guided on foot to the core repository.

STOP 1.1: Cores, Seismic Lines and Posters at Lamont-Doherty Earth Observatory, Palisades, NY

Location Coordinates: 41.004471°N, 73.908982°W: Core repository Laboratory, Geoscience Building, Lamont-Doherty Earth Observatory.

Duration: 1:00 hr.

Here we will examine cores, down-hole logs, seismic profiles, and some fossils from the New Jersey portion of the Newark Basin and in a more central position. These will relate directly to the outcrops will see after this stop.

Newark Basin Coring Project (NBCP) and Army Corps of Engineers (ACE) Cores

Stockton Formation - Princeton NBCP core and TW4: The facies of the Stockton Formation as seen in the Princeton core is closely comparable to the outcrops of the type area of the Stockton Formation near Stockton, New Jersey. Thick intervals of purplish, tan, and gray sandstone and minor conglomerate are interspersed with bioturbated red mudstone and muddy sandstone. Pedogenic features including cracks, slickensides, carbonate nodules, rhizoliths (root traces), and burrows are abundant.

Compare the red mudstone facies of the Stockton Formation in the Princeton Core with typical red mudstone from the nominal Stockton Formation of the TW4 core. Note that the huge sand-filled cracks seen in the TW4 mudstones are not seen in Princeton core mudstones. Also note the difference in color with the higher color saturation and slight purple tint of the TW4 mudstone. The TW4 facies resembles the nominal Stockton we will see in outcrop at Stop 1.2 (Fig. 24).

Lockatong Formation - Nursery and Princeton NBCP cores: Cores and logs: intervals of cores of exactly correlative lacustrine (Van Houten) cycles will be on display. Observe the decrease in thickness and change in facies from the Nursery core to Princeton, corresponding to the up-dip relationship between Nursery and Princeton and how that projects towards the hanging-wall side of the basin – the Granton Quarry area (Stops 1.3 and 1.5).

Also on display will be examples from these same cores of the lower Lockatong Formation, which changes dramatically in facies between Nursery and Princeton with correlation based on the magnetostratigraphy.

The trend from Nursery to Princeton is from thicker to thinner cycles, from finer to coaser grain, and a tendency for the lower Lockatong cycles to be replaced by red beds and tan and gray sandstone. This trend continues and is exaggerated from the Princeton area towards the northeast towards our field stops.

Passaic Formation – Somerset, Rutgers, and Titusville NBCP cores: Examples of stratigraphic overlap between the Rutgers and Titusville cores illustrates an extreme examples of lateral continuity. In particular are two siltstone layers only a few cm thick correlative between the two coring sites separated by 42 km. There is also a polarity transition just below these siltstones that serves as a corroboration of the hypothesis of correlation.

Examples of the single black-mudstone-bearing Van Houten cycle near the base of the Kilmer Member from the Somerset and Rutgers cores (11.5 km apart) will be on display. Note slight change in facies. As in the case above there is a polarity transition below and close to the base of this cycle and the base of the Member.

Passaic Formation and Orange Mountain Basalt – Martinsville core and ACE core PT-38: The upper few tens of meters of the Passaic Formation and its contact with the overlying Orange Mountain Basalt will

be shown. The interval on display in the two cores contains the base of the Exeter Member of the Passaic Formation, the remarkably continuous and thin polarity zone E23r, and the projected level of the ETE. At first glance there is not much to suggest anything particularly momentous is going on here. However, correlation between the Jacksonwald Syncline section (Exeter) in the southwestern Newark Basin, from where most of the pre-ETE and ETE biological data come from, and the Martinsville, ACE cores, and exposures (Stop 1.7) is highly corroborated by cyclostratigraphy (the deep water phase of lacustrine cycle at base of the Exeter Member, polarity zone E23r, and the base of the Orange Mountain Basalt.

There is scant biological data from the cores themselves, no sporomorphs, for example; however, the spinocaudatan (clam shrimp) *Shipingia olseni* is present within the fine mudstones in E23r in the Martinsville core, consistent with its presence in the Jacksonwald Syncline section (Kozur and Weems, 2005). Supposedly, the presence of this taxon is indicative of a Norian age and is the principle basis for the argument that a major hiatus, spanning millions of years, is present between the base Exeter Member and what we identify as the ETE (Kozur and Weems, 2005; 2010; Tanner and Lucas, 2015).

The key observation supporting the hiatus as stated by Kozur and Weems (2011) is that, "…the upper Norian faunas were dominated by very large conchostracans, while the Rhaetian (and Hettangian) conchostracan faunas are everywhere composed of very small forms." The lack of the early and middle Rhaetian clam shrimp zones and the presence of the large *Shipingia* just below the ETE in Newark Supergroup strata led to the hypothesis of this major hiatus. However, their hypothesis is falsified by the discovery of abundant large cf. *S. olseni* in late Rhaetian, largely marine strata in the North Germanic Basin underlain by strata contains the middle to late Rhaetian bivalve *Rhaetavicula contorta* and overlain by basal Liassic strata with psilocerid ammonites (Olsen and Kent, 2016).

Kent et al. (2016) note that, "…the recorded presence of the very short (~10 ka) Chron E23r immediately below CAMP basalts in three entirely separate basins, namely Newark (Kent and Olsen, 1999; Kent et al., 1995; Olsen et al., 1996a), Fundy (Deenen et al., 2011) and Argana (Deenen et al., 2010), makes such a major regional hiatus untenable. This is because the hiatus would require essentially identical intervals of nondeposition and/or erosion in all of these basins, so that somehow deposition halted just after or else each section was eroded to variable depths exactly down to just above Chron E23r, the shortest identified chron in the Newark-Hartford APTS. But not to be deterred, (Tanner and Lucas, 2015) do not regard such an argument as precluding a regional unconformity and speculate that a late Rhaetian episode of uplift along the entire rift axis might somehow have caused such precisely timed nondeposition or erosion of the exposed strata in all of the rift valleys prior to the flood basalt eruptions."

Examine the cores, and see if you can spot if there is any physical evidence for a hiatus.

In addition to the facies change seen across these three sites, from better cyclicity with dark gray shales in the deeper water units in the Jacksonwald syncline to the southwest, to obscure cyclcity in red beds in the northeast, there is also a parallel change from more or less consistent vertical patterns of cycles to a vertical pattern with fully fluvial conglomeritic facies below to a more marginal lacustrine facies above at the site of PT-38. The Jacksonwald area has been a major source of evidence on the initial ETE, including abundant Triassic-aspect crocodile-line tracks such as *Brachychirotherium* and *Apatopus*, while outcrops adjacent to the location of PT-38 have produced a post-initial-ETE assemblage of sparse sporomophs and macrofossil plants, and abundant footprints (Stop 1.7).

Preakness Basalt – ACE core PTI-3 and Lucent Technologies core MW-21D: ACE core PTI-3 was described by Tollo et al. (1990) and Tollo & Gottfried (1992). It contains both the pillowed lowest flow of the Preakness Basalt and the lower part of the second flow with the characteristic platy-prismatic jointing

that we will see in exposures at Stops 1.8 and 2.5. Lucent Technologies core MW-21D was cored in New Providence, NJ adjacent to the Lucent Technologies (formerly Bell Labs) complex at Berkeley Heights, NJ at 40.688342°, -74.396989°. This core site is 1.7 km northeast from the site (40.676546°, -74.409439°) from which Blackburn et al. (2013) obtained a zircon U-Pb CA ID-TIMS, Thorium-corrected ^{238}U-^{206}Pb age of 201.274±0.032 Ma from a gabbroid float in a stream cut of Preakness Basalt. Several well-developed gabbroid layers are present in Core MW-21D and samples from this core produced an indistinguishable, although as yet unpublished, age (T. Blackburn and J. Ramezani, pers. com., 2014). There is a small gabbroid roadside exposure directly in-line and between these two sites at (40.677774°, -74.408121°) from which we have a sample that will be on display.

This Preakness date along with others from intrusions associated with the other basalt flow formations of the Newark Basin, tested and precisely corroborated the hypothesis that the cyclicity seen in the syn-CAMP lacustrine strata was astronomically paced. The durations of the sequences between basalt flow formation based on U-Pb dates provided by Blackburn et al. (2013) are indistinguishable from the astrochronological estimates derived from Olsen et al. (1996b) and Whiteside et al. (2007).

Distance in miles (km)

Cumu-Lative	Point to Point	Route Description
10.0 (15.6)	0.3 (0.5)	Return to vehicles and proceed to exit, back to 9W southbound. Passing TW4 core site at left at (41.002829°, -73.910658°). Turn left onto Route 9W southbound.
10.7 (17.2)	0.7 (1.1)	Proceed south and turn left onto ramp for Palisades interstate Parkway (PIP) south.
10.8 (17.4)	0.1 (0.2)	Take ramp and enter PIP southbound. PIP follows ridge crest of the Palisades cuesta at about 1/3 stratigraphic thickness of the sill.
18.7 (30.1)	7.9 (12.7)	Take PIP southbound and take exit 1 on right for E Palisade Ave in Englewood Cliffs.
18.9 (30.4)	0.2 (0.3)	Take ramp for exit 1, keeping left.
19.0 (30.6)	0.1 (0.2)	Turn left onto E. Palisade Avenue
21.2 (34.1)	2.2 (3.5)	Turn right onto Hudson Terrace.
21.4 (34.4)	0.2 (0.3)	Continue straight onto Main St. This road follows a small fault with normal separation that offsets the Palisades ridgeline, dropping down to the left.
22.3 (35.9)	0.9 (1.4)	Turn left onto Henry Hudson Drive and into Palisades Interstate Park.
22.6 (36.4)	0.3 (0.5)	At circle take first right exit. Proceed downhill.
22.7 (36.5)	0.1 (0.2)	Turn right at Ross Dock Picnic area and park.

STOP 1.2: Ross Dock Picnic Area. Fort Lee, NJ

Location Coordinates: 40.860247°, -73.956157°: Parking for Ross Dock Picnic Area. Nominal Stockton Fomration, olivine zone in Palisade Sill.

Duration: 1:30 hr.

Here we will examine strata below locally exposed Lockatong Formation that is intruded by the Palisades Sill. Then we will look at the olivine zone on the way back to the bus.

Walk south along the path next to the river to its termination at the south tip of the park. At several places we will look at mudstones and sandstones of the Stockton. Walk 960 yards south along the river path to beneath the George Washington Bridge. Continue 887 yards farther south looking for outcrops at head height on the right (west) of the path. Depending on the plant cover you will see variegated (tan purple and red) cross-bedded arkosic sandstones and minor conglomerate interbedded with massive, intensely red-purple mudstone. The mudstone is cut by numerous large and deep ptygmatic sandstone-filled cracks that are often vertically boudinaged. This is the same facies we see in TW4 below the possible Lockatong (Stop 1.1).

Figure 24: Ptygmatic arkose-filled crack in massive, purplish-red mudstone of nominal Stocton Fomration at Stop 2.2. Cracks are about 54 cm wide but look wider because of "bleaching" of mudstone arohdn cracks.

Phytosaur locality (40.846613°, -73.963452°): At the end of the path along the Hudson is part of a set outcrops of some notoriety, having been the subject of page one of the 1910 Christmas Day pictorial section of the New York Times, entitled, "When the Giant Dinosaur Walked Down Broadway". Never mind that it was not a giant, or a dinosaur, or on Broadway! It is in fact a partial disarticulated postcranial skeleton of a large phytosaur (semi-aquatic, non-archosaur, crocodile-mimic pseudosuchian) that was recovered at the water's edge (Fig. 25) on private land then owned by the "three Goetschius brothers" just south of the park boundary. It appears to have come from the transition between an overlying arkose and red mudstone. The specimen was discovered in March or April of 1910 by Jesse E. Hyde, Daniel D. Condit, and Albert C. Boyle Jr., who were at the time graduate students of Prof. James F. Kemp of Columbia University (Hyde, 1911). They contacted Barnum Brown and W. D. Matthew at the American Museum of Natural History (AMNH) in New York City. The specimen was collected by Brown for the AMNH over a two-week period in late December 1910, after a few months of negotiations with the land owners. The phytosaur locality has been misidentified in most published reports, and was cited by the New York Times (December 21, 1910) as being "a half-mile south of the George Washington Bridge, opposite 155th St.", even though 155th St is closer to one mile south of the bridge! However Matthew (1911) and Hyde (1911) state that the specimen is from opposite 160th St., which is approximately 1/2 mile south of the bridge and there are outcrops still present on private land at (40.844472°, -73.965003°); The specimen is also commonly referred to as the "Fort Lee phytosaur", although it is actually from Edgewater The specimen (AMNH 4991; Fig. 27) consists of several posterior dorsal, sacral, and anterior caudal vertebrae, both femora, tibiae, and fibulae, a few dorsal ribs, many gastralia, and numerous osteoderms. Huene (1913) described the specimen and named it *Rutiodon manhattanensis*. Based on the structure of the ilium, the generic assignment is correct (Huber and

Lucas, 1993; Huber et al., 1993) but the specimen is indeterminate at the species level. This is the only vertebrate reported from this facies, but it suggests that further exploration might prove fruitful. AMNH 4991 is currently on exhibit in the Hall of Vertebrate Origins at the American Museum of Natural History in New York.

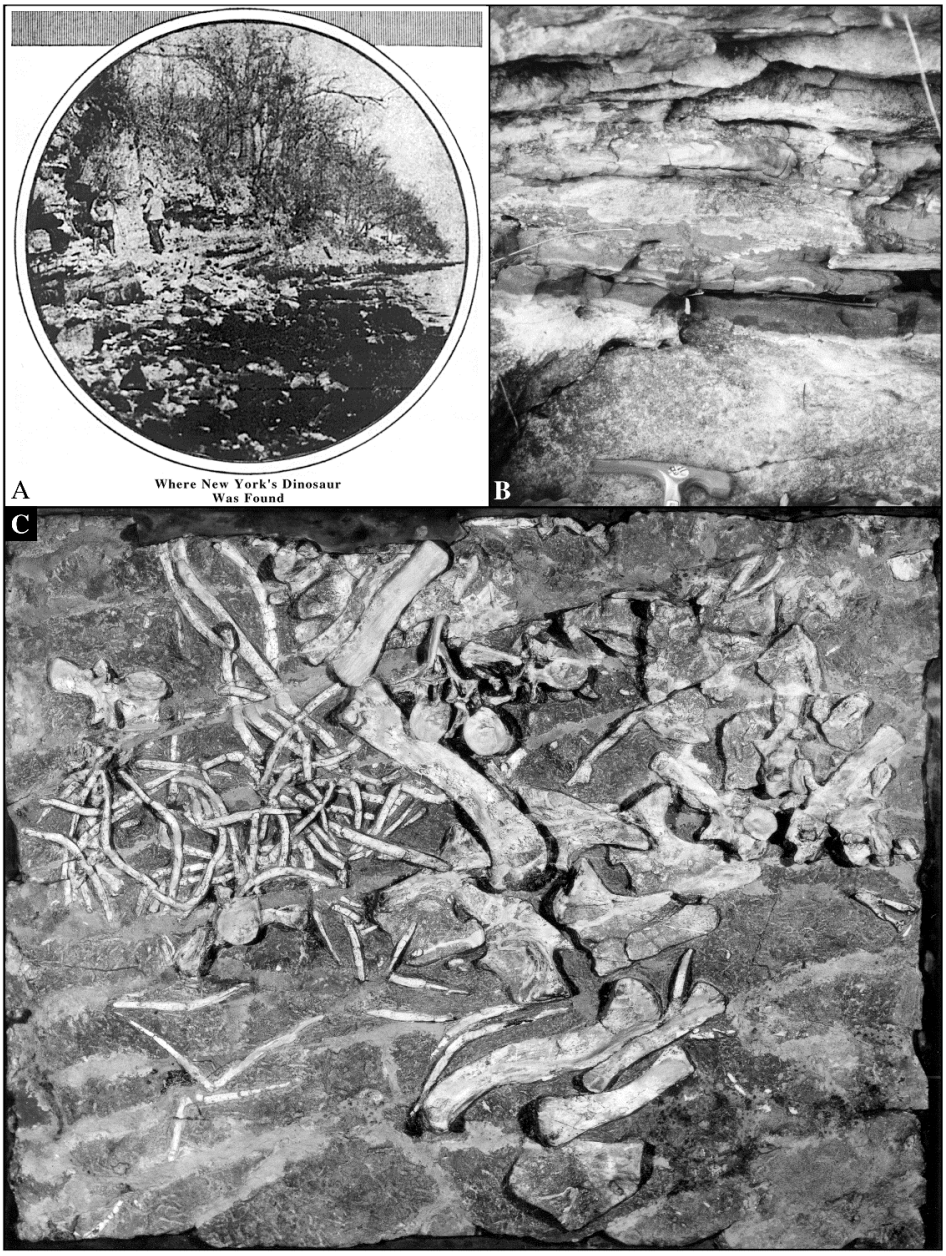

Figure 25: The phytosaur *Rutiodon manhattenesis* and outcrops at Stop 1.2, Stockton Formation: A, photograph from the front page of the magazine section of the New York Times for December 25, 1910, showing the location of the phytosaur skeleton just south of the boundary with the Palisades Interstate Park (Stop 3g) (with permission of the New York Times); B, photograph of typical lithologies (purple and red mudstones and tan arkose) at the north end of the outcrops shown in A; C, disarticulated partial skeleton of the large phytosaur Rutiodon manhattanensis (AMNH 4991) (courtesy of the American Museum of Natural History)

Take the switchback path that works its way up the hill to Henry Hudson Drive and proceed south toward the intersection with Main Street (Fort Lee) and the entrance to the park.

Weathered olivine zone of the Palisade Sill (40.846664°, -73.965107°): Exposure on the north side of road has weathering profile of the olivine zone that can be clearly seen here. The olivine zone is weathered to a very crumbly diabase that, according to Naslund (1998), still has many fresh looking olivine crystals. The olivine zone is about 10 to 15 m above the base of the Palisades Sill and its weathering produces an obvious bench along the escarpment, essentially paralleling the lower contact of the sill, as observed by Walker (1969).

Proceed north along the base of the sill on Henry Hudson Drive, keep track of the bench and note where sedimentary strata at the base of the sill are exposed. Also note the faint and fine layering visible on the diabase surfaces near the base of the sill. Beware of vehicles!

Slightly discordant base of sill and metamorphosed Lockatong Formation (40.851995°, -73.960580°): The thin-bedded to massive metamorphosed mudstones and siltstones, interbedded with tan arkosic sandstone, is typical of the lower Lockatong in this part of the basin, and it shows unequivocally that the red and tan units along the river are stratigraphically lower than Lockatong Formation. Of interest here is that as the sill cuts lower in the section, at either side of this outcrop, the strata become disrupted and the finer-grained appear to behave more competently while the coarser beds appear to have liquefied and partially and chaotically mixed with the diabase (Fig. 26). Note that the topographic bench tracking the olivine zone appears to bump upward here.

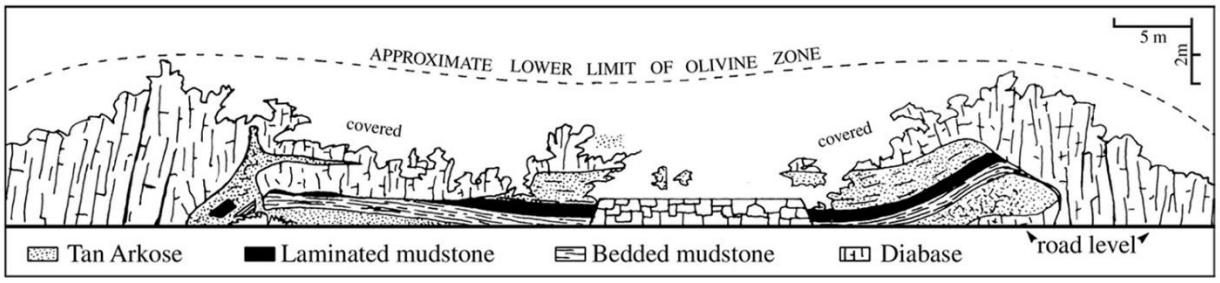

Figure 26: Sketch of discordant contact of Palisade sill and Lockatong Formation along Henry Hudson Drive just south of the George Washington Bridge at 40.851995°, -73.960580° (from Olsen, 1980).

Proceed north under the George Washington Bridge. The road basically follows the base of the sill.

Razor-edged contact between sill and Lockatong Formation (40.854159°, -73.959776°): Probably the best and most accessible contact between the Palisades Sill and underlying meta-sediments is here, where the contact tends to be planar, and very sharp, and although predominantly concordant, locally hops up or down in stratigraphy tens of centimeters. Note that over most of the exposure there is very little evidence of melting or assimilation and that fine-scale sedimentary structures are well-preserved despite proximity to the sill.

While these rocks are gray to nearly black, they contain no organic carbon. North along this same road, past the circle (at 40.862042°, -73.955783°), are exposures of similarly metamorphosed Lockatong Formation in a part of the stratigraphy (cylces W-5 and W-6 of the Nursery Member) that has been

traced along the base of the sill to Hoboken and correlated with the NBCP cores (Olsen, 1980c; Olsen et al., 1989; 1996a). Away from the sill, the fossiliferous (clam shrimp, ostrcodes, fish, and rare reptiles), microlaminated portions of the cycles have total organic carbon contents of 3 to 8 % (Manspeizer & Olsen, 1981), but here have essentially 0% organic carbon. Prior to larger scale metamorphism by the intrusions, the organic carbon content was probably in excess of 10%. This carbon, originally in the form of kerogen, was thermally cracked eventually to gas, finally methane and CO_2, presumably with ^{13}C-depleted isotopic ratios (δ13C of ~-28‰). These greenhouse gasses made their way into the atmosphere, but whether they did so catastrophically, contributing to the ETE greenhouse crisis and "initial isotopic excursion", or whether they leaked out slowly and assimilated without incident is unknown, although signs of disruption by escaping gas are certainly not obvious.

Proceed north to traffic circle.

Reclaimed quarry in lower Palisades Sill at traffic circle (40.857748°, -73.959041°): In this old quarry, the olivine zone is marked by a zone of deflected columns in the cliff face in fresh rock. Naslund (1998) notes flow banding is present within the olivine zone. You can project that zone of deflected column into the benchmarking the weathered olivine zone. What might the evidence be that the olivine zone represents a separate intrusive event or separate major pulse as suggested by Husch (1990), Puffer et al. (2009), and Block et al. (2015), and can you see any of the evidence here?

Proceed down steps at northwest side of circle and back to parking area.

Distance in miles (km)		
Cumu-Lative	Point to Point	Route Description
23.1 (15.6)	0.4 (0.6)	Return to vehicles and proceed to exit, back to Main street, Fort Lee. Turn right and Main Street, Fort Lee, becomes River Road, Edgewater, NJ.
26.3 (42.3)	3.2 (5.1)	Proceed south on river road. There are several exposures of Lockatong and Stockton formations along the base of the Palisades Sill along this route, described in Olsen (1980c). Keep left to stay on River Road. On Gorge Road to the right are excellent exposures of Lockatong Formation described by Olsen (1980c, 2003) and Colbert & Olsen (2001). These allowed the section at Granton Quarry above the Palisade Sill (Stop 1.5) to be concatenated with that of the sections below the sill.
26.7 (43.0)	0.4 (0.6)	Turn Right onto Church Road and Park along road.

STOP 3: Churchill Road Exposure of Dramatically discordant sill and Lockatong, North Bergen, NJ

Location Coordinates: 40.803242°, -73.994221°:

Duration: 0:30 hr.

This is a very large, virtually unstudied exposure of a dramatically discordant contact between the Palisade Sill and the Lockatong Formation (Fig. 27). "Measured" using GoogleEarth™ (which has large uncertainties in altitude) the shear face of the wall is about 39 m. Using this as a guide, and accounting for parallax (non-quantitatively), about 23.5 m of Lockatong is exposed and the sill cuts down through it all towards the southeast. About three large cycles, each consisting of a couplet of a complex of prominent tan sandstone beds and complex of mudstone beds, are present averaging about 7.8 m thick.

Given that the average thickness of a 20 kyr cycle in this area is about 1.5 m (Olsen, 2001), consistent with smaller scale alternations of laminated and non-laminated mudstones at this outcrop, it would suggest the larger cycle is an expression of the short eccentricity (~100 ka cycles). We will see more of this pattern at Granton Quarry at Stop 1.5.

Strata near the contact are deformed in a variety of ways. There are a number of blobby diabase intrusions that warp the surrounding strata, as well as several sheet-like ones that extend far from the main diabase body, and a series of small thrust faults (Fig. 27). This outcrop is very similar to that at Kings Bluff at Weehawken (Darton, 1890; Olsen, 1980c), except even more dramatic (Fig. 27). From here to the south near Weehaken, the base of the sill sits below the lowest well-developed mudstones on nominal Stockton Formation (Stop 1.4, below).

Figure 27: Dramatically discordant contact between Lockatong Formation and Palisade Sill. Sill cuts down section here to base of Lockatong at Stop 1.3.

Distance in miles (km)		
Cumu-Lative	Point to Point	Route Description
27.3 (43.9)	0.6 (1.0)	Return to vehicles and proceed back to River Road, turning right and proceed south to Walgreens parking lot. Turn right into parking lot of the Walgreens Pharmacy and park.

STOP 1.4: Palisades Sill contact with nominal Stockton Formation, North Bergen, NJ

Location Coordinates: 40.803242°, -73.994221°:

Duration: 0:30 hr.

This is another very large virtually unstudied exposure this time of largely concordant contact between the sill and underling Stockton Formation strata. “Measured” by GoogleEarth™, the cliff face is about 51 m high (consistent with topographic map) (Fig. 28). Based on photographs and accounting for parallax (non-quantiatively) about 14 m of mostly tan and white arkosic sandstone and minor pebbly sandstone with a minor bed of olive-gray sandy mudstone are exposed here below the sill. Several tan arkosic xenoliths are present, one of which remains attached at its south end, making a flame-like structure (Fig. 28). This outcrop has been described by Zakharova et al. (2016) and this specific xenolith compared with the arkosic xenolith in core TW4 (Stop 2.1).

This facies of tan arkosic sandstone is common below and in part above, typical Lockatong Formation. To the north it seems to interfinger with purple and red mudstones. While we are calling this Stockton

Formation, it is unclear if it is a lateral facies equivalent of the lowest Lockatong or time equivalent to part of the Stockton as it is represented in the central Newark basin.

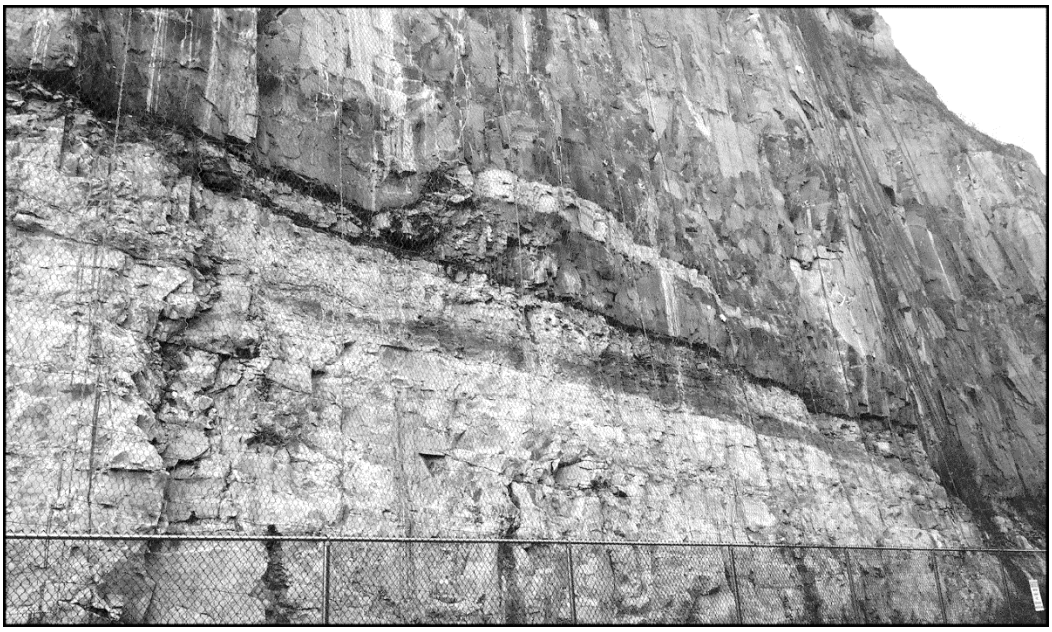

Figure 28: Xenolith still attached to underlying strata at Stop 1.4.

Distance in miles (km)

Cumu-Lative	Point to Point	Route Description
28.1 (45.2)	0.8 (1.3)	Return to vehicles and proceed to exit and turn left onto River Road, North Bergen. Turn sharp left onto River View Drive south.
28.7 (46.2)	0.6 (1.0)	Follow River View Drive south to 17th Street. Continue straight on 79th Street, North Bergen, NJ.
29.0 (46.7)	0.3 (0.5)	Continue on 79th Street. Make left and right "dog leg" on John F. Kennedy Boulevard, continuing on 79th Street.
29.4 (47.3)	0.4 (0.6)	Continue on 79th Street to Tonnelle Avenue (US Route 1 & 9) driving down dip-slope of Palisade cuesta, and cross into parking lot for Lowes Home Improvement Center, North Bergan, NJ and park.

STOP 1.5: Granton Quarry exposures of Lockatong Formation and Granton Sill, North Bergen, NJ

Location Coordinates: 40.807058°, -74.017908° and 40.807380°, -74.017774°.

Duration: 1:00 hr.

Leave vehicles and proceed to northeast corner of store. The following is adopted from Olsen (2003).

In the northeastern Newark basin, the outcrop belt of the Lockatong on both sides of the Palisades sill along the Hudson River is remarkably rich in vertebrate fossils, despite varying degrees of contact metamorphism. In this region, virtually all fine-grained facies and all cycles have some vertebrate body fossils. Here, only the Princeton, Nursery, and Ewing Creek members of the Lockatong Formation have

been positively identified. The Granton Quarry is the most famous of all the fossil localities in this belt and, in fact, the entire Newark Basin.

Remnants of the old Granton Quarry are preserved between the new Lowes Home Building Center on the south and Tonnelle Plaza (Hartz Mountain Industries) on the north. Granton Quarry was actively quarried for road metal, fill and rip rap during the 1950s and 1960s and was abandoned by 1970, whereafter it was slowly consumed by commercial developments and warehouses. Nonetheless, excellent exposures remain. The site has produced, and continues to produce, extraordinarily abundant fossils, especially vertebrates, and it is certainly one of the richest sites in North America for the Triassic (Fig. 29). This is also the best locality on this trip to see the details of Lockatong-type Van Houten cycles. Eleven such cycles with a thin-bedded to laminated division 2 are exposed on the sill-capped hill: seven are exposed on the south-facing exposure (Fig. 30) where we will see them first (40.807058°, -74.017908°), three additional cycles are exposed on the east-facing exposure; and all 11 cycles are exposed on the north-facing exposure, which is where we will examine them in more detail (40.807380°, -74.017774°). The base of the section appears to be 38-46 m above the contact with the Palisades Sill (Van Houten, 1969). This contact may be close to what was, prior to intrusion, the local Stockton-Lockatong formational contact. This section has been described in several papers including Van Houten (1969), Olsen (1980c; 2003), Olsen et al. (1989), and Colbert and Olsen (2001).

According to Van Houten (1969), these Lockatong hornfels include calc-silicate varieties in the middle carbonate-rich part, and extensively feldspathized and recrystalized diopside-rich arkose in the upper part. Some beds of arkose show well-developed cross-bedding. Because of the buff arkose at the top of nearly every cycle, these are the most visually-graphic of the detrital cycles seen on this field trip. Here, the many correlated changes occurring though individual cycles can be easily seen (Fig. 30).

Cycles G3 and G7 (Fig. 30) have produced representatives of all the known skeletal remains of Lockatong vertebrates, except definitive examples of the holostean *Semionotus*. The basal portions of division 2 of both of these cycles have extremely high densities of fossil fish,

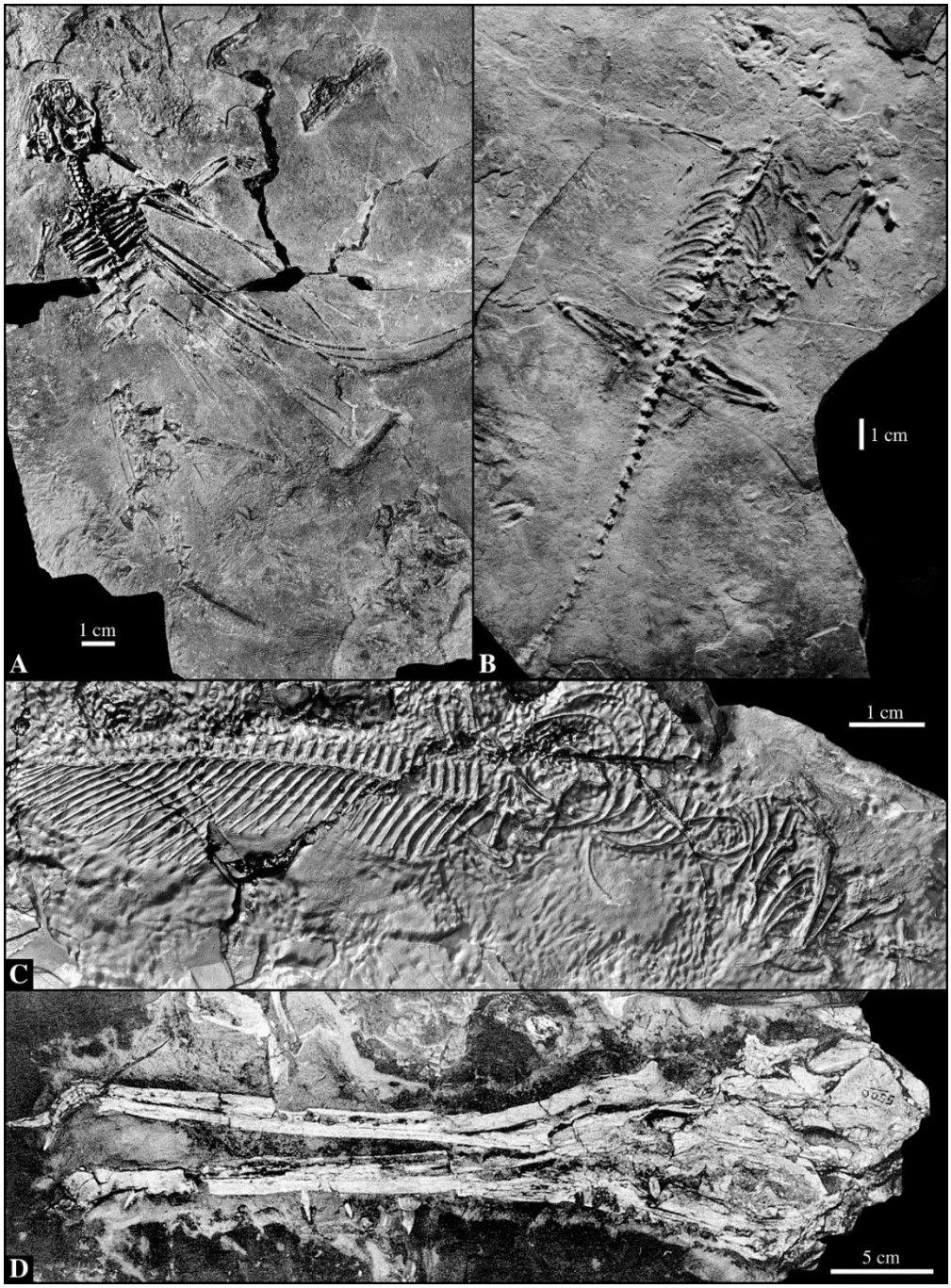

Figure 29: Reptiles from the Lockatong Formation at Granton Quarry (Stop 1.5): A, holotype specimen of *Icarosaurus seifkeri* from cycle G-3 (uncataloged AMNH specimen) (from Colbert, 1966; with permission of the American Museum of Natural History); B, female *Tanytrachelos ahynis* found by Steven Stelz, Trinny Stelz and James Leonard (New Jersey State Museum GP 22356); C, holotype specimen of *Hypuronector limnaios* from cycle G7 (AMNH 7759) (from Colbert and Olsen, 2001; with permission of the American Museum of Natural History); D, skull of cf. *Rutiodon carolinensis* found in float (AMNH 5500) (from Colbert, 1965; with permission of the American Museum of Natural History).

especially the coelacanth *Osteopleurus newarki (*Schaeffer, 1952). Small reptiles are also surprisingly abundant, and many important fish and unique reptile skeletons have been discovered here by dedicated amateurs and donated to various museums through the years (Colbert, 1965; 1966; Colbert and Olsen, 2001; Olsen et al., 1989; Schaeffer, 1952; Schaeffer and Mangus, 1971). Without a doubt, the three most spectacular skeletons of small reptiles found in the Lockatong Formation come from this site. These include the type specimen of the bizarre "deep-tailed swimmer", *Hypuronector limnaios* (Colbert and Olsen, 2001), the peculiarly-abundant and sexually dimorphic, tanystropheid *Tanytrachelos ahynis* (Olsen, 1979), and the gliding lepidosauromorph *Icarosaurus seifkeri* (Colbert, 1966) (Fig. 29). Larger remains occur as well, of which the most spectacular is the skull of a juvenile rutiodontine phytosaur (Fig. 29), but isolated phytosaur bones and teeth are fairly common and isolated vertebrae of a metoposaur amphibian also been found. This biotic assemblage is very different than that seen in post-ETE strata, but some of the elements are present just before the ETE, including phytosaurs and tanystropheids, both based on footprints in the Newark – *Apatopus* and *Gwynnedichnium*, respectively.

Cycles G8 through G11 overlap with the section on the east side of the Palisades Sill as exposed at Stop 4, as has been previously noted. A prediction of this correlation is that cycle W0 should be equivalent to G11. Examination of the easternmost outcrops at Granton Quarry of cycle G11 show that this is indeed the case. In fact, this cycle is distinctive in having a very pyrite-rich division 2 that has strikingly bright yellow and orange clay seams on weathering, a feature not seen in other Granton Quarry cycles. With the sections from both sides of the Palisades Sill combined, it is now possible to look at trends in

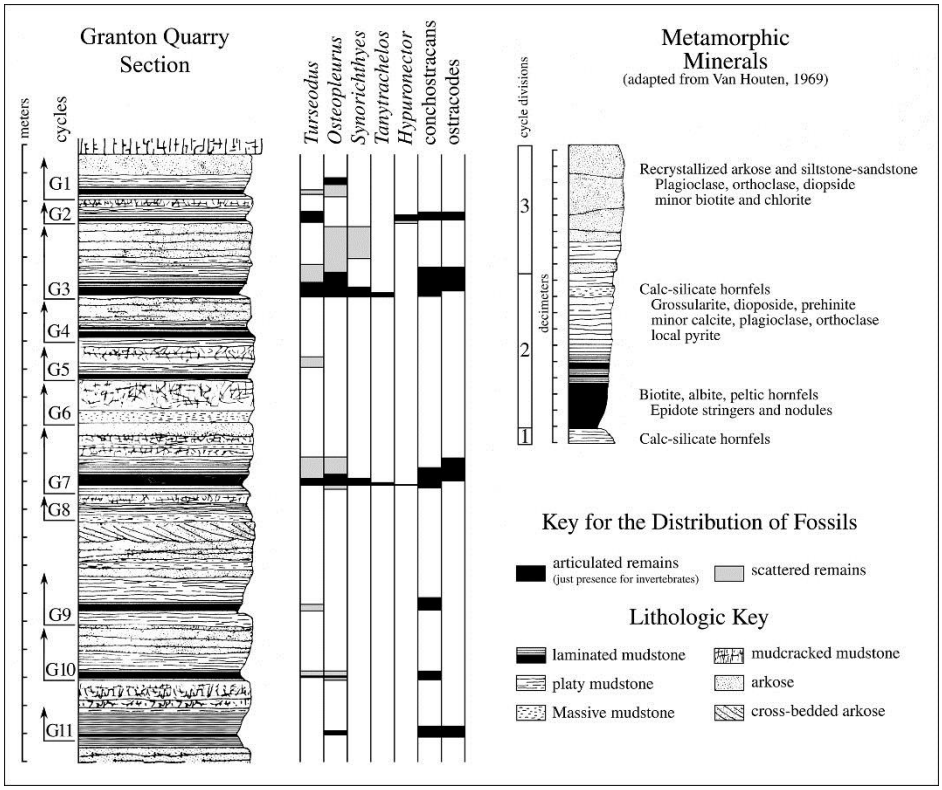

Figure 30: Mesured section at Granton Quarry, Stop 1.5. Section is based on measurenets from both sides of the promatory. Based on Olsen (1980b) and Olsen (2003). Metamorphic Minerals from Van Houten (1969). All of these cycles are still exposed.

lithology and biota at the scale of from a few thousand years (within one Van Houten cycle) to over 1 million years (i.e. three McLaughlin cycles) (Fig. 31).
Van Houten cycles thin to an average of about 1.5 m in this region, and at least some cycles from the drier phases of the 404 ky McLaughlin cycles appear to be entirely missing or replaced by tan arkose, accounting for the disproportionally low (18m) thickness of McLaughlin cycles in this area. If they scaled to the Van Houten cycles that are easily recognized, the McLaughlin Cycle should be ~20 x 1.5 m = 30 m thick. The couplets (i.e. varves) of microlaminated mudstones are thinner than their counterparts towards the center of the basin, but not in proportion to the thickness of the cycles, again suggesting a preferential omission of drier facies in each cycle.

This is an extension of the same thickness and coarsening trend in the Lockatong Formation that we have seen going from the Titusville to Nursery to Princeton NBCP cores (Stop 1.1). It is consistent with thinning onto the hinge margin of a half graben growth structure and incompatible with the strict version of the Broad Terrane hypothesis. The "missing" cycles and corresponding thinning of the McLaughlin cycles is consistent with offlap and bypassing on the hinge margin during lake lowstands and is also inconsistent with the strict version of the Broad Terrane. In fact, projecting that trend to the east and north, one would expect the Lockatong Formation to thin further and disappear entirely into sandstones, becoming unrecognizable, which is exactly what it does.

The stratigraphic sequence in the Hackensack Meadowlands, underlying the Granton sill to the west of the sill's dip slope, consists of arkosic tan sandstones, overlain by black shales (that surely represent much of the remainder of the Lockatong Formation), which are in turn overlain by red mudstones of the Passaic Formation (Parker, 1993). If something like the average accumulation rate, based on the

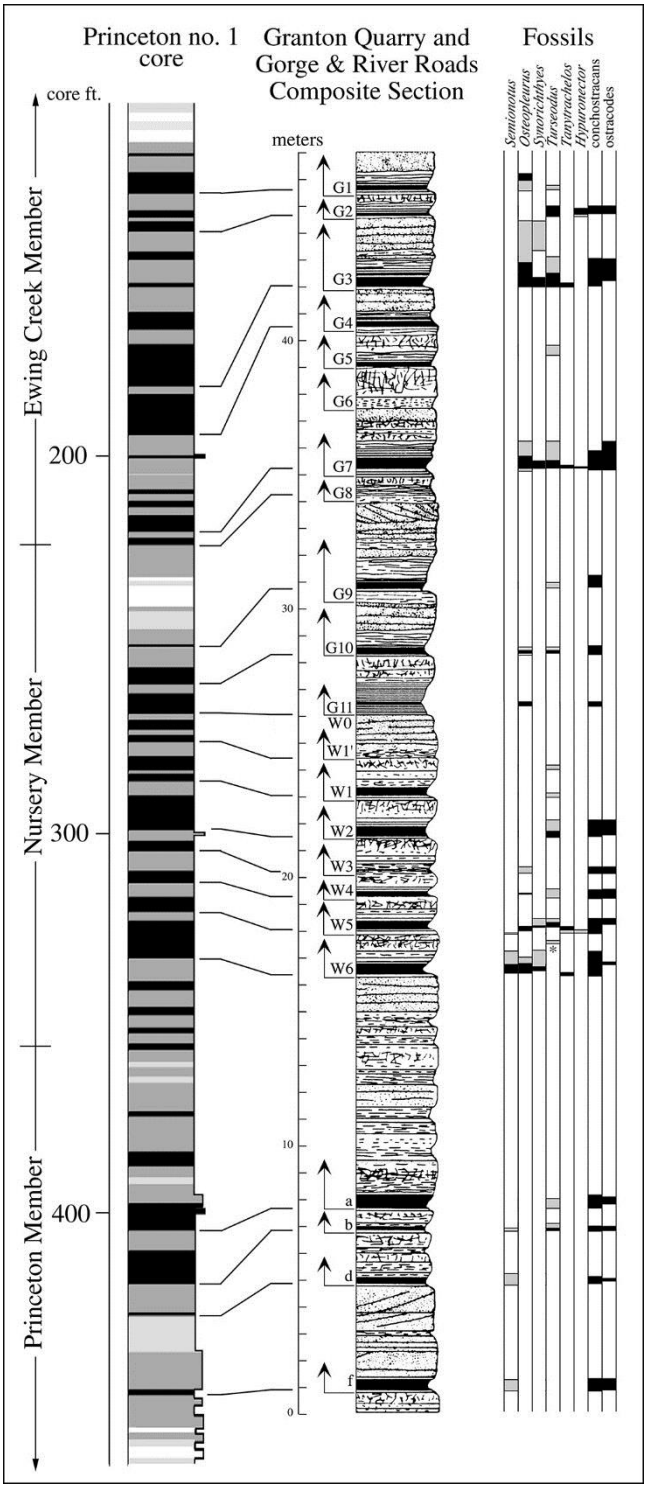

Figure 31: Composite section in vicinity of stop 1.2-1.5 with the distribution of fossils and correlation to the NBCP Princeton no. 1 core. Modified from Olsen (2003).

thickness of the Princeton, Nursery, and Ewing Creek members in the vicinity of North Bergen and Edgewater (i.e. 18 m/McLaughlin cycle), was maintained upward to the position of the Graters Member of the Passaic Formation (encountered in a boring; Lovegreen, 1974 cited in Parker, 1993), there is sufficient stratigraphic thickness in this area for the rest of the Lockatong and basal Passaic Formation.

At the south-facing exposures, cycles G1 and G2 are injected by diabase of the 20 m thick Granton sill (Van Houten, 1969), another component of the CAMP, which has protected the Lockatong Formation from erosion in this area. Because this sill is thin, and the Palisade Sill fairly remote stratigraphically, much of the sedimentary rock is not as metamorphosed as under the sill; some cycles still have considerable organic matter, especially noticeable in cycle G3 which on the south side of the Quarry is black with significant organic matter (Maliconico, 2010), but has little or none at the north end, where we are looking. The change in bone color tracks the thermal maturity as well: black where relatively low and white where high. Perhaps, the sandstones interbedded with the formerly organic-rich mudstones could act as conduits in the up-dip direction, venting methane and CO_2 into the atmosphere.

Distance in miles (km)		
Cumu-lative	Point to Point	Route Description
32.0 (51.5)	2.6 (4.2)	Return to vehicles and proceed to exit and turn right onto Tonnelle Avenue (US Route 1 & 9) south. Proceed southbound to ramp for NJ 3 on right.
32.6 (52.5)	0.6 (1.0)	Take ramp for US 3 and merge with US 3.
36.5 (58.7)	3.9 (6.3)	Continue on US 3 to exit for Polito Avenue on right.
37.4 (60.2)	0.9 (1.4)	Follow signs for Polito Avenue. Turn left onto Polito Avenue.
37.8 (60.8)	0.4 (0.6)	Turn right into parking area for 165 Polito Avenue, Lyndhurst, NJ 07071

STOP 1.6: Passaic Formation and Copper Prospect at Lyndhurst, New Jersey

Location Coordinates: 40.807357°, -74.108448°.

Duration: 0:45 hr.

Leave vehicles and proceed to view the adjacent exposures. The following is modified from Olsen et al. (2004).

We have moved considerably up section from earlier stops as well as deeper towards the depositional center of the basin, although we are still in a marginal facies. These exposures reveal most of the Kilmer Member of the Passaic Formation (~210 Ma, NBTS) (Fig. 4) exposed on the east side of a prominent ridge marking the western border of the New Jersey Meadowlands. This ridge is characterized by a heterogeneous assemblage of red mudstones and sandstones. However, there are a few purple and gray units present, and the eastern and stratigraphically lowest of these is parsimoniously interpreted as marking the base of the Kilmer Member (Fig. 4).

The Passaic Formation, characterized by extremely widespread units with a particularly well-developed “layer cake”-style stratigraphy, marks a stage in the tectonic evolution of the Newark rifts. Based on the very slow rates of thickening towards the faulted margins of the basin (Stop 1.1; Withjack et al., 2013), extension rates were slowing, the basin was filling towards its outlet, and the basin floors were extraordinarily wide and flat. The red Passaic and other central Pangean equivalents are the strata that most people think of when they think

Triassic. At yet a broader scale, the Passaic marks an interval where basins deeper within the arid belt and closer to the rifting axis began to receive considerable amounts of brine of marine origin with the consequent development of thick evaporite sequences (e.g. Osprey Salt of the Canadian Maritime margin).

Based on correlation to the central Newark Basin, albeit tentative, the exposures at this stop reveal the uppermost few meters of member T-U and the lower half of the Kilmer Member (Fig. 4). In the central Newark basin, the basal Kilmer Member includes a prominent Van Houten cycle with a well-developed black division 2. In the region around New Brunswick (NJ), this black shale and the underlying division 1 of this cycle are often rich in copper minerals, particularly chalcopyrite. At these outcrops in the northeastern Newark basin, the same Van Houten cycle apparently lacks black shale, instead having a purple shale with associated tan or white sandstones. The unit is still copper-mineralized, at least locally, and where intruded by thin diabase sills (2.2 mi) to the south-southeast in North Arlington (NJ), it was commercially exploited in what is supposed to be the oldest copper mine in North America – the Schuyler mine (Lewis, 1907). The exposures at this stop are almost certainly the prospect mentioned by Woodward (1944) on the Kingsland estate (located at - 40.8064893°, -74.1109759° http://geonames.usgs.gov/apex/f?p=gnispq:3:0::NO::P3_FID:877576), inspired by the Schuyler mine but never worked extensively. An exploratory shaft at least was opened, and the now-cemented entrance is still visible. Tan and white sandstones associated with purple and gray mudstone are exposed and mineralized with the same minerals as at the Schuyler mine, including chalcocite (black copper sulfide), chrysocolla (bluish-green copper silicate), malachite (green copper carbonate), and azurite (blue copper carbonate). It is noteworthy that there is no evidence of diabase at this location because the presence of an intrusive diabase sill has been used as an explanation for the copper minerailzation at the Schuyler mine (e.g., Woodward, 1944).

The overall section at this stop consists of lower red massive mudstones of member T-U, followed by the tan and white sandstones surrounding a purple well-bedded mudstone of the basal part of the Kilmer Member. This is succeeded by massive red mudstones, a well-bedded interval, and then red mudstones and fine sandstones with gypsum nodules. The overall stratigraphy is very similar to the expression of member TU and the Kilmer member in the NBCP cores we have seen at Stop 1.1.

A large collection of very well-preserved reptile footprints was made near here by Lawrence Blackbeer in the late 1960s (pers. comm., 1985; Olsen and Baird, 1986) (Fig. 32). Although the exact location was not recorded in detail, the lithology of the footprint slabs is consistent with the local expression of the Kilmer Member. This was confirmed by the discovery in 2002 of two well-preserved tracks during a field trip for IGCP 458 (Olsen, 2002) (by PEO and A.V. Hillebrandt,

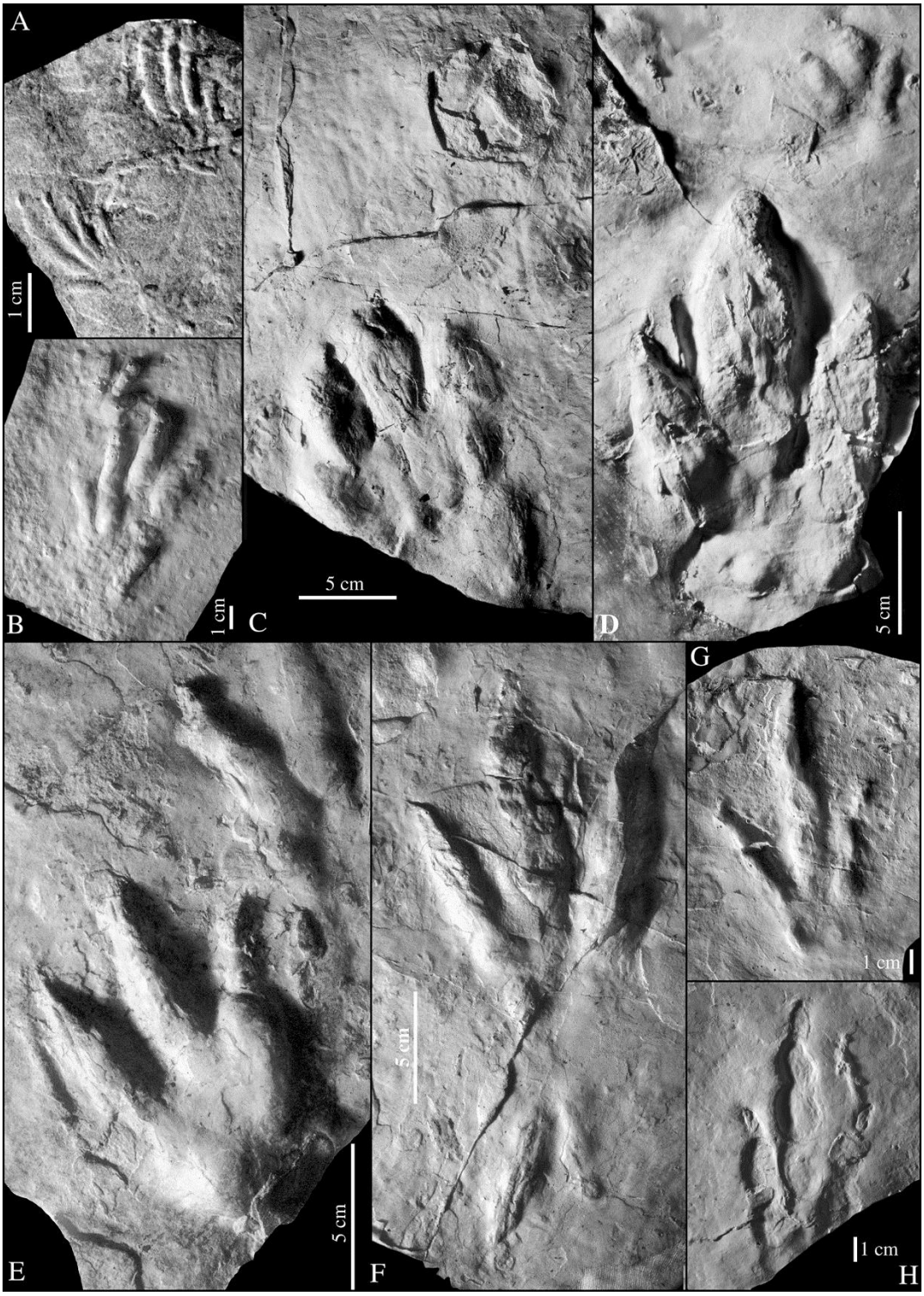

Figure 32: Footprints from Lyndhurst (Stop 1.6) or vicinity, Lawrence Blackbeer collection (all polysulfide casts): **A**, lepidosauromorph track *Rhynchosauroides* sp; **B**, probable suchian track *Brachychirotherium* sp.; **C**, probable suchian track *Brachychirotherium parvum*; **D**, silesaurian dinosauroform *Atreipus milfordensis*; **E**, ?saurischian dinosaurian track *Evozoum* sp.; **F**, theropod dinosaur tracks (brontozoid)

Anchisauripus sp. (above) and *Grallator* sp. (below); **G**, theropod dinosaur track (brontozoid) *Grallator* sp.; **H**, theropod dinosaur track (brontozoid) *Gral* c.f *lator* cf. *G. parallelus*.
June 8, 2002) in appropriate lithology from between the two prominent copper-bearing sandstones at this spot (Fig. 32).

This Norian age assemblage is distinguished in the Newark Basin by the presence of relatively large grallatorid (theropod dinosaur) footprints, up to the size of *Anchisauripus tuberosus*; this is the oldest level in the basin with such tracks. Relatively large examples of the plausibly non-dinosaurian dinosauriform (silesaurid?) track*, Atreipus milfordensis*, are present, along with a the possibly dinosauriform or poposaurid track *Evozoum* sp.[4] ("*Coelurosaurichnus*" sp. of Olsen and Flynn, 1989), as well as crocodile-line pseudosuchian track *Brachychirotherium parvum*, and the small lepidosaurian track *Rhynchosauroides* spp. This track assemblage records the beginning of the rise to ecological dominance of the dinosaurs, which in lower horizons are conspicuous by their relative rarity and small size. This assemblage is similar to that recovered from the Passaic Formation of Rockland County (see Stop 2.2).

Return to vehicles.

Distance in miles (km)		
Cumu-lative	Point to Point	Route Description
32.0 (51.5)	2.6 (4.2)	Return to vehicles and proceed to exit and turn left onto Polito Avenue. Proceed northbound to ramp for NJ 3 on right.
39.1 (62.9)	0.9 (1.4)	Take NJ 3 to merge with US Route 46, keeping right, take the exit immediately right for Valley Road.
46.2 (74.3)	0.2 (0.3)	Take ramp for Valley road keeping right and turn right onto Valley Road.
46.7 (75.2)	0.5 (0.9)	Proceed north along Valley Road (County Road 621) and turn left onto Four Seasons Boulevard.
47.0 (75.6)	0.3 (0.5)	Follow Four Seasons Boulevard and park in front of the "Club House".

STOP 1.7: ETE and E23r in uppermost Passaic Formation and Overlying Initial CAMP Basalt. Former Tilcon Quarry, Woodland Park, New Jersey[5]

Location Coordinates: 40.875964°, -74.188455°.

Duration: 0:45 hr.

Leave vehicles and proceed to view the adjacent exposures. The following is modified from Olsen et al. (2004).

The "Four Seasons at Great Notch Spa and Club" (K. Hovnanian) "adult community" occupies the site of a quarry that produced a very large amount of important stratigraphic, sedimentological, and

[4] Lockley & Lucas (2013) figured two polyurethane molds of PEO as *Evazoum* sp. (their Fig. 1A1, 1B1) but list the locality incorrectly as "from the Upper Triassic Wolfville Formation, Nova Scotia", when in fact they are from the Passaic Formation of New Jersey.

[5] It is possible that there may be no available exposures at this site at the time of our field trip. If that is the case we will visit an alternative exposure nearby possibly near Garrett Rock or Lambert Castle (40.899848°, -74.172896°).

paleobiological information, especially during the last few years as construction proceeded for the development. The quarry was owned and run by a series of
operators and is therefore known by various names, including: Little Ferry Asphalt, Union Building and Construction (UBC) Corporation, R.A. Hamilton, Dell Materials, and most recently Tilcon (the last operator). It has also been referred to as the "Clifton Quarry" and West Patterson Quarry (Gallahger & Hanczaryk, 2006).

The end Triassic extinction has left a rich, albeit asymmetrical, record in the northern Newark Basin. While most of the biological record below the ETE is from the southwestern Newark Basin, that above the initial ETE is from is northern part. Fortunately, the very short (~10m, <20ka) interval of reverse magnetic polarity lies in close proximity under the ETE allowing correlation that is independent of biostratigraphy (although in agreement with it).

Two main localities have provided nearly all of the biotic data in the Northern Newark Basin, both of which are now-abandoned quarries incorporated into Montclair State University and the now-abandoned quarry (this stop). The Montclair State locality (40.868368°, -74.194389° and vicinity) produced a good collection of footprints in the 1970s into the early 1980s with some excellent examples being represented by actual specimens or latex molds ending up in the Princeton collection at Yale, Peabody Museum (New Haven, CT) or the Donald Baird mold collection, now with PEO (the latter badly in need of archiving). Overwhelmingly dominant are brontozoid tracks, including a full size range from *Grallator* to *Eubrontes giganteus*. *Batrachopus* cf. *deweyii* is the only other form recognized. The Woodland Park quarry site, described by Olsen at al. (2004) and Gallagher & Hanczaryk (2006), produced large numbers of a full size range brontozoid dinosaur tracks including *Eubrontes giganteus*, several with unique preservation styles, abundant *Batrachopus deweyii* tracks, and the lizard-like track, *Rhynchosauroides* sp. Possibly thousands of tracks from this site have been examined by amateur collectors, with many finding their way into museum collections, notably the Princeton collection at Yale, the New Jersey State Museum (Trenton, NJ), and the Morris Museum (Morristown, NJ). Despite the very large numbers of tracks this site has produced there have been no examples of any other footprint taxa, nor any typical Triassic forms, some of which have been found nearby in lower strata (e.g., Baird, 1986) in Essex County.

As it was in 2011, when Tilcon was winding down its activity, the quarry exposes about 50 m of uppermost Passaic Formation and most of the 55 m thick lowest of three major flows of the 150 m thick Orange Mountain Basalt (Figs. 33 and 34). In this area, the uppermost Passaic Formation consists of two units of strongly contrasting facies: a lower interval of fluvial facies, and an upper unit of marginal lacustrine facies. The bulk of the upper Passaic in this region consists of upward fining cycles of relatively poorly sorted pale red conglomerate and pebbly sandstone with poorly defined trough cross bedding grading upward into massive red mudstones and sandstones (described by Parker et al., 1988). The units are intensely bioturbated, which is what obscures the bedding. This facies is overlain by red and gray mudstones and sandstones with more distinct bedding and excellent preservation of small-scale sedimentary structures, which are more heterogeneous than underlying units. There are cross-laminated sandstones with channel morphologies, tilted thin beds that toe laterally into mudstones suggestive of small deltas or crevasse splays, tabular beds of climbing ripple cross-lamination, and thin bedded mudstone beds suggestive of suspension deposits in standing water. Many sandstone beds are bound by clay drapes, and many surfaces are covered by ripples, desiccation cracks, and trace fossils, notably reptile footprints. The uppermost surface of this interval is covered by the Orange Mountain basalt and locally seems to have preserved some depositional relief, including small channels (Fig. 33).

Vertebrate footprint assemblages (Fig. 35) and floral remains from the upper facies completely lack all Triassic forms, indicating that the interval postdates the ETE.

Figure 33: Stop 1.7 as it appeared in 2004. North wall of quarry showing the lower flow of the Orange Mountain Basalt resting on Passaic Formation containing the ETE level and polarity zone E23r. Double arrow incated footprint-bearing levels in sandstone-and mudstone facies, a few meters below which is E23r in mixed pebbly sandstone-minor mudstone facies.

The thin reverse polarity interval E23r was identified in the north Quarry wall at about 16 m below the Orange Mountain Basalt in the coarser, fluvial, conglomeritic facies (Fig. 34) that is similar to normal Passaic formation in this area (Parker et al., 1988).

The coring transect of the Army Corps of Engineers (ACE) Passaic River Diversionary Tunnel Project passed through this area, and a series of short cores (<200 m) were recovered through the uppermost Passaic and lower Orange Mountain Basalt (Fedosh and Smoot, 1988; Tollo & Gottfried, 1992; Olsen et al, 1996a; Olsen et al., 2002). All of them show the same facies transition as seen at this stop. Reverse polarity zone E23r has been identified in these cores at the appropriate levels as well (e.g., ACE core PT-38: Stop 1.1).

The floral assemblage from discontinuous pods of gray mudstone and sandstone at this stop include abundant remains of *Brachyphyllum*, a cheirolepidiaceous conifer and less common fragments of the dipteridaceous fern *Clathropteris meniscoides*, a large variety of casts of stems and rhizoliths and poorly preserved pollen mostly of the genus *Classopollis*. This is a typical post-ETE assemblage very similar to that in the overlying Feltville Formation. The fern *Clathropteris meniscoides* is the source of the spores at the spore spike in the southwestern part of the Newark basin.

A quite remarkable feature of the assemblage from this site is that it records the appearance of the first truly large theropod dinosaurs, and increase in size (length) of over 20% that occurs at or just after the extinction level. A 20% increase in track length should scale to a doubling of mass, and thus this represents a very significant change in the top predators. As spelled out by Olsen et al. (2002), there are two obvious possible scenarios to explain the abrupt increase in size in theropod dinosaurs across the Triassic-Jurassic boundary in eastern North America (and globally). First, that the appearance of the much larger theropods represents a dispersal event from some unknown location, or second, that it

represents an evolutionary event. Thus far, we favor the second, evolutionary hypothesis for the appearance of large theropods and suggest that the abrupt increase in size is most easily explained by a sudden evolutionary response of the theropod survivors (which may have been quite small) to ecological release, operating at time scales of thousands of years. We hypothesize a response similar to that inferred for reptiles on modern islands lacking competitors. This evolutionary response hypothesis could be falsified by the discovery of equivalently large theropod bones or diagnostic *Eubrontes giganteus* (emphasis on the ichnospecies is important) tracks in unquestionably pre-ETE Triassic strata. Thus far these are wanting, contrary to assertions of, for example, Thulborn (2003), Lucas et al. (2006), and Lucas & Tanner (2008). In any case, this track assemblage suggests that the dramatic drop in non-dinosaurian diversity was caused by an extrinsic environmental catastrophe such as the CAMP, and the resulting drop in competitive pressure was the trigger for the global *spread* of large theropods. Sauropodomorph dinosaurs also survived the ETE, joining theropod and ornithischian dinosaurs to establish the familiar dinosaurian-dominated ecological pattern that dominated the terrestrial world for the next 135 million years.

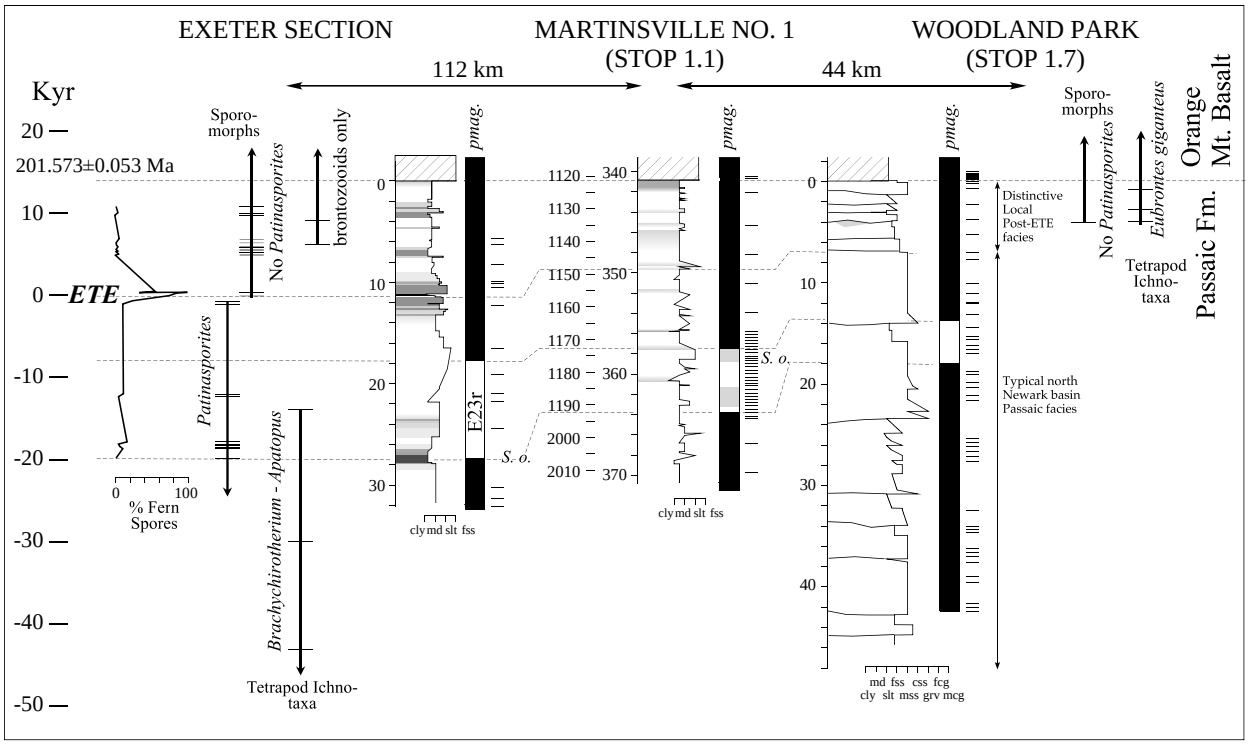

Figure 34: Physical, astro-, bio, and magnetic polarity stratigraphy of thee key sections around the ETE in the Newark Basin. Note the close correspondence with different lines of evidence. Black is normal polarity and white is reverse. *S. o*., marks occrences of the spinocaudatan *Shipingia olsenii*

The Orange Mountain basalt overlies the Passaic Formation and is a high-Ti quartz normative thoeliite (Puffer and Lechler, 1980; Tollo & Gottfried, 1992), a basalt type extremely widespread

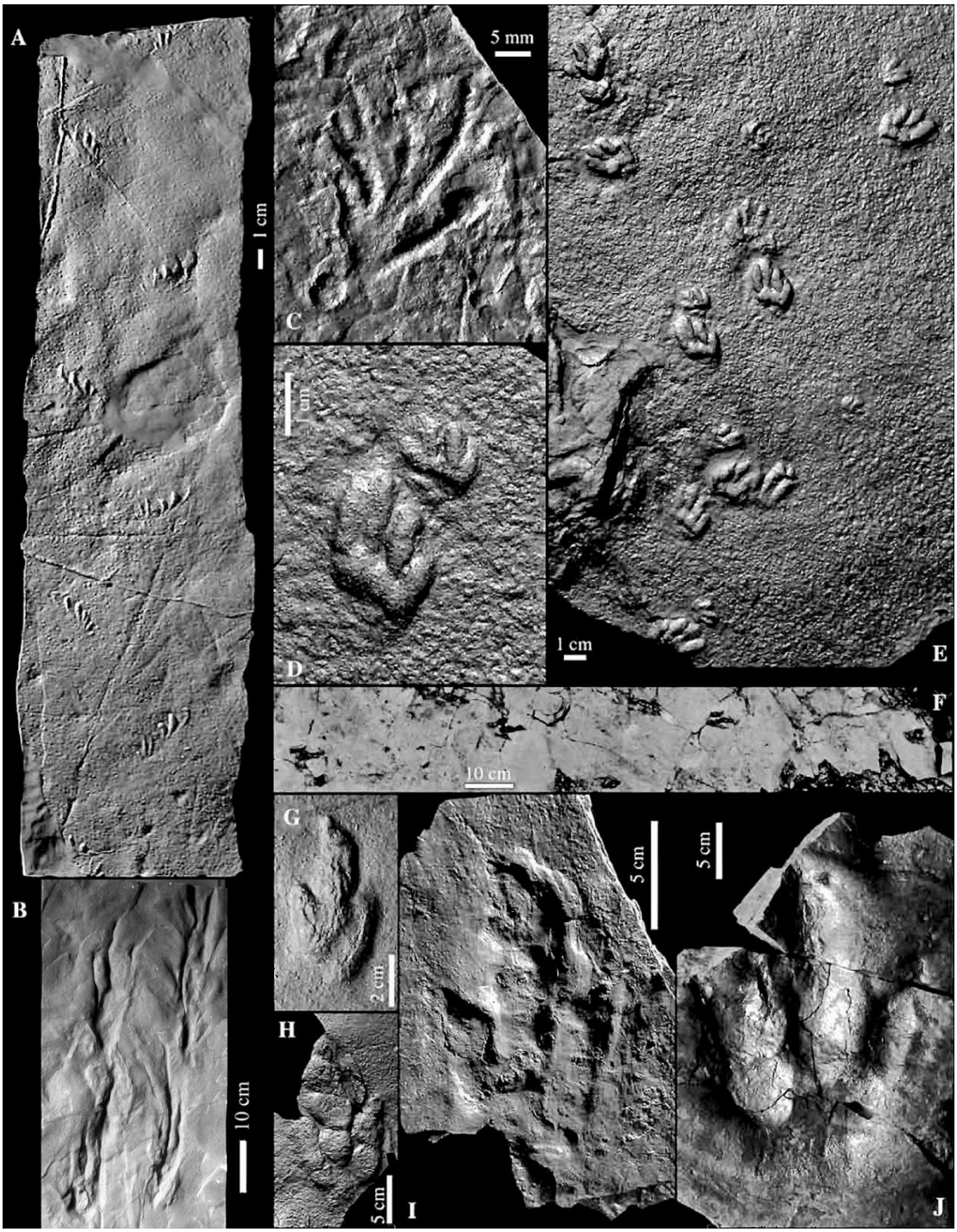

Figure 35: Post-ETE (latest Rhaetian) reptile footprints from the uppermost Passaic Formation at Stop 1.7: A, C, *Rhynchosauroides* n. sp.; B, swimming brontoozid tracks; D-E, *Batrachopus deweyii*; F, trackway of medium-sized brontozoid *Anchisauripus sillimani*; G, smaller brontozoid *Grallator* sp.; H, medium-sized brontozoid *Anchisauripus* sp.; I, medium brontozoid, *Grallator tuberosus*; J, largest and characteristic post-ETE brontozoid, *Eubrontes giganteus*.

in the CAMP as the initial flow type. While it is the oldest flow sequence in the Newark Basin, slightly older flows (by thousands to tens of thousands of years), occur in Nova Scotia and Morocco (Blackburn et al., 2013). Based on the connection of the zircon-bearing Palisade intrusion to the Orange Mountain Basalt flows in Rockland County, the ^{238}U-^{206}Pb age of the basalt is 201.520±0.034 Ma and that of the ETE is 201.564±0.015 Ma based on the zircon ages and astrochronology (Blackburn et al., 2013).

Distance in miles (km)		
Cumu-lative	Point to Point	Route Description
47.3 (76.1)	0.3 (0.5)	Return to vehicles and proceed to exit and turn left onto Valley Road (Passaic County Road 621).
49.3 (79.3)	2.0 (3.2)	Proceed north on Valley Road (Passaic County Road 621) to left turn onto New Jersey Route 19.
50.5 (81.3)	1.2 (2.0)	Proceed on New Jersey Route 19 to end and turn left onto Main Street, Patterson, NJ.
50.8 (81.8)	0.3 (0.5)	Follow Main Street north to left-right dogleg via Broadway to West Broadway (Passaic County Road 673).
51.3 (82.6)	0.5 (0.8)	Proceed on West Broadway to right turn onto Belmont Avenue (Passaic County Road 675).
53.4 (86.0)	2.1 (3.4)	Follow Belmont Avenue north to West Overlook Avenue, North Haledon, NJ and park in strip mall on left.

STOP 1.8: Upper Feltville Formation and lower Preakness Basalt, William Paterson University.

Location Coordinates: 40.951754°, -74.189353° (parking); 40.951150°, -74.192169° (quarry)

Duration: 1:00 h.

Leave vehicles at strip mall and walk about ~145 yards (~133 m) and enter woods down to creek). Proceed upstream ~130 yards (~ 119 m) observing outcrops of upper Feltville Formation to abandoned quarry in upper Feltville and basal Preakness Basalt. The following is modified from Olsen et al. (2003).

Manspeizer (1980) described this locality in that year's NYGSA guidebook noting the three basic units present. The upper Feltville Formation, a lower pillowed flow of the Preakness Basalt and a second massive and highly fractured flow of the Preakness Basalt (Fig. 36). The Feltville Formation exposed in the old quarry and adjacent stream consists of interbedded tan and red sandstones and red and gray and purple siltstones. The latter contain sporomorphs, conifer fragments, and wood. In terms of the cyclostratigraphy of the Feltville, this sequence is the interval of maximum precessional variability in the 100 ka cycle exhibiting the lowest precessional variability within its 405 ka cycle. The second flow of the Preakness has a ^{238}U-^{206}Pb age of 201.274±0.032 Ma, which is in complete agreement with its cyclostratigraphic age (Blackburn et al., 2013).

The basal flow of the Preakness as exposed here consists of a pillowed basalt complex and more massive flow lobes that fed the pillows, all of which show considerable vesicularity. This is Preakness flow P-1 of Tollo & Gottfried (1992) and is a distinct and mappable unit extending at least from the ACE core transect to the north near the border fault. It seems to be absent from at least West Orange (I-280) to near Somerville, NJ, but reappears along I-287 at Pluckemin, NJ. Olsen (1980a; 1980b) described outcrops of the lower flow but did not differentiate it from the overlying flow P-2 of Tollo & Gottfried (1992). At this locality there is little metamorphic effect on the underlying Feltville Formation, which to

be expected because P1 was extruded into water, presumably as deep as the thickness of the pillowed flow itself.

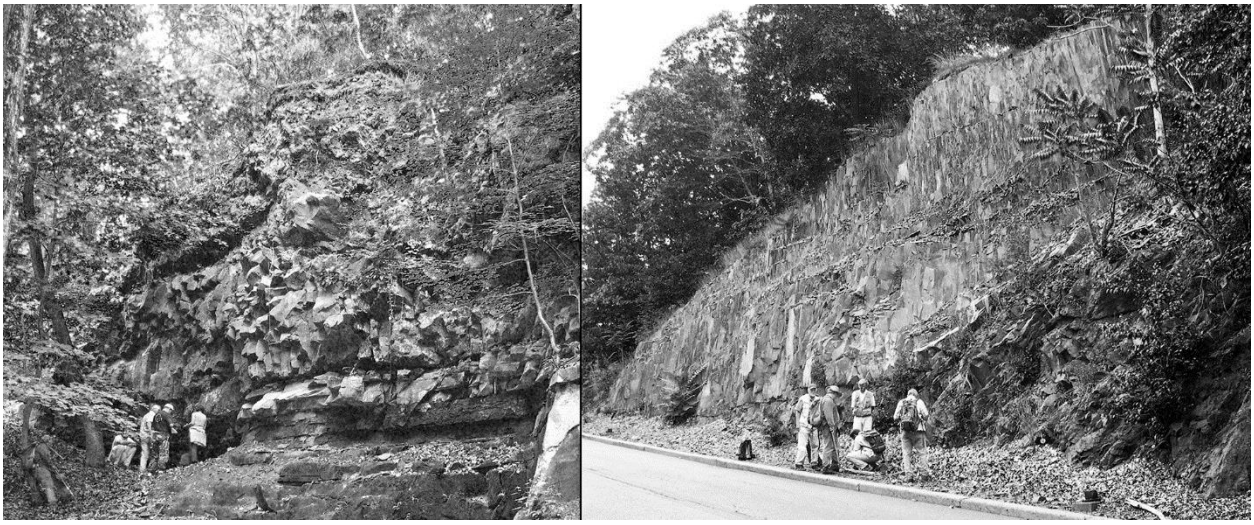

Figure 36: Preakness Basalt at Stop 1.8. Left, contact between upper Feltville Fomrtaion and pillowed and curivcolumnar flow 1 of the Preakness Basalt. Right, contact between flow 1 and 2 of the Preakness Basalt – John Puffer for scale.

Proceed from the quarry up the hill on the north to West Overlook Avenue and then to the west to exposures of basalt. The contact between P-1 and Tollo & Gottfried's (1992) flow P-2 can be seen here. P-2 is the very thick flow that is present all over the entire extent of the Preakness Basalt and is characterized by having an intense splintery or prismatic fracture (Faust, 1975) and gabbroid layers (Puffer & Volkert, 2001). Prévot & McWilliams (1989) noted that this flow has unusually low magnetic inclinations compared to the other Newark basin flows. They also found the same low inclinations in the second flow of the Hartford basin Holyoke Basalt and the Deerfield basin Deerfield Basalt. Hozik (1992) showed that the Sander Basalt shared the low inclinations unlike all the other basalts of the Culpeper basin. All of these low-inclination flows have the same chemistries (Puffer, 1992; 2003), all have gabbroid segregations, and all but the Deerfield Basalt have the characteristic splintery fracture. In the Hartford and Deerfield basins, a flow of similar chemistry but having a tendency to be pillowed is present below the flow with the low inclinations. As pointed out by Prévot & McWilliams (1989) these directions would seem to indicate correlation, and correlation within the time frame of secular variation, suggesting that these flows represent the same eruptive event of no more than 10s or 100s of years. The Sander flow with the low inclinations is over 200 m thick, and P-2 of the Preakness Basalt is more than 90 m thick, and if the flow extended from Massachusetts to Virginia, it would be one of the largest lava flows known on Earth.

In terms of environmental effects, rate as well as magnitude matters, and the eruption of this flow, if it was indeed one eruption, would have been among the largest flows known on Earth in terms of volume, and would have had significant global environmental effects. The largest single flow of the Columbia River Basalt is on the order of 5000 km^3 (Tolan et al., 1989), but if the Preakness and its equivalents averaged 100 m in thickness, spanned 800 km along strike, and were 100 km wide prior to erosion, it would have a volume of 8000 km^3. This does not include the area spanned by dikes of the same composition that extend well into Canada (McHone, 1996). Flow P-1 is highly vesicular at this locality and P-2 has very significant fracture porosity and permeability. The well-developed, platy-prismatic fracture in Flow P-2 is very well displayed here and could be very significant for sequestration. As previously discussed, Goldberg et al. (2009) argue that carbonation reaction in permeable zones of

basalt could provide a significant locus for carbon sequestration. However, while there is a large amount of porosity and permeability obvious here, it has yet to be demonstrated that it exists at depth in these ancient basalts.

Return to vehicles.

Distance in miles (km)		
Cumu-lative	Point to Point	Route Description
54.7 (88.1)	1.3 (2.1)	Proceed to exit onto West Overlook Avenue eastbound and turn left onto Belmont Avenue (Passaic County Road 675), heading north, and at end turn slightly left onto High Mountain Road.
55.6 (89.5)	0.9 (1.4)	Proceed on High Mountain Road and turn right onto Ewing Avenue.
57.6 (92.7)	2.0 (3.2)	Follow Ewing Avenue north and turn left onto ramp for New Jersey Route 208 N.
57.8 (93.1)	0.2 (0.3)	Take ramp and merge onto New Jersey Route 208 N
59.2 (95.3)	1.4 (2.3)	Proceed on New Jersey Route 208 N to merge onto US I-287 N.
59.6 (96.0)	0.4 (0.6)	Follow merge onto US Interstate I-287 N.
67.0 (107.9)	7.4 (11.9)	Proceed on I-287 N and rse the right 2 lanes to merge onto I-287 E/I-87 S toward Tappan Zee Br/New York City.
74.7 (120.3)	7.7 (12.4)	Follow I-287 E to take exit 14 on right for New York Route 59 toward Spring Valley/Nanuet.
74.9 (120.6)	0.2 (0.3)	Follow ramp keeping left, then turn left onto NY-59 East.
76.6 (123.3)	1.7 (2.7)	Follow NY-59 E to right hand turn to entrance for Double Tree, Nanuet.

End of Day 1.

DAY 2

Meeting Point: Parking Lot of DoubleTree by Hilton Hotel, 425 State Route 59, Nanuet, New York, 10954. Access is from the east-bound lanes of State Route 59.

Meeting Point Coordinates: 41.090694°N, 73.995438°W

Meeting Time: 8:00 AM (Both Days)

Distance in miles (km)		
Cumu-Lative	Point to Point	Route Description
0.0 (0.0)	0.0 (0.0)	Assemble in the parking lot of the DoubleTree, Nanuet. Leave Parking lot, turning right at entrance on to eastbound State Route 59, keep in right lane
0.1 (0.2)	0.1 (0.2)	Get on entrance ramp to Palisades Interstate Parkway South from NY-59 E
0.3 (0.5)	0.2 (0.3)	Merge onto Palisades Interstate Parkway South
8.4 (13.5)	8.1 (13.0)	Follow Palisades Interstate Parkway South to US-9W N/N Rte 9W N in Alpine. Take exit 4 from Palisades Interstate Parkway South
8.5 (13.7)	0.1 (0.2)	Turn right onto US-9W northbound.

9.4 (15.1)	0.9 (1.5)	Pass traffic light and turn right into campus of Lamont-Doherty Earth Observatory of Columbia University just before New York-New Jersey State line (Ludlow Lane).
9.7 (15.6)	0.3 (0.5)	Proceed to the front of the Geoscience building. Park and you will be guided on foot to the core repository.

STOP 2.1 - Cores, Seismic Lines and Posters at Lamont-Doherty Earth Observatory, Palisades, NY

Location Coordinates: 41.004471°N, 73.908982°W: Core repository Laboratory, Geoscience Building, Lamont-Doherty Earth Observatory.

Duration: 1:00 hr

Here we will examine cores, down-hole logs, seismic profiles, posters, and some fossils mostly from the Rockland portion of the Newark Basin near the northern terminus of the basin. These exhibits are meant to compliment the Stops of Day 1 and are related directly to the new seismic profiles across the basin in Rockland. These will relate directly to the outcrops will see after this stop.

Core TW4 on the Lamont Campus

We will examine the following features of Core TW4: 1) Diabase and xenolith; 2) Possible Lockatong Formation; 3) Nominal Stockton Formation; 4) High gamma sandstones without organics; 5) Gypsum-bearing red beds; Odd purple interval; Contact with Fordham Gneiss.

Core from the Tandem Lot

Metamorphosed lower Passaic Formation: Approximately 150 ft of core was collected from above and close to the Palisade Sill. Core is characterized by the presence of metamorphic minerals, most obviously epidote, and by peculiar colors, such as green and various shades purple and orange (Slater et al., 2012). Anhydrite, quartz, calcite, and feldspar cements are present. Sedimentary fabics suggest pedogenic nodular carbonates and fluvial or marginal lacustrine environments.

Cuttings and side wall cores from the Tandem Lot

Compare these cuttings and sidewall cores with the equivalent footages on the logs and with the seismic line to get a comprehensive perspective on the 6880 ft Tandem Lot drill hole.
Passaic Formation: Most Passaic formation washed cuttings look like they are nearly 100% sandstone because the mudstones wash out. We will show examples of the comparison between cuttings and sidewall cores.

Palisades Sill: Cuttings displayed will be from: 1) the upper part of the sill near the contact with the Passaic Formation; 2) the high gamma part of the sill plausibly from the zircon-bearing “sandwich horizon”; 3) from the middle part of the sill; 2) and the lower part of the sill, comparable to what is seen in the TW4 core.

Lockatong Formation: The cuttings are easily mistaken for gneiss, but the sidewall cores and FMI logs show that the section below the sill is similar to what we saw at Stops 1.3 and 1.5 consisting of alternating gray and dark mudstones and tan sandstones.

Fossils from the Passaic Formation of Rockland County

Fossils from the old Manhattan Trap Rock Company Quarry at Nyack Beach State Park (Stop 2.2): Large tetrapod, probably reptile burrows; a small theropod dinosaur (brontozoid) track, Grallator sp.; *Scoyenia*

(arthropod) burrows; and rhizoliths (root traces). The *Grallator* sp. track may be the only definitive dinosaur footprint from New York State.

Fossils from Snedeker's (or Waldberg) Landing, Haverstraw (41.173200°, -73.934633°): A small sandstone quarry located south of Haverstraw Beach State Park has produced a series of quite good and diverse fossils over the decades. On display will be the tetrapod trace fossils and fish scrap shown in Fig. 37, as well as additional *Cynodontipus* burrows, small very clear *Brachychirotherium* sp. tracks, and complex rhizomorphs (root traces).

Distance in miles (km)		
Cumu-lative	Point to Point	Route Description
10.0 (15.6)	0.3 (0.5)	Return to vehicles and proceed to exit. Passing TW4 core site at left at (41.002829°, -73.910658°). Turn right onto Route 9W northbound.
15.5 (24.9)	5.5 (8.9)	Proceed north to slight right turn onto Broadway, South Nyack.
19.0 (30.6)	3.5 (5.6)	Proceed north on Broadway though Nyack to end of Broadway and entrance to Nyack Beach State Park, keeping right entering park. Keep right, driving down to parking area near beach and Park.

STOP 2.2: Passaic Formation and Palisade Sill, Old Manhattan trap Rock Quarry, Nyack Beach State Park, Upper Nyack, NY.

Location Coordinates: 41.120639°, -73.911824° (parking, Station A); 41.121467°, -73.912095° (sandstone quarry, Station B); 41.121902°, -73.912009° (trap rock quarry, Station C).

Duration: 2:30 hr

Park vehicles at lot near beach on the Hudson and walk toward the brownstone Dutch colonial-looking “bathhouse” and the adjacent outcrops of Passaic Formation.

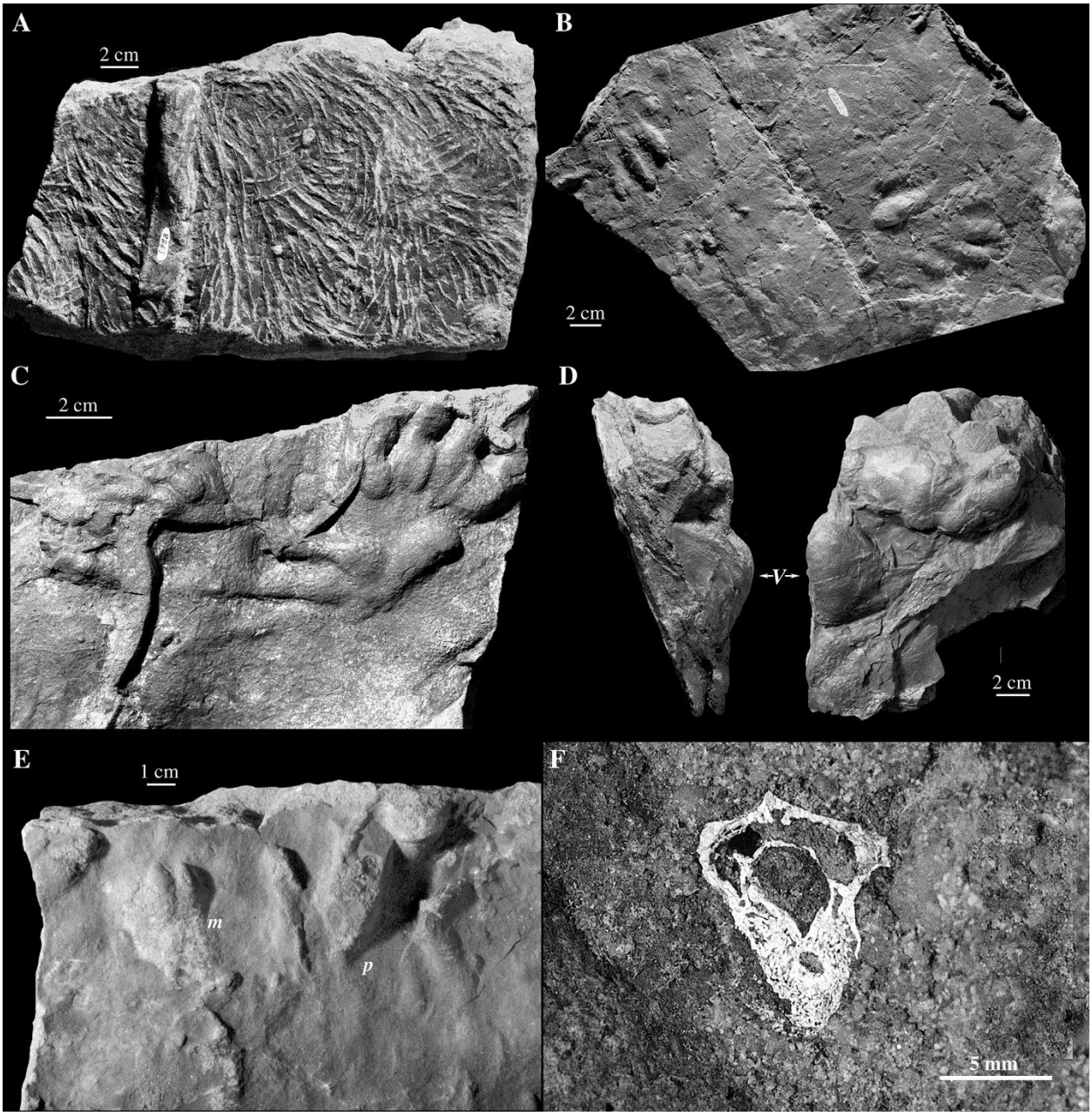

Figure 37: Fossils from near Haverstraw beach, Haverstraw, New York: A, the terminal marks of the tetrapod burrow *Cynodontipus* (YPM 8263); B, natural cast of partial trackway of *Brachychirotherium* cf. *B. eyermani* (YPM 8262); C, natual cast of manus-pes set of *Apatopus lineatus* and partial pes of *Brachychirotherium* cf. *B. eyermani* (YPM 7731); D, very deep natural cast of *Brachychirotherium* cf. B. *parvum* (AMNH uncataloged), V indicates digit V (five); E, natural cast of poor manus (m) and pes (p) set of ?*Atreipus* sp. (YPM 8553); F, partial *Semionotus* braincase (AMNH uncataloged) thought originally to be a tetrapod.

Nyack Beach State Park, is the southeastern component of a series of contiguous state parks including Hook Mountain State Park, Rockland Lake State Park, and Haverstraw Beach State Park all contained within Palisades Interstate Park. It hard to see it now, but this park was a huge active trap rock quarry in the nineteenth and early twentieth century (Fig. 38). Quarrying

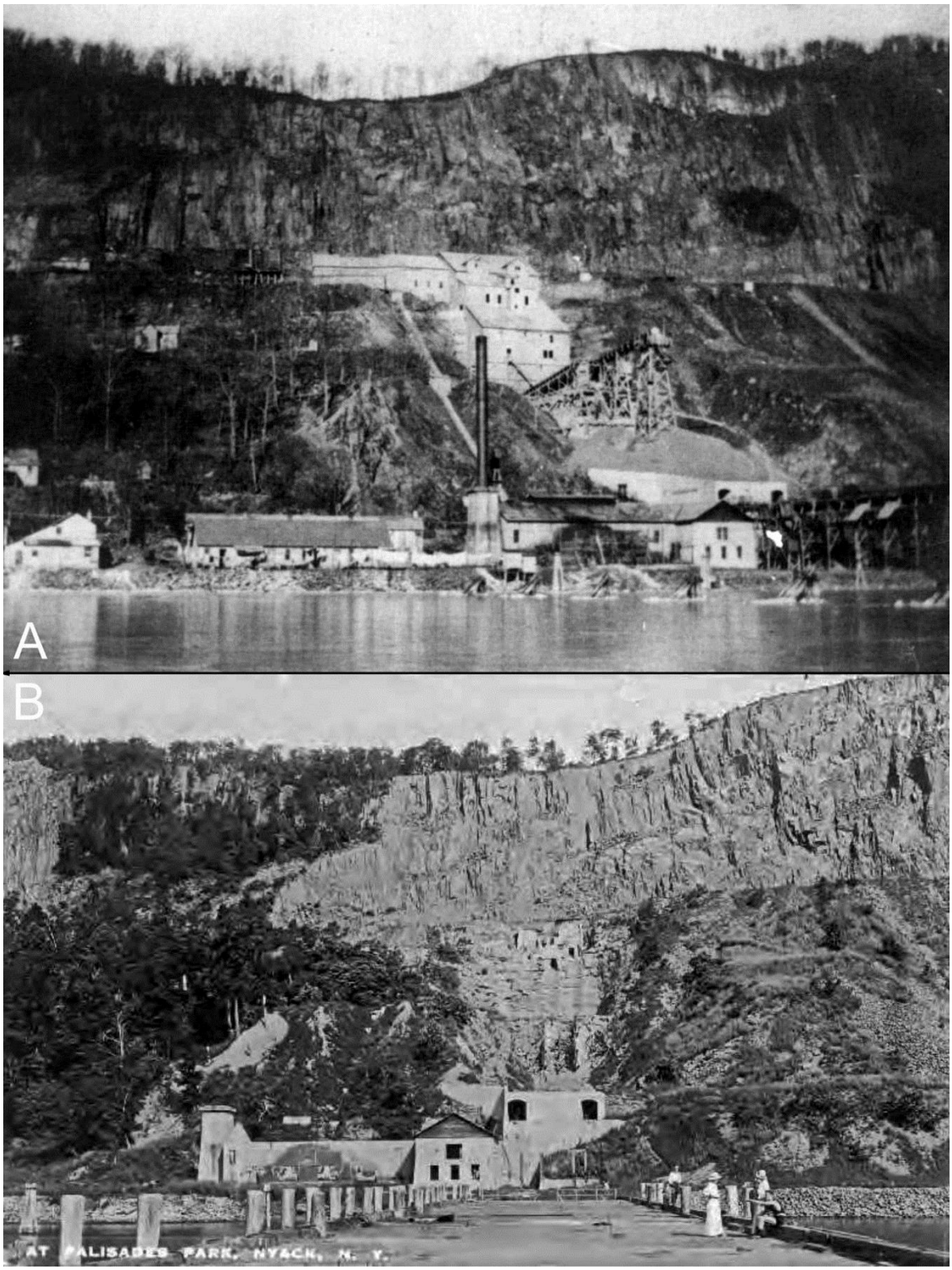

Figure 38: View of Nyack Beach and Hook Mountain state parks. A, is the Manhattan Trap Rock Company quarry and associated structures in full operation ca. 1909. B is the same area after 1912. Both frm Nyack Public Library.

may have begun for the red sandstone at this site by the middle 18th century and the quarry at Station B may have been part of the string of at least 30 (!) quarries extending from Upper Nyack to Piermont at the peak of the operations in the middle 19th century. The "Voorhis" Quarry at this site may have begun as one of these, but by the later 19th century, the quarry was focused on the diabase instead; the production of a higher quality "brownstone" had shifted to the Connecticut Valley (mostly of Jurassic age). In 1872, a huge stone crusher complex was built, eventually extending from the trap rock quarry floor to the river, filling the sandstone quarry as part of the Manhattan Trap Rock Company (OPRHP, 2013). The blasted diabase was dumped from the quarry floor (Station C) into the steam-engine-powered-crusher and sorting system and conveyed via belts down to a cement structure (still extant) on the north side of the brownstone powerhouse and then out on a long raised double pier where the crushed stone was loaded onto freighters on the Hudson (Fig. 38A). By the 1890s, the destruction of the Palisades cliffs and the associated blasting and crushing noise at Hook Mountain and elsewhere had become a conservation cause. In 1906, the authority of the Palisades Interstate Park Commission (the impetus for which was led by The New Jersey Federation of Women's Clubs) was extended by legislative action to Hook Mountain and north, and by contributions from members of the Rockefeller (the estate – Kykuit - of which was opposite the quarry), Harriman, and Perkins families, the Hook Mountain area and its quarries were purchased by the commission – ending quarrying by 1912. Many buildings of the complex were removed as was the rock crushing equipment, making the sandstone quarry again accessible (Fig. 38B). The Work Progress Administration (WPA) repurposed and rehabbed the powerhouse in 1936 as a bathhouse with a large fireplace and ballroom (OPRHP, 2013), which is the structure visible today at Station A.

The most extensive description of the geological aspects of the quarry was made by Kümmell (1900) when the Manhattan Trap Rock Company was operating at full-bore. Kümmell (pp. 27-28) notes: "At the time of my visit, the trap at the south end of the quarry could be seen cutting across the sandstone obliquely downward to the north, a distance of about 35 feet in 60. Thence it followed conformably the bedding planes and gradually regained its former elevation above sea level, though still at a lower geologic horizon. Its general elevation at the quarry is about 260 feet A. T. If the base of the trap kept to the same horizon which it has where it turns so abruptly eastward at Verdrietege Hook, the rise of the underlying sandstones up the dip would carry it from 620 to 6601 feet higher above sea level than it actually is at the quarry. The evidence seems conclusive therefore that the abrupt turn at Hook mountain north of Nyack, is due to the descent of the base of the sheet to a geologic horizon 600 or 700 feet lower than that occupied where it crosses the Rockland Lake-Nyack road." These observations are very important because they show that the crescentic offset of the Palisade ridge is not due to an anticline as sometimes presumed, but rather by the change in stratigraphic level intruded. Unfortunately, very few other detailed observations have been published on the extensive remaining aspects of the site, except for Savage (1968), and in fact the large sandstone quarry at Station B, seems to have escaped geologists' attention entirely until brought to the attention by Dr. William Menke (Columbia University) who found it while hiking. There are no published observations on the paleontology for the Passaic Formation at this site.

Figure 39: Fossils from the former Manhattan Trap Rock Quarry, Nyack Beach State Park. From left to right they are: small brontozoid theropod dinosauar track, Grallator sp.; large tetrapod burrow; complex bone fragment; bifurcating rhizomorph (root trace).

Station A, 41.120639°, -73.911824°: The handsome brownstone "bathhouse" is the repurposed part of the Manhattan Trap Rock Company complex of buildings. The tall brownstone tower-like structure on the south side of the building was the base of a large smokestack of the steam powerhouse of the plant (anonymous, 2011). We presume the sandstone for this building came from the quarry at Stop 2.2, Station B (below). Exposures behind the "bathhouse" are the lowest in this area and consist of a complex of bioturbated mudstones, micaceous reddish-brown sandstone, and some greenish-gray arkose (Savage, 1964). Some surfaces have dessication cracks and less disrupted clay bedding surfaces that could have tetrapod tracks. Carbonate nodules are present and carbonate and mud pellet intraformational conglomerates are present at the bases of some of the sandstones. According to Savage (1964) the paleocurrents are towards the northeast here, characteristic of many exposures in the Rockland part of the Newark Basin where they generally have easterly directions. This is distinctly different, as is the mineralogy, from the Stockton Formation as seen at Snedens landing where the paleocurrents are largely towards the west (Savage, 1964; Olsen, 1980b). Completely absent at this and the other exposures at this site are the red-purple massive mudstones with the very large ptygmatic arkose-filled dessication cracks seen in TW4 core and exposures at Stop 2.2, consistent with this section being upsection from those near the state-line.

From Station A walk 112 m SW along entry road to end of wall on right side of road. Turn northeast and walk up macadam path 39 m to entrance to trail at 41.120394°, -73.912492°. Walk 54 m northeast and turn sharp left up switchback trail. Walk 57 m southwest to right turn. Walk 90 m northeast to path to quarry. Go 41 m northeast into middle of old sandstone quarry.

Station B, 41.121467°, -73.912095°: This sandstone quarry was previously filled by the crusher complex of the Manhattan Trap Rock Company of the late 19th and early 20th century and prior to that it may have been the Voorhis sandstone quarry. More than 50 m of red mudstone and red and some tan sandstone are exposed. Fossils are abundant in the rubble from the quarry along its edges and down the slope to the east. Beware of broken glass, etc. Fossils are common (Fig. 39). *Scoyenia* (arthropod) burrows and clay rhizoliths (root traces) are abundant, sometimes obliterating bedding. At least one

brontozooid dinosaur track, *Grallator* sp., has been found along with one bone fragment. But most striking are the large flattened burrows, 10 to 15 cm wide, that are surprisingly common (four visits with four finds). We identified similar flattened cylindrical features as large roots at Stop 2.3, but they differ from roots in maintaining a relatively constant diameter and not branching. Instead they are consistent with tetrapod burrows. Such burrows indicate that these strata have intervals when they were above the water table for significant amounts of time. It is possible that skeletal remains could be found in such burrows and one should be alert to that possibility when looking about.

The section has several laterally persistent intervals of thin bedded siltstone and sandstone suggestive of shallow water lacustrine intervals seen in the Passaic Formation near Milford, NJ., and it is possible these were deposited during the wet phases of climatic precessionally paced Van Houten cycles.

Looking west and up towards the top of the quarry, you can see the remains of the cement portals for chutes from the trap rock quarry itself. These can be seen in Fig. 38B. The adjacent mudstones have a gray or purplish tint and the sandstones are large tan. We will see this again at Station C and the colors might be most simply explained by metamorphism approaching the sill contact.

Time permitting, we will leave the sandstone quarry and continue up the trail to the road up to the upper parking area.

Return 90 m southwest from middle of quarry and then 138 m southwest to switchback turn. Turn right and go 119 m to chair at last switchback turn before road. Turn left and go 98 m to entrance onto road. Turn right and walk northeast up road to parking area.

Station C, 41.121883°, -73.912208°: The upper parking area at Nyack Beach State Park occupies the former floor of the main part of the Manhattan Trap Rock Company Quarry. Observe jointing in sill: is this columnar jointing? At the far northern end of the quarry a “rotten” zone of diabase typical of the olivine zone of the sheet (Walker, 1969; Steiner, 1989).

Walk 90 m southwest to electrical service boxes. On right (northwest) 26 m is a continuous exposure on a promontory of metamorphosed Passaic Formation to the oblique, down to the west, contact with the Palisade Sill. Exposure is at 41.121486°, -73.913278°.

From the electrical boxes, proceed 44 m southwest to stone bathroom. Most of the blocks of this building are metamorphosed Passaic Formation. Many blocks exhibit nodular zones with epidote, presumably replacing carbonates. Walk back to electrical service boxes and go right down steps to road.

Walk 316 m southwest to guardhouse at entrance to park. Turn left and walk 353 m back to the parking area.

Distance in miles (km)		
Cumu-lative	Point to Point	Route Description
19.3 (31.1)	0.3 (0.5)	Leave Stop 2.2 onto N Broadway and turn right onto Larchdale Ave.
19.5 (31.4)	0.2 (0.3)	Continue on Larchdale and turn left onto N Midland Ave.
20.2 (32.5)	0.7 (1.1)	Continue on N Midland and turn right onto Christian Herald Rd.
20.3 (32.7)	0.1 (0.2)	Proceed on Christian Herald Rd and turn left onto N Highland Ave (US Rt. 9 S).
21.7 (34.9)	1.4 (2.3)	Follow N Highland Ave (US-9 S) to slight right onto S Highland Rd.
21.9 (35.2)	0.2 (0.3)	Take S Highland Rd and turn right onto Highland Ave.

22.1 (35.6)	0.2 (0.3)	Follow Highland Ave and turn right onto Bradley Parkway.
23.4 (37.7)	1.3 (2.1)	Continue on Bradley Parkway and turn right onto N Greenbush Rd. Park on left near fence for Stop 2.3.

STOP 2.3: Passaic Formation above Palisade Sill, large bedding surfaces with footprints and large burrows, Blauvelt, NY.

Location Coordinates: 41.085697°, -73.946738° (parking); 41.084403°, -73.946810° (main exposure of bedding planes).

Duration: 2:00 hr (Lunch)

Park vehicles on unpaved road and proceed 294 m south along N Greenbush Rd to break in vegetation at 41.083084°, -73.946247°. Proceed southwest 34 m at 232° (true N) to 41.084403°, -73.946810°, adjacent to large bedding surfaces. Proceed 54 m due west to a point (41.083117°, -73.946887°) on the bedding plane surface near the "discovery site" for the area.

Reptile footprints were originally found during reconnaissance of excavated rock surface by Paul Olsen and Robert F. Salvia in fall of 1972. Fossils were removed shortly thereafter and deposited in the State Museum of New York, in the case of footprints, and Yale University, in the case of bone and teeth fragments. After initial discovery and salvage, no more material was found until the preparation of this report. Excavation of the site for fill occurred prior to and had ceased by the time of the fossil discovery and since that time the site has lain fallow and is now partly covered by vegetation. However, much bedrock remains exposed.

The site consists of series of large bedding plane (dip slope) exposures comprised of variegated (gray, tan, purplish, greenish, and red) slightly metamorphosed mudstone and siltstone and arkosic sandstone of the Passaic Formation. The stratigraphic level may be correlative with one of the gray sequences further to the southwest within the basin.

The Palisades Sill outcrops to the east, north, and south of the site. From the attitude of the outcropping adjacent diabase on north, south, and east sides, it appears to be strongly discordant, cutting though the Passaic Formation at a high angle. Judging from what is known elsewhere where there are similar contacts and based on the visible metamorphism of the bedrock, the Palisades diabase probably underlies the Passaic Formation at this site at some depth, probably more than 10 feet and probably less that 500 feet.

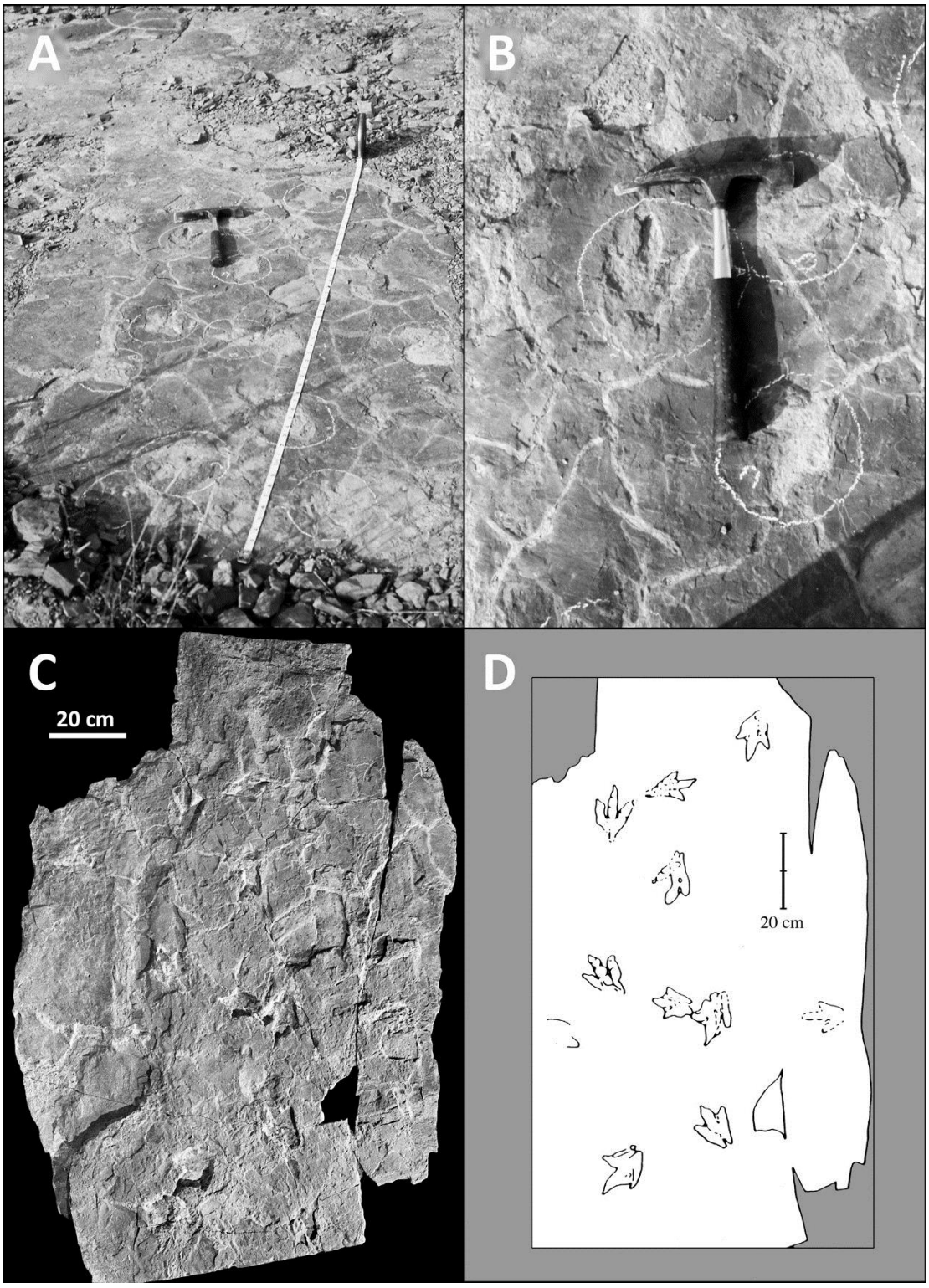

Figure 40: "Discovery slab" of trachs from Stop 2.3, Blauvelt , NY. A, Slab *in situ* prior to excavation. B, single dinosauriform track prior to excavation. C, after excavation preparation and montion at New York State Museum. D, drawing of same.

Four basic classes of fossils were found at the site: 1) reptile footprints; 2) tetrapod burrows; 3) possible teeth and bone scraps; and 4) rhizomorphs (natural casts of plant roots). Two areas you can see most of these features are centered at a north area (A: 41.083347°, -73.947186°) and a south area (B: 41.082287°, -73.946835°) with a 25 m radius.

1) Reptile Footprints: Reptile footprints were found in three places at the site. The first, "the discovery slab" was found in place with all of the tracks filled with white sandstone (Fig. 40) close to 41.083117°, -73.946887°. It was quarried out, taken to the New York State Museum and reassembled by the exhibition staff (briefly described by Olsen & Flynn, 1989). We (Paul Olsen and Robert F. Salvia) subsequently removed the white sandstone fill of the tracks. The slab in its present state reveal at least 12 three-toed footprints, each measuring about 12- 13 cm long (Fig. 40). The tracks have a shape typically associated with small dinosaurs and in fact they have been cited numerous times in the literature (e.g., Fisher, 1982) as the tracks of the small theropod dinosaur *Coelophysis*, which they are certainly not. Small coelophysid theropod dinosaurs such as *Coelophysis*, have a relatively long digit III (middle digit) on the foot producing bronozooid type tracks of the ichnogenus *Grallator*, but digit III on the tracks in the discovery slab is relatively short. On this basis alone, *Coelophysis* can be discounted as the track maker, even though coelophysid dinosaurs are known from strata both older and younger than this site in the Chinle Formation of the Southwestern United States (Irmis et al., 2011; Ramezani et al., 2014), and a small bronozooid was been found at stop 2.2 (Fig. 39).

The tracks on the discovery slab (Fig. 40) could belong to one of non-coelophysid dinosaurs known from the late Triassic, a non-dinosaurian dinosauromorph, or even a crocodile line archosaur convergent on dinosaurian form. Non-coelophysid dinosaurs such as the herrersaurid *Chindesaurus* do occur in North America (Irmis et al., 2007) and something like that could have made the track. However, only *Herrersaurus* proper has well preserved feet and these have a large digit 1 on the pes that should have impressed, but we do not see that in these tracks.
Atreipus (Olsen & Baird, 1986) is fair match to the footprints on the "discovery" slab in having a tulip-shaped hind track with a relatively short digit III for its size. Although *Atreipus* is usually found with forefoot impression, it is not rare to see trackways in which no forefoot impressions are present. Unfortunately, the tracks on the discovery slab are not well preserved enough for a positive identification. In any case, *Atreipus* can now, with some confidence, be assigned to a recently discovered group of non-dinosaurian dinosauromorphs, the silesaurs (such as *Silesaurus*). It is possible that poposaurs, a group of crocodile-relatives (suchian pseudosuchians) that evolved bipedal very dinosaur-like forms such as *Effigia okeeffeae* (Nestbitt, 2007), could have made these track, but *Effigia* too has a large digit 1 and so cannot be simply hypothesized to have made the discovery slab tracks. In summary, the tracks were not made by *Coelophysis* and may not have been made by a dinosaur.

Two occurrences of probably small quadrupedal forms were found on blocks that had been transported to the west edge of the property abutting Route 303 (Fig. 41). These were collected and given to the New York State Museum, although their present location is unknown. These small tracks probably belong to *Brachychirotherium* (a distant crocodilian relative that was not dinosaur-like), but they are actually too poorly preserved to identify.

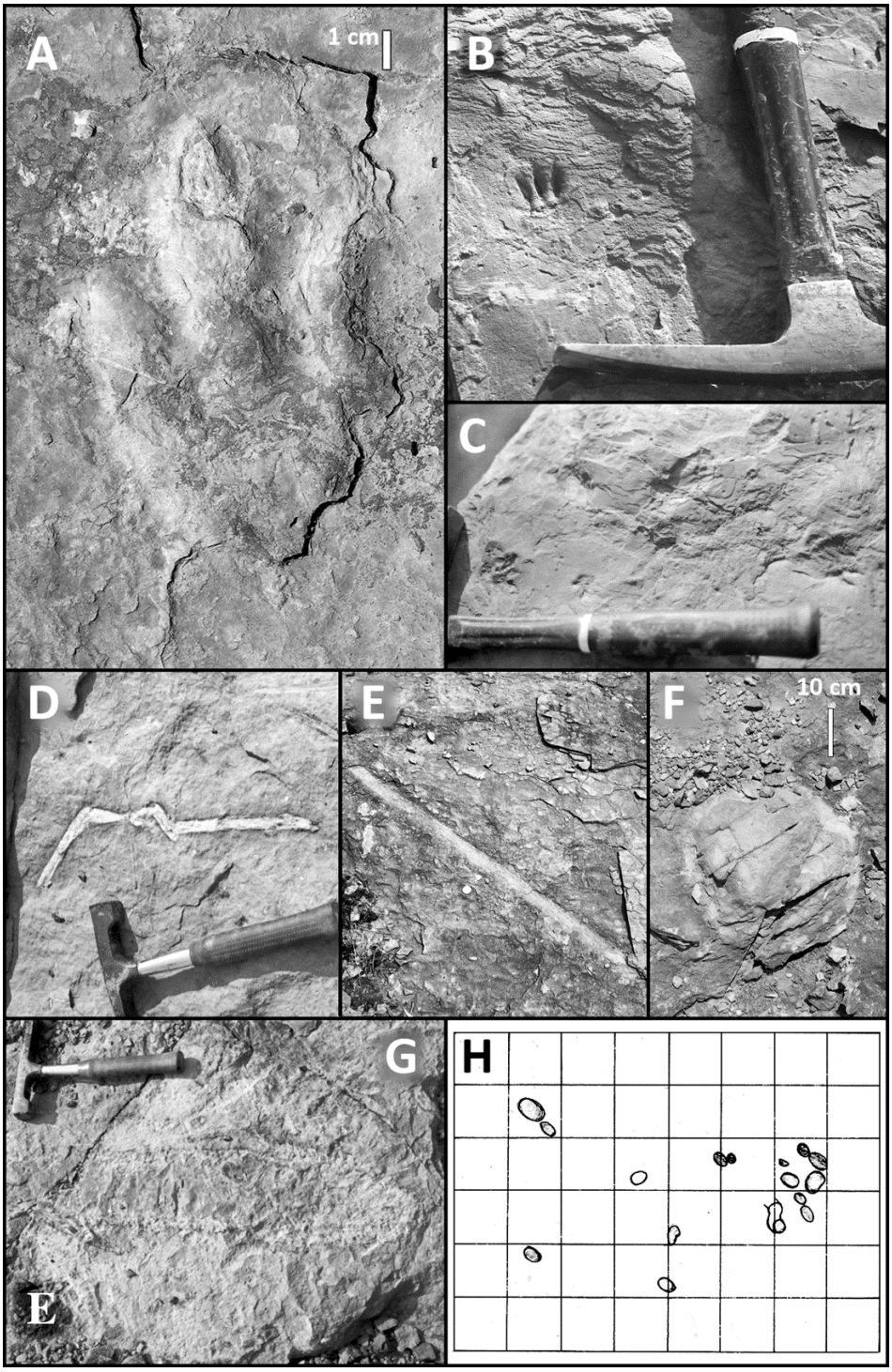

Figure 41: Other fossils from Stop 2.3: A, dinosaur-like possible *Atreipus* footprint (from area B); B, probable quadrupedal track (only one impression present, foot?), hammer for scale; C, very poor quadrupedal trackway, hammer for scale; D, whitish rhizomorph (root natural cast), hammer for scale; E, large root or stem cast, quarter (1.9 cm) for scale; F, large diameter tetrapod vertical burrow, same layer as D and E; G, large diameter horizontal burrow, hammer for scale; H, field sketch of possible tree trunks, same layer as F, grid is 2 ft (61 cm).

2) Tetrapod burrows: Large cylindrical casts are present (Fig. 41) in a greenish gray silty to fine sandy massive mudstone in the southwestern outcrops. Originally, Paul Olsen thought they were tree roots or trunk, but like the similar forms from Stop 2.2, they do not branch and are more simply interpreted as tetrapod burrows.

3) Possible teeth and bone scraps: A few small teeth and bone fragments were found. The shape of the probable teeth is superficially consistent with a phytosaurian reptile, but the metamorphism renders identification extremely difficult. The possible bone fragments are unidentifiable. These specimens were deposited in the vertebrate paleontology collection of the Peabody Museum of Yale University.

4) Rhizomorphs: A variety of rhizomorphs (root traces) are present throughout the exposed bedrock. These consist of whitish claystone natural casts in a greenish gray, silty to fine sandy massive mudstone (Fig. 41). They are present in most layers, but are especially obvious in the layers with the mapped tetrapod.

There have been several attempts at preserving this area via cooperative agreements between the land owner and Orangetown (the municipality), spearheaded by local residents (e.g., Town of Orangetown, 2009). Thus far, a firm arrangement has not been reached because of unfortunately timed economic downturns.

Backtrack to parking area.

Distance in miles (km)		
Cumu-lative	Point to Point	Route Description
23.9 (38.5)	0.5 (0.8)	Return to vehicles and leave Stop 2.3 onto N Greenbush heading north and Turn sharp left onto ramp towards NY-303, and keep right.
24.0 (38.5)	0.1 (0.1)	Go 0.06 m (335 ft) and turn right onto NY-303, and keep left.
24.1 (38.7)	0.1 (0.2)	Go north on NY-303, keeping left and turn onto N Palisades Center Dr, keeping left, and turn left onto ramp and merge onto I-287W/I-87 N.
27.8 (44.7)	3.7 (6.0)	Go west on I-287 W/I-87 N and take exit 14 for NY-59. Tandem lot on left was drilling site. Continue straight onto Forman Dr.
28.0 (45.0)	0.2 (0.3)	Follow Forman Dr and take right onto S Pascack Rd.
28.1 (45.2)	0.4 (0.6)	Take S Pascack Rd north and turn left onto Pipetown Hill Rd.
28.5 (45.8)	0.4 (0.6)	Proceed on Pipetown Hill Rd and turn left onto S Central Ave.
30.2 (48.5)	1.7 (2.7)	Go south on S Central Ave and continue onto Old Nyack Turnpike to left turn onto Saddle River Rd.
30.2 (48.7)	0.1 (0.1)	Take Saddle River Rd. 446 ft south and turn around and park to Stop 2.4.

STOP 2.4: Passaic Formation sandstone and conglomerate on New York State Thruway, Monsey, NY.

Location Coordinates: 41.101932°, -74.069205° (parking); 41.101801°, -74.067179° (main cut).

Duration: 0:45 hr.

NB! This site cannot be visited without a permit from the New York State Turnpike Authority and without proper safety attire.

Park vehicles near overpass for turnpike on east side of Saddle River Road. Leave the vehicles and proceed to north side of overpass. Go over fence and proceed east up to highway. At highway, stay to the outside (north) of the barricade and walk along cut to the east.

This cut exposes roughly 25 m of red pebbly sandstone and conglomerate and very minor mudstone. Conglomerates are dominated by Paleozoic sedimentary and metamorphic clasts. Highly irregular bedding with almost no preserved fine scale sedimentary structures, most simply explained by bioturbation by roots and burrows. This section was certainly deposited by fluvial processes, based on the apparent channel forms. This facies is typical of most of the Passaic Formation in the western half of Rockland County.

Backtrack towards vehicles.

Distance in miles (km)		
Cumu-lative	Point to Point	Route Description
30.6 (49.3)	0.4 (0.6)	Return to vehicles and proceed north on Saddle River Rd and turn left onto NY-59 west.
34.7 (55.9)	4.1 (6.6)	Proceed on NY-59 west and turn right onto Tilcon Rd.
34.8 (56.0)	0.1 (0.1)	Go north to gate on Tilcon Rd and park for Stop 2.5.

STOP 2.5: Upper Feltville Formation sandstone and conglomerate and lower flows of the Preakness Basalt, at former Tilcon, Union Hill Quarry, Village of Sufferen, Town of Ramapo.

Location Coordinates: 41.116395°, -74.145690° (parking); 41.117561°, -74.143347° (Station A); 41.117010°, -74.143702° (Station B); 41.116978°, -74.142732° (Station C).

Duration: 1:30 hr.

As mapped by Volkert (2011) Union Hill is underlain by an outlier of Preakness Basalt in a syncline with the Feltville Formation, Orange Mountain Basalt and uppermost Passaic Formation. Only the upper Feltville and lower Preakness Basalt, in which the trap rock quarry was developed, are exposed here, the rest being covered by Pleistocene till and Holocene deposits except for another small outlying area of basalt. We will examine the section from the top down in three stations, A, B, and C.

Station A, Preakness Basalt: The two lower flows of the Preakness Basalt are well exposed here and very similar to what we saw at Stop 1.8. The lowest flow is irregularly pillowed and the succeeding flow has a massive base and a typical, for the Preakness, entablature with well-developed, platy-prismatic jointing. The top of second flow is not exposed. Ratcliffe (1988) suggested that the western part of the quarry occupies a lower structural level than what is exposed on the east side. He suggested two possibilities: 1) a basalt flow complex flowing in a topographic depression west of the conglomerate; or 2) a westward-dipping or vertical fissure feeder surfacing in flow rocks. Ratcliffe notes that the pillowed zone was exposed at the deepest parts of the quarry so that (2) seems contradicted. This will be discussed on the exposures. However, there is little doubt that distinctive features of the Preakness Basalt, particularly its platy-prismatic jointing are very laterally persistent.

Station 2, Contact between Preakness Basalt and Feltville Formation: The contact between the uppermost Feltville Formation was well exposed during quarrying operations and was described by Ratcliffe (1980; 1988). Presently only some ledges of coarse dolostone conglomerate are exposed near where the contact projects. According to Ratcliffe (1980, p. 297), “Superb exposures at the south end of the quarry … show a vertical wall of coarse fanglomerate, enclosing a large boulder of brecciated dolostone in an apparent channel that, in turn, is overlain by an upward-fining cycle ending in fine red shale with greenish slate chips. Vesicular pillow lava directly overlies this shale.” Based on stratigraphic

position directly below the lowest flow of the Preakness Basalt, this is time-equivalent to the reddish and gray sandstones and mudstones at Stop 1.8.

Station 3, Wall of conglomerate of the upper Feltville Formation: This wall of brown conglomerate is a noticeably different color than typical red conglomerate of the Passaic Formation. According to Ratcliffe (1980, p. 297), "Clasts in the fanglomerate include epidote-rich hornblende granite gneiss, Silurian Green Pond conglomerate, dolostone clasts, and several cobbles of basalt pillows." Clasts of basalt other than pillows are present as well. The presence of these basalt clasts are evidence that these units are upper Feltville Formation. Volkert (2011) map the presence of Orange Mountain Basalt in this area on the basis of extrapolation from the Cushtunk, NJ area, although there is no direct observational evidence, close to Union Hill. However, Ratcliffe (1988) note that the chemistry of a small basalt outlier 2.4 km northeast of Union Hill (at around 41.133685°, -74.126122°) is indistinguishable from that the upper Ladentown flows to the northeast. The Ladentown flows are in turn part of the Orange Mountain Basalt (Blackburn et al., 2013; cf., Puffer, 1987; Puffer et al., 2009). This small basalt outlier projects to the conjectural Orange Mountain Basalt on the northeast limb of the Union Hill Syncline. That the Orange Mountain Basalt does not outcrop in this area is not indicative however, because it does not outcrop all along the east side of Camgaw Mounatin, where it is mapped by records of numerous water wells (Volkert, 2011). The hypothesized presence of the Orange Mountain Basalt in the Union Hill area could easily be tested by drilling.

Walk back towards vehicles.

Distance in miles (km)		
Cumu-lative	Point to Point	Route Description
34.9 (56.1)	0.1 (0.1)	Return to vehicles, turn around, and head south on Tilcon Road turning right onto Lafyette Ave (NY-59) west.
35.3 (56.7)	0.4 (0.6)	Take Lafayette Ave west (NY-59) and turn left onto Chestnut St.
35.5 (57.1)	0.4 (0.6)	Proceed on Chestnut Street and turn right onto Ramapo Ave.
35.5 (57.2)	0.1 (0.1)	Head toward Brook St and park for Stop 2.6.

STOP 2.6: Footwall of the Ramapo Fault Zone, Suffern, NY.

Location Coordinates: 41.115209°, -74.154462°.

Duration: 30 min.

Proceed to parking lot of train station and to walkway to Station (41.115038°, -74.154749°). Walk east and southeast 42 m and turn left before the chain link fence. Walk 36 m north-northwest to outcrop.

This outcrop is described as follows by Ratcliffe (1980) as cataclasite and fault fabric in cataclastic gneiss at Ramapo fault: "These small exposures of black, chlorite-coated, cataclastic, hornblende-granite gneiss are much more instructive than the exposures north of Suffern commonly visited by field trips. Excellent chlorite-slick surfaces dip in conjugate fashion northwest and southeast and exhibit down-to-the south right-oblique slip on southeast-dipping surfaces and down-to-the-west and left-oblique movement on southwest-dipping surfaces. The near-vertical attitude of the extension fractures here … suggests that the rocks of the footwall block … have not undergone rotation after formation of the cataclastic fabric."

Volkert (2011) mapped this outcrop as Mesoproterozoic hornblende granite of uncertain affinity with abundant xenoliths of well-foliated gneiss. According to Volkert's map, it is about 330 m northwest from

the mapped position of the Ramapo Fault and 75 m northeast from a NW-SE right lateral strike slip fault. Mapped foliations in the hornblende granite are to the southeast 30°-60° and a southeasterly dipping normal fault is shown on the immediate northwest.

It is worth noting that the mapped position of the fault does not correspond to the apparent escarpment of the Ramapo Mountains, and that nearly all outcrops are hundreds of meters within the footwall from it. Because the border faults of the Newark Basin tend to follow pre-existing structures, especially of Paleozoic age, brittle features that may have formed prior to the formation of the Newark basin proper may be hard to differentiate from Late Paleozoic structures. It is noteworthy that the position of the Ramapo Fault cannot be easily seen seismic profile, although that in part may be do to its relatively high angle here, structure parallel to the boundary fault are not as obvious at this site as one might hope.

Distance in miles (km)

Cumu-lative	Point to Point	Route Description
35.9 (57.7)	0.2 (0.3)	Return to vehicles, turn around, and head south on Ramapo Ave, turning right to continue of Ramapo Ave.
36.5 (58.7)	0.6 (1.0)	Continue on Ramapo Ave and right on top US-202 south (Ramapo Valley Rd).
37.3 (60.0)	0.8 (1.3)	Go south on US-202 to left turn onto ramp for merge onto NJ-17 north.
37.6 (60.4)	0.3 (0.5)	Head northwest on NJ-17 N and use left lanes to merge onto I-287 E/NJ-17 N towards Tappan Zee Bridge.
38.5 (61.9)	0.9 (1.4)	Take I-287 E/NJ-17 N north and use right two lanes to merge onto I-287 E/I-87 S towards Tappan Zee Bridge.
46.2 (74.3)	7.7 (12.4)	Take I-287 E/I-87 S towards Tappan Zee Bridge and take exit 14 for NY-59.
46.4 (74.6)	0.2 (0.3)	Take ramp and turn left onto NY-59 E from left lanes.
48.1 (77.4)	1.7 (2.7)	Proceed on NY-59 and turn right onto Rose Rd.
48.1 (77.4)	0.0 (0.0)	After 165 ft, turn right into Double Tree Inn.

END OF FIELD TRIP

TRIP B1: THE GEOLOGY OF STATEN ISLAND:

HARD ROCK GEOLOGY - SELECTED FIELD SITES

Alan I. Benimoff

Department of Engineering Science and Physics, College of Staten Island, Staten island, NY 10314

ABSTRACT

This field trip will visit two localities, namely the Staten Island serpentinite in the I-278 Road Cut and the Palisades Diabase at Graniteville Quarry Park in Staten Island, NY.

INTRODUCTION

John McPhee(1993) wrote: " Southeastern Staten Island is a piece of Europe glued onto an ophiolite from the northwest Iapetus floor".

Staten Island NY, a borough of New York City, approximately 13 miles long axis by 7 miles short axis, has a very diverse geology (e.g., igneous Rocks, metamorphic rocks, sedimentary rocks, cross bedded sediments, glacial deposits, glacial striations and grooves, kettle holes, beach deposits, streams, bluebelts and coastal features). This field trip will focus on the Diabase of the Palisades Sill at the Graniteville Quarry Park in Staten Island, NY and the Staten Island Serpentinite.

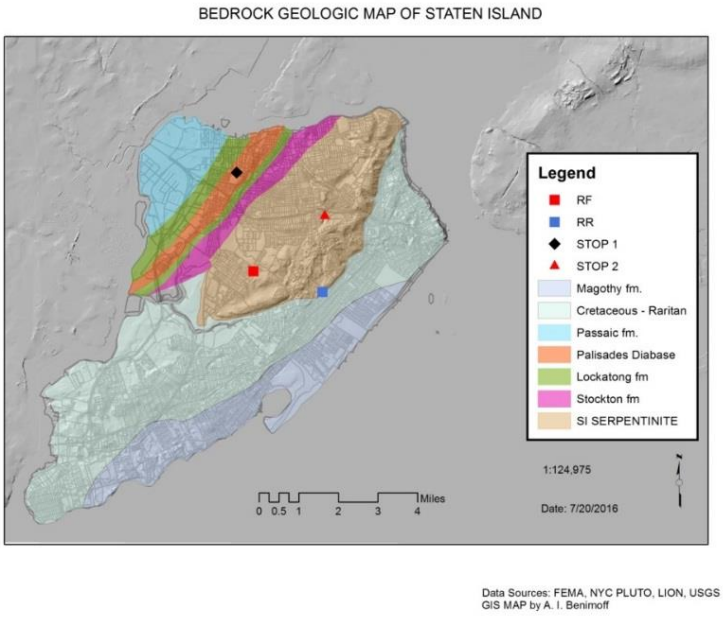

Figure 8: Geologic Bedrock map of Staten Island, NY Showing Locations of Field Stops 1 and 2. RF is near Rockland Avenue and Forest Hill Road; RR is at Lincoln Avenue and Richmond Road.

THE STATEN ISLAND SERPENTINITE

The Staten Island serpentinite (Figure 1) is a lens shaped NE-SW trending body, having a long dimension of 12 km and a width of 4.7 km. The ridge of serpentinite, makes up the bedrock in the northeastern section of Staten Island, and reaches an elevation of approximately 135 meters above sea level. The serpentinite body is part of a string of similar ultramafic bodies, extending throughout the Appalachians, from Alabama to Newfoundland (Figure 1). The serpentinite displays a sheared contact with the Hartland formation along its eastern margin (Lyttle and Epstein, 1987) and is uncomfortably overlain by the Triassic age Stockton formation of the Newark super group at the western margin. In places, the western contact is faulted. The southern and eastern margins of the serpentinite are overlain by the Raritan formation of cretaceous age. Pleistocene glacial deposits overlay most of the serpentinite. In cross section the serpentinite body is a wedge shaped pod, extending downward approximately 1.3 km (Yersak, 1977). The serpentinite is situated on Cameron's Line at the base of the Hartland Formation (Lyttle and Epstein, 1987). Hollick (1909) suggested that the Staten Island Serpentinite is a fault bounded horst block. Crosby (1914) and Miller (1970) share that interpretation.

The Staten Island Serpentinite is part of a discontinuous chain (Figure 2) of ultramafic bodies that extends from Alabama to Québec. The Staten Island body is the largest of four lenticular masses exposed in the New York City area that includes exposures at Hoboken, New Jersey, Western Manhattan, and Easton Bronx. It is a wide lens shape (Figure 1) that trends Northeast – Southwest and comprises the bedrock of northern Staten Island, although the Western boundary is not exposed. There is general agreement that the Staten Island Serpentinite is positioned on Cameron's line which defines the tectonic boundary of the western part of the Appalachian core zone. Lyttle and Epstein (1987) stratigraphically place (Figure 2) the Staten Island meta-peridotite and other related serpentinite bodies on Cameron's line conformably above member C of the Manhattan Schist but suggest that most of the peridotite lies east of Cameron's line at the base of the Hartland terrain.

Petrology

Germine (1982), Germine and Puffer (1981) and Puffer and Germine (1994) methodically examined samples of the Staten Island Serpentinite from 27 localities. They determined that about 66% of the serpentinite is lizardite and 27% chrysotile. Other predominate minerals are olivine, chromite, and magnetite together with minor talc, anthophyllite, relic pyroxene, chlorite, and magnesite. They concluded that the protoliths of the serpentinite body were harzburgite and dunite. The Staten Island serpentinite has been divided into two zones by Behm, (1954): a highly sheared outer serpentinite characterized by an abundance of talc, anthophyllite, and magnetite, and a relatively massive, under formed inner zone composed largely of partially serpentenite peridotite. Although now largely a serpentinite, the protolith was a peridotite that was serpentinized before or during Taconic tectonic emplacement. If the protolith was an ophiolite, most hydration to serpentine was probably introduced by heated deep marine water circulation near a spreading center. Most samples of peridotites dredged from the ocean floor are largely hydrated to serpentine and contain over 10% H_2O. Recent chemical analyses of selected Staten Island Serpentinite are shown in Tables 1 and 2 (Benimoff, 2015).

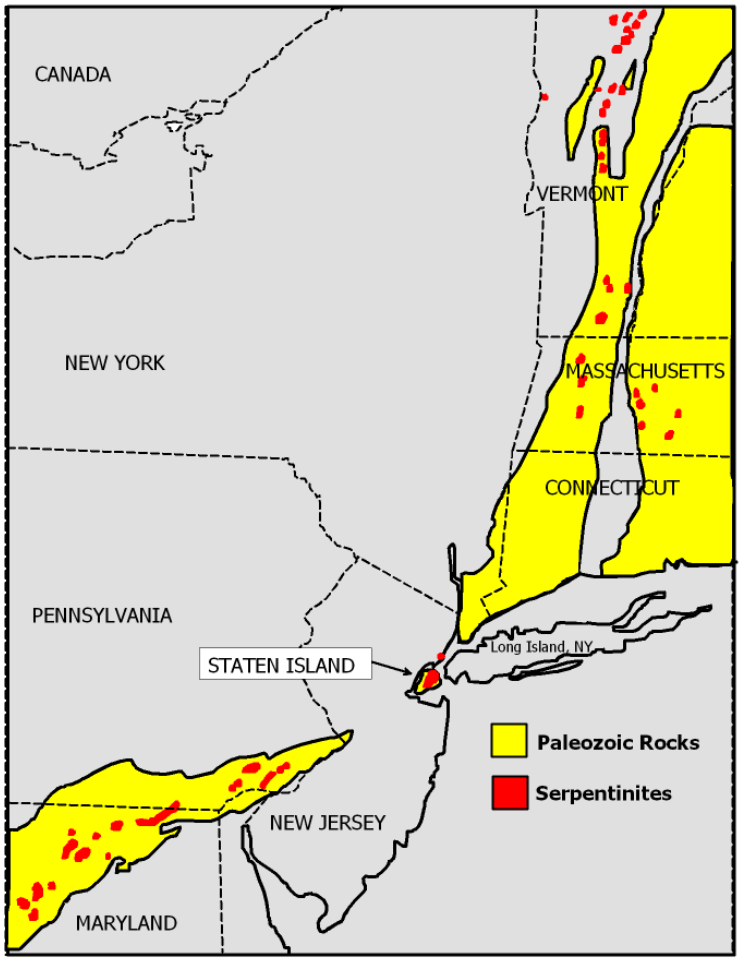

Figure 2: Serpentinite occurrences in the central and northern Appalachians appearing on the USGS "Tectonic map of the United States (modified from Puffer, 1996)

Clues as to the original protolith are found in some of the olivine rich samples, particularly from the North – Central portion of the ultramafic body. Unaltered pyroxene is rarely observed in any of the rock but phenocrysts of pyroxene that have been partially or completely altered to inter growths of chlorite, talc and oxide are common in some of the massive serpentinite. These altered pyroxene phenocrysts make up about 15% of subsamples and indicate that such rock was a harzburgite. Most samples of massive serpentinite where primary igneous textures are preserved, however, do not contain evidence of pyroxene and are probably dunite.

TABLE 1: Chemical Analyses of Serpentinite (Benimoff, 2015)

	Major Oxides (wt.%)										
	RR01	RR02	RR03	RR04	RR05	27801	27802	27803	27804	103401	103402
SiO2	36.40	32.95	37.08	34.27	36.27	37.08	37.77	34.26	37.11	37.33	35.83
TiO2	0.002	0.002	0.001	0.002	0.002	0.002	0.001	0.004	0.004	0.005	0.006
Al2O3	0.31	0.06	0.21	0.07	0.28	0.58	0.45	0.19	0.48	0.56	0.35
FeO*	6.63	5.60	6.23	6.29	6.70	6.52	6.14	6.45	6.22	6.39	6.71
MnO	0.087	0.086	0.094	0.084	0.085	0.101	0.085	0.101	0.087	0.099	0.090
MgO	39.97	42.11	38.79	40.68	39.74	39.12	38.25	39.78	38.02	38.89	39.82
CaO	0.02	0.01	0.04	0.01	0.02	0.06	0.18	0.02	0.22	0.06	0.02
Na2O	0.00	0.00	0.00	0.00	0.00	0.00	0.00	0.00	0.00	0.00	0.00
K2O	0.00	0.00	0.00	0.00	0.00	0.00	0.00	0.00	0.00	0.00	0.01
P2O5	0.000	0.000	0.000	0.000	0.000	0.000	0.000	0.000	0.000	0.000	0.000
LOI %	15.49	17.95	16.10	17.11	15.51	15.56	15.65	17.16	15.84	15.52	15.78
SUM	98.92	98.76	98.56	98.52	98.61	99.02	98.53	97.96	97.98	98.86	98.62
	Trace elements (ppm)										
Ni	2270	2706	2136	2373	2303	2198	2027	2264	2030	2171	2338
Cr	2344	1583	2505	3395	2015	2542	2398	2397	2519	1998	2145
V	21	9	13	12	22	21	22	13	27	23	21
Ga	0	0	1	1	0	2	1	1	1	0	0
Cu	7	5	5	3	6	12	6	6	6	6	6

RR01 – RR05 RR in Figure 1; 103401-103402 RF in figure 1RF; 27801 -27803 Stop 2 in Figure 1

TABLE 2 : REE Analyses and Other Trace Elements in ppm (ICP-MS) Benimoff, 2015)

Sample ID	RR01	RR02	RR03	RR04	RR05	27801	27802	27803	27804	103401	103402
La	0.090962	0.03474	0.15	0.085	0.076	0.077	0.06	0.141	0.25	0.086	0.034
Ce	0.206854	0.09085	0.304	0.184	0.183	0.174	0.142	0.282	0.451	0.214	0.098
Pr	0.021078	0.00907	0.03	0.016	0.016	0.017	0.014	0.031	0.047	0.024	0.01
Nd	0.08032	0.03696	0.102	0.059	0.061	0.055	0.053	0.122	0.178	0.086	0.05
Sm	0.014897	0.00855	0.008	0.007	0.008	0.008	0.007	0.019	0.032	0.012	0.011
Eu	0.0036	0.00408	0.008	0.002	0.005	0.002	0.003	0.012	0.024	0.003	0.012
Gd	0.013665	0.01071	0.015	0.011	0.014	0.01	0.011	0.027	0.034	0.01	0.01
Tb	0.003096	0.00189	0.003	0.003	0.002	0.003	0.001	0.006	0.009	0.002	0.002
Dy	0.022994	0.01978	0.021	0.019	0.023	0.021	0.018	0.064	0.063	0.016	0.02
Ho	0.005885	0.00589	0.005	0.005	0.008	0.006	0.006	0.018	0.019	0.006	0.006
Er	0.020287	0.02672	0.019	0.017	0.028	0.021	0.024	0.072	0.067	0.021	0.022
Tm	0.003708	0.00431	0.004	0.003	0.006	0.005	0.005	0.015	0.013	0.004	0.004
Yb	0.028288	0.03972	0.026	0.026	0.044	0.044	0.038	0.122	0.107	0.033	0.033
Lu	0.004632	0.00623	0.003	0.004	0.007	0.008	0.007	0.02	0.019	0.006	0.006
Ba	0.889996	0.51446	0.611	0.471	0.997	1.008	0.739	3.476	8.284	0.665	0.561
Th	0.046683	0.0231	0.041	0.037	0.042	0.038	0.035	0.036	0.052	0.046	0.025
Nb	0.032614	0.01118	0.028	0.142	0.027	0.028	0.021	0.05	0.073	0.036	0.008
Y	0.139294	0.17361	0.132	0.134	0.165	0.153	0.131	0.418	0.483	0.144	0.156
Hf	0.021136	0.00973	0.019	0.015	0.017	0.015	0.014	0.02	0.027	0.016	0.01
Ta	0.003095	0.00122	0.002	0.028	0.002	0.003	0.003	0.004	0.009	0.003	0.001
U	0.013377	0.00505	0.014	0.024	0.01	0.013	0.01	0.011	0.014	0.011	0.007
Pb	0.060827	0.06128	0.299	0.212	0.104	0.075	0.062	0.096	0.179	0.059	0.051
Rb	0.141584	0.26724	0.176	0.117	0.172	0.137	0.156	0.872	2.307	0.098	0.216
Cs	0.005796	0.00762	0.083	0.051	0.009	0.016	0.016	0.024	0.03	0.017	0.003
Sr	1.160683	0.28454	0.682	0.507	1.029	0.698	0.73	1.076	2.514	0.64	0.65
Sc	5.87434	1.86186	5.652	2.733	5.552	7.012	6.665	6.834	6.822	5.101	3.772
Zr	0.840324	0.3592	0.574	0.507	0.71	0.603	0.454	0.646	0.793	0.714	0.436

Ophiolite Emplacement

Most of the original olivine has been altered to serpentine but some samples contain as much as 50% olivine. The average olivine content of the Staten Island serpentinite is about 5% but it is absent from most samples. Where present, olivine typically occurs as relic anhedral micro – islands surrounded by serpentine that has replaced most of the individual grains or as larger grains thing by olivine. Further details of the petrology of the serpentinite are given in Behm (1954), Germine and Puffer (1981) and Puffer (1996). Puffer (1996) compares two mechanisms of serpentinite emplacement: Obduction of an ophiolite-suite member or a metamorphosed olivine cumulate zone in a layered gabbro magma chamber. Puffer (1996) supports the obducted ophiolite member since the serpentinite is associated with the Harland schist. Puffer (1996) concludes that the mode of emplacement of the New York area serpentinites is controversial but most evidence tends to favor Taconic obduction of the base of the Iapetus ophiolite sequence. Thus would force the placement of the New York area serpentinites into the

Taconic suture zone (Cameron's line) between the Hartland terrain and Manhattan C terrain. There is general agreement that the chemistry of olivine and spinel reflect the magmatic conditions of origin of highly serpentinized peridotite (Dick and Bullen, 1984; Arai, 1994; Kametesky et al., 2001: Metsger et al., 2002).

Recently Benimoff and Lupulescu (2008) sampled serpentinite samples from an excavation (Figure 2) for a shopping center in the Staten Island Serpentinite (N 40.5813° and W 74.1123°). The average composition of the serpentinite at this location is SiO_2 34.96, Al_2O_3 0.21, CaO 0.04, MgO 41.41, Na_2O<0.01, K_2O 0.03, Fe_2O_3 7.66, MnO 0.01, TiO_2 0.02, Cr_2O_3 0.44, and LOI 15.57 sum 100.36 wt. %. They reported Cr-spinel grains disseminated in the serpentinite; the grains are fractured and some are zoned with a Cr- rich core and Fe-rich rim. Electron microprobe analyses were used to compute the following empirical formulas for core (Fe^{+2} 0.70 Mg 0.28 Mn 0.02) Σ=1.00 (Cr 1.47 Al 0.39 Fe^{+3}0.14) Σ=2.00 O_4 and rim (Fe^{+2}0.88Mg 0.11Mn0.01) Σ=1.00 (Cr 0.7028 Al 0.01 Fe^{+3} 1.28) Σ=1.99 O_4 respectively. Cr numbers range from 94-99 in the rim to 79-87 in the core and the Mg numbers from 9-11 in the rim to 25-30 in the core indicating a probable dunite- harzburgite derivation. The core of the spinels analyzed in their study plot at the margin of the fore-arc peridotite region of Coish and Gardner (2004) in the (Cr/Cr+Al)sp vs. (Mg/Mg+Fe)sp diagram.

Recent work by Moores et al. (2000) describe a conflict in many ophiolite complexes that they call the "Ophiolite conundrum". The conflict is between "(1) structural and stratigraphic evidence for sea-floor spreading in a non–island arc environment and (2) geochemical evidence for derivation of magmas from highly depleted mantle similar to that found at present over subduction zones (suprasubduction zone settings)." Furthermore, oceanic paleogeography of the pre-suture ocean basin can be complex because dismembered ophiolitic rocks are associated with both MORB and arc-like igneous rocks (Tankut, et al. 1998). Ophiolite complexes can be divided into either Tethyan or Cordilleran (Moores et al. 2000; Wakabayashi and Dilek, 2003).

Coish and Gardner (2004) studied olivine samples from the meta-peridotite of the Vermont Appalachians in order to evaluate whether they were indeed parts of ophiolites, and if so in what tectonic environment they might have formed. They concluded through remnant olivine and chromite chemistry, that the peridotites probably formed in the fore- arc of an early Ordovician subduction zone. In their study they plotted Fo compositions of olivine against Cr/(Cr+Al)sp. It is clear that their Fo compositions fall mainly within the mantle array. They concluded that this represents conditions before serpentinization and regional deformation. Furthermore, they state that "the small Fo range is typical of residual peridotite, particularly harzburgite and dunite, and unlike cumulate rocks which tend to show lower Fo contents" (Arai, 1994). Their geochemical analyses on olivine and spinel support the hypothesis that their peridotites formed as highly-depleted mantle residues and they probably formed in a fore-arc, suprasubduction zone during the early Paleozoic. The data suggest that this serpentinite body probably formed in the same way as that described by Coish and Gardner (2004) for the serpentinite in the Vermont Appalachians namely in a fore-arc suprasubduction zone (Figure 3).

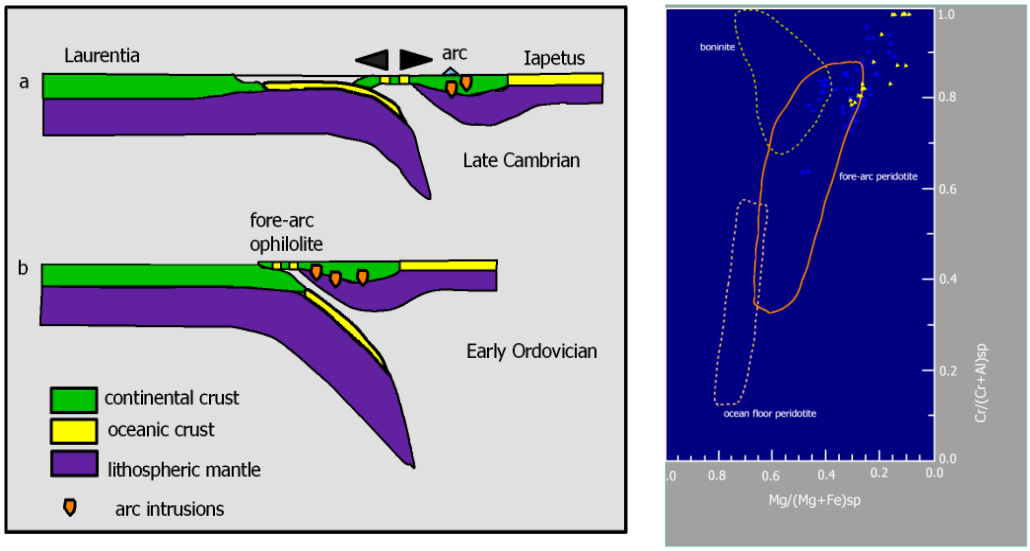

Figure 3 left: Modified from Coish and Gardner (2004). Figure 3 right: modified from Coish and Gardner (2004); Yellow triangles - chromian spinel from Benimoff and Lupulecu (2008). (+) Vermont (Coish and Gardner, 2004); Also shown are fields for ocean floor Peridotite (Dick and Bullen, 1984; Arai 1994b) harzburgite and dunite from hole 779A in the Mariana forearc (Parkinson And Pearce, 1998), and boninites (Arai, 1994a; Barnes and Roeder, 2001). Note that Cr-spinel compositions (Benimoff and Lupulecu, 2008) from the core plot within field of fore-arc peridotite

However, the occurrence of a suprasubduction zone peridotite in the Northern USA Appalachians (Coish and Gardner, 2004) is not clear evidence that the Staten Island serpentinite is a Cordilleran type. Puffer (2013) presents evidence the Staten Island ophiolite resembles the Wakabayashi and Dilek (2003) interpretation of a Tethyan ophiolite more closely than a Cordilleran type. Evidence includes the fact that the Hartland occurs above the Staten Island ophiolite (Figures 2 and 3). If the Hartland is interpreted as an accretionary complex is should instead exist beneath the ophiolite (Figure 4) to fit the Cordilleran description. Puffer (2013) also points out that the petrologic characteristics of undisputed accretionary complexes such as the Franciscan Formation of California are much different than Hartland rock. However, the issue is probably not settled.

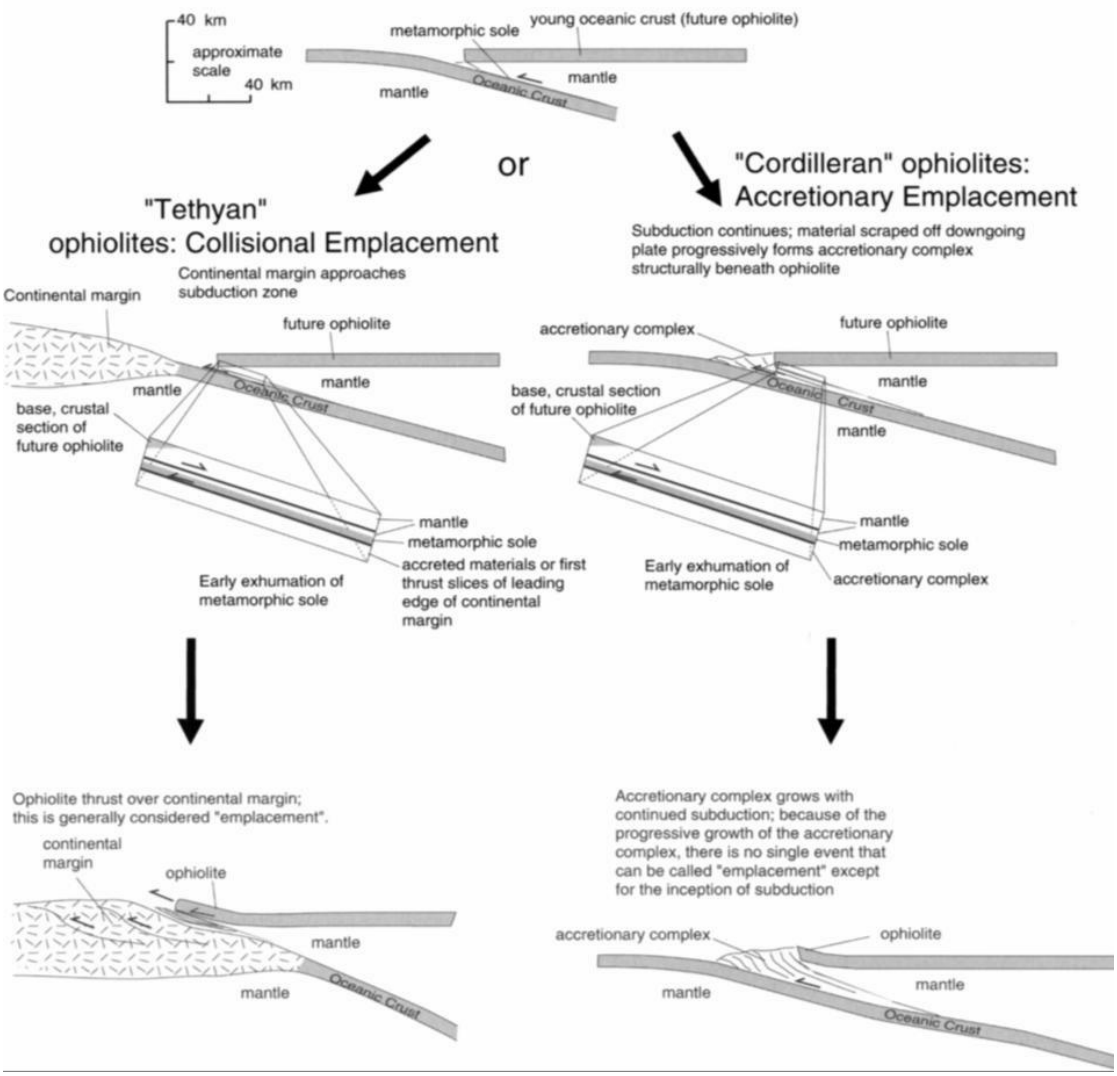

Figure 4. After Wakabashi and Dilek (2003): Emplacement of Tethyan and Cordilleran ophiolites. It should be noted that if a continental margin is attached to the plate subducting beneath a Cordilleran ophiolite, such an ophiolite may eventually be thrust over a continental margin, 'converting' it to a Tethyan-type ophiolite.

Further Geochemical Studies

Extended trace element patterns (figure 5) are characterized by a strong enrichment in Pb and a negative anomaly in Nb and Ti.

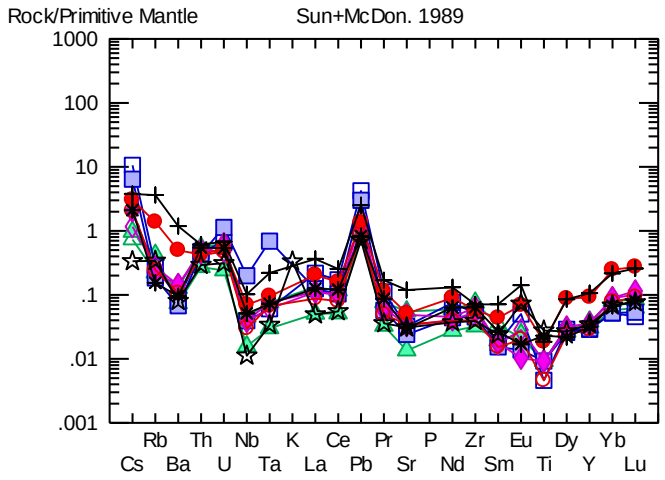

Figure 5. Mantle Normalized spider diagram (Sun and McDonough, 1989) of all samples from Table 2.

Three types of serpentinites are present in subduction zone, namely abyssal serpentinites, mantle wedge serpentinites and subducted serpentinites (Deschamps et. Al, 2013). Benimoff (2015) reported that most of the specimens of this study plot (La/Yb vs. Yb; U vs. Yb) in the abyssal serpentinite field(figure 6).

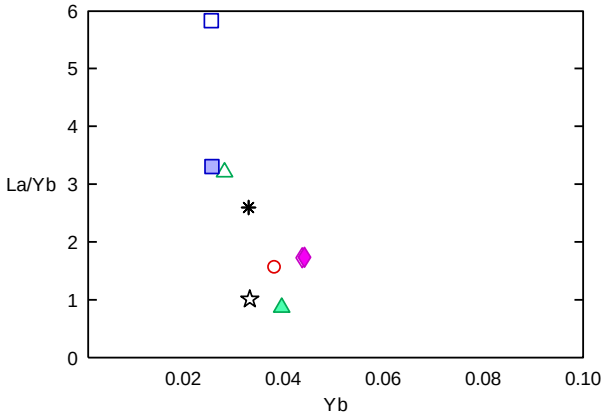

Figure 6 Serpentinites from this study plotted in La/Yb vs. Yb. These samples plot in the abyssal serpentinite field of Deschamps et al. (2013).

The Palisades Diabase on Staten Island at the Graniteville Quarry Park

Recent details on the Palisades Sill can be found in Puffer et al. (2010) and Puffer (2013). It is an exceptional occurrence wherein one can observe the parent of an igneous rock adjacent to that igneous rock. This is the case at the Graniteville Quarry Park (Stop 1) on this field trip where marginal fusion of a xenolith of sodium-rich Lockatong argillite enclosed in the basaltic magma of the Palisades sill resulted in coexisting silicic and mafic melts. This phenomenon was studied in detail by Benimoff and Sclar (1984) and Sclar and Benimoff (1993), and a summary of these studies is presented below. A xenolith of Lockatong argillite is exposed in the Palisades diabase in the Graniteville Quarry Park in Staten Island.

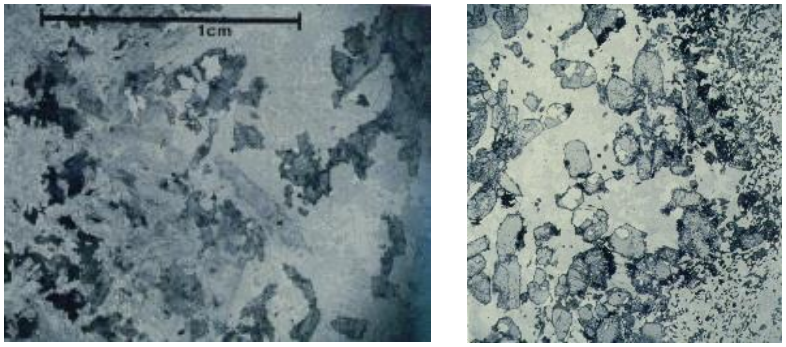

Figure 7: Photomicrographs of the Diabase Trondhjemite contact (right) and the Trondhjemite – Xenolith contact (left)

The xenolith has been recrystallized to a hornfels. It is a vertically dipping slab, 0.3 to 0.5m wide, and some 30 m long. The xenolith strikes N 30°W. The bottom of the xenolith is not exposed. Benimoff and Sclar (1984) concluded that the xenolith was derived from the Lockatong formation below the sill. Between the diabase and the hornfelsed xenolith is a sharply bounded interface zone of coarse-grained igneous rock (Figure 7). The interface zone ranges from 5 to 12 cm in thickness and completely surrounds the xenolith. They have categorized the coarse-grained rock of the interface zone as a melanocratic pyroxene trondhjemite.

The diabase at Graniteville is composed dominantly of plagioclase ($An_{61}Ab_{38.8}Or_{0.2}$) and augite ($En_{34-44}Fs_{17-31}Wo_{35-42}$) (Benimoff and Sclar, 1984). The augite contains exsolution lamellae of pigeonite on (001), and typically exhibits simple contact twinning on (100). A granophyric intergrowth of quartz and K-feldspar is present in minor amounts. Grains of titanomagnetite with oxidation lamellae of ilmenite and discrete grains of ilmenite are common.

The trondhjemite is composed dominantly of quartz-albite granophyre in which are enclosed large discrete crystals of albite and Ca-rich clinopyroxene (Benimoff and Sclar, 1984). Minor constituents include interstitial calcite, titanite, ilmenite, optically homogeneous titanomagnetite, nickelian and cobaltian pyrrhotites, apatite, and zinc sulfide (Sclar and Benimoff, 1993). The modal mineral percentages are clinopyroxene 38, albite 38, quartz 18, titanite 2.7, calcite 1.3, and opaques 2.0.

The xenolith is now a hornfels and exhibits a granoblastic texture. The hornfels is composed dominantly of albite and quartz and subordinantly of calcite, titanite, apatite, ilmenite, and actinolite. The modal mineral percentages are albite 66, quartz 30, titanite 2.3, calcite 0.9, apatite 0.5, and actinolite 0.3. The bulk composition of the xenolith is variable which is not unexpected for a rock of sedimentary origins. Normative albite ranges from 56.4 to 80.2 wt.%, whereas normative quartz ranges from 7.0 to 35.4 wt.%.

A core of the three contiguous rocks was cut into 1mm slabs and each slab was analyzed for major, minor and trace elements (Benimoff and Sclar, 1996). Concentration vs. distance profiles were constructed in order to see the distribution of these elements in the three contiguous rocks. This is the way nature distributed these elements. Further diffusional studies are planned.

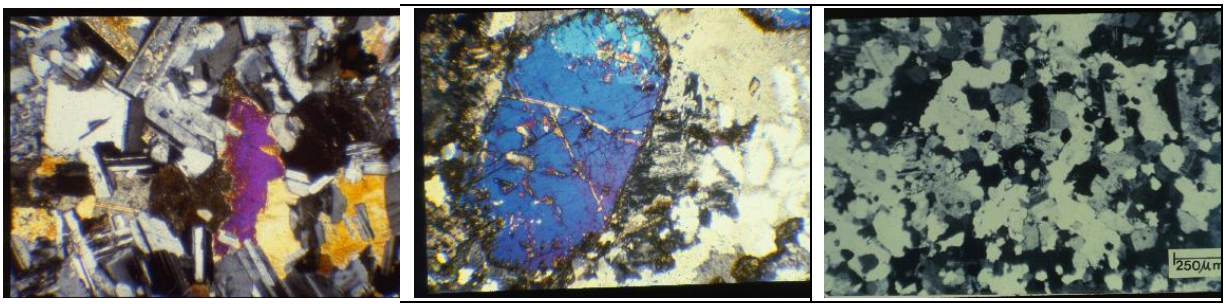

Figure 8. Photomicrographs of diabase, trondhjemite and xenolith

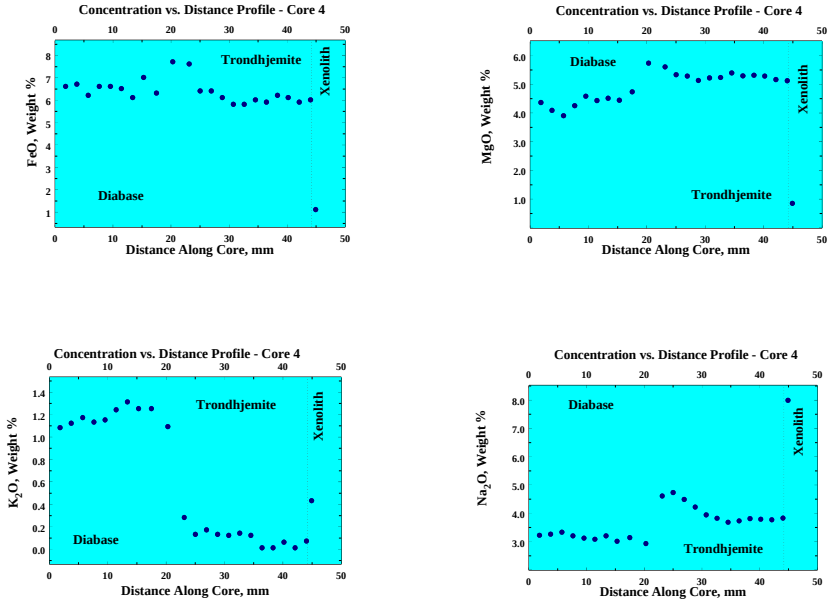

Figure 9 Concentration vs. Distance profiles. The diabase – trondhjemite contact is at 22mm in the core.

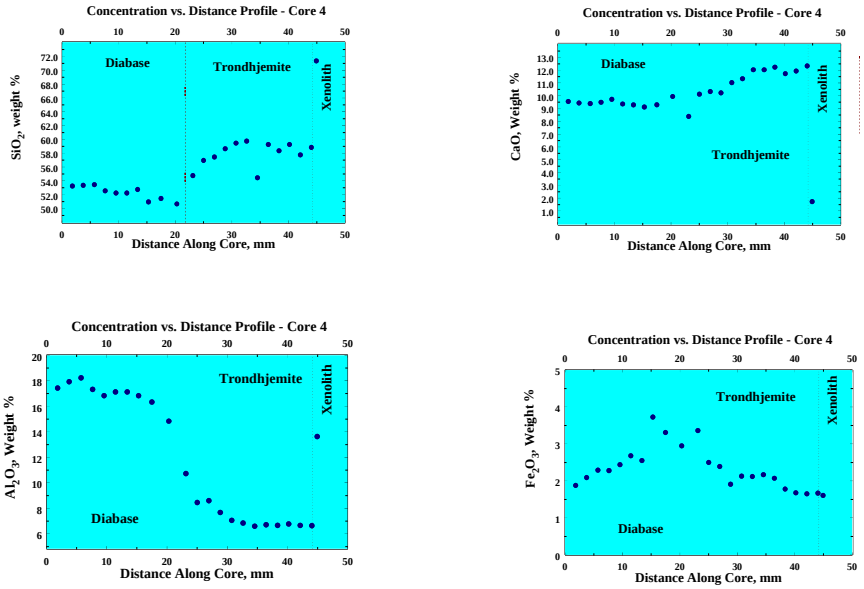

Figure 10 Concentration vs. Distance profiles. The diabase – trondhjemite contact is at 22mm in the core.

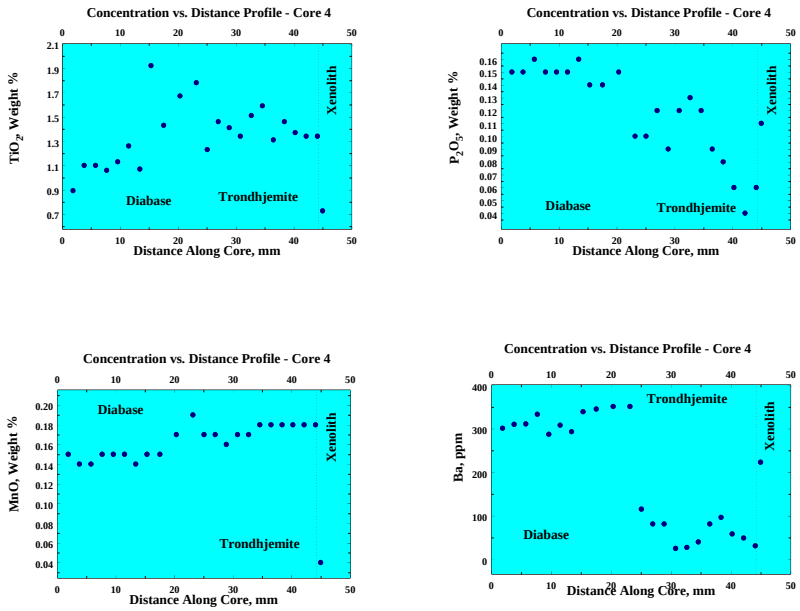

Figure 11 Concentration vs. Distance profiles. The diabase – trondhjemite contact is at 22mm in the core.

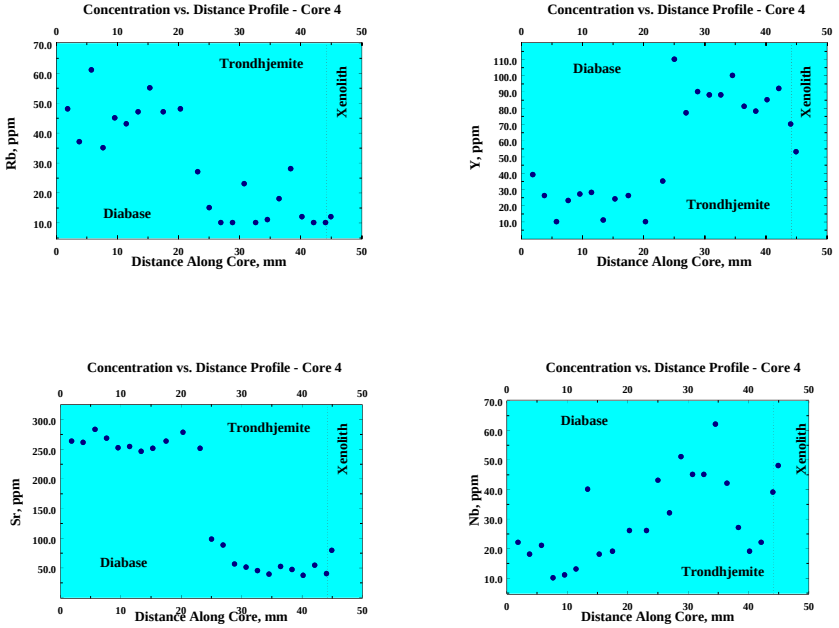

Figure 12 Concentration vs. Distance profiles. The diabase – trondhjemite contact is at 22mm in the core.

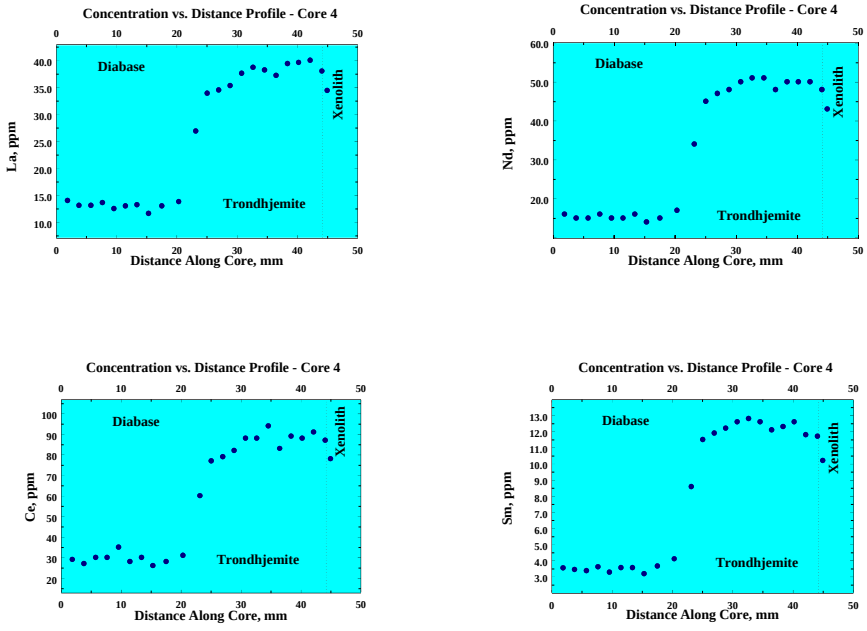

Figure 13 Concentration vs. Distance profiles. The diabase – trondhjemite contact is at 22mm in the core.

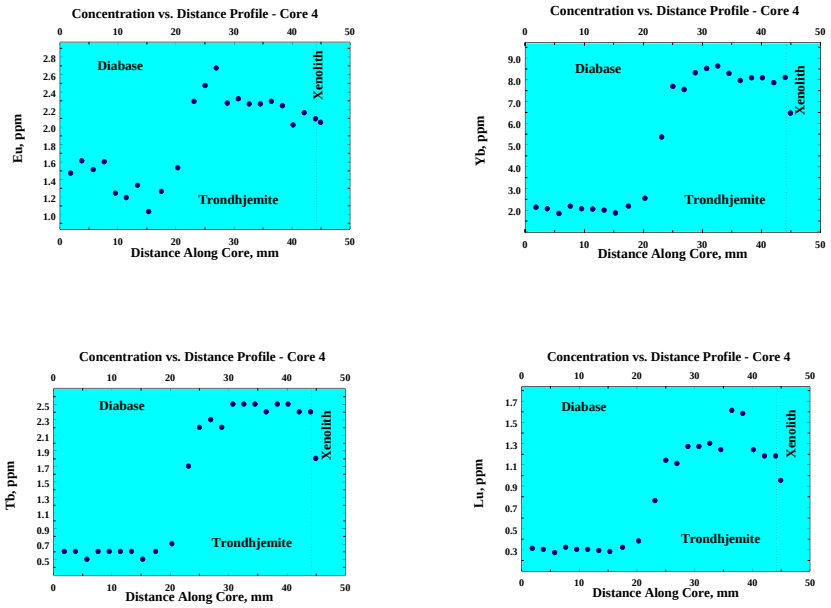

Figure 14 Concentration vs. Distance profiles. The diabase – trondhjemite contact is at 22mm in the core.

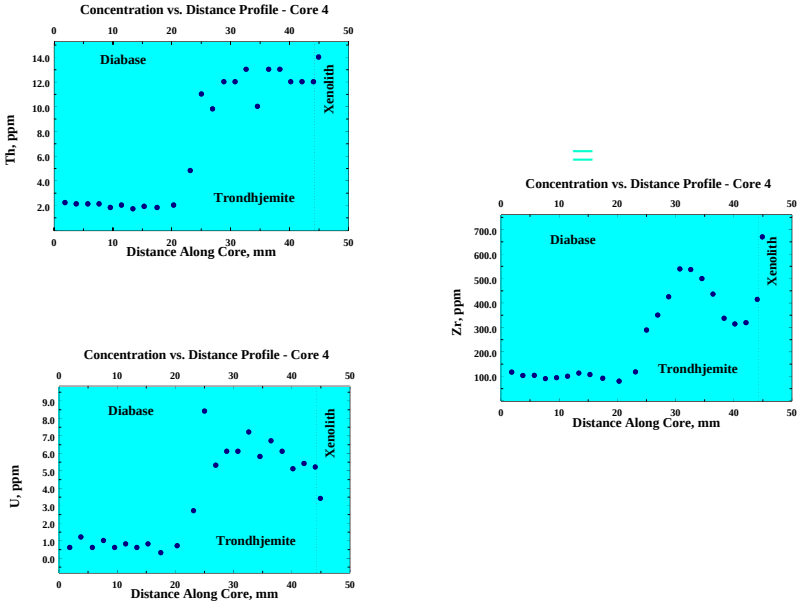

Figure 15 Concentration vs. Distance profiles. The diabase – trondhjemite contact is at 22mm in the core.

Benimoff and Puffer (2005) in their tri-modal fusion study of meta-argillites in the Palisades sill determined that there is virtually no mixing of the fusion zone melt with the early Jurassic diabase intrusion beyond about 1 mm from the contact and 2) assuming a typical sodic argillite xenolith, the iron, magnesium, and calcium depletion of the unbelted portion of the xenolith is balanced by enrichment of these elements in the fusion zone. The Palisades diabase disk cut 2 mm from the contact with the fusion zone is chemically the same as the disk cut 20 mm from the contact and is the same as a Palisades diabase sample collected 0.5 m from the contact. For example the 10 samples of Palisades diabase sampled within 20 mm of the contact maintain values of 1.3-1.5 percent K_2O, 291-346 ppm Ba, and 248-269 ppm Sr in distinct contrast to the0.01-0.08 percent K_2O, 10-70 ppm Ba, and 31-75 ppm Sr content of the fusion zone.

ACKNOWLEDGMENTS

Charles B. Sclar(diseased) contributed to a good part of this work on the Graniteville Quarry Park studies. Some of the work on the serpentinite studies comes from Benimoff and Puffer (2013).

REFERENCES CITED

Arai, S., 1994, Characterization of spinel peridotites by Olivine-Spinel compositional relationships; review and interpretation. Chemical geology, 113, 191-293.

Behm, J.J, 1954, The petrology of the Serpentinite of Richmond County (Staten Island). N.Y. Proceedings of the Staten Island Institute of arts and Sciences, V 16, p1-39.

Benimoff, A. I., 2015, Further studies of the Staten Island Serpentinite. Goldschmidt Abstracts, 2015 258.

Benimoff, Alan I. and Puffer, John H., 2005, Tri-modal fusion of meta-argillites along margins of early Jurassic diabase intrusions, New Jersey and New York. *Northeastern Geology and Environmental Sciences,* v. 27, no. 4, p. 265-275.

Benimoff A.I, and Puffer, John H., 2013, Overview of the Staten Island Serpentinite in Benimoff A.I. ed. , Igneous Processes During the assembly and Breakup of Pangaea: Northern New Jersey and New York City. 30th meeting of the Geological Association of New Jersey.

Benimoff, A. I., and Puffer, J.H., 2007, Effects of metasomatism and host rock fusion on the chemistry of early Jurassic palisades diabase in the Newark basin, *Geological Society of America Abstracts with Programs,* Vol. 39, No. 1, p. 94*

Benimoff, Alan and Lupulescu, Marian V., 2008, Zoned accessory Cr-spinel in the Staten Island serpentinite from a new Richmond road outcrop in Staten Island, NY, *GSA Abstracts with Programs* Vol. 40, No. 2

Benimoff, A. I. and Sclar, C. B., 1984, "Coexisting Silicic and Mafic Melts Resulting From Marginal Fusion of a Xenolith of Lockatong Argillite the Palisades Sill, Graniteville, Staten Island, New York" *American Mineralogist*, 69, 1005-1014.

Benimoff A. I., and Sclar C. B., 1996, Natural Cationic Diffusion Profiles Across a Liquid-Liquid Boundary Between Chemically Dissimilar Coexisting Magmas: a Trondhjemite-Diabase Interface *EOS, Transactions American Geophysical Union*, paper V21A-04.

Coish R.A. and Gardner P., 2004, Suprasubduction zone peridotite in the Northern USA Appalachians: Evidence from mineral Composition. Mineral. Mag. Vol. 64(4) 699-708.

Crosby, W.O., 1914, Physiographic relations of serpentine with special reference to the serpentine rock of Staten Island. Journal of Geology 22, No. 6, 582-592

Dick H.J.B and Fisher R.L., 1984, Mineralogical studies of the residues of mantle melting ; Abyssal and alpine peridotites. In J. Korbprobst, ed. Kimberlites II: The mantle and crust mantle relationships. 295-308. Elsevier, Amsterdam.

Deschamps, F., Godard,M., Guillot,S., and Hattori, K., 2013, Geochemistry of Subduction Zone serpentinites: A Review, Lithos 178, 96-127.

Dick H.J.B and Bullen T., 1984, Chromian spinel as a petrogenetic indicator in abyssal and Alpine –Type peridotites and spatially associated lavas. Contributions to Mineralogy and Petrology 86, 54-76.

Germine, M., 1982, Asbestiform serpentine and amphibole group minerals in the northern New Jersey area: Newark, New Jersey. Rutgers University, Master's thesis, 239 pp.

Germine, M., and Puffer, J. H., 1981, Distribution of asbestos in the bedrock of the northern New Jersey area: Environmental Geology, v. 3, p. 337-351.

Hollick C.A., 1909, notes in connection with specimens recently obtained from serpentinites of Staten Island N.Y. New York Academy of Sciences Annals, V19, p 315-317.

Kametsky, V.S., Crawford, A.J.and Meffre, S., 2001, Factors controlling chemistry of magmatic spinel: an empirical study of associated Olivine, Cr-spinel and melt inclusions from primitive rocks. Journal of Petrology, 42, 655-671

Lyttle, P and Epstein, J., 1987, Geologic Map of the Newark 1° x 2°Quadrangle, New Jersey, Pennsylvania and New York. USGS map I-1715.

McPhee, John, 1993, Assembling California, Farrar, Straus and Giroux, NY, 302 pages

Metsger, E.P., Miller, R.B. and Harper, G.D., 2002, Geochemistry and tectonic setting of the ophiolitic Ingalls Complex, North Cascades, Washington: Implications for correlations of Jurassic Cordilleran ophiolites. Journal of Geology 110, , 543-560.

Miller, W.H., 1970, Structural Geology and Tectonism of the Staten Island Serpentine,; Brooklyn College masters Thesis 67pages.

Moores, E.M., Kellogg, L.H. and Dilek, Y., 2000, Tethyan ophiolites, mantle convection, and tectonic historical contingency": A resolution of the "Ophiolite conundrum in Dilek Y, Moores E.M., Elthon D, and Nicolas A eds. Ophiolites and Oceanic Crust: New Insights from Field Studies and the Oceanic drilling program: Boulder Colorado, Geological society of America Special Paper 349, p 3-12.

Puffer, J. H., 1996, *in* Benimoff, A.I., Serpentinites of New York City and Vicinity, *in* Field trip Guide for the 68th Annual Meeting of the New York State Geological association, p.157-176.

Puffer, J. H., 2013, Igneous Processes During the assembly and Breakup of Pangaea Northern New Jersey and New York City: in Benimoff A.I. ed. , Igneous Processes During the assembly and Breakup of Pangaea: Northern New Jersey and New York City. 30th meeting of the Geological Association of New Jersey.

Puffer, J. H., and Germine, M., l994, The Staten Island Meta-Peridotite: *in* Benimoff, A.I., ed., Geology of Staten Island, New York, Field Guide and Proceedings, Geological Association of New Jersey, p. 1-25.

Puffer, J. H., Steiner, J.C., Block, K. and Benimoff, A.I., 2010, The Timing, Layering, Comagmatic Basalt flows, Granophyres, trondhjemites, and magma Source of the palisades intrusive System in Benimoff, A.I., ed., Field Trip Guidebook for the 82nd meeting of the New York State Geological association.

Sclar, C. B. and Benimoff, A. I., 1993, An Occurrence of Magmatic Sphalerite, *The Canadian Mineralogist,* 31, 3 691-694.

Sun, S., and McDonough, W. F., 1989, Chemical and isotopic systematics of oceanic basalts: Implications for mantle composition and processes, in Saunders, A. D., and Norry, M. J., eds., Magmatism in the ocean basins: Geological Society Special Publication, v. 42, p. 313-345.

Tankut, A., Dilek. Y and Önen, 1998, Petrology and geochemistry of the neo-Tethyan volcanism as revealed by the Ankara mélange, Turkey Journal of Vulcanology and Geothermal Research 85, 265-284

Wakabayashi, J. and Dilek, Y., 2003, What constitutes 'emplacement' of an ophiolite?" Mechanisms and relationship to subduction initiation and formation of metamorphic soles. In DILEK, Y. & ROBINSON P. T. (eds) Ophiolites in Earth History. Geological Society, London, Special Publications, v. 218; p. 427-447.

Yersak, T.E., 1977, Gravity Study of Staten Island and vicinity, Rutgers University, NewBrunswick, NJ Masters Thesis.

FIELD GUIDE AND ROAD LOG

DATE: SUNDAY, October 2, 2016
MEETING POINT: Graniteville Quarry Park

From NJ take the Goethals Bridge (I-278 EAST) and exit at Forest Avenue, make left turn onto Forest Avenue; drive 1.4 miles and park on right side south side of Forest Avenue between Van Name and Simonson Avenues meet at sign for Graniteville Quarry Park.

Meeting point Coordinates: Latitude +40.624689° ; Longitude -74.153697
Meeting Time: 9:00 AM

STOP 1. Xenolith fusion (trondhjemite) at Graniteville Quarry Park , Staten Island, NY

At this stop we will examine a xenolith of argillaceous Lockatong Formation enclosed in Palisades diabase that has undergone partial fusion to yield a pyroxene trondhjemite. The sodium-rich slab-like xenolith of argillite is 30 m long,, 0.5 m thick and strikes N 30° E with a vertical dip. The xenolith was derived from Lockatong located below the sill. One could think of this as ancient divergent plate boundary.

Distance in Miles			
Cumulative	Point to point		Route Description
0	0.3		Right turn on willow Road West
0.4	0.1		Enter NY 440 South
1.1	0.7		Bear right onto ramp for I-278 East
1.6	0.9		Enter I-78 east
3.3	1.7		Take Exit 12 Todt Hill Road
3.5	0.2		Right Turn onto Todt Hill road
3.6	0.1		Left Turn onto Lightner Avenue
3.7	0.1		Right Turn onto Melhorn Rd.
3.7	0.0		Park on Melhorn Road. +40.608940°; -74.11433° we will meet here. We will then walk east on Lightner Avenue and take the dead end road on the right. Proceed on trail downhill and take the trail on the left, proceed uphill and proceed north to outcrop. This is a filled in road cut for a now de-mapped road. I-278 is to the north. Do not enter I-278!

STOP 2: The Staten Island Serpentinite in the I - 278 Road Cut

This is an outcrop of Staten Island serpentinite that was emplaced during the Taconic Orogeny, during the assembly of Pangaea. The serpentinite was emplaced as an ophiolite along a plate suture between an island arc (Hartland Terrane) and sediments accumulating along the Laurentian continental margin(Manhattan schist). The serpentinite is composed of lizardite, chrysotile, antigorite and Olivine. chromite, magnetite, anthophyllite, magnesite and other accessory minerals. One could think of this as an ancient convergent plate boundary.

TRIP B2: NATURALLY OCCURRING FILTRATION SYSTEMS SEQUESTERING METAL CONTAMINANTS FROM HISTORICAL TAILING WASTES AT THE STERLING LAKE SMELTER COMPLEX, HUDSON HIGHLANDS, NEW YORK

SIVAJINI GILCHRIST
School of Environmental and Sustainability Sciences, Kean University, Union, NJ 07083

ALEXANDER E. GATES
Earth and Environmental Sciences, Rutgers University, Newark, New Jersey 07102

INTRODUCTION

Mining History

Over 15 million people in New York, New Jersey, Pennsylvania and Connecticut depend on the Highlands Region's (Fig. 1a) 800,000 plus acres of forested watershed for drinking water (Porter, 2008). Large-scale iron mining operations from 1730 to the early 20th century (Smock, 1889; Ransom, 1966) exposed the Highlands to environmental degradation. Although the region is recovering naturally, tailing wastes are still visible and chemically reactive impacting soil and water quality. In addition to iron mining, the Highlands were also exploited for sulfide ores (Gilchrist et al., 2009) but volumetrically spoils from iron mining operations were far greater than sulfide mining operations, the Sterling Lake iron smelter complex is one such example. This area was denuded of its forest to support the smelting operations. Waterfront property owners extract the lake water for potable use. Despite visible tailing wastes chemically decaying in the vicinity, water pH was found to be neutral when measured during a study of this site (Gilchrist et al., 2011). How is this possible if heavy metals are abundant in these tailing wastes?

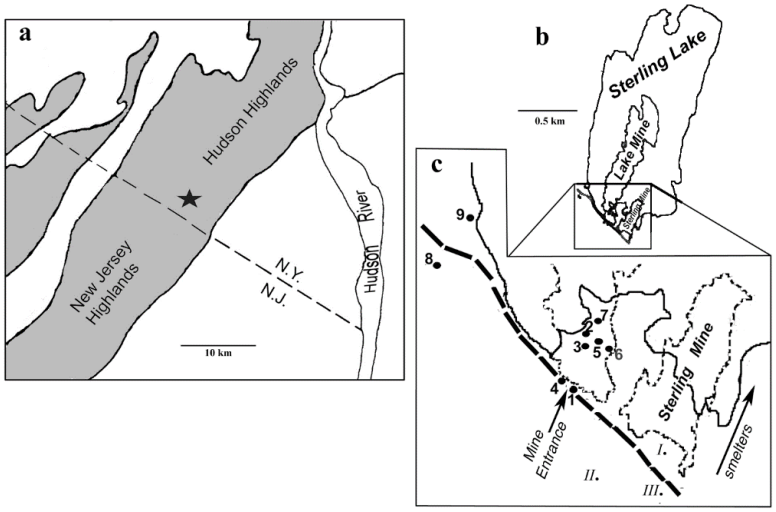

Fig. 1 (a) Study site, (b) Lake Mine and Sterling Mine represented by broken lines. Location of core sample collections indicated by numbered circles. Locations of water sample collections indicated by roman numerals (*I* stream water, *II* still water, *III* spring water). Grab and ash samples collected randomly around former smelter locations. Dashed line represents road. (Adapted from Gilchrist et al., 2011).

Soil cores and water samples were obtained from several locations at the site (Fig. 1b) and chemically analyzed to determine the extent of soil contamination. Geochemical results of the recovered soil cores were compared to regulatory standards and to background soils for the eastern USA (New York State Department of Environmental Conservation (NYSDEC) TAGM 4046, 2009) and the New Jersey Highlands soils (New Jersey Department of Environmental Protection & Energy (NJDEPE), 1993). Chemical analyses suggested that naturally occurring mechanisms are maintaining the neutral water pH. The Highlands Region is a desirable real estate for developers. It is hoped that obtaining answers to the natural recovery of an area impacted by past invasive destructive mining activities will fend off development to protect critical watersheds such as the Highlands region.

An active Panzhihua magnetite mining area in southwestern China yielded high concentrations of Ti, V, Cr, Mn, Zn, Cu, Pb and As in the area's soils (Yanguo et al., 2003) due to airborne depositions from mining and smelting activities. Elevated levels of Cd, Cu, Pb and Zn were found in another but sulfur-rich magnetite mine in central China (Zabowski et al., 2001). These limited studies show that magnetite mining operations can deliver significant metal contaminants to surrounding soils.

Site geology

This paper will provide a brief summary of the study conducted at the Sterling mines for purposes of the field trip scheduled for this conference. Detailed information can be found in Gilchrist et al. (2011). At this site, two abandoned iron mines belonging to the Sterling Lake group of iron mines in the Hudson Highlands of southeastern New York co-exist side by side (Smock, 1889; Hagner et al., 1963). Sterling Mine begins at the surface and continues under the lake (Colony, 1923; Hotz, 1953). The Lake Mine entrance begins at the surface and continues 1160 m out under the lake at a vertical depth of about 300 m below the lake surface (Colony, 1923; Hotz, 1953). Precambrian high-grade metamorphic and igneous crystalline rocks with embedded magnetite deposits are the primary rock types (Drake, 1984) at these sites. When mining operations ceased (1896 to 1921 (Ransom, 1966)) tailing wastes composed of calc-silicate gneiss, meta-volcanic gneiss, pegmatite and the magnetite ore were left abandoned and exposed to weather conditions. Ash and slag relics from surrounding historical furnaces located within the mining area are also visible.

Methods

Soil sampling

Detailed soil sampling method and analyses of soil cores, and water samples can be found in Gilchrist et al. (2011). Briefly, two sets of soil core samples were collected (Fig. 1b): Group A cores were collected at the most impacted areas from heavy mining activities and Group B core samples were collected at passive impacted areas. Each core was sub-sectioned, and prepared for ICP-OES analysis using the flux fusion method and acid digestion to determine chemical composition at various depths of the core (Fig. 2). Loss on ignition (LOI) analysis yielded soil organic matter content. Soil pH was measured using the slurry method (Eckert and Sims, 1995).

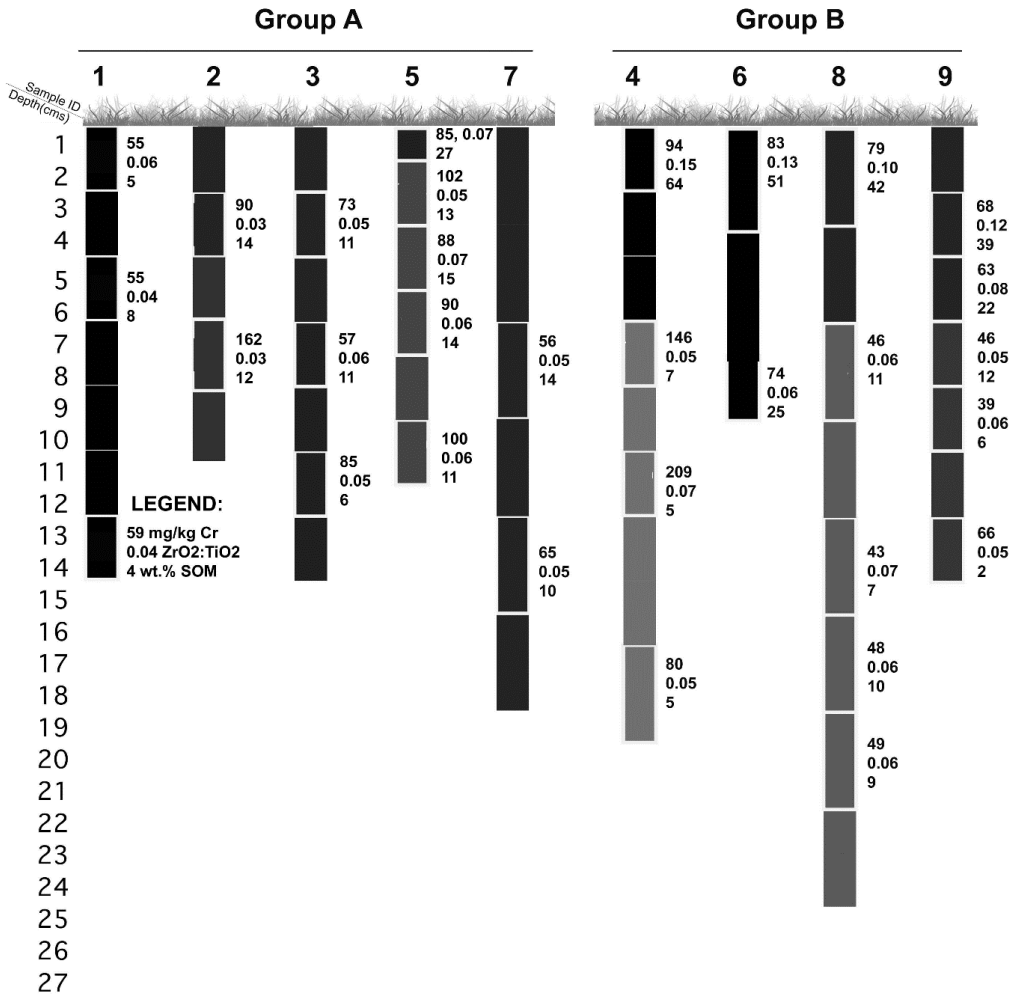

Fig. 2 Sample cores for Groups A and B. Values indicate Cr (mg/kg), ZrO2:TiO2 and SOM (wt%) in analyzed sub-sections. O-horizons are defined from 0–7 cm from the surface. (Adapted from Gilchrist et al 2011)

Rock standards, duplicates of these standards and laboratory blanks were used for precision analysis and recovery of elements in the standards. Results were within acceptable norms: laboratory blanks' values were less than 0.5wt % of any concentration measured for the field samples and recovery of the elements in the standards ranged 87 – 102%.

Water Sampling

An evaluation of metal concentrations in the water to determine whether these are being transported from the soils into the surface and groundwaters. Flowing water samples were collected from a stream flowing through Sterling Mine. Still water samples were collected from around the main entrance of Sterling Mine. Groundwater samples were collected from a spring that receives water through the

tailing piles (Fig. 1b). Collected samples were analyzed for heavy and trace metals by USGS laboratory in Denver, Colorado, using ICP-MS.

Determining metal source

Magnetite ($Fe^{+2}Fe^{+3}{}_2O_4$) and ilmenite ($Fe^{+2}TiO_3$) minerals are present at the site in the tailing piles and Cr can occur with these minerals (IETEG 2005). At Montclair State University, XRD was used to determine Cr-bearing minerals. When tailing piles oxidize and breakdown, Cr is released to the soils. Recalcitrant Cr-bearing minerals can also settle out into the slag and ash materials from ore smelting activities. Slag and ash wastes at the smelter complex were collected for Cr content determination.

To determine Cr content in the magnetite, samples were collected from magnetite-bearing waste rocks. Ilmenite, rare and less abundant than magnetite, was not studied for Cr content. At Montclair State University, samples of the collected magnetite minerals were subjected to a Vibrating Sample Magnetometer (VSM) to determine their purity. If pure, a characteristic hysteresis curve will be revealed.

Results and discussions

Soil characterization

At the most impacted areas (Group A), soil color ranged from dark grayish color to dark brown soils and at the less passively impacted areas (Group B) soil color ranged from very dark gray with yellowish brown and dark olive brown (Fig. 2). Several of the cores were enriched in soil organic matter i.e. greater than 5%, mostly in the top 7 cm from the surface. Whether the high SOM was a result of natural processes or contribution from charcoal-making activity during the mining era is unknown.

Soil pH

Soil pH values showed high spatial variability between Groups A and B and within each group (Table 1A). Sulfur contents were low in the soils and sulfate in waters were not significantly present, indicating sulfur minerals (Table 1B) are not prevalent or exist in insufficient quantities to contribute to soil acidity. It is thus believed that SOM may account for the soil acidity. Positive correlation of SOM with metals suggests retention of metals in soils as soluble chelates (Kabata-Pendias and Pendias, 1992).

Table 1A. Soil pH measurements of core samples. (Adapted from Gilchrist et al 2011)

	Group A cores					Group B cores			
	1	2	3	5	7	4	6	8	9
DI water	7.05	4.85	5.81	6.13	5.04	6.56	6.17	5.64	4.58
$CaCl_2 \cdot 2H_2O$ (0.01M)	5.91	3.9	4.46	4.76	3.95	5.69	4.79	4.53	3.65

Metals in soils

Cr, Ni and some major elements (i.e. Si, Ti, Al, Mg and P) exceed background soils of the New Jersey Highlands or the eastern USA (Table 1B). Group A soil samples showed higher concentrations of major metal-oxides than Group B soil samples. The concentrations were mainly in the O-horizons (Table 2). Iron was enriched in Group A soils, evident of slag and ash (Fe residuum rich) mixed into these soils.

Table 1B. Chemical composition of Groups A and B soil core samples. (Adapted from Gilchrist et al., 2011)

	Mean values[a]				EPA SSL[c] (residential)	Eastern USA[d] Background Soil Levels (NYSDEC)	NJDEPE[e] (Highland soils) Mean Values	World Soils[f] Median Values
	Group A (1,2,3,5 & 7)		Group B (4,6,8 & 9)					
Soil depth	0 – 6 cms	7 – 24 cms	0 – 6 cms	7 – 24 cms				
No. of sub-sections	(n = 8)[b]	(n = 8)	(n = 5)	(n = 11)				
Major Oxides (wt.%)								
Si	28.14	29.78	19.41	32.70	--[g]	--	--	28
Ti	0.48	0.52	0.31	0.43	--	--	--	0.4
Al	5.33	6.33	3.51	5.31	--	3.3	--	8
Fe	5.68	4.40	2.28	3.41	--	55 (max)	--	3.5
Mn	0.06	0.08	0.04	0.04	--	0.5 (max)	0.05	0.05
Mg	1.39	1.20	0.69	0.99	--	0.5 (max)	--	0.9
Ca	1.74	1.40	1.05	0.89	--	3.5 (max)	--	1.4
Na	0.87	1.00	0.61	0.88	--	0.8 (max)	--	1.0
K	0.97	1.12	0.62	1.01	--	4.3 (max)[h]	--	1.4
P	0.12	0.10	0.11	0.05	--	--	--	0.08
Trace Elements (mg/kg)								
Cr	79.80	84.30	77.31	76.99	230	40 (max)[h]	10	80
V	151.79	127.51	107.74	92.24	550	300 (max)	--	90
S (wt.%)	0.02	0.02	0.1	0.04	--	--	--	0.08
Zr	305.27	300.38	434.53	307.20	--	--	--	230
Ba	318.22	334.04	341.16	260.07	5500	600	--	500
Ni	52.96	51.74	45.49	45.62	1600	25 (max)	12	20

[a] Mean values of the analyte in all sampled sub-sections.
[b] n = number of sub-sections analyzed within the group.
[c] EPA SSL (soil screening levels, 2002) for residential soils. Cr value refers to total Cr.
[d] Eastern USA Background soil levels listed in NYSDEC TAGM 4046 (2009) for heavy metals.
[e] Soil data (n=17) extracted from counties (n=3) within the Highlands region compiled by NJDEPE (1993).
[f] World soil data compiled by Reimann and Caritat (1998).
[g] Dashed lines indicate no data available or not applicable because element is not considered a contaminant.
[h] New York State Background Levels also listed in NYSDEC TAGM 4046 (2009) for heavy metals.

Table 2. Mean concentrations of Cr, Oxides, SOM and divalent metals. Values in parentheses indicate correlation of oxides, SOM or divalent metals with Cr. (Adapted from Gilchrist et al 2011)

V	Cr (mg^{-kg})	Fe_2O_3 (wt.%)	Al_2O_3 (wt.%)	MnO (wt.%)	SOM (wt.%)	Ni (mg^{-kg})
Group A core samples (1,2,3,5 and 7)						
Upper soil sub-sections (0-6cms; n=8)	79.8	8.12 ***(0.17)***	10.07 ***(-0.49)***	0.08 ***(-0.28)***	13.37 ***(0.50)***	53.0 ***(0.52)***
Lower soil sub-sections (7-24cms; n=8)	87.1	6.29 ***(0.74)****	11.95 ***(0.92)*****	0.1 ***(-0.12)***	10.22 ***(0.32)***	51.74 ***(0.70)**
Group B core samples (4,6,8 and 9)						
Upper soil sub-sections (0-6cms; n=5)	77.31	3.26 ***(-0.66)***	6.63 ***(-0.92)***	0.05 ***(-0.49)***	43.59 ***(0.96)*****	45.49 ***((0.99)*****
Lower soil sub-sections (7-24cms; n=11)	77.0	4.87 ***(0.64)****	10.04 ***(0.49)***	0.05 ***(0.36)***	8.97 ***(-0.19)***	45.62 ***(((0.98)******

p-values: *p < .05. **p < .025. ***p < .005. ****p < .0005.

Chromium

Among the trace metals, Cr was more widespread than Ni and, hence, more emphasis was placed studying Cr source and its distribution at the site. Core samples contained elevated levels of Cr (Fig. 2). Group A soil profiled an irregular Cr distribution pattern while Group B showed Cr concentration in the top soils higher than at increasing depths. Passively impacted areas (i.e. Group B) are rich in SOM, which evidently resulted in a high correlation between SOM and Cr ($r = 0.96$, $p < 0.005$) in the O-horizons of these areas. The uppermost organic-rich layers at the site appear to act like a filtration/retention system for Cr, preventing vertical transportation. In the surface and ground waters, Cr concentrations were less than 1.5 ug/L, further evidence that the site's topsoil serve as filters and sinks for Cr released from the tailing piles and past ore-smelting operations. Manganese III, IV -(hydr)oxides are known to oxidize Chromium(III) to mobile Cr(VI) (Bartlett and James, 1979; Fendorf 1995; Stepniewska et al., 2004). But the absence of a negative correlation between Mn-Cr at the site indicates that some other factors may be inhibiting this association.

Chemical analysis for Cr in slag (100 mg/kg) and ash (200 mg/kg) materials confirmed these as possible Cr sources. Chromite can occur as an accessory mineral with magnetite ($Fe^{+2}Fe^{+3}{}_2O_4$) and ilmenite ($Fe^{+2}TiO_3$), which are present in calc-silicate rocks (Volkert and Drake, 1999), with magnetite more abundant (avg: 2.24–3.23wt.%) than ilmenite (avg: 1.1–1.37wt.%). If exposed to surface conditions, these chromite-bearing minerals can be a source of low-Cr in soils.

Two modes of Cr transportation from the sources are proposed: (1) Cr released from mining activities complexes with SOM and immobilizes as soluble chelates in the O-horizon, forming a first layer of a naturally occurring filtration/retention system; (2) Cr released in-situ in the lower soil horizons not complexed by SOM are sorbed and retained by soil-rich sesquioxides, forming a second layer of filtration/retention system.

Nickel

Several cores contained high Ni concentrations. Nickel retention is influenced by the abundance or lack of SOM, clay minerals and oxides in the soils (Nachtegaal and Sparks, 2003; Karathanasis and Pils, 2005). In this study, Ni showed a binding behavior similar to Cr. Nickel–SOM is strongly correlated when SOM is high relative to oxides, and vice-versa. A strong Ni-Fe correlation and a strong Ni-Al correlation were revealed in the lower layers of Group B soils as SOM decreases with depth. Ash contained 90 mg/kg of Ni compared to 50 mg/kg in the slag.

CONCLUSIONS

Against all odds, the once extensively mined area recovered with the return of the forest, a clean lake and streams with neutral pH waters. This is undoubtedly due to the naturally occurring filtration/retention systems at the site, both by the SOM and the sesquioxides in the lower soil horizons. The study was able to trace the Cr sources from the slag/ash to breakdown of the parent rock bearing magnetite and other Cr-bearing minerals. Whether these types of Cr filtration/retention systems can efficiently remove Cr in areas severely impacted by Cr contamination requires further study.

ACKNOWLEDGMENTS

The following institutions are acknowledged for laboratory, field and analytical assistance provided to this study: Montclair State University; USGS, Denver, CO; The Sterling Forest State Park, New York. The Dorr Foundation and the J.M. Kaplan Fund granted to Dr. Alexander Gates provided financial support for this work.

REFERENCES CITED

Bartlett, R.J., and James, B., 1979, Behavior of chromium in soils: III. Oxidation. J Environ Qual 8:31-35.

Colony, R.J., 1923, The magnetite iron deposits of southeastern New York. New York State Museum Bulletin, p. 249-250.

Drake, A.A., Jr. 1984, The Reading Prong of New Jersey and eastern Pennsylvania: An appraisal of rock relations and chemistry of a major Proterozoic terrane. In: Appalachians. Geological Society of America Special Paper. 194:75-109.

Eckert, D., and Sims, J.T., 1995, Recommended soil pH and lime requirement tests. In: Recommended soil testing procedures for the Northeastern United States, 2nd edn. Northeastern Reg Publ 493:16-18.

Fendorf, S.E., 1995, Surface reactions of chromium in soils and waters. Geoderma 67:55-71.

Gilchrist, S., Gates, A.E., Szabo, Z., and Lamothe, P.J., 2009, Impact of AMD on water quality in critical watershed in the Hudson River drainage basin: Phillips Mine, Hudson Highlands, New York. Environ Geol 57:397-409.

Gilchrist, S., Gates, A.E., Gorring, M., and Elzinga, E.J., 2011, Metal contamination and filtering in soil from an iron (magnetite) mine-smelter complex in the critical Hudson Highlands watershed, New York. Environ Earth Sci 63:1029-1041.

Hagner, A.F., Collins, L.G., and Clemency, C.V., 1963, Host rocks as a source of magnetite ore, Scott Mine, Sterling Lake, N.Y. Econ Geol 58:730-768.

Hotz, P.E., 1953, Magnetite deposits of the Sterling Lake, N.Y. Ringwood, N.J. area. US Geological Survey Bulletin, no. 982-F, p. 153-244.

Independent Environmental Technical Evaluation Group (IETEG), 2005, Chromium(VI) Handbook. Ed: Guertin, J., Jacobs, J.A., and Avakian, C.P. CRC Press, Florida, p. 4-6, 33-68.

Kabata-Pendias, A., and Pendias, H., 1992, Trace elements in soils and plants. 2nd edn. CRC Press, Florida, p. 66-67.

Karathanasis, A.D., and Pils, J.R.V., 2005, Solid-phase chemical fractionation of selected trace metals in some Northern Kentucky soils. Soil Sediment Contam 14:293-308.

Nachtegaal, M.,and Sparks, L., 2003, Nickel sequestration in a kaolinite-humic acid complex. Environ Sci Technol 37:529-534.

New Jersey Department of Environmental Protection & Energy (NJDEPE), 1993, Available via: http://www.state.nj.us/dep/dsr/soilrep.pdf. Accessed 15 Sept 2009.

New York State Department of Environmental Conservation (NYSDEC), 2009, Recommended soil cleanup objectives: heavy metals. TAGM 4046. Available via: http://www.dec.ny.gov/regulations/36325.html. Accessed 15 Sept 2009

Porter, D., 2008, Managing growth in America's communities. 2nd edn. Island Press, Washington DC, p. 122-124.

Ransom, J.M., 1966, Vanishing ironworks of the Ramapos: the story of the forges, furnaces, and mines of the New Jersey-New York area. Rutgers University Press, New Jersey, p. 177-214, 274-287.

Reimann, C., and Caritat, P. de, 1998, Chemical elements in the environment: factsheets for the geochemist and environmental scientist. Springer-Verlag, Berlin.

Smock, J.C., 1889, Iron mines and iron-ore districts in the State of New York. New York State Museum Bulletin, no. 7.

Stepniewska, Z., Bucior, K., and Bennicelli, R.P., 2004, The effects of MnO_2 on sorption and oxidation of Cr(III) by soils. Geoderma 122:291-296.

United States Environmental Protection Agency (USEPA), 2002, Supplemental guidance for developing soil screening levels for superfund sites, Appendix A-C. Available via: http://www.US EPA.gov/superfund/health/conmedia/soil/index.html. Accessed 15 Sept 2009.

Volkert, R.A., and Drake, A.A., 1999, Geochemistry and stratigraphic relations of middle proterozoic rocks of the New Jersey Highlands. US Geol Surv Prof Paper 1565-C.

Yanguo, T., Xianguo, T., Shijun, N., Chengjiang, Z., and Zhengqi, X., 2003, Environmental geochemistry of heavy metal pollutants in soil and stream sediment in Panzhihua Mining and Smelting area, Southwestern China. Chinese J Geochem 22:253-262.

Zabowski, D., Henry, C.L., Zheng, Z., and Zhang, X., 2001, Mining impacts on trace metal content of water, soil, and stream sediments in the Hei River Basin, China. Water Air Soil Poll 131:261-273.

FIELD GUIDE AND ROAD LOG

Meeting Point: Museum/Visitors Center (aka Frank L. Lautenberg Visitor Center) at 116 Old Forge Road, Tuxedo, NY 10987

Meeting Point Coordinates: 41.199^0 N, 74.255^0W

Meeting Date and Time: Sunday, October 2nd, 2016 at 9:00 AM

Directions from the conference (Distance in miles (km))

Cumulative	Point to Point	Route Description

1.3 (0.5)	1.3 (0.5)	Begin going east on Route 59 Take ramp onto Palisades Interstate Pkwy North (toward Bear Mt)
12.1 (19.5)	10.8 (17.4)	Take I-87 (NY Thruway) Westbound (toward Albany)
13.8 (22.2)	1.7 (2.7)	Take Exit 15A (NY17, toward NY-59/Sloatsburg/Suffern) and turn left onto Route 17.
16.9 (27.2)	3.1(5.0)	Take ramp toward Ringwood/Sterling Forest/West Milford and merge onto Sterling Mine Road.
20.5 (33.0)	3.6 (5.8)	Turn right onto Long Meadow Rd (Hwy 84)
20.8 (33.5)	0.3 (0.5)	Turn left onto Old Forge Rd *(If you reach Sterling Lake Corp you have gone a bit too far)*
21 (33.8)	0.3 (0.5)	Take first right to stay on Old Forge Rd *(If you reach Harriman Ct you went about 0.1 mile too far)*
		116 Old Forge Rd, Tuxedo Park, NY *(If you reach Reception Rd you have gone a bit too far)*

All 4 – 5 stops are short walking distances around the mining complex, including the visitors' center, which showcases a model of the underground mines and aboveground facilities before the whole operation was abandoned in the early 20th C. The exhibits also include samples of the rock types mined and other mining paraphernalia.

NYSGA: Geologic Diversity in NYC

TRIP B3: LATE PROTEROZOIC SHEAR ZONES OF THE WESTERN HUDSON AND NEW JERSEY HIGHLANDS

MICHAEL J. KALCZYNSKI and ALEXANDER E. GATES
Department of Earth & Environmental Sciences, Rutgers University, Newark, NJ 07102

ABSTRACT

Multiple phases of deformation associated with the Grenville orogeny are recorded in the rocks exposed in the northern Reading Prong of southeastern New York and northern New Jersey. The rocks of the Hudson and New Jersey Highlands are considered to have formed in an island arc or marine magmatic arc setting ca. ~1.3 Ga, as volcanics, volcaniclastics, and sedimentary rocks. Deposition terminated when continental collision resulted in the formation of a major mountain belt during the onset of the Grenville orogeny. Granulite facies metamorphism created the dominantly gneissic regional foliation and migmatization, with extensive pegmatite intrusion. During this time, the Ramapo and Reservoir faults were established as zones of major crustal weakness. Dioritic dike and stock intrusions occur shortly afterwards, but prior to the second event. The second Grenville deformational event was likely due to tectonic escape and resulted in the reactivation and creation of multiple dextral shear zones late in the Proterozoic.

The northeast-trending Ramapo and Reservoir fault zones were initially established during the earliest phase of the Grenville orogeny as ductile reverse faults. In the later phase, both zones were reestablished as ductile strike-slip faults. The shear sense is unequivocally dextral, evidenced by the multiple kinematic indicators such as S-C fabrics, rotated porphyroclasts, and asymmetric boudins. Evidence is also present for multiple subsequent reactivations, including later ductile and brittle fabrics.

Late in the Grenville cycle, a ~35 km wide zone of anastomosing near vertical mylonite zones overprinted early shallowly dipping foliations. Locally, shear zones in the western Hudson Highlands became dilational and extensive alteration and vein mineralization occurred. The veins formed in dilational right step-over jogs during the late stages of movement in northeast trending dextral shear zones. Locally buffered fluids controlled mineralization, resulting in calc-silicate, ferromagnesian, and quartz-sulfide assemblages. This process produced three zones: 1) a 'bleached' zone of altered wall rock adjacent to the vein, 2) an outer 'layered' zone in the vein, of ferromagnesian-rich bands, and 3) a core of massive magnetite ore and secondary minerals.

INTRODUCTION

The Reading Prong is a Grenville basement massif that forms part of the spine of the Appalachians, connecting the Blue Ridge and Green Mountain provinces, in Pennsylvania, New Jersey, New York, and into Connecticut (Fig. 1). It is composed of Grenville aged crystalline rocks that have largely been metamorphosed to granulite facies (see Drake, 1984). The Reading Prong is bounded to the west by deformed Paleozoic sedimentary rocks of the Valley and Ridge Province and to the east by the Piedmont Province. Known as the New Jersey Highlands and the Hudson Highlands in New York, it boasts a complex deformational history of multiple reactivations. The rocks of the highlands are interpreted to have formed in an island arc or magmatic arc as volcanics, volcaniclatics, and sedimentary rocks.

The details of the Grenvillian orogeny in the Appalachians are commonly difficult to decipher because of complex structural relations, lack of exposure, and pervasive granulite facies metamorphism, as well as extensive structural and metamorphic overprinting during the Paleozoic and Mesozoic locally (Ratcliffe, 1972; Bartholomew and Lewis, 1988; Krol *et al.*, 1992; Krol and Zeitler, 1994; Gates *et al.*, 2006). Gates (1995; 1998) and Gates and Costa (1998) proposed a major late Grenvillian dextral strike-slip event in the Reading Prong. This shearing was constrained to discrete faults, such as the Ramapo and Reservoir faults (Gates *et al.*, 2004), which were active well after peak Grenville tectonism and to lower temperatures (Gates *et al.*, 2006)(Fig. 2). Fundamental zones of crustal weakness that were established were reactivated multiple times during subsequent tectonic events. The rocks in these fault zones contain complexly overprinted mylonites, cataclasites, and breccias with distinct kinematics and mineralizations (Gates and Costa, 1998). Bimodal (diorite and granite) plutons intruded the area prior to the onset of a steeply southeast-dipping ~35 km wide dextral shear system that resulted from tectonic escape (Gates *et al.*, 2006).

The second event produced discrete zones of ductile deformation with a consistent dextral strike-slip shear sense and crenulation cleavage (Gates, 1998). Steeply southeast- to northwest-dipping 1 to 3 km wide zones of mylonite display extensive shallow northeast trending lineations, S-C fabrics, asymmetric boudins, asymmetric intrafolial folding, and rotated porphyroclasts locally (Gates, 1998). Late in their history, the shear zones crossed the brittle ductile transition and became dilational where extensive iron mineralization locally accompanied the shearing. Iron mineralized as magnetite veins in several shear zones exposed in the western Hudson Highlands following extensive fluid alteration of country rock and gauge mineral mineralization late in the Grenville orogenic cycle (Kalczynski and Gates, 2014). The veins are exposed at several abandoned magnetite mines within Harriman State Park. New modeling for the mode of formation of these magnetite deposits is discussed as well as reactivation history of the Ramapo and Reservoir fault zones.

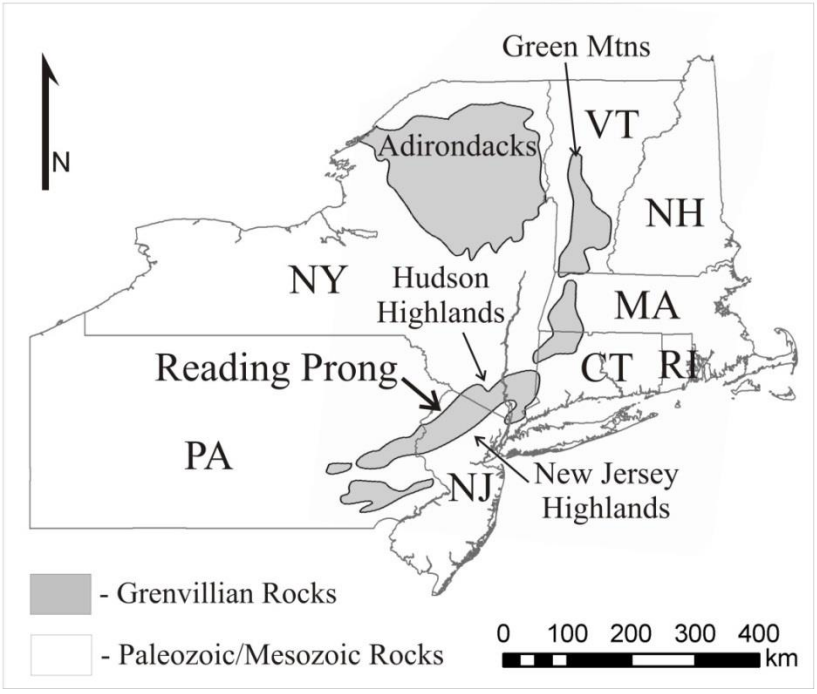

Figure 1. Map of the Northeastern United States showing distribution of Appalachian/Grenville rocks, the Reading Prong, and the Hudson and New Jersey Highlands.

GEOLOGY OF THE NEW JERSEY AND HUDSON HIGHLANDS

Several models currently exist for the formation of the crystalline bedrock of the Hudson Highlands. Recent geochemical investigations found that some of the rocks are of plutonic origin (Gundersen, 2004; Volkert and Drake, 1999; Volkert, 2001; Gates *et al.*, 2006), but based upon major element geochemistry, some of the layered gneisses have been interpreted to be volcanic (Helenek, 1971; Drake, 1984; Puffer and Gorring, 2005; Gates *et al.*, 2006). Gundersen (2004) and Volkert *et al.* (2010) proposed that many of these gneisses formed in an extensional backarc marginal basin, with a bimodal, volcanic origin whereas Gates *et al.* (2006) proposed formation of a volcanic pile with a volcaniclastic apron in an island arc or marine magmatic arc setting.

According to Gates *et al.* (2006), a volcanic pile initiated in an arc setting around 1.29 to 1.25 Ga (Volkert *et al.*, 2010), and is characterized by layered intermediate and mafic rocks, associated plutons, and volcaniclastic sediments. Continental collision of the arc with another continent (likely Amazonia) occurred during the building of the Rodinian supercontinent, ~1,050 to 1,020 Ma (Gates *et al.*, 2006). This sequence underwent granulite facies metamorphism, between 1,045 to 1,024 Ma associated with the Ottawan phase of the Grenville orogeny (Volkert *et al.*, 2010). Locally, anatexis produced migmatites, granite sheets, and the early pegmatites (Gates *et al.*, 2006). Subsequent diorite intrusions occurred around 1,008 Ma either the result of delamination at the end stages of the collision event, or the early dilational stages of a second tectonic event (Gates *et al.*, 2006). This second event is characterized by dextral strike-slip movement during a period of rapid uplift and unroofing at approximately 1,008 to 924 Ma (Gates and Krol, 1998). A ~35 km wide zone of anastomosing near vertical mylonite zones overprinted early shallowly dipping foliations. Total dextral offset was on the order of several hundred kilometers (Gates *et al.*, 2006).

Previous geologic mapping in this region sub divided gneisses based upon the individual varietal ferromagnesian minerals (Dodd, 1965; Dallmeyer, 1974). Considering that 80% of these rocks are quartzofeldspathic gneisses (Gates *et al.*, 2006), this paper follows the system proposed by Gundersen (1986), and adapted by Gates *et al.* (2006). Units are grouped into lithofacies based on various rock types, to define quartzofeldspathic, interpreted metasedimentary (calc-silicate, metapelite, and metapsammite), and metavolcanic (plagioclase-amphibole-pyroxene) assemblages.

Metavolcanic Gneiss

The metavolcanic unit consists of strongly banded sequences of inter-layered mafic and intermediate gneisses, with interpreted volcanic protoliths (Gates *et al.*, 2006). Compositional banding ranges in thickness from 5 cm to 5 m with varying quantities of each rock type. Mafic assemblages are composed primarily of medium to coarse grained amphibole, plagioclase, clinopyroxene and orthopyroxene, with minor sulfides and magnetite locally. Intermediate bands are primarily medium to coarse grained plagioclase and quartz, with minor amounts of amphibole, biotite, clinopyroxene and orthopyroxene. This unit also contains localized interlayers of interpreted metasediments such as, quartzite, marble, and calc-silicate gneiss, as well as migmatites. The contacts with the quartzofeldspathic unit are interstratal gradational.

Quartzofeldspathic Gneiss

The quartzofeldspathic gneiss ranges from massive to layered quartz-plagioclase gneiss to quartz-K-feldspar-plagioclase gneiss with lesser amounts of clinopyroxene, orthopyroxene, amphibole, and/or

biotite. Minor amounts of magnetite and garnet also occur locally. Compositional layering is defined by the proportions and species of ferromagnesian minerals. At the contact with the metavolcanic unit, it is also locally interlayered with quartzite and amphibole-pyroxene gneiss. Gradational contacts with the metavolcanic lithofacies, composition and mineralogy, and internal compositional layering suggest that this unit represents a volcaniclastic sequence (Gates *et al.*, 2006). Zircons analyzed from the quartzofeldspathic unit yield ages between 1,160 – 1,220 Ma for the zoned cores and between 1,000 - 1,080 Ma for the clear rims (Gates *et al.*, 2006).

Metasedimentary Gneiss

Throughout the western Hudson Highlands there are belts of rock considered to have sedimentary protoliths including metapelite, metapsammite, and calc-silicate gneisses interlayered with quartzite and marble. Belts of rock contain varying amounts of these lithologies interlayered at the scale of meters to hundreds of meters (Gates *et al.*, 2006). The calc-silicate gneiss is quartzofeldspathic containing diopside, K-feldspar, fluorapatite, titanite, scapolite, and amphibole. Tens of centimeters to meter-scale quartzite layers and discontinuous layers of diopside marble also occur in this unit. The metapelite consists of interlayered biotite-garnet gneiss with medium to coarse quartz, plagioclase, K-feldspar, and cordierite and sillimanite locally (Gates *et al.*, 2006). Zircons analyzed from the metasedimentary units yielded ages between 1,100 – 2,800 Ma for the zoned detrital cores and between 1,000 – 1,030 Ma for the distinct metamorphic rims (Gates *et al.*, 2006).

Diorite

Coarse to very-coarse grained black and white diorite dikes and bodies containing plagioclase, orthopyroxene, clinopyroxene, interstitial amphibole, and minor biotite, occur throughout the field area. Hornblende rims clinopyroxene which armors orthopyroxene, however orthopyroxene does not occur within sheared diorite. The diorite also grades to pyroxene-poor, anorthositic compositions locally (Gates *et al.*, 2003). Multiple small bodies of diorite are concentrated in certain areas, possibly indicating larger bodies at depth (Gates *et al.*, 2006).

Textures vary from coarse granoblastic to foliated and mylonitic with type II S-C fabrics (Lister and Snoke, 1984), exhibiting dextral shear sense (Fig. 2). Locally, the diorite contains xenoliths of gneiss, showing ductile contacts which are partially melted, forming a rind of coarse pegmatite granite. Granite also fills fractures in the diorite that opened after crystallization, but while the granite was still liquid (Gates *et al.*, 2006). Subhedral zircons with minimal to no zoning yielded a cluster of ages averaging 1,008 +/- 4 Ma (Gates *et al.*, 2006).

Figure 2. Lake Tiorati Diorite, with type II S-C fabrics and σ porphyroclasts indicating dextral shear sense.

Pegmatites

Two generations of pegmatites occur throughout the field area. The earliest dikes are white and contain K-feldspar, quartz, muscovite and minor garnet locally. They are concordant to semi-concordant to the gneissic foliation, commonly boudinaged and contain internal fabrics and deformed grains. Thickness of these dikes ranges from 1 cm to 1 m. The later pegmatitic dikes are pink and very coarse grained, containing K-feldspar and quartz with muscovite, amphibole, magnetite, pyroxene, titanite, and/or garnet locally, depending on the rock intruded. They are highly discordant, commonly within brittle faults and contain xenoliths of gneiss, mylonites, and mineralized rock. They show minor to no deformational fabrics, and thickness ranges from 1 to 10 m. They are also associated with small granite bodies (Gates *et al.*, 2006). Ar/Ar thermochronology of hornblende from the later pegmatite yielded an age of 923 +/- 2.8 Ma, and an age of 794 +/- 3.0 Ma from biotite samples (Gates *et al.*, 2006).

REACTIVATED ZONES OF THE NEW JERSEY HIGHLANDS

Ramapo Fault

The Ramapo fault zone is the boundary between the eastern and central highlands (Fig. 3). The northeast-trending Ramapo fault system in northern New Jersey and southeastern New York juxtaposes Middle Proterozoic crystalline rocks of the Reading Prong with Triassic and Jurassic sedimentary and igneous rocks of the Newark Basin along most of its length. The Ramapo fault system varies in thickness from approximately 5 km to 10 km along strike (Ratcliffe, 1980). It consists of many parallel to subparallel zones of well foliated to poorly to moderately lineated type II S-C mylonite (Lister and Snoke, 1984) and ultramylonite in Grenville gneisses (Fig. 4)(Gates and Costa, 1998). Primary kinematic indicators from the mylonite along the Ramapo fault system in northern New Jersey consistently exhibit reverse shearing sense, indicated by both σ-type and δ-type quartz porphyroclasts (Fig. 4B)(Passchier and Simpson, 1986).

Cores of the porphyroclasts define the southeast-dipping S plane and have tails of dynamically recrystallized quartz. Type B2a and type B2b quartz ribbons (Boullier and Bouchez, 1978) and dynamically recrystallized tails on porphyroclasts (Passchier and Simpson, 1986) define the C plane (Gates and Costa, 1998). The C' Plane, where present, is defined by asymmetric boudinage of quartz ribbons (Gates and Costa, 1998). Potassium feldspar and plagioclase also form σ-type and δ-type porphyroclasts (Fig. 4A)(Passchier and Simpson, 1986) with tails of recrystallized feldspar, quartz, muscovite and chlorite (Costa and Gates, 1998). Cores of these porphyroclasts also define the southeast-dipping S plane. The C plane is defined by porphyroclast tails. Edges of the feldspar porphyroclasts are commonly dynamically recrystallized (Gates and Costa, 1998). Plagioclase porphyroclasts have deformed twin lamellae. Feldspar porphyroclasts, less commonly, show pull-apart textures (Stauffer, 1970) that show antithetic shearing along cleavage planes (Gates and Costa, 1998). The ductile behavior exhibited by the feldspar porphyroclasts, indicates that the temperatures of this phase of deformation were in excess of 450 ± 50°C (Sibson, 1977; 1983; Tullis and Yund, 1977). This mineral response is consistent with deformation at middle to upper greenschist facies conditions (Simpson, 1985) (Gates and Costa, 1998).

C planes typically dip 40 to 50° towards the southeast. The average angle between S and C planes is 20°, but varies from 6 to 40°. C' planes where present, are spaced from 1.0 mm to 1.0 cm and oriented approximately 20 - 30° shallower than the C plane. Lineations of quartz, amphibole, and chlorite are consistently down dip (Gates and Costa, 1998). Chlorite and muscovite "fish" (Eisbacher, 1970; Lister

and Snoke, 1984) and aligned muscovite; tremolite and biotite define the southeast-dipping S-C fabric as well. Biotite commonly underwent reaction enhanced ductility (White *et al.*, 1980). C' planes commonly developed within the chlorite-rich zones (Gates and Costa, 1998).

Hornblende commonly underwent a brittle response. Pull-apart (Stauffer, 1970) hornblende porphyroclasts underwent reaction-enhanced ductility (White *et al.*, 1980) in which crude σ-type porphyroclasts evolved from antithetically sheared fragments. In these retrograded grains, metamorphic reactions generated chlorite, tremolite-actinolite, biotite, and muscovite as fillings within conjugate shear planes and as tails on porphyroclasts (Gates and Costa, 1998). The tails on some of the quartz porphyroclasts are pulled under or over the grain in a direction opposite to that indicated by the porphyroclasts. Some of the brittle hornblende grains show pull-apart textures with a shear sense opposite to that of the mylonitic matrix. Within some of the hornblende grains, the fractures formed during extension and fragmentation of the grain are V-shaped and are syntaxially filled first by amphibole and then by a chlorite-muscovite-quartz intergrowth. The amphibole is parallel to the fracture walls and indicates no rotation whereas the second growth indicates substantial rotation. V-textures could be used as kinematic indicators in single deformations (Hippert, 1993), but the textures described here are clearly composite and indicate a complex history (Gates and Costa, 1998).

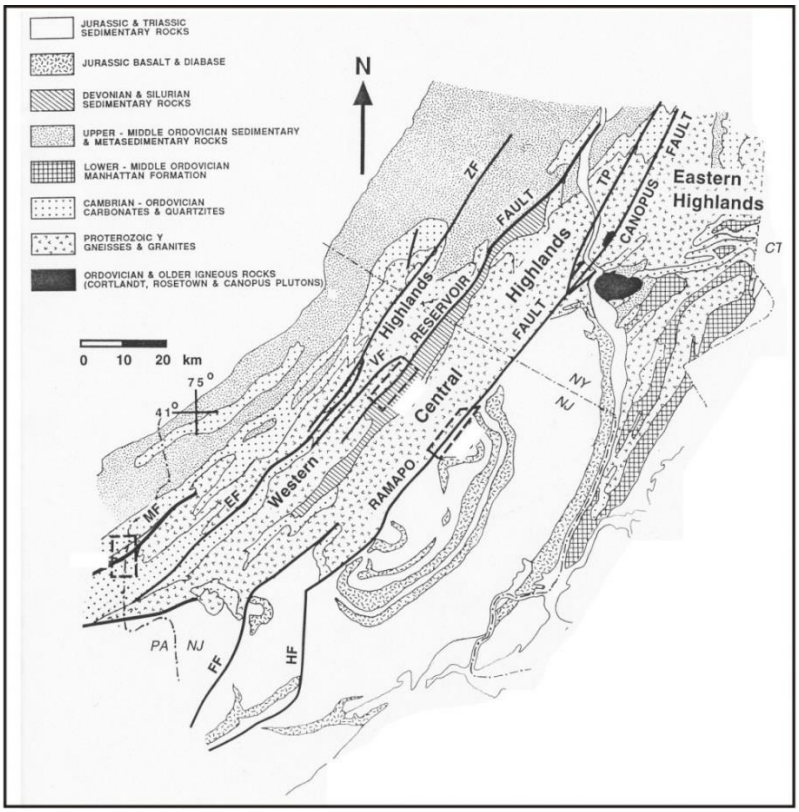

Figure 3. Geologic map of the northern Reading Prong, NY, NJ, and Pa, showing locations of the Ramapo and Reservoir faults (from Gates and Costa, 1998).

Within these mylonite zones of reverse movement, there is evidence for an earlier phase of normal movement at approximately the same metamorphic grade. Features such as intrafolial rootless isoclines and relict foliations, composite porphyroclasts, and V-shaped fractures with two syntaxial overgrowths (Fig. 4C) support this interpretation (Gates and Costa, 1998). The intrafolial folds and relict foliations occur primarily within quartz ribbons but also in within the fine-grained mylonitic matrix. Some

porphyroclasts and brittle pull apart grains exhibit evidence for two periods and directions of movement (Gates and Costa, 1998).

In addition to its development as a Grenville reverse fault (Ratcliffe, 1980), the Ramapo fault system has a long and complex reactivation history which includes up to five periods of fault movement. The dominate reverse ductile deformation which resulted in the development of the southeast dipping type II S-C mylonite (Fig. 4D) (Lister and Snoke, 1984) and ultramylonite zones is post-Grenville in age. The mineralogy and texture which are present are indicative of a lower grade deformation than those reached during the Grenville orogeny. Based on the deformation features and metamorphic grade of deformation (Simpson, 1985), the reverse mylonites and ultramylonites within the study area formed at mid- to upper greenschist metamorphic facies (Gates and Costa, 1998).

Cataclastic textures (Sibson, 1977) that overprint the early ductile and brittle-ductile fabrics indicate brittle strike-slip and normal reactivation of the southeast-dipping faults. Cataclastic seams (0.5 mm to 1.5 cm thick) offset grains and early fabrics are themselves offset by later faults (Gates and Costa, 1998). Southeast-dipping foliated greenish-gray to black gouge zones approximately 4.0 to 5.0 cm thick are commonly enriched in calcite and sheared antithetically (Gates and Costa, 1998). In addition, there are two generations of type I (Beach, 1975) quartz, calcite, and chlorite filled tension gashes and two generations of primary and secondary (Harding, 1974) planar, curvi-planar and listric brittle fault arrays with slickenlines (Gates and Costa, 1998).

Slickenside coated fault surfaces most commonly contain fibrous or stepped slickenlines of fine grained chlorite, tremolite-actinolite, limonite and calcite with lesser amounts of quartz and epidote. Two generations are evident by overprinting relations on single fault surfaces (Gates and Costa, 1998). Each generation of brittle faults includes four sets of moderate to steeply dipping faults. The early generation of steeply-dipping brittle faults includes east-southeast and west-northwest-dipping reverse faults; northeast and southwest-dipping normal faults and a conjugate set of north-northwest and south-southeast-dipping right-lateral strike-slip and east and west-dipping left lateral strike-slip faults. The later set of brittle faults includes south-southwest and north-northwest-dipping reverse faults, southeast and northwest-dipping normal faults and a conjugate pair of northeast and southwest-dipping right-lateral strike-slip and southeast-dipping left-lateral strike slip faults. An additional set of northwest and southeast-dipping right lateral strike-slip faults is present. Fault planes also developed P and T criteria kinematic indicators (Petit, 1987) and tension gashes filled with calcite, tremolite-actinolite, chlorite, and quartz (Gates and Costa, 1998).

The dominant ductile reverse mylonite fabric overprints a previously developed normal mylonitic fabric interpreted to be the result of Iapetan rifting as it predates Taconian deformation and postdates Grenville deformation (Gates and Costa, 1998). A Taconian age (450 – 460 Ma) has been assigned to reverse ductile movement on the Ramapo fault zone of southeastern New York based radiometric dates of plutonic and dike rocks of the Rosetown pluton and Cortlandt Complex (Ratcliffe, 1980; 1981; Ratcliffe *et al.*, 1982). During post-Ordovician and pre-Mesozoic activity mesoscopic synchronous primary and secondary brittle faults (Harding, 1974) and associated tension gashes (Costa, 1991) developed within the Ramapo fault system showing both reverse and strike-slip motion (Costa and Gates, 1998). Costa and Gates (1993) interpreted the strike-slip and reverse motion to be of the same generation and Alleghanian in age based on regional relations.

Overprinting slickenlines on a single fault plane allow the determination of a younger generation of brittle faults superimposed over the interpreted Alleghanian generation. This brittle phase of deformation corresponds with the southeast dipping normal faults which created the Newark basin (Gates and Costa, 1998). The Mesozoic sediments (Olsen, 1980) within the basin constrain the time of

faulting. During Mesozoic rifting primary and secondary brittle faults (Harding, 1974) and associated tension gashes also developed (Gates and Costa, 1998). The generation of overprinting cataclastic textures and fault gouge (Sibson, 1977) indicate faulting was under low temperature (<250°C) and shallow conditions (<10 km). An approximate north-northeast-trending maximum compressive direction is indicated by the complex fault array and tension gashes, requiring that the formation of the Newark basin had a transtensional component (Gates and Costa, 1998).

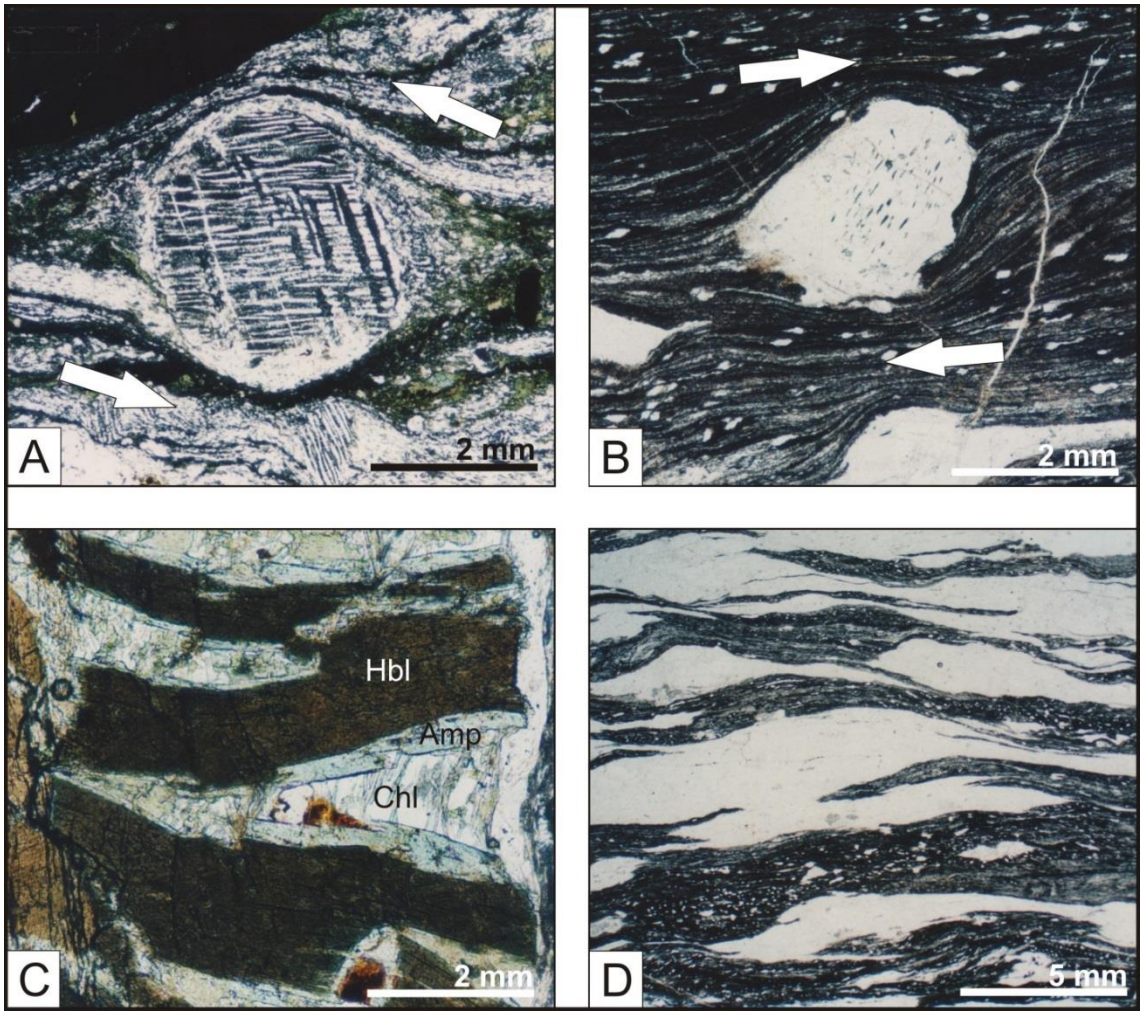

Figure 4. Photomicrographs of rocks from the Ramapo fault zone. Arrows show shear sense. A) Rotated porphyroclast of microcline. B) Rotated quartz porphyroclast. C) V-shaped fracture in a pull-apart hornblende porphyroclast. Composite filling of early amphibole and late chlorite-sericite-quartz intergrowth. D) S-C mylonite showing mylonitic fabric, quartz ribbons, and rotated quartz porphyroclasts.

Reservoir Fault

The Reservoir fault marks the boundary between the central and western Highlands. The shear zone is best developed in the Grenville gneisses of the Losee metamorphic suite (Lewis and Kummel, 1912; Hague *et al.*, 1956; Drake, 1984; Gates, 1993). The Reservoir fault is a multiply activated zone of weakness that forms the western boundary of the Silurian-Devonian Green Pond outlier. The vertical to

steeply northwest- and southeast-dipping shear zone extends from the Hudson Highlands, New York into the central New Jersey Highlands. Cataclastites and mylonites are best developed around Newfoundland, New Jersey within Grenville paragneisses that have been interpreted as being of metasedimentary origin (Lewis and Kummel, 1912; Hague *et al.*, 1956; Drake, 1984; Volkert, 1993). These rocks are dominantly layered amphibole, biotite, and pyroxene quartzofeldspathic gneisses and minor amphibolite gneiss (Gates and Costa, 1998). The quartzofeldspathic gneiss is interpreted as being derived from layered volcaniclastic and calcsilicate rocks (Drake, 1984; Gundersen, 1986) and contains scapolite, pyroxene, and garnet assemblages or plagioclase-pyroxene-amphibole-garnet assemblages (Malizzi and Gates, 1989). The gneisses were intruded by uraniferous pegmatite dikes along the Reservoir fault subsequent to or during granulite facies metamorphism (Malizzi and Gates, 1989).

Protoliths of the Reservoir fault rocks are preserved along the western margin of the fault and as xenoclasts and xenocrysts within the fault zone. The protolith is primarily a granitic to tonalitic paragneiss with antiperthite, varietal edenite to hornblende, and/or diopside and minor ilmenite, and apatite with a granoblastic to gneissic texture (Gates and Costa, 1998). Locally these rocks preserve early mylonitic textures. The amphibole in this rock is F-rich (1.5-2.0 wt.%) and Cl-bearing (up to 0.5 wt.%) (Gates and Costa, 1998). Feldspar is albite with exsolution lamellae of K-spar. There are also minor amounts of pyroxene-bearing amphibolite. In the fractured gneisses adjacent to the main fault zone, plagioclase, edenite-hornblende and locally, diopside are replaced by F-magnesiohastingsite along fractures and cleavage plains (Gates and Costa, 1998). Typically, the most complete replacement occurs closest to the fracture but, in many cases, the new mineral permeates the entire grain. Illmenite has overgrowths of titanite (Gates and Costa, 1998).

Brittle deformation of the granitic-tonalitic gneiss ranges from veining and fracturing in rocks adjacent to the fault to extensive fault breccia and cataclasite within the fault zone. Feldspar are fractured or granulated and commonly offset along microfaults that exploit mineral cleavage plains (Gates and Costa, 1998). The fractures are filled with amphibole, epidote, calcite, chlorite, and hematite. Quartz shows extreme lattice misorientation, much of which likely reflects submicroscopic cataclasis (Tullis and Yund, 1987) with minimal plastic deformation (Gates and Costa, 1998). Quartz also exhibits extensive fractures that are filled with essentially the same minerals as feldspar. Other minerals are offset along fractures and show extensive reaction textures (Gates and Costa, 1998).

In the mylonitic part of the shear zone, xenoclasts, xenocrysts, and coarse-grained neomineralized amphibole cores exhibit brittle deformation whereas fine-grained amphibole and chlorite display marginal plastic deformation (Gates and Costa, 1998). A well-developed S-C mylonitic fabric is formed in the amphibole-rich matrix including late C' planes (Simpson and Schmid, 1983). S planes are composed exclusively of fine-grained magnesiohstingsite and the cores of magnesiohstingsite porphyroclasts whereas C and C' planes are fine-grained ferro-actinolite and actinolite with variable amounts of chlorite (Gates and Costa, 1998).

Larger grains of F-magnesiohastingsite including porphyroclasts cores commonly exhibit varying amounts of brittle fracturing primarily as microfaulting along cleavage planes and subsequent bending of the microfault blocks with Cl-magnesiohstingsite and chlorite filling the fractures. These large grains also commonly exhibit mantles and asymmetric tails of fine-grained and aligned Cl-magnesiohstingsite, ferro-actinolite and actinolite and form rotated σ-type (Gates and Costa, 1998). According to Gates and Costa (1998), seemingly solid cores of F-magnesiohastingsite porphyroclasts show that most of the rims and even inner cores, in some cases, are granulated and overgrown by epitaxial Cl-magnesiohastingsite with 1.0 to as much as 2.4 wt.% Cl but with little to no F. The outer edge of the porphyroclast in turn is rimmed by ferro-actinolite and actinolite. The S-C fabric, rotated porphyroclasts, and offset brittle

grains including pull-aparts consistently show a dextral transcurrent sense of shear (Gates and Costa, 1998).

Overgrowths and fracture fillings on Cl-magnesiohastingsite are optically continuous ferro-actinolite and actinolite and subsequently actinolite + chlorite. Unlike the magnesiohastingsite, the ferro-actinolite is more commonly intergrown with other minerals (Gates and Costa, 1998). Assemblages include fine-grained epidote, albite, titanite, apatite, pyrite, and locally muscovite and biotite but they are still dominated by amphibole. These minerals occur in shear bands and in veins that parallel foliation. Biotite also shows a transition from F-rich to Cl-rich compositions within ferro-actinolite and actinolite bearing assemblages (Gates and Costa, 1998).

Small pockets within the fault zone contain extensive breccia and cataclasite that lack foliation. The matrix of these rocks is primarily actinolite. In the well-developed cataclasite parts of the shear zone, rounded xenoclasts of both protolith and cataclastic fault rock range up to 0.5 m but most relict components are 0.5 to 1.0 mm xenocrysts of quartz and feldspar. The xenoclasts and xenocrysts float in a matrix of randomly oriented 0.1 to 0.5 mm actinolite with minor chlorite, biotite, albite, apatite, epidote and rare pyrite (Gates and Costa, 1998).

The retrograde metamorphism that accompanied shearing is reflected in mineralogical changes. The observed protolith assemblages in granitic-tonalitic gneiss are: diopside + low Ca feldspar (antiperthite) + quartz + ilmenite, or edenite-hornblende + low Ca feldspar (antiperthite) + ilmenite ± scapolite ± garnet (Gates and Costa, 1998). These assemblages were produced during peak granulite facies metamorphism. The first retrograde assemblage is magnesiohastingsite which is locally potassian and consistently a flouro-amphibole + titanite ± albite ± pyrite (Gates and Costa, 1998). Amphibole makes up about 90 to 95% of this assemblage. The early magnesiohastingsite is F-rich but subsequent magnesiohastingsite became progressively more Cl-rich. Amphibole analyses with equal parts of F and Cl (~1%) are common (Gates and Costa, 1998). The latest magnesiohastingsite observed is Cl-rich and contains no F. These data indicate that metamorphic fluids underwent a transition from F-rich to Cl-rich compositions that was synchronous with movement on the Reservoir fault (Gates and Costa, 1998). Ferro-actinolite-rich assemblages succeeded the magnesiohastingsite assemblages and include albite, epidote, titanite, apatite, biotite, and chlorite. The final retrograde amphibole is actinolite and it is virtually always associated with chlorite in varying proportions (Gates and Costa, 1998). Other common associations include epidote, apatite, albite, titanite, and biotite. These later assemblages are most common in cataclasites with random grain orientations (Gates and Costa, 1998).

The Reservoir fault zone has a history of multiple periods of activity. Previous workers have suggested that it underwent Alleghanian movement (Hull *et al.*, 1986; Mitchell and Forsythe, 1988), and that it is still active, producing regular low magnitude earthquakes (Ratcliffe, 1980). It has been proposed to have had Mesozoic (Lewis and Kummel, 1912), Acadian (Finks, 1990), Taconian (Ratcliffe, 1980), and some form of Precambrian movement (Hull *et al.*, 1986), but these phases of motion are not as easily documented (Gates and Costa, 1998).

Based on overprinting relations, the mechanical response of the minerals and the chlorite-bearing assemblages of the fault rocks, shearing postdated peak granulite facies metamorphism associated with the Grenville orogenesis (Gates and Costa, 1998). Because quartz appears to straddle the brittle-ductile transition, the temperature of deformation of this strike-slip event appears to have been approximately 300 ± 50°C (Tullis and Yund, 1977) or less, which is consistent with the chlorite + actinolite + albite assemblages (Gates and Costa, 1998). On the other hand, the presence of F-rich fluids and halogen-rich fluids in general indicates that it is related to Proterozoic metamorphism (Gates and Costa, 1998). The edenite and hornblende in the protolith Reservoir fault rocks have similar F contents to the F-

magnesiohastingsite within the fault rocks. Such high F contents and halogen content in general are common in amphiboles and biotite within rocks that underwent Grenville metamorphism in the Reading Prong (Gundersen, pers. comm., 1994). Such concentrations of halogen-rich amphibole within fault zones or otherwise do not occur within the Paleozoic sedimentary rocks of the Green Pond outlier (Gates and Costa, 1998). Other occurrences of amphibole mineralization within the New Jersey Highlands are also restricted to late fault zones within crystalline rocks (Kalczynski and Gates, 2014), though Paleozoic sedimentary rocks are common in the area. Based on occurrence and composition, the movement accompanying amphibole mineralization on the Reservoir fault is late Middle to Late Proterozoic in age (Gates and Costa, 1998).

Because movement sense is unequivocally dextral, it is likely late Middle Proterozoic (Gates and Costa, 1998). Costa and Gates (1993) have identified normal movement on the nearby and parallel Ramapo fault. They propose that this movement is Late Proterozoic to earliest Cambrian and related to the opening of the Iapetus. These results are consistent with the interpretation of Iapetan rift deposits of Drake (1984) in the western Reading Prong. Based on orientation, inferred orientation of the maximum compression direction, and regional relations, the dextral strike-slip faulting on the Reservoir fault is more consistent with the earlier movement on the Ramapo fault (Ratcliffe *et al.*, 1972) than Iapetan rifting although oblique extension cannot be ruled out (Gates and Costa, 1998).

The timing of the multiple movement periods on the Reservoir Fault is poorly constrained by both geochronology and the stratigraphy of the area (Gates and Costa, 1998). Clearly the dominate deformation in the Green Pond outlier is Late Paleozoic Alleghanian and compressional in nature (Hull *et al.*, 1986; Mitchell and Forsythe, 1988; Herman and Mitchell, 1991) and the Reservoir fault was certainly active during this event (Gates and Costa, 1998). Malizzi and Gates (1989) proposed that this movement may have been dextral transpressional rather than simply compressional. Hull *et al.* (1986) and Malizzi and Gates (1989) speculated on Grenvillian movement on the fault, possibly recorded by gneissic foliation and aligned uraniferous pegmatites. The Reservoir fault was active several times during the Paleozoic and Mesozoic (Gates and Costa, 1998). Ratcliffe (1980), Mitchell and Forsythe (1988) and Malizzi and Gates (1989) documented two post-deformational phases of movement, one of which preserved the Green Pond outlier through west-side-up movement. Lewis and Kummel (1912) and Ratcliffe (1980) considered the entire Green Pond outlier to be preserved in a Mesozoic graben, the Reservoir fault having had normal movement. Finks (1990) proposed that the thick, high energy Devonian sedimentary rocks were deposited in a restricted dextral transtensional pull-apart basin, accounting for its separation from the Catskill depocenter to the west (Gates and Costa, 1998). Ratcliffe (1980) proposed Taconian movement on the zone as well as neotectonism, marked by the low intensity of earthquakes

MINERALIZED ZONES OF THE HUDSON HIGHLANDS

Within the western Hudson Highlands, half-kilometer wide shear zones, formed within the ~35 km-wide anastomosing dextral strike-slip shear system (Gates *et al.*, 2004), and contain concordant to slightly discordant mineralized ore veins (Fig. 5). The northeast trending zones are defined by steeply dipping foliations, penetrative mineral lineations, and type II S-C mylonites with dextral kinematic indicators (Fig. 2). The vein-wall rock contact is generally sharp and semi-concordant to the mylonitic foliation, but slightly discordant and uneven locally.

The veins and their contacts are characterized by three distinct zones sub-parallel to the wall rock boundary (Fig. 6). The unaltered wall rock, grades into a 1 to 2 cm thick 'bleached zone' that is lighter in

color and marked by the alteration of the original wall rock minerals. The bleached zone is in contact with the mineralized vein. The bleached zone is not uniformly distributed throughout the deposits, and in some areas the mineralized vein is in direct contact with wall rock.

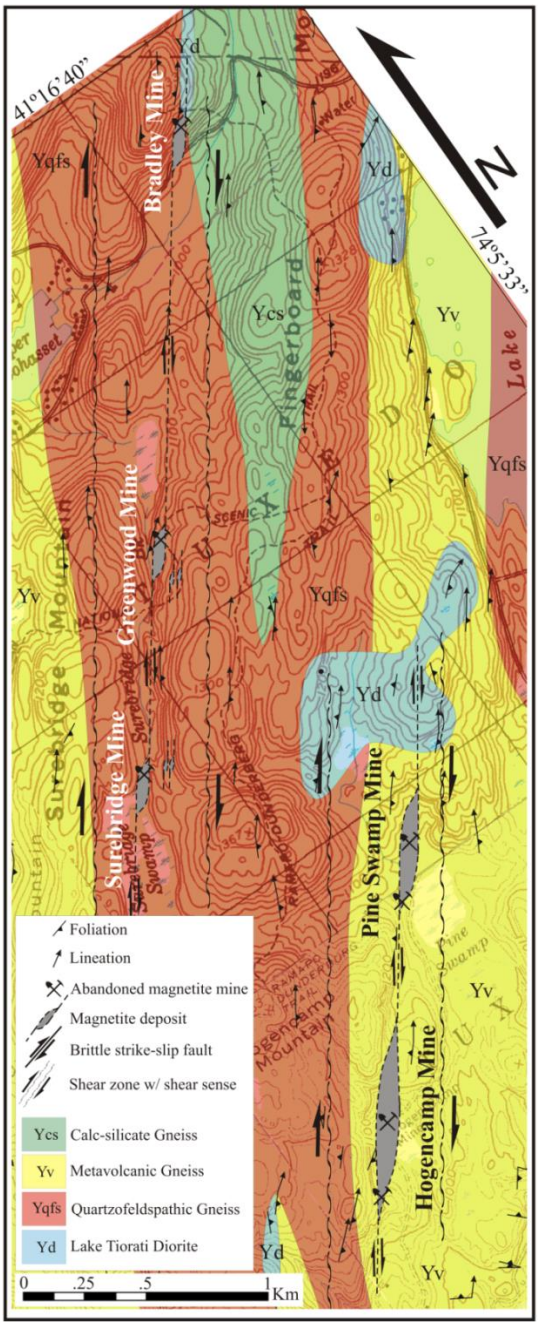

Figure 5. Geologic map of the Hudson Highlands study area, located within Harriman State Park, NY.

The mineralized vein is characterized by two distinct zones, a layered sequence adjacent to the wall rock and a core of primarily very coarse, massive minerals (>2 cm). The layered sequence is characterized by distinct, dark colored bands of fine to medium grained, pyroxene, amphibole, and/or biotite-rich assemblages, which range in thickness from 2 to 10 cm and have gradational to sharp contacts. The cores of the veins are characterized by medium to very coarse, magnetite ore, randomly oriented

amphibole and pyroxene gangue minerals, and late stage interstitial cementing minerals (Fig. 7). Thickness of the vein ranges from 2 to 15 m and length is ~10 m to 1 km. The thickness of the ore zone ranges from 1 to 10 m and length is ~100 to 500 m. The narrow zones that connect the magnetite deposits are typically composed of randomly oriented to aligned pyroxenes and amphiboles with minor magnetite, biotite, and/or quartz. The zones are commonly intruded by late pegmatite dikes that contain the mineralized rock as xenoliths.

Bleached zone mineral assemblages, vein material, and late-stage cementing minerals vary by location within the mineralized zones. In areas of calcium-rich country rocks, clinopyroxene/calcite rich mineral assemblages dominate the bleached zone and the vein assemblages. In areas of quartzofeldspathic country rock, amphibole/quartz assemblages dominate the layered and massive vein material, whereas areas with iron and sulfide-rich country rocks (metavolcanics), contain orthopyroxene/sulfide-rich vein assemblages. Pyroxenes vary by location between diopside, and iron-rich orthopyroxenes, whereas amphiboles are mainly chlorine- and fluorine-rich magnesiohastingsite (Gates, 1995) and potassichastingsite (Lupulescu *et al.*, 2009).

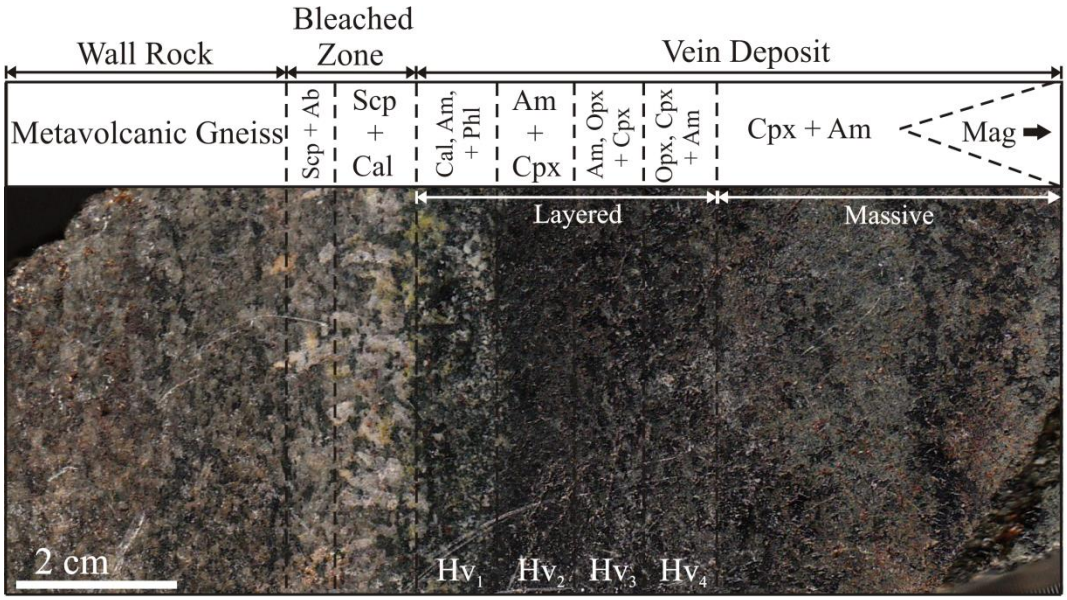

Figure 6. Sample from the Hogencamp deposit, showing banded mineral assemblages across the wall rock, bleached zone, mineralized vein contact. Layered and massive vein assemblages, and layers Hv_1-Hv_4 are also shown.

The southeastern-most shear zone contains the Hogencamp and Pine Swamp deposits. The mineralized vein that hosts both deposits is ~3 km long and ranges in thickness from 2 to 10 m at the mine locations to as little as one meter in the narrow zones that connect them. Country rock in this area includes metavolcanic and quartzofeldspathic gneiss, with diorite, calc-silicate, and marble locally.

Hogencamp Mine

The Hogencamp deposit lies in the southern portion of the shear zone. The sheared wall rock is dominated by metavolcanic gneiss, with calc-silicate gneiss and marble locally. The vein is continuous for about one kilometer.

The bleached zone is characterized by fine-medium grained calcite (~15%) and scapolite (~15%), and the alteration of pyroxene to amphibole (~45%), with phlogopite (<10%), albite (<10%), and minor fluorapatite locally (<5%). The layered vein is composed of 'bands' of individual fine-medium grained amphibole-, clinopyroxene-, and orthopyroxene-dominated assemblages, also containing calcite and phlogopite at the bleached zone contact (Fig. 6).

Layered vein banded assemblages are designated Hv_1-Hv_4 (Fig. 6). Hv_1, the assemblage adjacent to the bleached zone, is composed dominantly of amphibole (~70%) and interstitial calcite (~15%) with minor clinopyroxene and (<10%) phlogopite (<5%). Hv_2 is mainly fine-medium grained amphibole (~60%) and clinopyroxene (~40%). Hv_3 is dominated by fine-medium amphibole (~45%) with lesser amounts of clinopyroxene (~35%) and orthopyroxene (~20%), whereas Hv_4 is dominated by medium grained orthopyroxene (~50%) and clinopyroxene (~30%) with lesser amounts of amphibole (~20%). The central massive vein is characterized by very coarse magnetite ore and coarse gangue minerals of clinopyroxene, amphibole, and biotite, cemented by interstitial calcite.

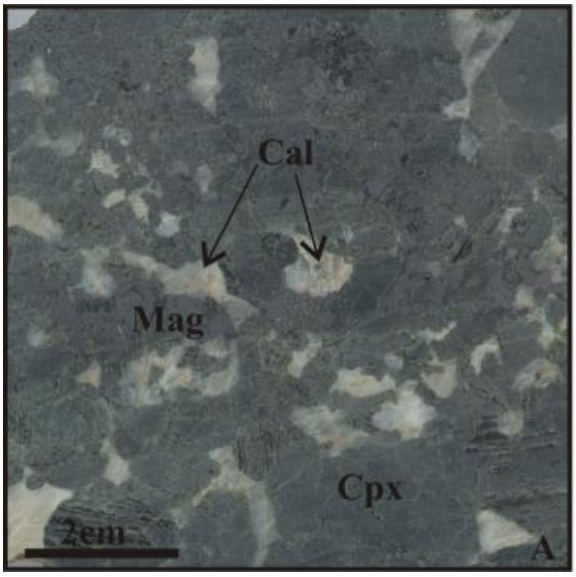

Figure 7. Massive vein from the Hogencamp deposit; clinopyroxene and magnetite with interstitial calcite.

Pine Swamp Mine

The Pine Swamp deposit lies along strike about one kilometer northeast of the Hogencamp deposit. The vein that hosts the Pine Swamp deposit is about 500 m long, with minor semi-concordant veins in the northern extent of the deposit. This vein lies primarily in quartzofeldspathic gneiss and sulfide-bearing metavolcanic gneiss country rock, which varies between interlayered mafic and intermediate gneiss.

The bleached zone is primarily defined by retrogression of medium grained pyroxene to amphibole (~80%), but also contains minor amounts of fine-medium grained scapolite (<10%), biotite (~5%), and fluorapatite (<5%) locally. Medium-coarse grained orthopyroxene (~75%) and amphibole (~15%) dominate the narrow layered vein, with minor quartz (~10%). The massive vein contains magnetite ore and medium-coarse grained orthopyroxene (>80%) and amphibole (<20%) gangue minerals. The minerals in the massive vein are cemented by sulfide minerals, mainly pyrite and pyrrhotite. Large euhedral magnetite and sub-euhedral orthopyroxene are contained by amphibole and interstitial sulfides.

Geochemistry

Samples were collected at each of the mines, across the wall rock-bleached zone boundary, for chemical analysis. Small, cm-scale samples were removed from the unaltered wall rock and from the bleached zone at each locality. Wall rock chemistries were averaged at each sampling location to reduce variations due to compositional heterogeneity in the cm-scale samples of gneiss (Grant, 2005). The geochemistry of the wall rock and bleached zone samples were compared to constrain elemental gains and losses into the metasomatic fluids within the zone. Grant's Isocon analysis (1987), after Gresens (1967) equation for metasomatic alteration was applied to the bulk oxide geochemistry results and density calculations. In doing so, constant alumina or titanium was assumed. The results from the isocon analysis (by percent volume change) were then used to determine the amount of each oxide gained or lost in grams per 100 grams of bulk wall rock (Δg/100g). The final mass transfer results were averaged for each of the deposits to constrain 'overall' gains and losses into the bleached zones (Table 1). Bulk rock chemistries were also acquired in cm-scale bands across layered vein material from Hogencamp Mine (Table 2). The locations of the bands are shown in Figure 6.

Average metavolcanic wall rock compositions from the Hogencamp deposit resemble an intermediate igneous rock, with 61.4% silica, 14.0% aluminum, 7.2% calcium, 6.7% iron, 4.1% potassium, and 3.6% magnesium and sodium (Table 1). The bleached zone had significant gains in calcium (6.5g), iron (~5.3g), and magnesium (2.8g), with lesser gains in titanium (~0.3g), manganese (<0.1g), and phosphorus (<0.1g), and losses in silica (3.8g), potassium (3.1g), and sodium (0.3g). On average, about 7.8 grams of material was added to the bleached zone, per 100 grams of wall rock. Averaged wall rock from the Pine Swamp deposit is similar to Hogencamp, with 63.7% silica, 14% aluminum, 7.1% iron, 6.3% calcium, 4.5% sodium, 3.2% magnesium, and 1.3% potassium. On average, the Pine Swamp bleached zone gained iron (2.4g), magnesium (~1.2g), potassium (~1.0g), and calcium (0.6g), with minor gains in titanium (~0.2g), manganese (<0.1g), and phosphorus (<0.1g), and losses in silica (~1.4g), sodium (~0.7g), and aluminum (~0.3g) per 100 grams of wall rock. An overall net gain of about 3.1 grams per 100 grams of wall rock was added to form the bleached zone (Table 1).

Table 1. Average wall rock bulk oxides and calculated mass transfer into the bleached zone.

Oxide	Hogencamp Mine		Pine Swamp Mine	
(wt%)	Wall	(Δg/100g)	Wall	(Δg/100g)
SiO_2	61.44	-3.81	63.65	-1.39
TiO_2	0.70	0.28	0.81	0.19
Al_2O_3	14.04	0.00	14.04	-0.28
Fe_2O3	6.66	5.25	7.10	2.44
MnO	0.12	0.07	0.09	0.01
MgO	3.58	2.80	3.23	1.17
CaO	7.24	6.50	6.30	0.62
Na_2O	3.55	-0.30	4.50	-0.66
K_2O	4.10	-3.08	1.26	0.95
P_2O_5	0.15	0.07	0.17	0.03
Total	101.57	7.78g	101.16	3.08g

Table 2. Bulk oxide geochemical results (in wt.%) from layered vein material.

Oxide	Hogencamp Vein			
(wt%)	Hv_1	Hv_2	Hv_3	Hv_4
SiO_2	48.00	47.13	45.98	44.76
TiO_2	0.22	0.32	0.32	0.32
Al_2O_3	11.18	7.93	7.49	8.62
Fe_2O_3	13.06	13.95	12.10	11.59
MnO	0.25	0.27	0.20	0.17
MgO	6.08	8.59	11.73	13.25
CaO	17.58	20.45	21.42	18.58
Na_2O	1.86	0.91	0.65	0.91
K_2O	0.67	0.28	0.50	1.06
P_2O_5	0.49	0.79	1.30	1.02
Total	99.42	100.61	101.69	100.27

Bulk chemical composition of the layered vein material from Hogencamp Mine resembles that of a mafic to ultramafic igneous rock (Table 2). Silica progressively decreases from 48-44.8% into the vein, whereas magnesium increases from 6.1-13.3%. Iron shows a small net loss from 13.1-11.6%, inward whereas alumina and soda decrease progressively away from the wall and increase into the innermost analyzed

layer, from 11.2-7.5% and 1.9-0.7% respectively. Potash decreases close to the wall rock from 0.7-.3%, but increases to 1.1% in the innermost layer. Similarly, calcium and phosphorus progressively increase but then decrease in the innermost layer from 17.6-21.4% down to 18.6%, and 0.5-1.3% down to 1.0%, respectively. Titanium remains relatively stable around 0.2-0.3% across all layers.

Model of Formation

During the later stages of dextral shearing and uplift (~1,008 - 924 Ma), temperature and pressure decreases of the country rock and high fluid pressure caused the shear zones to cross the brittle-ductile transition and dilational right step-over structures formed. Country rock, still in excess of ~700°C from the waning stages of granulite facies metamorphism (~1,024 Ma), was intruded by diorites and associated pegmatites (~1,008 Ma), and later pegmatites. Acid-rich fluids derived from amphiboles and micas in metavolcanic country rock liberated iron, migrated towards the fault zones, and filled the dilational fractures.

These metamorphic fluids flushed into and filled the fractures and equilibrated with wall rocks through exchange reactions (Fig. 8A). The earliest fluids altered wall rock into bleached zone assemblages (Fig. 8B). Changes in chemistries into the bleached zone, at the wall of the vein, relative to unaltered country rock reflect the exchange of various chemical species to and from the buffered fluids. Fluid fluxes were high enough to alter wall rock to different assemblages in the bleached zone. Partially buffered to the composition of local country rocks, these fluids were transported and mixed along strike during seismically induced pumping events, dilating the structures further. The fluids encountered and mixed with fluids from other sections of the fault and changed in composition, finding favorable physical and/or chemical conditions for mineralization within the dilational areas in the fault zones (Fig. 8C).

Pressure drops and fluid mixing at the dilational segments of the faults caused certain species in the fluids to become supersaturated and prompted precipitation. Minerals precipitated in the confined cracks, and resulted in the early layered vein deposits, primarily composed of alternating pyroxene- and amphibole-rich assemblages (Fig. 8C). Nucleation sites were primarily along the walls, and only allowed for fine- to medium-grained crystal growth. The layered vein assemblages provide mineralogical, textural, and geochemical evidence for seismic pumping and the local mixing of fluids, and REE concentrations are evidence of regionally closed system behavior (Kalczynski and Gates, 2014). By the time the first layer of vein assemblages was deposited in the vein fractures, bleached zone forming exchange reactions ceased, as the fluids were no longer in contact with original wall rock, and country rock temperature and fluid pH no longer permitted exchange reactions to occur.

The buffered fluids contributed to layered vein assemblages, as they mixed and flushed along the fault zones. In areas of calc-silicate country rock (Hogencamp deposit), abundant calcium was mobilized into the fluids and resulted in calcium-rich vein assemblages, dominated by clinopyroxene, calcite, amphibole, scapolite, and minor micas (Fig. 9). In quartzofeldspathic and metavolcanic country rock (Pine Swamp deposit), silica was abundant, and most mobilized during mass transfer and vein deposition. Silica-enriched assemblages are dominated by amphibole, orthopyroxene, scapolite, quartz, and/or sulfides.

With continued dilation, large fluid volumes were introduced to and trapped in larger cavities, and the dominant mode of mineralization favored massive deposits (Fig. 8D). Mineralization along the faults eventually sealed fluids in the fault zones and dilational segments as the system became closed, even at the local level. Fluids became iron and volatile-rich as other chemical species were depleted through crystallization. Fluid ratios increased, depressing crystal nucleation sites and aiding in element mobility

allowing massive magnetite and ferromagnesian-rich assemblages, including euhedral crystals, to form in these cavities (Fig. 8D). Fluid pressure in these large cavities was also lower than surrounding country rock, dropping the solubility of iron and prompting mineralization. Mixing of carbonate-rich fluids neutralized the acidic fluids, also lowering the solubility of magnetite, further promoting precipitation. Temperature and pressure decreases limited the crystallization reactions, dominantly mineralizing magnetite and the few other gangue minerals.

As chemical species were depleted crystallizing the massive gangue minerals, the remaining dissolved iron oxidized and was deposited as the massive magnetite bodies. Locally buffered fluids also contributed to the gangue minerals of the massive assemblages. Clinopyroxene and interstitial calcite formed in deposits near calc-silicate and marble (Hogencamp), and orthopyroxene/amphibole and interstitial quartz and/or pyrite formed in deposits near quartzofeldspathic and metavolcanic country rock (Pine Swamp). Late in the massive vein mineralization process the interstitial minerals (calcite, quartz, and sulfides) overprinted the massive assemblages (see Kalczynski and Gates, 2014).

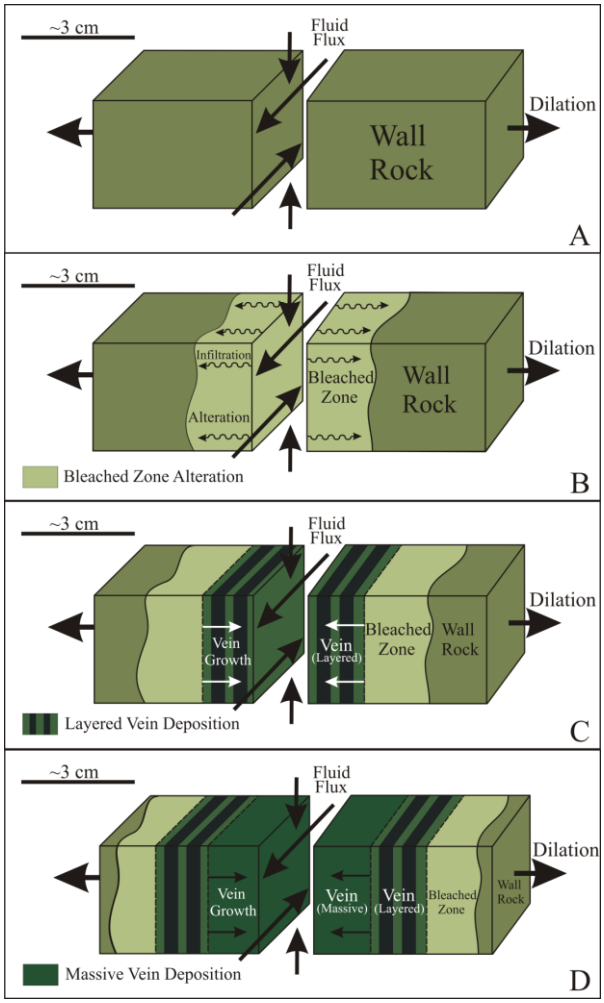

Figure 8. Schematic block model of the formation of the vein deposits. (modified after Weisenberger and Bucher, 2010).

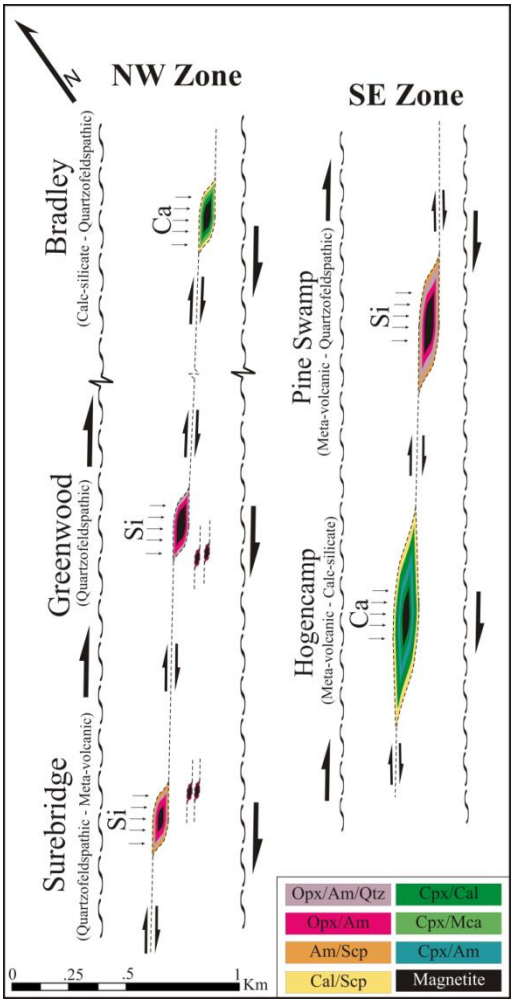

Figure 9. Schematic diagram of the vein deposit's dominate mineral assemblages, and sources of some chemical species.

LATE PROTEROZOIC TECTONIC HISTORY

A volcanic pile formed about 1.2 Ga in an island arc or marine magmatic arc setting characterized by layered intermediate and mafic rocks, and associated plutons and volcaniclastic sediments (Gates *et al.*, 2001). This sequence underwent granulite facies metamorphism, about 1,050 Ma associated with the Ottawan phase of the Grenville orogeny (Gates *et al.*, 2003). Locally, anatexis produced migmatites, granite sheets, and the early pegmatites (Gates *et al.*, 2003). The Ramapo and Reservoir fault zones were activated as ductile reverse faults. Subsequent diorite intrusions occurred around 1,008 Ma, either the result of delamination at the end of the first event, or the early dilational stages of the next event (Gates *et al.*, 2003). This second event is characterized by dextral strike-slip movement during a period of rapid uplift and unroofing at approximately 1,008 Ma to 924 Ma (Gates and Krol, 1998). Thick anastomosing zones of mylonite formed, overprinting previous features. Offset reached upwards of 100's of kilometers (Gates *et al.*, 2003). Both Ramapo and Reservoir fault zones were reactivated as ductile dextral strike-slip faults. Strike-slip shearing continued during rapidly decreasing temperatures, resulting in smaller, local shear zones crossing the brittle-ductile transition and becoming dilational (Gates *et al.*, 2003). Regionally derived, but locally chemically buffered fluids resulted in the mineralization of magnetite vein assemblages in dilational shear zones. The vein assemblages reflect the changing chemistries of the fluids from changes in flux, fluid buffering source, chemical, and/or physical conditions (Kalczynski and Gates, 2014).

CONCLUSIONS

The Grenville event in the New Jersey and Hudson Highlands of the central Appalachians was formed in a fourfold tectonic scenario (Gates *et al.*, 2003).

1. Deposition of volcanic and volcaniclastic sediment within a subduction zone complex ca 1.2 Ga.
2. Continental collision of the arc with another continent to the east during the building of the Rodinian supercontinent occurred at ca. 1,050-1,020 Ma. Granulite facies metamorphism and extensive pegmatite intrusion accompanied this event.
3. After orogenesis ceased, dioritic melts intruded the area, ca. 1,008 Ma., accompanying period of extension or mantle delamination.
4. Strike-slip shearing resulting from tectonic escape probably lasted from 1,008-980 Ma or later. There was a rapid decrease in temperature during this event resulting in the shear zones crossing the brittle-ductile transition and becoming dilational. Extensive mineralization occurred within these dilational fractures.

FIELD GUIDE AND ROAD LOG

Meeting Point: West parking lot of the Double Tree Inn, located at 425 NY-59, Nanuet, NY, 10954.

Meeting Point Coordinates: 18T 0584372mE, 4549264mN

Meeting Time: 8:30 AM

Distance in Miles (km)		Route Description
Cumulative	Point to Point	
0.0 (0.0)	0.0 (0.0)	Assemble in the western parking lot of the Double Tree Inn in Nanuet, NY.
0.3 (0.5)	0.3 (0.5)	Head East on NY-59 E toward Rose Rd.
0.5 (0.8)	0.2 (0.3)	Use the right lane to take the ramp to Palisades County Rd N.
9.9 (15.9)	9.4 (15.1)	Merge onto Palisades Interstate Parkway N.
10.1 (16.3)	0.2 (0.3)	Take exit 14 for Willow Grove Rd toward Letchworth Village.
11.6 (18.7)	1.5 (2.4)	Turn left onto Willow Grove Rd.
15.1 (24.3)	3.5 (5.6)	Merge onto Kanawauke Rd.
15.4 (24.8)	0.3 (0.5)	At the Kanawauke traffic circle, take the second exit and stay on Kanawauke Rd (Route 106).
16.0 (25.7)	0.6 (1.0)	Continue on Kanawauke Rd for 0.6 miles until reaching the bridge over the eastern-most extent of Little Long Pond. If needed, parking can be found a quarter mile east on Kanawauke Rd at the picnic area (lavatory facilities). Walk 100 feet to the north-west on Kanawauke Rd to the first road-cut (Stop 1, Fig. 11).

STOP 1: Unsheared Metavolcanic Gneiss, Harriman State Park, NY

Location Coordinates: 18T 0573484mE, 4565104mN

Strongly interlayered intermediate and mafic gneisses with migmatitic bodies, just outside of the SE shear zone. Mafic layers are characterized by assemblages of clinopyroxene and amphibole with minor plagioclase, magnetite, sphene, and apatite. Intermediate layers are mainly plagioclase with minor quartz, apatite, amphibole, and biotite. The felsic leucosome is composed of coarse plagioclase, quartz, and K-feldspar, which form veins and clots including classic “net veining”. Minerals exhibit preferred orientations in the gneiss and appear granular in the leucosome. Late stage K-feldspar pegmatites can also be observed in this outcrop, containing mafic gneiss xenoliths.

Gneisses exhibit a strongly banded, intermediately dipping, foliation that strikes N-NE. Isoclinal intrafolial folds can also be observed, with axis following similar orientation. This deformation is indicative of main stage Grenville tectonism, and was unaffected during the later tectonic event, associated with the formation of the ore deposits. Contrast these rocks with Stop 2.

Distance in Miles (km)		Route Description
Cumulative	Point to Point	
16.0 (25.7)	0.0 (0.0)	Head west on route 106 for roughly 600 feet to the large peninsula protruding into Little Long Pond. Proceed 250 feet to the south to reach the tip of the peninsula (Stop 2, Fig. 12).

STOP 2: Southeastern Shear Zone Boundary, Harriman State Park, NY

Location Coordinates: 18T 0573272mE, 4565124mN

Several meter scale lozenge and cigar shaped boudins of mafic gneiss are contained within mylonitic quartzofeldspathic gneiss, with folded biotite and local amphibole-rich layers. The layers appear contorted and wrap around the mafic bodies. The encased mafic gneiss is similar to that of Stop 1, however it also contains contorted folds and veins of magnetite. The long axis of the bodies and fold axis appear sub-parallel, and shallowly plunge to the northeast.

Both Stops 1 and 2 are similar in composition and therefore grouped within the same metavolcanic sequence. Long axis and fold axes roughly parallel shear zone boundaries and fabrics within. This location is at the edge of the southeastern dextral, strike-slip shear zone. Deformation steadily increases to the northwest, into the central shear zone, characterized by a steepening of planar fabric and increase in intensity of linear fabric. The contrast of the features at Stop 1 with Stop 2 shows the difference between the first main Grenville and second strike-slip events.

Distance in Miles (km)		**Route Description**
Cumulative	**Point to Point**	
16.0 (25.7)	0.0 (0.0)	Locate the gated path directly on the opposite side of Kanawauke Rd. Walk this path heading north for a quarter mile, to the intersection with Dunning Trail (E-W trending). Head roughly northeast on Dunning Trail for about a half mile until you reach several large holes in the ground, and the path crosses a small stream. Hike upstream for roughly 100 feet until you are almost cliff side. A linear open pit mine should be visible to the southwest and a large mine shaft to the northeast into the cliff, beneath Cape Horn (Stop 3, Fig. 13).

STOP 3: Hogencamp Mine, Harriman State Park, NY

Location Coordinates: 18T 0573790mE, 4566280mN

Hogencamp Mine lies in the southern part of the mineralized zone. Here the sheared wall rock is dominated by quartzofeldspathic and amphibole-pyroxene (metavolcanic) gneisses with interlayered calc-silicate gneiss and marble locally. Hogencamp Mine was active from the earliest to latest 18th century. It is characterized by a series of meter to several meter scale horizontal and vertical mine shafts and open pit mines. The mines can be traced along strike for up to a kilometer. The mineralized zone that hosts Hogencamp Mine is roughly 6 kilometers long and extends into Pine Swamp Mine (Stop 4). The vein ranges in thickness from 3 to 15 meters at the mine locations to as little as one meter in the narrow zones connecting the deposits. The Hogencamp Mines can be followed to the southwest from this location for up to a kilometer.

The vein-wall rock contact is sharp and semi-concordant to mylonitic foliation. On the small-scale it appears slightly discordant, crosses foliation and erodes into the wall rock. This is best observed in the open pit mine, directly in front of the northeastern most mine shaft, below Cape Horn (Fig. 10). Here, the bleached zone is characterized by the deposition of calcite and scapolite, and retrogression pyroxene to amphibole, also containing phlogopite, calcite, and minor apatite locally. Earliest vein deposit is characterized by layered amphibole, orthopyroxene, and clinopyroxene, later by massive clinopyroxene and magnetite, cemented by late stage, interstitial calcite in the ore zone. Clinopyroxene and localized magnetite are euhedral, forming doubly terminated crystals, thought to have crystallized in cavities. The veins are also intruded by very coarse grained pegmatites which contain xenoliths of the mafic vein material.

Figure 10. Hogencamp (Stop 3, left) and Pine Swamp (Stop 4, right) Mines.

Distance in Miles (km)		Route Description
Cumulative	Point to Point	
16.0 (25.7)	0.0 (0.0)	Back on Dunning Trail, walk east than north-northeast, another half mile until you reach a large swamp to the east, and a large, steep hillside to the west, littered with dark-colored mine tailings. Locate the makeshift path on the hillside. Take this path uphill for about two hundred feet, until your reach the entrance to the mine (Stop 4, Fig. 13).

STOP 4: Pine Swamp Mine, Harriman State Park, NY

Location Coordinates: 18T 0574253mE, 4566795mN

Pine Swamp Mine lies in the northern part of the shear zone within the same mineralized vein which hosts Hogencamp Mine, roughly one kilometer alone strike (NE). Pine Swamp is also characterized by a 3 to 12 meter horizontal mine openings and several, meter scale open pit mines (Fig. 10). The mines that compromise the Pine Swamp deposit can be traced along strike for several hundred meters, with minor semi-concordant offshoots in the northern extent of the deposit. This portion of the hydrothermal vein lies dominantly within sulfide-bearing quartzofeldspathic gneiss country rock, which contains interlayered metavolcanic gneisses. The bleached zone is primarily defined by retrogression of pyroxene to amphibole, also containing minor amounts of scapolite, and apatite locally. Orthopyroxene and amphibole dominate the narrow layered vein and thick massive sequences followed by the magnetite deposits. Massive minerals are locally cemented by late stage sulfide minerals, mainly pyrite and pyrrhotite. The flat wall adjacent to the mine proper is yellow to rust colored, due to the weathering of the sulfide-rich country rock. Massive minerals orthopyroxene, amphibole, and substantial magnetite can also be observed.

Distance in Miles (km) Cumulative	Point to Point	Route Description
16.0 (25.7)	0.0 (0.0)	Take Dunning Trail south and west back to the first intersection of paths. Head south on the first path, to exit back at the gated entrance.
16.7 (26.9)	0.7 (1.1)	Drive east on Kanawauke Rd to Kanawauke Circle, and take the third exit to head north on Seven Lakes Drive.
19.1 (30.7)	2.4 (3.9)	Continue north on Seven Lakes Drive until reaching Lake Tiorati. Stop 5 is a large road cut, ~650 feet north of Cedar Pond Rd, on the left (west) side of the Seven Lakes Drive. Please park vehicles as far on the shoulder closest to the lake as possible. Lavatory facilities and additional parking can be found ~3/4 of a mile north on Seven Lakes Drive at Tiorati Circle.

STOP 5: Lake Tiorati Diorite, Harriman State Park, NY

Location Coordinates: 18T 0575665mE, 4568681mN

Pluton of coarse- to very coarse grained black and white speckled diorite. On the south side of the outcrop, the diorite is equigranular in texture with random grain orientation. It contains a roof pendant of well-foliated biotite quartzofeldspathic gneiss that exhibits crenulation cleavage. The xenolith contains a drag fold along its contact with the diorite. It also contains a rim of granitic pegmatite that connects to pegmatite and quartz veins within the diorite. The diorite contains plagioclase and hornblende and clinopyroxene but with brown cores or orthopyroxene. Other phases include magnetite and ilmenite. In the northern part of the exposure, the diorite is crossed by anastomosing mylonite bands. The mylonite strikes northeast and is near vertical. Lineations plunge shallowly to the northeast. Kinematic indicators include rotated porphyroclasts and S-C fabric. Where it can be determined, shear sense is consistently dextral.

Subsequent to the first tectonic event which included the nappe emplacement and granulite facies metamorphism, there was a period of intermediate plutonism. The xenolith was deformed and metamorphosed prior to intrusion. The xenolith became more ductile as a result of the heat of the pluton. Thus, drag folds formed along its edges as it fell into the magma. The magma was hot enough to cause partial melting of the rim of the xenolith, producing a granitic melt. The diorite crystallized at a higher temperature than the granitic melt. Fractures opened in the newly crystallized rock and the remaining granitic melt squeezed into them forming the veins. Later deformation produced the mylonitic fabric in the diorite. This outcrop is at the eastern edge of a large dextral strike-slip shear zone with similar orientation.

Distance in Miles (km) Cumulative	Point to Point	Route Description
21.6 (34.8)	2.5 (4.0)	Turn around on Seven Lakes Drive to head southbound.
26.7 (43.0)	5.1 (8.2)	At the Kanawauke Circle, take the first exit onto Kanawauke Rd (Route 106).
27.6 (44.4)	0.9 (1.4)	Continue onto NY-17A westbound. Stop 6 is a large road cut on the northern (right) side of 17A. Park on the shoulder of the road, and proceed onto the outcrop.

STOP 6: 17A Indian Hill Mylonite Zone, Tuxedo, NY

Location Coordinates: 18T 0567611mE, 4565080mN

The rock is biotite quartzofeldspathic mylonite gneiss with interlayers of biotite gneiss locally, interpreted to have a volcaniclastic origin. The mylonite is well foliated and lineated and composed of

plagioclase, quartz, potassium feldspar, and biotite. This mylonite exhibits well developed kinematic indicators including S-C fabric, reverse shear cleavage (RSC), rotated porphyroclasts, and shear bands. These kinematic indicators show a consistent dextral shear sense. The width of the zone and the low S-C angle indicate significant offset during the second event. Because this shear zone developed in biotite-rich gneiss, it displays kinematic indicators better than most zones. It is another in the series of anastomosing dextral shear zones that were produced during the second event. The gneiss is interpreted to have a volcaniclastic origin.

Distance in Miles (km)		**Route Description**
Cumulative	**Point to Point**	
28.1 (45.2)	0.5 (0.8)	Head West on NY-17A W toward Clinton Rd.
29.5 (47.5)	1.4 (2.3)	Make a U-turn at Clinton Rd.
36.5 (58.7)	7 (11.3)	Turn right to merge onto NY-17 S.
36.8 (59.2)	0.3 (0.5)	Use the right lane to take the NY-17 S/Interstate 87 S/New York Thruway ramp to Interstate 287.
37.8 (60.8)	1 (1.6)	Merge onto I-87 S/NY-17 S.
38.6 (62.1)	0.8 (1.3)	Use the right lane to take exit 15 for NY-17 S/I-287 S toward New Jersey.
39.2 (63.1)	0.6 (1.0)	Continue onto I-287 S (entering New Jersey).
52.7 (84.8)	13.5 (21.7)	Keep Right to stay on I-287 S.
52.8 (85.0)	0.1 (0.2)	Take exit 52A-52B for NJ-23 toward Riverdale/Wayne/Butler.
53.1 (85.5)	0.3 (0.5)	Keep left at the fork, follow signs for State Highway 23 and merge onto NJ-23 S/State Highway 23 S.
53.7 (86.4)	0.6 (1.0)	Merge onto NJ-23 S/State Highway 23 S.
53.7 (86.4)	0 (0)	Slight right onto West Parkway.
54.2 (87.2)	0.5 (0.8)	Turn right onto West Parkway. Stop 7 is located in a small (Foot Hill) park on the right (northwest) side of West Parkway, closest to I-287. Park in the parking lot and proceed to the outcrop ~100 feet to the west of the parking lot.

Figure 11. Stop 7. Outcrop of Ramapo fault zone, located in Riverdale, NJ.

STOP 7: Ramapo Fault Zone, Riverdale, NJ

Location Coordinates: 18T 0557739mE, 4536780mN

The northeast-trending Ramapo fault zone is the major border fault which juxtaposes the Proterozoic gneisses of the New Jersey Highlands with the Mesozoic sedimentary and igneous rocks of the Newark Basin. Width of the fault zone varies from approximately 5 to 10 km (Ratcliffe, 1980). Abundant moderate to steep southeast-dipping zones up to 25 m thick are developed within the granitic gneisses of the fault zone and exhibit mesoscopic S-C mylonite fabric. The fault zone is also intruded by mafic dikes which have been subsequently sheared during brittle reactivation. The Ramapo fault zone originally developed as a reverse right-lateral strike-slip fault during the Grenville orogeny (Ratcliffe, 1980) and has a long and complex kinematic history which included four to five recognizable episodes of fault movement. Despite the long history of reactivation of the zone there is no strong evidence of any post-Mesozoic or neotectonic movement. The mylonites within the Ramapo fault zone consistently indicate top to the northwest reverse faulting. These zones were reactivated under mid- to upper-greenschist facies conditions during the Taconic orogeny approximately 450 to 460 Ma (Ratcliffe, 1980) (Costa and Gates, 1993).

This exposure is located in Foot Hill Park at the end of West Parkway in Riverdale, New Jersey (Fig. 11). The entire exposure consists of ultramylonite of the Ramapo fault zone. Glacial striations oriented essentially north-south have polished the surface of the exposure. The alternating black and white/gray bands of foliation dip moderately to the southeast. The black bands are composed of fine-grained foliated chlorite, whereas the white/gray bands are quartzofeldspathic. Both quartz and feldspar deformed in a ductile manner, and are extensively dynamically recrystallized. Small grains of pyrite are present within the foliation.

Distance in Miles (km)		**Route Description**
Cumulative	**Point to Point**	
54.2 (87.2)	0 (0)	Head north on West Parkway (left out of the Foot Hill Park parking lot).
54.7 (88.0)	0.5 (0.8)	Keep Left to continue onto Boulevard.
57.6 (92.7)	2.9 (4.7)	Use any lane to turn left at the 1st cross street onto NJ-23 N.
68.1 (109.6)	10.5 (16.9)	Continue on NJ-23 N.
68.1 (109.6)	0 (0)	Slight right toward Canistear Rd.
68.2 (109.8)	0.1 (0.2)	Turn left onto Canistear Rd.
68.2 (109.8)	0 (0)	Turn left at the 1st cross street onto NJ-23 S/Paterson Hamburg Turnpike S.
68.7 (110.6)	0.5 (0.8)	Continue on NJ-23 S for half a mile. Park on the right hand shoulder (west side) of NJ-23 S, just before the road-side barrier and the shoulder narrows. Walk down the hill and cross the stream at the narrow portion. Continue to walk southbound along the western edge of Oak Ridge Reservoir for ~half a mile. The exposures are just around the bend of the reservoir, at the reservoirs edge, facing southward.

STOP 8: Reservoir Fault Zone, West Milford, NJ

Location Coordinates: 18T 0542826mE, 4546228mN

This stop illustrates how hydrothermal chemical and resulting mineralogical changes in a fault zone can change deformation style from brittle to ductile. We will observe undeformed protolith (granitic gneiss), hydrothermally mineralized cataclasite (brittle), and mylonite (ductile) of the mineralized zone. The undeformed to slightly deformed rock is mapped as pyroxene gneiss and interpreted as a metasedimentary sequence. The rock consists of diopside-, amphibole- and rarely scapolite-bearing granitic to quartz dioritic gneiss with sparse interlayered amphibolite gneiss and pegmatite veins. The faulted rocks are cataclasite and breccia with mainly rounded blocks and clasts of granitic-quartz dioritic gneiss.

The matrix material is composed of ~95% randomly oriented actinolite with minor epidote, albite, chlorite, and sulfides although finely ground xenocrystic phases from the gneiss are locally abundant. Thin ductile shear zones can be found in this outcrop but the structures observed are primarily the result of brittle deformation coupled with hydrothermal activity that produced the amphibole-sulfide mineralization. After formation through hydrothermal alteration, the amphibole-rich matrix underwent ductile deformation forming an S-C mylonite, more typical of rocks found in the center of the fault zone. The ductile deformation produced a strong foliation with significantly reduced grain size. Kinematic indicators include dragged foliation, S and C bands, rotated porphyroclasts, and offset markers showing a consistent dextral strike-slip sense (Gates, 1993).

Distance in Miles (km)		**Route Description**
Cumulative	**Point to Point**	
68.7 (110.6)	0 (0)	Back-track to return to the road side and vehicles.
81.1 (130.5)	12.4 (20.0)	Head south on NJ-23 S.
81.4 (131.0)	0.3 (0.5)	Use the right lane to merge onto I-287 N via the ramp to Mahwah.
81.4 (131.0)	0 (0)	Merge onto I-287 N.
88.0 (141.6)	6.6 (10.6)	Keep left to stay on I-287 N (entering New York).
96.0 (154.5)	8 (12.9)	Use the right 2 lanes to merge onto I-287 E/I-87 S toward Tappan Zee Bridge/New York City.
103.7 (166.9)	7.7 (12.4)	Take exit 14 for NY-59 toward Spring Valley/Nanuet.
103.9 (167.2)	0.2 (0.3)	Use the left 2 lanes to turn left onto NY-59 E.
105.6 (169.9)	1.7 (2.7)	Return to Double Tree Inn at 425 New York 59, Nanuet, NY, 10954. Destination will be on the right.
		END TRIP

REFERENCES CITED

Bartholomew, M.J. and Lewis, S.E., 1988, Peregrination of Middle Proterozoic massifs and terranes within the Appalachian orogen, eastern U.S.A.: Trabajos de Geologia, v. 17, p. 155-165.

Beach, A., 1975, The geometry of en-echelon vein arrays: Tectonophysics, v. 28, p. 245-263.

Boullier, A.M. and Bouchez, J.-L., 1978, Le quartz en rubans dans las mylonites: Bull. Soc. Geol. Fr., v. 20, p. 253-262.

Costa, R.E., 1991, Structural evolution and neotectonics of the Ramapo fault system, northern New Jersey: Dept. of Geological Sciences, Rutgers University, Newark, unpublished Master's thesis, 83 p.

Costa, R. and Gates, A.E., 1993, Multiple episodes of movement on the Ramapo fault system, northern New Jersey, *in* Puffer, J.H. (ed.), Geologic Traverse across the Precambrian Rocks of the New Jersey Highlands: Geological Association of New Jersey Field Guide and Proceedings, v. 10, p. 168-195.

Dallmeyer, R.D., 1974, Metamorphic history of the northeastern Reading Prong, New York and Northern New Jersey: Journal of Structural Geology, v. 15, p. 325-359.

Drake, A.A. Jr., 1984, The Reading Prong of New Jersey and eastern Pennsylvania, An appraisal of rock relations and chemistry of a major Proterozoic terrane in the Appalachians, *In* Bartholomew, M.J. (ed.), The Grenville Event in the Appalachians and Related Topics, Geological Society of America Special Paper 194, p. 94-109.

Dodd, R.T. Jr., 1965, Precambrian geology of the Popolopen Lake quadrangle, southeastern New York: New York State Museum and Science Service Map and Chart Series, No. 6, 39 p.

Eisbacher, G.H., 1970, Deformation mechanisms of mylonite rocks and fractured granulites in Cobequid Mountains, Nova Scotia, Canada: Geological Association of America Bulletin, v. 81, p. 2009-2020.

Eugster, H.P., 1986, Minerals in hot water: American Mineralogist, v. 71, p. 655-673.

Finks, R.M., 1990, The Green Pond outlier as a Silurian right-lateral transpressional basin: Geological Society of America, Abstracts with Programs, v. 22, p. 15.

Gates, A.E., 1993, Chemical changes in mylonites and cataclasites of the Reservoir fault zone, New Jersey, *in* Puffer, J.H. (ed.) Geologic Traverse across the Precambrian Rocks of the New Jersey Highlands, Geological Association of New Jersey Field Guide and Proceedings, v. 10, p. 148-167.

Gates, A.E., 1995, Middle Proterozoic dextral strike-slip event in the central Appalachians- Evidence from the Reservoir fault, NJ: Journal of Geodynamics, v. 19, p. 195-212.

Gates, A.E., 1998, Early compression and late dextral transpression within the Grenvillian Event of the Hudson Highlands, NY, USA, *in* Sinha, A.K. (ed.), Basement Tectonics 13; Dordrecht, The Netherlands, Kluwer Academic Publishers, p. 85-98.

Gates, A.E., and Costa, R.E., 1998, Multiple reactivations of rigid basement block margins: Examples in the northern Reading Prong, USA, *in* Gilbert, M. C. and Hogan, J.P. (eds.), Basement Tectonics 12: Central North America and Other Regions; Dordrecht, The Netherlands, Kluwer Academic Publishers, p. 123-153.

Gates, A.E. and Krol, M.A., 1998, Kinematics and thermochronology of late Grenville escape tectonics from the central Appalachians: Geological Society of America, Abstracts with Programs, v. 30.

Gates, A.E., Valentino, D.W., Gorring, M.L., Chiarenzelli, J.R., and Hamilton, M.A., 2001, Bedrock geology,

geochemistry and geochronology of the Grenville Province in the western Hudson Highlands, New York, *In* Gates, A.E. (ed.), Geology of the Lower Hudson Valley: New York State Geological Association Guidebook, p. 177–204.

Gates, A.E., Valentino, D.W., Chiarenzelli, J., Gorring, M., and Hamilton, M., 2003, Field Trip to the Western Hudson Highlands: 2003 Long Island Geologists Conference, 30 p.

Gates, A.E., Valentino, D.W., Chiarenzelli, J.R., Solar, G.S., and Hamilton, M.A., 2004, Exhumed Himalayan-type syntaxis in the Grenville Orogen, northeastern Laurentia: Journal of Geodynamics, v. 37, p. 337–359.

Gates, A.E., Valentino, D.W., Gorring, M., Thern, E.R., and Chiarenzelli, J.R., 2006, Rodinian collisional and escape tectonics in the Hudson Highlands, New York, *In* Pazzaglia, F.J. (ed.), Excursions in Geology and History: Field Trips in the Middle Atlantic States, Geological Society of America Field Guide 8, p. 65-82.

Grant, J.A., 1986, The isocon diagram—a simple solution to Gresens' equation for metasomatic alteration: Economic Geology, v. 81, p. 1976–1982.

Grant, J.A., 2005, Isocon analysis: A brief review of the method and applications: Physics and Chemistry of the Earth, v. 30, p. 997-1004.

Gresens, R.L., 1967, Composition–volume relationships of metasomatism: Chem. Geol., v. 2, p. 47–55.

Gundersen, L.C.S., 1986, Geology and geochemistry of the Precambrian rocks of the Reading Prong, New York and New Jersey - Implications for the genesis of iron-uranium-rare earth deposits, *In* Carter, L.M.H. (ed.), USGS Research on Energy Resources -1986 Programs and Abstracts, US Geological Survey Circular, v. 974, p. 19.

Gundersen, L.C.S., 2004, Tectonics and metallogenesis of Proterozoic rocks of the Reading Prong: Journal of Geodynamics, v. 37, p. 361-379.

Hague, J.M., Baum, J.L., Hermann, L.A., and Pickering, R.J., 1956, Geology and structure of the Franklin-Sterling area, New Jersey: Geological Society of America Bulletin, v. 68, p. 435-473.

Harding, T.P., 1974, Petroleum traps associated with wrench faults: American Association of Petroleum Geologists Bulletin, v. 58, p. 1290-1304.

Helenek, H.L., 1971, An investigation of the origin, structure and metamorphic evolution of major rock units in the Hudson Highlands: PhD Thesis, Brown University.

Herman, G.C. and Mitchell, J.P., 1991, Bedrock geologic map of the Green Pond Mountain region from Dover to Greenwood Lake, New Jersey: New Jersey Geological Survey, Geologic Map Series 91-2.

Hippert, J.F.M., 1993, 'V'-pull-apart microstructures: a new shear sense indicator: Journal of Structural Geology, v. 15, p. 1393-1403.

Hull, J., Koto, R., and Bizub, R., 1986, Deformation zones in the Highlands of New Jersey, *in* Husch, J.M. and Goldstein, F.R., (eds.), Geology of the New Jersey Highlands and Radon in New Jersey, Geological Association of New Jersey Field Guide, v. 3, p. 19-67.

Kalczynski, M.J. and Gates, A.E., 2014, Hydrothermal alteration, mass transfer, and magnetite mineralization in dextral shear zones, western Hudson Highlands, New York, United States. *Ore Geology Reviews* v. 61, p. 226-247.

Krol, M.A., Gosse, J., Hedlund, C., Messina, T., Tenore-Nortrup, J., Winslow, D., and Zeitler, P., 1992, 40Ar/39Ar constraints in the extent of both Paleozoic and and Mesozoic thermal overprinting of Reading Prong basement adjacent to the Newark basin, EOS Transactions, American Geophysical Union Abstracts with Programs, v. 73, p. 279.

Krol, M.A. and Zeitler, P.K., 1994, 40Ar/39Ar constraints on regional thermal resetting of alkali feldspars from the Newark basin and adjacent Reading Prong, Eighth International Conference on Geochronology, Cosmochronology and Isotope Geology, U.S. Geological Survey Circular, v. 1107, p. 180.

Lister, G.S. and Snoke, A.W., 1984, S-C mylonites: Journal of Structural Geology, v. 6, p. 617-638.

Lewis, J.V. and Kummel, H.B., 1912, Geologic map of New Jersey (1910-1912), New Jersey Dept. of Conservation and Economic Development, Atlas Sheet 20.

Lupulescu, M. and Gates, A.E., 2006, Iron deposits from Hudson Highlands, NY: Systematics, mineralogy, mineral chemistry and tectonic setting: Geological Association of New Jersey Field Guide and Proceedings, v. 23, p. 46-59.

Malizzi, L. D. and Gates, A. E., 1989, Late Paleozoic deformation in the Reservoir Fault zone and Green Pond Outlier: N. Y. State Geological Assoc. Field Trip Guidebook, v. 61, p. 75-93.

Mitchell, J.P. and Forsythe, R., 1988, Late Paleozoic non-coaxial deformation in the Green Pond outlier, New Jersey Highlands: Geological Society of America Bulletin, v. 100, p. 45-59.

Olsen, P.E., 1980, Triassic and Jurassic formations of the Newark basin, in (Manspeizer, W. eds) Field studies of New Jersey Geology, New York State Geological Association Guidebook, v. 52, p. 1-39.

Passchier, C.W. and Simpson, C., 1986, Porphyroclast systems as kinematic indicators: Journal of Structural Geology, v. 8, p. 831-843.

Petit, J.P., 1987, Criteria for the sense of movement on fault surfaces in brittle rocks: Journal of Structural Geology, v. 9, p. 597-608.

Puffer, J.H. and Gorring, M.L., 2005, The Edison magnetite deposits in the context of pre-, syn-, and post-orogenic metallogenesis in the Grenville Highlands of New Jersey: Canadian Journal of Earth Sciences, v. 42, p. 1735-1748.

Ratcliffe, N.M., Armstrong, R.L., Chai, B.H., and Senechal, R.G., 1972, K-Ar and Rb-Sr geochronology of the Canopus pluton, Hudson Highlands, New York: Geological Society of America Bulletin, v. 83, p. 523-530.

Ratcliffe, N.M., 1980, Brittle faults (Ramapo fault) and phyllonitic ductile basement rocks of the Ramapo seismic zones, New York and New Jesrey, and their relationship to current seismicity, *in* Manspeizer, W. (ed.). Field studies of New Jersey Geology, New York State Geological Association Guidebook, v. 52, p. 278-311.

Ratcliffe, N.M., 1981, Cortlandt-Beemerville magmatic belt: a probable late Taconian alkali cross trend in the central Appalachians: Geology, v. 9, p. 329-335.

Ratcliffe, N.M., Armstrong, R.L., Mose, D.G., Seneschal, R., Williams, N., and Baiamonte, M.J., 1982, Emplacement history and tectonic significance of the Cortlandt Complex, related plutons, and dike swarms in the Taconide zone of southeastern New York based on K-Ar and Rb-Sr investigations: American Journal of Science, v. 282, p. 358-390.

Sibson, R.H., 1977, Fault rocks and fault mechanics: Jour. Geol. Soc. London, v. 123, p. 191-213.

Simpson, C. and Schmid, S.M., 1983, An evaluation of criteria to deduce the sense of movement in sheared rocks: Geological Society of America Bulletin, v. 94, p. 1281-1293.

Simpson, C., 1985, Deformation of granitic rocks across the brittle-ductile transition: Journal of Structural Geology, v. 7, p. 503-511.

Stauffer, M.R., 1970, Deformation textures in tectonites: Canadian Jour. Earth Sciences, v. 7, p. 498-511.

Tullis, J.A. and Yund, R.A., 1977, Experimental deformation of dry Westerly granite: Journal of Geophysical Research, v. 82, p. 5705-5718.

Tullis, J.A. and Yund, R.A., 1987, Transition from cataclastic flow to dislocation creep of feldspar: Mechanisms and microstructures: Geology, v. 15, p. 591-595.

Volkert, R.A., 1993, Geology of the Middle Proterozoic rocks of the New Jersey Highlands, in (Puffer, J.H., ed.) Geologic Traverse across the Precambrian Rocks of the New Jersey Highlands, Geological Association of New Jersey Field Guide and Proceedings, v. 10, p. 23-55.

Volkert, R.A. and Drake, A.A. Jr., 1999, Geochemistry and stratigraphic relations of Middle Proterozoic rocks of the New Jersey Highlands: U.S. Geological Survey Professional Paper 1565-C, 77 p.

Volkert, R.A., 2001, Geologic setting of Proterozoic Iron, Zinc, and Graphite Deposits, New Jersey Highlands: Society of Economic Geology Guidebook Series, v. 35, p. 59-73.

Volkert, R.A., Aleinikoff, J.N., and Fanning, C.M., 2010, Tectonic, magmatic, and metamorphic history of the New Jersey Highlands: New insights from SHRIMP U-Pb geochronology: Geological Society of America Memoirs, v. 206, p. 307-346.

White, S.H., Burrows, S.E., Carreras, J., Shaw, N.D. and Humphreys, F.J., 1980, On mylonites in ductile shear zones: Journal of Structural Geology, v. 2, p. 175-187.

TRIP B4: LOWER TO MIDDLE DEVONIAN ROCKS OF THE DELAWARE WATER GAP NATIONAL RECREATION AREA, NEW JERSEY: FRACTURE AND LITHOLOGIC CONTROL ON ROCK-SHELTERS, KARST AND GROUNDWATER FLOW

DON MONTEVERDE
New Jersey Geological and Water Survey, Trenton, 08624

RON WITTE
New Jersey Geological and Water Survey, Trenton, 08624

ABSTRACT

Kittatinny Mountain is a major ridge that crosses eastern Pennsylvania, through northwestern New Jersey and into southern New York. It is underlain by Middle Silurian Shawangunk Formation, a resistant quartz sandstone to quartz-pebble conglomerate that separates younger Silurian and Devonian carbonate and clastic sediments on the west from Cambrian and Ordovician flysch and platform carbonates to the east. Kittatinny Mountain displays a change in structural trend from northeastward to northward near an exposure of Upper Ordovician nepheline syenite, part of the Beemerville Intrusive Complex. Westward this same structural trend is marked by upright and northwest directed overturned folds and well developed cleavage in Pennsylvania, which becomes a broad zone of gently dipping formations generally devoid of a penetrative cleavage in New Jersey. Here outcrop widths of the units are doubled. Tight and overturned folding with cleavage development and an associated decrease in outcrop width reappears farther to the north across the New York border. This undeformed zone widens to the west creating bowed margins on maps and DEMs with the syenite body at the center of the bow.

Did the Beemerville Intrusive Complex form a rigid block that created a strain shadow against Alleghenian westward directed compressional deformation? Preliminary field data in conjunction with regional gravity and seismic reflection studies while not definitively pointing to this hypothesis as the only possible conclusion it also does not negate it as a possible answer. Other possible explanations exist including indentor-controlled variability and margin-controlled geometry for example which require further research. At this point we favor an interaction with a foreland obstacle, the Beemerville Intrusive Complex.

The strain shadow creates an impact on weathering and groundwater flow as compared to the more highly deformed regions to the north and south. Karst development has to date only been found within the strain shadow, mainly in the Onondaga Limestone where beds dip uniformly gently to the northwest. Here joints, enlarged by dissolution, dominantly control groundwater flow. Other reactions of weathering to this change in structural style along strike are investigated such as joint cave development in non-carbonate rocks.

Key words: Devonian, shadow zone, cleavage, fracture

INTRODUCTION

The advent of DEM's (digital elevation models) and Lidar (acronym for Light Detection and Ranging) as well as Google Earth has allowed the investigation of the detailed landscape without leaving the office.

These tools are especially helpful with the geology of northwestern New Jersey. Using these tools, one sees a long curving ridge stand out in the topography that trends westerly out of eastern Pennsylvania, turning more northeasterly through New Jersey and more northerly into New York. Its name depends on its location, Blue Mountain in Pennsylvania, Kittatinny Mountain in New Jersey, and Shawangunk Mountains in New York (figure 1). It also forms a geological time break in that older rocks from Ordovician to Mesoproterozoic lie to the east and the younger rocks ranging from Silurian and younger to the west. One particular feature is an apparent nearly doubling of the outcrop width in New Jersey between Kittatinny Mountain and the Delaware River. Several different belts of rocks increase in width across the Culvers Gap, Branchville, Milford and Port Jervis South quadrangles (figure 1).

The best place to observe this morphologic change in the field is from High Point State Park in northwestern New Jersey. At the High Point monument (figure 1), beautiful vistas are open in all directions that offer a good vantage point to observe the changing topographic expression of the regional landscape. The visible topography is mostly controlled by the underlying bedrock with locally a blanket of thick glacial deposits. The ridge is the Middle Silurian Shawangunk Formation with the younger Bloomsburg Red Beds forming the western slope of Kittatinny Mountain. In a visual traverse beginning in the northwest, the distant ridges comprise the gently tilted Devonian and younger rocks of the Appalachian Plateau termed the Poconos in Pennsylvania and Catskills in New York. Northward is the termination of the Shawangunk Mountains/Formation. Eastward, there is a multilayered assemblage of rocks in both type and time. Just below the overlook the sandstone, greywackes and slates of the Ordovician Martinsburg Formation are visible. Farther afield are well-defined ridges in the Hudson and New Jersey Highlands consisting of Mesoproterozoic metamorphic rocks related to the Grenville Orogeny. A linear valley between the low lying Martinsburg ridges and the metamorphic ridges, named Kittatinny Valley in New Jersey, contains a belt of Cambrian and Ordovician carbonate rocks that lay in a recess position due to their higher degree of erosion. Southward, Kittatinny Mountain swings westward into Pennsylvania.

This field trip is not to investigate the reasons for this increased width of the exposed Middle Devonian through Middle Silurian rocks, though we will present two possible explanations. The field trip will offer examples of how the structural imprint, related to this increase of the outcrop belt, plays a role in many different features such as karst, groundwater flow, and habitation by early man.

Regional Geology

Martinsburg Formation represents the oldest units in this study (figure 2). It comprises several different members that vary along strike, all of which formed from turbidite deposition into a deep linear foreland basin. In northwestern New Jersey, the Martinsburg comprises three members. The Bushkill is a ribbon slate that forms the base of the turbidite deposition into a deepening basin that developed on a subsiding Cambrian and Ordovician carbonate bank. The Ramseyburg Member, which overlays the Bushkill and displays an increase of grain size with the addition of interbedded greywacke sands. These

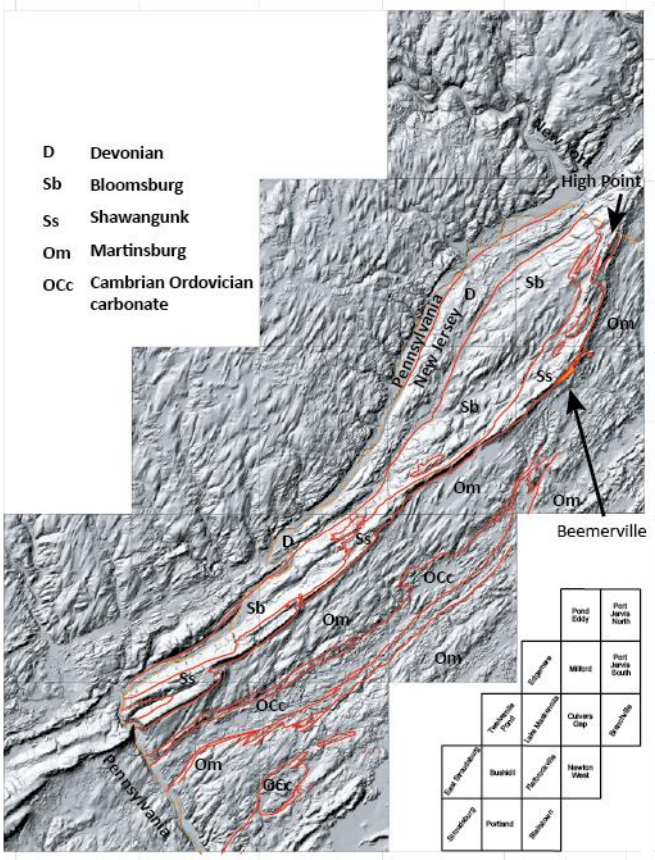

Figure 1. Regional digital elevation model (DEM) map of the Kittatinny Mountain region of New Jersey. Base map is a compilation of 16 DEM quadrangles with a 5x vertical distortion and a southeast looking illumination.

two units are found across northwestern New Jersey and into Pennsylvania (Drake and Epstein, 1967). McBride (1962) studied Martinsburg sedimentology and noted deposition occurred both downslope (northwestward) and parallel (southwest-northeast trending) to the basin axis. The third and youngest regional member of the Martinsburg varies by location and displays a pronounced along-strike morphology in the foreland basin. The Penn Argyl Member in eastern Pennsylvania, with its thick slate beds and associated commercial slate quarries, maps out a deeper depositional environment within the basin. Thick sandstone beds with rare shale ripups of the locally occurring High Point Member suggest a more proximal deposit to the sediment flow (Drake, 1991). McBride (1962) showed that Martinsburg paleoflow in New Jersey parallels the bathymetric basin axis towards the southwest; whereas sediments located farther westward were carried northeast both possibly accounting for the deep sedimentation of the Penn Argyl. The Martinsburg was considered late Middle Ordovician age (Parris and Cruikshank, 1992), but due to refining time boundaries (Cooper and Sadler, 2012), the same fossil assemblage is now considered Upper Ordovician (Dalton and others, 2014) with deposition synorgenic in the Taconic Orogeny.

The ridge forming Shawangunk sits with an angular unconformity on the Martinsburg. It consists of thin- to thick-bedded quartz and feldspathic sandstone, quartzite, and quartz-pebble conglomerate. Clasts are primarily quartz, with some dark-gray argillite and black chert (as long as 5 cm (2 in)) in poorly- to well-sorted, planar tabular to trough cross-bedded sandstone. It developed as a clastic wedge, deposited under an alluvial fan to braided stream environment, after the uplift of the Martinsburg foreland basin at the close of the Taconic Orogeny (Epstein, 1993; 2001; Epstein and Epstein, 1972). Gray and Zeitler, (1997) showed the sediment provenance of the pebbles in the Shawangunk as an uplifted and unroofed Grenville terrain from the southeast. An angular unconformity, commonly termed the Taconic unconformity, forms the basal contact separating the Shawangunk from the Martinsburg, and varies in angular divergence along strike (figure 3; Epstein and Lyttle, 1989; 2001). Only a 5° to 10° difference in bedding exists on its few exposures across New Jersey. Exposures in eastern Pennsylvania continue the gentle angular difference (Wintsch and others, 1996) into central

System	Series	Formation			Thickness (feet)
DEVONIAN	Middle	Marcellus			1000-1150
		Onondaga			270
	Lower	Schoharie			100-150
		Esopus			180-300
		Oriskany Group	Ridgeley Sandstone	Glenarie	0-16
			Shriver Chert		50-85
		Helderberg Group	Port Ewen Shale		150
			Minisink Limestone	Alsen	11-14
			New Scotland		65-78
			Coeymans		40-90
SILURIAN	Upper	Rondout			23-45
		Decker			50-82
		Bossardville Limestone			12-110
		Poxono Island			500-800
	Middle	Bloomsburg Red Beds			1,500
		Shawangunk			1500
ORDOVICIAN	Upper	Martinsburg			9,000-12,000

Figure 2. Regional stratigraphic column (modified from Epstein, 2001)

Pennsylvania, near Hamburg, where a near 90° angular divergence exists, though the contact could represent a fault zone (Lash and others, 1984). In New York, the angular difference also increases. Here the Shawangunk is eroded away and a younger unit, the Upper Silurian-Lower Devonian Rondout rests atop the Martinsburg.

Lying within the Martinsburg is the Beemerville Intrusive Complex. This complex includes two nepheline syenite bodies, several diatremes and associated dikes that intrude the Martinsburg Formation. Maxey (1976) described another nepheline syenite body that intruded into the Shawangunk. This occurrence, however, may actually represent glacial erratics of late Wisconsinan age as there is no evidence of any contact metamorphism. Also, westerly glacial striations and syenite erratics found west of Kittatinny Mountain (Monteverde and Witte, 2012) show how the late Wisconsinan glaciation could have deposited these large blocks of syenite on the Shawangunk as described by Maxey (1976).

Previous workers have outlined several other igneous bodies related to the Beemerville complex, which is also called Beemerville Intrusive Suite (Drake and Monteverde, 1992). These include several diatremes near the syenite bodies and others in a small cluster farther to the southeast (Spinks, 1967; Maxey, 1976; Drake and Monteverde, 1992). Xenoliths within the diatreme include Mesoproterozoic Grenville metamorphics, lower Paleozoic dolomites and the Martinsburg, showing the magma traversed the entire geologic column of that time of New Jersey.

Ratcliffe and others (2012) used U-Pb TIMS method on titanite that yielded a 447±2 Ma age for the Beemerville complex. Several fission-track ages explain the cooling history of the intrusion. Eby (2004, 2012) calculated a fission-track age on titanite of 420 ± 6 Ma mean to mark the cooling to a ~275° C and a younger age of. 156 ± 4 Ma. The high resolution age date of Ratcliffe and others (2012) places the Beemerville intrusive older than Shawangunk deposition.

The Bloomsburg Red Beds, an Upper Silurian red, fining-upwards clastic unit grades into and overlies the Shawangunk Formation. A complete fining-upwards sequence contains a basal medium-grained, cross- to planar-bedded sandstone with an erosional base that grades upwards through fine-grained, laminated sandstone/ siltstone and into a shale (Epstein and Lyttle, 1987; Prave and others, 1989; Alcala, 1990; Epstein, 2001b). Locally fining-upward sequences may be poorly defined and missing the shale cap. Bloomsburg sediments mark the transition from braided to meandering stream environments with rare paleosols (Epstein, 2001b; Driese and others, 1991) into marginal marine to brackish water marking a minor marine transgression (Epstein, 1971; Metz, 2000). Similar to the Shawangunk, sediment was transported westward and northwestward. Due to its increased iron content metamorphic rocks such as Grenville rocks uplifted and exposed by the Taconic Orogeny have been suggested as their sediment source (Epstein, 2001).

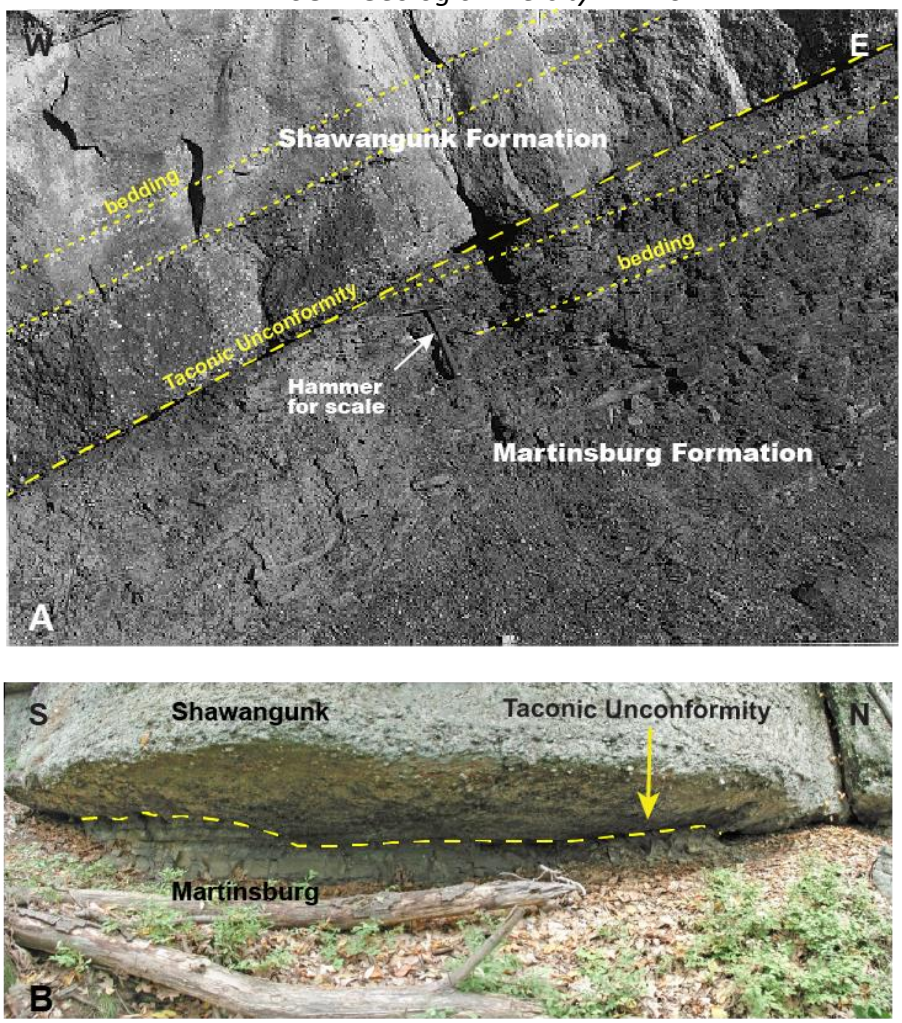

Figure 3 - Exposure of the Taconic unconformity. A) exposure looking north taken during construction of Interstate Route 84 in New York by Epstein. Note slight angular divergence between the Shawangunk and Martinsburg sediments. B) exposure looking west taken south of Sunrise Mountain in Stokes State Forest, New Jersey by Monteverde. Surface shows evidence of minor slip.

Generally, shallow marine waters blanketed this region for the remainder of the Silurian as shown by the sediments of four different units, Poxono Island Formation, Bossardville Limestone, Decker and Rondout Formations. Poxono Island and overlying Bossardville are dominantly carbonate deposited near sea level in highly saline and/or brackish water in intertidal to supratidal flats and partly lagoonal paleoenvironments (Epstein and others, 1967; Barnett, 1970; Epstein, 1986; 2001). Marine waters deepened in the Decker Formation as noted by its fine to coarse calcareous quartz sandstone and associated limestone beds. Epstein and others (1967) and Denkler and Harris (1989) interpreted the quartz sand-bearing lithofacies as deposited in a barrier bar environment. Abundant trace (Metz, 2003a) macrofossils and localized biohermal facies are present in the limestone beds. Their depositional environments include a biostromal bank to shallow subtidal crinoidal meadow (Epstein and others, 1967; Barnett, 1970; Denkler and Harris, 1989). Sediments of the younger Rondout Formation indicate a return to very shallow brackish water conditions that periodically dried up such as in restricted lagoonal and tidal flat paleoenvironments (Herpers, 1951a; Epstein and others, 1967; Epstein and Epstein 1969; Barnett, 1970). Denkler and Harris (1988) used conodonts to place the Silurian-Devonian boundary within the middle of the Rondout.

The Helderberg Group, which is dominantly composed of limestones, marks relative tranquil marine conditions before the onset of the Acadian orogenic event. Basal sediments of the Helderberg contain several different formations, which will be combined here as the Coeymans interval. Biogenic limestone units vary along strike with some stromatoporoid biostromes with massive tabulate corals. Multiple authors have suggested that the biohermal facies formed isolated patch reefs close to sea level (Precht, 1982; 1984; 1989; Finks and Raffoni, 1989; Raffoni and Finks, 1989). We will visit an example of this reef material at stop 4. Fossils, including ichnofossils are abundant in this lithologic interval (Epstein and others, 1967; Spinks, 1967; Barnett, 1970; Precht, 1982; 1984; 1989; Finks and Raffoni, 1989; Raffoni and Finks, 1989; Metz, 2003b). Limestones from this interval formed under high-energy, shallow subtidal conditions (Epstein and others, 1967; Spinks, 1967; Barnett, 1970) and are capped by calcareous quartz-pebble conglomerate and sandstone interpreted as a barrier beach deposit (Epstein and others, 1967; Spinks, 1967).

A thick sequence of siliceous, calcareous, fossiliferous shale with argillaceous, fossil-rich limestone interbeds of the New Scotland Formation blankets the older rocks formed in deeper water (Epstein and others, 1967; Epstein and Epstein, 1969). Overlying the New Scotland and depending on location is either a fine grained limestone to the southeast (Minisink Limestone) (Epstein and others, 1967; Monteverde, 1992) or a medium-to fine-grained highly fossiliferous limestone associated with either the Becraft Limestone (Weller, 1902) or Alsen Formation of New York (Rickard, 1962; Barnett, 1970). Deposition in deeper waters formed irregularly bedded calcareous silty shale to shaly siltstone of the Port Ewen that caps the Helderberg Group.

New Jersey again proved to be the location for changes in deposition patterns. Going into New Jersey from Pennsylvania the Lower Devonian Oriskany Formation/Sandstone was subdivided into shale, sandstone, limestone and chert of the Shriver Chert, which grades upwards to coarse-grained calcareous sandstone of the Ridgeley Sandstone (Epstein, 2001). Along strike, the Shriver and Ridgeley change over to entirely limestone of the Glenerie Limestone. Sea level lowering that was initiated during Port Ewen deposition continued into the Oriskany.

The Wallbridge Unconformity, a major regional unconformity, failed to develop in this region due to the deep water paleodepositional environment of the Oriskany (C. Ver Straeten, written communication, 2004). The upper part of the Oriskany marks a regional transgression (Johnson and others, 1985; Ver Straeten, 2001a).

Esopus and Schoharie formations that grade from argillaceous siltstone and sandstone into siliceous or calcareous siltstone, sandstone and localized limestone depict several sea level cycles (Epstein, 2001a; Ver Straeten, 2001a; 2001b). Several K-bentonites located in the basal Esopus have yielded $^{207}Pb/^{208}Pb$ ages of 408.3$\pm$1.9 Ma (Tucker and others, 1998; Ver Straeten, 2002; 2003).

The Schoharie grades upwards into the Lower to Middle Devonian Onondaga Limestone (termed Buttermilk Falls Limestone on Drake and others, 1996 and Monteverde, 1992). Onondaga lithologies grade from a basal limestone containing variable black chert through an argillaceous limestone and into a chert rich limestone that caps the unit. A bentonite bed correlated to the Tioga Ash bed is located in the upper Onondaga (Epstein and others, 1974). Ver Straeten notes several Tioga A-G K-Bentonite beds within the upper Onondaga or at the contact with the

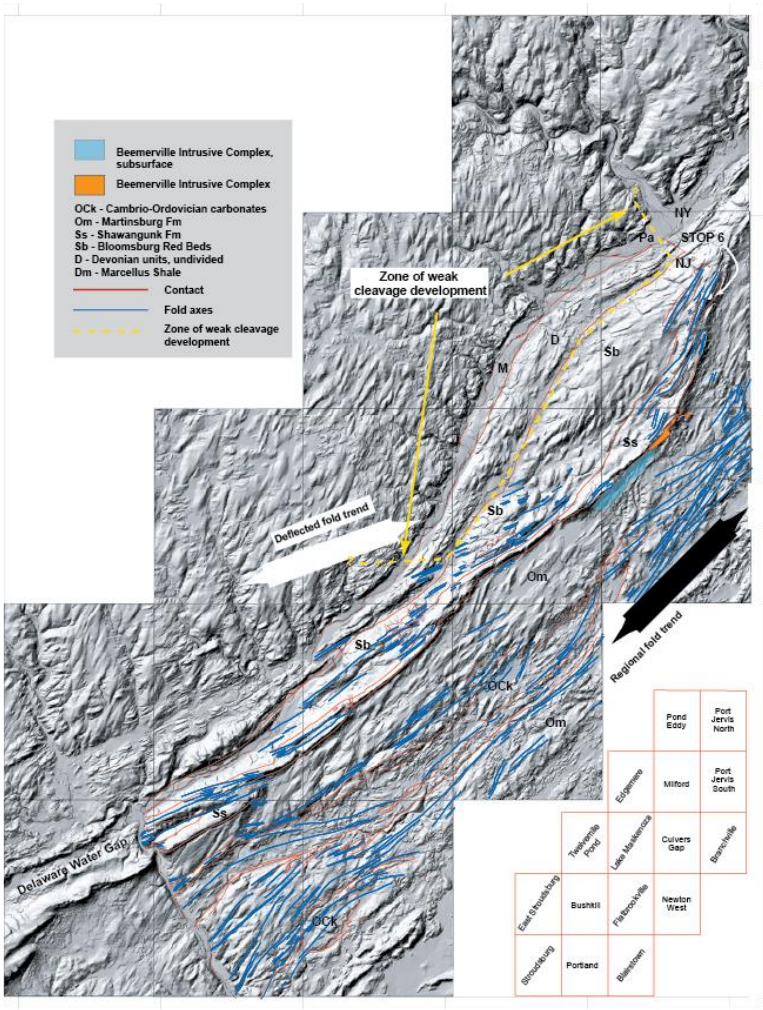

Figure 4. Regional structural interpretation of the Kittatinny Mountain region of New Jersey. Map depicts the outcrop location of the Beemerville Intrusive Suite shown in orange as well as the subsurface extension in blue, identified by Ghatge et al., 1992. The outcrop width of the Shawangunk and Bloomsburg increases markedly behind the intrusion. Fold trend deflects in the Silurian Devonian and also the Ordovician sedimentary units along the southern area of the intrusion. Base map is a compilation of 16 DEM quadrangle and has a 5x vertical distortion and a southeast looking illumination.

Marcellus. Tucker and others (1998) calculated 391.4±1.8 Ma $^{207}Pb/^{208}Pb$ age for the Tioga K-Ash bed.

Workers in eastern Pennsylvania and around the New York outcrop belt have subdivided the Onondaga into three to four members based on lithologic and paleontologic criteria that corresponds to variable sea level conditions (Epstein, 1984; Inners, 1975; Ver Straeten, 1996a; 1996b; 2001). Shallow water conditions prevailed during deposition of the basal Edgecliff Member's cherty limestone, but the argillaceous limestone of the overlying Nedrow Member suggests a deepening water environment. Shallow water conditions prevailed for the cherty limestone of the Moorehouse Member. This complete sea level cycle is repeated in the upper part of the Moorehouse Member into the youngest Onondaga Member, the Seneca Member (Ver Straeten, 2001).

The youngest rocks in northwestern New Jersey are thin-bedded dark-gray shales of the Middle Devonian Marcellus Formation, the shale-gas unit. Ver Straeten and others (1994), Ver Straeten and Brett (1995) and Ver Straeten (2001a) suggested the Marcellus should be elevated to "subgroup" status.

They place the Union Springs and Oatka Creek formations under the Marcellus. These formations are further subdivided into the shaly Bakoven and overlying Stony Hollow calcareous siltstones and sandstones, both within the Union Springs. The Oatka Creek was subdivided into 4 members that do not occur in New Jersey. The black shales mapped as Marcellus in New Jersey (Kummel, 1940) correlate to the Bakoven Member of the Union Springs. They are pyritic and contain a dwarf fauna indicative of an oxygen poor basin developed below wave base. These rocks are part of a prograding delta plain that culminates in the Catskill delta (Herpers, 1951b; Epstein, 1986; Faill, 1997).

DATA

Field Data

Regional field mapping allows an understanding of the influence of the different formations and a possible timing of events. The stratigraphy of this region has been known since before the map of Lewis and Kummel (1914). More recent detailed 1:100,000 and 1:24000 scale mapping has updated this early map product with recent advances in stratigraphy and structural interpretations (Epstein and others 1967; Spink, 1967; Monteverde, 1992; Drake and Monteverde, 1992; Drake and others, 1996; unpublished field data of Epstein and Monteverde). Mapping has shown that the trend of Kittatinny Mountain deflects at the Beemerville intrusive outcrop (figure 4; Drake and others 1996). Field data from both published and unpublished field mapping was analyzed to qualify the apparent change in structural orientation on both sides of the Beemerville outcrop. Structural data was subdivided geographically and stratigraphically. Data from the Lake Maskenozha (Monteverde, 1992) and Flatbrookville (unpublished data of Epstein and Monteverde) field mapping were combined as representative of structures south and west of the change in ridge trend and outcrop width increase. To the north, data was combined from Culvers Gap (Monteverde, 1992), Branchville, (Drake and Monteverde, 1992), Milford and Port Jervis South quadrangles mapping (unpublished field mapping of Epstein, Monteverde and Witte) for both the region of increased outcrop width and the change into a northern trend. It should be noted that the change from gentle dipping formations into the more northern steeply dipping beds were not sampled in sufficient quantity as mapping stopped at the NY-NJ state line. More mapping into New York is needed to create a more complete data set. Changes in dominant sediment type and age were reviewed independently. Martinsburg data (OM) collected east of the ridge was analyzed separately due its different sedimentology and being Ordovician age and was the only unit to have experienced any deformation from the Taconic Orogeny as well as younger deformational events. The younger units were subdivided more along rheological criteria such that the clastic Shawangunk and Bloomsburg Red Beds (S/B) were combined and separated from the dominantly carbonate Poxono Island through Marcellus (PIM) forming two separate data sets.

Field data is not conclusive. No statistics were run on this data and all interpretations are based on a visual inspection. Bedding data across all three sedimentary formation subdivisions show a strong agreement with the visual DEM data in that bedding south of the ridge trend changes strike more easterly than the more northerly strikes to the north (figure 5). Both show moderate dips and signs of folding. Cleavage differs in trend between the north and south OM data (figure 5). This trend difference is repeated in the S/B data but not as

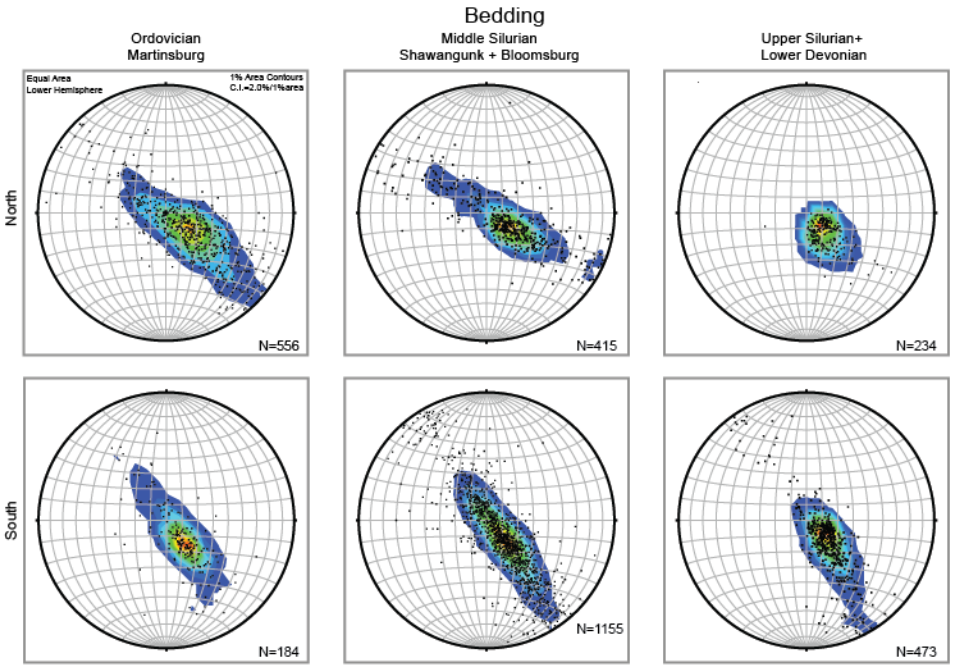

5a

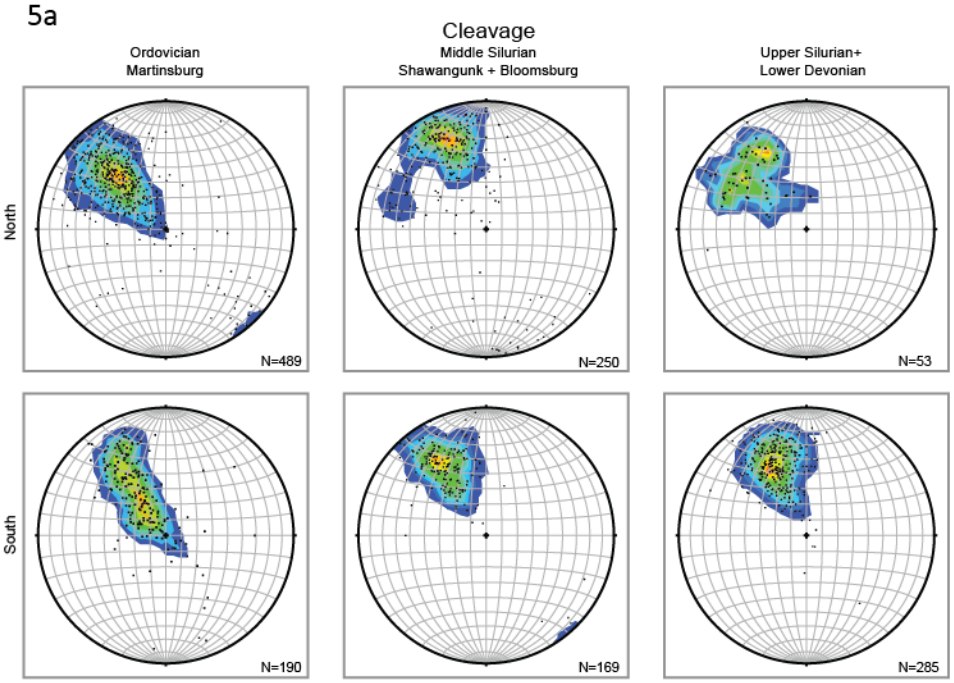

5b

Figure 5. Equal area, lower hemisphere stereonet plots of regional data plotted using program of Allmendinger and others (2013) and Cardozo and Allmendinger (2013). Plots are divided into north and south segments as described in the text. Number of data points shown in lower right corner of each plot. Contour interval is 1% area. a) displays poles to bedding, b) poles to cleavage, c) displays bedding cleavage interseection, d) poles to joints.

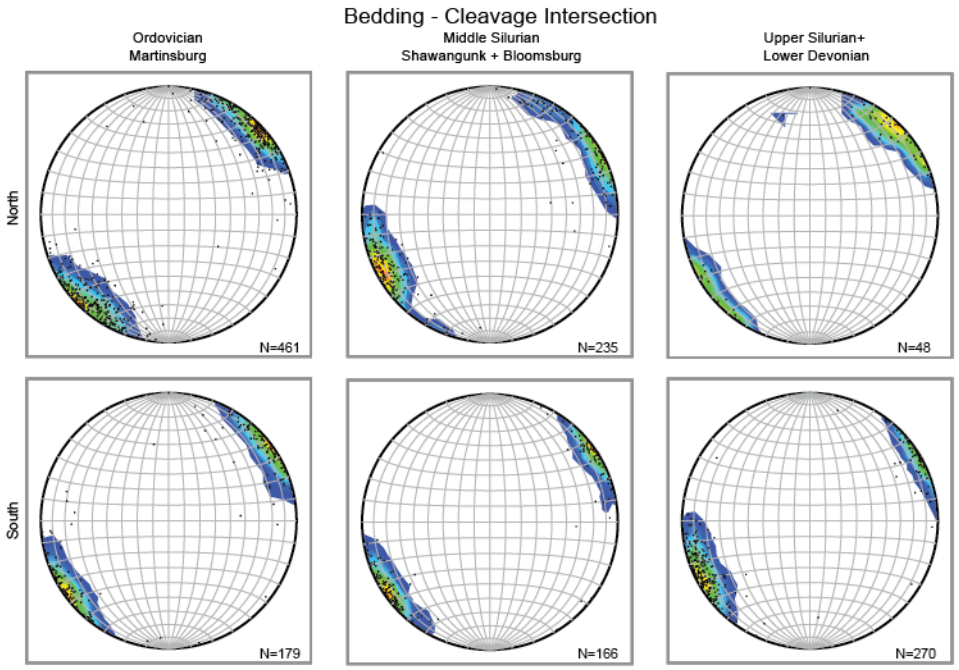

5c

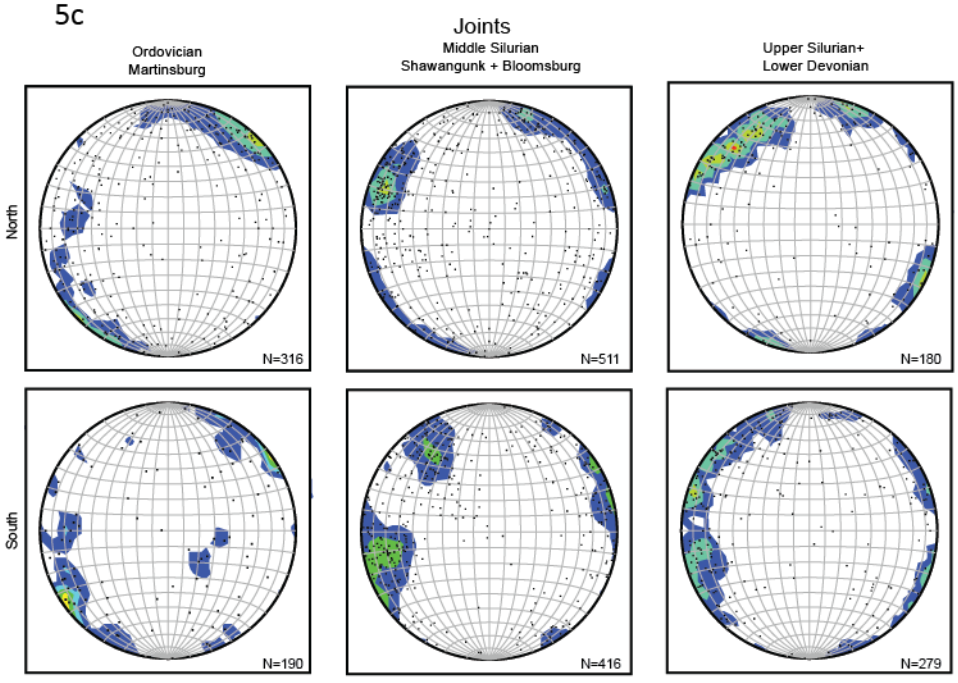

5d

clearly. Cleavage trends across the three southern sediment groups show a gradual rotation to more easterly strikes. Northern data display a strong rotation to a more easterly strike from OM to S/B with PIM presenting a broad maximum that "generally" parallels S/B trends. However, one must remember the general lack of cleavage in the northern PIM formations.

Bedding cleavage intersections somewhat mimic the cleavage trends (figure 5). South OM and S/B data display similar trends with PIM rotating slightly towards the east-west trend. Northern

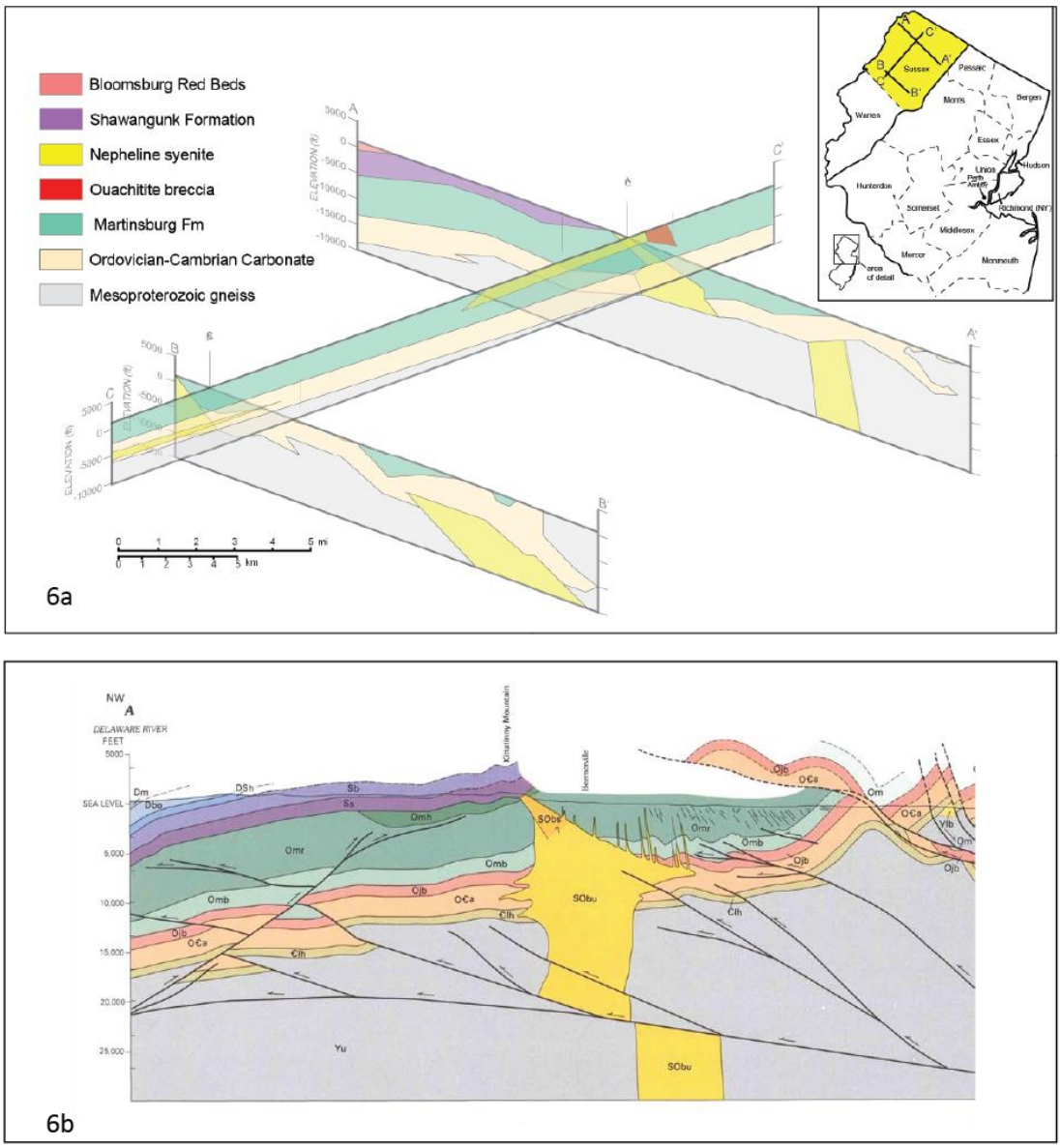

Figure 6. Results of gravity investigation to define the laterial extent of the Beemerville intrusive bodies (Ghatge and others, 1992). a) Modeled results of gravity data. Note that cross section have uniform scale but of variable depths. Two bodies were modeled on section A-A' that are interpreted as cut by a reverse fault, b) dip cross section from Herman and others (1996) showing intrusive bodies cut by thrust faults. Section does not conincide with located away from gravity sections. Unit SObu on section b represents the intrusive body, Sb=Bloomsburg, Ss=Shawangunk, Omh/Omr/Omb=Martinsburg, Ojb/OCa/Clh = Cambrian and Ordovician platform carbonates, Yu=Mesoproterozoic metamorphic units individed.

OM trends again shows a strong reorientation to the east-west trend, but more so that the South data. This compares to the north OM data trending more northerly than the south OM data. The north PIM is more diverse but has two slight maximums that correlate to either the OM or S/B both of the north. Again, the north PIM data are limited due to reduced cleavage development in the wider outcrop band.

Joint data is not that diagnostic (figure 5). They have a wider distribution and less defined maximums. Part of this reflects the data acquisition method in that all joints were given equal

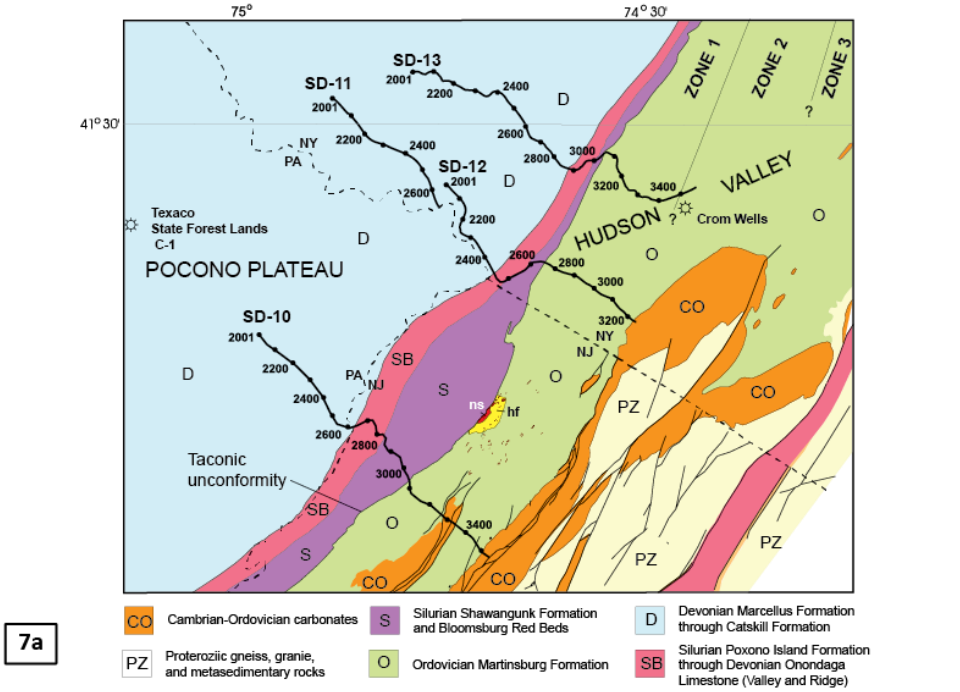

7a

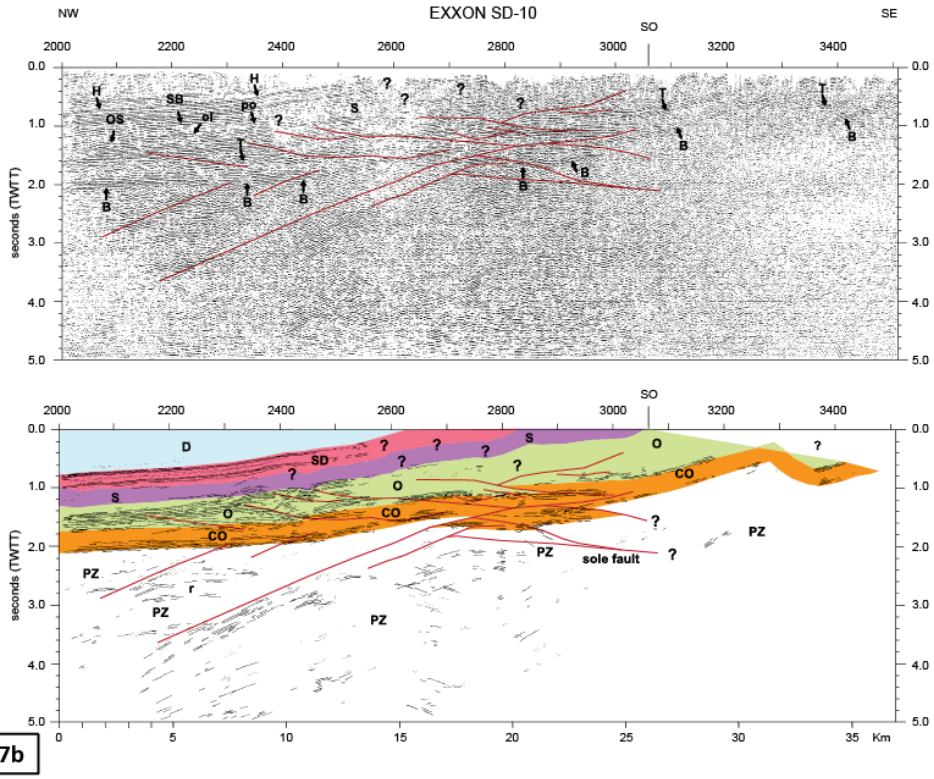

7b

Figure 7. Location map of Exxon seismic lines and geological cross section based on 1:24,000 scale field mapping. b) Exxon seismic-reflection profile SD-10. Geologic interpretations are shown for both the migrated, full display (top) and the conventional line drawing (bottom). PZ – Proterozoic, B – upper boundary of PZ unit, CO – Cambrian and Ordovician carbonates, T – upper boundary of CO unit, O – Ordovician Martinsburg flysch, OS – upper

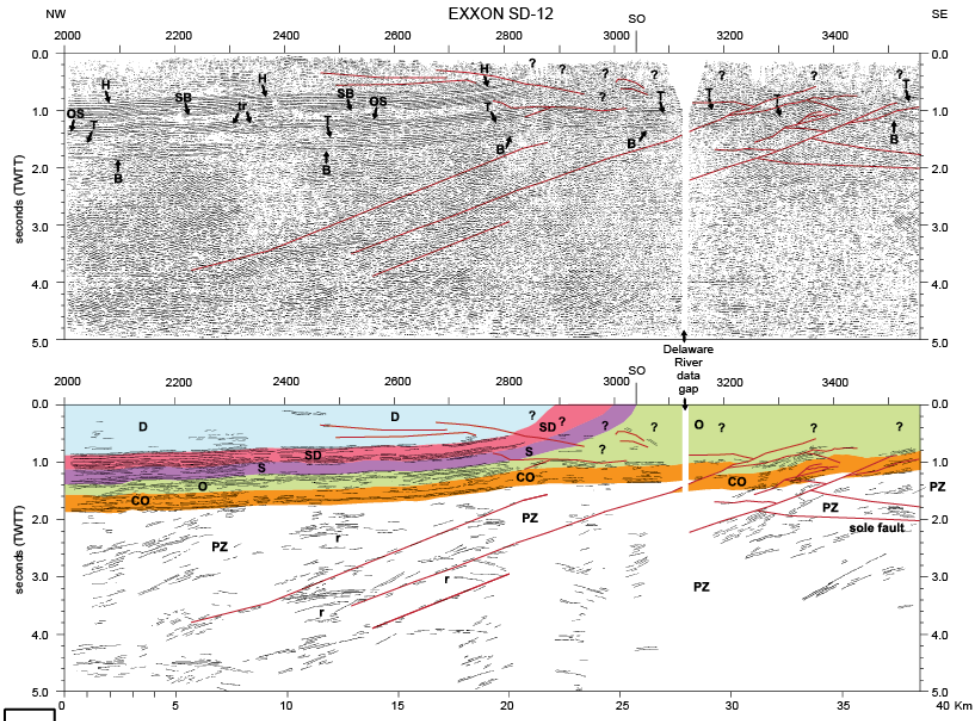

7c

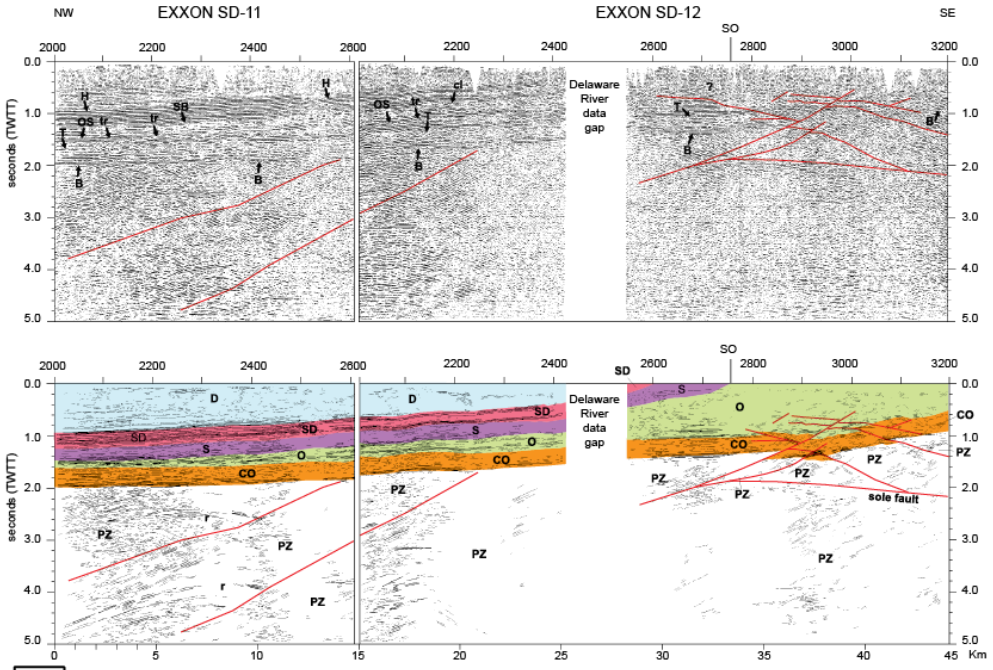

7d

Figure 7. (continued) boundary of O unit, S – Silurian molasse, SB – upper boundary of S unit, SD– Silurian and Devonian, undivided, H – upper boundary of SD unit, D – Devonian undivided, r – rollover, ol– onlap, po – pinch out. SO on map is location of the Taconic unconformity. Heavy red lines are faults. (modified from Herman et al., 1997). c) Exxon seismic-reflection profiles SD-11 and SD-12, abbreviations same as 7b. d) Exxon seismic-reflection profiles SD-13, abbreviations same as 7b

weight at each outcrop even though one particular trend may have been repeated multiple times at a single bedrock exposure.

Geophysical Data

The surface expression of the Beemerville Intrusive complex has long been known (Aurousseau and Washington, 1922; Spink 1967; Zartman and others, 1967; Drake and Monteverde, 1992; Drake and others, 1996), but not its subsurface extent. Jagel (1990) and Ghatge and others, (1992) used gravity and magnetic geophysical methods to investigate the subsurface continuation of the intrusive complex (figure 6). Their model greatly increased the subsurface extent of the Beemerville and showed that the sill thickened up to 2,000 ft (610 m) with a lateral extent of 5 mi (8 km) to the southwest following regional strike of Kittatinny Mountain. Farther to the south, a second southwest-trending syenite sill was modeled within Ordovician and Cambrian platform carbonates that thicken towards the northwest (figure 6). Ghatge et al. (1992) further suggested that the main intrusive body thickened dramatically with depth and also separated into two distinct bodies possibly offset by southeast-dipping Alleghanian thrust movement (Herman and others 1996). They modeled an extension of the pluton 5.5 miles (8.8 km) southeastward that thickened to 2 miles (3.2 km) at 7000 ft (2133 m) depth.

Exxon Co. USA collected three dip-trending seismic lines across Kittatinny Mountain and onto the Pocono Plateau (figure 7; Herman and others, 1997). Strata are combined into six seismic packages on the basis of seismic characteristics including Proterozoic basement (PZ), Cambrian and Ordovician carbonates (CO), Martinsburg (O), Shawangunk and Bloomsburg (S), Poxono Island through Onondaga Limestone (SB), and finally Marcellus into the Catskill Formation (D, figure 6). Fault displacement is primarily in pre-Shawangunk units (units PZ, CO and O) and shows a series of blind, gently easterly-dipping thrust faults in the east and younger moderately west-dipping antithetic faults in the western sections. Some blind faults end in broad and open cover folds in younger units and faulting just cuts the base of the Silurian on profile SD-10 suggesting post Taconic movement. Line SD-13, the farthest north line images steepened S and SB sections and an increased foreland-directed faulting into Devonian seismic units. It showed the return to the more highly deformed sections that continue northward. Profiles SD-10 and SD-12 image a broad region of Bloomsburg deposition as they sampled along the edges of the strain shadow (figure 7) Herman and others (1997) suggested this change marks a gradation into the increased foreland deformation of the Silurian and Devonian units (Marshak and Tabor, 1989; Burmeister and Marshak, 2006).

DISCUSSION

The structures in this region including some within the Martinsburg relate to Alleghenian deformation. Offield (1967) suggested that a broad fold in the Martinsburg is the deformational signature of the Taconic in this region. Epstein and Lyttle (1987; 2001) were able to separate Taconic from Alleghanian structures in their work with the Shawangunk and Martinsburg in the Ellenville area of New York. They interpreted that the Taconic only left gentle upright folds in the Martinsburg adjacent to the Shawangunk contact. Herman and others (1997) concluded similar ideas that the post-Taconic collisional event only left broad open folds in this region. In their research they uncovered an unpublished report by Merchant and Teet (1954) of the New Jersey Zinc Company that also advanced this idea. Cleavage age in the Martinsburg also has come into question as to whether it relates to the Taconic or Alleghenian Orogeny (see Monteverde and Witte, 2012) for a further discussion of this topic). Cleavage orientation between the Martinsburg and Shawangunk/Bloomsburg are very similar with the overlying rocks in close orientation (figure 5). Epstein and Lyttle (1987) have also proposed a different

strain shadow to cleavage development in the Martinsburg proximal to the Shawangunk outcrop. These many sources conclude that the margin here in northwestern New Jersey was one of broad open folds at the end of the Taconic.

So the question becomes what occurred during the Alleghenian deformation event to account for the strain shadow in the Silurian and Devonian units in northwestern New Jersey? One hypothesis to explain this supposed strain shadow in northwestern New Jersey involves the Beemerville Intrusive Complex, at and near the Shawangunk-Martinsburg contact. Spink (1967, 1969, 1972) first suggested this model. It was thought to be similar to a water wave deflecting after hitting a stone. This would create a larger area behind the stone which does not feel the wave's influence. Some data could support the hypothesis that the Beemerville Intrusive Complex acted as a wall or buffer creating a 'strain shadow' to the Alleghanian tectonic strain propagation into the foreland. There is a marked difference in the amount of both penetrative and mechanical strains recorded in the Silurian and Devonian from eastern Pennsylvania through New Jersey and into New York (figure 4). Cleavage development in Upper Ordovician through Lower Devonian sediments displays similar regional trends southwest of Wallpack Center, New Jersey through Stroudsburg, Pennsylvania with the exception of a slight eastward overall trend in Lower Devonian units in relation to the older rocks (figure 5). This cleavage is penetrative in that it appears in most units as an intense southeast-dipping, closely spaced, locally slaty regional cleavage. Some units such as the Esopus with its high clay content developed a well-developed cleavage that is a defining characteristic used in bedrock mapping (Alvord and Drake, 1971). Within this 'strain shadow' the Esopus is almost devoid of cleavage as are the rest of the Devonian units. Locally some units express a hint of a spaced cleavage, but it is not penetrative. Cleavage plotted for these rocks on figure 4 is a poorly developed spaced cleavage.

Fold formation also differs across the region behind or west of the Beemerville intrusive. No folds exist within Poxono Island Formation and younger units within the strain shadow west of the Beemerville intrusive. Glacial sediments blanket most of the Bloomsburg so fold patterns are obscure, though its outcrop width is greatly increased suggesting little to no folding. Along strike south of Wallpack Center the Bloomsburg through Onondaga sediments delineate tight, upright to northwest directed overturned folds. Along the edge of the southern strain-shadow, several fold trends diverge by up to 20^{o} from the northeast-southwest regional orientation into a more west-southwest direction (Monteverde, 1992). This fold deflection hints of involvement of the Beemerville Intrusive Complex in affecting stress propagation. A similar though muted trend appears with the Martinsburg fold pattern east of the pluton. Similar steep to overturned bedding occurs to the north just across the New Jersey border into New York, along Trilobite Mountain and farther northward. Within the strain shadow, these units display very gentle (8-30^{o}NW) uniform dips which affects and enhances the groundwater flow and sinkhole development (see stops 1 and 2 on this trip).

Not all data supports the 'strain shadow' hypothesis. The Shawangunk and overlying Bloomsburg rests atop the Martinsburg and Beemerville. Shawangunk folds do not show any apparent change related to their location along Kittatinny Mountain. Overturned beds are found directly southwest of the exposed' and subsurface extension of Beemerville as indicated by the gravity surveys (Jagel, 1990; Ghatge and others, 1992). There is a decrease in overturned panels near to the pluton compared to those along strike to the southwest. Also, the mapped Shawangunk outcrop belt does not double its width behind the intrusion, similar to the Upper Silurian and Devonian units. This puts in question the validity of the buffering of tectonic strain in the Shawangunk by the pluton. The most dramatic increase in the outcrop is seen in the Bloomsburg.

There are many other possible scenarios to explain the geometry of deformational fronts (Macedo and Marshak, 1999). One of these options as a mechanism for the strain shadow effect is the morphology of

the indenter plate during the Alleghenian Orogeny. In this model, promontories on the indenter accounting for the stronger deformational signature of Pennsylvania and New York and a recess covering the Beemerville area, created a lower deformational event. Could the outcrop width increase in the Bloomsburg be due to broad fold formation overlying thrusting as interpreted on the seismic by Herman and others (1997)? But if so, how would that account for the absence of cleavage in the younger units? All these questions and hypotheses need further work to evaluate their validity.

IMPACTS

The strain shadow impacts how the rocks react to normal weathering, which is the theme of this trip. Witte (personal commun, ongoing field work) performed detailed mapping of karst development in the Onondaga Limestone across northwestern New Jersey. His results have highlighted a dramatic preference for sinkhole development in regions of low dip, specifically within the strain shadow. Here the local joint trends are the major drivers of sinkhole formation and associated swallow holes, springs and groundwater flow networks. This will be explored in Stops 1 and 2. The diminished cleavage development in the Esopus along the southern boundary of the strain shadow also shows the larger impact of joint development. These localized joint openings were enlarged under the influence of postglacial weathering and possibly glacial ice wedging during the waning stages of deglaciation as will see at Stop 3.

REFERENCES CITED

Alcala, M.L., 1990, Stratigraphy, sedimentology, and petrography of some Upper Silurian rocks in southeastern New York: New York City College of the City University of New York, Department of Geology, unpubublished M.A. thesis, 39 p.

Allmendinger, R. W., Cardozo, N. C., and Fisher, D., 2013, Structural Geology Algorithms: Vectors & Tensors: Cambridge, England, Cambridge University Press, 289 pp.

Alvord, D.C., and Drake, A.A., Jr., 1971, Geologic map of the Bushkill quadrangle , Pennsylvania-New Jersey, US Geological Survey, Geologic Quadrangle Map, GQ-908, scale 1:24,000.

Aurousseau, M., and Washington, H.S., 1922, The nephelite syenite and nephelite porphyry of Beemerville, New Jersey, Journal of Geology, v.30, p.571-586.

Barnett, S.G., 1970, Upper Cayugan and Helderbergian stratigraphy of southeastern New York and northern New Jersey, Geological Society of America, Bulletin, v.81, p.2375-2402.

Cardozo, N., and Allmendinger, R. W., 2013, Spherical projections with OSXStereonet: Computers & Geosciences, v.51, no.0, p.193 - 205, doi: 10.1016/j.cageo.2012.07.021

Cooper, R.A., and Sadler, P.M., 2012, The Ordovician Period, in Gradstein, F.M., Ogg, J.G., Schmitz, M.D., and Ogg, G.M., The Geologic Time Scale Volume 2, Elsevier, p.489-524.

Dalton, R.F., Volkert, R.A., Monteverde, D.H., Herman, G.C., and Canace, R.J., 2014, Bedrock geologic map of the Hamburg quadrangle, Sussex County, New Jersey, new jersey Geologic and Water Survey, Geologic Map Series, GMS 14-3, 6p. scale 1:24,000.

Denkler, K.E., and Harris, A.G., 1988, Conodont-based determination of the Silurian-Devonian boundary in the Valley and Ridge Province, Northern and Central Appalachians, *in* Sando, W.J., Contributions to paleontology and stratigraphy: U.S. Geological Survey Bulletin 1837, p.B1-B13.

Drake, A.A., Jr., 1991, The High Point Member (Upper Ordovician) of the Martinsburg Formation in northern New Jersey and southeastern New York, in, Drake, A.A., Jr., editor, Contributions to new Jersey geology, US Geological Survey Bulletin 1952, p.B1-B9.

Drake, A.A., Jr., and Epstein, J.B., 1967, The Martinsburg Formation (Middle and Upper Ordovician) in the Delaware Valley Pennsylvania-New Jersey, in US Geological Survey, Bulletin 1244-H, p.H1-H16.

Drake, A.A., Jr., and Monteverde, D.H., 1992, Bedrock Geologic Map of the Branchville Quadrangle, Sussex County, New Jersey, US Geological Survey, Geologic Quadrangle Map GQ-1700, scale 1:24,000.

Drake, A.A., Jr., Volkert, R.A., Herman, G.C., Monteverde, D.H., Houghton, H.F., Parker, R.A., and Dalton, R., 1996, Geologic map of New Jersey: northern bedrock sheet; U.S. Geological Survey Miscellaneous Field Studies Map, I-2540A, scale 1:100,000.

Driese, S.G., Fischer, M.W., Easthouse, K.A., Marks, G.T., Gogola, A.R. and Schoner, A.E., 1991, Model for genesis of shelf sandstone sequences, southern Appalachians: paleoenvironmental reconstruction of an Early Silurian shelf system, in Swift, D.J.P., Oertel, G.F., Tillman, R.W., and Thorne, J.A., editors, Shelf Sand and Sandstone Bodies: Geometry, Facies and Sequence Stratigraphy: International Association of Sedimentologists Special Publication No.14, p.309-338.

Eby, G.N., 2004, Petrology, geochronology, mineralogy, and geochemistry of the Beemerville alkaline complex, northern New Jersey, in Puffer, J.H. and Volkert, R.A., editors., Neoproterozoic, Paleozoic, and Mesozoic intrusive rocks of northern New Jersey and northeastern New York, 21st Annual Meeting, Geological Association of New Jersey, Mahwah, NJ, p.52-68.

Eby, G.N., 2012, The Beemerville alkaline complex, northern New Jersey, in Harper, J. A., ed., Journey along the Taconic unconformity, northeastern Pennsylvania, New Jersey, and southeastern New York: Guidebook, 77th Annual Field Conference of Pennsylvania Geologists, Shawnee on Delaware, PA, p.85-91.

Epstein, J.B., 1993, Stratigraphy of Silurian rocks in Shawangunk Mountain, southeastern New York, including a historical review of nomenclature: U.S. Geological Survey Bulletin 1839L, 40p.

Epstein, J.B., 2001, Stratigraphy in the region of Delaware Water Gap National Recreation Area: *in,* Inners, J.D., and Fleeger, G.M., editors, 2001 a Delaware River odyssey, Guidebook, 66th Annual field conference of Pennsylvania Geologists, Shawnee-on-Delaware, PA, p.1-13.

Epstein, J.B., and Epstein, A.G., 1969, Geology of the Valley and Ridge Province between Delaware Water Gap and Lehigh Gap, Pennsylvania, *in,* Subitzky, S., editor, Geology of selected area in New Jersey and eastern Pennsylvania and guidebook of excursions, Rutgers University Press, New Brunswick, New Jersey, p.132-205.

Epstein, J.B., and Epstein, A.G., 1972, The Shawangunk Formation (Upper Ordovician (?) to Middle Silurian) in eastern Pennsylvania: U.S. Geological Survey Professional Paper 744, 45p.

Epstein, J. B., and Lyttle, P. T., 1987, Structure and stratigraphy above, below, and within the Taconic unconformity, southeastern New York, *in* Waines, R. H., editor, Guidebook, 59th Annual Meeting of the New York State Geological Association, Kingston, NY, p. C1-C78.

Epstein, J. B. and P. T. Lyttle, 2001, Structural relations along the Taconic unconformity between New York, New Jersey, and Pennsylvania, *in*, Inners, J. D. and Fleeger, G. M., editors, 2001—a Delaware River odyssey, Guidebook, 66th Annual Field Conference of Pennsylvania Geologists, Shawnee-on-Delaware, PA, p.22-27.

Epstein, A.G., Epstein, J.B., Spink, W.J., and Jennings, D.S., 1967, Upper Silurian and Lower Devonian stratigraphy of northeastern Pennsylvania, New Jersey, and southeasternmost New York: US Geological Survey, Bulletin, 1243, 74p.

Ghatge, S.L., Jagel, D.L., and Herman, G.C., 1992, Gravity investigations in Sussex County, New Jersey: New Jersey Geological Survey Geologic Map Series 92-2.

Gray, M.B., and Zeitler, P.K., 1997, Comparison of clastic wedge provenance in the Appalachian foreland using U/Pb ages of detrital zircons, Tectonics, v.16 (1), p.151-160.

Herman, G.C., Monteverde, D.H., Schlische, R.W., and Pitcher, D.M., 1996, Foreland crustal structure of the New York recess, northeastern United States, Geological Society of America, Bulletin, v.109, p.955-977.

Herman, G.C., Monteverde, D/H., Volkert, H.F., Houghton, H.F., Parker, R.A., Drake, A.A.,Jr., and Dalton, R.F., 1996, Cross section of the Valley and Ridge, Highlands, and Piedmont geologic provinces, northern and central bedrock sheets, New Jersey, in Drake, A.A., Jr., Volkert, R.A., Herman, G.C., Monteverde, D.H., Houghton, H.F., Parker, R.A., and Dalton, R., Geologic map of New Jersey: northern bedrock sheet; U.S. Geological Survey Miscellaneous Field Studies Map, I-2540A, scale 1:100,000.

Jagel, D.L., 1990, A gravity and magnetic model of the Beemerville Intrusive Complex, Beemerville, New Jersey: New Brunswick, New Jersey, Rutgers University, M.S. thesis, unpaginated.

Lash, G.G., Lyttle, P.T., and Epstein, J.B., 1984, Geology of an accreted terrane: the eastern Hamburg Klippe and surrounding rocks, eastern Pennsylvania, in, Guidebook for the 49th Annual Field Conference of Pennsylvania Geologists, Wyomissing, Pennsylvania, 151p.

Macedo, J., and Marshak, S., 1999, Controls on the geometry of fold-thrust belt salient, Geological Society of America, Bulletin, v.111, p.1808-1822.

Maxey, L.R., 1976, Petrology and geochemistry of the Beemerville carbonatite-alkalic rock complex, New Jersey, Geological Society of America Bulletin, v.87, p.1551-1559.

McBride, E.F., 1962, Flysch and associated beds of the Martinsburg Formation (Ordovician), central Appalachians, Journal of Sedimentary Petrology, v.32, p.39-91.

Merchant, J. S., and Teet, J. E., 1954, Kittatinny limestone, Sussex County, New Jersey: Ogdensburg, New Jersey, New Jersey Zinc Company, Progress report on file at the New Jersey Geological Survey (Trenton, New Jersey), 24 p.

Metz, R., 2000, Ancestral horseshoe crab (suborder Synziphosurina) from the Bloomsburg Red Beds (Upper Silurian) of northwestern New Jersey, Northeastern Geology and Environmental Sciences, v.22, p.227-231

Metz, R., 2003a, Ichnology of the upper Silurian Wallpack Center Member (Decker Formation), northwestern New Jersey, Northeastern Geology and Environmental Sciences, v.25, p.116-125.

Metz, R., 2003b, Lower Devonian trace fossils from shallow marine deposits, Shawnee Island Member of the Coeymans Formation, northwestern New Jersey, Northeastern Geology and Environmental Sciences, v. 25, p.206-214.

Monteverde, D.H., 1992, Bedrock geologic map of the New Jersey portions of the Culvers Gap and Lake Maskenozha quadrangles, Sussex County, New Jersey: New Jersey Geological Survey Geologic Map Series 92-1, scale 1:24,000.

Monteverde, Don and Witte, Ron, 2012, STOP 7: Lusscroft Farm and the Beemerville syenite, in Harper, J. A. editor, Journey along the Taconic unconformity, northeastern Pennsylvania, New Jersey, and southeastern New York. Guidebook, 77th Annual Field Conference of Pennsylvania Geologists, Shawnee on Delaware, PA, p.314-334.

Monteverde, D.H., and Epstein, J.B., in prep., Bedrock geology of the New Jersey and New York portions of the Milford, Pa-NJ and Port Jervis South NY, NJ and PA quadrangles, New Jersey Geological Survey, scale 1:24,000.

Parris, D.C., and Cruikshank, K.M., 1992, Graptolite biostratigraphy of the Ordovician Martinsburg Formation in New Jersey and contiguous areas: New Jersey Geological Survey, Geological Survey Report 28, 18 p.

Prave, A. R., Alcala, M. L. and Epstein, J. B., 1989, Stratigraphy and sedimentology of Middle and Upper Silurian rocks and an enigmatic diamictite, southeastern New York, *in* Weiss, D., editor, Guidebook, 61st Annual Meeting of the New York State Geological Association, p.121-140.

Ratcliffe, N.M., 1981, Contact relations of the Cortlandt Complex at Stony Point, New York, and their regional implications. Geological Society of America Bulletin, v.79, p.777-786

Ratcliffe, N.M., Tucker, R.D., Aleinikoff, J.N., Amelin, Yuri, Merguerian, Charles, and Panish, P.T., 2012, U-Pb zircon and titanite ages of late-to post-tectonic intrusions of the Cortlandt- Beemerville magmatic belt, CT, NY, and NJ: Relation to Iapetan closure in the Taconian orogeny. Geological Society of America Abstracts with Programs, v.44, n 2, p.73.

Spink, W.J., 1967, Stratigraphy and structure of the Paleozoic rocks of northwestern New Jersey: New Brunswick, Rutgers University, unpublished Ph.D. dissertation, 311p.

Spink, W.J., 1969, Structural geology in the region of Beemerville nepheline syenite pluton [abst.]: New Jersey Academy of Science Bulletin, v.14 p.62.

Spink, W.J., 1972, Differential tectonic transport around a nepheline syenite pluton in northwestern New Jersey [abst.]: Geological Society of America, Abstracts with Programs, v.4, p.46.

Ver Straeten C.A., 2001a, Event and sequence stratigraphy and a new synthesis of the Lower to Middle Devonian, eastern Pennsylvania and adjacent areas: *in,* Inners, J.D., and Fleeger, G.M., editors, 2001 a Delaware River odyssey, Guidebook, 66th Annual field conference of Pennsylvania Geologists, Shawnee-on-Delaware, PA, p.35-53.

Ver Straeten C.A., 2001b, The Schoharie Formation in eastern Pennsylvania: *in,* Inners, J.D., and Fleeger, G.M., editors, 2001 a Delaware River odyssey, Guidebook, 66th Annual field conference of Pennsylvania Geologists, Shawnee-on-Delaware, PA, p.54-60.

Wintsch, R.P., Kunk, M.J., and Epstein, J.B., $^{40}Ar/^{39}Ar$ whole-rock data constraints on Acadian diagenesis and Alleghanian cleavage in the Martinsburg Formation, eastern Pennsylvania, American Journal of Science, v.296, p.766-788.

Zartman, R.E., Brock .M.R., Heyl, A.V., and Thomas H.H., 1967, K-Ar and Rb-Sr ages of some alkali intrusive rocks from central and eastern United States, American Journal of Science, v.265, p.848-870.

FIELD GUIDE AND ROAD LOG - Lower to Middle Devonian rocks of the Delaware Water Gap National Recreation Area, New Jersey: fracture and lithologic control on rock-shelters, karst and groundwater flow

by

Ron W. Witte, Don H. Monteverde, and Steve Domber – New Jersey Geological and Water Survey

Meeting Point: Doubletree by Hilton Hotel, Nanuet, New York.

Meeting Point Coordinates: 41.090°N, 73.995°W

Meeting Time: 8:00 AM. **Note** road log starts at last I-84 West exit (exit 1, bottom of ramp) before entering Pennsylvania. Don Monteverde will meet the group on Sunday morning and shepherd the caravan to Stop 1a (Brau Kettle, Delaware Water Gap National Recreation Area, Sandyston Township, New Jersey. Directions to the start of the official road log are as follows:

Get on Palisades Interstate Pkwy N in West Nyack – 0.5 miles (0.8 km).

Follow Palisades Interstate Pkwy N to Highlands. Take exit 18 from Palisades Interstate Pkwy N -

16.5 mi (26.6 km).

Continue to Woodbury and continue on US-6 W – 7.3 miles (11.7 km).

Take I-84 W to Exit 1 - 35.1 miles (56.5 km). Field guide road log starts at end of off-ramp.

Cumulative in miles (km)	Point to Point in miles (km)	Route Description
0.0 (0.0)	0.0 (0.0)	Bottom of I-84 ramp, turn left on U.S. Route 6 West.
0.1 (0.2)	0.1 (0.2)	Left on State Route 23 South.
0.8 (1.3)	0.7 (1.1)	Right on County Route 653 (Clove Road) South.
5.6 (9.0)	4.8 (7.7)	Pass Montague Mini Mall on left, site of Stop 4.
8.1 (13.0)	2.5 (4.0)	Left on U.S. Route 206 East.
9.8 (15.8)	1.7 (2.7)	Right on County Route 645 South to Hainesville.
10.6 (17.1)	0.8 (1.3)	Right on County Route 646 West (Jager Road).
12.0 (19.3)	1.4 (2.3)	Arrive at Stop 1a. Park on right shoulder below culvert.

STOP 1a: Jager Road (near Brau Kettle), Sandyston Township, New Jersey

Location Coordinates: 41.263°N, 74.824°

Sample collecting and the use of rock hammers is not permitted in Delaware Water Gap National Recreation Area without a research permit. Most outcrops and other features provide more than adequate inspection. If needed, trip leaders will provide samples for examination.

Guidebook figures for each field stop are listed at the end of their respective sections. A full-color field guide will be handed out to trip participants the morning of the field trip by Don prior to the group leaving the hotel. Additional copies will be available at Stop 1a.

STOPS 1a and 1b) – Jager Road and Old Mine Road – Karst Geology and the Onondaga Limestone: Joint-controlled karst, regional structures, sedimentology of the Onondaga Limestone, shallow groundwater flow, and Brau Kettle.

Location and logistics

Stop 1 lies in the Milford quadrangle in the Delaware Water Gap National Recreation Area (fig. 1-1) along the western edge of New Jersey's Valley and Ridge Physiographic Province. The Delaware River, which forms the border between Pennsylvania and New Jersey, flows southwestward through Minisink Valley. Wallpack Ridge borders on Minisink Valley in New Jersey and it rises as much as 300 feet (91 m) above the valley's floor. At Stop1, the Onondaga Limestone underlies the ridge's northwest flank forming a gentle dip slope that extends to Minisink Valley. The western side of Minisink Valley in Pennsylvania is bordered on by a 300-foot-high (91 m) escarpment held up by the Mahantango Shale.

Stop 1will consist of two parts: 1a will be a short hike along the upper reach of an unnamed creek that flows near Jager Road. Park along the north side of Jager Road below culvert 1 (fig. 1-2). Additional parking for a few more cars is found below culvert 2 along the south side of Jager Road. We will meet near culvert 1 for a short discussion on karst and the Onondaga Limestone. Return to your cars at the end of the hike (culvert 3) and drive down the hill to the parking area at intersection of Jager and Old Mine

Road (fig. 1-2). Depending on the number of participants, a short discussion on Brau Kettle well will be held in the parking area or near Brau Kettle.

Geologic Setting

Bedrock in the Wallpack Ridge area consists of Silurian and Devonian carbonate and siliciclastic (sandstone, siltstone, and shale) sedimentary rocks that overlie the Bloomsburg Red Beds and uniformly dip northwest forming a monocline (fig. 1-3). These units comprise fifteen geologic formations (fig. 1-4), but may be grouped into six lithotypes (fig. 1-3) when studying karst at regional scales.

Wallpack Ridge is long, narrow, and slightly sinuous, extending 25 miles (30 km) from Wallpack Bend on the Delaware River to Tristates, New York (fig. 1-5). Its width varies between 0.7 and 1.7 miles and its highest elevation is 928 feet (283 m). Topography consists of short, rocky northeast-trending strike-ridges and benches with long slopes forming the ridge's northwestern flank. Wallpack Ridge consists of three sections (southern, middle and northern) based on the ridge's topographic trend (fig. 1-5). The southern and northern sections trend about N 55° E while the middle trends about N 26° E. The middle is also the widest section because its rock formations dip to the northwest much less steeply than those in the southern and northern parts (see the manuscript accompanying this trip for a discussion of these differences).

Minisink and Wallpack Valleys lie on either side of Wallpack Ridge. Both are narrow, deep, and trend southwest following belts of weaker rock. The valleys were also the former sites of a planned hydroelectric and water storage project by the Army Corps of Engineers. A dam planned for construction at Tocks Island would have flooded Minisink Valley upstream to Port Jervis, New York, and Wallpack Valley upstream to Layton. The reservoir would have provided storage capacity of nearly 250 billion gallons. After years of controversy, Congress de-authorized the project in 1992.

Kittatinny Mountain (fig. 1-5) is a prominent ridge that separates far northwest New Jersey from Kittatinny Valley, and runs from the Shawangunk Mountains in New York southwestward through New Jersey into Pennsylvania. It rises as much as 1500 feet above the floor of Minisink Valley and is underlain by the Shawangunk Formation, a tough and highly weathering-resistant quartzite and quartz-pebble conglomerate. The lower area northwest of the mountain that extends to Wallpack Valley is largely underlain by the Bloomsburg Red Beds and is included with Kittatinny Mountain.

Stop1 lies about 28 miles (45 km) north of the late Wisconsinan terminal moraine. Nearby glacial deposits (Witte, 2012) include valley train, meltwater terrace, and outwash-fan deposits laid down during systematic deglaciation of Minisink Valley. The Dingmans Ferry, Montague moraines mark a minor pause or slight readvance of the Minisink Valley lobe. Elsewhere, thin till covers most of the bedrock slopes with thicker till forming small drumlins and aprons on north-facing slopes. Thick deposits (up to 10 feet (3 m) of eolian sand blanket the lower slope of Wallpack ridge with a small field of sand dunes covering the outwash plain just upvalley from Brau Kettle.

Onondaga Limestone and Karst

A large number of karst features were detected along Wallpack Ridge in the Delaware Water Gap National Recreational Area (DEWA) during the recent mapping of surficial deposits in northwestern New Jersey (Stone and others, 2002; Witte (2012). Sinking streams, springs, a few small caves, and numerous small sinkholes were located with most all of the features found overlying the Onondaga Limestone, especially in the area between Dingmans Ferry and Montague, New Jersey (fig. 1-6).

The Onondaga Limestone in New Jersey was never formally divided into members (fig. 1-7) as it had been in New York (Oliver, 1954) and Pennsylvania (Epstein, 1984) (fig. 1-4). However, it was informally divided

(Herpers, 1952) into a lower section that is devoid of or contains only sparse chert (fig. 1-8a) and an upper section that contains abundant chert (fig. 1-8b). Cook (1868) had also observed this bipartite division near Dingmans Ferry where the Onondaga Limestone represented the noncherty limestone and the Corniferous Formation represented the cherty limestone.

Oliver (1954) codified the previous lithologic divisions of the Onondaga into formal members. From oldest to youngest they included the Edgecliff, Nedrow, and Moorehouse members. The Seneca, previously named by Vanuxem (1839), was retained as the Onondaga's youngest member. In Pennsylvania, Epstein (1984) divided Willard's (1939) Buttermilk Falls Limestone into, from oldest to youngest, the Foxtown, McMichael, and Stroudsburg Members. Inners (1975) added the Echo Lake member to the formation in part based on recognizing the Tioga Ash Bed in an Onondaga outcrop near Stroudsburg, Pennsylvania. Ver Straeten and others (2001) have added that the four members of the Buttermilk Falls are "exact correlatives" of the Onondaga Limestone and its four members in central New York. The terms Buttermilk Falls Limestone of Willard (1939) and the members of Epstein (1984) and Inners (1975) will be abandoned." For this study, the authors accept the New York stratigraphic division of the Onondaga into the Edgecliff, Nedrow, Moorehouse, and Seneca members rather than the Buttermilk Falls divisions of Pennsylvania. Whether or not all four members occur in New Jersey remains to be seen.

The Stroudsburg stratigraphy (Buttermilk Falls or Onondaga divisions) have only been traced as far as Wallpack Bend by Epstein (1984), and Ver Straeten (2001 and others) have correlated the four members to central New York via central Pennsylvania (Selinsgrove area). A direct correlation along strike from Stroudsburg, Pennsylvania through New Jersey to New York (fig. 1-9) has not been done. Recent mapping in New Jersey (Drake and others, 1996, and Monteverde, 1992) show both the Buttermilk Falls and Onondaga Limestones with the former continuing across the Delaware River into New Jersey at Wallpack Bend, and the latter continuing from New York into New Jersey at Tristates (fig. 1-9). Mapping was based on the Buttermilk Falls being more argillaceous (darker gray and finer-grained) and cherty than the Onondaga. The gradational boundary between the two limestones (Monteverde, personal commun., 2016) occurs near Montague, New Jersey (fig. 1-9) in the northern part of the outcrop belt.

Oliver (1956) noted that the Edgecliff and Morehouse members are recognizable but greatly changed at Port Jervis and that Willards (1936) Buttermilk Falls Limestone is the approximate equivalent of the Onondaga at Port Jervis. If this correlation is correct, then its lower cherty unit has been replaced by a noncherty or sparsely cherty unit of the "lower Onondaga" in the study area. Oliver and others (1962) indicated that the Edgecliff southwest of Wawarsing is a thinner, darker, and finer-grained limestone with little chert and recognized mainly by its large crinoid columnals. The large columnals were also noted by Epstein (1984) in his Foxtown Member, the basal part of the Buttermilk Falls and Spink (1967) described the occurrence of large crinoid columnals as abundant in the basal section of an Onondaga outcrop near Dingmans Ferry along Dingmans Ferry – Layton Road (the southwest edge of the karst-study area near Stop 2). The columnals have been also found by the author's near Spink's Dingmans Ferry outcrop. Elsewhere, they have not been observed in New Jersey. Spink (1967) also noted that the base of the Onondaga where it lies in contact with the Schoharie consists of a five-foot thick limestone bed characterized by an anastomosing network of silt. A similar bed was observed about 2.5 miles northeast of Stop 1a where it overlies a two-foot thick bed of nodular limestone that may represent the Onondaga - Schoharie contact. Based on the above observations it appears that the Edgecliff Member does extend into the study area where it is represented by sparsely-cherty, thin to medium-bedded, dark gray, fine-grained, flaggy to nodular limestone.

Oliver (1956) indicated that the Nedrow Member becomes indistinguishable from the Moorehouse in the southeastern New York outcrop belt and at Wawarsing, New York; the Moorehouse rests directly on the Edgecliff. The Moorehouse at Port Jervis, New York is about 190 feet (58 m) thick (Oliver, 1962). Given

that the overall thickness of the Onondaga in the study area is estimated at 200 feet (91 m) (Drake and others, 1996) to 250 feet (76 m) (Spink, 1967), then the Onondaga consists of a thin Edgecliff overlain by a much thicker Moorehouse. No exposures of the Seneca Member have been found in southeastern New York because it has been replaced by the lower part of the Marcellus Formation (Oliver, 1956).

Based on Oliver's (1956, 1962) descriptions of the Onondaga in southeastern NY, the presence of large crinoid columnals in New Jersey, and the informal division of the Onondaga into a lower noncherty member and an upper cherty member (Herpers, 1952; this study) it appears that Edgecliff and Moorehouse Members make up the Onondaga Limestone in the study area and that the majority of the sinkholes are found in the Edgecliff and lower part of the Moorehouse. The four-member stratigraphy of Pennsylvania's Buttermilk Falls (Epstein, 1984 and Inners, 1975) and the more recent Onondaga revision by Ver Straeten and others (2001) has not been traced through New Jersey into New York, specifically the Nedrow member. Main reasons for this include: 1) Lateral facies changes along strike from pure to argillaceous limestone and noncherty to cherty limestone are common in the Onondaga as shown by Oliver (1956 and 1962). This is also shown by faunal changes (Oliver, 1956) where "south from Leeds the Edgecliff thins, the coral fauna disappears, the rock becomes finer-grained and darker, and the light-gray chert is replaced by dark chert." 2) The Onondaga in New Jersey is largely found along the northwestern flank of Wallpack Ridge where it forms a dip slope of 8 to 30 degrees. Because of this geometry, there are few outcrops where thick sections are exposed, prohibiting a detailed examination of the limestone and mapping of its members. 3) The upper section of the Onondaga in many places is covered by thick glacial outwash and postglacial alluvium in the Delaware River valley, possibly concealing the thin Seneca member.

Karst Features

Sinkholes - Sinkholes are the most common karst features mapped on the Onondaga Limestone. More than one hundred sinkholes or clusters of closely-spaced sinks have been located (fig. 1-6) on a two-mile long section of Wallpack Ridge, south of Montague, New Jersey. As much as 15 feet (6 m) deep and 100 feet (34 m) in length, they formed in areas where the Onondaga Limestone is overlain by Late Wisconsinan till and in places, thin eolian sand. Most are oval- or trough-shaped with their long-axis oriented parallel to primary joints found in the local rock. Sinks may occur alone or in small groups that are aligned with local joints. Most sinks or sink clusters are aligned along a 040° to 020° trend with a few sinks aligned around a cross-joint trend of 120°. Also, most sinkholes are not found along streams or in places where they may receive concentrated surface runoff.

Sinkholes chiefly occur as two types. The first are solution sinks that form shallow surface depressions in the overlying surficial substrate (fig. 1-10). They do not exhibit an open throat or show evidence of recent collapse. They typically form over large open joints that have been covered by thin till and in some places postglacial eolian sand. Most of these sinks probably formed shortly after deglaciation, representing places where thin (< 20 feet (6 m) thick) surficial materials slowly filled subsurface voids chiefly by collapse, which resulted in the formation of a shallow depression or sag of overlying materials.

The second kind are solution sinks (fig. 1-11). They are generally smaller, have steep walls, and an open throat. They represent places where surficial material has been undermined, collapsing into a soil void and creating a steep-walled sink. They probably form more rapidly than soil-collapse sinks and may represent periods of episodic movement whereas solution sinks form more slowly representing a period of more steady and gradual collapse. Many of these do exhibit bedrock in the sink's walls and most are found along the intersection of major joints.

Sinkholes are typically found in three different topographic settings: 1) Many sinks lie adjacent to the up slope side of a rocky strike ridge (fig. 1-11). These sinks are rock-walled or at least partially lined by

bedrock, 2) Additional sinks are found along topographic benches or on gentle dip slopes. Many of these occur in closely-spaced groups and outcroppings within them are uncommon. In rare instances, several closely-spaced sinks that formed along cross joints are found on gentle slopes. 3) more rarely they occur at the base of a dip slope where slope meets the valley floor.

Sinking streams and springs – Many small streams that flow over the Onondaga Limestone disappear or more rarely emerge at various places along the stream's course. Often these streams lose flow or completely disappear over the course of a few hundred feet. Mostly, water sinks through thin alluvium into bedrock through small open joints and voids. In a few places, seepage is much more dramatic, the stream flowing into a small sink or large void (swallow hole). About 1800 feet upstream from Brau Kettle (fig. 1-2), approximately 70 percent of stream flow disappears into an opening about 2 feet in diameter (Stop1a-1). The remaining water seeps into the streambed within the next 200 feet. Downstream, two additional swallow holes have been identified, but the creek bed is typically dry except during periods of heavy precipitation. Whether these swallow holes are the source for Brau Kettle remains to be investigated.

Springs are common and range from small ephemeral seeps to larger year-round flows (> 300 gallons per minute (gpm)). Springs typically discharge along either 1) abrupt changes in slope along bedding or joints or 2) the surficial – bedrock contact (till-rock interface). In places, deposits of calcareous tufa (Stop 2a) are found just downstream from where the spring emerges. Brau Kettle is a peculiar spring. During dry times of the year the kettle is a small soil collapse sinkhole, while during the wetter periods it fills with water and discharges to a nearby creek. The spring and its relationship to a nearby well are discussed at Stop 1b.

Caves – Several small caves have been discovered in the study area. Most have openings that are just large enough for a person to fit through, and then quickly diminish in size. No large caverns have been discovered in the karst study area, although the size of a few sinkholes suggest that bigger caves may exist. About two miles northeast of Montague, two larger caves, Vulture (fig. 1-12) and a more recently found unnamed cave have been located in the Onondaga Limestone. These represent the largest known Onondaga caves in New Jersey.

Cutters and limestone pavements – The Onondaga's long dip slope and thin surficial cover provides many places where limestone pavement crops out at the surface (also occurs along some of the streams). Bare areas of rock exhibit deep fissures (max depth – 10 feet (3 m), and max width 2 feet (0.5 m) that break the rock surface up into large rectangular blocks (fig. 1-13). They are chiefly the result of dissolution along joints that mostly occurred beneath a layer of thin soil. Given their size, many of these fissures are older than the Late Wisconsinan glaciation (24 ka); formation of extensive joint dissolution prior to the Late Wisconsinan glaciation. Glacial erosion during the last glaciation removed soil and loose rock from the land. In most places, the glacially eroded limestone pavement was covered by thin till. In places where till was not deposited or where the thin surficial material was eroded by postglacial slope erosion, the pavement is exposed.

Karst Formation

Several factors contributed to the formation of karst on the Onondaga Limestone. Most importantly, is that the limestone is susceptible to dissolution by surface water and groundwater, especially those parts of the formation that are a purer limestone. Because the rock formations that topographically lie above the Onondaga consist largely of siliclastic rocks, water that drains through them becomes slightly acidic. Also, rainwater that seeps through organic-rich soil in the area becomes slightly acidic. Over time, these waters dissolve the calcium carbonate that makes up the Onondaga Limestone.

Because the Onondaga has a very low primary permeability, water moves through the rock chiefly along fractures. Over time, these fractures widen by dissolution, and where flow is concentrated along fractures, dissolution is accelerated. Eventually, larger, connected conduits are formed, highly magnifying the rock's secondary permeability. Water flow through the Onondaga occurs mainly along solution–enlarged joints and to a lesser degree along bedding.

Two dominant joint trends have been measured in the Onondaga (figs. 1-2 and 1-13). The first (called here J1) is a 020º to 030º set that nearly parallels bedrock strike. They have long, straight traces that typically penetrate the rock more than several meters. The second (called here J2) is a 110º to 120º set that nearly bisects bedrock strike. These cross-joints typically have irregular traces and in most places are shorter than J1. Penetrative depth is typically less, being no more than a couple of meters and the joints tend to be much more bedding terminated than J1. Because joint intersections are especially prone to dissolution, larger voids may develop. Overtime, a connected system of conduits forms along systematic joints in the limestone. These joints are likely Alleghenian age (325 to 260 mya) and mostly formed as extensional fractures.

The shallow dip of the limestone beds also promotes dissolution by creating a larger surface area of limestone. In this section of the Wallpack Ridge the thin- to medium-thick beds of the Onondaga dip about 10 degrees or less. Elsewhere, the limestone dips as much as 35 degrees, most notably in the southern and northern sections (fig. 1-3). Because of this difference, the width of the Onondaga outcrop belt in the area most prone to karst formation is two to three times greater.

Although the primary conduits of subsurface flow are joints, some beds of the Onondaga are more prone to dissolution due to their higher calcium carbonate content (fig. 1-14). The trend and shape of sinkholes and open fractures indicates that water flow occurs mainly along systematic joints. However, based on outcrop observations, flow along bedding cannot be discounted and locally may be an important contribution to overall flow through the limestone.

Chert content will also affect dissolution. Most of the sinkholes occur in the lower part of the formation (interpreted in this report to be the Edgecliff and lower part of the Moorehouse members) where chert content is very low. Elsewhere, in the upper part of the formation where chert is more abundant, sinkholes are rare. Chert may lessen the effects of dissolution by retarding the growth of conduits along joints.

Finally, rocks along the middle section of Wallpack Ridge lack cleavage or it is only weakly formed whereas rocks along the southern and northern sections have a pronounced steeply-dipping southeast cleavage (fig. 1-5). Because cleavage planes may also act as conduits of subsurface flow, their absence here may have led to the concentration of water flow along joints, which accelerated rates of dissolution. The diminution of cleavage in the study area may be related to a large body of igneous rock that lies beneath Kittatinny Mountain near the village of Beemerville, New Jersey. The intrusive rock principally consists of syenite. It was emplaced sometime during the Ordovician period about 340 million years ago. The location of the Beemerville intrusive may have reduced the tilting of sedimentary strata to the west, and insulated these rocks from forces that produced cleavage. The large bulge found along Kittatinny Mountain (fig. 1-5) is a topographic manifestation of the strain shadow that could have occurred northwest of the intrusive when these rocks were deformed during the Alleghenian Orogeny. A more robust discussion on cleavage and jointing may be found in the paper by Monteverde and Witte.

Glaciation and Karst

There are no known dates for the age of karst features in DEWA or the nearby caves. Because the DEWA sinks formed on late Wisconsinan glacial (till) and postglacial deposits (eolian sand), we can estimate a

maximum age at about 18,000 years based on the age of the late Wisconsinan deglaciation in northern New Jersey. Because glaciers erode rock and soil, most all of the sinks older than the last glaciation have been destroyed. The age of the subsurface conduits and voids that lie beneath the sinks is unknown, but based on their size they existed prior to the last ice age. Given the short time since deglaciation, it is doubtful whether any of these depressions were formed by postglacial subsidence related to solution weathering.

Several sinks occur in eolian sand, which was deposited in postglacial time prior to the growth of extensive vegetation (period of time between deglaciation and the growth of an extensive boreal forest; 15 – 12 ka). Sinks that formed after this eolian phase suggest a possible link between glaciostatic rebound and lowering of regional groundwater levels. Most sinks do not appear active because they lack an open throat and show no evidence of recent subsidence. There probably has not been extensive dissolution of the Onondaga since the late Wisconsinan glaciation. Glacial till was deposited over pre-existing voids and open fractures. Over time, this material settled, creating the many small sinks in the park.

STOP 1a (41.263°N, 74.824°W)

Presenters – Ron Witte and Don Monteverde

Location 1a-1 – Creek bed just downstream from culvert 1 (fig. 1-15) near Schoharie – Onondaga contact.

Features - Large solution joints, Onondaga Limestone (Edgecliff Member) and swallow hole along left bank.

Discussion – Here the Onondaga limestone forms the creek bed, which is primarily a bedding-plane dip slope cut by several large solution joints (fig. 1-16). The rock is a thin to medium-bedded, fine-grained, faintly nodular, non-cherty, sparsely fossiliferous limestone. Given its proximity to the Schoharie contact, the limestone probably belongs to the Edgecliff Member. Large crinoid columnals that are used to define Onondaga's base have not been found near stop 1. However, the scarcity of outcrops due to dip slope geometry and burial by glacial cover in this area makes their discovery fortuitous at best. The main point to take away from this "blah, blah, blah" discussion is that the lower Onondaga in Karst Park is non- to sparsely-cherty and that is where many of the sinkholes occur.

Systematic joints in the Onondaga generally are aligned along two major trends (fig. 1-2). Enlargement of these joints and their intersections over time by dissolution, as well as minor bedding-plane dissolution has resulted in an extensive, integrated network of subsurface conduits (will discuss further at Stop 1b, Brau Kettle). The long axis of oval to trough-shaped sinks and lines of multiple sinks in Karst Park are aligned along these trends showing that karst features are strongly controlled by jointing (probably not an epiphany to most, but the lead geologist at this stop has a surficial geology background and is amused by simple observations). Solution along joints has resulted in various forms. In most places, joint surfaces are straight-walled to slightly curvilinear. Elsewhere, digitate forms (fig. 1-16) are observed, the result of dissolution along closely-spaced orthogonal to perpendicular joint sets. Also, in a few places, short, narrow openings occur that suggest a distinctive vertical component to dissolution.

A small swallow hole is found along near base of cascades, along the stream's left bank below the roots of a small tree (fig 1-17). The swallow hole is following a large joint (020° trend), draining southwest. It is now partially covered in debris (mostly gravel). Scraps of screening and rebar (also found at other swallow holes) show manmade interference with natural flow conditions. These efforts generally fail, but once in a great while they're thwarted by inquisitive geologists (ask Don). Most of the time this area was

observed, about 70% of stream flow entered the swallow hole. Remaining flow continued downstream toward the left-hand bend eventually disappearing into the channels coarse alluvium. Over the last few years, flow many times has been observed to continue downstream past the bend to Stops 1a-2, 1a-3, and 1a-4 (fig. 1-15). The main reason for this is that the swallow hole at Stop1a-1 has become partially blocked with gravel and debris, material washed in during periods of storm-related discharge or maybe Don (the geologist not the rock) had something to do with it.

Head downstream to Stop 1a-2 either by following the stream bed (only if it's dry) or by following the stream's left bank. The small pit you pass on your right supplied sand to local denizens. The sand is eolian, blown off late Wisconsinan glacial outwash braid plains in nearby Minisink Valley. The sand is part of an extensive eolian sheet that has been found as much as 200 feet (61 m) above the valley floor. Just north up Stop 1-b, small sand dunes as much as 5 feet (2 m) high, cover the east side of the valley (a story for another time).

Location 1a-2 – Creek bed downstream from left hand bend.

Features - Buried swallow hole below slump, Onondaga joint-blocks, coarse gravel bar.

Discussion – Stream flow to location 1a-2 is rare. During a field trip to this area in February, 2016, the typical view of stream flow downstream from culvert 1 (the one where the stream disappears before the bend) was not so typical. Upon arriving at location 1a-2, two observations stood out: 1) most stream flow (~ 75 %) was disappearing into an area of boulder alluvium beneath a small slump along the channel's right side (fig. 1-18) and the remaining flow was diverted around a coarse gravel bar (located just upstream from the slump) to a small swallow hole located along the streams left bank at Stop 1a-3.

The sinking stream was probably draining into a large open joint that may have been open for observation at one time. However, recently slumped sediment (eolian sand overlying till) and Onondaga joint-blocks have covered the swallow hole. It appears that under natural conditions, variable discharge along reaches between swallow holes may be due to blockage of swallow holes upstream. Over time, the cyclical filling and emptying of swallow holes (collapse into sink holes or erosion by running water) has resulted in a complex stream flow history. Also, heavy precipitation may overwhelm the capacity of the swallow holes to drain the creek, and channel bars may also divert flow around or to swallow holes.

Onondaga joint blocks here are non-cherty and sparsely fossiliferous limestone similar to that at Stop 1a-1. Given the gentle dip of bedding (< 15°), this limestone and outcrops downstream probably belong to the Edgecliff member.

Location 1a-3 – Creek bed just downstream from Stop1a-2.

Feature - Swallow hole along left bank in collapsed till.

Discussion – The swallow hole (fig. 1-19) is a small sinkhole formed mostly in till that underlies the left steam bank and hillslope. Shallow bedrock in the stream channel just downstream from this location suggests that bedrock is very near the surface below the sink. It is very probable that this sink overlies a large solution joint or solution joint intersection. Again, it's very rare for surface drainage to reach this location, but this year's February storm was severe with runoff heightened by frozen ground and melting snow.

Location 1a-4 –stream channel just upstream from culvert 2.

Features – Small cave along right stream bank, joints, Onondaga Limestone

Discussion – The intersection of a large solution joint (114° ~v) and creek channel (possibly JI) forms the opening to a small cave (fig. 1-20). The entrance is 28 inches (71 cm) wide and 32 inches (81 cm) high with

the top of the entrance formed by soil and tree roots. Bedding is 021° 10° NW, similar to bedding at Stop 1a-1. The large solution joint that forms the cave entrance trends 114 degrees and has nearly vertical to slightly scalloped sides (possibly eroded by sediment laden water). The 114° trend is part of a regional set of cross joints that cluster around 120 degrees. The cave floor from its entrance extends about 5 feet (2 m) before it drops another 3 feet (1 m) into a gravel choked opening. During periods of very high stream flow, the creek partly flows into the cave and over the years its floor near the entrance has filled with sand and fine gravel. As elsewhere, a small grate near the entrance does prevent most of the coarse sediment from entering the cave.

The Onondaga here is very fine grained, non-cherty, thin to medium bedded and slightly flaggy limestone. In places, silty (?) laminae with bedding parallel, curvilinear traces mark the rock's weathered surface (fig. 1-20).

Location 1a-5 – stream channel downstream from culvert 2.

Features – Spring, small reservoir and box.

Discussion - Several small springs are located along south side of Jager Road. Here the small reservoir and box (fig. 1-21) are typical structures used to collect water where it is often directly piped down slope to another holding area. The springs and seeps found along the south side of Jager Road discharge at or very near the till/rock contact. The small stream-cut valley topographically cuts this contact and together with the northwest dip of bedding creates favorable conditions for the emergence of springs. Given the occurrence of open solution joints along the rock's surface springs probably represent areas where water flow has been concentrated.

The new retaining wall was built after flood waters from then Tropical Storm Sandy (10/29/2012) washed out the road, nearly removing most of the eastbound lane.

Location 1a - 6 – just downstream from culvert 3.

Features – small swallow hole along right bank near right concrete abutment. Located at base of steep slope.

Discussion – Lastly, if we look downstream from culvert 3, you'll notice a small opening (22" wide (56 cm) by 16" (41 cm) high) along the stream's right bank just below the concrete abutment (fig. 1-22). Just past the opening the swallow hole's floor drops 3 to 4 feet into a small trough that trends about 55 degrees. The trough walls are partially bounded by outcrop, suggesting that this opening is following a large solution joint. Similar to the cave at Stop 1a-4, soil and tree roots form a ceiling. The opening has increased in size four fold over the last two years. Presumably, decreased subsurface discharge upstream due to sediment infilling of swallow holes, has increased discharge in the creek's lower reaches. These hydraulic modifications are episodic and may only take one or two good storms to greatly alter stream flow.

Below culvert 3 (fig. 1-15) most of the stream drains into the swallow hole directly or seeps through the gravelly alluvium adjacent to it. Downstream the creek is usually dry until input from a small spring below culvert 4. From here discharge seeps into boulder alluvium within 100 feet (30 m) of where the spring enters the channel. Normally the creek is dry downstream until it picks up outflow from Brau Kettle.

Please return to your cars and drive to the small parking area at the end of Jager Road and Stop 1b, Brau Kettle. The group will assemble in the parking area (fig. 1-2). Given the limited space around Brau Kettle, we may discuss Brau Kettle and the Anson Johnson well before taking the short hike to the kettle.

Cumulative in miles (km)	Point to Point in miles (km)	Route Description
12.3 (19.8)	0.3 (0.5)	Arrive at Stop 1b. Intersection with Old Mine Road. Park in area across intersection.

STOP 1b (41.263°N, 74.829°W)

Presenters – Steve Domber and Ron Witte

Location – 125 feet south of Old Mine Road and Jager Road intersection.

Features – Brau Kettle (spring and sinkhole)

Brau Kettle is a unique sinkhole-spring located along the eastern edge of Minisink Valley near the intersection of Jager Road and Old Mine Road in Sandyston Township, New Jersey (fig. 1-2). References to the kettle go back to the early French and Dutch settlers. The name was likely derived from the Dutch word for "brewing" or "boiling" (Dalton, 1976), a fitting description of the spring during discharge.

The kettle (fig. 1-23) is a conically shaped depression approximately 10 feet (3 m) deep by 20 feet (6 m) wide with its floor located in till. The sloping walls of the kettle are in thin wind-blown sand and till. Depth to rock is unknown, but given the kettle's geometry and discharge history, it is assumed that the Onondaga Limestone is very near the kettle's floor. Brau Kettle can be classified as an intermittent spring that varies from dry, to partially filled, to spilling; with highly variable fill and spill periods. A hydrogeologic investigation of Brau Kettle and its relationship to the Onondaga Limestone commenced in 2008 by the New Jersey Geological and Water Survey under a research permit granted by the National Park Service. This investigation consisted of measured hourly water level data using an ADR logger from the kettle and a nearby domestic well, precipitation data, and kettle discharge measurements.

It is hypothesized that the kettle was formed when a near-surface solution feature (joint or joint intersection) in the Onondaga Limestone enlarged to the point where the overlying surficial materials collapsed creating a sinkhole. Over time the flowing groundwater removed most of the finer materials leaving a boulder lag on the kettle's floor. Because the kettle is well above the Delaware River near the base of Wallpack ridge, groundwater only rises in the kettle during wet recharge periods. Farther downstream (closer to the Delaware River) is a series of perennial springs which discharge (in a boil-like fashion) through glacial outwash and postglacial alluvium. The lower elevation springs can be thought of as the perennial "base-line" discharge points and the kettle can be thought of as the overflow or relief valve when groundwater levels are elevated and discharge is high through the local joint-controlled hydrogeologic system.

Figure 1-24 shows selected water-level elevation data for the kettle and a nearby domestic well and precipitation data. The numbered descriptions below refer to the corresponding number on Figure 1-24. 1) Dashed grey line is elevation of base of kettle outlet channel; kettle elevations above this indicate that the kettle is discharging to the adjacent stream. When the green line is flat at approximately 434 feet (132 m), the kettle is dry. 2) Water levels in the well and kettle increase in response to precipitation/recharge on Oct 28th. 3) Water levels in the kettle and well recess. 4) Rate of decline increases once kettle stops flowing out outlet. 5) Kettle is dry while water level in well continues to decline. 6) Increase in well water levels due to small precipitation/recharge event, but not high enough to come above base of kettle. 7) Water levels in well increases and kettle temporarily fills in response to precipitation/recharge event. 8) Kettle fills and begins to discharge out outlet, water levels in well increase. 9) Note that water levels follow

similar trend, but are at different elevations since well water level represents a composite water level from multiple zones in the aquifer; whereas kettle represents only the upper-most zone in the aquifer.

Figure 1-25 shows the period when a square notched weir was installed in the Brau Kettle outlet channel and used to measure discharge. Calibration of the manual and data recorder measurements was poor with an R-squared error of 0.79 and seepage around the edges of the weir was observed after several months of operation. The discharge estimates should be assumed approximate at best. The kettle and domestic well water level elevation can be seen rising and falling in response to recharge events as described in Figure 1-24. Discharge is observed to have occurred in the wetter winter months when Evapotranspiration is low and recharges rates and water levels are typically highest. Discharge also periodically occurs during the summer and fall for short durations when heavy rains cause significant but temporary increases in water levels. Discharge rates hover in the 500 to 1000 gpm range and peak as high as 3,500 gpm. This would make the kettle a 3rd order spring and fairly large for what is typically observed in New Jersey. Also of interest is that a nearby stream channel (located approximately 100 feet (30 m) to the north and lower in elevation that the base of the kettle) is typically dry when the kettle is actively discharging. This suggests that groundwater flow is highly constrained along joint-controlled flow paths.

Lastly, because springs may be used to determine the health of the aquifer, floral and faunal studies have been conducted throughout New Jersey (biologists and geologists working together, hmmmm. another sign of the apocalypse). Figure 1-26 shows a recent monitoring of Brau Kettle where a brook trout was captured. An additional study by NJGWS, monitors spring chemistry and temperature. Water samples collected between 10/18/2012 and 7/26/2013 show a range of pH between 7.0 and 7.5 with temperature ranging between 8.6 to 12.0 centigrade.

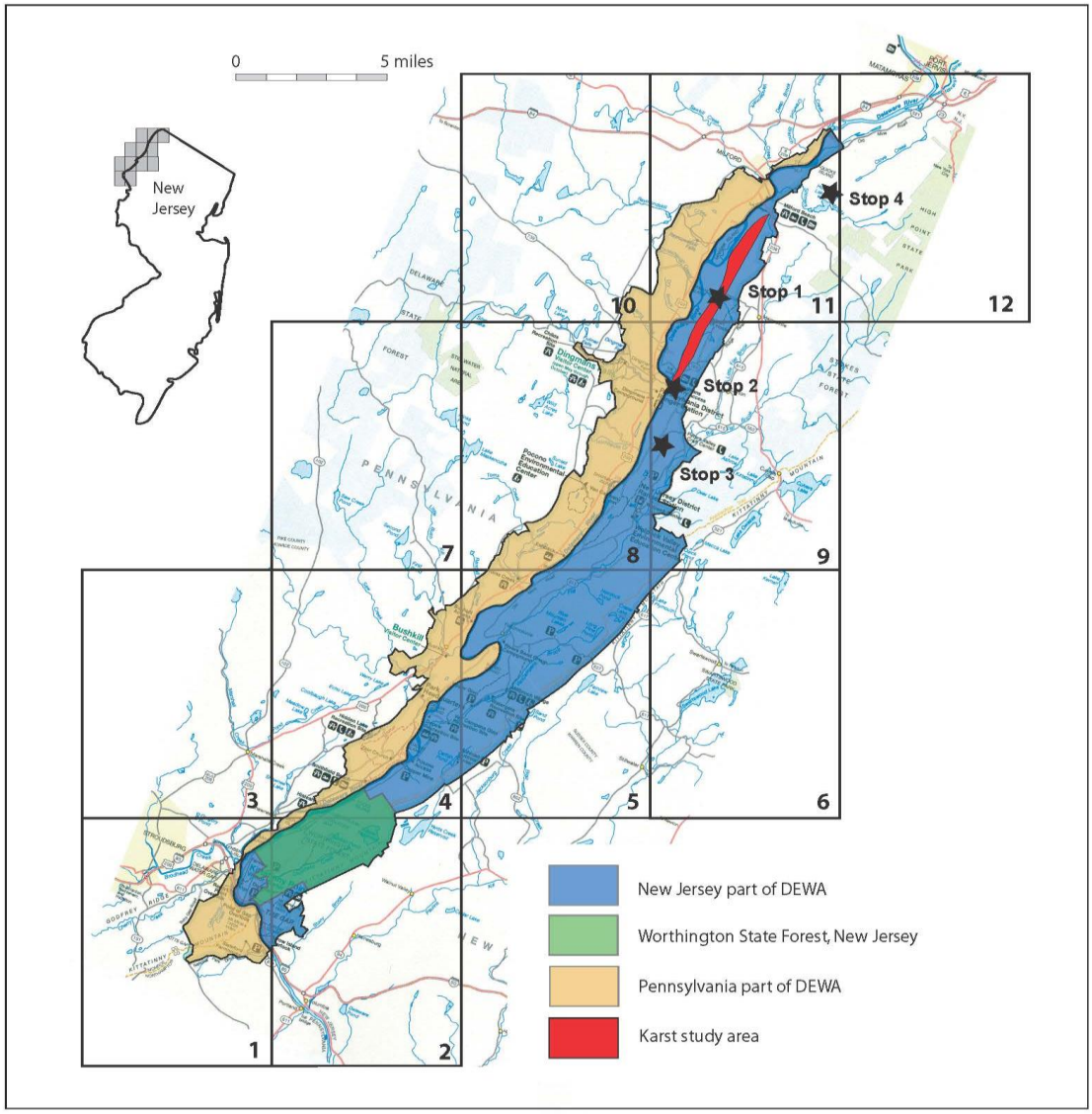

Figure 1-1. Location of Delaware Water Gap National Recreation Area (DEWA) in New Jersey and Pennsylvania, karst study area, field stops, and location of U.S. Geological Survey 1:24,000 quadrangles. 1. Stroudsdburg, 2. Portland, 3. East Stroudsburg, 4. Bushkill, 5. Flatbrookville, 6. Newton West, 7. Twelvemile Pond, 8. Lake Maskenozha, 9. Culvers Gap, 10. Edgemere, 11. Milford, 12. Port Jervis South.

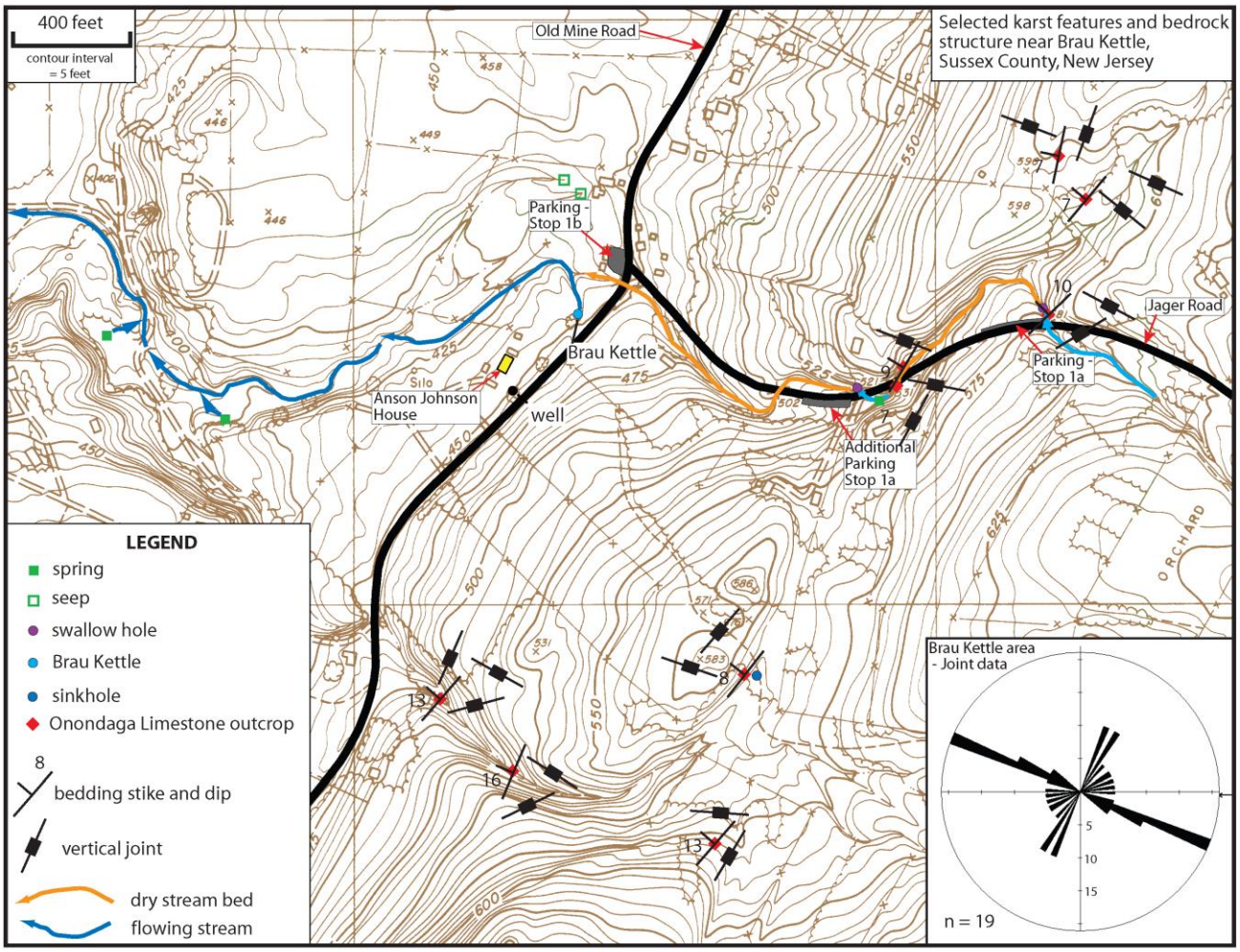

Figure 1-2. Stop 1 location map, karst features, and joint data for the Brau Kettle area.

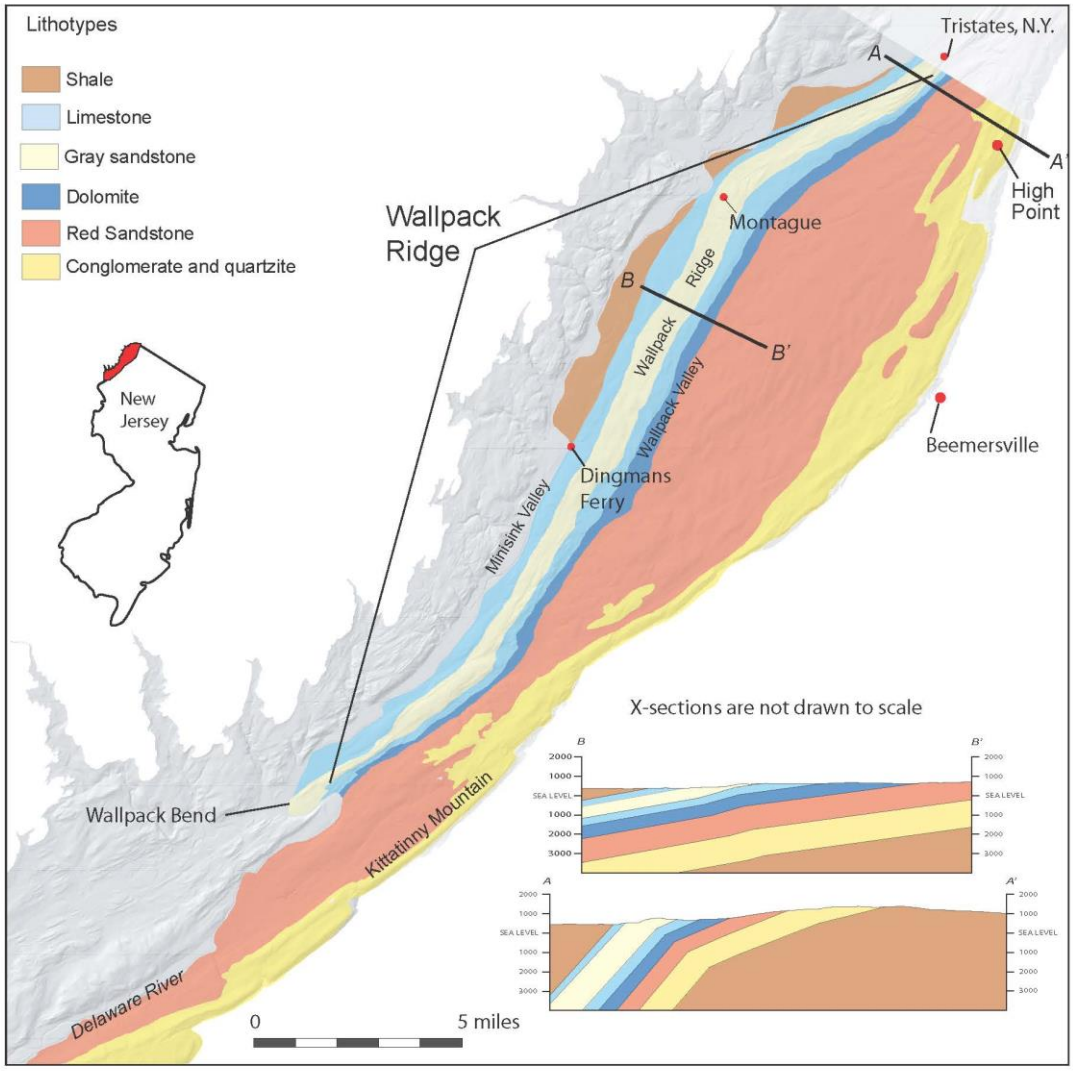

Figure 1-3. Simplified bedrock map of New Jersey in the vicinity of Wallpack Ridge. Modified from Drake and others (1996). The Onondaga Limestone forms the most westerly limestone.

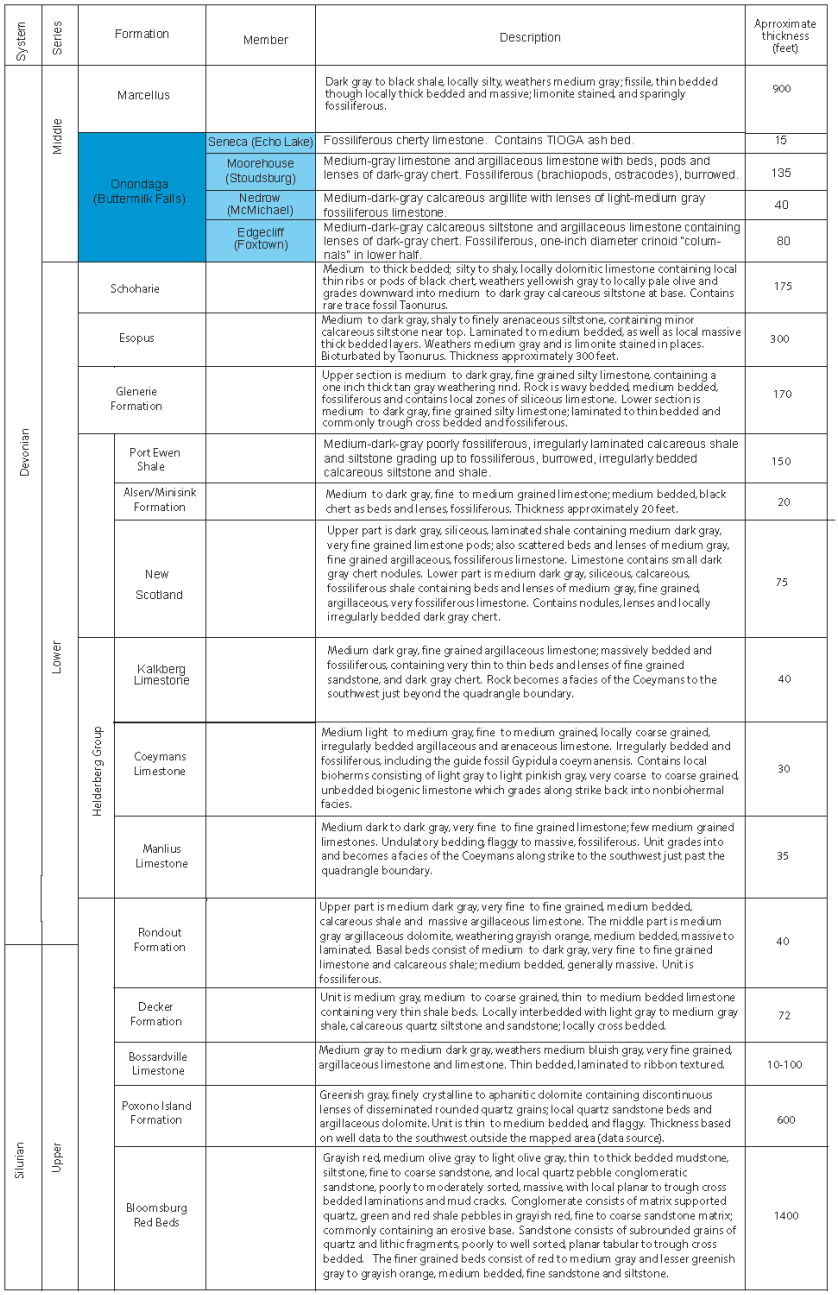

System	Series	Formation	Member	Description	Aprroximate thickness (feet)
Devonian	Middle	Marcellus		Dark gray to black shale, locally silty, weathers medium gray; fissile, thin bedded though locally thick bedded and massive; limonite stained, and sparingly fossiliferous.	900
		Onondaga (Buttermilk Falls)	Seneca (Echo Lake)	Fossiliferous cherty limestone. Contains TIOGA ash bed.	15
			Moorehouse (Stoudsburg)	Medium-gray limestone and argillaceous limestone with beds, pods and lenses of dark-gray chert. Fossiliferous (brachiopods, ostracodes), burrowed.	135
			Nedrow (McMichael)	Medium-dark-gray calcareous argillite with lenses of light-medium gray fossiliferous limestone.	40
			Edgecliff (Foxtown)	Medium-dark-gray calcareous siltstone and argillaceous limestone containing lenses of dark-gray chert. Fossiliferous, one-inch diameter crinoid "column-nails" in lower half.	80
	Lower	Schoharie		Medium to thick bedded; silty to shaly, locally dolomitic limestone containing local thin ribs or pods of black chert, weathers yellowish gray to locally pale olive and grades downward into medium to dark gray calcareous siltstone at base. Contains rare trace fossil Taonurus.	175
		Esopus		Medium to dark gray, shaly to finely arenaceous siltstone, containing minor calcareous siltstone near top. Laminated to medium bedded, as well as local massive thick bedded layers. Weathers medium gray and is limonite stained in places. Bioturbated by Taonurus. Thickness approximately 300 feet.	300
		Glenerie Formation		Upper section is medium to dark gray, fine grained silty limestone, containing a one inch thick tan gray weathering rind. Rock is wavy bedded, medium bedded, fossiliferous and contains local zones of siliceous limestone. Lower section is medium to dark gray, fine grained silty limestone; laminated to thin bedded and commonly trough cross bedded and fossiliferous.	170
		Helderberg Group	Port Ewen Shale		Medium-dark-gray poorly fossiliferous, irregularly laminated calcareous shale and siltstone grading up to fossiliferous, burrowed, irregularly bedded calcareous siltstone and shale.	150
			Alsen/Minisink Formation		Medium to dark gray, fine to medium grained limestone; medium bedded, black chert as beds and lenses, fossiliferous. Thickness approximately 20 feet.	20
			New Scotland		Upper part is dark gray, siliceous, laminated shale containing medium dark gray, very fine grained limestone pods; also scattered beds and lenses of medium gray, fine grained argillaceous, fossiliferous limestone. Limestone contains small dark gray chert nodules. Lower part is medium dark gray, siliceous, calcareous, fossiliferous shale containing beds and lenses of medium gray, fine grained, argillaceous, very fossiliferous limestone. Contains nodules, lenses and locally irregularly bedded dark gray chert.	75
			Kalkberg Limestone		Medium dark gray, fine grained argillaceous limestone; massively bedded and fossiliferous, containing very thin to thin beds and lenses of fine grained sandstone, and dark gray chert. Rock becomes a facies of the Coeymans to the southwest just beyond the quadrangle boundary.	40
			Coeymans Limestone		Medium light to medium gray, fine to medium grained, locally coarse grained, irregularly bedded argillaceous and arenaceous limestone. Irregularly bedded and fossiliferous, including the guide fossil Gypidula coeymanensis. Contains local bioherms consisting of light gray to light pinkish gray, very coarse to coarse grained, unbedded biogenic limestone which grades along strike back into nonbiohermal facies.	30
			Manlius Limestone		Medium dark to dark gray, very fine to fine grained limestone; few medium grained limestones. Undulatory bedding, flaggy to massive, fossiliferous. Unit grades into and becomes a facies of the Coeymans along strike to the southwest just past the quadrangle boundary.	35
Silurian	Upper		Rondout Formation		Upper part is medium dark gray, very fine to fine grained, medium bedded, calcareous shale and massive argillaceous limestone. The middle part is medium gray argillaceous dolomite, weathering grayish orange, medium bedded, massive to laminated. Basal beds consist of medium to dark gray, very fine to fine grained limestone and calcareous shale; medium bedded, generally massive. Unit is fossiliferous.	40
			Decker Formation		Unit is medium gray, medium to coarse grained, thin to medium bedded limestone containing very thin shale beds. Locally interbedded with light gray to medium gray shale, calcareous quartz siltstone and sandstone; locally cross bedded.	72
			Bossardville Limestone		Medium gray to medium dark gray, weathers medium bluish gray, very fine grained, argillaceous limestone and limestone. Thin bedded, laminated to ribbon textured.	10-100
			Poxono Island Formation		Greenish gray, finely crystalline to aphanitic dolomite containing discontinuous lenses of disseminated rounded quartz grains; local quartz sandstone beds and argillaceous dolomite. Unit is thin to medium bedded, and flaggy. Thickness based on well data to the southwest outside the mapped area (data source).	600
			Bloomsburg Red Beds		Grayish red, medium olive gray to light olive gray, thin to thick bedded mudstone, siltstone, fine to coarse sandstone, and local quartz pebble conglomeratic sandstone, poorly to moderately sorted, massive, with local planar to trough cross bedded laminations and mud cracks. Conglomerate consists of matrix supported quartz, green and red shale pebbles in grayish red, fine to coarse sandstone matrix; commonly containing an erosive base. Sandstone consists of subrounded grains of quartz and lithic fragments, poorly to well sorted, planar tabular to trough cross bedded. The finer grained beds consist of red to medium gray and lesser greenish gray to grayish orange, medium bedded, fine sandstone and siltstone.	1400

Figure 1-4. Stratigraphic column and description of rock formations found in the New Jersey part of the karst study area. Mapping of karst features indicates that lithology (purer limestones are more susceptible to dissolution), thickness (thicker formations are more susceptible to karst formation), and structure (low dip of bedding combined with long dips slopes, and high joint density) are important indicators of a formation's susceptibility to form karst. Onondaga members from Oliver (1954) and Vanuxem (1839). Buttermilk Falls (Willard, 1939) members from Epstein (1984) and Inners (1975). Figure modified from Epstein (2001).

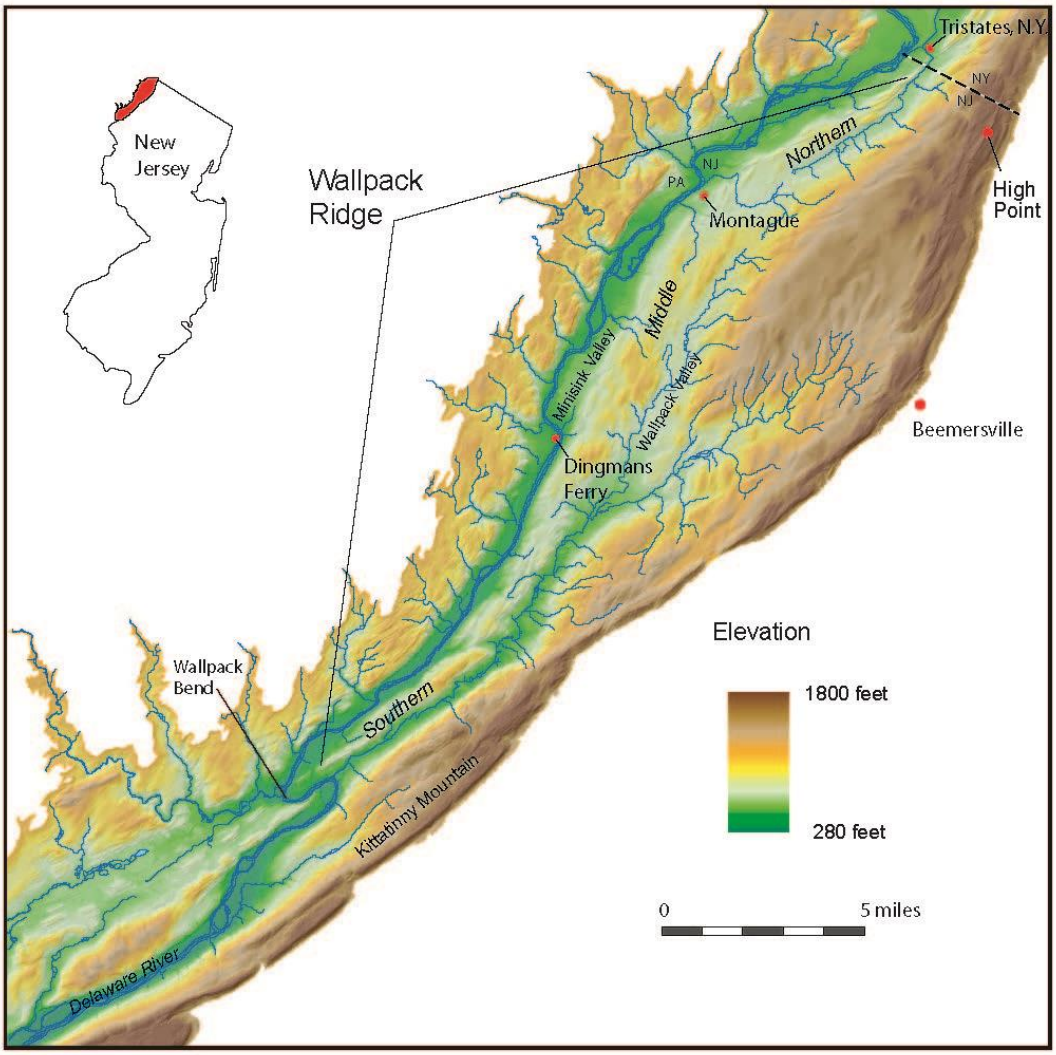

Figure 1-5. Color shaded-relief map of Wallpack Ridge and surrounding area.

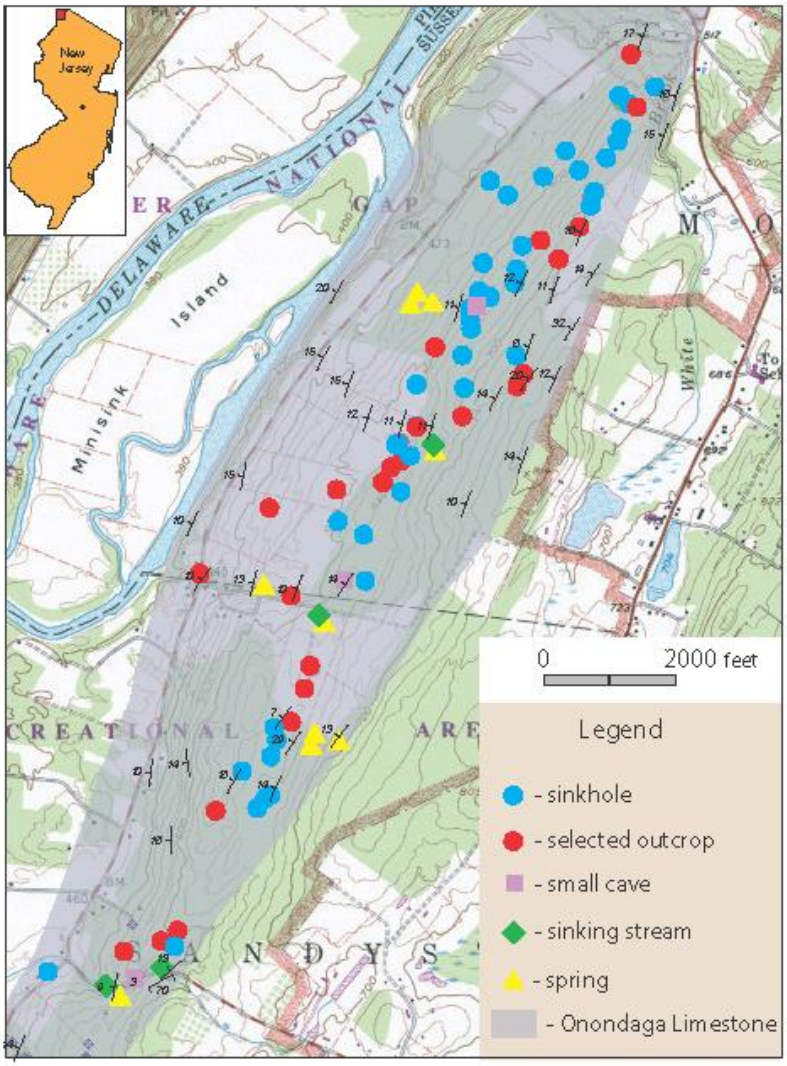

Figure 1-6. Karst features mapped on Wallpack Ridge between Jager Road and U.S. Route 206, Delaware Water Gap National Recreation Area. Sinkholes may be solitary or form small clusters that are aligned with joints in the Onondaga Limestone.

Rogers, 1840	Cook, 1868	Lewis and Kummel, 1915	Herpers, 1952	Spinks, 1967	Drake and Others, 1996
Fossiliferous limestone of the Delaware, base of Formation VIII	Corniferous (Cherty) Limestone and Onondaga Limestone (both are sometimes known as the Upper Helderberg Limestones) and they are not divided.	Onondaga Limestone	Onondaga Limestone: lower (Onondaga Limestone of previous workers) and upper member (Corniferous Limestone of previous workers).	Onondaga Limestone	Buttermilk Falls Limestone and Onondaga Limestone
Light blue and gray limestone, some argillaceous beds, many layers contain fossils. 200 feet thick.	Cornifierous - light blue, very fine-grained, uniformly-bedded limestone, argillaceous limestone with chert composing half the rock. Fossils are not common. Onondaga recognized as an encrinite and it does not form any considerable stratum. 600 feet thick (includes what is now mapped as the Schoharie Formation.)	Hard, cherty, regularly-bedded (3 to12 inches thick) limestone. Thickness is unknown (includes what is now mapped as the Schoharie Formation.)	Lower member – gray, fine-grained fossiliferous limestone with little or no chert; upper member – dark gray cherty limestone (equivalent to the Buttermilk Falls Limestone of Willard (1936) in northeastern Pennsylvania.	Fine- to medium-grained, medium-dark to dark gray, flaggy to massively-bedded limestone. Dark gray chert is commonly present in nodules and irregular layers. Fossils are common in the lower part of the formation. 250 feet thick.	Buttermilk Falls Limestone – light to medium-light gray, thin- to medium-bedded, fossiliferous limestone, flaggy, clayey to silty limestone and nodular black chert. Onondadga Limestone – Light-medium-gray, fine-grained, thin- to thick-bedded fossiliferous limestone. Black chert is more abundant in the upper half of the unit. 200 feet thick.

Figure 1-7. Nomenclatorial history of the Onondaga Limestone in New Jersey. Early studies were highly influenced by work in central New York where the Onondaga Formation was first described by Hall (1839) for cherty limestones in Onondaga County and the term "Corniferous" was first used by Eaton (1828) to discuss the same rocks. Later Drake and others (1996) combined Pennsylvania's Buttermilk Falls limestone (Willard, 1836) with the Onondaga as a undivided map unit noting that a facies change occurs in New Jersey along the northern part of the outcrop belt.

Figure 1-8. Onondaga Limestone in New Jersey showing typical exposures. Photo A - noncherty, thin- to medium-bedded, nodular fine-grained limestone. The outcrop is near the base of the formation and is located near Stop 1a. Photo B - cherty, thin- to medium-bedded fine-grained limestone. The outcrop is near Dingmans Ferry spring (Stop 2d). Earlier workers in New Jersey (see fig. 1-7) had informally divided the limestone into a lower noncherty unit (named the Onondaga Limestone) and an upper cherty unit (named the Corniferous Limestone). Photos by R. Witte.

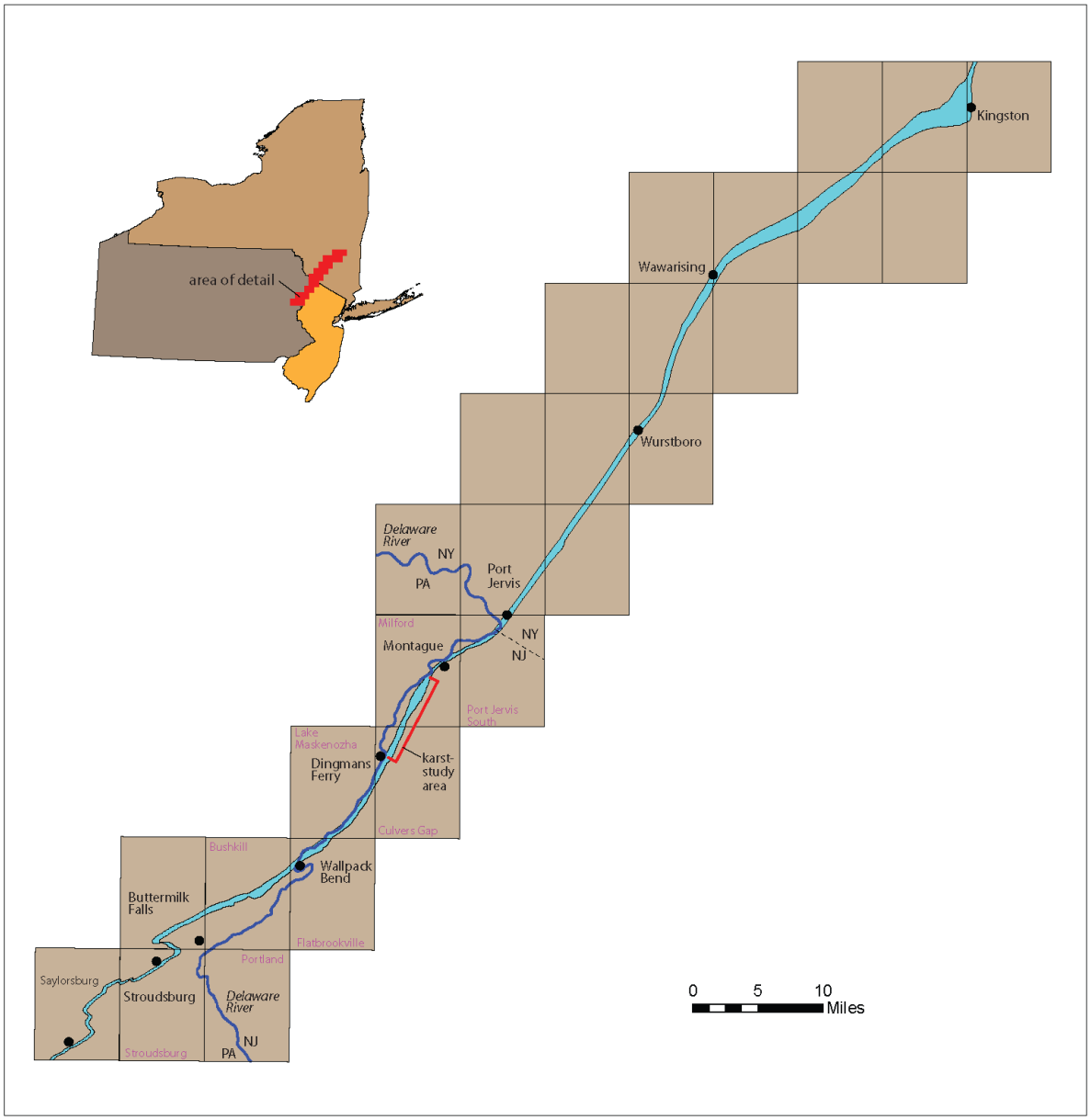

Figure 1-9. Location of the Onondaga Limestone outcrop belt between Kingston, New York and Saylorsburg, Pennsylvania, index of 7 1/2 minute topographic quadrangles, and places named in report. Only quadrangles in New Jersey named. Modified from Oliver (1956, figure 2) and Epstein (1984, figure 1).

Figure 1-10. Solution collapse sinkhole over the Onondaga Limestone. Delaware Water Gap National Recreation Area. Photo by R. Witte.

Figure 1-11. Soil collapse sinkhole over the Onondaga Limestone. Delaware Water Gap National Recreation Area. Photo by R. Witte.

Figure 1-12. Vulture Cave in the Onondaga Limestone, Delaware Water Gap National Recreation Area, Montague, New Jersey. The cave opening is about 4 feet (1.2 m) in diameter. The cave is partially filled with sand and debris deposited by the Delaware River during floods. Photo by R. Witte.

FIgure 1-13. Cutters J1 (054°) and J2 (146°) in the Onondaga Limestone, Delaware Water Gap National Recreation Area. Photo by R. Witte.

Figure 1-14. Bedding plane dissolution in the Onondaga Limestone. Photo by R. Witte.

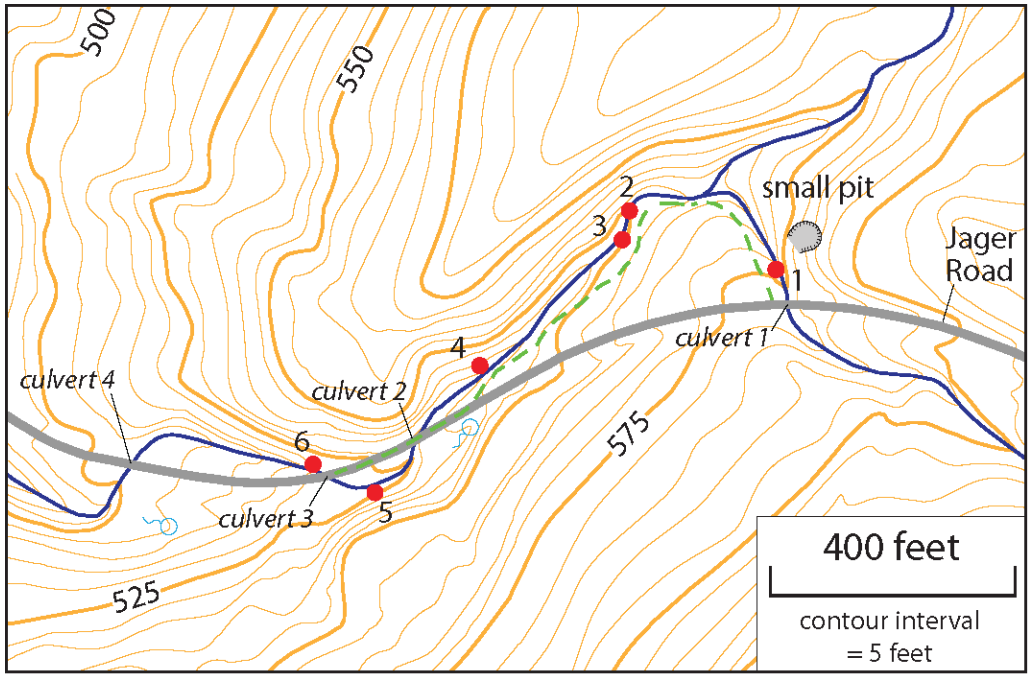

Figure 1-15. Site map of Stop 1a with numbered areas along route (green-dashed line) keyed to discussion and photographs in guidebook.

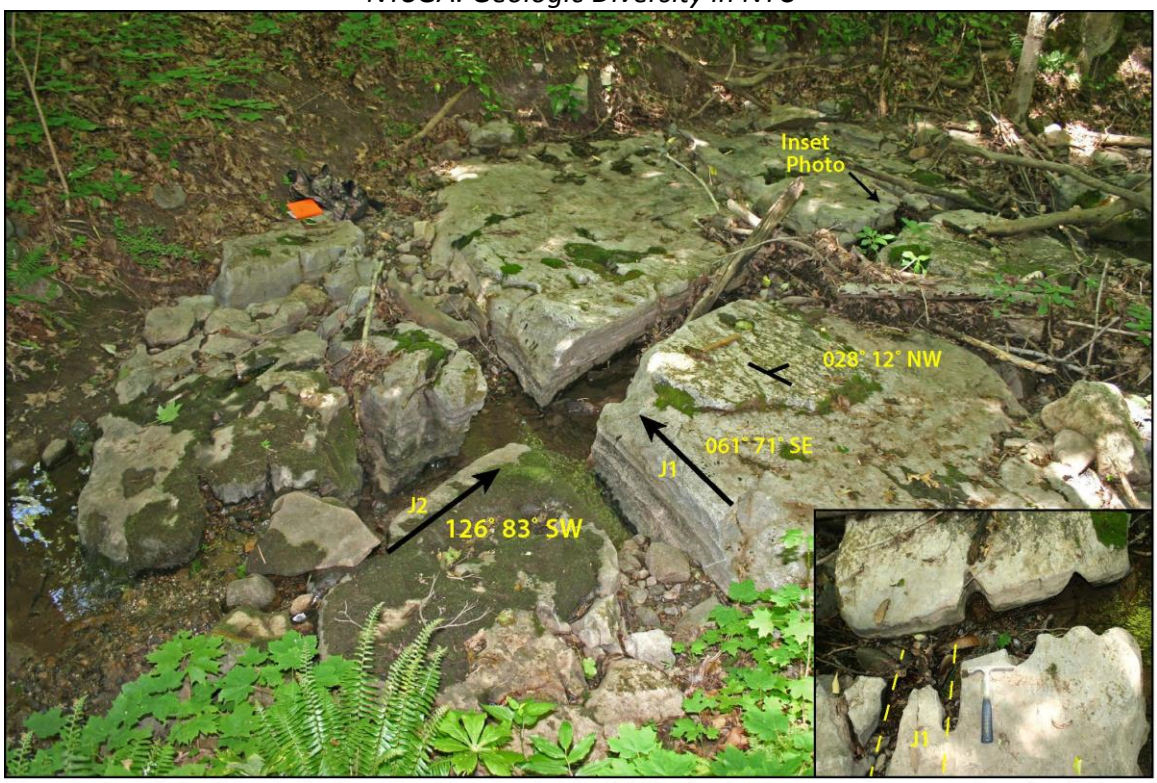

Figure 1-16. Solution joints in the Onondaga Limestone's Edgecliff Member just upstream from a small swallow hole and downstream from culvert 1. Water flows from left to right, rock hammer and fieldbook for scale. Inset photo shows dentate solution weathering along J1 joints. Water flow is right to left with hammer for scale. Photos by R. Witte.

Figure 1-17. Swallow hole formed in J1 joints, located along the left stream bank and downstream from culvert 1. Water flow is from left to right, hammer for scale. Photo by R. Witte.

Figure 1-18. Upstream view of debris-covered swallow hole below slump. Tree on right side of photograph is about 18 inches in diameter. Photograph was taken after a significant rain event in February 2016. Most of the time the flow does not reach this far downstream. The inset photo shows the slight depression formed in bouldery alluvium above what is assumed to be another large solution joint. This photo was taken a few weeks later and shows only a trickle of water (flow is from right to left). Note that secondary flow around a coarse gravel bar (main photo)diverts stream flow away from the buried swallow hole. Since swallow holes occupy positions along channel banks, stream flow to these features may be constrained by gravel bars and other debris (mostly fallen trees). Photos by R. Witte.

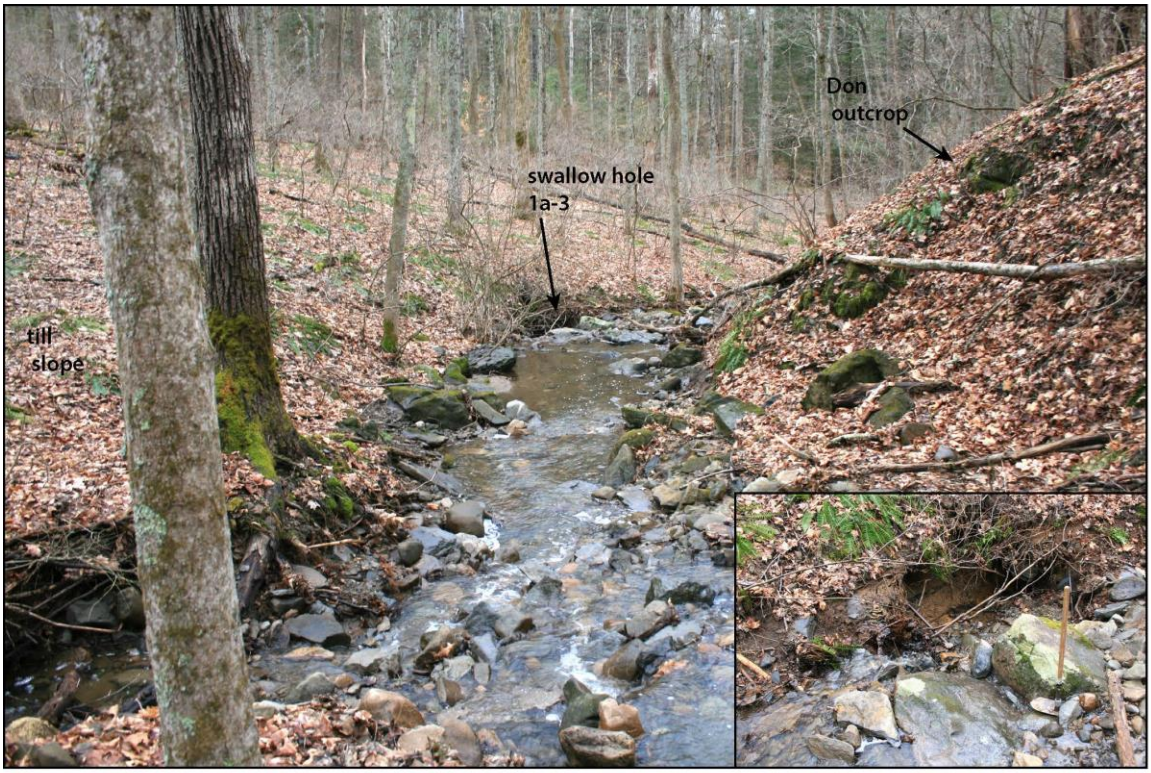

Figure 1-19. Downstream view (from end of gravel bar) and inset photo (shovel for scale) of the swallow hole located at 1a-3. Photos by R. Witte.

Figure 1-20. Small cave opening (28 inches (71 cm) wide by 32 inches (81 cm) high) located along the channel's right bank just upstream from culvert 2. Entrenching shovel is 32 inches long. Bedding (021˚ 10˚ NW) dips away from the viewer. The cave opening follows a large solution cross-joint (J2 - 114˚) about 5 feet (1.5 m) across a sediment-filled floor before it drops another 3 feet (1 m) into a very small passage. The Onondaga here is noncherty, thin to medium bedded, very fine-grained limestone. In places (inset photo taken to the right of shovel, mechanical pencil for scale), wavy, silty laminae parallel bedding. On weathering surfaces these stand out in greater relief compared to the more limy beds that weather out in negative relief. Photo by R. Witte.

Figure 1-21. Small spring located just downstream from culvert 2. Over the years the low reservoir wall has been undercut resulting in the formation of a small sinkhole. Local denizens (inset photo) are the green-headed frog and orange long-tailed salamander, both common inhabitants of springs and seeps in karst areas. Spring photo by R. Witte and inset photo by Jon Inners.

Figure 1-22. Sinkhole along right stream bank below culvert 3. Opening is 22 inches (56 cm) wide by 16 inches (41 cm) high. The subsurface cavern beneath the sink is about 4 feet (1.2 m) deep and over 7 feet (2.1 m) in length. The inset photo shows that the sink lies over a large solution channel (~ 055°). Typically, discharge from the spring upstream from culvert 3, drains into a gravelly area of alluvium near the sink. The sink has expanded over the last decade because of increased stream flow to this part of the channel, which was largely caused by the blockage of swallow holes upstream.

Figure 1-23. Seasonal views of Brau Kettle. The blue-capped standpipe housed the ADR logger that recorded water level and temperature. Photo A shows the kettle flowing during the late winter, typically a period of high groundwater levels in the Onondaga Limestone. Photo B shows the kettle partially filled, either filling or draining in response to summer thunder storms. During this period, water levels may fluctuate greatly in response to rapid changes in groundwater levels in the shallow karst aquifer. Photos by R. Witte.

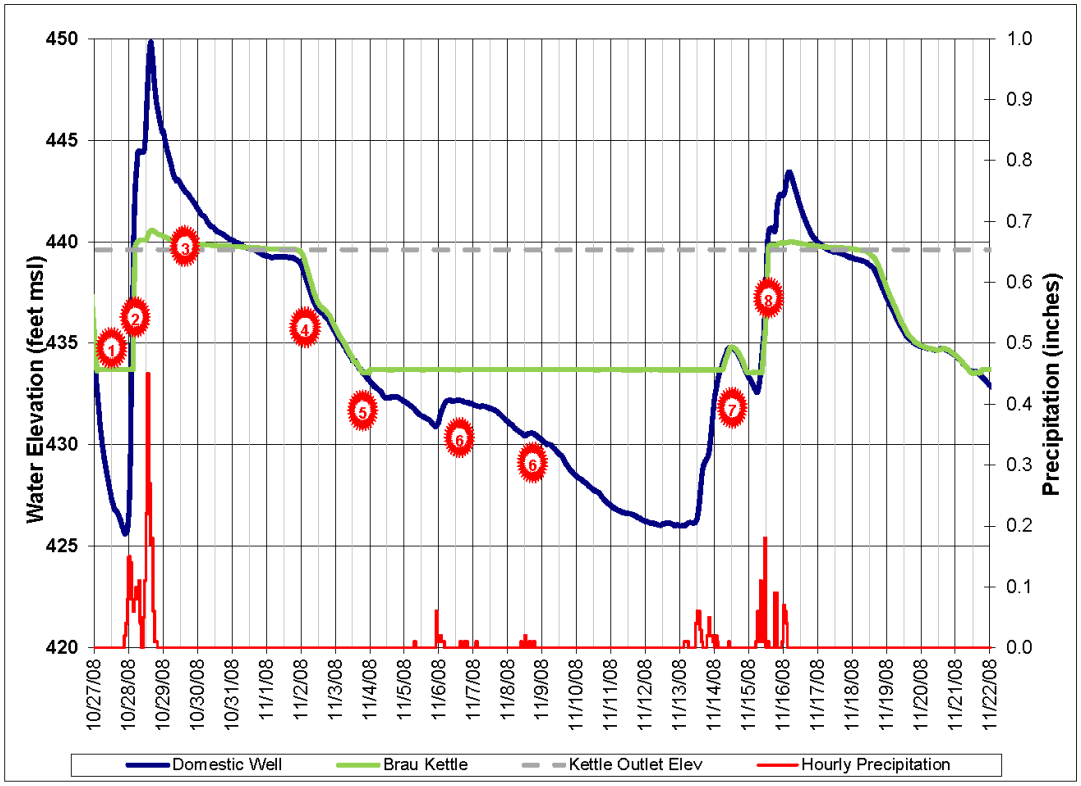

Figure 1-24. Daily water level and precipitation data for Brau Kettle and nearby domestic well at the Anson Johnson House from/27/2008 to 11/22/2008.

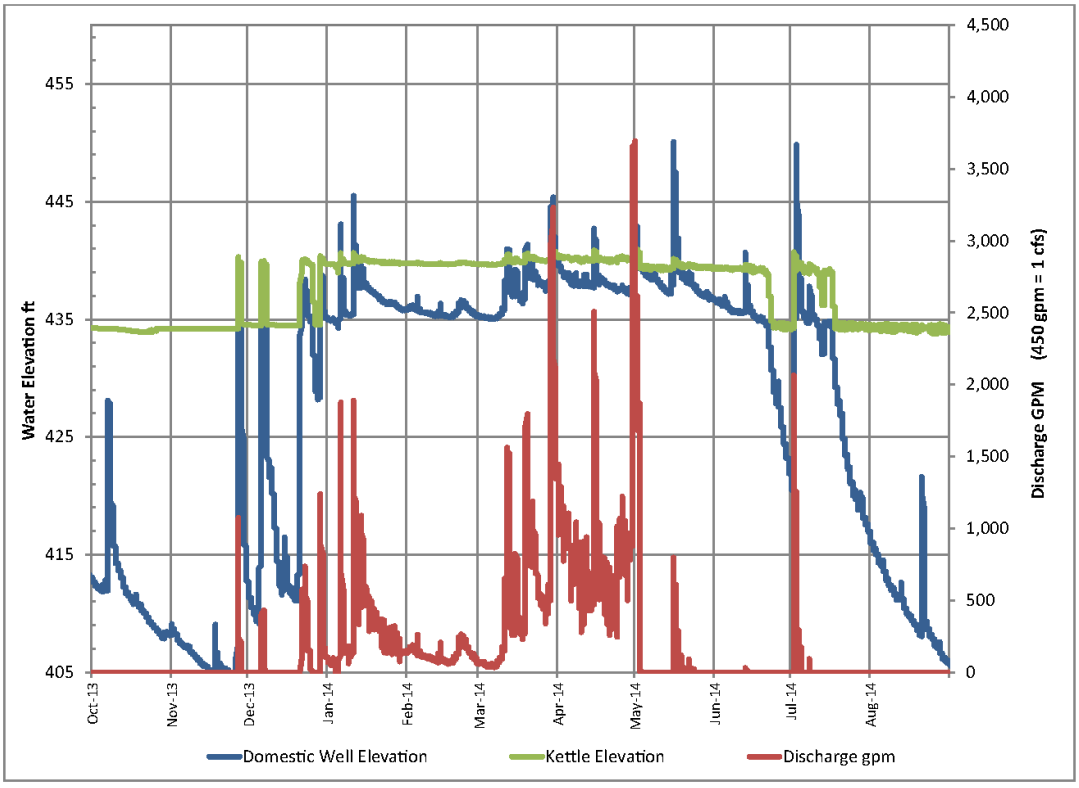

Figure 1-25. Water levels for the Anson Johnson House domestic well and Brau Kettle, and Brau Kettle discharge from October, 2013 to August, 2014.

Figure 1-26. NJDEP, Bureau of Freshwater and Biological Monitoring conducting a fish survey at Brau Kettle. Inset photo shows a mature 9 inch (23 cm) Brook Trout (netted in main photo) hiding amongst till stones on the Kettle's floor. Photos courtesy of Brian Henning (New Jersey Department of Environmental Protection, Bureau of Freshwater and Biological Monitoring).

Directions to STOP 2- Turn right out of parking area and head south on Old Mine Road.

Cumulative in miles (km)	Point to Point in miles (km)	Route Description
		Turn left onto Old Mine Road (south).
12.4 (20.0)	0.1 (0.2)	Pass Anson Johnson house well on right.
15.5 (24.9)	3.1 (5.0)	Cross County Route 560 (Tuttles Corner - Dingman Road) and continue on Old Mine Road.
15.8 (25.4)	0.3 (0.5)	Turn left into parking area, Old Dingman Road, Stop 2.

STOP 2 – Old Mine Road and Old Dingmans Road near Dingmans Ferry – Dingmans Ferry Spring, Tom Quick Cave, and Onondaga Limestone: solution and non-solution fractures, chert in the Onondaga Limestone, Amerind chert quarrying, and spring chemistry.

Field Stop leaders – Ron Witte, Don Monteverde, and Steve Domber.

Location and logistics

Stop 2 is located in the Culvers Gap quadrangle within the Delaware Water Gap National Recreation Area (DEWA) on the northwest slope of Wallpack Ridge. This field stop (fig. 2-1) is divided into two parts: 2a will consist of a short hike up Old Dingman Road and through the woods to Dingmans Ferry spring. After a short discussion, the group will cross a small stream (typically dry) and continue north through the woods to a large hill and outcrops of cherty Onondaga. **Safety Alert**. Be very careful traversing the steep slope and narrow game trail past Tom Quick Cave to the discussion area. The group will congregate along the west side of the hill for discussion and much arm waving by trip leaders especially by the one whose first name matches the rock's geo-abbreviation.

Geologic Setting

The same as Stop 1. We are still on the northwest flank of Wallpack Ridge formed here by a gentle dip slope of the Onondaga Limestone. In most places, the slope is covered by thin till. Along the Delaware River, glacial and postglacial terraces flank the river. The field stop route will traverse the lower and older part of the Onondaga first followed by a short ascent to the younger part of the formation. The lower part of the Onondaga is noncherty (similar to that observed at Stop 1-1a) whereas the upper part is very cherty. Large crinoid columnals that define the base of the limestone were observed by Spink (1967) along County Route 560, located about one mile (1.7 km) from the parking area. The columnals were confirmed by the trip leaders and several more were found nearby along strike.

Stop 2a – Dingmans Ferry Spring (41.220°N, 74.855°W)

Location – Lower slope of Wallpack Ridge.

Features – Dingmans Ferry spring, large solution joints, Onondaga Limestone (Edgecliff Member) and tufa.

Discussion – The spring (fig. 2-2) flows out of a large solution joint (070°), and emerges from a large opening at the base of a slope break. From here it spills downstream, cascading over a lag of till stones before coalescing into single channel. A very large oak tree (5-foot (1.5 m) diameter) stands sentient next

to the spring, drinking its cool water for centuries. Building ruins below near Old Mine Road (fig. 2-1) and a nearby spring box suggest settlers used the spring for potable water. Evidence of Amerind history in the area (Schrabisch, 1915) suggest the refreshing spring water was enjoyed well before this wild area was settled by colonists. Given the proximity of the spring, cave, and chert resource to each other, this area was probably sacred to the Minsi Lenapi that lived along the banks of the Delaware river.

Tufa, porous calcium carbonate (fig. 2-3), covers many of the rocks near the spring. It was deposited by emerging spring water, following a decrease in pressure (subsurface to atmospheric) resulted in the precipitation of $CaCO_3$. Water samples collected by NJGWS show pH values ranging from 7.25 to 7.42 and total dissolved solids ranged from 161 to 179 ppm; all measurements typical for springs in this area.

The nearby creek bed (fig. 2-1) is lower along contour from the spring and is typically dry. Here the Onondaga Limestone forms the creek bed, primarily a bedding-plane dip slope cut by several large solution joints (fig. 2-4). The limestone exposed along the creek bed is a thin to medium-bedded, faintly nodular, non-cherty limestone with some fossils. Its lithology is similar to the Onondaga observed at Stop 1a, so it may belong to the Edgecliff member. Similar to the situation at Brau Kettle, the lower and dry creek next to the spring shows that groundwater flows along strata-bound solution joints. Upstream a few small seeps discharge into the channel and a small wetland also drains into the channel as well as a small stream that flows off the hillslope above the spring and well above the Schoharie – Onondaga contact. Present hydrologic conditions do not explain erosion observed along the creek. Perhaps the channel may have been cut by glacial meltwater or postglacial stream flow prior to a change in subsurface drainage and the formation of Dingmans Ferry spring.

Recently, the spring's small stream was diverted to a larger channel (fig. 2-1). Spring discharge can now be observed flowing into the dry channel just upstream from the culvert on Old Mine Road. This manmade diversion was in response to erosion abatement and icing along Old Mine Road.

Proceed across dry (hopefully) creek bed and head upslope. **Safety Alert**. Be very careful crossing channel. If wet, the sloping rock surface is very slippery and may also be covered by leaves and moss. Also, watch out for a paper wasp nest near the south side of the dry creek. Hopefully, these insects will vacate the premises before our trip.

Stop 2b (41.221°N, 74.855°W)

Location – Hill overlooking the Delaware River near Dingmans Ferry and the only privately owned toll bridge across the Delaware River. Add history of Dingmans Ferry.

Features - there are three things to see, 2b-1) possible evidence of Amerind chert utilization, 2b-2) Tom Quick Cave, and 2b-3) cherty Onondaga Limestone (flinty Don). Depending on the group size, slope conditions, and whether we're on schedule, we may stop at all three locations (fig. 2-1).

Discussion -

2b-1 – Slope below outcrop.

There are many small chert fragments and a quartzite hammerstone (fig. 2-5) near the base of a tree. Because tree root growth may concentrate rock fragments on the surface (old mapping trick in areas of sparse outcrop), their occurrence here may not indicate Amerind working of this chert resource. However, some chert fragments exhibit conchoidal fractures and the hammerstone's tip has been broken in a way to suggest it was used as a tool. Also, the hammerstone fits remarkably well into the palm of your hand. Amerinds quarried and collected chert throughout Wallpack Ridge to provide blanks for tools and projectile points (Phillip LaPorta, personal commun., 1996)). Given the location of this hill overlooking the Delaware River, proximity to Amerind encampments situated on alluvial terraces near Dingmans Ferry

(Schrabisch, 1915), and abundance of chert in the Onondaga here, this site would have been a prime location to collect chert. It may have been quarried from the outcrop or collected from loose rock on the slope below. Typically, larger pieces of chert were knapped into smaller blanks at the outcrop and then carried back to encampments where they were further worked into tools such as scrappers and projectile points. Hopefully, the evidence presented shows that this site was actively used to process chert. At least that's our story (spring, cave, chert) and we're sticking by it.

2b-2 – Tom Quick cave.

The cave is a long, narrow slot (fig. 2-6) that runs about 25 feet (8 m) along a large joint (027°). Given the attitude of bedding (043° 12° NW) and proximity to a steep slope down dip, the cave is probably a fracture cave that formed when a very large joint block moved downslope by creep., and not the result of solution weathering. However, the initial enlargement of the joint by solution weathering cannot be discounted. In addition to creep, movement may have been aided by root growth and ice wedging. Also, evidence for solution weathering beneath cherty limestone (Stop 2b-3) may have contributed to detachment along bedding along the base of the joint block. Above the cave small sinkholes are found that are aligned along the 027° fracture.

Eye witness accounts (Bathgate, 1916) of a small room at the cave's terminus about 55 feet from its entrance suggest the cave may have been larger than its current size. During a return visit, Bathgate could only proceed about 20 feet into the cave. One of the cave walls had moved closing off the passage. This account suggests that the cave may consist of several joint blocks that at times may move independently from one another.

As with most caves, local lore provides interesting stories where fact is not easily separated from fiction. The cave is named after Tom Quick Jr., who may have used the cave as a hideout during the mid-1700's following one or several Indian skirmishes (Dalton, 1967). Supposedly, Tom's father, Tom Quick Sr. was mortally wounded in a raid when the family was cutting ice on the Delaware River (njherald.com/article/20151206/ARTICLE/312069975#).

Currently the cave is closed by the National Park Service in order to protect bats from a deadly fungus that causes white nose syndrome.

2b-3 – Cherty Onondaga Limestone outcrop along west side of hill.

This face offers a good opportunity to investigate the cherty beds of the upper Onondaga. Originally named the Corniferous Limestone (Cook, 1868) based on similarities cherty limestones found in Pennsylvania and New York. This 14 foot-high (4.3 m) outcrop shows an abundance of chert nodules dispersed throughout the outcrop (figure 2-7). The chert nodules vary from 2 to 3 inches (5-7.5 cm) across. Close inspection shows areas where the chertification was incomplete yielding a dark gray mottled appearance. Associated with this incomplete certification are intriguing very thin parallel black curving lines that are commonly associated with the mottled spots (fig. 2-7, inset photos). There is no preferred orientation of these thin bands, which we suggest may relate to the secondary chert-forming process. Further study is needed to completely understand this appearance.

Due to the absence of a preferred fracturing in these beds the chert would be more easily worked and highly prized by the original inhabitants of this region. Farther to the north this same cherty upper part of the Onondaga is highly cleaved which would greatly inhibit the ability to work those cherts into usable points. Beds are generally wavy with variable thickness of 3 to 8 inches (7.6-20.3 cm). At the base of this outcrop are two small solution openings (fig. 2-8) in generally chert-free beds. The solution appears to occur at the intersection of the bedding plane and some weakly developed joints trending 068°. This minor

bedding plane solution may have enhanced joint-block movement down slope which led to the development of Tom Quick cave.

Given its high chert content and younger stratigraphic position relative to the basal Onondaga, we believe we are looking at the Moorehouse Member (possibly its upper part). We have not encountered the Nedrow Member in our mapping because it may not be here because it may be indistinguishable from the Edgecliff or Moorehouse Members (Oliver, 1956) or because of its shaly nature it does not outcrop along the Onondaga dip slope. The Tioga bentonite, which defines the Seneca-Moorehouse contact has not yet been encountered in western New Jersey, but as stated in the long discussion preceding Stop 1a we believe the Seneca lies mostly buried beneath alluvium and glacial outwash making its identification problematic.

Return to parking area by retracing steps to flatter area above the creek and follow slope to Old Mine Road (fig. 2-1). For more adventurous types, straight down the hill is the shortest route. Mind you, if you fall and incapacitate yourself will give you a bottle of whiskey, GPS your position, and notify the Park Rangers at the end of the trip.

Directions to Lunch Stop (Peters Valley). Turn left onto Old Mine Road (south) from parking area along Old Dingman Road.

Cumulative in miles (km)	Point to Point in miles (km)	Route Description
16.5 (26.6)	0.7 (1.1)	Continue straight on Wallpack Road (south). Do not turn right onto Old Mine Road.
17.5 (28.2)	1.0 (1.6)	Turn right into driveway toward picnic pavilion at Peters Valley.

Lunch Stop – Peters Valley (41.197°N, 74.851°W), which is on route to Stop 3 (Bevans Rock Shelter). Park in upper lot near picnic pavilion (fig. 2-9). Rest rooms are located at the bottom of the hill across the street from the gallery. Please take a moment to stop by the gallery and checkout the many fine works of the local artisans.

Peters Valley School of Craft is a non-profit corporation, founded in 1970 in partnership with the National Park Service to promote and encourage education and excellence in craft. Peters Valley School of Craft's programs include adult summer workshops, youth programs, opportunities for artists, special studio programs, public exhibitions, demonstrations, and outreach. Peters Valley School of Craft maintains studios in eight disciplines: blacksmithing, ceramics, fiber surface design, fiber structure, fine metals, photography, special topics and woodworking. Description from https://www.nps.gov/dewa/planyourvisit/peters-valley.htm.

For more information about Peters Valley School of Craft and the programs offered, visit the campus at 19 Kuhn Road, Layton, NJ 07851, call (973) 948-5202 or visit their website at petersvalley.org.

We'll probably spend about 45 minutes here and then take the short drive over to Stop 3 (Bevans Rock Shelter). Turn right onto Wallpack Road to continue trip.

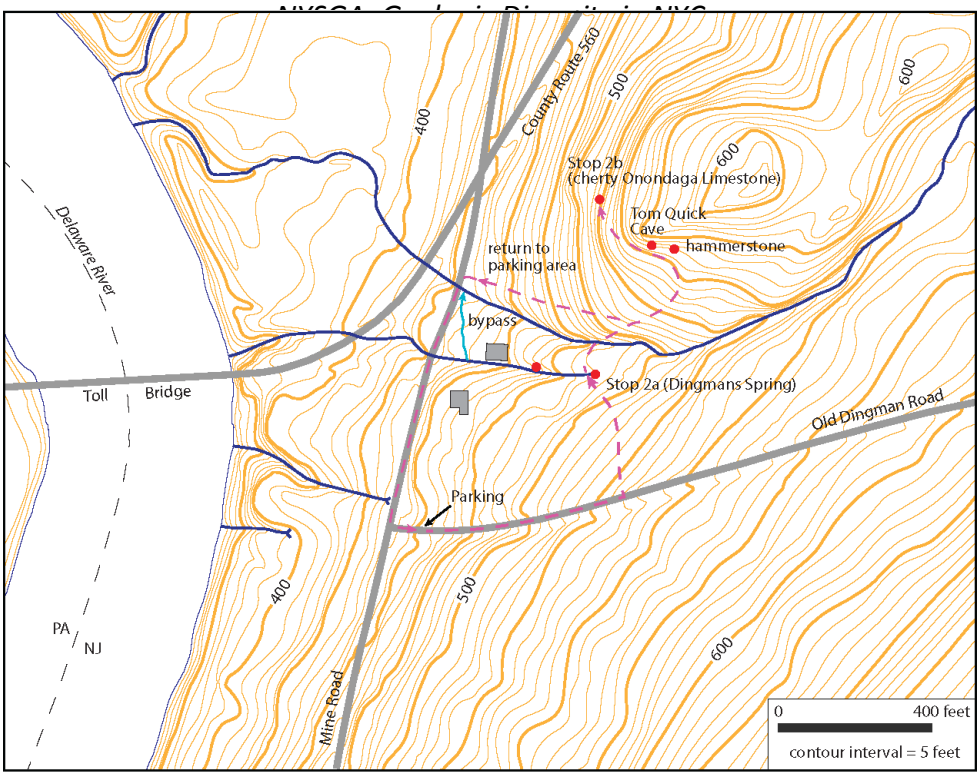

Figure 2-1. Site map of Stop 2 with areas labelled along route (purple-dashed line) keyed to discussion and photographs in guidebook.

Figure 2-2. Dingmans Ferry spring, Delaware Water Gap National Recreation Area, Sandyston Township, New Jersey. The spring flows from a large opening along the lower slope of Wallpack Ridge. Large oak tree to the right is 5 feet in diameter. Closer inspection (inset photo) shows that the spring's discharge is directed along a solution joint that trends about 060°. Photo by Jon Inners.

Figure 2-3. Moss-covered tufa (porus calcium carbonate) encrusting cobblestone at Dingmans Ferry spring. Photo by R. Witte.

Figure 2-4. Onondaga Limestone (bedding dip slope) in stream channel just north of Dingmans Ferry spring. Except for a few small seeps, the channel is typically dry, while the spring flows year round. The solution joints (one noted along arrow, 071˚) have a similar orientation as the joint where the spring emerges. The channel floor (measured along slope contour) is lower than the spring, showing that groundwater flow is highly controlled by joints and vertical zonation between beds. Photo by Jon Inners.

Figure 2-5. Chert fragments and quartzite hammerstone (right side of pencil) found on slope below outcrop of cherty Onondaga Limestone. Note indents along left side of hammerstone that could easily accommodate thumbhold and fingerholds. The stone's pointed end exhibits small impact marks, suggesting it may have been used to knap larger pieces of chert into smaller blanks. These were later carried back to encampments where they were worked into tools and projectile points. Photo by Don Monteverde.

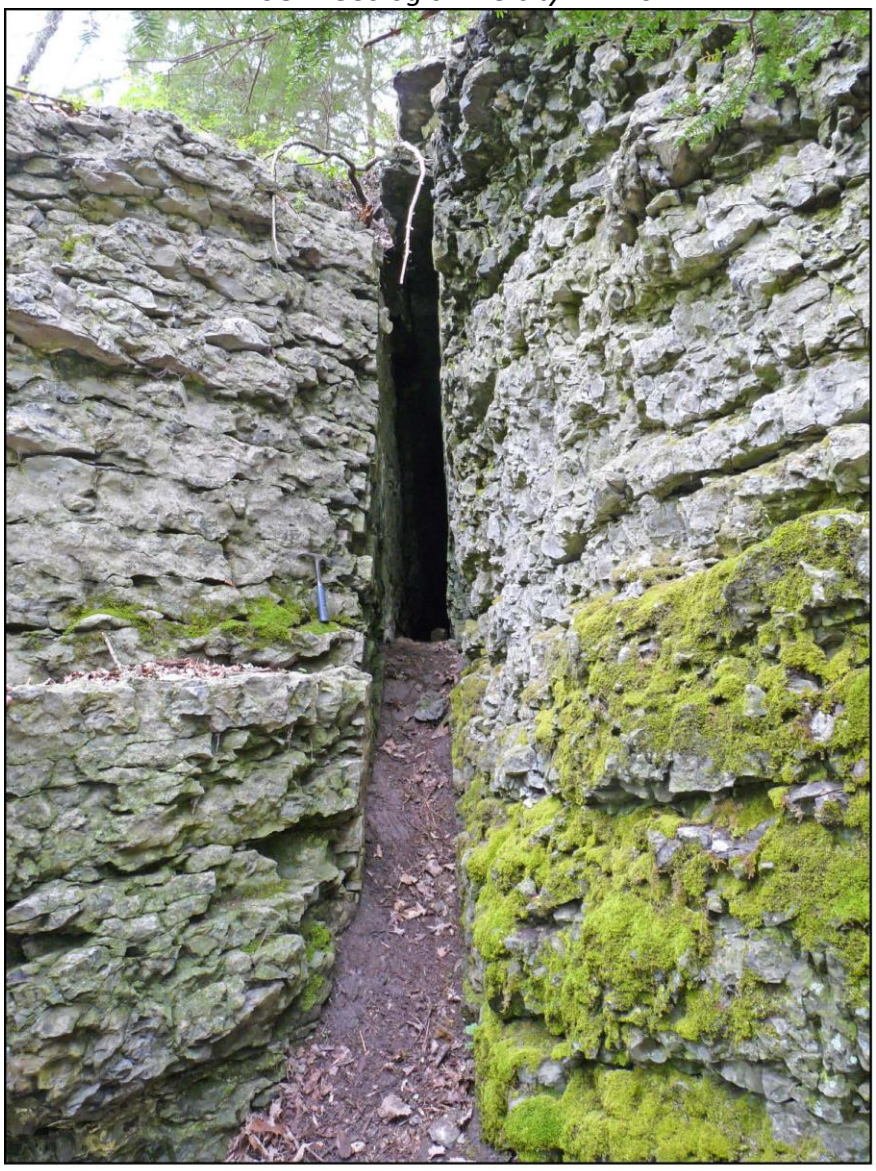

Figure 2-6. Entrance (w = 1.15 ft. (.35 m), ht = 8.2 ft. (2.5 m)) to Tom Quick cave, rock hammer for scale. The cave follows a enlarged vertical joint (027˚) about 30 feet (9 m) long. Bedding = (043˚, 12˚ NW). Based on bedding attitude and proximity along a steep slope the cave's fracture may have become enlarged by mass movement (downslope creep) rather than solution weathering. Photo by R. Witte.

Figure 2-7. Outcrop of chert-bearing Onondaga Limestone showing many dark gray to black chert nodules. Note mechanical pencil for scale. The abundance of chert places this exposure in the Moorehouse Member of the Onondaga. The overlying Seneca is also chert bearing, but is separated from the Moorehouse by the Tioga Ash bed which has not yet been found in New Jersey. Bedding (009˚ 13˚ NW, towards the viewer) is quite wavy, probably due to the original nodular sedimentology and the secondary chertification. Beds have a very rough parallel fracture pattern that does not commonly propagate upwards into adjoining beds. Inset photos A and B. Examples of thin, parallel dark silica (?) bands associated with locations of incomplete chertification. Band alignment is only parallel locally and there is no preferred orientation across the outcrop. They are associated with dark gray patches of incomplete chertification. Photos by Don Monteverde.

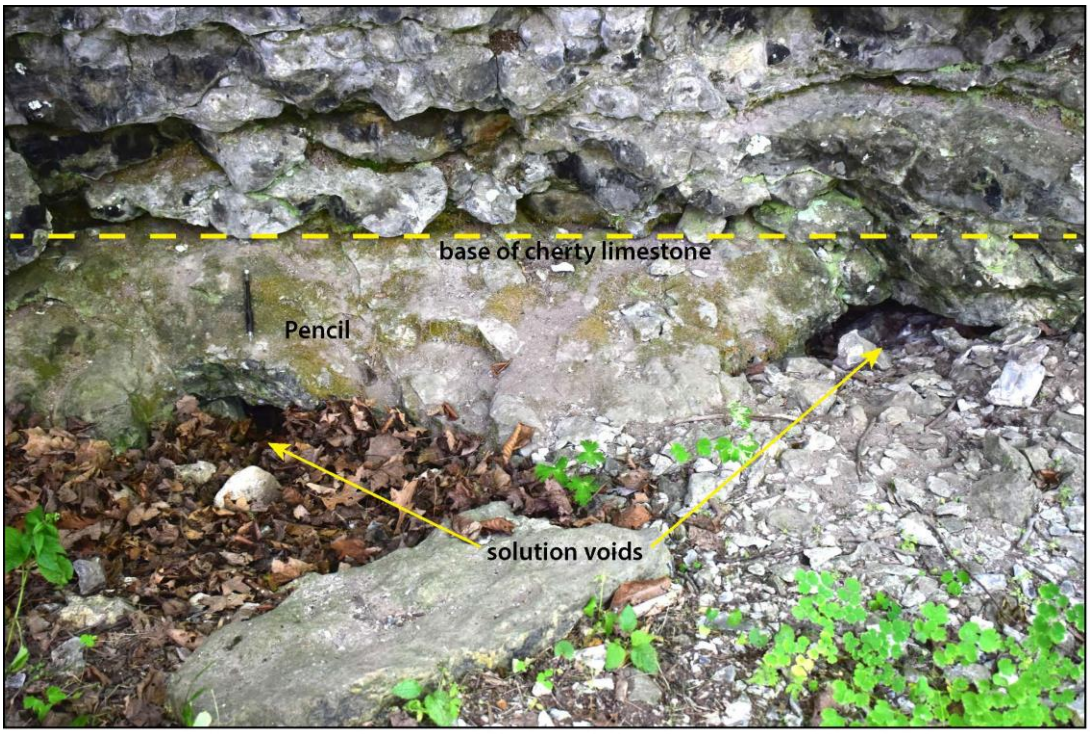

Figure 2-8. Two small solution voids in a limestone-rich bed beneath cherty limestone. Pencil for scale. The voids appear to have formed along a joint (068˚ 83˚ SW) - bedding (009˚ 13˚ NW) intersection. Photo by Don Monteverde.

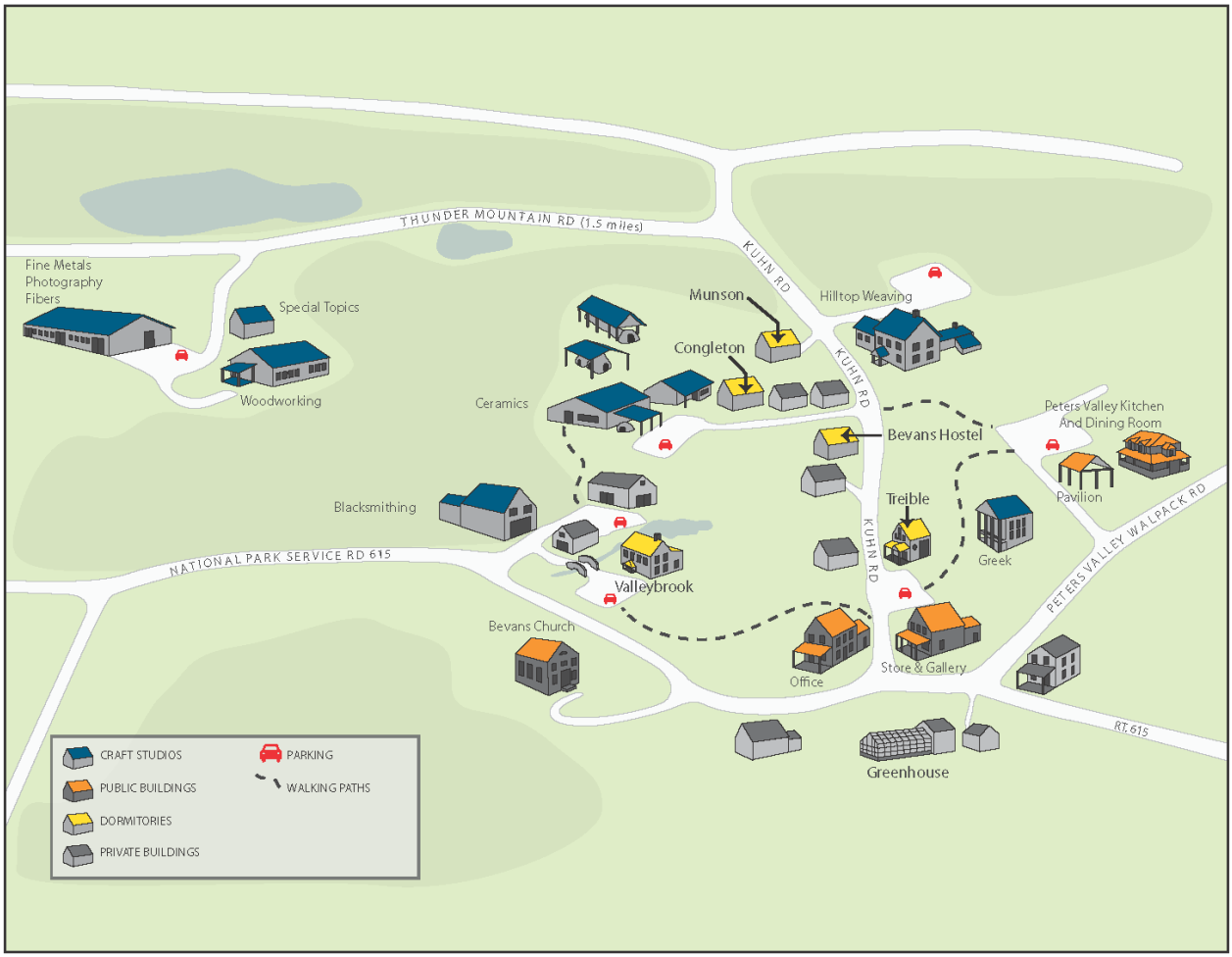

Figure 2-9. Campus map of Peters Valley. We'll stop for lunch at the pavilion. Please feel free to check out the store and gallery. Rest rooms are located across the street from the gallery along the right side of the office.
Map from - www.petersvalley.org/images/file/pv_student_map-8_5inx11in-trifold-inside.pdf

Directions to STOP 3 - Turn right out of driveway onto Wallpack Road (south).

Cumulative in miles (km)	Point to Point in miles (km)	Route Description
17.6 (28.3)	0.1 (0.2)	Turn right onto Kuhn Road (west), next to Peters Valley Gallery.
18.3 (29.5)	0.7 (1.1)	Turn left onto Thunder Mountain Road, park in small area about 100 feet past turn off. Arrive at Stop 3.

STOP 3 – Bevans Rock Shelter, Esopus Formation, fracture caves, Amerind history.

Location Coordinates (parking area): 41.194°N, 74.863°W

Field Stop leaders – Ron Witte, Don Monteverde, and Ted Pallis.

Location and logistics

Stop 3 is located in the Culvers Gap quadrangle in the Delaware Water Gap National Recreation Area (DEWA) on Wallpack Ridge above Peters Valley (fig. 1-1). The exact location of the rock shelter is not shown in order to protect the cultural integrity of the site. Follow trip leaders to secret parking area and then we'll proceed by foot to the rock shelter. The large outcrop near the parking area is the Esopus Formation, a very thin to thin-bedded, very fine-grained sandstone. Bedding is 046° 16° NW and the outcrop is cut by a well-developed cleavage (081° 72° SE).

Geologic Setting

The Bevans Rock Shelter (fig. 3-1) sits high on Wallpack Ridge about one mile (1.6) km from both the Delaware River and Flat Brook in Wallpack Valley. The rocks in the shelter area are oldest to youngest are the Glenerie Formation and Ridgely Sandstone of the Oriskany Group, Esopus Formation, Schohaire Formation, and the Onondaga Limestone (fig. 3-2). All formations dip northwestward with the Onondaga forming a long dip slope to the Delaware River. The Ridgely Sandstone, which consists of thick-bedded quartz-pebble conglomerate and coarse quartz sandstone (Monteverde, 1992) may not be present over the Glenerie at the shelter, but it has been observed nearby to the south, where it thickens along strike to Wallpack Bend and reaches a maximum thickness of 32 feet (9.8 m).

Oriskany through Onondaga time represents a sea-level cycle where 1: the Oriskany Group represents a carbonate shelf to clastic sequence (beach and nearshore fluvial deposits), 2: the Esopus Formation represents deeper water deposition marked by very low fossil content and occurrence of the trace fossil Zoophycus, 3: the Schohaire Formation is a transitional unit that marks a return to shallower seas, and 4: the Onondaga represents a carbonate shelf sequence, which in places contains patchwork reefs.

The shelter rocks over the years have had several interpretations. Henry Kummel's field sheets (1895, on file at NJGWS, Trenton, New Jersey) show that the Cauda Galli Grit (now recognized as Esopus) was mapped at the shelter with the Oriskany contact located just east of the shelter. Meredith Johnson, during a visit to the shelter in 1938 (NJGWS permanent notes on file at NJGWS, Trenton, New Jersey), indicated that the shelter rocks belonged to the Oriskany Limestone. Johnson also noted that base of the shelter contained "numerous small brachiopods of the type similar to *Anoplotheca flabellites*. Herpers (1952) noted that a contact between the Oriskany and Esopus occurs at the shelter and that the lower fossiliferous zone belongs to the *Acrospirifer murchisoni* zone of the Oriskany. Monteverde (1992)

showed that the shelter lies within the Esopus Formation. Hmmm. multiple interpretations of the same outcrop, let's see if we can add to the confusion.

Discussion

Geology of Bevans rock shelter.

Take ten geologists to an outcrop and you'll wind up with 10 different interpretations. An old witticism to be sure, but one with a kernel of truth to it. Who's right and who's wrong? We'll present the facts and you can make up your own minds. Esopus, Oriskany, or both?

The outcrop at Bevans rock shelter looks much different than the Esopus outcrop near the parking area and above the shelter, which is a dark gray, noncalcareous, very fine-grained sandstone with a well-formed cleavage. The trace fossil *Zoophycos* is also found throughout the shelter's rocks. The shelter's roof rock (fig. 3-1) is similarly described so we're confident that this part of the shelter is Esopus. The 10.5 feet (3.2 m) section (fig. 3-1) below the roof is much different. The rock here is mostly (we did not check every bed) a thin- to medium-bedded, calcareous, very fine-grained sandstone where cleavage is not nearly as well-formed as it is in the overlying rocks. Throughout the shelter's back wall solution voids up to 6 inches (15 cm) in diameter (most are less than 2 inches (5 cm)) are found along bedding (fig. 3-3). Also, a few dark gray, calcareous concretions (fig. 3-3) occur along bedding about midpoint between the shelter's roof and floor. *Zoophycos* occurs throughout this section to at least 2 feet above the shelter's floor (fig 3-4). Lastly, a thin bed of small brachiopods (fig. 3-3) occurs about 5.4 feet (1.6 m) from the shelter's floor. Presumably, these are the same brachiopods observed by Johnson and Herpers, which were interpreted to be Oriskany fauna (fig. 3-3). Biostratigraphically, this is a mixed zone where Oriskany and Esopus faunas are transitional. Lithostratigraphically, a contact occurs between noncalcareous and calcareous sandstone at or just below the shelter's roof. As far as we are aware, no one has described *Zoophycos* in the Oriskany. However, Brett and others (2009) indicated that a few Oriskany brachiopods were transitional into the Esopus. Spink (1967) also noted, that the lower Esopus contact in places is "gradational through an interval of several feet in which arenaceous and calcareous siltstones become interbedded with, and then are replaced by, silty limestones." Spink's silty limestones are probably the Glenerie Formation.

Given the best available data (one of Don's favorite terms of escapism) and similarity to Spink' s description of the Esopus-Glenerie contact, the shelter section below the roof represents the basal, transitional facies of the Esopus Formation. The Oriskany contact lies just to the east, buried beneath a bog that flanks the shelter. However, if you want to place the contact elsewhere, that's fine, just publish your work after we retire.

Geomorphology

The rock shelter and the smaller caves on its flanks (fig. 3-5) were shaped by glacial erosion and postglacial mass weathering. The main shelter, with its resistant Esopus roof, was chiefly formed where the easily eroded transitional Esopus rock was removed by glacial plucking and abrasion. The scalloped surfaces on the shelter's back wall (fig. 3-3f) appear to be glacially scoured. Also, the absence of loose rock beneath most of the shelter's roof suggests this material was removed by glacial erosion. Admittedly, some of this material may lie buried in the bog that lies adjacent to the shelter. However, given the large size of current joint blocks in and around the shelter, one would expect that some of this material should be here on the floor of the open part of the shelter. Other than smaller stones, this material was probably not moved by the shelter's past inhabitants.

Over time, part of the shelter's roof and walls have collapsed (specifically the north end). The result of postglacial frost wedging and slump where joint blocks became dislodged and fell away from the outcrop. Similarly, the fracture caves on the shelter's flanks may have been formed by frost wedging. However, because bedding dips into the hillside, the movement of these very large joint blocks was not helped by gravity as it was at Tom Quick Cave (Stop 2-c). Another possibility is that ice wedging may have occurred during glaciation. Specifically, during deglaciation when overlying ice was thin and freeze-thaw cycles much more robust.

The smaller cave in the shelter (fig. 3-5) appears to be largely a result of mechanical weathering along a nearly vertical 096° joint that intersects the shelters back wall. However, dissolution in the lower Esopus beds may have aided the cave's formation.

Archaeology of the Bevans Rock Shelter

The Beans rock shelter (fig. 3-6), located in Sandyston Township, Sussex County is a prominent rock shelter that was used by Native Americans during the Late Archaic (3000 B.C to 1000 B.C.) and Woodland (1000 B.C. to 1550 A.D.) periods. This rock shelter sits about 300 feet (91 m) above the Delaware River, located halfway between the Delaware and Wallpack Valleys. The shelter has an eastern exposure and lies adjacent to a narrow bog. It has an overhanging roof that projects up to 20 feet outward from the rock face, creating a sheltered space underneath. The habitable area of the shelter consists of three parts (fig. 3-7). To the south (near fireplaces "a" and "b") lies a typical overhanging rock, 24 feet long, which projects eight feet outward about 10-14 feet above the floor. In the center (near dislodged rocks), another overhanging rock, 22 feet long, has a roof 8 feet high projecting 6 feet, and is protected in front by two detached masses of rock, one small, the other large, lying 5 feet from the rear wall. The central section has a higher degree of enclosure due to the two detached blocks which hold up the roof and form the eastern wall. At the right is a cave-like compartment (near fireplaces c and d), 16 feet long, 4 1/2 feet wide and 6 feet high. This northern section offers the most protection. All three parts lie in an approximate straight line at the foot of a low cliff and their total length is about 62 feet. The dirt floor underneath the rock is level and composed of light sand mixed with rocks.

Two archaeological surveys were conducted here, one from 1912-1913 by Max Schrabisch, archaeologist and writer and another in 1931 led by Dorothy Cross (State Archaeologist and Curator for the New Jersey State Museum). Several local collectors also reported finding material in the main shelter from time to time, but none of this was officially recorded.

Max Schrabisch partially excavated the Bevans rock shelter while making an archaeological survey of Sussex County for the state from 1912 - 1913. In the summer of 1931, from June 8 to July 7, the New Jersey State Museum and the University Museum, Philadelphia, sponsored the complete excavation of the four shelters at the Bevans Rock shelter under the direction of Dorothy Cross. These two surveys uncovered many artifacts or traces of human habitation. During the first excavation by Schrabisch, the southern open shelter (location b, fig. 3-7) yielded the most aboriginal remains while the middle section contained the least. The rear was smoke-stained and discolored by ancient fires but no relics were found on the surface. Native American relics were found from three inches to two feet below the surface. Items included both plain and ornamented pot shards, deer bones, projectile points (identified as arrow and spear points), multiple tools (drill, pestles, hammers, blades), net sinkers, many flint and jasper flakes, and at least 1000 pieces of pottery (most cord-marked) belonging probably to approximately 20 different pots were found in the three parts of this rock shelter. Also, several fire pits were excavated (fig. 3-7), some

of which contained mussel shells. Figures 3-8 and 3-9 are some of the artifacts collected during the Schrabisch survey.

A second excavation was conducted in 1931 Led by archaeologist Dorothy Cross (fig. 3-10). Altogether, the second excavation produced 102 various stone artifacts (some of which included arrow points, blades, scrappers, one possible hoe, hammerstones, net sinkers, one maul, one anvil, and one rubbing stone), 11 bone artifacts, 1,428 potsherds (both cord-marked and plain), 100 fresh-water *Unio* shells (whole and fragmentary), three crinoid stems (possibly used as jewelry) and several thousand whole and fragmentary animal bones, a fragment of a trade pipe, and a lead bullet. Three undisturbed pits were found during this excavation. All pits showed traces of fire action and contained refuse material.

Both archaeologists who excavated the site came to different conclusions about the habitation of the site. According to Schrabisch, "based on the materials found here, the rock shelter was tenanted more or less permanently and perhaps used for winter quarters. The fireplaces suggest cooking and the pottery indicates that the women and children accompanied the men and shared their quarters." Cross believed "the Bevans shelters were used as temporary abodes and this is attested to by the absence of permanent household equipment. Almost all of the artifacts can be associated with hunting and fishing, either directly or indirectly; though the number of potsherds is a little greater than would have been associated with a hunting or fishing camp." Cross further stated that "if the entire contents of the shelter were available, more definite conclusions might be drawn" regarding Amerind habitation.

Figure 3-1. Bevans rock shelter looking northeast. Past the collapsed roof blocks to the left is a narrow vertical fracture that leads to a small cave (the enclosed part of the shelter). The roof and upper part of the shelter's back wall contain the trace fossil *Zoophycus*, a common fossil in the Esopus Formation. Near the base of the back wall, small brachiopods (*Anoplotheca flabellites*) have been found, a common fossil in the Oriskany. Note odd fellow in the shadows for scale.

System	Series	Formation		Member	Description	Aproximate thickness (feet)
Devonian	Middle	Marcellus			Dark gray to black shale, locally silty, weathers medium gray; fissile, thin bedded though locally thick bedded and massive; limonite stained, and sparingly fossiliferous.	900
		Onondaga (Buttermilk Falls)		Seneca (Echo Lake)	Fossiliferous cherty limestone. Base contains Tioga ash bed.	15
				Moorehouse (Stoudsburg)	Medium-gray limestone and argillaceous limestone with beds, pods, and lenses of dark-gray chert. Fossiliferous and burrowed.	135
				Nedrow (McMichael)	Medium-gray calcareous argillite with lenses of light-gray fossiliferous limestone.	40
				Edgecliff (Foxtown)	Medium-dark-gray calcareous siltstone and argillaceous limestone containing lenses of dark gray chert. Fossiliferous, one-inch diameter crinoid columnals in lower half.	80
	Lower	Schoharie			Medium to thick bedded; silty to shaly, locally dolomitic limestone containing local thin ribs or pods of black chert, weathers yellowish gray to locally pale olive and grades downward into medium to dark gray calcareous siltstone at base. Contains rare trace fossil Taonurus.	175
		Esopus			Medium to dark gray, shaly to finely arenaceous siltstone, containing minor calcareous siltstone near top. Laminated to medium bedded, as well as local massive thick bedded layers. Weathers medium gray and is limonite stained in places. Bioturbated by Taonurus. Thickness approximately 300 feet.	300
		Oriskany Group	Ridgely Sanstone		Medium-gray, medium- to thick-bedded quartz-pebble conglomerate and coarse quartz sandstone. Sand grains are moderately well sortd and subrounded. Rock has a carbonate cement and contains abundant braciopods. Unit occurs west of Peters Valley and thickens to the southwest.	0-32
			Glenerie Formation		Upper section is medium to dark gray, fine grained silty limestone, containing a one inch thick tan gray weathering rind. Rock is wavy bedded, medium bedded, fossiliferous and contains local zones of siliceous limestone. Lower section is medium to dark gray, fine grained silty limestone; laminated to thin bedded and commonly trough cross bedded and fossiliferous.	55-170

Figure 3-2. Description of rock units near Bevans rock shelter. Modified from Epstein (2001). Onondaga members from Oliver (1954) and Vanuxem (1839). Buttermilk Falls (Willard, 1939) members from Epstein (1984) and Inners (1975). Ridgely Sandstone description from Monteverde (1992).

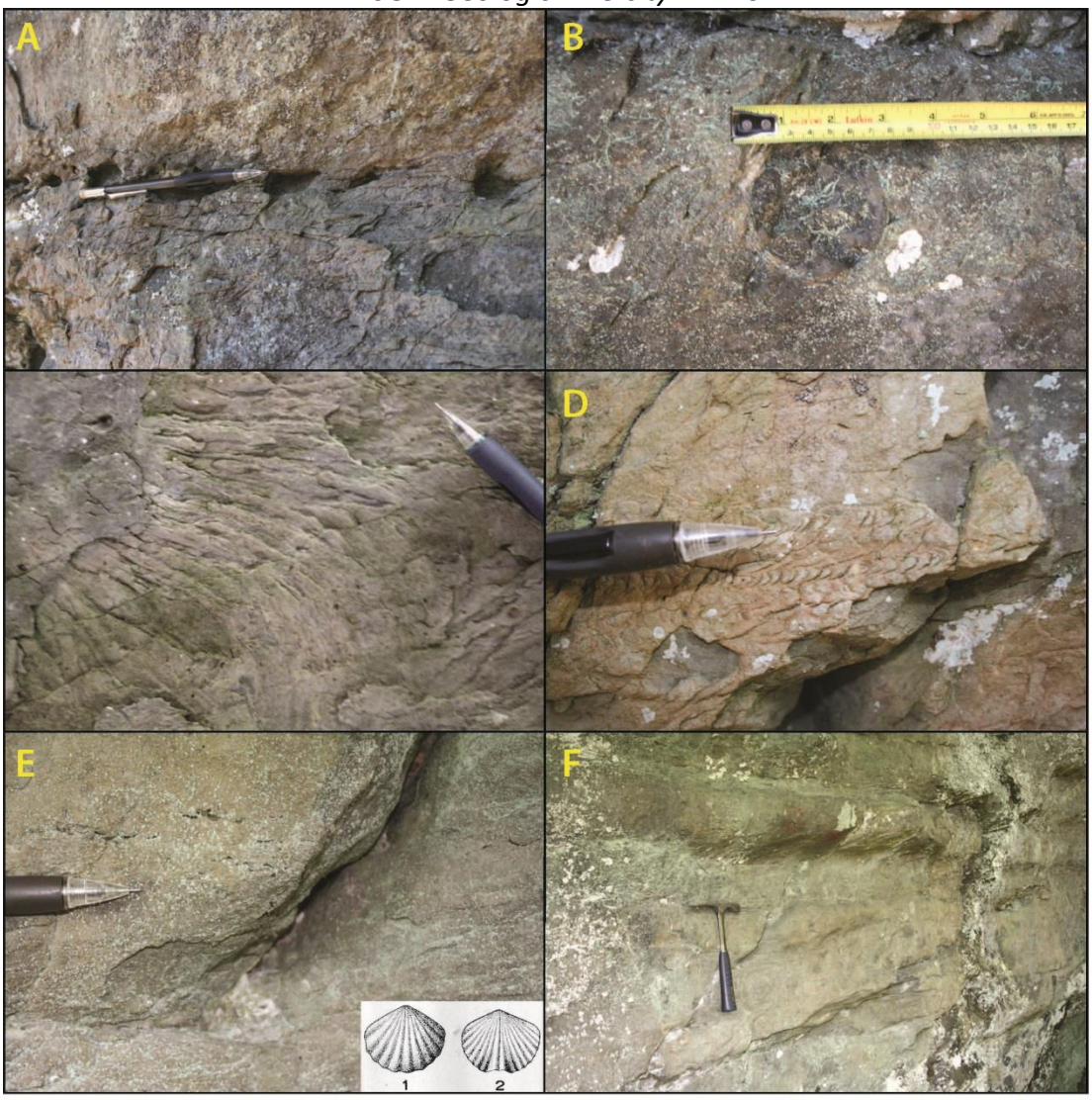

Figure 3-3. Features along the back wall of the Bevan rock shelter: A) solution voids along bedding , B) calcareous concretion, C) *Zoophycos* (planar view, bottom of roof rock), D) *Zoophycos* (cross-sectional view), E) small brachiopods (dark-curved lines - *Anoplotheca flabellites*?), inset illustration from Weller (1903, Plate XLIX), *Anoplotheca flabellites* (1) complete pedicle valve and (2) complete brachial valve collected near Layton, New Jersey, and F) glacial scour. Photos by R. Witte. Photo of planar view of *Zoophycos* by Yelena Stroiteleva (NJGWS).

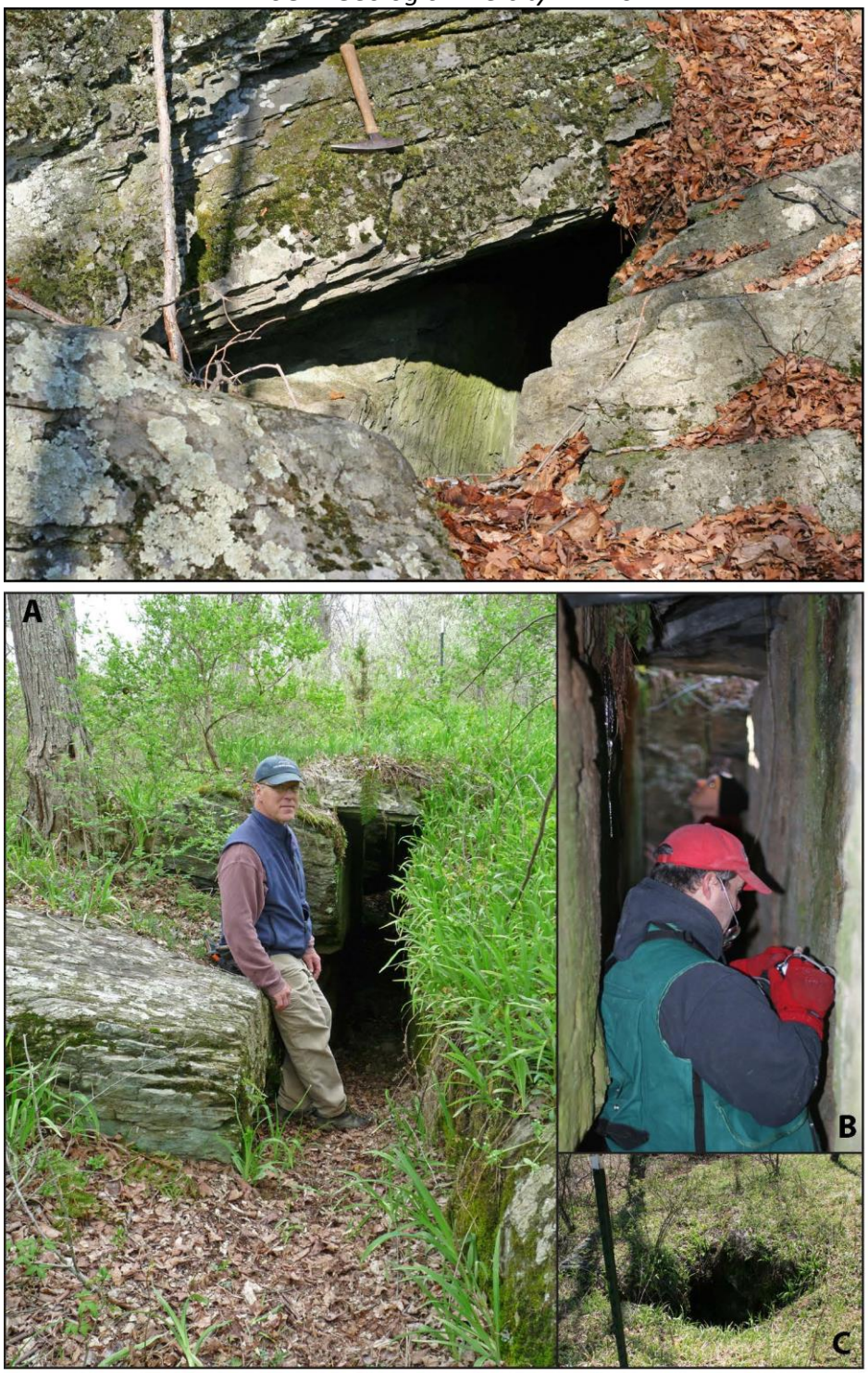

Figure 3-4. Upper photo. Small fracture cave located on the southwest side of the Bevans rock shelter. Bedding (010˚ 18˚ NW) dips right to left. The cave is about 12 feet (3.7 m) in length and follows a nearly vertical joint that trends 019˚. Lower photo. Fracture cave located on the northeast side of the Bevans rock shelter. Follows 017˚ joint. (A) Cave entrance, bedding dips left to right into hillside. B. Don Monteverde and Ron Pristas (NJGWS) collecting joint data during a much colder time of the year. Cave length is 27 feet (8.2 m). C. Small sinkhole (about 4 feet (1.2 m) in diameter) that formed over the far end of the cave where a cross joint (098˚) cuts the cave's walls. Photos by R. Witte and photo A by Jon Inners.

Figure 3-5. Small cave along the back wall of the rock shelter. Joint blocks, cut by 019° (parallel to shelter wall) and 096° (cross joint into the cave) joints, have collapsed forming the shelter within a shelter. Photo by R. Witte.

Figure 3-6. Bevans Rock Shelter (looking west), c. early 1930's. Photo from New Jersey State Museum.

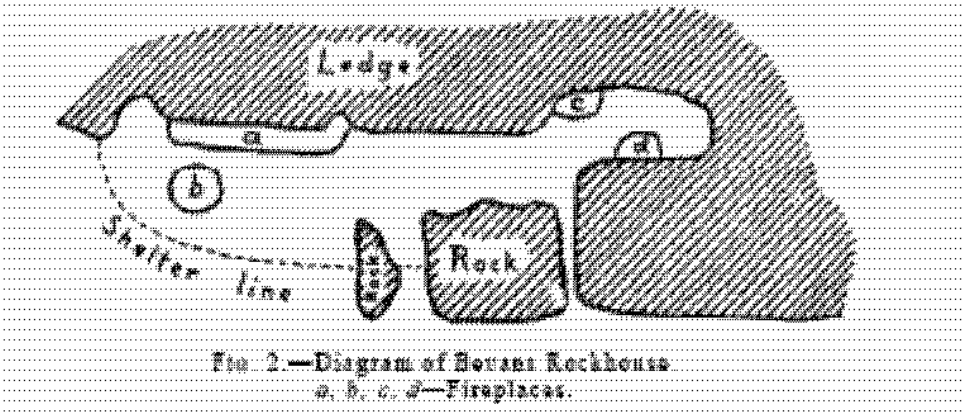

Figure 3-7. Diagram of Bevans rock shelter with location of fireplaces from Schrabisch, 1915.

Figure 3-8. Tools and pointed projectiles from the New Jersey State Museum Collection; Max Schrabisch Excavation, 1912 - 1913.

Figure 3-9. Rope-designed pottery fragments from the New Jersey State Museum Collection; Max Schrabisch Excavation, 1911 - 1912.

Figure 3-10. Dorothy Cross, October 21, 1931 at the Bevans rock shelter. Photo from New Jersey State Museum.

Directions to STOP 4 – Turn right on Kuhn Road (east) toward Peters Valley.

Cumulative in miles (km)	Point to Point in miles (km)	Route Description
19.0 (30.6)	0.7 (1.1)	Turn left onto County Route 615 North (Bevans Road) toward Layton. Intersection is just pass Gallery and Wallpack Road on left.
21.0 (33.8)	2.0 (3.2)	Village of Layton.
21.3 (34.3)	0.3 (0.5)	Turn left onto County Route 645 North toward Hainesville.
24.1 (38.8)	2.8 (4.5)	Village of Hainesville.
25.1 (40.4)	1.0 (1.6)	Turn left onto U.S. Route 206 West.
26.9 (43.3)	1.8 (2.9)	Turn right onto County Route 653 North (Clove Road).
29.4 (47.3)	2.5 (4.0)	Turn right into Montague Mini Mall and arrive at Stop 4. Stop 4 is behind self-storage facility behind the Sussex Bank, stay to right when entering mini mall."

STOP 4: Montague Mini Mall, Montague, NJ

Location Coordinates: (41.313°N, 74.756°W)

Field Stop leader – Don Monteverde.

Location and logistics

Stop 4 is located in the Milford quadrangle along Clove Road behind the Montague Mini Mall (fig. 4-1). An exposure of the Coeymans Limestone was uncovered during quadrangle-scale mapping around 1990. A short discussion will precede a good look at this unique exposure. Please do not use your hammers at this site. We wish to protect the outcrop from further degradation so others can also enjoy this interesting outcrop.

Fractures and Weathering

This outcrop was originally excavated in the 1980's during the construction of a self-storage facility. Since its initial exposure, the outcrop has been weathering fairly rapidly. Both regional strike and cross strike joints were originally evident across these fossil-rich carbonate beds. The strike joints, probably through dissolution and freeze thaw have forced large carbonate joint blocks to break away. Some, I am sure have been picked up for ornamental rocks in personal gardens. Only a single strike joint is visible on the back of the outcrop in the trees. However, a nice cross joint which exposes several thick calcite-filled veins lies near the southern part of this rock body (figure 4-2). The calcite veins appeared to have dissolved faster than the surrounding bedrock which enhanced the formation of large loose blocks.

Even though the fractures here tie in with the main theme of this trip, they were just used as bait to allow us to include this field stop. So read on through the following explanation and enjoy an unusual carbonate outcrop in northwestern New Jersey.

Regional Geology

Rocks of Middle Silurian through Lower Devonian age trend northeast-southwest across northwestern New Jersey (figure 4-2). To the east, gentle, upright folds occur in the Middle to Upper Silurian

Shawangunk Formation and Upper Silurian Bloomsburg Red Bed. Moving up section and still eastward of our present location, lies the Upper Silurian through Lower Devonian Poxono Island Formation, Bossardville Limestone, Decker and Rondout Formations and Manlius Limestone. All are locally covered by surficial deposits. The Lower Devonian Coeymans Formation, the lower part of the Helderberg Group, is exposed in front of us. Continuing westward and sparsely exposed lies the rest of the Helderberg Group including from oldest to youngest, the Kalkberg Limestone, New Scotland and Alsen Formations and Port Ewen Shale. As one migrates still farther westward towards the Delaware River the successively younger northwest-dipping units consist of the Glenerie Formation of the Oriskany Group, Esopus (seen at stop 3) and Schoharie Formations, the Onondaga Limestone (seen at stops 1 and 2) and lastly the Marcellus Shale. Regional investigations suggest that the Bloomsburg is the youngest folded unit while the remaining younger unfolded units dip gently northwestward (Monteverde, 1992, Monteverde and Epstein, unpublished data, Drake and others, 1996). Folds in these units reappear immediately south of Wallpack Center (Monteverde, 1992) and to the north across the New York state line into Port Jervis.

Silurian and Early Devonian sediments record the paleoenvironmental change from the end of the Taconic Orogeny into the oncoming Acadian Orogeny. Workers have mapped the changing continental sediments of the Shawangunk into the marginal marine sediments of the Bloomsburg Red Beds (Epstein and Epstein, 1969, 1972). The Bloomsburg displays different sedimentary assemblages indicative of fluvial, estuarine, lagoonal, tidal flat and offshore bar and beach paleoenvironments. These rocks continue to grade upwards into the Poxono Island and Bossardville that mark the continuing transgression through a brackish supratidal and intertidal flats depositional environment into a carbonate depositional environment (Epstein and others, 1967; Barnett, 1970, Epstein, 1986). The overlying Decker Formation witnessed a developed carbonate shelf with minor clastic sediment influx as well as locally developed biostromal reef complexes consisting of possible corals $\pm$ stromatoporoids(?). Time progressed and the sediments of the Rondout mark a relative sea level fall into restricted lagoonal and tidal flat paleoenvironments (Herpers, 1951; Epstein and others, 1967; Epstein and Epstein, 1969). Denkler and Harris (1988) used conodonts from the Rondout to identify the Silurian to Devonian boundary.

Sediments of the overlying lower part of the Helderberg Group record a deepening and corresponding marine transgression. The Manlius Limestone suggests changes from lagoonal and intertidal environments to the high-energy conditions of a carbonate shelf/ shoal and associated patch reefs of the Coeymans Formation (Epstein and others, 1967; Barnett, 1970; Smosna, 1989). Succeeding deeper shelf settings are observed in the Kalkberg sediments and into the argillaceous limestones of the New Scotland Formation (figure 4-3). In this region the overlying Alsen Formation records a minor regression and redeposition of fossiliferous cherty limestone. The same regression is marked in eastern New York by crinoidal grainstones of the Becraft Limestone. Sea level returned to subtidal conditions as shown by the Port Ewen Shale sediments (Barnett, 1970), which marked the end of the Helderberg Group deposition.

Epstein and others (1967) subdivided the different Helderberg formations into members from eastern Pennsylvania to southern New York (figure 4-4). The different members highlight the regionally shifting paleoenvironment along this carbonate margin. Because the descriptive terminology of carbonate units differs from clastic units, one not actively working in these units may become confused with respect to their meaning. Therefore, figure 4-5 outlines the terminology originally devised by Dunham, (1962), and subsequently modified by Embry and Klovan, (1971) so a non-carbonate geologist can understand the meaning of the discussion.

The Shawnee Island Member of the Coeymans Formation is the sole unit exposed at this stop. In the woods to the east the older Thacher Member of the Manlius Limestone is exposed. he overlying Kalkberg

and New Scotland locally emerge from the Pleistocene cover to allow their mapping along strike to the northwest and southwest.

Patch Reefs and Flank Paleoenvironments

Along its outcrop belt from eastern Pennsylvania through western New Jersey, eastern New York and westward into central New York, the Coeymans Formation contains at least 14 isolated reef deposits (Oliver, 1960; Rickard, 1962; Epstein and others, 1967; Isaacson and Curran, 1981; Precht, 1982, 1984, 1989; Smosna, 1989). Nine-reefs have been documented in the Deansboro Member of the Coeymans Formation in the Syracuse, New York region and the remaining are in the Shawnee Island Member in northeastern Pennsylvania and northwestern New Jersey (figure 4-6). Each Shawnee Island build up is a patch reef with a central core ranging up to 160x70 m and 15 m thick, accompanied by associated flank beds (figure 4-7) (Epstein and others, 1967; Precht, 1982, 1984, 1989; Finks and Raffoni, 1989; Raffoni and Finks, 1989).

Flank Beds

Reef flank facies consist of bedded bioclastic reef debris that thin away from the reef proper (James and Bourque, 1992) (fig. 4-7). Wilson (1975) differentiates two separate facies, that of flank beds and talus. Bioclastic debris is the exclusive sediment of flank beds, while talus also contains lithoclastic material. Lithoclastic material consists of partially lithified micritic material ripped up from underlying beds. Talus facies deposits are rare compared to flank bed facies (Wilson, 1975). Tucker and Wright (1990) suggest that these flank deposits only form near wave base and are therefore grainstone dominated. High energy waves and currents washed over these skeletal debris deposits and removed all micritic material (Smosna, 1989).

Reef flanks, as seen here, contain a high content of reef debris. This material lies broken and fragmented without any accompanying micritic or lithoclastic material. Fragmental hemispherical *Favosites* and crinoids constitute the greatest percentage of debris (fig. 4-7). Scarce stromatoporoids are also exposed. Rare brachiopods are present, though I have yet to find any good examples. Crinoids, although not typically part of a reef complex, are exposed here as broken fragments that commonly weather in relief. The character of the limestone beds indicates a reef flank paleoenvironment. The absence of micritic material and lithoclasts suggests an environment above wave base, in strong currents, but not reef proximal enough to be considered talus. The corresponding reef could be south of this exposure as indicated by this outcrops apparent coarser grain size in that direction. Finks (oral communication, 2001) suggested that this site is proximal to a patch reef, currently not exposed.

Relative abundance of the different bioclastic material varies over the outcrop. Corals exist across the outcrop, but they dominate in the southern beds. Crinoids occur as dispersed debris and also concentrated as bed load. They are moderately sorted in the absence of coralline material. Stromatoporoids, distantly related to modern sponges are less common across the exposure.

Grain size is variable across the exposure with a general north-south trend across the central beds. A rudstone texture from fragmented hemispherical corals appears more common in the south. Across the outcrop towards the north a general grainstone texture developed from smaller coralline debris exits. The oldest beds remain as a wackestone to packstone across the outcrop that changes through younger beds as fragmental crinoid lenses that grade into a bioclastic rudstone. Having trouble following this discussion without a figure showing outcrop geometry

Local Reefs

One of the Shawnee Island reef examples occurs in Montague Township only 1.5 miles (2.4 km) south-southeast of this stop. First documented by Epstein and others (1967), it has subsequently been studied by Precht (1982, 1984, 1989), Finks and Raffoni (1989) and Raffoni and Finks (1989). Precht (1989) described four zones that follow the successive reef growth stages of stabilization, colonization, diversification and domination (figure 4-8) as described by James and Bourque (1992). The four growth stages of Precht (1989) are:

1. Deposition of massive bedded crinoidal packstones to grainstones that stabilized the substrate.
2. Large domal and branching forms of the tabulate coral Favosites colonize the substrate, initiating reef formation.
3. Development and diversification of reef core where bafflestones, floatstones, and framestones predominate. Reef growth includes branching tabulate corals, (Cladopora and Favosites), domal and planar tabulate corals (Favosites), rugose corals, and domal and laminar stromatoporoids.
4. Massive stromatoporoids overgrown by laminar and encrusting stromatoporoids and encrusting algae predominate and develop into bindstones and framestones under shallow water conditions. Diversity of tabulate corals and stromatoporoids diminishes drastically as compared to lower stages.

James and Wood (2010) suggested that tabular stromatoporoids locally bound with other material have been found in rough-waters, but as they commonly do not have an encrusting habit, they would not fare well in the surf zone (figure 4-9). Hydrodynamics of the different stromatoporoid forms control where they would have the best chance to flourish. Those with low profiles would have the best chance to grow under high turbulent waters while encrusting forms are more common in reef margin environments (Cole and others, 2015). Forms that developed below wave base included bulbous, domal and dendroid forms (James and Wood, 2010).

Finks and Raffoni (1989) and Precht (1989) suggested that deeper, more open water existed north of the Montaque reef. The reefs formed and prograded across gently northward-sloping sea floors in 33-66 feet (10-20 m) water depth (Smosna, 1989; Precht, 1989) (figure 4-11). Reefs built up to sea level and higher energy flow conditions (Epstein and others 1969; Finks and Raffoni, 1989; Precht, 1989).

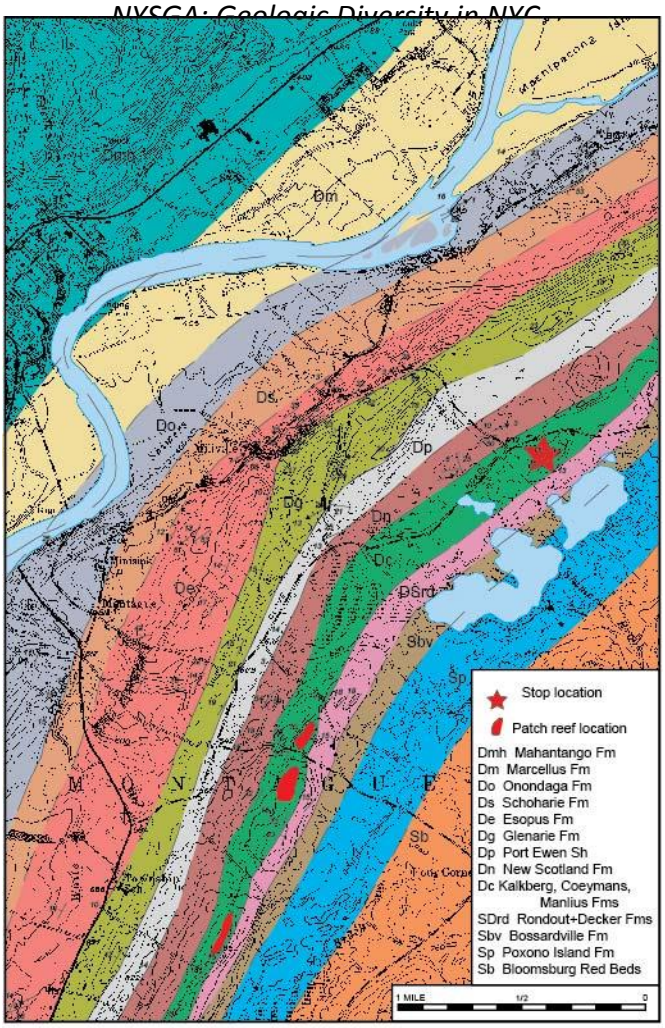

Figure 4-1. Location map of Stop 4 within the Milford PA-NJ quadrangle along Clove Road in Montague, New Jersey. Star marks the actual stop location. Geological map displays Lower Devonian to Upper Silurian sedimentary units by Monteverde and Epstein, unpublished. Southeast of the stop location are several patch reefs within the Shawnee Island Member of the Coeymans Formation identified by Epstein and others (1967), Spinks (1967) and Finks and Raffoni (1989).

Figure 4-2. Photograph looking north at a cross joint surface within the Coeymans Fm limestone that exposes two different solution gaps identified by arrows created by dissolution of calcite-filled discontinuous veins. Third arrow locates a calcite vein that slowly dissolving. Dashed line identify bedding trend. Pencil and geologic compass for scale.

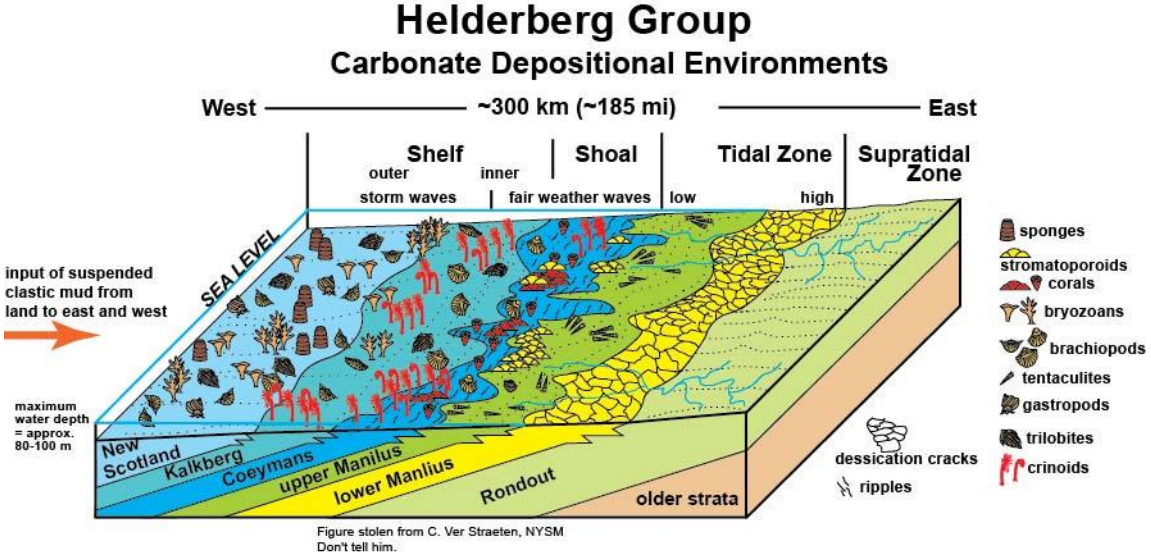

Figure 4-3. Diagram depicting the deepening marine paleoenvironments through the Helderberg Group formations. Associated fossil types for each water depth are also shown. Graphic from Ver Strataen.

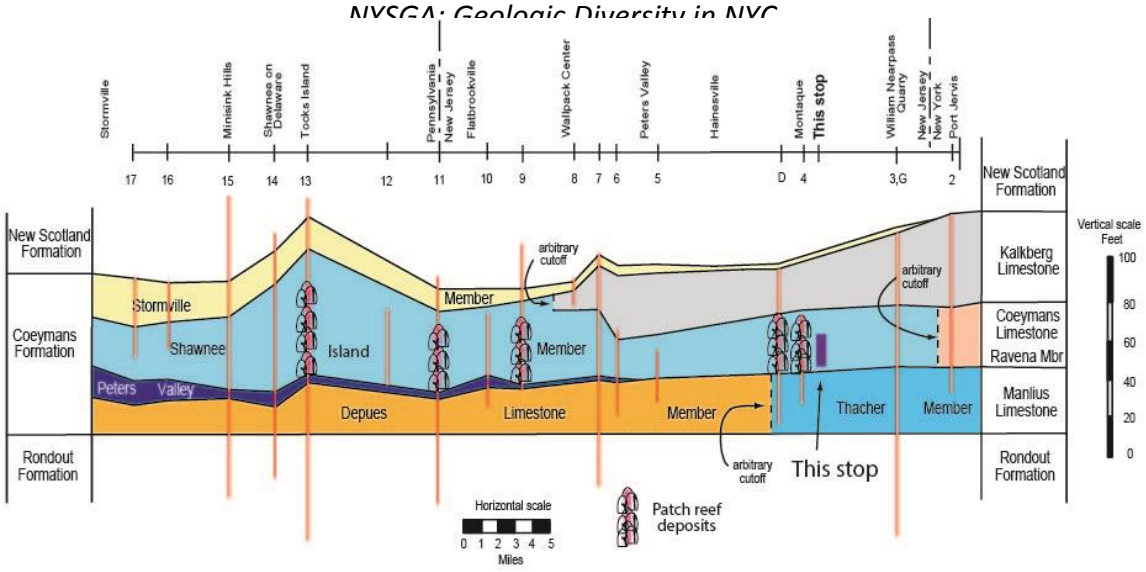

Figure 4-4. Fence diagram portraying the relationship of different members of the Coeymans Formation from eastern Pennsylvania through western New Jersey and into New York. Four patch reefs are identified in the Shawnee Island Member. Numbered measured sections are from Epstein and others (1967) and lettered sections from Spinks (1967).

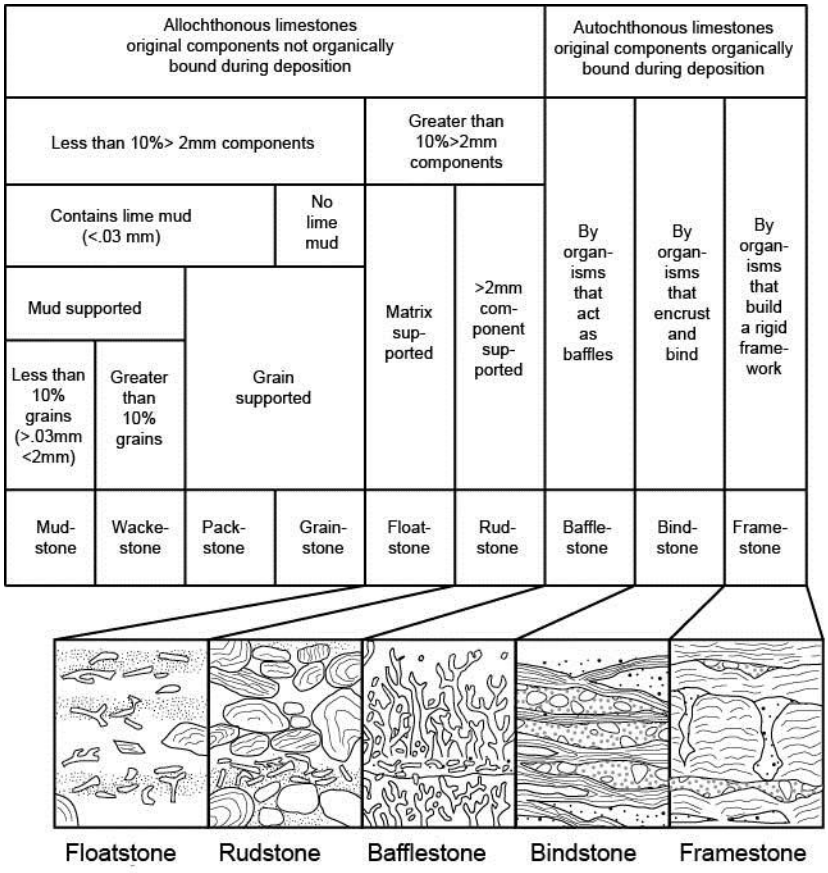

Figure 4-5. Carbonate classification as devised by Dunham (1962) and later modified by Embry and Klovan (1971). It should be noted that bafflestone, bindstone and framestone are commonly applied to reef facies while floatstone and rudstone are more indicative of flank deposits.

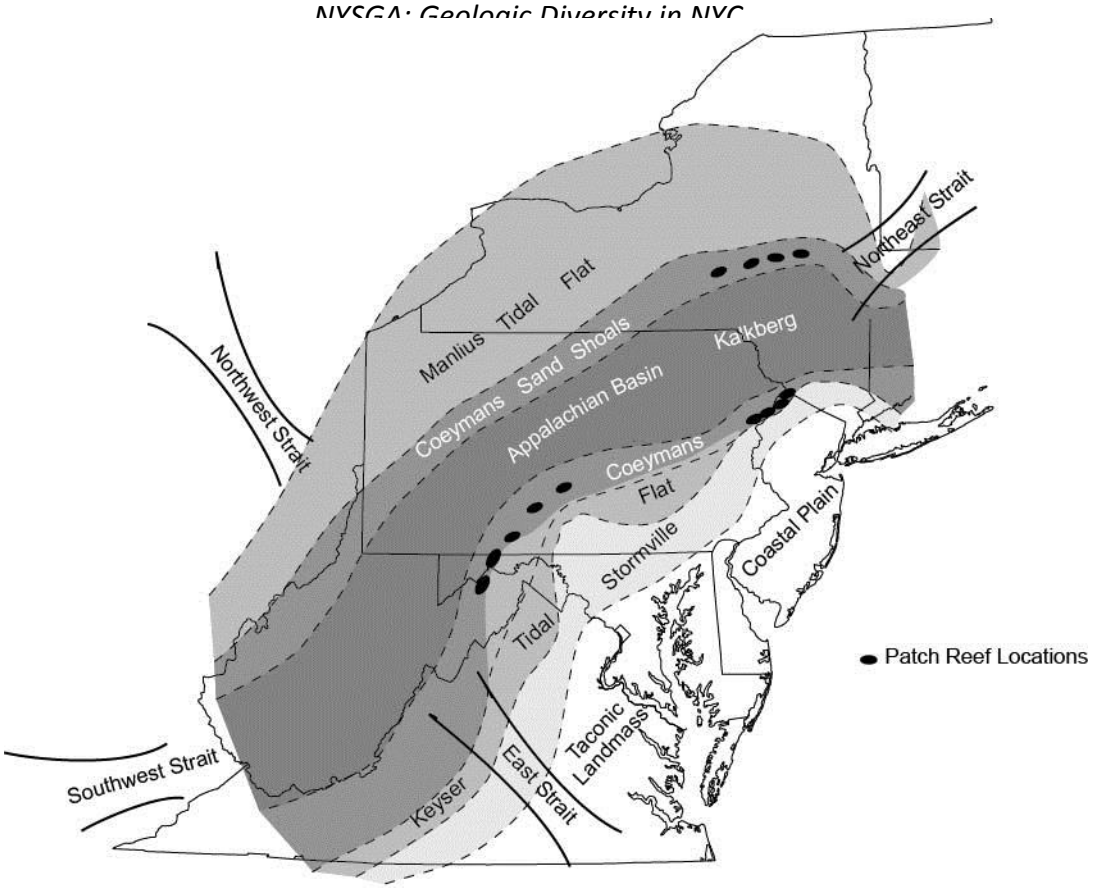

Figure 4-6. Regional map of known reef facies within the Coeymans Formation across central Appalachians Modified from Precht (1989) and Smosna (1989).

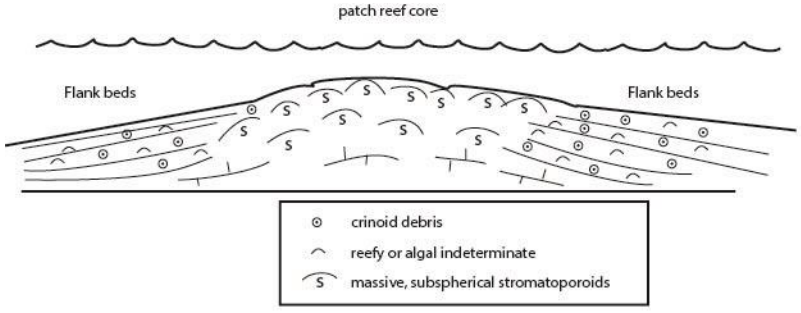

Figure 4-7. Devonian stromatoporoid patch reef portraying flank beds containing crinoidal debris. As reefs prograde both horizontally and vertically towards sea level they may grow additional cores and flank beds. Windward and leeward sides have been identified at the Montague reef (Finks and Raffoni, 1989). Shapes tend to be elongate and trend parallel to depth contours. Modified from Wilson (1975).

STRUCTURE	STAGE		LIMESTONE	DIVERSITY	SHAPE
REEF	Climax	Domination	Bindstone Framestone	Low	Laminate Encrusting
		Diversification	Framestone Bindstone	High	Domal Massive Lamellar Branching Encrusting
MOUND	Pioneer	Colonization	Bafflestone Floatstone	Low	Branching Lamellar
		Stabilizatiion	Grainstone Rudstone	Low	Skeletal Debris

Figure 4-8. Description of the different growth stages of reefs. Precht (1989) established a similar growth pattern for the nearby Montague patch reef. Modified from James and Bourgue (1992)

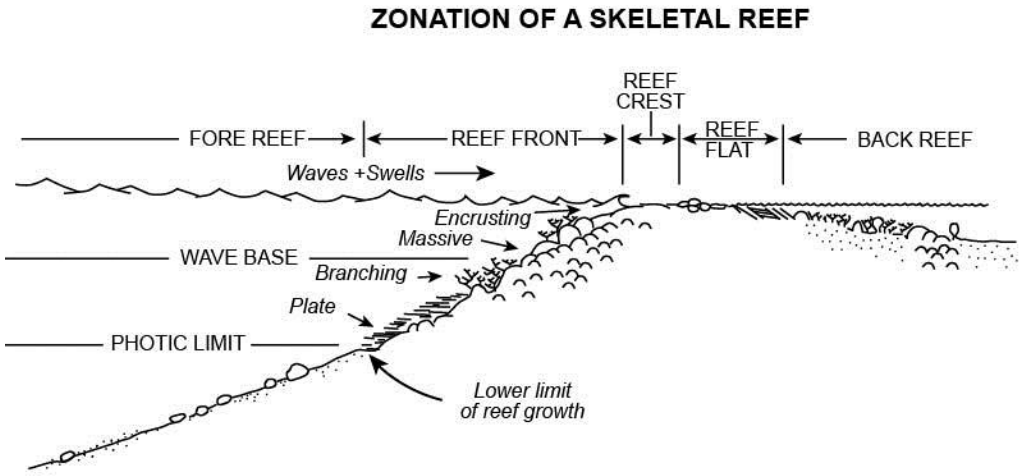

Figure 4-9. Generalized architecture of a Lower Devonian reef containing stromatoporoids. Modified from James and Wood (2010).

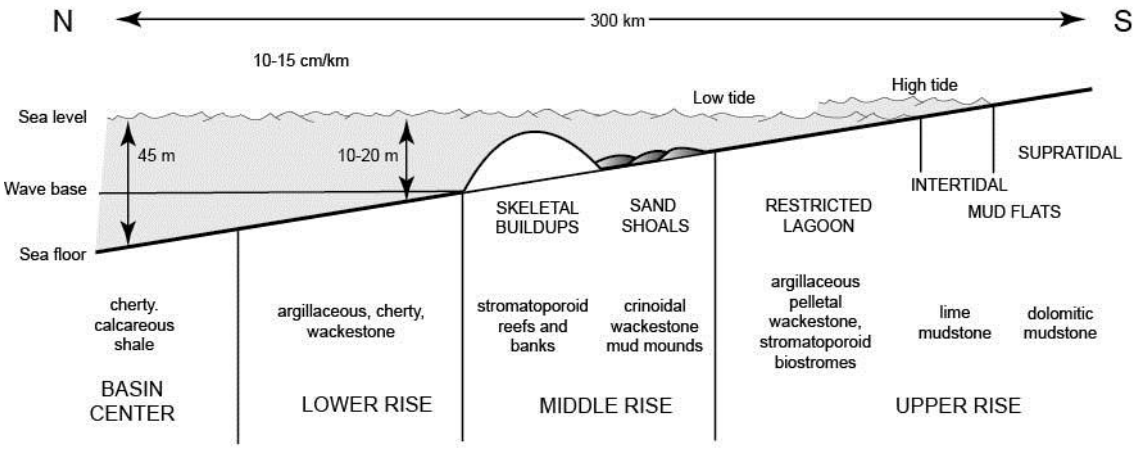

Figure 4-10. Paleoenvironmental ramp reconstruction of Lower Devonian Coeymans deposition on the southeastern side of the margin. Similar geometries existed in the Syracuse region except the geographic directions were reversed. Modified from Smosna (1989)

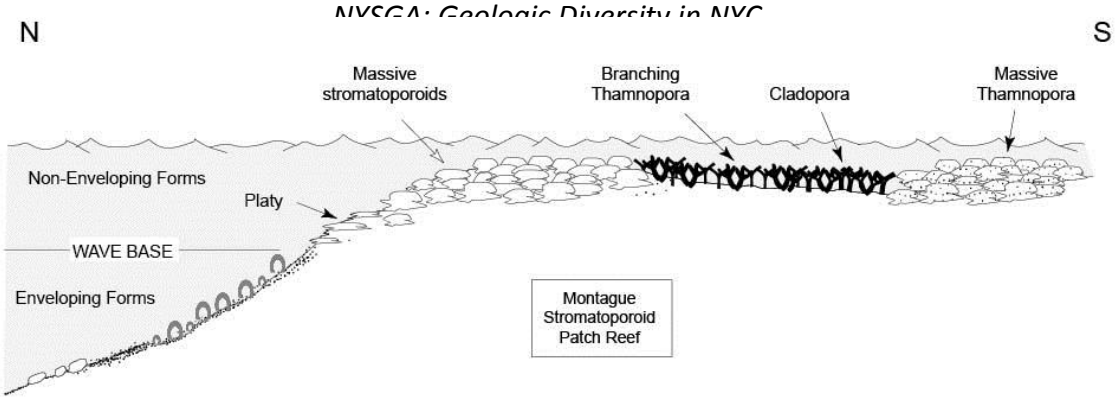

Figure 4-11. Construction of a Lower Devonian stromatoporoid reef (James and Bourque, 1992) altered to account for the different coral densities across the Montague reef as defined by Finks and Raffoni (1989).

REFERENCES CITED

Barnett, S.G.,III, 1970, Upper Cayugan and Helderbergian stratigraphy of southeastern New York and northern New Jersey: Geological Society of America Bulletin, v.81, p. 2375 2402.

Bathgate, W. R., 1916, www.njherald.com/article/20160110/ARTICLE/301109973#

Cole, S.R., Haynes, J.T., Lucas, P.C., and Lambert, R.A., 2015, Faunal and sedimentological analysis of a latest Silurian stromatoporoid biostrome from the central Appalachian Basin, Facies, 61:12.

Cross, Dorothy, 1948, The Bevan's Rock Shelters, Bulletin of The Archaeological Society of New Jersey, No. 1, 1948, J. Alden Editor.

Denkler, K.E. and Harris, A.G., 1988, Conodont-based determination of the Silurian-Devonian boundary in the Valley and Ridge Province, Northern and Central Appalachians, US Geological Survey, Bulletin 1837, p. B1-B16.

Drake, A. A., Jr., Volkert. R. A., Monteverde, D. H., Herman, G. C., Houghton, H. H., Parker, R. A., and Dalton, R. F., 1996, Bedrock geologic map of northern New Jersey: U.S. Geological Survey Misc. Geol. Inv. Map I-2540-A, scale 1:100,000.

Dunham, R.J., 1962, Classification of carbonate rocks according to depositional texture, in, Ham, W.E., editor, Classification of carbonate rocks, American Association of Petroleum Geologists, Memoir 1, p. 108-121.

Epstein, A.G., Epstein, J.B., Spink, W.J., and Jennings, D.S., 1967, Upper Silurian and Lower Devonian stratigraphy of northern Pennsylvania and New Jersey, and southeastern most New York: U.S. Geological Survey Bulletin 1243, 74p.

Epstein, J. B., 1984, Onesquethawan stratigraphy (Lower and Middle Devonian) of northeastern Pennsylvania: U.S. Geological Survey Professional Paper 1337, 35 p.

_____, 2001, Stratigraphy in the region of the Delaware Water Gap National Recreation area, *in* Guidebook for the Sixty-sixth Annual Field Conference of Pennsylvania Geologists, (eds.), Inners, Jon D., and Fleeger, Gary M., p. 1-13.

Epstein, J.B., and Epstein, A.G., 1969, Geology of the Valley and Ridge Province between Delaware Water Gap and Lehigh Gap, Pennsylvania, field trip 1 B, in Subitzky, Seymour, ed., Geology of selected areas in New Jersey and eastern Pennsylvania and guidebook to excursions: New Brunswick, New Jersey, Rutgers University Press, p.132 205.

_____, 1972, The Shawangunk Formation (Upper Ordovician(?) to Middle Silurian) in eastern Pennsylvania, US Geological Survey Professional Paper 744, 45p.

Finks, R.M., and Raffoni, M.P., 1989, Ancient land surfaces in and around the Green Pond Outlier, a Devonian coral reef, and "Taconian Islands" revisited, Weiss, d., editor, New York State Geological Association 6^{1s}t Annual Meeting, p.93-120.

Herpers, H., 1951, The stratigraphy of the Rondout Limestone in New Jersey: New Jersey Geological Survey Geologic Series, Bulletin 60, p.1-13.

_____, 1952, Silurian and Devonian Stratigraphy, Field Trip B: *in* Guidebook of field trips: Eighteenth Annual Field Conference of Pennsylvania Geologists.

Inners, J. D., 1975, The stratigraphy and paleontology of the Onesquethaw Stage in Pennsylvania and adjacent states: Unpub. Ph. D. thesis, University of Massachusetts, Amherst, Mass., 666 p.

Isaacson, P.E., and Curran, H.A., 1981, Anatomy of an Early Devonian carbonate buildup, central New York, Journal of Paleontology, v. 55, p. 1225-1236.

James, N.P., and Bourque, P-A., 1992, Reefs and mounds, in, Walker, R.G., and James, N.P., editors, Facies models, response to sea level change, Geological Association of Canada, p. 323-345.

James, N.P., and Wood, R., 2010, Reefs, in, James, N.P., and Dalrymple, R.W., editors, Facies models 4, Geological Association of Canada, p. 421-448.

Monteverde, D. H., 1992, Bedrock geologic map of the New Jersey portions of the Culvers Gap and Lake Maskenozha quadrangles, Sussex County, New Jersey: New Jersey Geological Survey Geologic Map Series 92-1, scale 1:24,000.

Oliver, W. A., Jr., 1954, Stratigraphy of the Onondaga Limestone (Devonian) in central New York: Geol. Soc. America Bull., v. 65, p. 621-652.

_____, 1956, Stratigraphy of the Onondaga Limestone in eastern New York: Geol. Soc. America Bull., v. 67, p. 1441-1474.

_____., 1960, Rugose corals from reef limestones in the Lower Devonian of New York, Journal of Paleontology, v. 34, p. 59-100.

_____, 1962, The Onondaga Limestone in southeastern New York: New York State Geol. Assoc., Guidebook to field trips, 34th Ann. Mtg.: Port Jervis, N.Y., p. A2-A6.

Precht, W.F., 1982, The paleoecology and structure of the Late Silurian-Early Devonian patch reef, northwestern New Jersey, American Association of Petroleum Geologists, v. 66, p. 1173, abstract.

_____, W.F., 1984, Diagenesis of Coeymans (Lower Devonian) patch reefs, northern Appalachian Basin, American Association of Petroleum Geologists, v. 68, p. 1927, abstract.

_____, 1989, Lower Devonian reefs of the Coeymans Formation in the northern Appalachian Basin; in, Geldsetzer, H.H.J., James, N.P., Tebbutt, G.E., editors, Reefs; Canada and adjacent areas, Canadian Society of Petroleum Geologists, Memoir 13, p. 514-519,

Raffoni, M.P., and Finks, R.M., 1989, Orientation, growth-form, and species distribution in a lower Devonian coral/sponge reef, Geological Society of America, Abstracts with Programs, v.22, no. 2, p.60.

Rickard, L.V., 1962, Late Cayugan (Upper Silurian) and Helderbergian (Lower Devonian) stratigraphy in New York, New York State Museum and Science Service, Bulletin 386, 157p.

Schrabisch, Max, 1915, Indian Habitations in Sussex County New Jersey. Geological Survey of New Jersey. Bulletin 13. Union Hill: Dispatch Printing Co, 1915.

Smosna, R., 1989, Paleogeographic reconstruction of the Lower Devonian Helderberg Group in the Appalachian Basin, in, McMillan, N.J., Embry, A.F., and Glass, D.J., editors, Devonian of the World, Volume 1: Regional Syntheses, Canadian Society of Petroleum Geologists, p. 265-275.

Spink, W. J., 1967, Stratigraphy and structure of the Paleozoic rocks of northwestern New Jersey: unpublished Ph.D. dissertation, Rutgers University, 311 p., 10 pls., and 64 figs.

Stone, B. D., Stanford, S. D., and Witte, R. W., 2002, Surficial geologic map of northern New Jersey: U.S. Geological Survey Miscellaneous Investigations Map Series, scale 1: 100,000.

Tucker, M.E., and Wright, V.P., 1990, Carbonate sedimentology, Blackwell Scientific Publications, Cambridge, Massachusetts.

Vanuxem, L., 1839, Third annual report of the geological survey of the third district: New York State Geological Survey, Annual Report 3, p. 241-285.

Weller, S. B., 1903, The Paleozoic Faunas: New Jersey Geological Survey, Report on Paleontology, v. 3, 462 p.

Willard, Bradford, 1936, The Onondaga Formation in Pennsylvania: Jour. Geology, v. 44, p. 578-603.

_____, 1939, Middle and Upper Devonian, in Willard, B., Swartz, F. M., and Cleaves, A. B., The Devonian of Pennsylvania: Pennsylvania Geological Survey, 4th ser., General Geology Report 19, p. 131-253.

Wilson, J.L., 1975, Carbonate facies in geologic history, Springer-Verlag, New York, New York, 471p.

Witte, R. W., 2012, Surficial Geologic Map of a Part of the Milford Quadrangle, Sussex County, New Jersey and Pike County, Pennsylvania: New Jersey Geological Survey Open-file Map OFM 96, scale: 1 to 24,000.

TRIP B6: LATE AND POST-IGNEOUS MINERALIZATION OF THE ORANGE MOUNTAIN BASALT AND THE CO-MAGMATIC PALISADES SILL

JOHN H. PUFFER
Dept. of Earth & Environ. Sciences, Emeritus, Rutgers Univ. Newark, NJ 07102.

KARIN A. BLOCK
Dept. of Earth and Atmospheric Sciences, City College of New York, NY 10031.

CHRIS LASKOWICH
Geologist, 14 Old Rifle Camp Road, West Paterson, NJ 07424.

MICHAEL DORSEY
Geologist, Tilcon NY Inc, 162 Old Mill Rd., West Nyack, NY.

ABSTRACT

The three Orange Mountain basalt flows are typical in most respects to other occurrences of HTQ-type CAMP basalt. However, some unusual to rare mineralization and structures are associated with the flows. Unusually high quality zeolite mineralization is associated with an Orange Mountain pillowed flow while high quality prehnite is found associated with highly vesiculated subaerial structures and historically important copper mineralization is associated with metasomatism at the base of the first flow. A distinct and uniform 4 m thick black layer at the base of the first flow contains up to 35 volume percent fine grained disseminated calcite and is overlain by a 4 m thick white albite enriched micro-vesicular layer that has locally thickened into diapir shaped structures containing vesicles up to a meter across. We propose that these mineral and structure associations are the result of a complex sequence of high temperature hydrothermal activity heated by the underlying intrusion of co-magmatic Palisades diabase magma and by subsequent low temperature hydrothermal activity associated with later pulses of Palisades magma and by post igneous burial dewatering.

INTRODUCTION

Safety considerations

The field trip accompanying this chapter will include rock quarry sites. Therefore, for your protection, hard hats, steel-toe boots, long pants, and eye-goggles, must be worn while visiting these sites. Stay a safe distance away from quarry or road-cut walls where loose rock may fall, and be sure to wear goggles when trimming rock samples. Be aware that using a steel hammer as a chisel can cause steel splinters to fly off.

Geological Setting

Extrusives

The Orange Mountain Basalt together with the overlying Preakness and Hook Mountain flows are part of the Central Atlantic Magmatic Province (CAMP) that is distributed across eastern North America, northeastern South America, northwestern Africa, and southern Europe (Marzoli et al., 2011). High precision age dating (Blackburn et al., 2013) indicates that the Orange Mountain basalt extruded 201.56 Ma and defines the end of Triassic extinction at the Triassic-Jurassic boundary. Recent isotopic evidence (Merle et al., 2014) and trace element evidence (Whalen et al., 2015) indicates that the Orange Mountain Basalt originated from a subduction-enriched mantle source as originally proposed by Puffer (2003).

The trap-rock quarries of Lower and Upper New Street expose Orange Mountain basalt consisting of three flows (OMB1, OMB2, and OMB3) from the base to the top of the formation. The first flow is a 60 to 70 m thick subaerial flow, the second flow is about 40 m thick unit that near Paterson is alternately pahoehoe and pillowed. The third flow is subaerial and about 30 m thick. The three flows are locally discontinuous throughout parts their entire geographic distribution but wherever drill cores through the flows have been logged three flows have been reported. The three flows are separated by scoraceous flow tops and thin discontinuous beds of intertrappen red-bed sediment.

Intrusives

In addition to the Palisades Sill which is exposed roughly parallel to the Hudson River from Staten Island to Rockland County, the Palisades Intrusive System includes several small co-magmatic shallow sills such as the Arlington Sill, and dikes such as Laurel Hill and several larger co-magmatic intrusion located in west-central NJ such as the Byram diabase, Stockton diabase, Lambertville Sill, Belle Mountain diabase, Pennington Mountain diabase, and Baldpate Mountain diabase. The central portion of the Palisades sill is about 300 m thick and dips to the west at about 10 to 15 degrees. Puffer et al. (2009) present evidence that the lower half of the central Palisades geochemically resembles the Orange Mountain Basalt while the upper half more closely resembles the Preakness Basalt. They proposed that the Palisades intruded as a series of pulses that broke through to the surface and extruded as basalt flows. Block et al. (2015) present supporting evidence for the multiple pulse model and show that with each successive pulse additional fractionated residual melt was carried north where thick layers of iron enriched granophyre accumulated. The Haverstraw Quarry that we will visit is located near the north end of the Palisades and is, therefore, enriched in fractionated rocks.

The late igneous history of the first magma pulse of the lower Palisades contrasts with the late igneous history of late pulses. The principal difference is the development of common granophyre layers in the upper Palisades and thick pegmatoid layers in the co-magmatic Preakness basalt that are absent in the lower Palisades and co-magmatic Orange Mountain basalt (Block et ., 2015). To date no pegmatoids have been found in the Orange Mountain basalt, although we encourage all field trip participants to continue the search.

Objective

The purpose of this chapter and field trip is to examine the late and post-igneous mineralization of the Orange Mountain Basalt and co-magmatic lower Palisades Sill. In particular we will describe our recent and ongoing research activity pertaining to the precipitation of zeolites, prehnite, carbonates, and albite in the Orange Mountain Basalt. We will focus on events and processes that began immediately after the Palisades diabase sill was intruded and secondary events that began after the Orange Mountain basalt was extruded. Our presentation will, therefore, include 1. The highly localized fusion of sediments at the

igneous contacts of the Palisades sill and Orange Mountain basalt. 2. The development of historic commercial copper concentrations at the lower contact of the Orange Mountain basalt. 3. The effects of high-temperature hydrothermal activity on the Orange Mountain basalt, particularly the development of a highly unusual and highly altered "white layer" associated with volcanic diapirs that invaded the still mushy lava core and the development of a basal layer within a meter of the lower contact that has been infused with up to 35 % very fine grained calcite. 4 The effects of medium to low-temperature hydrothermal activity associated with the precipitation of coarse grained sulfates, particularly anhydrite, and glauberite, in vesicles and the alteration of pillow rinds. 5. The precipitation of a secondary population of fine grained albite near the base of the Orange Mountain basalt and 6. The effects of burial metamorphism including the recrystallization of hydrothermal mineral assemblages to form coarse grained zeolite facies minerals, calcite and prehnite.

1. SEDIMENT FUSION

In addition to the development of a thick hornfels in the Lockatong Formation below the Palisades sill and a thin hornfels at the base of the Orange Mountain basalt, there are well documented occurrences of fusion at the base of the Palisades sill and at the base of the Orange Mountain basalt. The fusion occurrences are not continuous and were presumably localized by concentrations of salts capable of fluxing the sediments within a meter or less from the Palisades intrusion and rarely the Orange Mountain extrusion.

The base of the Palisades intrusive system

Fusion products at the base of the Palisades include granitic and syenitic components of some migmatites, and a network of leucocratic trondhjemite dikes that occupy parallel cooling joints in the Jurassic diabase intrusions. Detailed field descriptions of these occurrences including precise locations of samples analyzed for Table 1 are found in Benimoff and Puffer (2000). These fusion products are exposed at several sites along the margins of Jurassic intrusions throughout the northeastern New Jersey and Staten Island, New York. Four of the most carefully studied field occurrences include:

1. Migmatites at the base of the Palisades Sill at Ross Dock, Palisades Park near the George Washington Bridge.

Flow of the diabase through Lockatong argillite has excavated a few channel-like cuts several meters across that truncate underlying Lockatong bedding planes. In addition, anticlinal dome-like structures that rise a few meters into overlying diabase have been observed. It is at these dome-like structures where most fusion has taken place.

Three clearly exposed domes occur within 2 km of Ross Dock near the George Washington Bridge where partial fusion has occurred resulting in migmatites consisting of granitic rock veined with black laminated rock. The major element compositions of the granitic rock and the surrounding dark rocks appear in Table 1. The bedding at these domed structures is disrupted and may have involved movement of volatiles derived from brackish groundwater within the lacustrine Lockatong sediments. The host rock of the migmatite is dark gray laminated meta-siltstone. The chemical composition of the meta-siltstone host rock is consistently intermediate between the black biotite enriched refractory portion of the migmatite and the granitic component (Table 1).

2. Trondhjemite dikes exposed along an I-95 road cut through the Palisades Sill, at Fort Lee, New Jersey.

A group of three parallel and vertical trondhjemite dikes are exposed within the upper 70 meters of the Palisades Sill along a major road-cut along Interstate 95 (Figure 1). Several thin calcite veins up to 12 cm thick have precipitated into joints approximately parallel to the trondhjemites. The trondhjemite dikes are near vertical and strike N 27° E parallel to a major joint set of cooling cracks in the sill. Five samples across the width of the 4.5 m thick dike were selected for chemical analysis (Table 1). Some of the calcite veins contain about 10 percent sulfides and probably precipitated out of hydrothermal vapors injected into cooling shrinkage joints in the Palisades from a Lockatong sedimentary source.

The trondhjemite dikes are leucocratic holocrystalline microphanerites composed almost exclusively of quartz and albite. The rock is porous and most of the pores are miarolitic cavities. The microtexture observed in thin section is unusual because it consists of a granophyric intergrowth of quartz and albite. Polished thin sections reveal an intergrowth of clear grains of quartz in a turbid matrix of albite; ilmenite, hematite and skeletal sphene grains are also present. Most quartz grains are in approximately parallel optical continuity. This texture is interpreted as resulting from simultaneous crystallization of quartz and albite from a eutectic melt. The total iron is very low (<1.8%) and the silica is very high (77 - 80% , 34 - 41.5% normative quartz). Na_2O (6.5-7%; 54-60% normative albite) is exceptionally high and K_2O is extremely low (0.04%). In addition, CaO and MgO are each less than 1%. The trondhjemite dikes are interpreted by Benimoff and Puffer (2000; 2005) as the fusion products of previously metasomatised Lockatong hornfels.

Figure 1. Photograph of 4.5 m thick trondhjemite dikes at I-95 roadcut through the Palisades Sill, Fort Lee, New Jersey.

3. Migmatites near the upper contact of the Stockton diabase intrusion exposed along a stream cut at Brookville, New Jersey.

Migmatite composed of pink syenite and a refractory residue composed of black biotite, chlorite, and calcite is exposed along the banks of a stream that flows along the upper contact of the early Jurassic

Stockton Diabase sill (a Palisades correlative) with the Lockatong Formation. The Stockton Diabase is approximately 500 m thick and is truncated by a southeast-dipping normal fault near the migmatite occurrence.

The syenite component of the migmatite is a holocrystalline phanerite containing 15 modal percent black euhedral amphibole prisms in a matrix of mottled pink and white feldspar. Electron microscopy reveals that the amphibole is zoned with an Mg -rich core and an Fe- rich rim. The Mg -rich core is a sodic kaersutite and the Fe rich rim is a sodic magnesium hastingsite. Around the amphibole is an extremely fine intergrowth of oligoclase surrounded by K-feldspar that shows reverse rapakivi texture.

The Lockatong meta-argillite hornfels at Brookville is composed principally of sodic plagioclase and biotite with minor but variable pyroxene, amphibole, chlorite, calcite and muscovite. Quartz is conspicuously absent. Van Houten (1965; 1971) has studied the hornfels above the sill near Brookville and describes it as "metamorphosed calcareous feldspathic argillite", a variely of detrital cycle meta-argillite. It is similar to the detrital cycle hornfels exposed under the Palisades sill at Fort Lee although it contains less pyroxene and more sodium. Olsen (1980) describes the detrital cycle hornfels as dark gray laminated meta-siltstone. Chemical analyses of this dark gray hornfels appear in Table 1.

Fusion of the hornfels produced syenite and a black biotite and chlorite refractory residue exposed within 3 meters of the Stockton sill. MgO and Fe_2O_{3T} were highly partitioned into the refractory residue reaching concentrations of 11 and 15 percent respectively (Table 1). Most other elements in the syenite and hornfels host rock maintain approximately consistent levels indicating high degrees of partial fusion.

4. Fusion at the base of the Orange Mountain basalt

Puffer et al. (1993) have presented evidence of fusion of sediment under the OMB1 flow at the discontinued Tilcon (UBC) Quarry at Paterson. They described a thin (up to 1 m) layer of sediment fluxed by salt that was melted at the base of the 70 m thick OMB1 extrusion. During fusion K_2O was strongly partitioned into residual sediment while Na_2O was partitioned into the melt phase resulting in a gray vesicular aphanitic rock composed of microphenocrysts and microlites of albite set in an optically irresolvable reddish-brown groundmass containing vesicles filled with calcite and pumpellyite. The rock is characterized by 8.0 percent Na_2O, 0.03 percent K_2O, and 73 percent normative albite. The composition of the fused sediment closely resembles the composition of a network of 0.5 to 2 m thick trondhjemite dikes that have penetrated the Palisades sill at Fort Lee, New Jersey that have also been interpreted as the product of sediment fusion (Benimoff and Puffer 2000; 2005). In the case of the Tilcon (UBC) Quarry occurrence, salt enriched Passaic siltstone containing 1.5 percent K_2O and 3.3 percent Na_2O was entrained and fused, based on analyzed samples collected 10 m below the base of OMB1. In the case of the Fort Lee occurrence Lockatong argillite containing 4.0-6.4 percent Na_2O and 3.3 to 5.2 percent K_2O (Van Houten 1965) was fused. In both cases the composition of the trondhjemitic melt plots very close to the binary eutectic of the Qtz-Ab phase diagram as described by Benimoff and Puffer (2005).

The sediment fusion layer at the base of OMB1 is absent at most lower contact exposures but is about 0.25 m thick along the east wall of the UBC quarry. Elsewhere at the UBC quarry a thin layer of travertine is exposed along the base of OMB1.

Petrologic controls on fusion

Figure 2 is a Quartz-Nepheline-Kalsilite phase diagram at 1 kilobar illustrating the petrologic control on the composition of fusion products. The composition of the trondhjemite dikes and the fusion zone at the base of the Orange Mountain basalt in particular plots almost exactly at the binary quartz-albite eutectic point. It is also true that the composition of Lockatong hornfels sampled at Graniteville, New York also plot close to the eutectic but the hornfels have undergone considerable metasomatic alteration from their previous sedimentary composition, chiefly a major decrease in virtually all potassium content. Details of these relationships are found in Benimoff and Puffer (2005).

Fusion of the hornfels at Brookville has generated a syenite that is also depicted in Fig. 2. The hornfels is compositionally intermediate between the black biotite enriched refractory residual portion of the migmatite and the igneous syenite portion. The same relationship is also seen at Ross Dock where again the hornfels is compositionally intermediate between the black biotite enriched refractory residual portion of the migmatite and the granite portion (Table 1). It is noteworthy that the composition of the Ross Dock granite plots very close to the ternary minimum of the Quartz-Albite-Orthoclase phase diagram (Table 1).

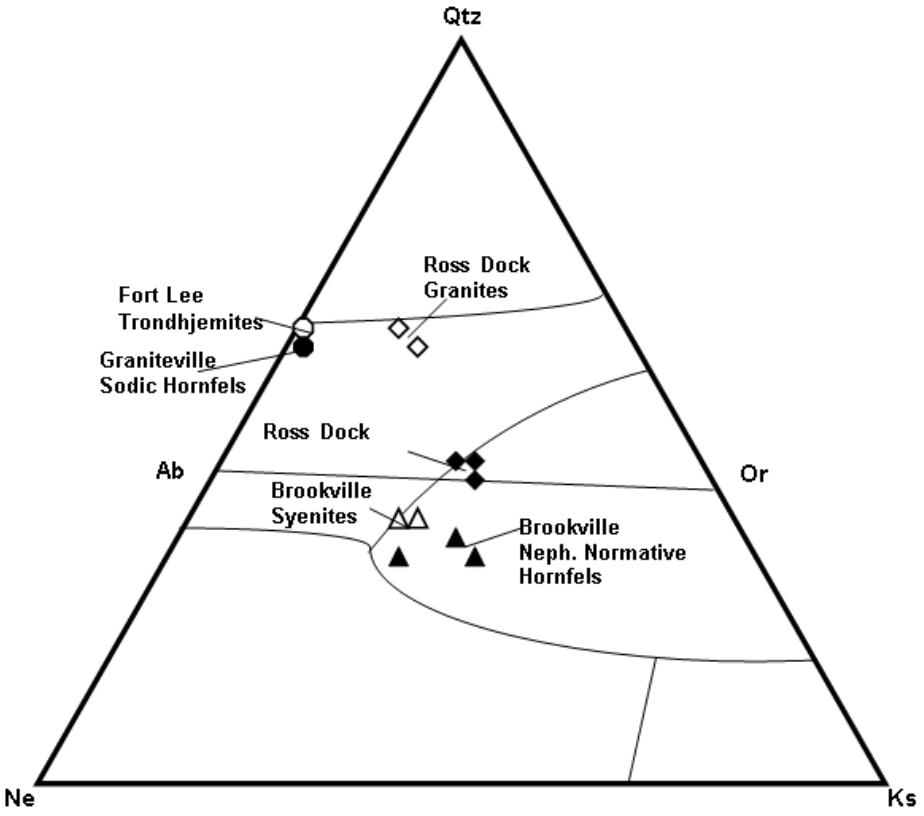

Figure 2. after Benimoff and Puffer (2005). Quartz-Nepheline-Kalsilite phase diagram at 1 kilobar with trondhjemite, granite, syenite compositions together with their respective hornfels sources. Trondhjemites from Fort Lee (open circles) plot close to the eutectic point along the Ab-Qtz boundary. Granite from the George Washington Bridge site plot close to the thermal valley of the Quartz-Albite-Orthoclase system and syenites from Brookville plot close to the Albite-Orthoclase-Nepheline-Kalsilite minimum.

Table 1. Chemical composition of trimodal fusion prodcts and their host rocks at three sites, New Jersey and New York

Location	Stockton Sill at Brookville NJ			Palisades Sill at Ross Dock			Palisades at Fort Lee
Structure	Migmatite			Migmatite			trondhjemite dikes
Rock Type	Syenite	Residue	Int-hornfels	Granite	Residue	K-hornfels	
Sample #	av. 5	B11c	B-10	G2E-L	G12D1	G2BD	av. 5
Color	pink-gray	black	dark gray	pink	black	dark gray	white
SiO_2	55.64	38.4	51.33	76.17	53.52	55.4	78.42
TiO_2	0.84	0.83	0.81	0.22	0.93	0.91	0.57
Al_2O_3	18.13	14.14	17.2	12.77	17.63	17.6	11.67
Fe_2O_{3t}	5.16	14.84	9.88	0.62	8.87	8.4	1.54
MnO	0.06	0.17	0.06	0.01	0.13	0.08	0.01
MgO	1.87	10.98	5.24	0.62	6.92	4.59	0.16
CaO	3.34	5.3	2.65	0.29	0.53	0.65	0.68
Na_2O	7.32	0.54	7.29	5.04	2.78	4.68	6.85
K_2O	4.34	5.22	4.81	3.05	7.35	5.4	0.04
P_2O_5	0.27	0.61	0.31	0.09	0.16	0.15	0.14
LOI	0.98	8.45	1.52	1.34	2.31	1.38	0.53
Total	97.95	99.48	101.1	100.22	101.13	99.24	100.61
ppm:							
Rb	97	68	63	64	99	73	7
Sr	569	239	297	392	1180	1120	39
Y				0.23	0.57	0.41	37
Zr	165	149	157	151	119	116	466

2. COPPER MINERALIZATION

The copper ores of the Newark Basin have been described by Weed (1902, 1903, 1911), Lewis (1906, 1907), Woodward (1944), Puffer (1984; 1987a; b), Robinson (1987), Robinson and Woodriff 1987), Robinson and Sears 1987), Puffer and Proctor (1992, 1994), Sclar and Moses (1995), Cattafi et al., 1998), and Puffer and Graham (2005). Genetic interpretations by these authors are wide ranging but in most (but not all) cases have addressed the close association of the copper mineralization with the Orange Mountain Basalt.

All of the 29 Mesozoic Cu mines of New Jersey described by Lewis (1906, 1907) are found along the upper or lower contact of the Orange Mountain Basalt or near thin early Jurassic dikes and sills that intrude the Passaic Formation. Copper ore is most commonly found in: 1) Passaic hornfels within 1 m below the base of the Orange Mountain Basalt; 2) Passaic hornfels within 1 m above or below thin shallow dikes and sills of Orange Mountain composition and; 3) in Orange Mountain Basalt within 2 m above the base of the first flow (Figure 3) or within 1 m below flow tops. A few very minor copper occurrences are found in unmetamorphosed red-beds of the Passaic Formation.

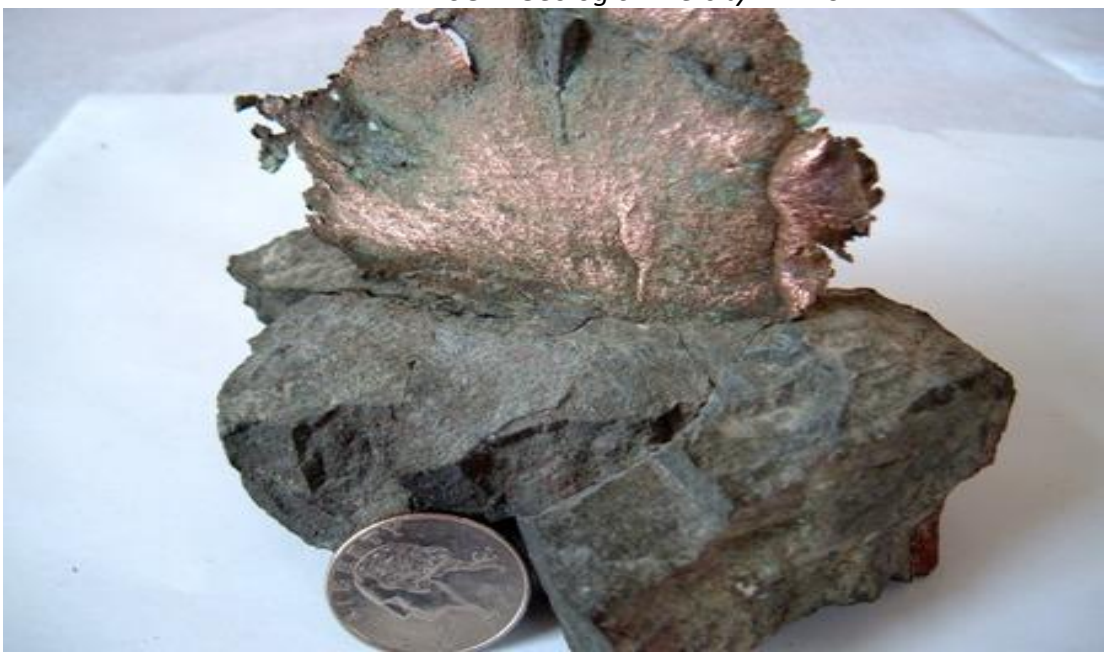

Figure 3. Sheet of native copper in basalt joint sampled at the Chimney Rock trap-rock quarry, New Jersey

Each of these mine locations have been visited by the principal author of this report (except for Glen Ridge and Newtown). In most cases there is very little that remains of the former workings except for occasional samples of discarded ore and host-rock. However, the underground workings at the Schuyler mine at North Arlington were examined on several occasions throughout 1970-1980 by the principal author and good exposures of ore and country rock are also still accessible at the mines near Somerville N.J., particularly the American Mine.

Chalcocite, native copper, and chrysocolla are found in most ore samples together with minor malachite, and cuprite. Pyrite is a common gangue mineral in samples of hornfels and trace amounts of chalcopyrite is found in most samples of massive basalt. Chrysocolla is easily observed at most mine exposures, and flakes and sheets of native copper are readily observed in high grade samples. However, observation of disseminated chalcocite and native copper typically requires microscopic observation of polished sections.

Proposed Origin - The diversity of the Mesozoic copper deposits of New Jersey make it impossible to categorize all of them into any one USGS (Cox and Singer, 1986) or Canadian Geological Survey (Eckstrand el al., 1995) genetic model. However with few minor exceptions the best fit is the USGS "Basaltic Cu" model which is approximately equivalent to the CGS "Volcanic redbed copper" model. Characteristics of "Basaltic Cu" deposits that apply to most of the Mesozoic Cu deposits of New Jersey include:

1.) Host rock is subaerial to shallow marine (brackish water) basalt and interbedded red-beds.
2.) Ore textures include precipitation in basalt amygduloids and in adjacent sediments with high original porosity.
3.) Association of ore with copper-rich basalt (90-405 ppm) and interbedded red-beds.
4.) An intercontinental rift tectonic setting.

5.) A native copper – chalcocite ore
6.) A gangue of hematite, quartz, chlorite, and zeolites.

A few New Jersey copper deposits comply in all respects to the "Basaltic Cu" model, particularly the deposits located within the amygduloidal flow-top of the Orange Mountain basalt including the Pluckamin (Hoffman) mine. In agreement with the "Basaltic Cu" model a close association of copper mineralization with subaerial basalt or comagmatic intrusives is a characteristic of all the larger deposits of New Jersey. However, copper in the mines at the base of the Orange Mountain basalt was probably precipitated in surface muds, probably boiling "mud-pots", in the solfateria that with little doubt characterized the Newark Basin immediately preceding the extrusion of the Orange Mountain basalt (Figure 4). The underlying Palisades Sill and shallow off-shoots fed these copper rich flows as it intruded beneath wet Passaic redbed sediment.

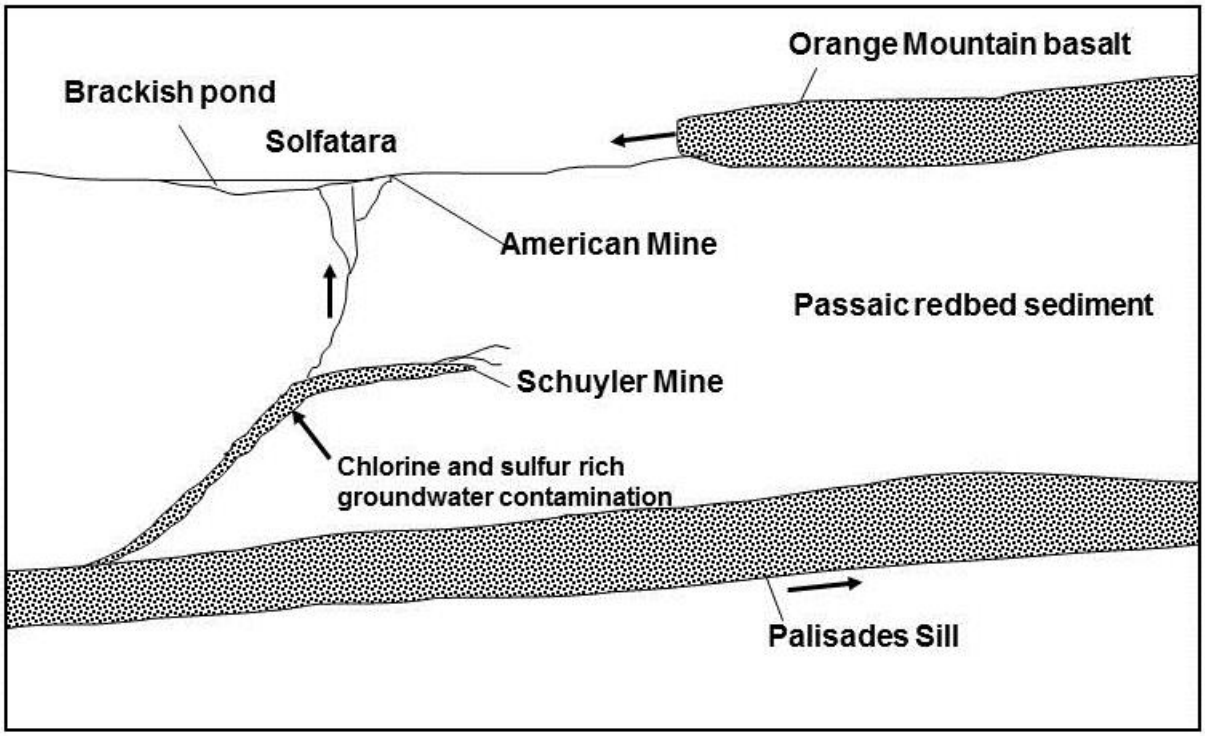

Figure 4. Idealized cross section through Passaic redbeds illustrating the leaching of copper from diabase into epithermal brines followed by movement to solfatara vents at the surface. Copper precipitation in explosion breccia occurred wherever thin diabase offshoots encountered wet sedimentary horizons as at the Schuyler Mine.

Hydrothermal water circulation through the intrusive system of diabase could have leached considerable copper during the entire cooling history of the sill as first proposed by Lewis (1906). Copper leached from the intrusive system would have been driven toward the surface as complex ions in hydrothermal solutions. Some copper was probably concentrated in the muds of solfatara or may have formed small Besshi-type hot-spring precipitates at the bottom of any water bodies. Where shallow diabase sills encountered wet muds, hot-spring-type explosion breccias would have formed, such as those of the Schuyler mine (Figure 5) together with a network of thin veins.

Figure 5. Explosion breccia sampled at the Schuyler mine consisting of diabase clasts in sandstone.

Several additional examples of Basaltic Cu deposits are listed by Cox and Singer (1986) and Eckstrand et al (1995) including the Keweenaw and Denali deposits, in the US, the Redstone, Sustut, and White River deposits in Canada and the Manto and Buena Esperanza deposits of Chile.

3. HIGH-TEMPERATURE HYDROTHERMAL ACTIVITY

3a. Development of the "white layer" and the "diapirs" of the Orange Mountain Basalt

Extrusion of the OMB1 flow onto a very active geyser field would have resulted in the injection of alkali vapors into the flow. However, deep upward penetration into or through the flow would not occur if the lava was rapidly flowing. Instead, any vapor plume encountering a rapidly advancing flow would have been dragged downstream to form a vesicular layer such as the layer we describe as the White Layer (Figs. 6 and 7a,b). An initially thick OMB1 flow may have blocked or sealed off a geyser field. However, it is likely that the full 70 m thickness of the OMB1 flow was not reached during first encounter with any such vents and reached full thickness only after subsequent inflation between the overlying vesicular lava crust and the vesicular (white) layer. This interpretation of the origin of the white layer is a departure from the less dynamic origin previously proposed by Puffer and Laskowich (2012) but best fits all the evidence.

The white layer is about 4 m thick throughout the greater Paterson area and is characterized by its white to light gray color due to albite and calcite content and its microvesicular texture. High-temperature reactions between the alkali vapors of the proto-white layer and basalt lava occurred before solidification of the OMB1 flow. The pressure of the overlying 50 m portion of the OMB1 flow kept most vesicles from expanding. However, once forward flow subsided some vesicles locally coalesced into large mega-vesicles that carried some white layer up into the still unsolidified core zone to form diapir shaped bodies (Fig. 7b) that are typically 7 m across and penetrate 4 m to 30 m above the top of the white layer.

The vesicules of the diapirs are typically 2 to 100 cm across and in many cases have collapsed to form lenses of breccia up to 4 m across. The chemical composition of the white layer is about the same as the core zone except for considerable sodium enrichment (4.5 vs 2.1 % Na_2O) and calcium depletion (6.5 vs 10.5% CaO). It is suspected that at least some of the sodium enrichment is the result of high-temperature hydrothermal reactions.

The unusually high temperatures that drove the circulation of hydrothermal activity including geysers and hot springs during the extrusion of the lower Orange Mountain flow was due to the co-magmatic intrusion of the underlying Palisades sill and associated shallow sill offshoots.

Figure 6. White layer (4 m thick) exposed near the base of OMB1 at the Prospect Park Quarry.

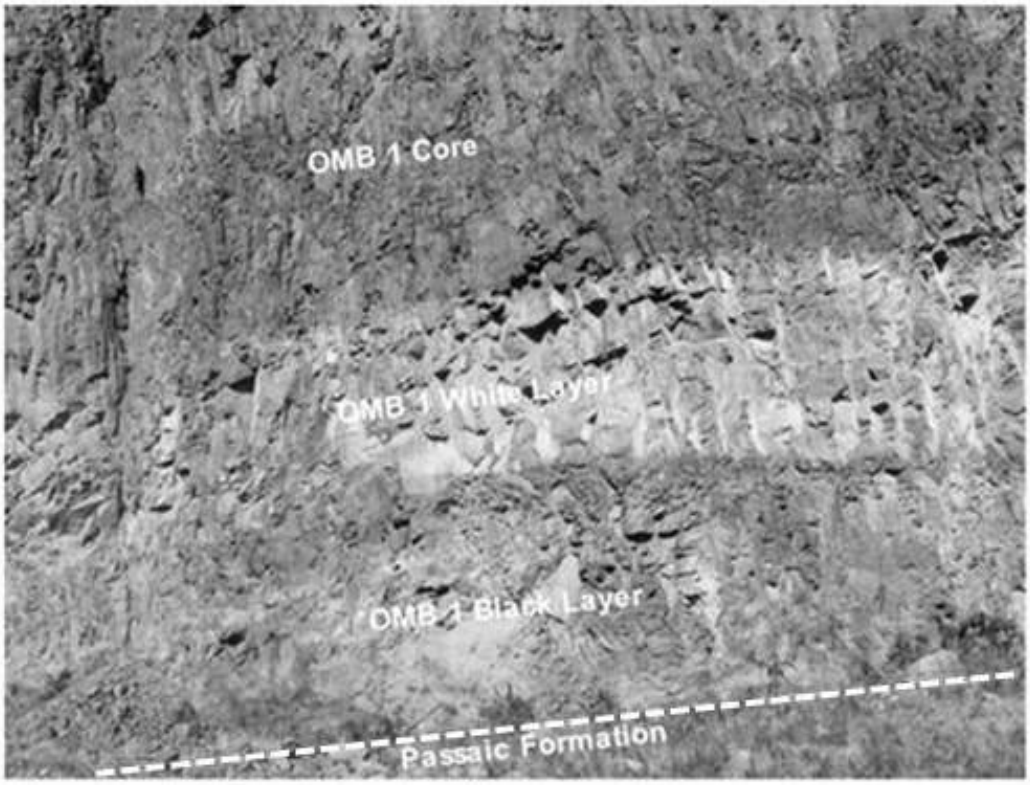

Figure 7a. Close up photograph of Black, White, and Core layers at UBC Quarry. White layer is about 4 m thick; black layer is 5 m thick.

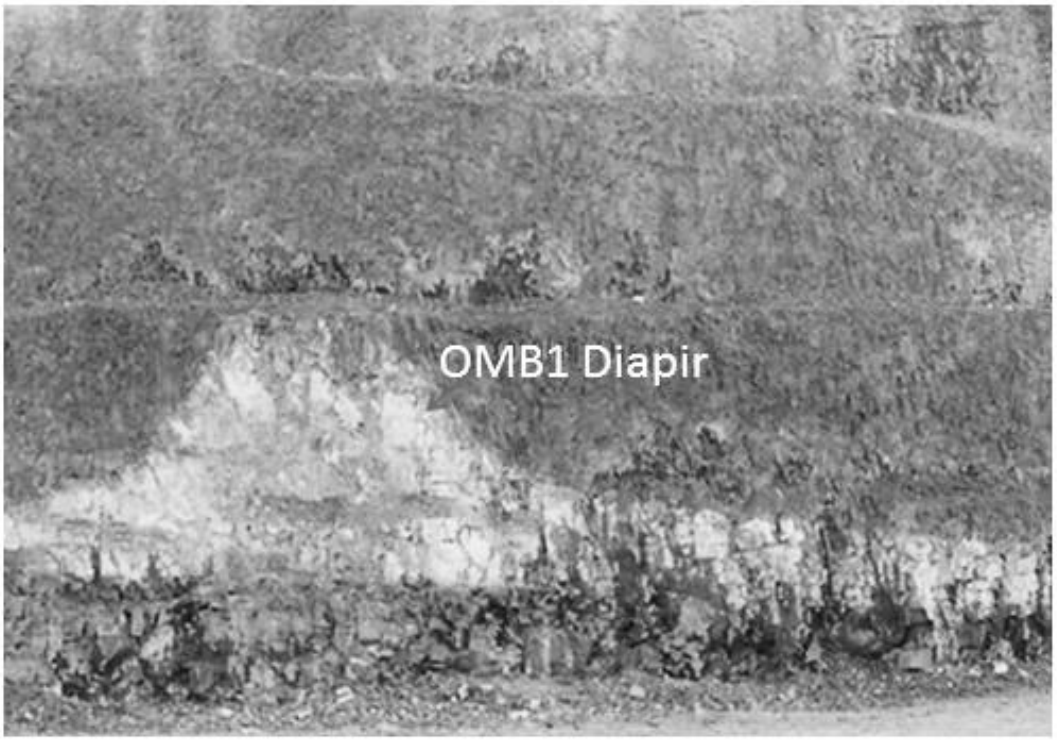

Figure 7b. Diapiric intrusion of white layer into the overlying still molten flow interior at Prospect Park Quarry.

3b. The "Black Layer" and fine grained calcite precipitation

The lowermost 3 to 5 m thick layer of the Orange Mountain basalt exposed throughout the Paterson area is characterized by its black color and absence of a vertical joint pattern. In outcrop and in hand specimen none of the layer appears to be altered. However, the lower 2/3 of the layer and the lowest 1.5 m thickness of the layer in particular is extremely altered and has been replaced by up to 35 % calcite. The calcite is very fine grained, resembling a quench phase in distinct contrast with the white veins and encrustations of coarse-grained sparry calcite found in vugs within the white layer or in vesicular flow tops. The melting point of aragonite is only 825 C and if fluxed with brine would melt at still lower temperatures. The thin layers of banded yellow travertine that are commonly found at the base of several Paterson area exposures of Orange Mountain basalt, however, do not appear to have melted.

Steinen et al. (1987) describe hot springs that penetrated through the entire thickness of the Talcott basalt (a co-magmatic correlative of the Orange Mountain found in Connecticut) and locally resulted in total replacement of basalt with carbonates. Therefore, it is more likely that superheated vapors supersaturated with carbonates at the base of the flow diffused into the lava flow as described by Steinen et al. (1987).

4. MEDIUM TO LOW-TEMPERATURE HYDROTHERMAL ACTIVITY

As the superheated vapor that formed under and within the basalt flow began to cool a variety of medium to low-temperature hydrothermal reactions occurred.

4a. Clay-palagonite alteration

Berger et al (1987) has shown experimentally that not much happens to basalt lava when it reacts with seawater except for some clay alteration of thin glass rinds. Mg, Al, Fe, and K increase in the glass while Si, Ca, Na decrease in the glass. None of these alteration effects have occurred in the White Layer or in the pillow basalts of OMB2. In addition, Rosenbauer et al (1983) have shown that reaction of Na-Cl solutions or seawater with basalt does not produce spilitic alteration. However, Bischoff and Seyfried (1978) have experimentally shown that more sustained exposure to warm seawater (or presumably basin brine) at 70 C^o at 1 bar results in an increase of Mg, Na, and K in the basalt and loss of Ca and Si to solution, similar to what has occurred in the basalt of the White Layer and in the pillow basalts of OMB2.

4b. Anhydrite-Glauberite precipitation

Another result of the initial cooling of basin brine contained within the white layer is the precipitation of abundant anhydrite in vesicles. Hajash and Chandler (1981) have experimentally reacted seawater with basalt in a 200 to 500 C^o range at pressures up to 1000 bars and found that anhydrite precipitates at high temperatures in response to decreased pressures. Bischoff and Dickson (1975) experimentally examined basalt-seawater reactions at 200 C and found that originally slightly basic solutions of seawater become acid as Ca and SO_2 are diminished during anhydrite precipitation and that K^+ is quickly leached into the aqueous phase. They found that the composition of the resulting acid solution is similar to those of the Icelandic geothermal fields. This is also the stage in the sequence when most SO_2 and then finally HCl emissions would have occurred.

5. FINE GRAINED ALBITE PRECIPITATION

Albitization of basalt is difficult to accomplish using seawater or Na-Cl solutions, generally producing insignificant amounts of albite compared to natural spilites (Rosenbauer et al 1988) or the albitized basalt of the White Layer and pillow basalts. However, increased confining pressures under overlying volcanic flows and accumulating sediments eventually reached the special environmental and geochemical conditions proposed by Rosenbauer et al., (1988) as most conducive to the albitization of basalt. They have experimentally demonstrated that albitization of basalt is maximized at pressures of 400 bars, 350 C, 3.4 m NaCl, excess silica, an absence of strong acidity and therefore minimal dissolved Mg. The porous and permeable portions of OMB1 were presumably saturated with basin brine during burial and the base of the OMB1 flow was also presumably subjected to the flow of heated brine. Reaction with silicate wall rock would eventually neutralize the brine and saturate it with silica. Reoccurring volcanism and intrusive activity associated with the extrusion of the Hook Mt Basalt could have generated temperatures of about 350 C. Reaction of basalt with deep circulation of neutral Mg-depleted basin-brine in this environment would result in sodium metasomatism (spilitization or albitization) that is a characteristic of the white layer and the pillow basalts of the OMB2 flow. Re-precipitation of Ca released by Na substitution in plagioclase resulted in the abundant calcite found in the vesicles and breccia of the white layer and in the interstices of the pillow basalt of OMB2. Similar calcite found in the vesicles of a basalt pillow from the co-magmatic Talcott Formation has been described by Greenberger et al., (2015) together with considerable albitization.

6. BURIAL METAMORPHIC ACTIVITY / POST IGNEOUS HEATING EVENT

Alt et al. (1986) described hydrothermal alteration throughout a 1 km section of MORB. They described zeolites, coarse grained calcite, and prehnite precipitating in sheeted dikes at 100-250 C at a depth of 1075.5 m. As burial sequentially loaded the Palisades sill, the OMB, the Preakness, and the Hook Mountain basalts zeolites and prehnite were progressively precipitated. The fact that zeolites and prehnite are common among the Hook Mountain basalt indicates that at least 1000 m of sediment must have been deposited over them. Stratigraphic evidence (Olsen et al., 1996) indicates that 3000 m of sediment was indeed deposited over the Hook Mt basalts.

Most of the zeolite and prehnite mineralization did not require metasomatism; instead the authigenic minerals including clays were simply recrystallized isochemically. Where excess calcium was present, as in the case of the white layer and diapirs, abundant prehnite precipitated. Where excess sodium was present, as in the case of the pillow basalts of OMB2, abundant zeolites precipitated. Abundant calcite precipitated wherever the porosity of the basalt permitted transmission of CO_2. A similar study of zeolite and prehnite mineralization of the basalts of Greenland (Neuhoff et al., 1997) has shown that zeolite precipitation occurred rapidly during and just after volcanism. Prehnite precipitation occurred at 3000 m.

NYSGA: Geologic Diversity in NYC

FIELD GUIDE AND ROAD LOG

Meeting Point: Double Tree Inn, Nanuet, New York

Meeting Point Coordinates: (41.0922914, 73.996757)

Meeting Time: 8:30 AM

Distance in miles

Cumu-lative	Point to Point	Route Description
0.0	0.0	Assemble in the parking lot of Double Tree Inn.
0.23	0.23	Start out going east on NY- 59.
0.5	0.27	Turn slight right onto ramp.
1.31	0.81	Merge onto PIP N/Palisades Interstate Pkwy.
3.85	2.54	Merge onto I-87 W/I-287/New York State Trwy via EXIT 9W toward Albany.
4.73	0.88	Take EXIT 14A.
6.86	2.13	Merge onto Garden State Parkway Connector (Portions toll).
18.94	12.08	Garden State Parkway Connector becomes GSP S/Garden State Pkwy (toll) (Crossing into New Jersey).
19.33	0.39	Take EXIT 159.
19.41	0.08	Keep left at the fork in the ramp.
19.59	0.18	Keep right at the fork in the ramp.
22.78	3.19	Merge onto I-80 W toward Paterson.
23.29	0.31	Take EXIT 57C.
23.29	0.02	Turn left onto CR 509/Main St.
23.85	0.56	Turn left onto (638)/Grand St.
24.27	0.42	Turn left onto (633)/New St. Proceed 0.42 miles south on New Street then turn left into PNC Bank parking lot across from Hugo Street. Follow path into Lower New Street Quarry.

STOP 1: Lower New Street Quarry, Woodland Park, NJ.

Location Coordinates: (40.9044069, 74.1913619)

The Lower New Street Quarry (Fig. 8) is located in a wooded lot at 100 New Street, Paterson, New Jersey adjacent to Route 80 east, in Passaic County, and is mapped within the Paterson Quadrangle. It is one of several trap-rock quarries cut into the Orange Mountain basalt of New Jersey. High quality specimens of prehnite (Fig. 9), analcime, chabazite, datolite, heulandite, pectolite, natrolite, stilbite, and amethyst have been found in at Lower New Street and in the adjacent Upper New Street quarry located on the east side of New Street. This secondary mineral assemblage in the context of Paterson area trap-rock quarries has been described by Fenner (1910), Schaller (1932), Drake, (1943), Mason (1960), Sassen (1978), Peters et al. (1980), Peters (1984), Cummings (1985, 1987), Kent and Butkowski (2000),

Imbriacco (2009, 2010) Sinkankas, J. (1964), Puffer and Student (1992), Puffer and Laskowich (2012), and Laskowich and Puffer (in press).

Subaqueous pillowed OMB2 at base of quarry

At the base of the Lower New Street quarry, in a trench along the south end of the quarry wall, excellent exposures of pillow basalt provide evidence of subaqueous extrusion. Pillows are an important characteristic of the OMB2 flow wherever it has been described. Most of the pillows are large (about one meter across) and are coated with a dark green palagonite rind. Subtle differences in shape and distribution have enabled Manspeizer (1980) to distinguish between pillows, flow lobe pillows, and bedded pillow buds although some of the distinctions among sub-types are based on observation made at other quarries including the Upper New Street quarry that was cut into the OMB2 flow.

Subaerial pahoehoe OMB2 (OMB3?) on quarry wall

Flat pahoehoe surfaces, pahoehoe toes, collapsed and open lava tubes, large lower flow vesicles, and massive to columnar joint systems are exposed along the quarry wall of the Lower New Street quarry. In contrast to the pillows observed in the trench at the base of the quarry the elongate ellipsoidal structures exposed on the quarry wall are here interpreted as subaerial pahoehoe toes. The criteria for distinction between pillows and pahoehoe toes was presented by Manspeizer (1980) as first established by Macdonald (1953):

Pahoehoe toes

- Major axis of the ellipsoid 3 or 4 times the cross sectional axis.
- Concentric structures in cross section.
- Moderately to highly vesicular or amygdaloidal.
- Vesicles elongate tangentially to edge or not at all.
- Lava tubes are common, resulting in central cavities.
- Radial joints are poorly developed or absent.

Pillows

- Major axis of ellipsoid less than 3 or 4 times the cross sectional axis.
- Radial structures well developed.
- Moderately to poorly vesicular or amygdaloidal.
- Vesicles elongate radially, especially near the edge.
- Lava tubes are rare.
- Radial joints are well-developed and conspicuous in cross section.

These criteria continue to be generally accepted among volcanologists. Although not all of the ellipsoid dimensions of the pahoehoe toes exposed on the quarry wall appear to be more than 3 times the cross section axis, the criteria is based on the maximum dimension of the cross section axis which is not typically exposed in outcrop. It is, however, apparent that lava tubes are common across the quarry face. Each of these tubes have been lined to varying degrees with prehnite. Most of these tubes have collapsed or partially collapsed under the weight of late OMB3 flow inflation resulting in horizontal layers of breccia cemented with prehnite.

At a central location on the south-west quarry wall a smooth flat surface dipping northward about 15 degrees is interpreted as a subaerial pahoehoe surface. Similar surfaces are not commonly found throughout the OMB1 and OMB3 flows despite their generally recognized acceptance as subaerial flood basalt flows. The pahoehoe surface exposed here marks the transition of a subaerial flow lobe before it

was buried by a thick layer of massive tholeiitic basalt. Some columnar cooling joints are apparent in the upper quarry wall together with large vesicles that are a characteristic of OMB1, again, generally accepted as subaerial.

Secondary Mineralization

In general, the most of the prehnite (Fig. 8) that we have found among Orange Mountain basalt exposures throughout New Jersey is contained within subaerial structures including diapirs, large partially filled vesicles, half-moon vesicles, and vesicular flow-tops (Puffer and Laskowich, 2012). In contrast, the most productive zeolite collecting is largely confined to the pillows of the OMB2 flow with some notable exceptions. The prehnite to zeolites abundance ratio throughout the Lower New Street quarry above the pillow layer is typical of Orange Mountain subaerial exposures elsewhere and is quite high. There is no definitive explanation for this. However, the zeolites found in the Orange Mountain basalt are much more highly hydrated than prehnite and in most cases are sodic in contrast to prehnite which contains calcium as the only significant octahedral cation. Perhaps preferential salt water contamination of the pillowed layers during extrusion is a controlling factor. Geochemical evidence (Puffer and Student, 1992; Tollo and Gottfried, 1992) indicates that the zeolite enriched pillowed portions of OMB2 contain up to 5.34 percent Na_2O compared to a typical OMB concentration of 2.4 %.

Figure 8. Prehnite from Lower New Street Quarry, Paterson New Jersey.

Distance in miles Cumu-lative	Point to Point	Route Description
24.69	0.42	Start out going northeast on (633)/New St toward Hugo Ave.
24.56	0.98	Turn right onto (638)/Grand St.
25.03	0.47	Turn left onto CR 509/Main St.
25.26	0.23	Turn slight left onto CR 509/West Broadway.
25.36	0.10	Turn left onto Ryle Ave.
25.44	0.08	Turn left onto Ryle Rd. The cliff face exposes the black and white layers at the base of the Orange Mountain basalt.

STOP 2: Very Strange White and Black Layers at base of first Orange Mt basalt flow, Woodland Park, NJ

Location Coordinates: (40.9212118, 74.1771544)

At Stop 2 we will sample the White and Black layers of OMB1 exposed along Ryle Road at the Paterson Animal Shelter near the north end of Totowa Road (Fig. 9). Large slabs of basalt fallen to the base of the cut allow close inspection of pipe vesicles at the base of the black layer. Note the microvesicular texture of the White Layer and the black spherical shaped structures 1 to 3 mm across that comprise about 80% of the Black Layer. They are best observed with a hand lens. These spherical structures were interpreted by Puffer and Laskowich (2012) as collapsed bubbles that formed too early in the cooling history of the basalt to prevent closure of lava behind them.

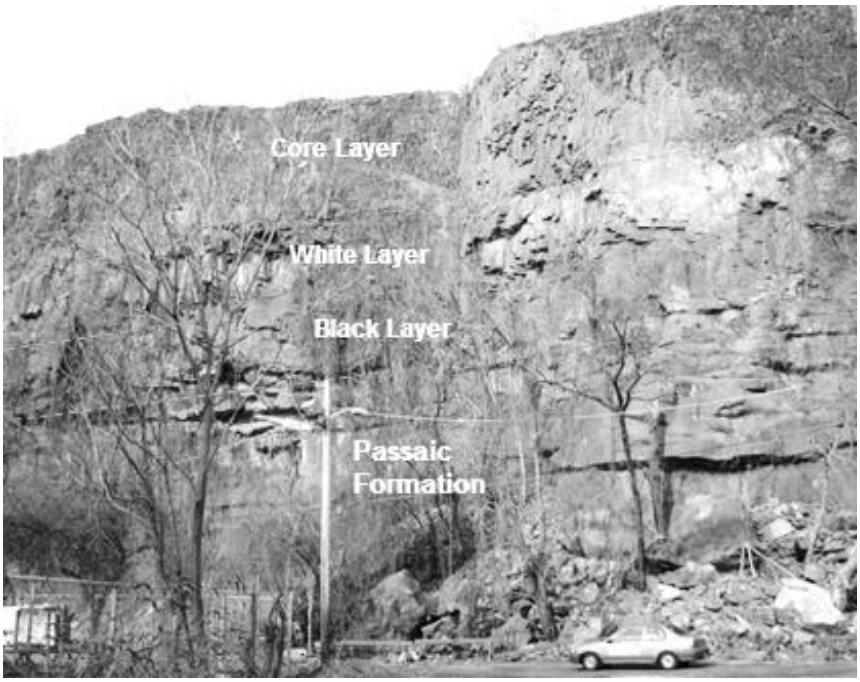

Figure 9. OMB1 Core, White, and Black layers exposed along Ryle Road.

Distance in miles Cumulative	Point to Point	Route Description
25.52	0.08	Start out going north on Ryle Rd toward Ryle Ave.
25.62	0.19	Turn right onto Ryle Ave.
25.85	0.23	Turn right onto CR 509/West Broadway.
26.04	0.19	Turn slight right onto CR 509/Main St.
26.41	0.37	Turn right onto CR 648/Market St.
26.49	0.08	Turn right onto (639)/Spruce St.
26.57	0.08	(639)/Spruce St becomes CR 639/McBride Ave. Lunch stop at Libby's Lunch (optional).

STOP 3: Orange Mountain Basalt at Great Falls, Paterson, NJ

Location Coordinates: (40.9141809, 74.1841325)

We plan to stop across from the Libby's Lunch Restaurant within a three minute walk from the edge of the cliff overlooking Great Falls. Simply walk toward the US flag at the falls (Fig. 10). The upper-middle 70 % of the OMB1 flow is exposed. An abandoned hydroelectric power plant can be seen on the bank of the Passaic River. Common half-moon vesicles are exposed along upper surfaces of basalt.

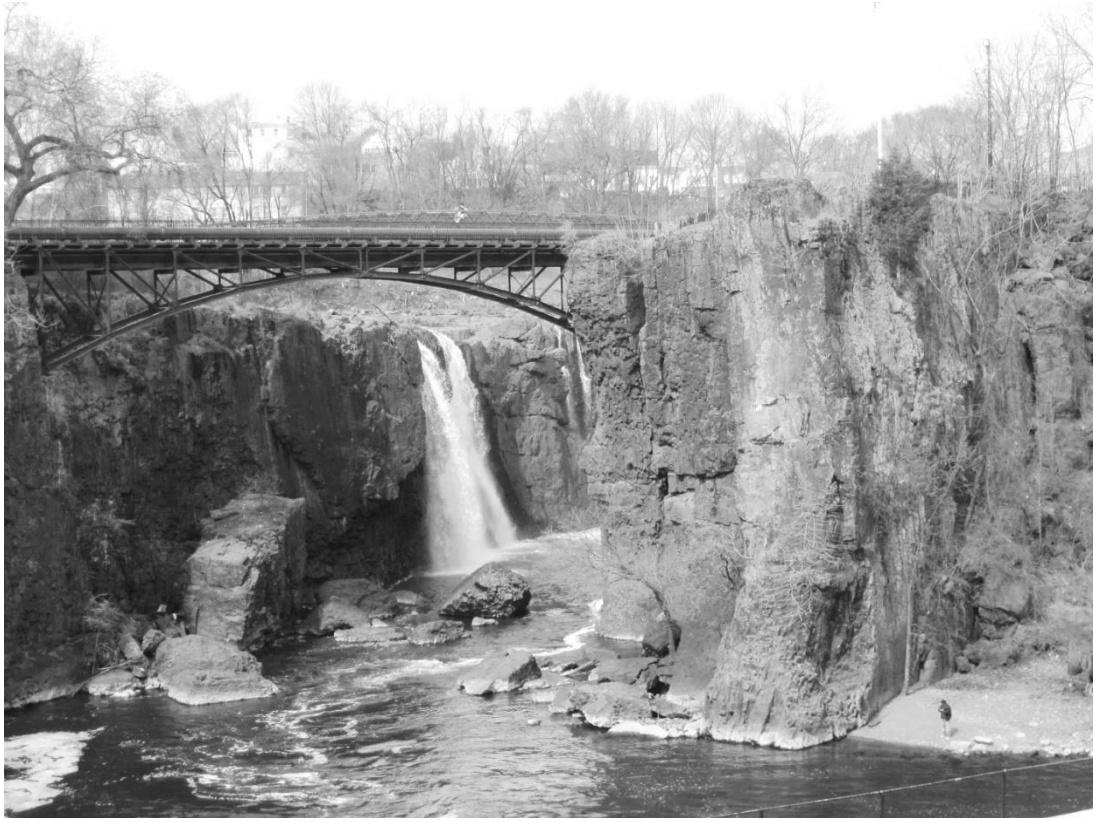

Figure 10. Great Falls, Paterson, New Jersey.

Distance in miles Cumulative	Point to Point	Route Description
26.65	0.08	Start out going east on CR 639/McBride Ave toward (639)/Spruce St.
26.85	0.20	Stay straight to go onto (639)/Spruce St.
26.96	0.11	Turn left onto Oliver St.
27.23	0.27	Stay straight to go onto NJ-19 S.
31.15	3.92	Merge onto I-80 E.
31.59	0.44	Take EXIT 62A-B.
32.16	0.57	Take EXIT 62A.
32.28	0.12	Keep left at the fork in the ramp.
32.35	0.07	Keep left at the fork in the ramp.
44.35	12.00	Merge onto GSP N/Garden State Pkwy (Portions toll) (Crossing into New York).
46.14	1.79	Garden State Pkwy becomes Garden State Parkway Connector.
47.51	1.37	Merge onto I-87 E/I-287/New York State Trwy.
49.25	1.74	Merge onto NY-59 via EXIT 14.
50.24	0.99	Merge onto NY-304 N.
51.56	1.32	NY-304 N becomes State Hwy 304.
56.10	4.54	State Hwy 304 becomes NY-304.
56.28	0.18	Turn left onto Berts Rd.
56.33	0.05	Turn left onto Long Clove Rd. Park vehicles at the Tilcon Quarry parking lot.

STOP 4: Tilcon Haverstraw Quarry in Palisades SIll, Haverstraw, NY.

Location Coordinates: (41.173221, 73.953693)

The trap-rock quarry at Haverstraw (Fig. 11) is owned and operated by Tilcon Corp. and is located on the west bank of the Hudson River. We will exit our bus at the mine office located at 66 Scratchup Road.

Tilcon N.Y., part of the Oldcastle Materials group, operates a crushed stone quarry in Haverstraw, New York. The quarry first began mine operations in 1927 and has since expanded to cover 112 acres. The majority of stone crushed in the northern Rockland County quarry ships out on barges down the Hudson River to terminals in New York City and Long Island where it will be used for construction projects including asphalt and concrete.

The quarry produces crushed diabase, known as “trap rock” in the construction industry. The stone is first blasted from the quarry’s rock faces before being crushed by the primary crusher, which is visible from the entrance of the mine. From the primary crusher, stone is sent through a tunnel under Route 9W to the secondary plant where it is crushed and screened to ensure proper size for construction usage/applications. Once the stone passes a quality test, it is transported to customers via trucks or barges.

The quarry sits on the Northern extent of the Palisades sill. The top of the quarry by the radio antenna is 580ft above sea level. The current quarry floor is -220ft. Cores drilled down from this level show another 160ft of diabase before intersecting the lower contact with the Newark group sedimentary sequence (Moore 2015). The diabase is columnar jointed in the south west corner of the quarry and dips sharply in the north east. This sharp dip causes the northeast faces to appear less defined and there is more rubble on the benches. The eastern face also shows evidence of faulting with no displacement. There is evidence of slickensides on some of the rock mined. Inside some of these faults and also in some joints mineralization of primarily calcite occurs (Delcos 2003).

The quarry has exposed both upper and lower contacts between the palisades sill and the surrounding sedimentary rocks of the Newark basin. The lower contact was intersected while constructing a conveyor tunnel under 9W (Delcos 2003). Unfortunately, the contact was covered by concrete upon completion of the tunnel. The upper contact is exposed on one of the uppermost benches on the North West face. This contact has only been recently exposed by mining operations. The upper contact zone is not clearly defined in the quarry. This is evident in The Western side of the mine where overburden is being stripped to expose more diabase. This stripped area has a horst and graben structure making it difficult to find the contact.

The Haverstraw Quarry is one of only two Quarries actively mining the Palisades sill diabase, the other is Tilcon's West Nyack Quarry.

Probably the first thing that most visitors to the Haverstraw Quarry notice is the impressive depth of the open pit. Thirteen 50 foot benches have been cut into the Palisades Sill that have exposed the lower few meters of the overlying Lockatong Formation (a non-marine meta-siltstone/argillite) and about 700 feet (about 230 m) of the Palisades Sill. Drilling into the base of the quarry has penetrated another 200 feet (65 m) of Palisades; therefore about 78% of the total thickness of the Palisades sill is visible along the quarry walls. The upper contact is rarely exposed; however at Haverstraw a distinctly red hornfels is exposed. Some of the Lockatong hornfels has dropped down along normal faults to form a graben at the southern quarry wall. The northern end of the sill becomes increasingly dike-like and at Haverstraw dips to the south at about 15 degrees.

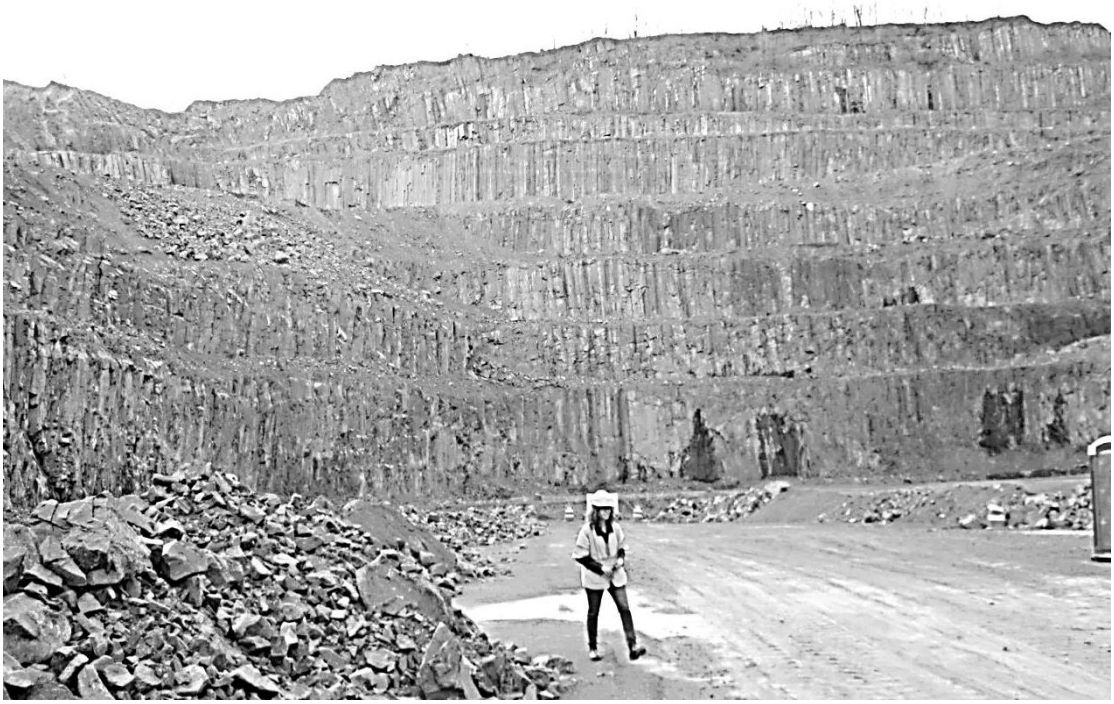

Figure 11. Quarry walls of the Haverstraw Quarry. Note the well-developed columnar jointing.

Some of the late to post-magmatic structures and textures that are exposed in the walls of the quarry include granophyres and pegmatoids. However, it is important to point out that these structures are confined to the upper Palisades. The geochemistry of the upper Palisades does not resemble the Orange Mountain basalt which is the principal objective of this chapter. The exception is the thin layer of upper chill zone that represents the upper portion of the first pulse of Palisades magma. All late pulses have intruded between the initial upper and lower chill zones. However, we have not yet analyzed samples of diabase from the upper chill zone at Haverstraw and it is possible that some late pulses intruded parallel to and above the initial chill zone, although evidence of hornfels layers or chill zone contained within the sill have not yet been found.

Granophyres

Ferrogranophyres are defined as rocks primarily composed of residual liquid with > 55% SiO2 and > 14% FeOT. In Fort Lee, NJ these constitute the sandwich horizon where the upper and lower crystallization fronts meet. The granophyre assemblages at this location exhibit significant deuteric alteration exemplified by pyroxenes almost entirely replaced by amphibole, sericitized plagioclase, and abundant myrmekite.

Gabbroids/Pegmatoids

In Upper Nyack, ferrogranophyres adopt a gabbroid/pegmatoid texture and occur from ~ 200 m to ~ 300 m. At 84 m where FeO_T reaches a maximum of 18%, the texture corresponds to a coarse ferrodiorite with abundant skeletal opaques, large euhedral plagioclase, and interstitial pyroxene. Higher in the section, (124 m to180 m) the ferrodiabase exhibits a similar texture to that observed at 84 m. Hornblende often replaces pyroxene along the rims and is accompanied by alteration products of plagioclase (sericite). From 168 m to 250 m the most evolved differentiates are ferrogranophyres containing abundant interstitial myrmekite and opaques, and exhibiting evidence of hydrothermal

alteration. There is evidence of sheared fabrics possibly caused by transport of residual liquid northward, and resulting in changes in the mineral assemblages near the solidus temperature.
At the Haverstraw quarry, smeared lenses of light-colored granophyric pegmatoid are apparent near the upper contact (Fig. 12). These lenses have been previously interpreted as products of segregation of liquid expelled from crystal mush accumulated on the floor of the magma chamber (Ragland and Arthur, 1985) and has been dubbed a 'pocket pegmatite' (Steiner et al. 1992). In places where pocket pegmatites occur, large crystals grow against the facies boundaries as a result of rapid crystal growth likely due to saturation with an deuteric fluids.

Zeolite veins

Most of the mineralized veins exposed in the wall of the Haverstraw occupy thin (0.25 to 2 cm) joints that cut through the diabase at an angle to the columnar joint system. These joints are commonly mineralized with calcite, stilbite, prehnite, chabizite, and other zeolites as mono-mineralic veins or mixtures. Where there has been displacement along joints the slickensides are typically coated with chlorite or amphiboles.

Figure 12. Fine to medium grained chill-zone diabase near the upper contact of Palisades Sill exposed at the Haverstraw Quarry. From top to bottom are red-bed sediments and slightly metamorphosed hornfels of the Lockatong Formation overlying a red v-shaped notch containing possibly fused sediment. Light gray lenses of pegmatoid oriented parallel to the upper contact have been described in detail by Steiner et al., 1992 and interpreted as pockets of residual liquid that accumulated after expulsion from a crystal mush.

Distance in miles		
Cumu-lative	Point to Point	Route Description

56.38	0.05	To return to the Double Tree Inn start out going east on Long Clove Rd toward Berts Rd.
56.56	0.18	Turn right onto Berts Rd.
62.38	5.82	Turn right onto NY-304/State Hwy 304. Continue to follow NY-304.
62.74	0.36	NY-304 becomes State Hwy 304.
63.12	0.38	State Hwy 304 becomes NY-304 S.
63.23	0.11	Take the exit.
63.33	0.10	Turn right onto Smith St.
63.61	0.28	Turn right onto NY-59 and exit vehicles at the Double Tree Inn parking lot.

REFERENCES CITED

Alt, J.C., 1986, Hydrothermal alteration of a 1 km section through the upper oceanic crust, Deep Sea Drilling Project hole 504B: Mineralogy, chemistry and evolution of seawater-basalt interactions: J. of Geophysical Research, v. 91, p. 10,309-10,335. doi: 10.1029/JB091iB10

Benimoff, A., and Puffer, J. H., 2005, Tri-modal fusion of meta-argillites along margins of early Jurassic diabase intrusions, New Jersey and New York. Northeastern Geology & Environmental Sciences: v. 27, p. 265-275.

Benimoff, A. and Puffer, J. H., 2000, Syenitic and trondhjemitic fusion at Mesozoic diabase intrusion contacts with sedimentary rocks of northern New Jersey and Staten Island: Field-trip Guidebook, 35th Annual Meeting of the Northeastern Section, Geological Society of America, New Brunswick, New Jersey, 46 pp.

Berger, G., Schott, J., and Loubet, M., 1987, Fundamental processes controlling the first stage of alteration of a basalt glass by Seawater: an experimental study between 200° and 320°C: Earth and Planetary Science Letters, v. 84, p. 431-445.

Bischoff, J.L., and Dickson F.W., 1975, Seawater-basalt interaction at 200°C and 500 bars: Implications for origin of sea-floor heavy-metal deposits and regulation of seawater chemistry: Earth and Planetary Science Letters, v. 25, p. 385-397.

Bischoff, J.L., and Seyfried, W.E., 1978, Low Temperature basalt alteration by sea water: an experimental study at 70°C and 150°C: Geochemica et Cosmochimica Acta, v. 43, p. 1937-1947.

Blackburn, T.J., Olsen, P., Bowring S.A., Mclean, N., Kent, D., Puffer, J.H., McHone, G., Rasbury, T., and El-Touhami, M., 2013. Zircon U-Pb Geochronology Links the End-Triassic Extinction with the Central Atlantic Magmatic Province: Science. v. 340, p. 941-945. With supplementary materials pp. 1-15, references, and tables.

Block, K.A; Steiner, J.C.; Puffer, J.H.; Jones, K.M.; and Goldstein, S.L., 2015. Evolution of late stage differentiates in the Palisades Sill, New York and New Jersey: Lithos v. 230, p. 121-132.

Cattafi, P.P; Mahon, J.C; Shaw, M.F; Stefanik, A; Syred, T.A; Villacis, J.P; and Puffer, J.H., 1998, The American Mine Copper Deposit of New Jersey." The Economic Geology of Central New Jersey. Field Guide and Proceedings; Fifteenth Annual Meeting of the Geological Association of New Jersey.

Cox, D.P., and Singer, D.A., 1987, Mineral Deposit Models: U.S.G.S. Bull 1693, 380 pp.

Cummings W.L. 1985, Mineralization at the Millington quarry, New Jersey: Rocks and Minerals, v. 60, p. 213-218.

Cummings W.L. 1987, Mineralization at the Fanwood & Summit Quarries, New Jersey: Rocks and Minerals, v. 62, p. 150-159.

Delcos, Lawrence. 2003, 8-10R Tilcon New York, Inc. Haverstraw Quarry Geologic Report of Proposed Operations from 2003 Through 2006. Earth Tech, 1-4. (not available to the public).

Drake, H.Y. 1943, The quarry at Upper Montclair, N.J.: Rocks and Minerals, v. 18, p. 332-333.

Drake, A.A., Jr., Volkert, R. A., Monteverde, D.H., Herman, G. C., Houghton, H. F., Parker, R. A., Dalton R. F., 1996. Bedrock geologic map of Northern New Jersey: U.S. Geol. Survey Miscellaneous Series Map 1-2540-A, scale 1:100,000.

Eckstrad, O.R., Sinclair, W.D., and Thorpe. R.I., 1995, Geology of Canadian mineral deposit types (No. 8): Geological Survey of Canada.

Fenner, C.N. 1910, The Watchung basalt and the paragenesis of its zeolites and other secondary minerals: New York Acad. Sci. Annals, v. 20**,** p. 93-187.

Greenberger, R.N., Mustard, J.F., Cloutis, E.A., Mann, P., Wilson, J.H., Flemming, R.L., Robertson, K.M., Salvatore, M.R., and Edwards, C.S., 2015, Hydrothermal alteration and diagenesis of terrestrial lacustrine pillow basalts: Coordination of hyperspectrial imaging with laboratory measurements: Geochemica et Cosmochemica Acta, v. 171, p. 174-200.

Hajash, A.H., and Chandler, G.W., 1981, An experimental investigation of high-temperature interactions between seawater and rhyolite, andesite, basalt and peridotite: Contrib. mineral. Petorl., v. 78, p. 240-254.

Imbriacco, F.A. 2009, The Braen Quarry, Haledon, Passaic County, New Jersey: Mineralogical Record, v. 40, p. 511-524.

Imbriacco, F.A. 2010, The Fanwood Quarry, Somerset County, New Jersey: Mineralogical Record, v. 41, p. 161-174.

Jahns, R. H., and Burnham, C. W., 1969, Experimental studies of pegmatite genesis: A model for the derivation and crystallization of granitic pegmatites: American Journal of Science, v. 64, p. 843-864.

Kent, B.P. and Butkowski, B. 2000, Mineral of the Millington Quarry, Somerset County, New Jersey: Mineralogical Record, v. 31**,** p. 399-411.

Laskowich, Chris and Puffer, John H. (in press) Prehnite and zeolites in the volcanic structures of the Orange Mountain Basalt, Paterson, New Jersey. The Mineralogical Record.

Lewis, J. V., 1906, The Origin and Relations of the Newark Rocks: The Newark (Triassic) Copper Ores of New Jersey; Properties of Trap Rocks for Construction: New Jersey Geological Survey Series Pt. III, p. 97-172.

Lewis, J.V., 1907, The Newark (Triassic) Copper Ores of New Jersey: Annual Report of the State Geologist For the Year 1906, p. 131-164.

Lewis, J.V. 1907, Copper Deposits of the New Jersey Triassic: Econ. Geol., v. 2, p. 244-257.

Lowenstem J. B., et. al., 1991, Evidence for Extreme Partitioning of Copper into a Magmatic Vapor Phase: Science, v. 252, p. 1405-1409.

MacDonald, G.A. 1953, Pahoehoe, aa, and block lava: American Journal of Science, v. 251, p. 169-191.

Manspeizer, W. 1980, Rift tectonics inferred from volcanic and clastic structures. In Manspeizer (editor) Field studies of New Jersey geology and guide to field trips. *52nd Annual Meeting of the New York State Geological Association*, Rutgers University, Newark New Jersey p. 314-350.

Marzoli, A., Jourdan F., Puffer J.H., Cupone, T., Tanner L. H., Weems, R.E., Bertrand H., Cirilli, S., Bellieni G., and De Min A. 2011, Timing and duration of the Central Atlantic magmatic province in the Newark and Culpeper basins, eastern U.S.A.: Lithos, v. 122, p. 175-188.

Mason, B.H. 1960, Trap rock minerals of New Jersey: New Jersey Geological Survey Bulletin 64.

Merle, R., Marzoli, A., Reisberg, L., Bertrand, H., Nemchin, A., Chiaradia, M., Callegaro, S., Jourdan, F., Bellieni, G., Kontak, D., Puffer, J., and McHone, G., 2014. Sr, Nd, Pb and Os Isotope Systematics of CAMP Tholeiites from Eastern North America (ENA): Evidence of a Subduction-enriched Mantle Source: Journal of Petrology. v. 55, p. 133-180.

Moore, Nathan, Bogdan Kevin. 2015, Preliminary Report: Haverstraw 2014 Core Drilling Program. Continental Placer Inc. (not available to the public).

Neuhoff, P.S., Watt, W.S., Bird, D.K., and Pedersen, A.K., 1997, Timing and stryctural relations of regional zeolite zones in basalts of the East Greenland continental margin: Geology, v. 25, p. 803-806.

Olsen, P.E., 1980, Fossil great lakes of the Newark Supergroup in New Jersey. *in* Manspeizer, W. (Ed.) Field studies of New Jersey geology and guide to field trips*:* New York State Geological Association, 52nd Annual Meeting, Newark, New Jersey, Rutgers University, p. 352-398.

Olsen, P.E., Kent, D.V., Cornet, B., Witte, W.K., and Schlische R.W., 1996, High-resolution stratigraphy of the Newark rift basin (early Mesozoic, eastern North America): GSA Bulletin. v. 108, p. 40–77.

Peters, J.J. 1984, Triassic traprock minerals of New Jersey: Rocks and Minerals, v. 59, p. 157-183.

Peters, T.A., Peters, J.J. and Weber, J. 1980, Famous mineral localities: Paterson, New Jersey: Mineralogical Record, v. 9, p. 157-179.

Puffer, J. H., 2003, A reactivated back-arc source for CAMP Magma: in Hames, W. E., McHome, J. G., Renne, P. R., and Ruppel, C. (editors) The Central Atlantic Magmatic Province: Insights From Fragments of Pangea: American Geophysical Union Geophysical Monograph 136, p. 151-162.

Puffer, J. H., 1984, Copper Mineralization of the Newark Basin, New Jersey : *In* Puffer J. H. (editor) Igneous Rocks of the Newark Basin: Petrology, Mineralogy, Ore Deposits, and Guide to Field Trip: Geological Association of New Jersey, 1st Annual Field Conference, p. 127-136.

Puffer, J.H., 1987, The Palisades Sill and Watchung Basalt Flows, Northern New Jersey. *In* Geological Society of America Centennial Field Guide-Northeastern Section, Geological Society of America, p. 91-96.

Puffer, J.H., 1987, Copper Mineralization of the Mesozoic Passaic Formation, Northern New Jersey. *In* Vassiliou, A, H. (editor), Process Mineralogy VII, The Metallurigical Society of AIME-SEM p. 303-313.

Puffer, J.H., 1992, Eastern North American Flood Basalts in the Context of the Incipient Breakup of Pangea. In Puffer, J. H., and Ragland, P. C., (Editors) Eastern North American Mesozoic Magmatism: Geological Society of America, Special Paper 268, p. 95-119.

Puffer, J. H. and Graham, G. E., 2005, Genetic classification of Mesozoic copper deposits of New Jersey using contemporary USGS and CGS criteria: *in* Gates, A. E. (editor), Newark Basin – View From the 21st Century, Geologic Association of New Jersey Field Guide and Proceedings, v. 22, p. 13-38.

Puffer, J.H., Block, K.A., Steiner, J.C., 2009. Transmission of Flood Basalts through a Shallow Crustal Sill and the Correlation of Sill Layers with Extrusive Flows: The Palisades Intrusive System and the Basalts of the Newark Basin, New Jersey, U.S.A: The Journal of Geology, v. 117, p. 139–155

Puffer, J. H., Benimoff, A. I., and Sclar, C. B., l993, Thermal metamorphism of sediments at the basal contact of the Orange Mountain Basalt, Paterson, New Jersey: Geological Society of America, Abstracts with Program, Burlington, Vermont, v. 25, p. 72.

Puffer, J. H., and Proctor, T., 1992, Copper Mineralization at the Base of the Orange Mountain Basalt, Newark Basin, New Jersey. Geological Society of America, Annual Meeting, Cincinnati, Ohio, Abstracts With Program, v. 24, p. 23.

Puffer, J. H., and Proctor, T., 1994, Distribution of Copper in the Orange Mountain Basalt, Related Diabase Dikes, and Underlying Passaic Formation, New Jersey. Geological Society of America, Annual Meeting, Seattle, Washington, Abstracts with Program, v. 26, p. A-402.

Puffer, J. H., and Student, J.J. l992, The volcanic structure and eruptive style of the Watchung Basalts, New Jersey*: in* Puffer, J. H. and Ragland, P. C., (editors) Eastern North American Mesozoic Magmatism: Geological Society of America, Special Paper v. 268, p. 261-279.

Puffer, J.H. and Laskowich, C. 2012, Volcanic diapirs in the Orange Mountain flood basalt: New Jersey, USA: Journal of Volcanology and Geothermal Research, v. 237-238, p. 1-9.

Ragland, P. C., and Arthur, J. D., 1985, Petrology of the Boyds diabase sheet, northern Culpeper basin, Maryland: U.S. Geological Survey Circular, no. 946, p. 91-99.

Robinson, G. P., Jr., 1987, Base and Precious Metals Associated with Diabase in t Newark, Gettysburg, and Culpeper Basins of the Eastern United States - A Review. In Froelich, A.J., and Robinson, G. R., Jr. (Editors) Studies of the Early Mesozoic Basins of the Eastern United States, U. S. Geological Survey Bulletin 1776, p. 303-319.

Robinson, G. R., Jr. and Woodriff, L.G., 1987, Characteristics of Base-Metal and Barite Vein Deposits Associated With Rift Basins: Geology of the Early Mesozoic Basins of North America. In Froelich, A. J.., and Robinson, G. R., Jr. (Editors) Studies of the Early Mesozoic Basins of the Eastern United States, U. S. Geological Survey Bulletin 1776, p. 377-390.

Robinson, G. R., Jr., and Sears, C, 1987, Inventory of Metal Occurrences Associated with the Early Mesozoic Basins of the Eastern United States. *In* Froelich, A. J., and Robinson, G. R., Jr. (Editors) Studies of the Early Mesozoic Basins of the Eastern United States, U. S. Geological Survey Bulletin 1776, p. 265-302.

Rosenbauer, R.J., Bischoff, J.L., and Zierenberg, R.A., 1988, The laboratory albitization of mid-ocean ridge basalt: J. of Geology, v. 96, p. 237-244.

Rosenbauer, R.J., Bischoff and Radtke, A.S., 1983, Hydrothermal alteration of greywacke and basalt by 4 m NaCl: Econ. Geol., v. 78, p. 1701-1710.

Sassen, R. 1978, Natrolite and associated secondary minerals at the Chimney Rock Quarry, Bound Brook, New Jersey: Mineralogical Record, v. 9, p. 25-31.

Sclar, C. B., and Moses, C. O., 1995, The Depositional Mechanism of Primary Native Copper in the Newark Basin of New Jersey. Abstracts and Program, Northeastern and Southeastern Sections, Geologic Society of America, Annual Meeting, v. 27, p. 125.

Steiner, J. C., Walker, R. J. Warner, R.D., Olsen, T.R., 1992, A cumulus-transport-deposition model for the differentiation of the Palisades Sill. In Puffer and Ragland (editors) Eastern North American Mesozoic Magmatism: The Geological Society of America Special Paper 268. p. 193-208.

Schaller, W.T. 1932, The crystal cavities of the New Jersey zeolite region: U.S. Dept of the Interior Geological Survey Bulletin, v. 832, p. 90 pp.

Sinkankas, J. 1964, Mineralogy for Amateurs: Von Nostrand Reinhold Company, New York, 585 pp.

Steinen, R.P., Gray, N.H., and Mooney, J., 1987, A Mesozoic carbonate hot-spting deposit in the Hartford Basin of Connecticut: J. of Sed. Pet., v. 57, p. 319-326.

Svensen, H., Planke, S., Chevallier, L., Malthe-Sørenssen, A., Corfu, F. and Jamtveit, B., 2007. Hydrothermal venting of greenhouse gases triggering Early Jurassic global warming: Earth and Planetary Science Letters, v. *256*(3), p. 554-566.

Tollo R.P. and Gottfried, David, 1992, Petrochemistry of Jurassic basalt from eight cores, Newark Basin, New Jersey: Implications for the volcanic petrogenesis of the Newark Supergroup: in Puffer, J. H. and Ragland, P. C., (editors) Eastern North American Mesozoic Magmatism: Geological Society of America, Special Paper 268, p. 233-259.

Van Houten, F.B., 1965, Composition of Triassic Lockatong and associated formations of Newark Group, Central New Jersey and adjacent Pennsylvania: American J. of Science, v. 263, p. 825-863.

Van Houten, F.B., 1971. Contact metamorphic mineral assemblages, late Triassic Newark group, New Jersey: Contributions to Mineralogy and Petrology, v. *30*(1), p.1-14.

Weed, W. H., 1902, Copper Deposits of New Jersey: *In* Annual Report of the State Geologist for the Year 1901. Geological Survey of New Jersey, p. 125-139.

Weed, W.H., 1903, Copper Deposits of New Jersey. *In* Annual Report of the State Geologist For theYear 1902, p. 125-137.

Weed, W.H., 1911, Copper Deposits of the Appalachian States. United States Geological Survey Bulletin 455.

Whalen, L.,E. Gazel, C. Vidito, J. Puffer, M. Bizimis, W. Henika, and M. J. Caddick, 2015, Supercontinental inheritance and its influence on supercontinental breakup: The Central Atlantic Magmatic Province and the breakup of Pangea, AGU Publications, Geochem. Geophys. Geosyst., v. 16, 23 pp, doi:10.1002/2015GC005885.

Woodward, H. P., 1944, Copper mines and mining in New Jersey: Dept of Cons. and Dev. State of New Jersey, Bull., v. 57, 156 pp.